Development, Experimentation, and Implementation of a Gap Damper System to Limit Displacements in Extreme Ground Motions

by

Taylor A. Rawlinson

A dissertation submitted to the Graduate Faculty of
Auburn University
in partial fulfillment of the
requirements for the Degree of
Doctor of Philosophy

Auburn, Alabama
May 10, 2015

Keywords: Base-isolation, Earthquake Engineering, Energy Dissipation, Seismic Pounding

Approved by

Justin D. Marshall, Chair, Associate Professor of Civil Engineering
James S. Davidson, Professor of Civil Engineering
Mary L. Hughes, Lecturer and Assistant Chair for Undergraduate Studies in Civil Engineering
Andrzej S. Nowak, Professor and Chair of Civil Engineering

Abstract

Studies have shown the effectiveness of providing supplemental energy dissipation in base-isolated structures to reduce displacements at the isolation level, often with consequences to superstructure performance. A previous analytical study demonstrated the benefits of providing this energy dissipation at a specified gap larger than the design displacement. The gap before engagement allows the base isolation system to meet performance criteria in varying levels of ground excitation. Use of this 'gap damper' device eliminates undesirable effects often exhibited with large amounts of supplemental damping at lower intensity motions. Using and expanding upon results from an analytical study, the primary purpose of this research was to develop devices for practical implementation. Development of the devices demanded simplicity, feasibility, economy, and reliability to be an effective option in building design and construction. Multiple designs were proposed, and a final design was chosen based on selection criteria and finite element analyses. The device was designed and tested in Auburn University's Structural Research Lab.

Experimental results were compared with theoretical model results to verify behavior and make necessary adjustments for design of a shake table experiment at the University of Nevada-Reno's Earthquake Engineering Lab. In addition, results were calibrated with detailed finite element analyses to investigate system behavior that could not be achieved in the lab testing environment.

With demonstrated benefits from analytical and experimental testing, a detailed design procedure was developed for practical implementation of a gap damper system. Using the design

procedure, a case study building was analyzed in OpenSees and SAP2000 for a comparison basis and demonstration of practical modeling techniques. The results of the case study clearly show the reduction of displacements at the isolation level with some consequences in the superstructure for extreme ground motions. Overall, the gap damper system shows promise in providing a performance-based system that can effectively reduce isolation level displacements without affecting response in low-to-moderate level intensity motions.

Acknowledgments

My doctoral work at Auburn would not have been possible without the help of a supporting cast. Dr. Marshall has provided me with invaluable assistance throughout my academic tenure, challenging me to become an independent thinker and problem solver. I owe my success to his continued investment in me as young professional and support in my academic endeavors. In addition, I would like to thank other members of my committee for their continued interest in my success. Dr. Davidson, through classes and research, has taught me a tremendous amount during my time at Auburn. I appreciate his interest in my work and have enjoyed working for him as a teaching assistant. The time commitment from Dr. Nowak is truly appreciated as well as his department responsibilities offer little spare time.

Dr. Hughes has left a lasting impression of my time at Auburn that I will never forget. Her continued advice, support, and encouragement has been essential to my success. Words cannot quantify my appreciation for her role in my development as a person and academic. Her husband Carl has also been a fantastic resource and friend that has devoted a large amount of time into teaching and helping me with school and personal projects. I owe a large amount of my practical development to Billy Wilson and Andy Weldon. Their advice and patience with laboratory work was essential for the success of my experimental work.

I would also like to thank my fellow graduate students and friends whose camaraderie has made Auburn a very enjoyable place to study and live the last six years. My time at Auburn has allowed me to make friends that will last a lifetime. In particular, my good friend Dave Mante has

been instrumental in my success. His practical problem solving background and support has always provided a great environment in which we challenge each other to be the best in our respective fields. My friend and colleague Patrick Koch was also critical to the early success of my project, always challenging me with his intellectual curiosity.

In addition to my colleagues at Auburn, our collaborators at the University of Nevada-Reno have been an integral part of my doctoral work. Dr. Ryan's continued advice and assistance has challenged me to become a better researcher. Hamed Zargar's commitment and passion has been invaluable to the joint success of the project. Working together with our collaborators provided both sides of the project an opportunity to learn and utilize each other's strengths.

Parents, grandparents, and extended family have continually offered love and support throughout my research endeavors. The hard work and determination necessary to complete a doctoral program was instilled by my mother's strong character. And lastly, my fiancée Alana has been my greatest influence throughout my doctoral work. I truly appreciate her patience and understanding of my long hours, especially towards the end of my dissertation. Being able to see her at the end of a long day always provided the extra motivation to finish my work. Our journey has only just begun in Auburn and I'm excited for our future together.

Table of Contents

List of Tables

List of Figures

Chapter 1. Introduction

When tasked with designing a structure, engineers and researchers continue to develop innovative solutions to create economical, functional, and sustainable results, blending aspects of science and mathematics. Within the scope of structural design exist two primary types of loading; gravity and lateral loads. Gravity loading is the most predictable loading, consisting of the dead loads, live loads, and other loads resisted vertically by the building. Adequate resistance to combinations of loads must be provided by all structural elements, including both strength and serviceability requirements with appropriate margins of safety. Lateral loading primarily consists of wind loads and seismic loads, which require very different design approaches. Wind design relies on elastic analysis to resist the demand provided by service-level wind conditions and large wind events. Due to the relatively infrequent occurrence and the magnitude of demands from seismic events, design in the elastic realm is impractical and uneconomical for earthquake loading. Therefore, structural engineers rely on inelastic behavior and energy dissipation from structural elements to resist the large forces imparted on the structure during seismic events.

1.1 Defining the Problem

The emphasis in the United States design codes is primarily focused on providing life safety and collapse prevention, rather than preserving the integrity of the structure during a seismic event. Seismic events continue to attract global attention, with valid concerns about the safety and resiliency of structures. The 1994 Northridge, California earthquake demonstrated the need to consider a multi-faceted approach to design. Although many structures met their performance

objectives, the damage costs exceeded $25 billion dollars with costly interruption in infrastructure (National Institute of Standards and Technology, 1994). In addition, the 1995 Kobe, Japan and more recently the 2010 Chile, 2011 New Zealand, and 2011 Tohoku, Japan earthquakes have stressed the importance of evolving seismic design. The challenge earthquake engineers currently face is in the development of multi-objective structures that are not only structurally sound, but also economically viable for a large range of potential ground excitations.

Most structures rely on the lateral resisting elements of a structural system to dissipate energy in a seismic event, sometimes utilizing supplemental energy dissipation devices such as viscous dampers, viscoelastic dampers, metallic yielding devices, and friction devices. Each device has its own inherent strengths and weaknesses that are evaluated for design. Within the last 30 years, the emergence of base-isolation has provided a proven option for seismic hazard mitigation. By creating a horizontally flexible layer between the structure and ground, the goal of base-isolation is to uncouple the structure from the ground motion. The flexible layer lengthens the natural period with primary first mode response at the isolation interface, reducing forces and interstory displacements in the superstructure. The base-isolators also provide beneficial damping that limits displacements at the base and dissipates earthquake energy input. The increased cost for a base isolated building is often justified for essential facilities that are vital for post-event response, such as hospitals and government structures.

Adoption of base-isolation has increased rapidly internationally with lagging adoption in the United States. Increased research in recent years is intended to fully understand base-isolation behavior and further develop and proliferate the technology. The evolution of base-isolation is fully covered within the literature review in Chapter 2. Concerns have been raised about the performance of base-isolated structures in extreme near-fault ground motions (Hall J. F., Heaton,

Halling, & Wald, 1995). Near-fault pulses can create large displacements at the isolation level that cause the structure to collide with the surrounding moat wall or damage isolators due to stability failures. Since base-isolation is typically used for the protection of essential facilities, ensuring resilience and post-event survival of the structure in extreme ground motions is requisite for the community as they recover from the aftermath of the earthquake. Limiting isolation level displacement can be achieved through a number of means, thoroughly covered within the scope of the literature review. Designing a base-isolated structure that is only resilient to extreme earthquakes is not ideal, as the structure is much more likely to be exposed to small to moderate events within its design life. Ideally, a system should be developed that responds appropriately for more frequent events and transitions behavior for more extreme events. This research effort seeks to accomplish this task by allowing traditional base-isolated behavior for small to moderate events and activates a secondary system to limit displacements in extreme events, all through passive mechanisms.

1.2 The Proposed Solution

The solution proposed in this work combines traditional base-isolation with a secondary form of energy dissipation to create a phased behavior that utilizes the strength of each device. As alluded to previously, base-isolated structures perform very well in small to moderate seismic events and this performance should be maintained. The primary problem occurs in extreme events with large displacements at the isolation level. The novel idea presented in this research involves triggering a secondary form of energy dissipation at a specified displacement in order to reduce the possibility of catastrophic collisions with the surrounding moat wall or isolator failures. Using passive energy dissipation such as viscous dampers, friction dampers, or hysteretic devices, the secondary system provides enough energy dissipation to reduce displacements with little effect on the superstructure,

with no need for an external energy supply. Due to the delayed activation, or gap, and the secondary energy dissipation, the name for the system developed within the scope of this research is coined the "gap damper system".

Many options exist for the gap damper system, therefore research was necessary to fully understand the available alternatives. Through an analytical parametric study, the type and amount of energy dissipation necessary for the desired behavior was determined. In addition, the most practical, reliable, and economical option was determined for actual implementation within a structure. The resulting system is effective in both directions, in addition to meeting other objectives presented in Chapter 3. Providing a system that is able to passively adapt to varying levels of ground excitation is a marketable and viable option for the earthquake design community.

1.3 Scope of Work

The gap damper system was developed through a collaborative effort between the University of Nevada at Reno (UNR) and Auburn University (AU), with specific tasks designated for each side of the project in addition to joint project tasks. The scope of this research is broad, initially encompassing a large array of possible system combinations. The initial task was completed by UNR, was to analytically and numerically investigate the gap damper concept and to determine the type of supplementary dissipation that was desirable to decrease base displacements while maintaining acceptable accelerations in the superstructure. This was accomplished through a large parametric study that varied isolation level properties and evaluated energy dissipation capacity of various supplemental systems relative to the base-isolated systems. The results of this parametric study were further evaluated at AU by evaluating sensitivity of the systems to ground motion suite selection, displacement demands, and superstructure modeling assumptions.

Using the results of the parametric study, the researchers at Auburn University were tasked to develop a practical implementation of the desired gap damper system found in the parametric study. This was accomplished by clearly defining a number of design objectives necessary for the success of the system and developing a practical system that was able to meet these objectives. Once developed, the further scope of the AU research involved designing, fabricating, and testing the gap damper system in order to ensure the desired real behavior of an analytical system. A full analysis of the data was conducted to evaluate important trends and make recommendations for the shake table testing. After completion of the component tests at AU, a finite element model was developed to evaluate the aspects of the system that could not be fully evaluated in the laboratory. Results from the experiment were compared to the finite element analyses to ensure the model showed similar global behavior. Once the validity of the coarse mesh was verified, a fine mesh was added to evaluate localized behavior of the system.

Lastly, a design criteria was developed for implementation of a gap damper system in a practical design of a structure. The design procedure clearly lays out the process necessary for the complete design of a system, with recommended design values and details based on the conclusions of the research. A three-dimensional case study building was introduced and the design procedure was implemented using two analytical models for a comparison of performance. Results of the study are presented to evaluate the overall performance of the gap damper system and to assess the applicability of the design procedure.

1.4 Organization of Dissertation

The organization of this dissertation is meant to mimic the steps taken in developing, analyzing, and testing the gap damper system.

Chapter 2 provides a thorough literature review, starting from basic seismic fundamentals and transitioning into earthquake engineering design. Base-isolation, although only a few decades old, has been extensively researched and developed. This review highlights some of the advancements and concerns in the field of base-isolation. In addition, a gap damper system requires supplemental energy dissipation, therefore a literature review on energy dissipation techniques is also provided.

Chapter 3 introduces the concept of the gap damper system. A parametric study is outlined and the results of the study are explained. Using the results from the study, the options available for practical implementation of a gap damper device are presented and qualitatively compared. A description of the final design chosen for implementation in a prototype device to be tested at Auburn University's Structural Research Laboratory is provided.

Chapter 4 presents the component design and experimental program conducted at Auburn University. Full design details are presented with explanation of the design considerations. The laboratory experiment is introduced, and includes prototype design calculations and description of the experimental procedure. The results of the tests are fully analyzed, providing insight towards gap damper behavior and implementation in further shake table tests.

Chapter 5 overviews the finite element analysis portion of the project. Modeling details are presented as well as a comparison of the model results to laboratory values. The model was used to evaluate behavioral features of the gap damper system that were unable to be captured in the laboratory experiment.

Chapter 6 is a collaborative chapter with researchers from the University of Nevada-Reno; a discussion of the development of design guidelines for a gap damper system for practical application is provided. The design guidelines integrate the current design procedures for base-

isolated structures with findings from the gap damper research. In addition, a case study is presented, comparing the analyses of a model building in two different structural analysis software packages. The case study provides significant insight towards the practical implementation of a gap damper system.

Chapter 7 summarizes the work completed in the dissertation. Conclusions are presented as well as recommendations for future work.

Chapter 2. Literature Review

2.1 Introduction

A structural engineer is tasked with the design of structures for both gravity and lateral loads. Gravity systems are typically straightforward to design, using strength and serviceability limit states and providing an adequate load path. Lateral loading consists of two primary types of loads, wind and seismic. Depending on the location and site conditions of the structure, wind or seismic loads may govern the design of the lateral load resisting system. For seismic design, codes in the United States are intended to provide levels of seismic protection based on the probabilistic assessment of the seismic hazard given the location of the structure. Given the high amount of uncertainty with seismic events and the large amount of energy imparted to the structure, seismic design would be economically impractical if the design required the structure to remain elastic. In addition, to strengthen a structure involves increasing the size of structural elements which consequentially increases the stiffness. With a larger stiffness, the natural period decreases and acceleration in the building increases which requires further strengthening.

Figure 2-1 illustrates the performance objectives of the U.S. design code. The design basis event (DBE) has a probability of exceedance of 10% in 50 years which would result in a high level of damage to an ordinary structure. In addition, a medium level event with a 20% probability of exceedance in 50 years would result in a moderate amount of damage to an ordinary structure. This illustrates the relatively high probability of structural damage during the life of a structure, a fact the general public or a client would often find disturbing.

Seismic Hazard			Tolerable Impact			
			Building Occupancy and Use (Category)			
Event	Occurrence	Probability of Exceedence	Infrequent (I)	Ordinary (II)	Critical (III)	Essential (IV)
Small	Frequent	50% in 30 years (43-year MRI)	Moderate	Mild	Mild	Mild
Medium	Occasional	20% in 50 years (225-year MRI)	High	Moderate	Mild	Mild
Large (DBE)	Rare	10% in 50 years (475-year MRI)	Severe	High	Moderate	Mild
Very Large (MCE)	Very Rare	2% in 50 years (2,475-year MRI)	Severe	Severe	High	Moderate

Mild impact means there is no loss of structural strength and stiffness, and the building is safe to occupy. Nonstructural systems are fully operational, and the overall extent and cost of damage is minimal.

Moderate impact means there is some structural damage, but such damage is limited and repairable. There may be delay in occupancy. Nonstructural systems are operational but may require repair. Emergency systems remain fully operational. The extent and cost of damage is significant in some areas.

High impact means there is significant damage to structural components (but "no large falling debris"). Repair is possible, but significant delays in occupancy are expected. Nonstructural systems are inoperable; emergency systems are significantly damaged, but remain operational.

Severe Impact means there is significant structural damage, but the gravity-load carrying system is still intact. Occupancy and repair may not be possible or feasible. There may be multiple casualties.

Figure 2-1. Performance Objectives of the U.S. Design Code (Judd & Charney, 2014)

Since the structure could potentially experience damage during its design life, the structural engineer must incorporate inelastic behavior in the design. Using proper detailing, structural elements can dissipate large amounts of energy through yielding. Therefore, structures must have ductile members that allow large inelastic deflections without collapsing. Ordinary structures designed in the United States are only required to provide "life safety" during a design basis event, meaning structural and nonstructural elements may be damaged beyond repair but the occupants will survive (NEHRP, 2009). This prescriptive approach to design often has undesirable consequences. A typical performance curve of a structure is shown in Figure 2-2.

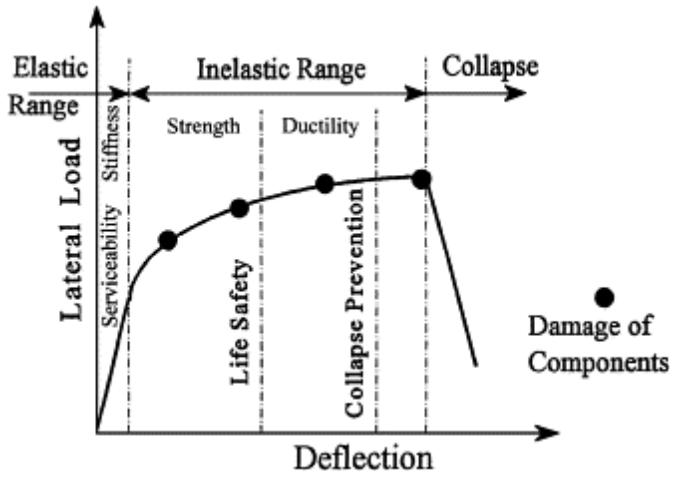

Figure 2-2. Performance Curve (Ghobarah, 2001)

Although structures met the life safety performance objective, the damage present in code compliant structures after the 1994 Northridge, California and 1995 Kobe, Japan earthquakes created large economic losses due to repairs and loss of use (Ghobarah, 2001). For example, the Olive View Medical Center in Sylmar, California resisted floor accelerations of 2.8g in the Northridge event without structural damage, yet was evacuated for days due to damage of sprinkler and water lines (Bertero & Bertero, 2002). Even though the structure achieved the life safety objective, the facility was not operational due to non-structural damages. Essential facilities such as hospitals should be immediately operational after an event to ensure post-event safety of local residents. These problems have created a need to evolve a performance-based approach that outlines expected performance of structures (structural and non-structural) at varying levels of ground motion intensity.

Bertero & Bertero (2002) recommend at least two performance levels for design, stressing the need for a more probabilistic approach to design, including structural and non-structural loss. In recent years, further attempts have been made to develop performance-based seismic design. The FEMA P-58 methodology is a culmination of a decade's worth of research with the Applied

Technology Council to develop a methodology and tools to assess structural performance (Applied Technology Council, 2012). Using building information, response quantities, fragilities, and consequence data, the FEMA P-58 methodology seeks to quantify human life loss, direct economic loss, and indirect losses such as repair time resulting from a probabilistic assessment. The FEMA P-58 provides a Performance Assessment Calculation Tool (PACT) which is a software developed specifically for the cost analysis of structures built under seismic provisions (Applied Technology Council, 2012).

With the trend moving towards a performance-based seismic design, the challenge will be to develop structural designs that are able to achieve these performance objectives. One way to meet these objectives is to develop structural elements that are multi-phased, meaning they change based on seismic demand in the structure. In particular, the goal of this research effort is to accomplish multiple performance objectives through the use of a novel "gap damper" device used to limit base level displacements in base-isolated structures. The gap damper system proposed allows a base-isolation system to respond traditionally under low-to-medium intensity motions and to engage a supplemental energy dissipation mechanism for high intensity motions. Additional energy dissipation is necessary in order to mitigate potential pounding with a surrounding moat wall or other buildings in extreme earthquakes (return period over 2475 years). In order to accomplish this task a full literature review was necessary to understand the options for the project. The literature review encompassed base-isolated structures (Section 2.2), base-isolation concerns (Section 2.3), and supplemental energy dissipation techniques (Section 2.4).

2.2 Base Isolation

Base-isolated structures exhibit a unique approach to seismic design in which the structure is uncoupled from the ground, reducing the effects of the motion. The uncoupling can be

accomplished with rollers, balls, cables, rocking columns, and soft soils (Naeim & Kelly, 1999). By placing a horizontally flexible layer between the ground and structure, the fundamental natural period of the structure is lengthened and the floor accelerations and inter-story drift demands are drastically reduced compared to conventional structures, as evident in Figure 2-3. The increased natural period allows the superstructure to remain mostly elastic for design level events, allowing the structure to be operational immediately after the event. This makes base-isolation appealing for essential buildings such as hospitals or government facilities that must be operational during and after an event in order to save lives. Another interesting application is in the seismic isolation of bridge decks with elastomeric bearings, allowing not only the desired seismic properties but also the needed flexibility in the structure necessary for temperature effects (Kunde & Jangid, 2003).

The basic elements required of a base-isolated system, as described by Buckle & Mayes (1990), are 1) a flexible mounting to lengthen the natural period of the structure, 2) an energy dissipation technique to reduce relative displacements between the ground and superstructure, and 3) rigidity under low loads for occupant comfort for service level laterals loads. Figure 2-3 illustrates these concepts by showing a) conventional structure attached to the ground with potentially large forces in the superstructure, b) an isolated rolling structure that provides no energy dissipation capacity and no rigidity against low lateral loads, and c) a successfully isolated building that provides horizontal flexibility, with energy dissipation in the form of a lead rubber bearing with enough stiffness to resist service lateral loads.

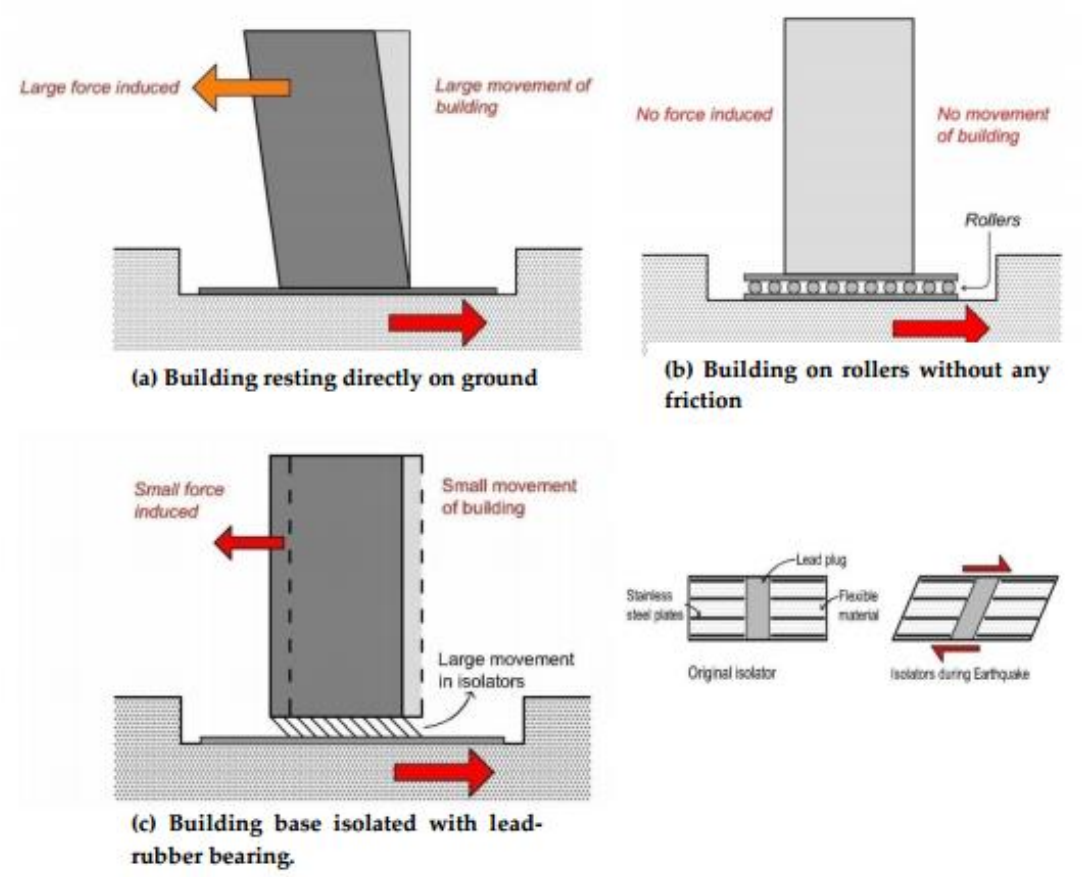

Figure 2-3. Principle of Base Isolation (Buchanan, et al., 2011)

2.2.1 The History of Base-Isolation

The concept of base-isolation has existed since the 19th century but has only been adopted in the last few decades. The first known record of seismic isolation is a double concave rolling ball bearing patented in 1870 as an "Earthquake-proof building" (Warn & Ryan, 2012). One of the first known research endeavors with base isolation was conducted in 1885 by Englishman John Milne at the University of Tokyo. Experimenting with structures built on various sized balls that slid in cast-iron saucer-like plates, he was able to accomplish an isolated system that performed well in an earthquake (Naeim & Kelly, 1999). Hundreds of similarly-devised isolation concepts were proposed over the next hundred years, however none were adapted due to lack of practicality and

skeptical designers (Buckle & Mayes, 1990). Interesting observations were made after early 20th century earthquakes when some unreinforced masonry buildings survived while neighboring buildings perished. The ones that survived were mistakenly allowed to slide on the grade beams, isolating the building from the foundation (Buckle & Mayes, 1990). Additionally, Frank Lloyd Wright designed the Imperial Hotel in Tokyo, which was founded on a thick layer of soft soil and survived the 1923 Tokyo Earthquake. Evidence of the success of base-isolation, and whether this was the actual intent of Wright's design, is debatable (Buckle & Mayes, 1990).

The practicality of base isolation has only been realized in the last 35 years as the development of multi-layered elastomeric bearings progressed. These bearings use alternating layers of rubber and steel which allow them to carry the large gravity loads from the structure while providing the horizontal flexibility necessary to isolation the superstructure (Naeim & Kelly, 1999). The first modern use of base-isolation was for a government building in Wellington, New Zealand in 1981, which used an elastomeric layered steel and rubber bearing containing a lead core for hysteretic energy dissipation. The technology was first used in the United States in 1985 in Rancho Cucamongo, California with the isolation of the Foothill Communities Law and Justice Center through the use of high-damping rubber bearings. Around the same time, the first modern day sliding system was developed utilizing spherical sliding surfaces to achieve isolation objectives while relying on friction for energy dissipation (Taylor & Aiken, 2011).

From 1985 to 1997, an average of three seismic isolation projects were completed a year in the U.S. while production in Japan had been increasing rapidly, reaching a total of 600 buildings by the year 2000 (Taylor & Aiken, 2011). One project of note in the U.S. was the retrofit of San Francisco City Hall in 1998, adding 530 rubber bearings with lead cores at the base of each column and shear wall (Figure 2-4). This retrofit extended the natural period of the building to 2.5 seconds

for a design earthquake with 18 to 26 inches of relative lateral movement (Chopra, 2012).

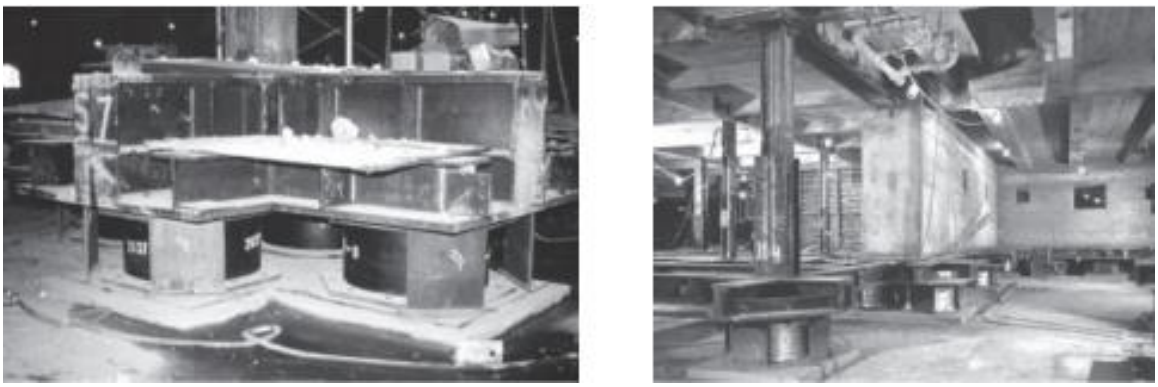

Figure 2-4. Isolators at the Base of Columns and Shear Walls (Chopra, 2012)

2.2.2 Isolation Methods

The two primary methods of seismic isolation involve elastomeric (natural rubber, high damping rubber and lead-rubber) and sliding bearings, each of which are reviewed in this section.

2.2.2.1 Elastomeric Bearings

One of the most common forms of seismic isolation utilizes hard rubber and steel shims, as shown in Figure 2-5. Rubber layers are meant to provide the horizontal flexibility necessary for the isolation of the structure and the steel shims are intended for vertical stiffness so that the bearing does not bulge under the large building weight. In the manufacturing process, natural or synthetic rubber is layered with steel shims in a mold in alternating fashion and then heated in order to vulcanize and bond the rubber to the steel (Warn & Ryan, 2012). A rubber cover provides protection from environmental effects (Lake & Lindley, 1967). Steel plates are typically attached at the top and bottom for connection to the foundation and structure.

There are two primary types of regular elastomeric bearings, low damping natural rubber and high damping rubber. Low damping rubber only provides 2-3% of critical damping at 100%

shear strain, with a linear stress-strain distribution up to 150% shear strain. Concurrent supplemental energy dissipation is necessary with the low damping bearings to limit isolator level displacements (Warn & Ryan, 2012). High damping rubber bearings are created by adding carbon black to the rubber which makes the bearings stiffer but provides beneficial energy dissipation (Naeim & Kelly, 1999). The difference between the behavior of the low and high damping rubber is evident in Figure 2-5, which shows the hysteresis loops of the two types of isolators. The wider hysteresis loops (Figure 2-5b) for the high damping rubber indicate the effectiveness in energy dissipation, while the narrow hysteresis loops (Figure 2-5a) for the natural rubber indicate the need for supplemental energy dissipation.

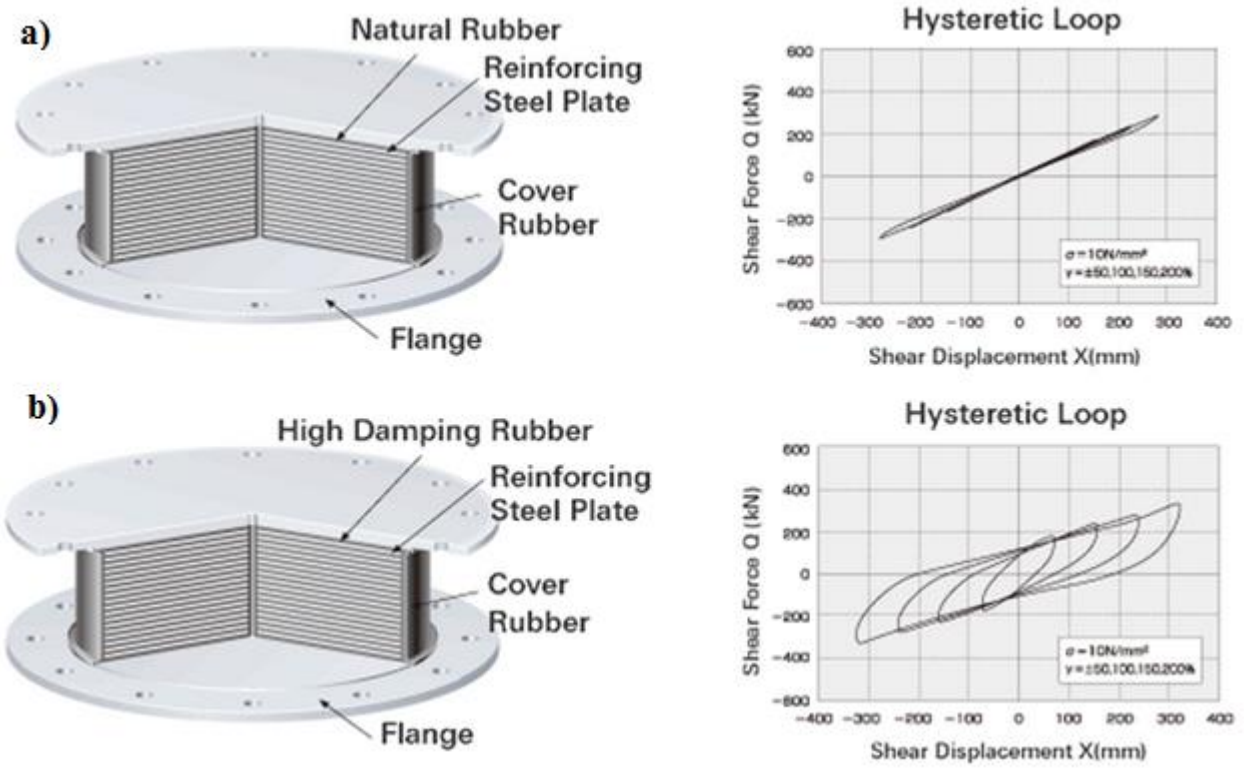

Figure 2-5. a) Natural "Low Damping" Rubber Isolator with Hysteresis b) High Damping Rubber Isolator with Hysteresis (Bridgestone Corporation, 2014)

Warn & Ryan (2012) introduce a few important fundamental elastomeric bearing calculations necessary to understand system properties. The horizontal stiffness (Equation 2-1) of the bearing (K_h) is a function of the shear modulus (G), area of the bonded rubber (A_b), and the total thickness of the rubber layers (T_r):

$$\mathbf{K_h = \frac{GA_b}{T_r}} \qquad \textbf{Equation (2-1)}$$

The compression modulus (E_c) for an individual, solid, circular incompressible rubber layer is:

$$\mathbf{E_c = 6GS^2} \qquad \textbf{Equation (2-2)}$$

where S is the shape factor defined in Equation 2-3 and illustrated in Figure 2-6:

$$\mathbf{S = \frac{Loaded\ Area}{Area\ Free\ to\ Bulge}} \qquad \textbf{Equation (2-3)}$$

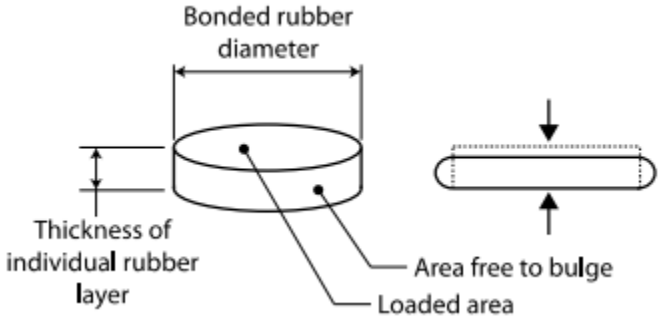

Figure 2-6. Rubber Layer (Warn & Vu, 2012)

Vertical stiffness (K_v) is defined as

$$\mathbf{K_V = \frac{E_c A_b}{T_r}} \qquad \textbf{Equation (2-4)}$$

meaning that the ratio between vertical and horizontal stiffness in a bearing is

$$\mathbf{\frac{K_V}{K_h} = 6S^2} \qquad \textbf{Equation (2-5)}$$

With shape factors typically ranging from 15 to 30, the exponential relationship between the two stiffnesses means the vertical stiffness is considerably higher than the horizontal stiffness. This high vertical stiffness leads to a high natural frequency in the vertical direction, which can

potentially cause problems with amplification of the vertical high frequency ground motions (Warn & Vu, 2012).

2.2.2.2 Lead Rubber Bearings

A modified and commonly used version of the elastomeric bearing is the lead-rubber bearing. The bearings are similar to the natural rubber bearings but utilize a lead plug in the core of the isolator for hysteretic energy dissipation (Figure 2-7). This potentially eliminates the need for supplemental energy dissipation in the base level for low intensity ground motions.

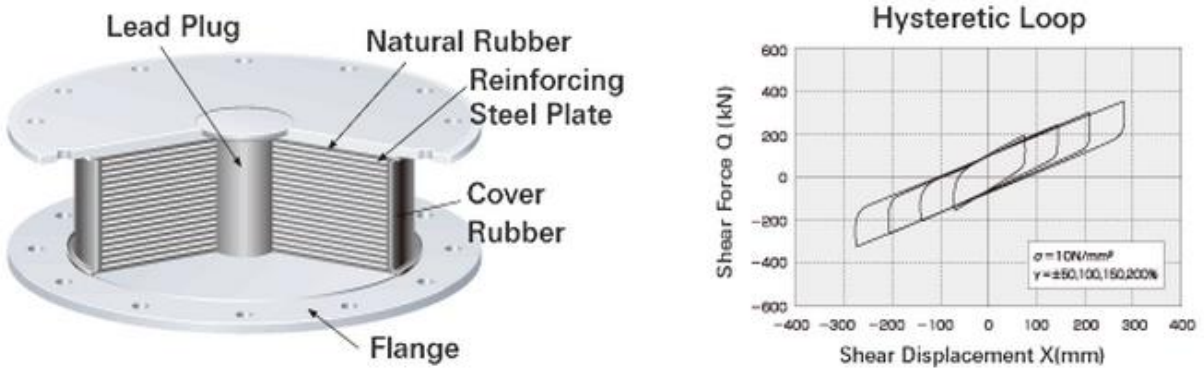

Figure 2-7. Lead-Rubber Bearing (Bridgestone Corporation, 2014)

Warn & Ryan (2012) identify a few of the important equations that characterize the force-displacement relationship of the lead-rubber bearings. The hysteretic strength (Q_d) is defined as a function of the shear yield strength of the lead core (σ_L) and area of the lead core (A_L):

$$\mathbf{Q_d = \sigma_L A_L} \qquad \textbf{Equation (2-6)}$$

with the secondary stiffness (K_d) representing the stiffness of the rubber, given in Equation 2-1, the horizontal effective stiffness (K_{eff}) at a given displacement (d) can be determined as:

$$\mathbf{K_{eff} = \frac{Q_d}{d} + K_d} \qquad \textbf{Equation (2-7)}$$

with the bilinear force-displacement relationship is shown in Figure 2-8. As evident from the figure, the effective stiffness and resulting natural period are functions of the displacement. Other

parameters of concern in the figure are the yield force (F_y) which is the point of stiffness transition and the elastic stiffness (K_e) which is the initial stiffness of the isolator, typically valid up to 1 inch of lateral displacement and responsible for controlling service loads (Dynamic Isolation Systems, 2014). The EDC, or energy dissipated per cycle, is the area contained in the hysteresis loop, which is a measure of the damping capability of the isolator.

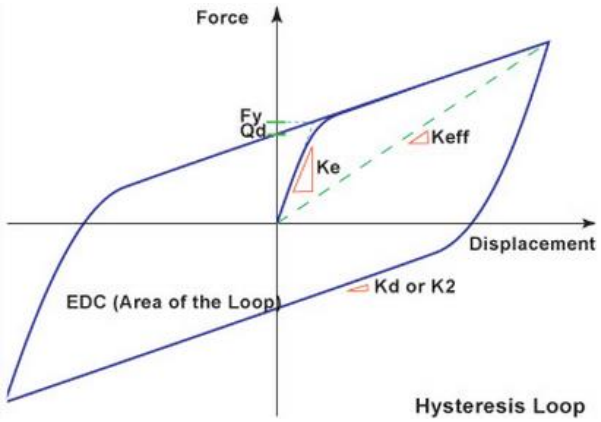

Figure 2-8. Bilinear Characterization of the Lead-Rubber Bearings (Dynamic Isolation Systems, 2014)

2.2.2.3 Sliding Bearings

Another type of isolation is achieved through the use of sliding bearings. Although this can be accomplished in a number of ways, the first practical use of a sliding bearing was in the form of a Friction Pendulum System (Zayas, Low, & Mahin, 1987). Using a slider resting on a concave surface, the two surfaces are coated with polytetrafluoroethylene (PTFE) to allow sliding; this action provides beneficial friction energy dissipation during relative movement. The concave surface is necessary for the re-centering of the device as a flat friction surface would require springs to restore the structure to its original position (Figure 2-9).

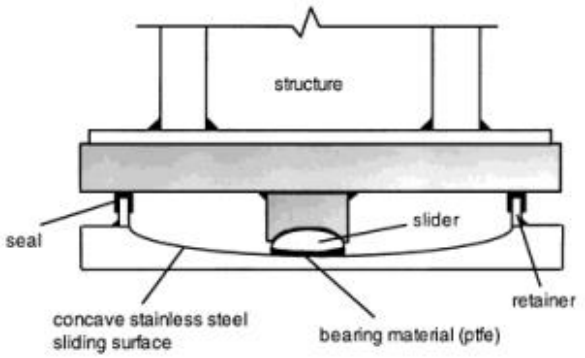

Figure 2-9. Friction Pendulum System (Almazan, de la Llera, & Inaudi, 1998)

The force-deformation behavior of a friction pendulum system is similar to that of the lead-rubber bearings shown in Figure 2-8 but with a variation in parameter equations. Similar to the elastomeric bearings, Warn & Ryan (2012) identified some of the important equations for friction pendulum bearings. The hysteretic strength (Q_d) is defined as a function of the coefficient of friction (μ) and the weight carried by the isolator (W):

$$\mathbf{Q_d = \mu W} \qquad \textbf{Equation (2-8)}$$

The secondary stiffness (K_d) defined as a function of the weight (W) and radius of curvature (R):

$$\mathbf{K_d = \frac{W}{R}} \qquad \textbf{Equation (2-9)}$$

The natural period (T_N) of the isolator is:

$$\mathbf{T_N = 2\pi\sqrt{\frac{R}{g}}} \qquad \textbf{Equation (2-10)}$$

where g is the acceleration of gravity. This expression is the equation for the fundamental period of a pendulum. This means that the natural period of a friction pendulum device is only dependent on the radius of curvature and not on the mass of the structure (Al-Hussaini, Zayas, & Constantinou, 1994).

More recently friction pendulum devices have been adapted to include multiple pendulum mechanisms. A double pendulum was developed by Fenz and Constantinou (2006) that had two

varying concave surfaces on the top and bottom plates of the bearing surface. By varying concave surfaces and friction coefficients of the contact surfaces, a multi-staged pendulum device was developed to achieve multiple performance objectives. Furthermore, a triple pendulum device was developed by EPS, Inc. that included four concave surfaces and three pendulum mechanisms (Morgan & Mahin, 2011). The increasing friction resistance with increasing base displacement creates a three-stage response that reduces potentially large base displacement demands in larger seismic events. The complex behavior is best illustrated in Figure 2-10, which shows the progression of the device through the three pendulum mechanisms. The force required to activate each stage increases based on the relationship between the radius of curvature and friction coefficient.

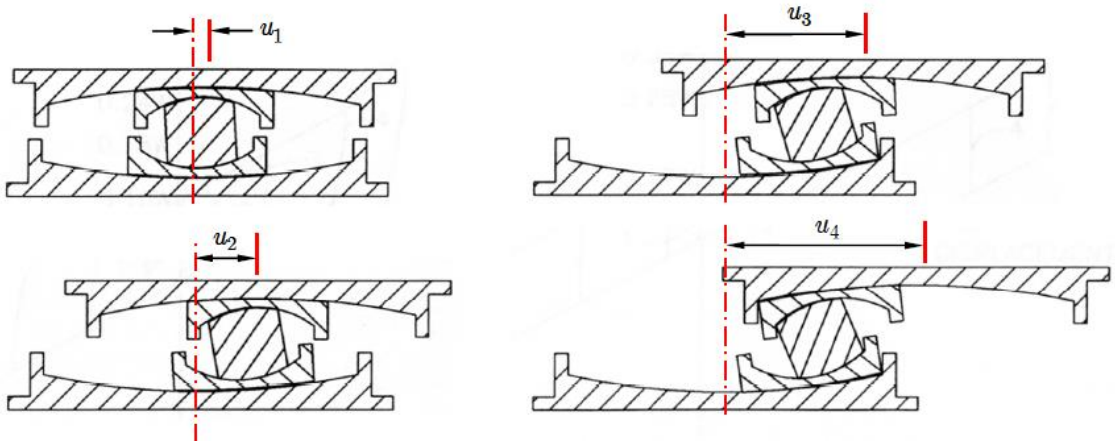

Figure 2-10. Stages of the Triple Pendulum System (Morgan & Mahin, 2011)

2.2.2.4 Other Base Isolation Methods

Although elastomeric and sliding bearings are the primary methods of base-isolation, a few other designs have been proposed involving rolling mechanisms. One method involves a rolling system proposed by Lin & Hone (1993) which isolates the building by allowing the building to roll on the foundation. Although very effective in reducing the transmission of earthquake forces into the

structure, the major drawback of the system is the large magnitude of residual displacements at the base level due to a lack of re-centering capabilities. An interesting system proposed by Jangid & Londhe (1998) attempts to resolve this issue by isolating the building using elliptical rollers, shown in Figure 2-11. This system is found to be more effective than the circular rolling rods, with decreasing effectiveness at large superstructure natural periods.

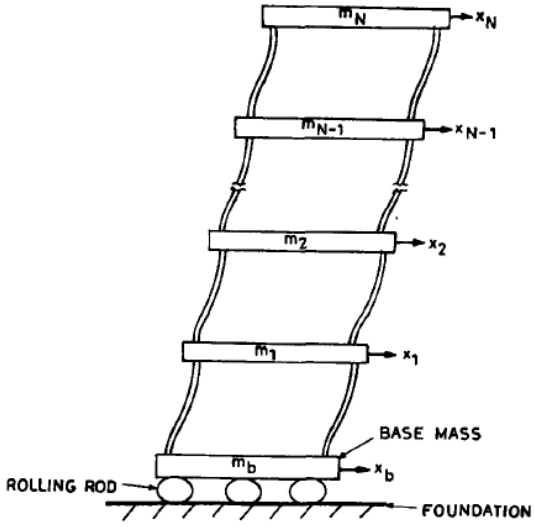

Figure 2-11. Elliptical Rolling Base-Isolation (Jangid & Londhe, 1998)

2.2.3 Base Isolation Research

With the rise of base-isolation implementation, there has been a tremendous amount of research surrounding the subject in the last 30 years. This section is intended to identify some, but not all, of this research; including analytical studies, experimental studies, and performance evaluations of existing buildings during seismic events.

2.2.3.1 Analytical Studies

Adequate comparison between conventional structures and base-isolated structures was lacking for years until the development of design provisions for base-isolated buildings and bridges. Lin & Shenton III (1992) completed one of the first analytical comparisons of code compliant

buildings using the 1990 Structural Engineers Association of California (SEAOC) *Recommended Lateral Force Requirements and Commentary* for base-isolated buildings designed to 25%, 50%, and 100% of required strength (SEAOC, 1990). The study was meant to determine the equivalent design force level for a base-isolated building relative to a fixed-base building. For both a steel concentrically braced frame and moment frame structure, the base-isolated buildings designed at 25-50% of the strength provision performed at least as well as the fixed-based structure in a 54 ground motion, non-linear time history analysis. Generally speaking, the base-isolated braced frame outperformed the moment frame structure.

Around the same time, Nagarajaiah, Reinhorn, & Constantinou (1991) completed a 3-dimensional analysis of base-isolated structures. Capturing the non-linear behavior of the isolation systems, elastomeric or sliding, was difficult with existing algorithms, therefore a new solution was developed. This solution was verfied with experimental results of a ¼-scale six-story base-isolated friction pendulum system. Using the new algorithm solution, an analytical comparison of a friction pendulum system and a lead-rubber bearing system was made for a six-story reinforced concrete structure. For the given design, the friction pendulum system was more effective at reducing base level displacements; the response was larger in the superstructure with higher interstory drifts.

2.2.3.2 Experimental Studies

Preliminary studies demonstrated the potential benefits of base-isolation and with increasing interest, many experimental studies were completed in order to verify behavior.

One of the first experimental studies of elastomeric bearings was done by Kelly & Hodder (1982) in the evaluation of lead and elastomeric bearings using a 1/3-scale, five-story, three-bay isolated structure. The tests were meant to not only verify the effectiveness of base-isolation, but

also to identify the rubber material and central core materials that were best for isolation systems. Figure 2-12 shows the response of the isolated structures in comparison to the fixed-base structure, indicating at least 10 times the reduction of acceleration in the isolated superstructure. The lead filled elastomeric bearings were determined to be the most effective at reducing the acceleration in the structure, in addition to limiting displacements at the base level due to the energy dissipation of the lead core. Although the 40 durometer bearings showed promising acceleration reduction, the flexibility without the lead core produced large base displacements.

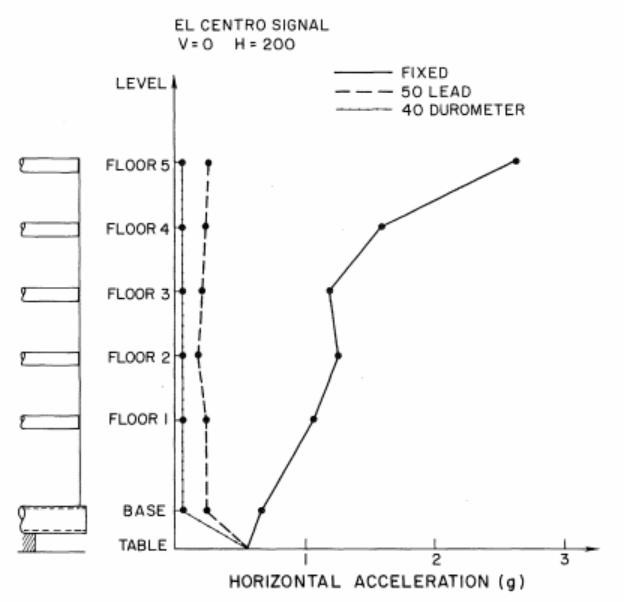

Figure 2-12. Comparison of Fixed-Based Structure to Elastomeric Bearings (Kelly & Hodder, 1982)

Building on previous research of Zayas, Low, & Mahin (1987), Mokha, Constantinou, Reinhorn, & Zayas (1991) experimentally evaluated a ¼-scale six-story building isolated with four friction pendulum bearings. The six-story building was used to evalute resistance to overturning that may be possible due to a large height-to-width aspect ratio. The study showed the overall effectiveness and robustness of the friction pendulum system to varying seismic inputs. The isolated structure was able to remain elastic up to six times the peak shake table acceleration values

of the fixed-base structure for one ground motion. In addition, the analysis techniques proposed by Constantinou, Mokha, & Reinhorn (1990) for friction pendulum systems were verified with experiemental results.

Wolff & Constantinou (2004) tested a total of 27 configurations in the six-story model pictured in Figure 2-13 with an emphasis on secondary systems (fire sprinkler systems, drop ceilings, etc). The configurations were a mix of fixed-base and base-isolated buildings isolated with elastomeric, lead-rubber, and friction pendulum bearings with and without supplemental damping. The superstructures used were a steel moment frame, symmetrically braced frame, and asymmetrically braced frame. A major observation of the study is that the addition of supplemental damping to the system substantially and negatively impacted the performance of the building, an important point that will be discussed further in Section 2.3.2. In addition, the floor accelerations were found to be largely dependent on the substructure period, with the moment frame accelerations exceeding the braced frame, primarily because the fixed-base period of the braced frame is much smaller than the isolation period. Smaller peak floor velocity and drift values were found in the buildings isolated using friction pendulum systems. Generally speaking, the highly nonlinear systems such as the friction pendulum systems and a combined elastomeric and sliding system offered the best protection of building contents. In addition, results were compared to analytical results demonstrating about a 15% disjoint between measured and analytical values.

Figure 2-13. Six-Story Base Isolated Model Structure (Wolff & Constantinou, 2004)

Dolce, Cardone, & Ponzo (2007) compared the response of a reinforced concrete frame isolated with four different types of isolation systems. The isolation systems consisted of rubber-based, steel-based, and shape memory alloy based isolation, and a hybrid system with shape memory alloys and hysteretic components. The shape memory alloy systems have the capability of dissipating large amounts of energy and returning to the original unstressed state. All systems offered excellent strutural performance relative to fixed-base structures but no system optimally reduced base displacements, base shear, and floor accelerations. For instance, the rubber-based system offered a substantial reduction in floor acceleration at a cost of increased base displacements and base shear coefficient. The authors suggest that the type of isolation system should largely depend on the design objectives of the structure.

More recently, a large full-scale collaborative project was completed at "E-Defense" using the world's largest shake table in Japan. Sasaki, et al (2012) demonstrated the effectiveness of both lead-rubber bearing and triple friction pendulum systems in the testing of a five-story steel moment frame subjected to bidirectional motions, in addition to vertical excitations. A large reduction in superstructure acceleration is evident in Figure 2-14, which compares the ratio of acceleration response of the fixed-base structure (Fix) to the triple pendulum bearing (TPB) and lead-rubber bearing (LRB) systems. The ratio of less than one for the base-isolated systems indicates that both systems are effective in reducing acceleration in the superstructure. The three applied excitations were vastly different to test the robustness of the system to different ground motions, including a frequent motion (Westmorland), long duration subduction motion (Iwanuma), and a near-fault motion (Rinaldi). A mass eccentricity was also introduced in order to capture the isolator resistance to torsion; the triple-pendulum bearing provided a better mitigation of torsion than the lead-rubber bearings.

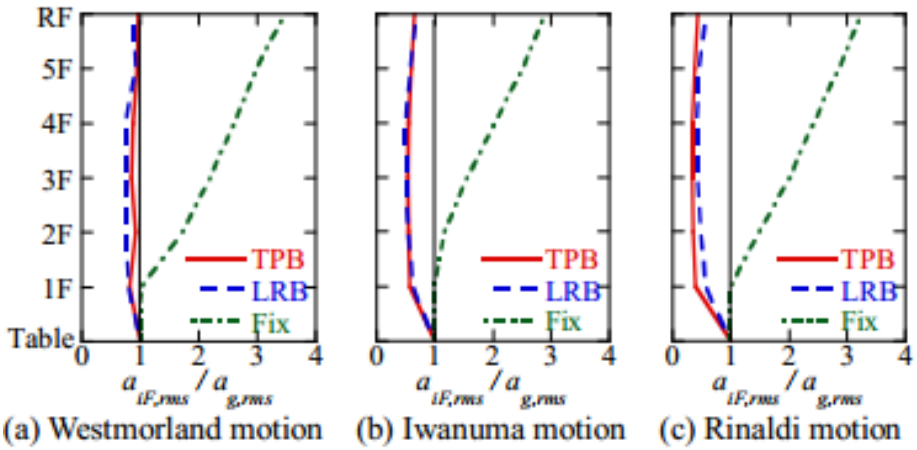

Figure 2-14. Response Acceleration Comparison for Three Ground Motions (Sasaki, et al., 2012)

2.2.3.3 Performance Evaluations

Given the relative infrequency of seismic events and the relatively new emergence of base-isolation, there have only been a few instances where existing base-isolated structures have been exposed to ground motions. These performance evaluations are obviously one of the most important factors in assessing the performance of base-isolated structures, as they are not conducted in a controlled analytical or lab environment.

Stewart, Conte, & Aiken (1999) evaluated the response of four base-isolated buildings during six earthquakes in California. The structure evaluated included the Los Angeles Fire Command and Control Building, Los Angeles USC Hospital, Foothills Communities Law and Justice Center in Rancho Cucamonga, and the Seal Beach Building in Seal Beach, CA. This study primarily dealt with the observed isolator mechanical properties compared to the properties assumed for modeling in order to evaluate the appropriateness of design and modeling procedures. Although the structures experienced the desired frequency reduction for large ground motion pulses, the reduction was not nearly as substantial as design suggested for design basis earthquakes. The stiffness and damping present in the isolators were evaluated and found to be extremely dependent on the amplitude of the ground motions. For small shear strain levels, the stiffness in the isolators was measured to be higher than predicted and showed a significant reduction in stiffness with an increase in shear strain. The study suggests that incorporating fully-softened stiffness and damping values determined from experimental evaluation may not provide the most accurate portrayal of as-built behavior, and the authors suggest a careful consideration of ground motion amplitude when designing for small to moderate earthquakes. This practice may result in an increase in superstructure participation and subsequent nonstructural damage.

Mikras & Deoskar (1996) present a comparison of an analytical model and observed behavior of a base-isolated building subjected to the 1994 Northridge Earthquake. A previously

proposed model generally predicted accurate response of the structure and a simplified modal analysis procedure was further developed to predict superstructure response. Analysis of the data indicated that the isolation system was able to reduce the acceleration in the superstructure by 45%.

Nagarajaiah & Sun (2000) evaluated the response of the USC Hospital Building in response to the Northridge earthquake in 1994. This building has a total of 149 isolators that are a mix of lead-rubber bearings for the exterior columns and elastomeric bearings for the interior columns (Figure 2-15). Calibrating an analytical model with measured values obtained from sensors during the ground motions allowed a full evaluation of the system performance. Although the spectral acceleration was only 30% of the design values, the study suggests appropriate behavior of the structure would be realized for future stronger events as well. The Northridge event had significant energy in the higher modes that were eliminated due to the presence of the base-isolation system. The superstructure remained elastic, with peak roof acceleration reduced to less than 50% of peak ground acceleration and superstructure drift was less than 30% of code requirements. Period lengthening was evident with an estimated 15% damping in the fundamental mode of vibration.

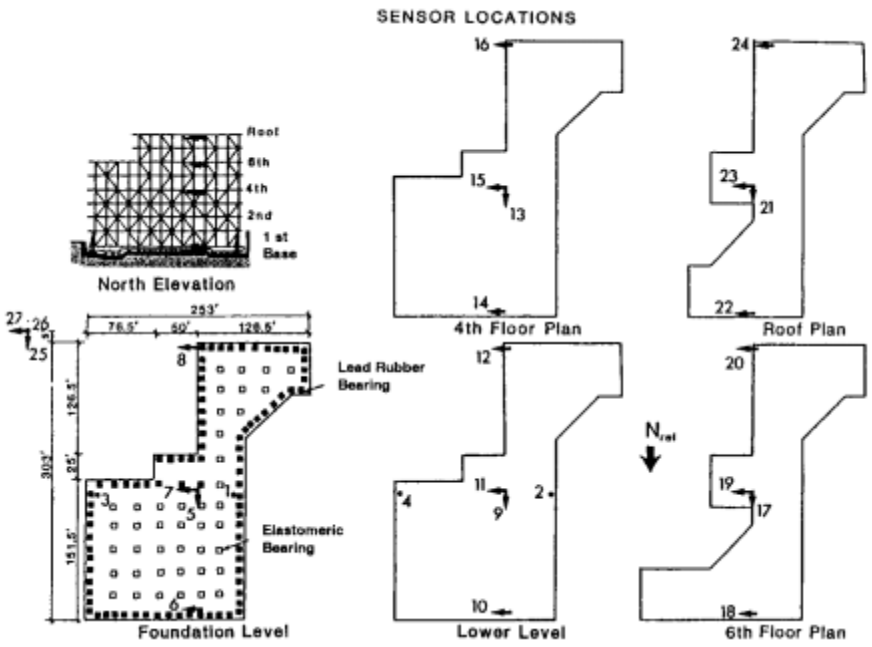

Figure 2-15. USC Hospital Elevation, Plan Views, Isolator Layout, and Sensor Locations (Nagarajaiah & Sun, 2000)

Kani, Takayama, & Wada (2006) give a thorough review of the seismic performance of Japanese base-isolated structures. Over a dozen isolated buildings were surveyed after the 2004 Niigata-Chuetsu (M6.8) and 2005 Fukuoka West-Offshore earthquakes (M7.0), focusing on damage as well as human perception of movement. The damage was limited to non-structural damage, if any at all, in all of the isolated buildings while neighboring conventional structures experienced costly damages. Overall, occupants and owners were very satisfied with the performance of the structures, often citing very little perception of any ground vibration.

Roussis, Constantinou, Erdik, Durukal, & Dicleili (2003) detail the failure of the isolation system protecting the Bolu Viaduct in the Duzce, Turkey earthquake of 1999. The viaduct was built close to a fault with a combination of sliding friction bearings and yielding steel hysteretic devices that did not meet current design requirements. Displacement demand capacity required by the code was 790 mm while the sliders only allowed 210 mm of movement. Unfortunately, even if designed according to code, analyses indicate that the structure would have surpassed

design requirements by 600 mm, suggesting the near-source effects of ground motion can be troublesome for isolated structures.

2.2.4 Adaptive Base-Isolation Systems

One of the primary concerns with isolation systems, further discussed in Section 2.3.1, is the large displacement demand in the base level of the isolation system that can lead to structural pounding or isolator instabilities. In order to mitigate this problem, fully active and semi-active control systems have been proposed for use alongside the base isolation system, which allows adaptation to varying intensities of excitation using control algorithms and a power supply. Using sensors, actuators, and a feedback loop, active control can potentially eliminate building movement by countering with an opposing force. Although thoroughly researched worldwide, implementation of such systems is rare due to large costs, maintenance issues, reliance on external power, and concerns of the reliability of the feedback control (Spencer Jr. & Nagarajaiah, 2003)

Semi-active control is a rapidly developing area in the field of civil engineering. The devices do not impart any mechanical energy into the structural system, but have properties that can be altered in order to reduce the structural response. Examples include controllable fluid dampers, controllable friction devices, variable stiffness devices, and variable-orifice fluid dampers. Many semi-active devices are able to operate on battery power, making it an appealing option because of the adaptability of the systems without the use of an external power source (Asteris, 2008).

Controllable fluid dampers offer simplicity and reliability of semi-active control in the form of electrorheological (ER) and magnetorheological (MR) devices. Reversible behavior between a viscous fluid and a semi-solid fluid is achieved by inducing an electric or magnetic field as needed to dissipate energy (Spencer Jr. & Nagarajaiah, 2003). ER fluids have been thoroughly researched and remain limited in use due to a limited yield stress range, high voltage requirements, low level of safety, and

intolerability to fluid impurities. In recent years, magnetorheological (MR) fluid dampers, as illustrated in Figure 2-16, have become a more attractive option for semi-active controllable fluid dampers. MR fluid is able to achieve much higher yield stresses than ER fluids in addition to requiring much less power, and exhibiting resilience to temperature changes and fluid impurities (Spencer Jr. & Sain, 1997).

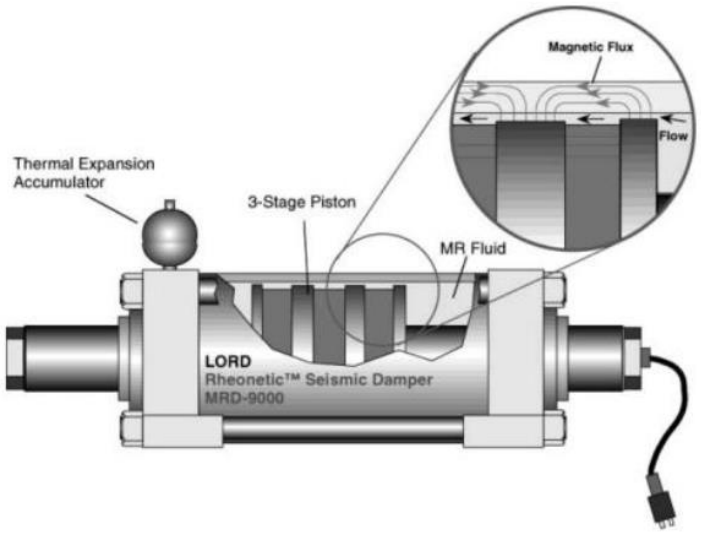

Figure 2-16. Magnetorheological Fluid Damper (Spencer Jr. & Nagarajaiah, 2003)

Due to that fact that this is a developing field, there are still many inherent problems to be resolved. Complex algorithms that are not yet optimal are involved in relaying information from sensors to the control center. Reigles & Symans (2005) completed a quantitative comparison of ten peer-reviewed "smart" semi-active isolation systems. The performance metrics involved the isolation system deformation, superstructure accelerations, and superstructure interstory drifts. Systematically evaluating all of the systems led to a conclusion that although semi-active control shows promise, there is still a need to advance the technology to be competitive with less complex passive systems. In addition, direct comparisons between semi-active and passive systems are difficult to make due to the variability of damping.

2.2.5 Design for Base-Isolation

The first attempt to incorporate design provisions for seismic isolation was in the mid-1980s by the Structural Engineers Association of California (SEAOC). The provisions were adopted by the 1991 Uniform Building Code and were not mandatory for design. The National Earthquake Hazard Reduction Program's (NEHRP) *Recommended Provisions for Seismic Regulations for New Buildings* developed isolation design provisions that were adopted by the Uniform Building Code (UBC) which was eventually replaced by the International Building Code (IBC) in 2000 (ASCE, 2004). Currently the NEHRP serves as the primary resource document for the American Society of Civil Engineers *Minimum Design Loads for Buildings and Other Structures* (ASCE 7-10) in the design of isolated buildings (NEHRP, 2009). These provisions provide isolator design displacements, superstructure design criteria, and testing protocol for the isolators.

The *General Design Requirements* of the seismic provisions of NEHRP (2009) specify a seismically isolated structure should be able to:

1. *Resist minor and moderate levels of earthquake ground motions without damage to structural elements, nonstructural components, or building contents; and*
2. *Resist major levels of earthquake ground motion without failure of the isolation system, without significant damage to structural elements, without extensive damage to nonstructural components, and without major disruption to facility function.*

Design for base-isolated buildings is not much different than design for fixed-based buildings. The primary difference is that the lateral loads for the isolated superstructure are less than for a fixed-base structure. *The Primer on Seismic Isolation* (ASCE, 2004) emphasizes that although similar to typical seismic design, there are a few important general design issues that need to be addressed with isolation systems, including:

- Selection of an adequate lateral force resisting system with a natural period much shorter than the isolation level natural period. Mass and stiffness irregularities should also be avoided in order to allow the isolation system to be fully effective.
- Special consideration should be given to the diaphragm above the isolation plane so that the loads can be adequately transferred to the superstructure.
- Uplift of isolators due to large overturning moments should be avoided if possible.
- The structure should be able to accommodate vertical deformations present with most isolation mechanisms.
- The longevity and durability of the isolator should be evaluated and considered in design.
- Careful consideration of the site specific ground motion characteristics. A building near an active fault may experience large velocity pulses that create a large displacement demand on the isolation level, further discussed in Section 2.3.1.
- Division of design responsibilities between the structural engineers and the isolator manufacturers in a way that provides the most efficient and economical results.
- A seismic gap must be provided around the perimeter of the building in order to accommodate the horizontal movement. This gap must be covered or precautions must be taken to avoid accidents or disruption of the isolation system. In addition, utilities and pipelines must accommodate the relative movement across seismic gaps.

Design in the U.S. differs from other places in the world due to the requirement of a large restoring force in order to reduce permanent lateral displacements (Constantinou, Whittaker, Kalpakidis, Fenz, & Warn, 2007). In addition, base-isolated structures are typically designed beyond performance objectives set forth in the code, furthering the perception that base-isolated systems are too expensive for typical building projects (Erduran, Dao, & Ryan, 2011). With the

relatively new emergence of base-isolation and the movement toward performance-based design, isolation design codes will continue to evolve.

2.3 Base Isolation Concerns

As with any emerging technology, skepticism and design concerns have hindered the widespread adoption of base isolation. This section is meant to identify some, but not all, of the concerns with base isolation and to identify some of the research done in these areas.

2.3.1 Base Level Displacement Demand

A number of studies have highlighted the concern of large displacements in the isolation layer. Although displaying proven effectiveness in design level earthquakes, the benefit of base-isolation is often lost in more extreme events or near-field events. A near-field region of an earthquake is defined as the region within several kilometers of the fault rupture zone's projection on the surface (Iwan, 1997). A recent study found that peak base displacements associated with near-fault motions are 37-58% larger than those associated with far-fault motions (Pant & Wijeyewickrema, 2014).

Hall J. F., Heaton, Halling, & Wald (1995) emphasize the potential for large "displacement pulses" in base-isolated buildings due to near-source effects. The study suggests that the current distances between a base-isolated structure and a moat wall could be far exceeded in a structure subjected to a pulse. Even in a moderate (M7.0) earthquake in California, the study indicates that collapse is possible in base-isolated structures due to contact with the moat wall. In particular, an analytical study was completed indicating that a 3-story structure with a 40 cm moat width (distance from structure to surrounding moat wall) would require at least 60 cm and an additional 10% damping in the isolators to avoid a collision with the surrounding moat wall. Significant

yielding was present in the structure even when the moat wall distance was increased. The study questions the validity of building base-isolated structures in near-source regions.

The 1997 Uniform Building Code (UBC) significantly increased near-source factors, attempting to accommodate the large displacement demands (Hall & Ryan, 2000). Figure 2-17 shows the effects of a simulated (M7.0) blind-thrust earthquake, comparing the UBC near-source factors, N_V, and the simulated peak ground displacements and velocity. The results indicate that the near-source factors may be inadequate in accommodating the large demands in the structure.

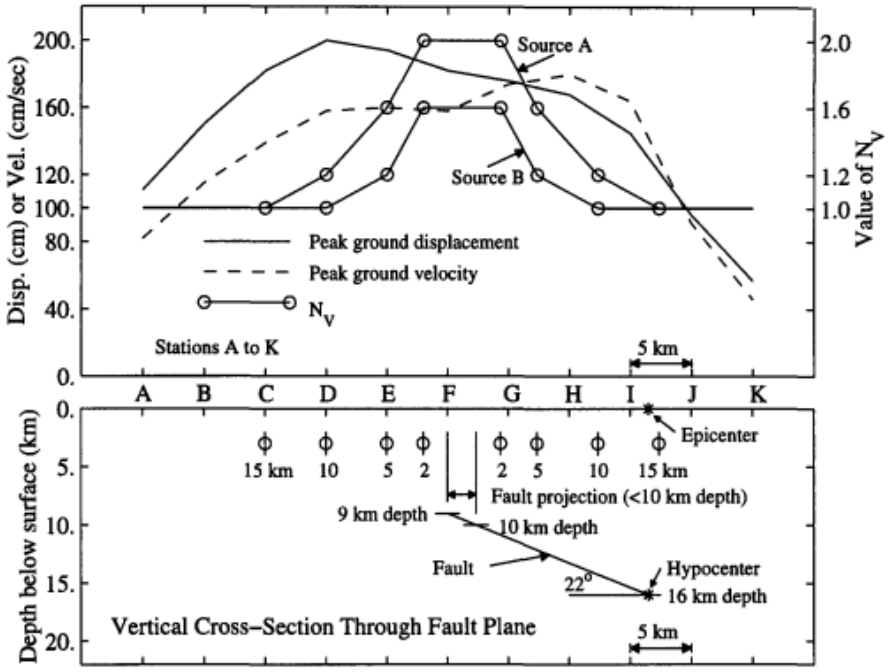

Figure 2-17. Near-Source Effects (Hall & Ryan, 2000)

More recently, Erduran, Dao, & Ryan (2011) compared a minimally code-compliant conventional fixed-based structure with a base-isolated structure. The results of the study indicate that the demands of the isolated structure are much less than those for the fixed base structure in the maximum considered earthquake (Figure 2-18a). Story drifts and accelerations are significantly reduced in the isolated structure, with significant inelastic response observed in only one out of twenty ground motions. The study did not account for the displacement limit state of the isolators,

which would probably reduce the effectiveness of the base-isolated structure. Significant isolator displacements were observed for most of the ground motions (Figure 2-18b).

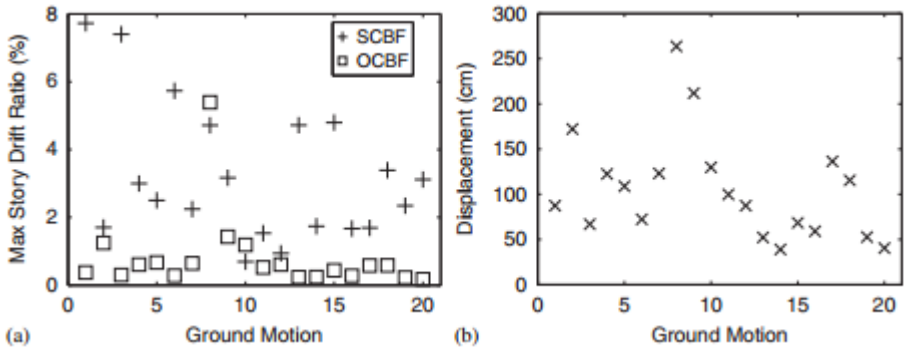

Figure 2-18. a) Comparison of Story Drift Ratio of a Fixed-Base (SCBF) and Base-Isolated (OCBF) Structure b) Isolator Displacement Demands (Erduran, Dao, & Ryan, 2011)

In addition to concerns with impacting the moat wall at large displacements, another concern is with the stability of the isolators at large displacements due to large overturning secondary moments. Experimental evaluation of the triple pendulum device exhibits relatively stable behavior at large displacements, even with a presence of uplift in extreme earthquakes (Morgan & Mahin, 2011). With elastomeric bearings, as the displacement increases, the critical load, horizontal stiffness, bearing damping, and bearing height are all affected (Nagarajaiah & Ferrell, 1999). The results of the Hall & Ryan (2000) study indicate that the large lateral displacements seen at the isolation level would require bearings of a very large diameter for stability. This leads to stiffer isolation bearings which makes it difficult to achieve longer natural periods. The study indicates that supplemental damping may be necessary to reduce the displacements.

2.3.2 Damping in Base-Isolated Buildings

With the concern of large displacement in the isolation layer, the natural inclination is to add damping to the system in order to reduce the displacements. A considerable amount of research

has been completed to evaluate the effect of adding supplemental damping to base-isolated structures. Stemming from the research involving near-source factors, Hall & Ryan (2000) also investigated the effect of adding supplemental damping to the isolation level. Values of 10%, 20%, and 30% of critical damping were added to the structure. Optimal performance was found in the 10% to 20% range, with larger roof accelerations found for higher values of damping. The research suggests there is an optimum value of damping which can balance cost and overall performance.

Makris & Chang (2000) evaluated the type of energy damping that may have the best influence on the response of isolated structures. A parametric study was completed comparing the response of different viscous, viscoplastic, and friction damping mechanisms subjected to near-source ground motions. Favorable results were observed from most mechanisms, but a combination of viscous and friction energy dissipation was deemed the most attractive due to a reduction of the isolator displacements without a large increase in base shears and accelerations. Jangid & Kelly (2001) acknowledge that supplemental damping may be beneficial for pulse-type ground motions but voice concern about the performance of a highly damped isolation system in moderate and more frequent broadband ground motions. An isolation system designed primarily for near-source effects will be more rigid in a moderate earthquake, which could subject the building to high accelerations.

Wolff & Constantinou (2004) completed an experimental shake table study on isolation systems with an emphasis on the secondary system response. Secondary systems (nonstructural, contents, etc.) are primarily sensitive to story drifts, floor velocities, and floor accelerations and can be very costly to replace. The experiment concluded that the addition of damping devices to

a lightly or highly damped system provides little benefit to structural response. Friction pendulum devices were observed to provide the best protection of secondary systems.

With considerable debate on the effect of supplemental damping and displacement restraints in isolation systems, the code has stringent requirements for the evaluation of the system. If a displacement restraint is added to an isolation system, Section 17.2.4.5 of ASCE 7-10 (ASCE/SEI, 2010) has specific design requirements detailed below:

1) *Maximum considered earthquake response is calculated in accordance with the dynamic analysis requirements of Section 17.6* [Dynamic Analysis Procedures], *explicitly considering the non-linear requirements of the isolation system and the structure above the isolation system.*
2) *The ultimate capacity of the isolation system and structural elements below the isolation system shall exceed the strength and displacement demands of the maximum considered earthquake.*
3) *The structure above the isolation system is checked for stability and ductility demand in the maximum considered earthquake.*
4) *The displacement restraint does not become effective at a displacement less than 0.75 times the total design displacement unless it is demonstrated by analysis that earlier engagement does not result in unsatisfactory performance.*

2.3.3 Pounding

The major concern with large isolator displacements is that seismic pounding with the moat wall that surrounds the building can occur, sending a shock wave through the building. This can lead to substantial superstructure yielding or even collapse.

The Fire Command and Control building in Los Angeles experienced an accidental impact in the Northridge earthquake due to incorrect construction. Nagarajaiah & Sun (2001) were able to evaluate the observed response using instruments present on the building and to develop analytical impact models. The impact excited higher modes of response, increasing the acceleration from 0.22g at the base to 0.32g at the roof. The results of the study indicated that the base isolation system was effective in the North/South direction but in the East/West direction, where the impact was observed, base shear and drift demands increased. The effectiveness of the isolation was reduced, indicating that seismic impact should be avoided.

An experimental analysis of a collision with a moat wall was completed by Miwada et al. (2012) using an existing base isolated building that was to be replaced. The building was loaded with a jack and then allowed to freely vibrate, making contact with the surrounding moat wall. The collision resulted in large accelerations in the superstructure and inelastic damage. In addition, a rocking behavior was observed after each impact due to the vertical stiffness of the isolation layer.

Masroor & Mosqueda (2012) recently completed an experimental evaluation of pounding in extreme events and the effects of superstructure response. A ¼-scale, three-story structure was designed with an emphasis on proper scaling in order to capture the inelastic response due to impact. The properties of the moat wall and gap distance were varied in order to capture different impact stiffnesses and velocities. The results indicate that the response is largely dependent on the gap distance, moat wall properties, and impact velocity. Acceleration response was largely amplified at the base level and increased uniformly in the other stories (Figure 2-19). Interstory drifts were largely sensitive to the moat wall type, with increased drifts associated with large pounding forces resulting from stiffer moat walls and increased impact velocities.

The overall conclusion of the study was that pounding of base-isolated structures can potentially have damaging consequences on structural performance. Pounding should be avoided, even in the most extreme events.

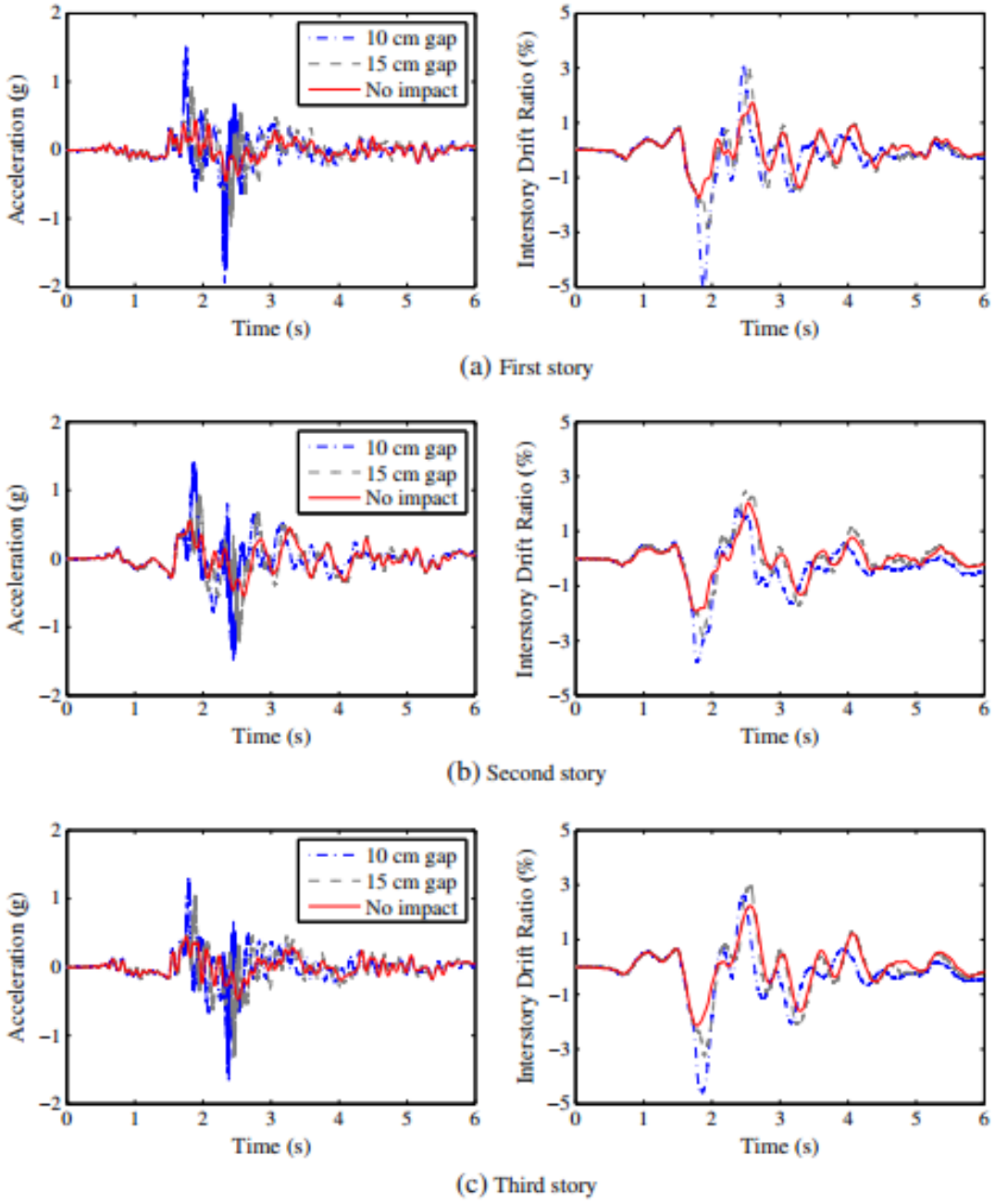

Figure 2-19. Moat Wall Impact Testing (Masroor & Mosqueda, 2012)

2.3.4 Base- Isolation Cost

The rate of adoption of base-isolation in the U.S. has not kept pace with other areas of the world. There are currently about 125 seismically isolated buildings in the U.S. while there are more than 6500 in a Japan and several hundred in China (Taylor & Aiken, 2011). Slow implementation in the U.S. is due to many factors, including lack of industry knowledge, prohibitive design codes, and perceived high cost of isolation systems. Although full life-cycle cost benefit analyses may indicate the advantages of a base-isolation system in comparison to a conventional structure, the initial costs are often the deterring factor (Arendt, Earle, & Meyers, 2010). In addition, base-isolated structures are typically designed beyond performance objectives set forth in the code, furthering the perception that base-isolated systems are too expensive for typical building projects (Erduran, Dao, & Ryan, 2011). Even though isolated structures offer immediate occupancy of the structure, the economic benefit is not realized by insurers in the U.S. who could provide attractive discounts in insurance premiums. These incentives already exist for fire and hurricane-resistant building materials and make the larger initial costs more bearable for clients (Taylor & Aiken, 2011).

In order to make a direct comparison between fixed-base and base-isolated structures, numerous recent studies have compared the response of minimally code compliant buildings (Erduran, Dao, & Ryan (2011), Sayani, Erduran, & Ryan (2011), and Shenton III & Lin (2011)). Substantial reduction in drift and acceleration can be seen in the base-isolated structures in comparison to fixed-base structures but this is accompanied with larger upfront design, construction, and material costs. Cutfield et al. (2014) used a professional cost estimator to calculate the difference between a conventional and base-isolated 3-story building (Table 2-1). Although 14% reduction in structural framing is evident in the base-isolated structure, an overall

12.5% increase in building cost is evident when accounting for other aspects of the isolation system. The breakdown of the estimated costs of the isolation layer is found in Figure 2-20.

Table 2-1. Cost Estimates for a Conventional and Base-Isolated Building (Cutfield M. R., Ryan, Buckle, & Ma, 2014)

	Fixed base SCBF ($)	Base isolated OCBF ($)	Percent increase
Foundation	265,000	331,000	+24.9%
Structural framing	1,387,000	1,193,000	-14.0%
Isolation layer	-	1,973,000	-
Non-structural elements	6,793,000	6,793,000	0%
Utilities	7,845,000	7,845,000	0%
Total building cost	15,931,000	17,776,000	+11.6%
Recommended budget	24,067,000	27,081,000	+12.5%

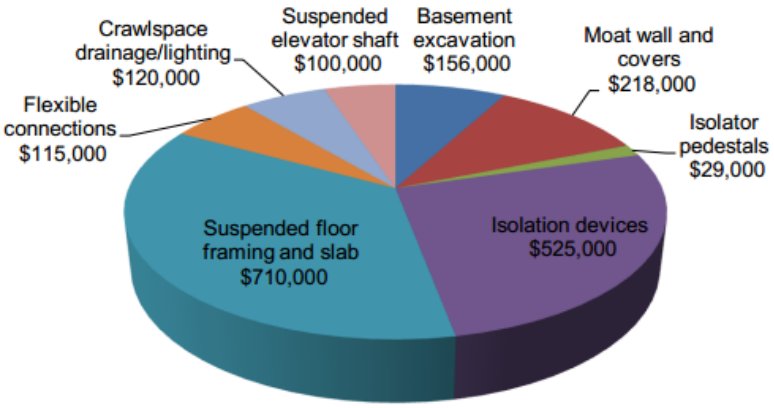

Figure 2-20. Isolation Layer Costs (Cutfield M. R., Ryan, Buckle, & Ma, 2014)

Given the increased performance of isolated systems at an increased initial cost, life cycle analyses are necessary to demonstrate potentially beneficial long-term costs of base-isolated structures. Ryan et al. (2010) estimated annual loss of an isolated braced frame to be about 1⁄4 of a conventionally braced frame using a probabilistic response assessment developed by Miranda & Aslani (2003). Recently, Cutfield et al. (2014) completed a life cycle analysis of conventional and base-isolated buildings within the framework of the FEMA P-58 life-cycle methodology demonstrating potentially advantageous life-cycle performance of base-isolated structures. Given

the infancy of the P-58 methodology, continued research is still necessary to fully understand the potential benefits and drawbacks of base-isolation given a large dependence on assumptions. One of the major findings of the study was that the majority of the contribution of expected losses in base-isolated buildings was due to structural pounding in extreme events. This justifies the need to limit the displacements at the isolation level in rare events.

2.3.5 Summary

The purpose of this section was to identify some of the existing concerns with base-isolated structures. The issues highlighted in this section are all associated with the creation of a gap damper system. The gap damper system seeks to limit large displacements in the isolation level by providing supplemental damping at a preset displacement. Since pounding with the surrounding moat wall is identified as a potentially dangerous result in an extreme earthquake, the gap damper system hopes to alleviate this risk. In addition, the gap damper system utilizes a delayed activation of the supplemental damping so as to not impact response in more frequent events. Finally, to be a practical option, the gap damper system must be cost effective in comparison to traditional systems.

2.4 Supplemental Seismic Energy Dissipation

The gap damper system proposed in this research utilizes passive energy dissipation in addition to a base-isolation system in order to reduce displacements at the isolation layer. Research summarized in the previous section indicated that the addition of supplemental energy dissipation can effectively reduce displacements, but the means to achieve this energy dissipation is not described. The purpose of this section is to review some of the current methods of providing supplemental passive energy dissipation in structures.

2.4.1 Velocity-Dependent Passive Control

Velocity-dependent, often referred to as rate-dependent, passive control devices rely on relative motion for energy dissipation. They are typically cost effective and can be used in the design of a new structure or added to existing structures to provide additional protection (Chopra, 2012). The two most typical rate-dependent devices are viscous fluid dampers (VFD) and viscoelastic dampers (VED), with typical hysteretic behavior shown in Figure 2-21. Damping values can vary largely depending on the type and implementation of damping device.

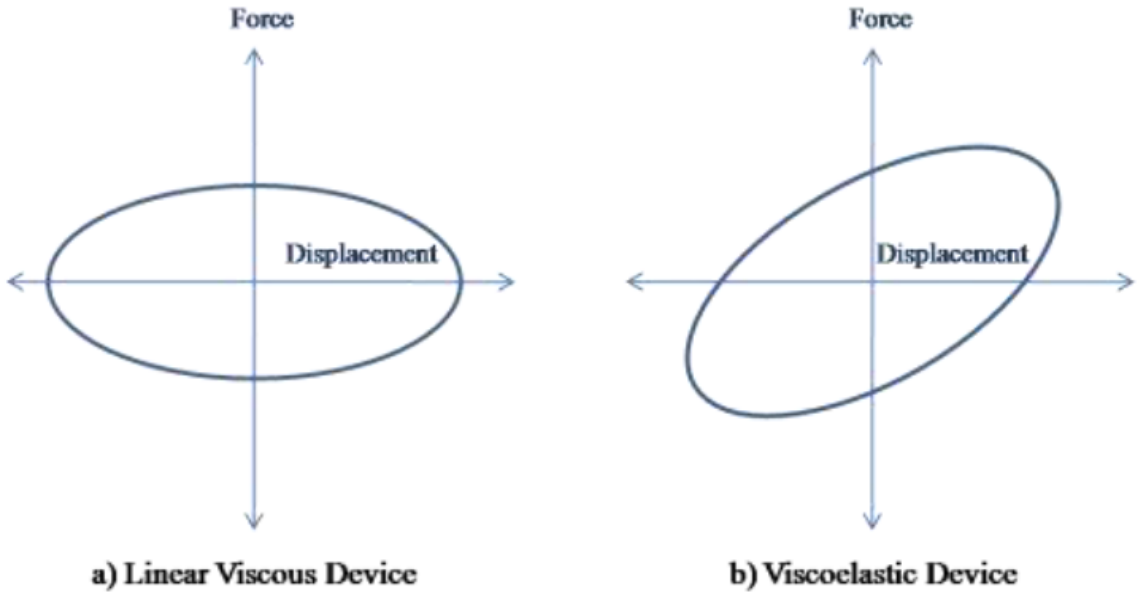

Figure 2-21. Velocity-Dependent Hysteresis Comparison

2.4.1.1 Viscous Fluid Dampers

Viscous fluid dampers consist of a cylinder filled with a fluid, typically silicon, and a piston with orifices on the face (Figure 2-22a). The travel of the piston through the fluid inside the cylinder dissipates energy. Although the device is operational and stable at various temperatures and frequencies, the viscous properties of the damper do vary (Reinhorn, Constantinou, & Li, 1995). Viscous fluid dampers can be either linear or nonlinear depending on the arrangement of the

orifices on the face of the piston. The linear hysteresis loop has an elliptical shape (Figure 2-21a) but as the nonlinear exponent approaches 0.3, the hysteresis loop is nearly rectangular (Lee & Taylor, 2001). Inclusion of viscous fluid dampers in an elastic steel structure shaking table experiment have shown reduction in story drift and shear forces of 30% to 70% in addition to improving drift response in inelastic systems (Reinhorn, Constantinou, & Li, 1995).

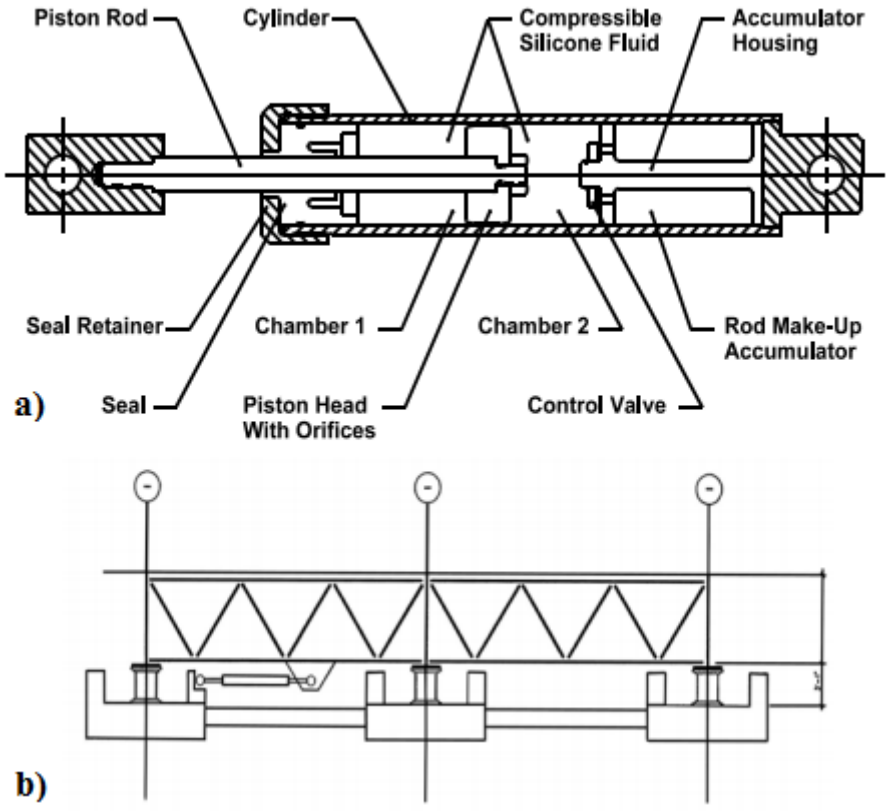

Figure 2-22. a) Typical Viscous Fluid Damper b) Damper in Base-Isolated Structure (Hussain, Lee, & Retamal, 1998)

Viscous dampers can be added to any form of base-isolated structures in order to provide supplemental damping to the system. For high damping rubber bearings, achieving high levels of damping may be difficult, especially at large displacements. In addition, the rubber compounds may be sensitive to environmental and fatigue conditions. Manufacturing dampers with a slight preload can also assist in re-centering of the device, in addition to providing some initial stiffness.

These reasons all make viscous dampers an attractive option to use in parallel to a base-isolated system (Figure 2-22b). Viscous dampers have been shown to reduce base displacement by up to 50%, permitting the elastomeric isolators to be reduced in size and decreasing overall costs. Projects of note that utilize base-isolation systems and dampers in parallel include the San Bernardino Medical Center, located near the intersection of two major fault lines, and the Los Angeles City Hall which utilizes viscous dampers both at the isolation level and in the superstructure (Hussain, Lee, & Retamal, 1998).

2.4.1.2 Viscoelastic Dampers

Viscoelastic devices utilize layers of copolymers to dissipate energy in shear deformation (Chopra, 2012). Figure 2-21b illustrates a typical hysteresis configuration for a VE device which utilizes a viscoelastic material, such as high-damping natural rubber, sandwiched between two metal plates. The ability to reach strains up to 500% before failure means that the device can dissipate energy over a large range of deformation (Marshall, 2008). Variation in temperature can significantly impact the performance of a viscoelastic device. An increase of 10°C can alter material storage and loss modulus from 30% to 50% at low frequencies and even more at higher frequencies, meaning that a fluctuation in temperature could largely affect the energy dissipation capability (Reinhorn, Constantinou, & Li, 1995). This is typically not an issue for seismic events because of the short duration but can cause problems for strong wind events due to a build-up of heat over repeated strain cycles. The development of newer rubber materials has decreased the variability in performance and increased the energy dissipation capacity (Marshall, 2008).

As evident in Figure 2-21b, viscoelastic devices do provide additional stiffness to a system. Although this will decrease the natural period of the structure and thus increase the seismic response, the period is typically only shortened by about 10% to 20%, which is much less than the

effect of most metallic displacement-dependent devices (Chopra, 2012). Although primarily used for wind excitation, considerable research has been performed in recent years on VE dampers for seismic protection. One dynamic analysis demonstrates the effectiveness of installing VE dampers between seismic joints or sky bridges between structures. As evident in Figure 2-23, displacements were significantly decreased, especially if the natural frequencies of the connected structures were different (Kim, Ryu, & Chung, 2006). A full discussion of the use of viscoelastic materials in base-isolated structures was presented in Section 2.2.2.1.

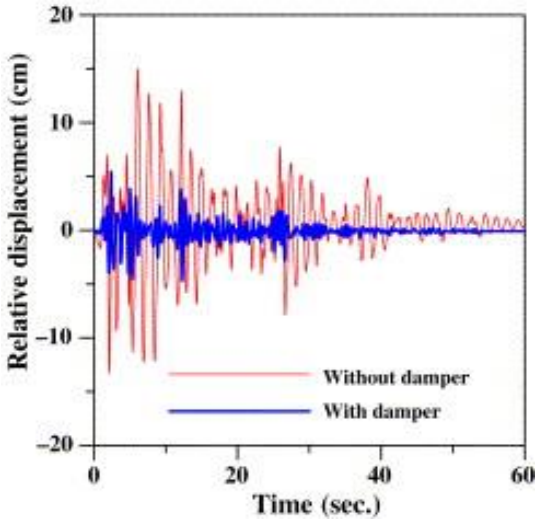

Figure 2-23. Viscoelastic Devices Used to Reduce Relative Displacements between Two Adjacent Structures (Kim, Ryu, & Chung, 2006).

2.4.2 Displacement-Dependent Passive Control

Another type of passive control, which is rate-independent (or velocity-independent), is often referred to as "hysteretic". Use of these rate-independent devices significantly affects seismic response due to a high elastic stiffness which can drastically shorten the natural period of the structure. Although the seismic hazard may significantly increase, the large inelastic capabilities are appealing for energy dissipation. The two most common classes of hysteretic devices are

metallic yielding devices and friction devices. The hysteretic behavior of each is represented in Figure 2-24.

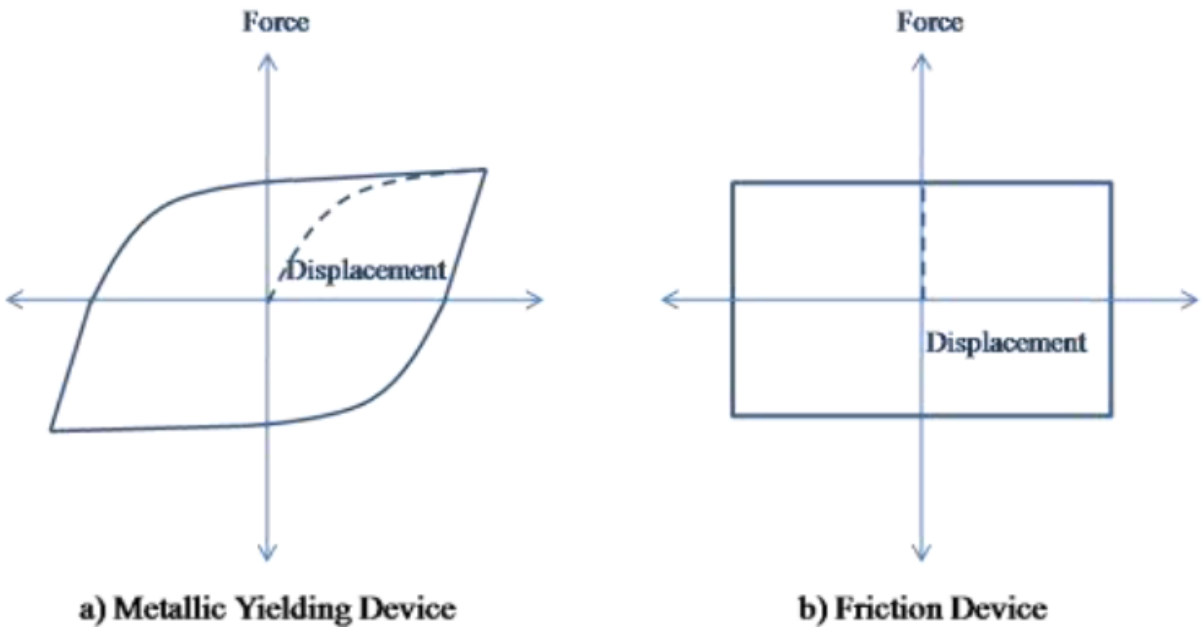

Figure 2-24. Displacement-Dependent Hysteresis Comparison

2.4.2.1 Metallic Yielding Devices

Metallic yielding devices rely heavily on the inelastic action of the metal, typically mild steel, to dissipate energy. Numerous devices and configurations have been designed, researched, and implemented with success. One such application involves adding damping and stiffness (ADAS) elements as a link at the top of a chevron braced configuration (Figure 2-25). Multiple plates are arranged in a parallel formation and dissipate energy through flexural yielding. The unique tapered design of the plate is intended so that the plates can act in double curvature, yielding across the entirety of the plate and therefore dissipating more energy (Alehashem, Keyhani, & Pourmohammad, 2008). The TADAS (Triangular Added Damping and Stiffness) device is similar except it utilizes a triangularly shaped plate and therefore single curvature to dissipate energy.

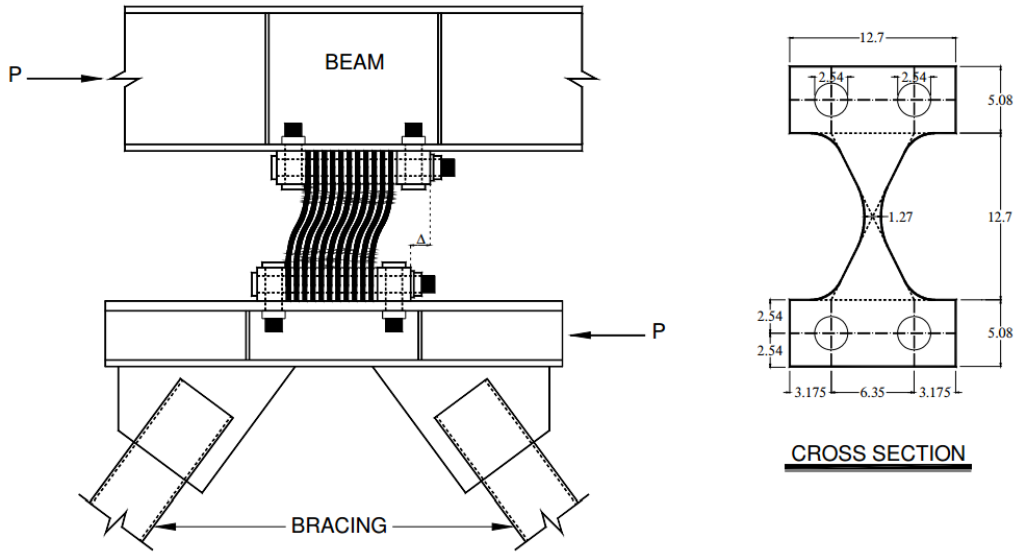

Figure 2-25. Added Damping and Stiffness (ADAS) Device (Alehashem, Keyhani, & Pourmohammad, 2008)

Seismic events such as Northridge 1994 and Loma Prieta 1989 raised concerns about typical braced frames due to poor performance under cyclic loading (Sabelli, Mahin, & Chang, 2009). Buckling restrained braces (BRB) offer a solution to this problem by encasing a steel core in a concrete filled tube in order to restrain the brace from lateral buckling. BRBs are beneficial because they are able to dissipate roughly the same amount of energy in both tension and compression, eliminating the erratic and inefficient behavior of typical concentrically braced frames. Figure 2-26 shows the typical arrangement of a BRB using a cruciform yielding steel bar encased in a steel tube and mortar to prevent buckling. The design of the steel core may vary depending on the manufacturer but the fundamentals of behavior remain the same. Nonlinear dynamic analyses and experimental testing of the braces have demonstrated reliable behavior with improved interstory drifts and substantial ductility capability (Sabelli, Mahin, & Chang, 2009). The ability of BRBs to dissipate energy somewhat equally in tension and compression could

potentially be advantageous if hysteretic energy dissipation is necessary for the gap damper system.

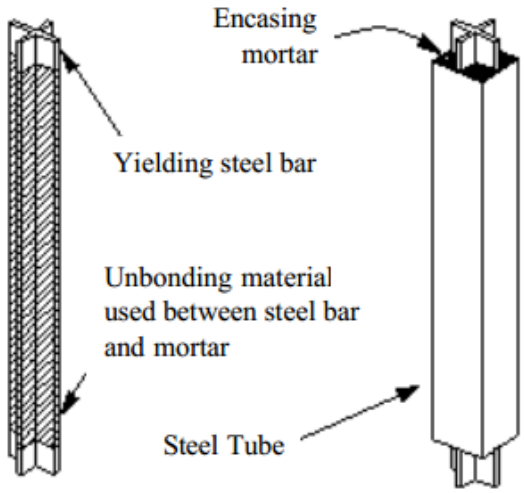

Figure 2-26. Buckling Restrained Brace Assembly (Sabelli, Mahin, & Chang, 2009)

An increasingly popular metallic device used for seismic protection incorporates shape memory alloys (SMA). During excitation, the alloys have the ability to dissipate energy through a stress-induced solid-to-solid phase transformations (Song, Ma, & Li, 2006). The change in stress during a ground motion causes a phase transformation from austenite to martensite and then back again to austenite, resulting in a hysteretic behavior and energy dissipation. The primary advantage of SMA systems is the ability to self-center, providing life safety after an event.

Wilde, Gardoni, & Fujino (2000) proposed a base isolation system that combined laminated rubber bearings and SMAs. Analytical models demonstrated that the SMA bars provided additional damping capacity for moderate earthquakes while providing damping and displacement control for more extreme earthquakes. Dolce, Cardone, & Marnetto (2001) developed and tested a Nitinol-based SMA used as the primary source of energy dissipation in parallel with a rolling isolation system. The system was able to carry 600 kN and up to 180 mm displacement with an overall effectiveness at dissipating energy. Alvandi & Ghassemieh (2014)

provide a thorough review of some of the more recent applications of shape memory alloys in base-isolated structures. Overall, the review suggests the feasibility and effectiveness of shape memory alloys when used with isolation systems.

Japanese designs typically favor the use of supplemental hysteretic damping devices such as helical and U-shaped dampers and lead dampers (Morgan & Mahin, 2011). The U-shaped steel dampers can either be integrated with the elastomeric bearing or installed separate from the bearings (Figure 2-27). The dampers are designed so that the yielding of the steel is spread over the length of the device to avoid high strains and low-cycle fatigue (Buchanan, et al., 2011). In addition to spherical bearings, lead dampers and helical steel dampers are found in Japenese isolated buildings (Figure 2-28).

Figure 2-27. a) U-Shaped Steel Damper with Integrated Rubber Bearing b) U-Shaped Steel Damper Separate from Isolator (Nippon Steel & Sumitomo Metal Corporation, 2014)

Figure 2-28. Lead Dampers (Front) and Helical Steel Dampers (Back) (Mori Living, 2011)

2.4.2.2 Friction Devices

Friction devices are another commonly used means for dissipating large amounts of energy. Once the device reaches a "slip force", friction is utilized as two solid bodies slide against one another. The mechanism slips in both tension and compression and creates a rectangular hysteresis behavior, as shown in Figure 2-24. These devices do add stiffness to the system, the natural periods are only shortened by about 10% to 20% (Chopra, 2012). The devices are often favored in design due to reliable behavior under varying load amplitude and frequencies (Reinhorn, Constantinou, & Li, 1995). Slotted bolted connections (SBC) are a type of friction device often used due to the relative ease of design, construction, and availability of commercial materials (Levy, Marianchik, Rutenberg, & Segal, 2000). As seen in Figure 2-29, the bolts connect two plates together with a clamping force. Once the slip force is reached, the coefficient of friction and bolt compression dissipate energy through heat. Initially SBCs used two steel surfaces to generate friction but experimental results showed that brass on steel contact creates a more uniform behavior (Grigorian & Popov, 1994).

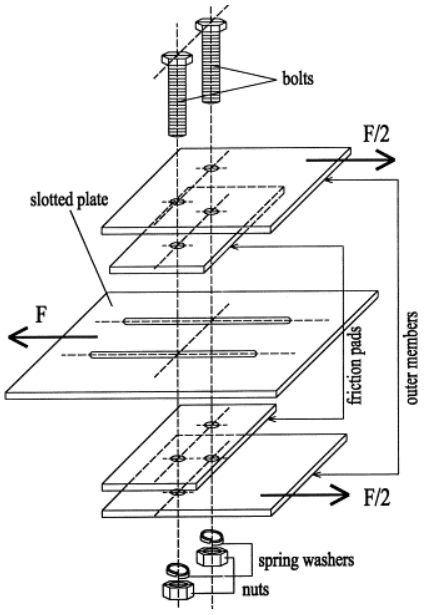

Figure 2-29. Typical Slotted Bolted Connection (Balendra, Yu, & Lee, 2001)

As detailed in Section 2.2.2.3, friction pendulum devices are extensively used in base-isolation as a means of isolating the superstructure from the ground and providing beneficial friction energy dissipation. In addition, studies from Makris & Chang (2000) and Hall & Ryan (2000) indicate that supplemental friction energy dissipation may be beneficial in reducing isolator displacements with minimal consequences in the superstructure.

2.4.3 Multi-Phase Systems

The gap damper system is a phased system, allowing the base-isolation system to resist low-to-moderate earthquakes and activating supplemental energy dissipation for extreme earthquakes. Passive multi-phased systems are increasingly desirable in seismic protection because of the ability to meet multiple performance objectives. The purpose of this section is to identify some the previous research involving multi-phase passive control.

The multi-phase nature of multi-phase passive control systems has been explored in the past, showing promising results in many different applications. Weidlinger & Ettouney (1993) developed a sequential coupling system that utilized dynamic slip and multi-phase behavior in order to improve response. Using a repeated slip-resistance sequence within a structural system, a significant reduction in deformation response was achieved. This can be accomplished by properly detailing special connections, such as bolts in slotted holes, in steel, reinforced concrete, and prestressed concrete structures, as illustrated in Figure 2-30. A simple single-degree-of-freedom (SDOF) model suggested a sequential coupling system could reduce acceleration response by up to 70% with residual displacements of less than 10% of standard systems.

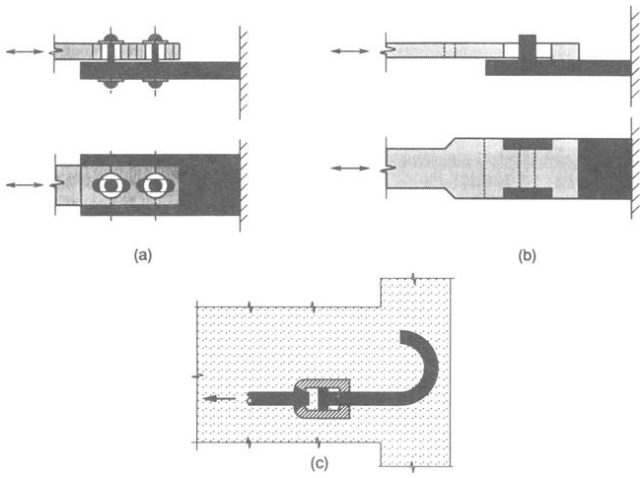

Figure 2-30. Sequential Connection Schematics (Weidlinger & Ettouney, 1993)

More recently, Marshall & Charney (2010) developed a multi-phase passive control device combining a viscoelastic high-damping rubber sandwich damper and a buckling restrained brace. Backed up with a moment resisting frame for initial stiffness and redundancy, the system was developed in order to take advantage of the each material for varying levels of seismic excitation. The behavior of the system is comprised of three main phases. The first phase, involving the VE sandwich damper and moment frame, is designed to provide sufficient stiffness and damping for service level wind conditions and small to moderate seismic events. The next phase involves the transition from the VE device to the BRB, which occurs at a specified gap size that is a percentage of the moment frame yield displacement. The lockout of the secondary phase occurs due to a slotted bolted connection on the outer plates of the sandwich damper (Figure 2-31). The final phase involves the BRB, which adds significant stiffness and energy dissipation capacity to the system for larger seismic events. The overall result is a device that can variably respond to levels of lateral force and primarily restrict damage to a replaceable BRB.

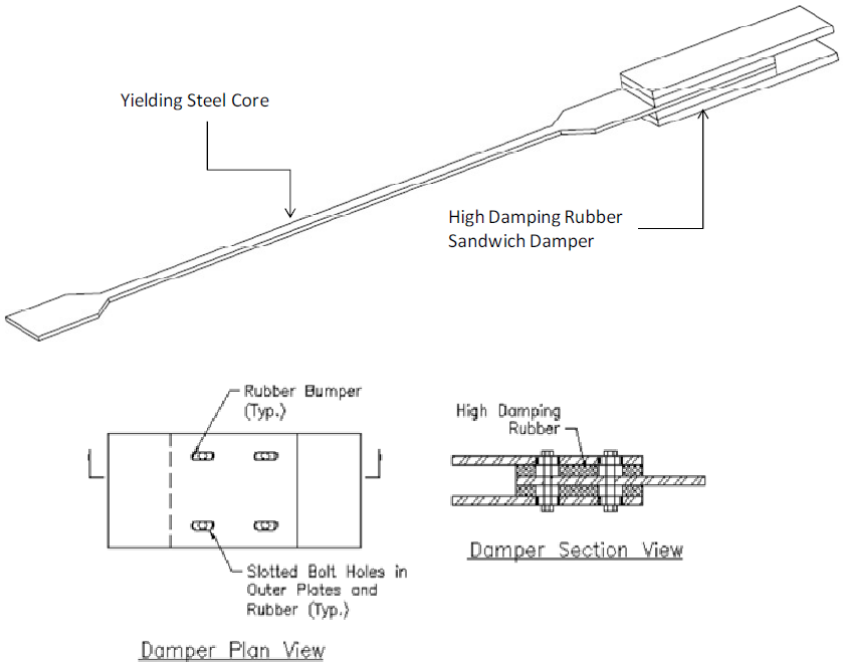

Figure 2-31. High-Damping Rubber Sandwich Damper Schematic (Marshall, 2008)

An analytical study was performed on a 9-story steel moment frame designed with the novel device and other multi-phase arrangements. Viscous fluid dampers, rather than viscoelastic materials, as well as a range of transition gap sizes were also considered. Other arrangements of the system were also considered (Figure 2-32). Arranging a system in a parallel formation provides damping throughout the entire duration of excitation, whereas the series formation only allows damping in the first phase. Response parameters such as acceleration, base shear, drift, and residual displacements all showed marked improvement over conventional systems. Rawlinson & Marshall (2014) furthered the study by completing an exhaustive parametric study evaluating the multi-phase configurations and the sensitivity to seismic hazard, system arrangements, component strength ratios, and transition displacements (gaps). An incremental dynamic analysis compared hundreds of systems on the basis of total acceleration, base shear, and element ductility demand. Results of the study offer significant insight towards the development of multi-phase passive devices.

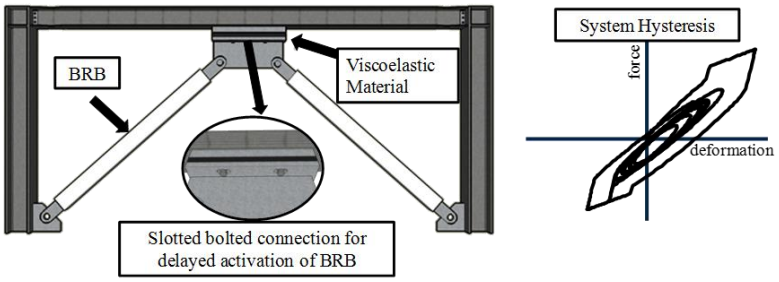

a) Viscoelastic device in series with a buckling-restrained-brace

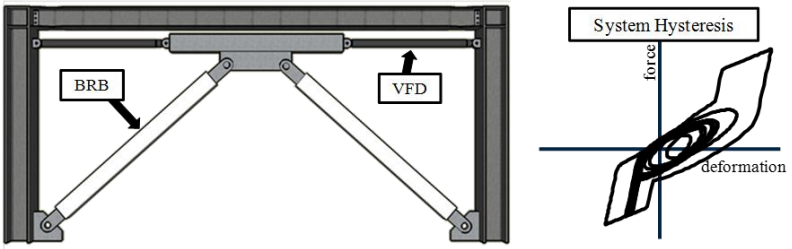

b) Viscous fluid damper in series with a buckling-restrained-brace

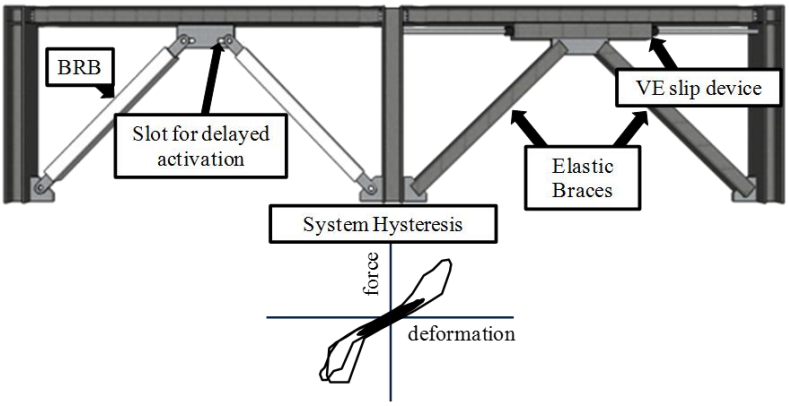

c) Viscoelastic device in parallel with buckling-restrained-brace with a slot for delayed activation

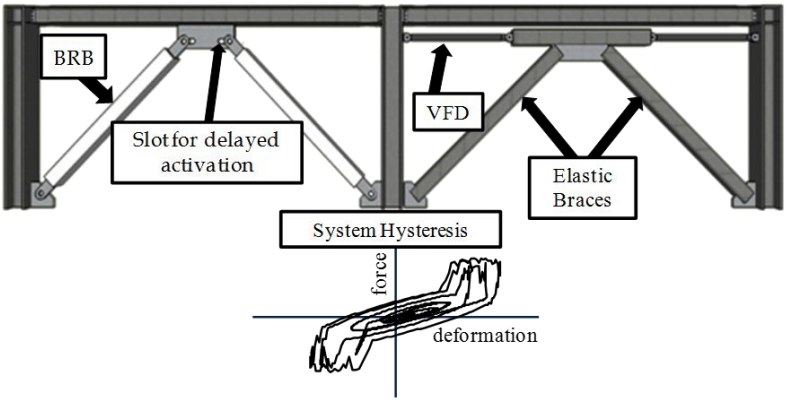

d) Viscous fluid damper in parallel with buckling-restrained-brace with a slot for delayed activation

Figure 2-32. Multi-Phase Passive Control Devices (Rawlinson & Marshall, 2014)

In addition to active and semi-active control, a few multi-phase passive mechanisms have been developed that are able to modify base-isolation response depending on displacement demands. Kelly, Beucke, & Skinner (1980) developed a skid system that engaged under large isolator displacements in order to dissipate energy and provide a fail-safe mechanism. The device works by allowing a beam attached to the ground level to make contact with a girder in the structure. The clearance between the beam and the girder allows conventional isolation behavior until the axial shortening of the elastomeric bearings at large displacements closes the gap. Contact of the girder and beam provide beneficial coulomb friction energy dissipation that reduces displacements. The 1/3-scale shake table testing indicated that although the isolators failed, the fail-safe skid system was able to prevent collapse with a minimal increase in superstructure acceleration.

Wang (2009) developed a passive two-step control damping (PTCD) device that provides a two-stage damping behavior that is displacement controlled. Using a mechanical system, the device does not need to rely on external power, sensors, or algorithms. Although applicable in multiple situations, the device is particularly appealing for base-isolated structures that need additional energy dissipation at large displacements. The experimental study paired the device with a roller isolation bearing, limiting isolation level displacements and providing better superstructure performance.

Han, Xianhua, & Du (2008) experimented with a "soft-collision" mechanism in order to mitigate displacements in the isolation layer. A large parametric experimental study was completed on 28 different systems including steel springs (Figure 2-33a), U-shaped buffers, and compound U-shaped buffers with lead inserts (Figure 2-33b). A direct relationship was found between the rigidity of the system and the reduction in isolation layer displacement. The trade-off

was in the superstructure interstory drift which increased as the rigidity of the buffer increased. These mechanisms were unable to provide much damping to the system.

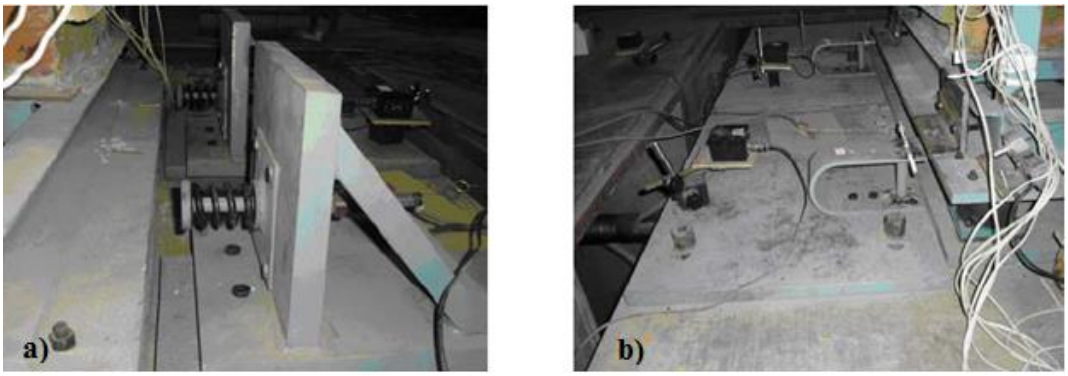

Figure 2-33. Soft-Collision Mechanisms a) Steel Spring b) Compound U-Shaped Compound Device (Han, Xianhua, & Du, 2008)

2.5 Summary

The purpose of this chapter was to give a thorough review of literature in the field of base-isolation and seismic protection. The history, application, and types of base-isolation were outlined along with important fundamental concepts of isolation systems. Analytical, experimental, and observational research was reviewed, suggesting base-isolation as a great option for seismic protection. As with any emerging technology, there are some hindrances in the full adoption of isolation technologies, especially in the U.S., where prohibitive design codes and costs have stunted growth potential.

In addition to cost and design, some of the other base-isolation concerns were identified in the literature. Displacement demands in the isolation level, especially in large near-field earthquakes, are a major concern as impact with the surrounding moat wall could potentially collapse the structure. In order to mitigate these large displacements, many have incorporated supplemental energy dissipation. There are mixed opinions as to the effectiveness of providing

this damping as displacements are controlled at the base level with consequential effects in the superstructure. A system with substantial damping to mitigate base-level displacements may not be the most effective in more broadband ground motions. Finally, a brief review of supplemental energy dissipation devices was presented. The gap damper requires the activation of supplemental energy through the use of viscous, viscoelastic, hysteretic, and/or friction devices.

There is a significant gap in the state-of-the-art technology covering base-isolation systems that can meet the objectives of more frequent ground motions while also protecting the structure in an event that has a significant displacement demand. A few base-isolation systems exist that accomplish multi-objective goals, such as the Triple Pendulum Device (Morgan & Mahin, 2011) and friction skid-system (Kelly, Beucke, & Skinner, 1980), but that do not necessarily encompass the same novel ideas as the gap damper system. Results of the research effort can provide valuable insight towards a system that could substantially change the way seismic isolation is perceived worldwide.

Chapter 3. Conceptual Development of a Gap Damper System

3.1 Introduction

Base-isolation systems and some of the innovative developments in the field in the last few decades were introduced in the literature review in Chapter 2. Some of the potential issues with the technology in its current state were also discussed. There remains a significant concern about the large displacement demands in isolators in extreme ground motions, which could lead to a pounding response as the building collides with the surrounding moat wall. In order to curtail potential pounding response, a "gap damper" system has been proposed to reduce the displacements in the base level. By introducing a significant amount of energy dissipation in the base level, the goal of this system is to reduce the base level displacements while also minimizing consequential superstructure response. This is accomplished through a phased behavior, allowing traditional base-isolated behavior up to a threshold displacement and activating supplemental energy dissipation for large displacement demands. The intention of this chapter is to introduce the overall concept of the gap damper system and explain the details of a parametric study.

An important aspect of this research is that the work was done collaboratively between researchers at Auburn University and the University of Nevada-Reno. While some tasks were clearly split amongst the researchers, others involved a group effort. This dissertation describes the efforts of both parties in order to provide proper context, but will clearly indicate if a task was not completed within the scope of this doctoral work.

3.2 Gap Damper Concept

A paper entitled *"Exploring the Gap Damper Concept to Control Seismic Isolation Displacement Demands"* fully describes the concept of a gap damper device; a summary is provided in this section (Zargar, Ryan, Rawlinson, & Marshall, 2012).

In order to control isolator displacements, the gap damper device triggers passive supplemental damping at a desired displacement. This provides a phased behavior that allows for traditional base-isolated behavior in low to medium intensity ground motions and provides beneficial energy dissipation for high intensity motions with larger displacement demands. The conceptual system can be achieved through many means of energy dissipation, such as viscous, hysteretic, or combinations thereof, but the overarching principle of the system remains that there is a gap, in which the base-isolation system is the only lateral resistance, followed by the activation of supplemental energy dissipation, hence the name "gap damper". Although potentially effective in reducing displacements, the caveat of the gap damper system is that the type of energy dissipation and amount of energy dissipation can largely effect the superstructure by increasing the acceleration and story drifts. The goal of this research is to strike a balance between limiting the isolator level displacements while creating as little negative superstructure effect as possible.

The fundamental concept of the gap damper system utilizes an equal energy approach (Figure 3-1). The design level displacement (D_D) is associated with the design basis earthqauke, having a return period of 475 years. A maximum considered earthquake (MCE) has a displacement demand (D_{MCE}) associated with a return period of 2475 years. Collision with the surrounding moat wall would be detrimental to the superstructure response, therefore the goal of the gap damper is to reduce isolation level displacement to a displacement less than the distance between the structure and moat wall. The maximum displacement in the isolation system is restricted to 10% beyond

the MCE displacement ($1.1*D_{MCE}$), the minimum distance to the surrounding moat wall. The bilinear force-displacement relationship in Figure 3-1 represents a typical isolator hysteresis up to $1.375*D_{MCE}$, which is 25% beyond the moat wall location. The distance from 0 to $0.6*D_{MCE}$ is considered the initial gap size, in which the supplemental energy dissipation is not active and the isolator is the only form of lateral resistance. The threshold of $0.6*D_{MCE}$ is generally greater than the design displacement, D_D.

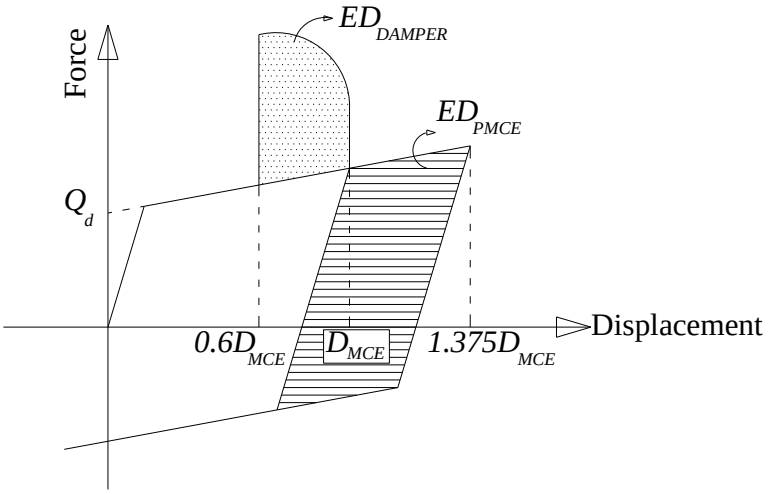

Figure 3-1. Equal Energy Approach

The equal energy concept utilizes the energy dissipated by the isolator (ED_{PMCE}) from $1.0*D_{MCE}$ to $1.375*D_{MCE}$ and providing supplemental energy dissipation capacity to compensate for the $0.6*D_{MCE}$ to $1.0*D_{MCE}$ (ED_{DAMPER}), theoretically reducing the displacement to acceptable levels. The ratio of ED_{DAMPER} to ED_{PMCE}, Energy Dissipation Level (EDL), is not necessarily ideal at 1. A large portion of this research endeavor involves the investigation of EDL values that balance displacement at the base level without inducing large superstructure accelerations. Although Figure 3-1 illustates ED_{DAMPER} as a viscous damping mechanism, the energy dissipation could be accomplished through other means.

Figure 3-2 represents the theoretical response of a hysteretic gap damper system subjected to a harmonic load with increasing amplitude. Using an elastic-perfectly plastic energy dissipation

element, Figure 3-2a represents a gap damper ssytem that has reached the gap threshold of 0.6*D_{MCE}, but has not yielded the damping elements. As the amplitude of the input motion is increased, yielding occurs in the hysteretic element, leading to permenant deformation in the element (Figure 3-2b). Although the hysteretic element yields, the gap between the hyteretic elements in the positive and negative directions remains the same distance (2*0.6*D_{MCE}, or 1.2*D_{MCE}). Therefore, if a gap damper system engages at -0.6*D_{MCE} for a distance of 0.1*D_{MCE}, the system will engage at +0.5*D_{MCE} in the opposite direction. Figure 3-2c and Figure 3-2d show continued accumlation of residuals in the gap damper system. These residuals could be beneficial or damaging to overall performance of the system.

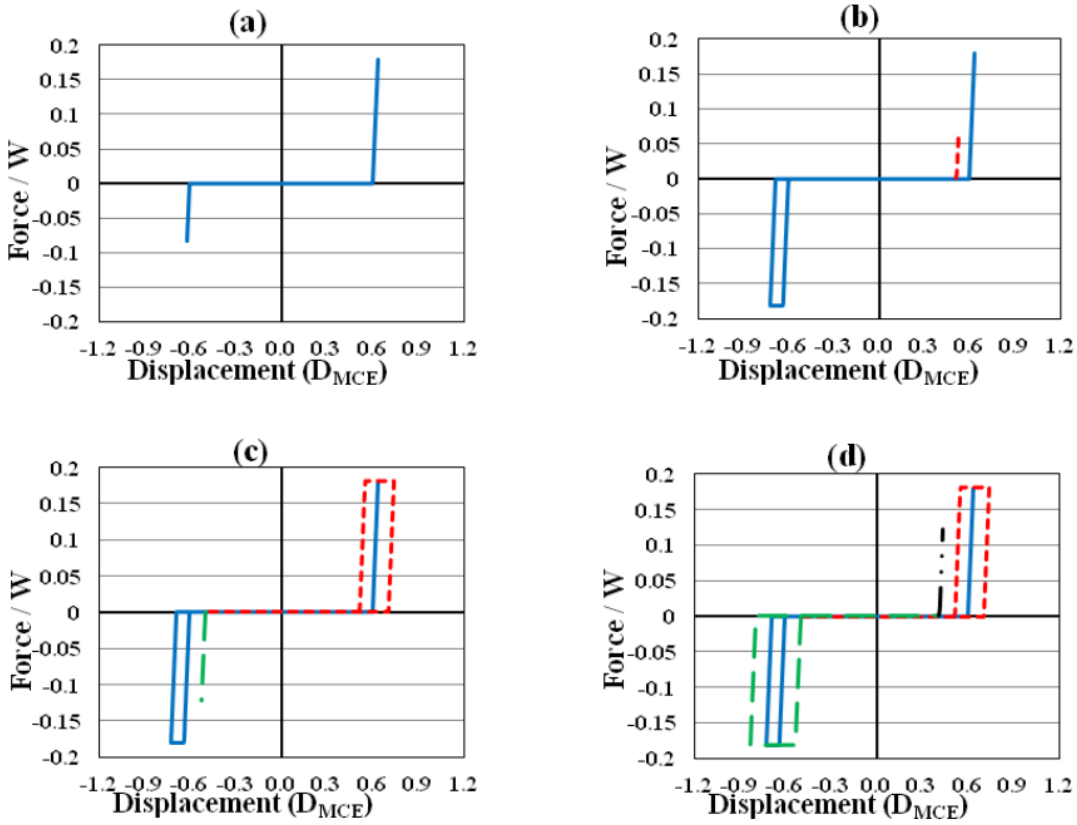

Figure 3-2. Hysteretic Gap Damper Behavior with Increasing Amplitude

A preliminary analysis of the gap damper system was executed to compare the efficiency of the system in comparison to a traditional base-isolated system. This was accomplished using a

reference base-isolated system with a natural period (T_M) of 3.0 seconds and isolator damping (ξ) of 15%. The Erzincan, Turkey ground motion of 1992 was scaled to reach a displacement of 1.375*D_{MCE} in the reference structure, 25% beyond the moat wall location, analyzed for both a viscous and hysteretic gap damper system. The solid black lines in Figure 3-3 indicate the location of the moat wall and shows the traditionally base-isolated structure exceeding this displacement. The hysteretic gap damper device (Figure 3-3a) reduces the displacement to a level that barely makes makes contact with the moat wall, while the viscous gap damper device (Figure 3-3b) reduces the displacement below the moat wall location, indicating that the system was able to achieve the intended goal.

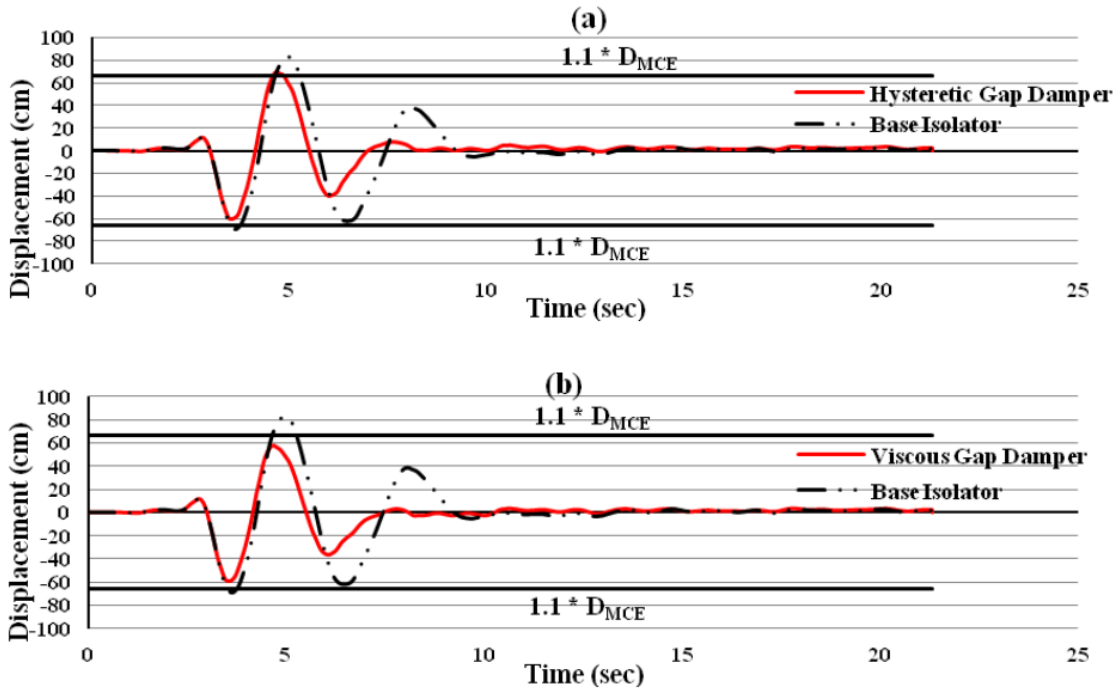

Figure 3-3. Isolator-Level Displacement Time History Comparison of a Base-Isolated System to a Gap Damper System Subjected to the 1992 Erzincan Turkey Ground Motion for a) Hysteretic Gap Damper and b) Viscous Gap Damper

The displacement control evident in the gap damper system comes with a trade-off of increasing the superstructure accelerations. Similar to the displacement criteria established as the moat wall location (1.1*D_{MCE}), an acceptable acceleration criteria was developed for the

superstructure as three times the median peak roof acceleration of the superstructure when subjected to a suite of design level ground motions ($3*A_{DM}$). Figure 3-4a illustrates that although the hysteretic element is not as effective at reducing isolator level displacement, the superstructure accelerations remain within an acceptable range. Figure 3-4b illustrates the contrary, as the gap damper system was able to reduce the displacements to an acceptable level, but at a cost of large acceleration spikes in the superstructure. These results only model the effects of the activation of the gap damper system and do not consider the pounding that would be present if the structure were to contact the moat wall.

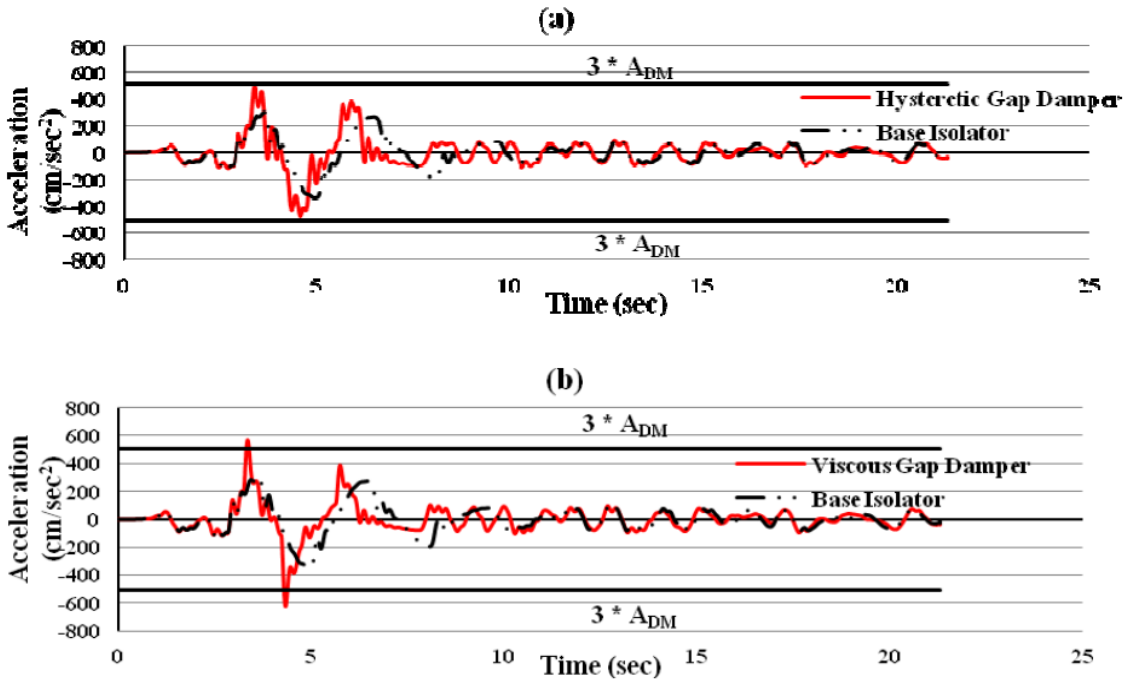

Figure 3-4. Roof Acceleration Time History Comparison of a Base-Isolated System to a Gap Damper System Subjected to the 1992 Erzincan Turkey Ground Motion for a) Hysteretic Gap Damper and b) Viscous Gap Damper.

The acceleration spikes present in the gap damper systems are due to a sudden increase in force, as shown in Figure 3-5. Upon activation of the supplemental energy dissipation devices, the energy is transferred to the superstructure. The force in the hysteretic device is displacement-dependent while the force in the viscous device is velocity-dependent, suggesting that the

performance of the device could vary based on the frequency content of the ground motion. The engagement of the gap damper systems at different displacements is also evident in Figure 3-5, as residual displacements accumulate throughout the ground motion.

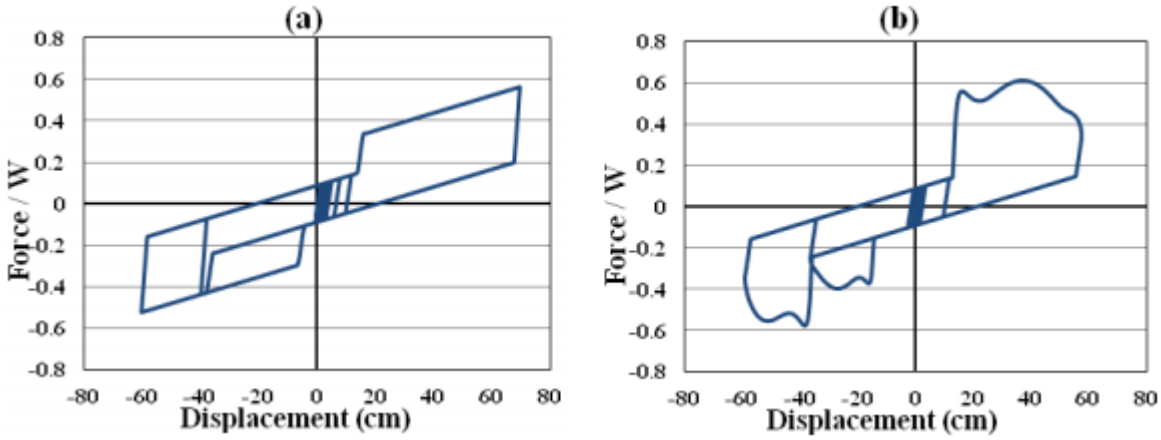

Figure 3-5. Force-Displacement Relationship of the Base-Isolation System Paired with a) Hysteric Gap Damper and b) Viscous Gap Damper

This brief introduction to the gap damper concept clearly indicates the potential for such systems, but further investigation is necessary. Although hysteretic and viscous gap damper results were presented in this section, different combinations of hysteretic and viscous models in the form of hybrid systems could provide the desired performance. Due to the relative trade-off between displacement reduction in the isolator level and acceleration in the superstructure upon activation of the gap damper system, it is evident that a parametric study was necessary in order to identify systems with the best performance.

3.3 Parametric Study

A large parametric study was completed at the University of Nevada-Reno prior to the start of the Auburn University research. The details are published in a paper entitled *"Feasibility study of a gap damper to control seismic isolator displacements in extreme earthquakes"* (Zargar, Ryan, &

Marshall, 2013). This section provides an overview of the essential aspects of the parametric study necessary to provide proper context for this doctoral work.

3.3.1 Model Details

The model considered for the parametric study was a simple two degree-of-freedom shear structure, pictured in Figure 3-6a. A superstructure mass M and base mass 0.25M were chosen to represent a typical low-rise base-isolated structure with a superstructure natural period of $T_s = 0.5$ seconds and a damping ratio of $\xi_s = 5\%$. The hazard selected has a short period spectral acceleration (S_{MS}) of 2.2g and a 1.0 second spectral acceleration (S_{M1}) of 1.11g. Superstructure stiffness (K_s) was determined in order to achieve the desired natural period of the superstructure.

The base-isolation system was assumed to have a bilinear force-deformation relationship shown in Figure 3-6b, typical for a lead-rubber bearing. As described previously, the objective of the gap damper system was to limit the displacement to less than the moat wall location of $1.1*D_{MCE}$. According to ASCE 7-10 Chapter 17, the maximum considered earthquake displacement (D_{MCE}) can be determined as:

$$\mathbf{D_{MCE} = \left(\frac{g}{4\pi^2}\right)\frac{S_{M1}T_M}{B_M}} \qquad \textbf{Equation (3-1)}$$

where B_M is the damping factor determined using the ASCE 7-10 Table 17.5-1 and T_M is the natural period of the isolation system, determined using the effective secant stiffness of the isolator (K_M) at D_{MCE} and mass of the entire superstructure (1.25M):

$$\mathbf{T_M = 2\pi\sqrt{\frac{1.25M}{K_M}}} \qquad \textbf{Equation (3-2)}$$

The initial stiffness (K_i) of the isolator is in the elastic range of the lead core with lead core yielding at 1.0 cm (D_y). Post-yield stiffness of the isolator (K_d) is a function of isolator material properties but can also be found using Equation 3-3:

$$K_d = \frac{K_M D_{MCE} - Q_d}{D_{MCE}} \qquad \textbf{Equation (3-3)}$$

where Q_d is the characteristic strength of the isolator at zero displacement, defined as:

$$Q_d = \frac{K_M \xi_M D_{MCE}}{2(D_{MCE} - D_y)} \qquad \textbf{Equation (3-4)}$$

where ξ_M is the effective isolator damping, which varies from 10% to 25% of critical damping. In addition, the isolator natural periods (T_M) considered varied from 2.5 seconds to 4.0 seconds to represent various base-isolation characteristics. All systems were calibrated using MCE properties, meaning the design level natural period and damping characteristics were not equivalent. Using a design spectrum with code-specified design values $S_{DS} = 2/3*S_{MS}$ and $S_{D1} = 2/3*S_{M1}$, an iterative approach yielded a design natural period (T_D) that was less than the MCE value and a damping value (ξ_D) that was larger than the MCE value.

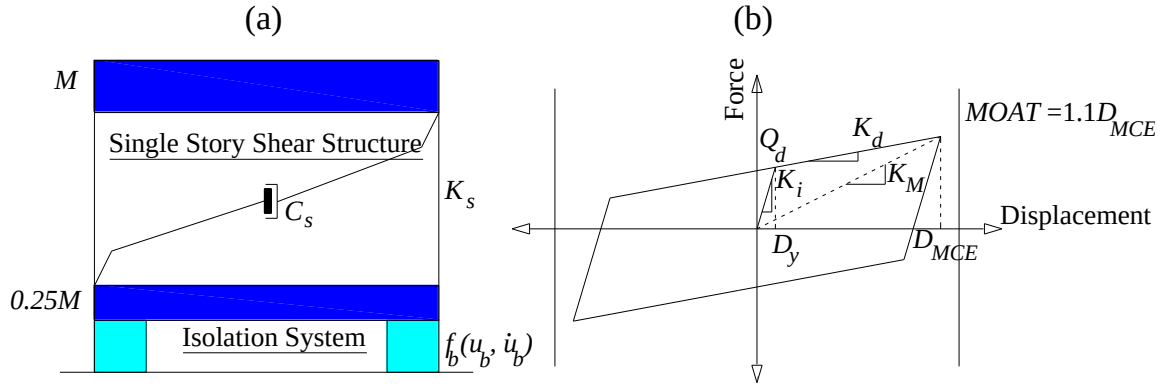

Figure 3-6. a) Two Degree-of-Freedom Base-Isolated Model b) Bilinear Isolation System Hysteresis

A total of five potential combinations of hysteretic and viscous energy dissipation elements were considered for the parametric study, which included hybrid systems consisting of both hysteretic and viscous systems. The systems considered were single-phase and multi-phase systems. Single-phase systems engage one or two dissipative elements at the same time while

multi-phase systems use a staged activation of dissipative devices that engage at different specified displacements. Figure 3-7 demonstrates the five models considered in the parametric study.

The five systems considered in the study are outlined below:

1. A hysteretic gap damper that utilizes an elastic-perfectly plastic spring for supplemental energy dissipation. The hysteretic element becomes active due to the stiffness increase of the gap element at $0.6*D_{MCE}$. The gap element is placed in series with the hysteretic element to form an element that is parallel to the bilinear spring representing the isolator behavior. An illustration representing the model can be found in Figure 3-7a, and the hysteretic response to a harmonically increasing excitation found in Figure 3-8a.
2. A viscous gap damper utilizes a viscous dashpot in series with a gap element. The overall behavior is similar to the hysteretic gap damper system with the viscous dashpot used in place of the hysteretic element. The use of the viscous dashpot means that the system is velocity-dependent, which is potentially advantageous for large velocity pulses often observed in near-fault motions. Although a linear dashpot was initially used (power of 1), other damping exponents were explored later in the study. An illustration representing the model can be found in Figure 3-7b, and the hysteretic response to a harmonically increasing excitation found in Figure 3-8b.
3. The Kelvin gap damper is a single-phased model that combines both the hysteretic element and viscous element in parallel. Similar to the previous models, these elements are placed in series with a gap element but allow hybrid energy dissipation from both elements in a single-phase system. An illustration representing the model can be found in Figure 3-7c, and the hysteretic response to a harmonically increasing excitation found in Figure 3-8c.

4. The two-phase viscoelastic gap damper is a multi-phase system that combines a viscous dashpot with a linear elastic spring. This is classified as a multi-phase system because the activation of the dashpot and spring occur at two different displacement thresholds. Similar to the other systems, the supplemental energy dissipation is not active until $0.6*D_{MCE}$. When the gap element locks out, the viscous dashpot is initially the only dissipative element active until $0.8*D_{MCE}$, when an elastic spring is activated and utilized in parallel to the dashpot. An illustration representing this multi-phase model can be found in Figure 3-7d, and the hysteretic response to a harmonically increasing excitation found in Figure 3-8d.
5. The last system considered is a two-phase viscoplastic gap damper. This multi-phase system is similar to the two-phase viscoelastic gap damper except for the utilization of an elastic-perfectly plastic hysteretic spring rather than an elastic spring. Similar to the previous system, the viscous dashpot is activated at $0.6*D_{MCE}$ and the hysteretic spring becomes active at $0.8*D_{MCE}$. Both dissipative elements act independently of one another and accumulate separate residual displacements. An illustration representing this multi-phase model can be found in Figure 3-7e, and the hysteretic response to a harmonically increasing excitation found in Figure 3-8e.

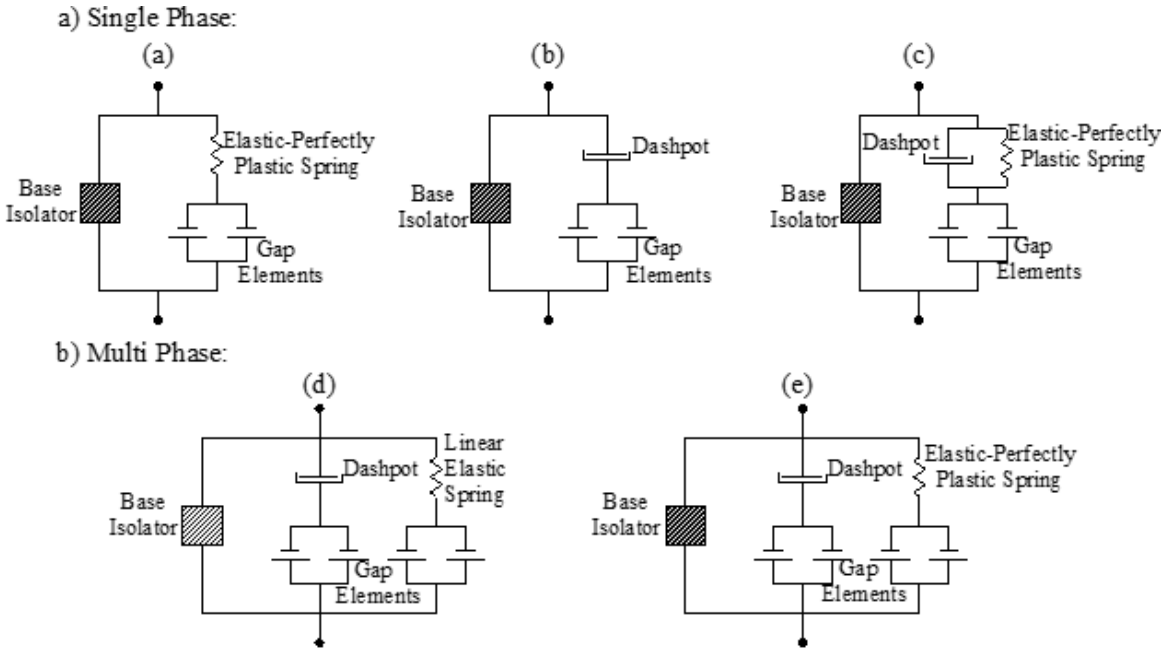

Figure 3-7. Gap Damper Models Considered: a) Hysteretic b) Viscous c) Kelvin d) Two-Phase Viscoelastic, and e) Two-Phase Viscoplastic

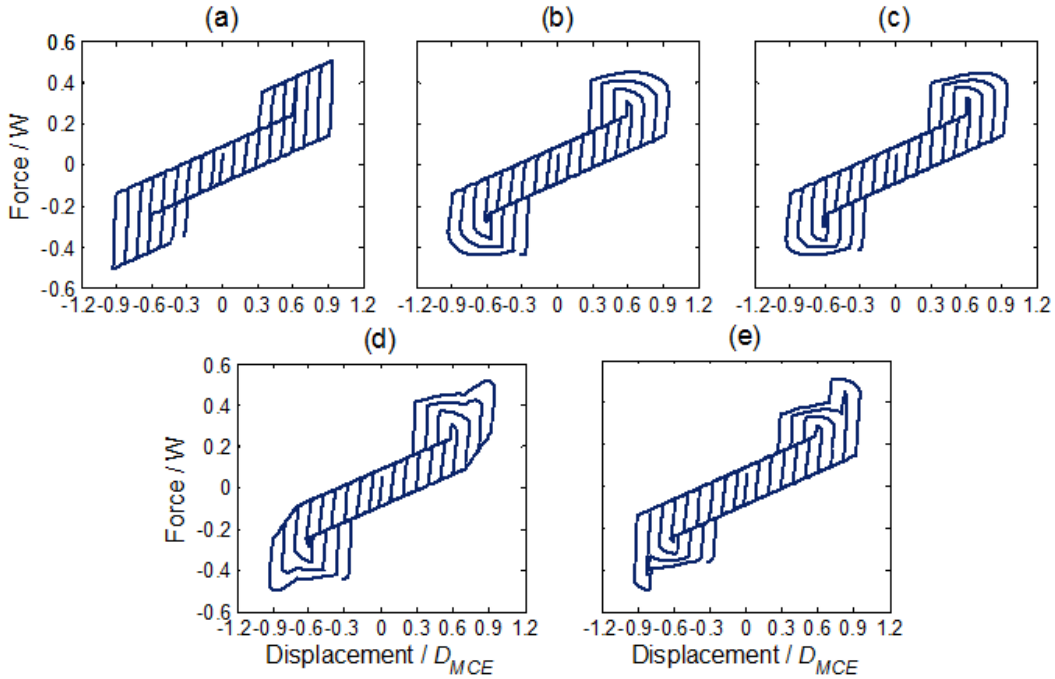

Figure 3-8. Cyclic Representation of the Gap Damper Models Considered a) Hysteretic b) Viscous c) Kelvin d) Two-Phase Viscoelastic, and e) Two-Phase Viscoplastic

For the original parametric study, a suite of 24 ground motions were chosen using the PEER NGA database (Chiou, Daragh, Gregor, & Silva, 2008) and motions from the SAC Steel Project (Somerville, Smith, Puntamurthula, & Sun, 1997). The motions were scaled so that a system without a gap damper would have a displacement demand of 1.375* D_{MCE}, 25% beyond the moat wall location of 1.1* D_{MCE}. When a gap damper system was subjected to the larger "over moat scale factors", the objective was to reduce the displacement at least 25%. The set of motions were also scaled to meet the design displacement (D_D) in order to establish acceleration demands in a design-based earthquake. Scale factors varied based on the natural period and damping present in the isolation system. The 24 final ground motions were the result of the elimination of motions with a peak ground acceleration (PGA) greater than 1g or a scale factor greater than 3. Details of the ground motions selected are presented in Table 3-1.

Table 3-1. Ground Motions for the Parametric Study

GM #	NGA	Earthquake	Station	Magnitude	Distance (km)	PGA (g)
1	NA	Loma Prieta, USA, 1989	Los Gatos Pres. Ctr. (SAC la23)	7.00	3.50	0.42
2	NA	Loma Prieta, USA, 1989	Los Gatos Pres. Ctr. (SAC la24)	7.00	3.50	0.47
3	NA	Northridge, USA, 1994	Sylmar-Olive View Hosp. (SAC la 27)	6.70	6.40	0.93
4	NA	Elysian Park Fault	Simulated (SAC la33)	7.10	10.70	0.78
5	NA	Elysian Park Fault	Simulated (SAC la34)	7.10	10.70	0.68
6	NA	Elysian Park Fault	Simulated (SAC la35)	7.10	11.20	0.99
7	NA	Elysian Park Fault	Simulated (SAC la36)	7.10	11.20	1.10
8	NA	Palo Verdes Fault	Simulated (SAC la37)	7.10	1.50	0.71
9	NA	Palo Verdes Fault	Simulated (SAC la38)	7.10	1.50	0.78
10	NA	Palo Verdes Fault	Simulated (SAC la39)	7.10	1.50	0.50
11	NA	Palo Verdes Fault	Simulated (SAC la40)	7.10	1.50	0.63
12	NGA 1084	Northridge, USA, 1994	Sylmar Conv. Sta. (SCS052)	6.70	5.35	0.61
13	NGA 0527	N. Palm Springs, USA, 1986	Morongo Valley (MVH135)	6.06	12.07	0.21
14	NGA 1120	Kobe, Japan, 1995	Takatori (TAK090)	6.90	1.47	0.62
15	NGA 0821	Erzican, Turkey, 1992	Erzican (ERZ-NS)	6.69	4.38	0.52
16	NGA 1605	Duzce, Turkey, 1999	Duzce (DZC180)	7.14	6.58	0.35
17	NA	Imperial Valley, USA, 1940	El Centro (SAC la01)	6.90	10.00	0.46
18	NA	Imperial Valley, USA, 1979	Array 05 (SAC la03)	6.50	4.10	0.39
19	NA	Imperial Valley, USA, 1979	Array 05 (SAC la04)	6.50	4.10	0.49
20	NA	Imperial Valley, USA, 1979	Array 06 (SAC la05)	6.50	1.20	0.30
21	NA	Imperial Valley, USA, 1979	Array 06 (SAC la06)	6.50	1.20	0.24
22	NA	Landers, USA, 1992	Barstow (SAC la07)	7.30	36.00	0.42
23	NA	Landers, USA, 1992	Yermo (SAC la10)	7.30	25.00	0.36
24	NGA 0723	Superstition Hills, USA, 1987	Parachute Test Site (B-PTS225)	6.54	0.95	0.46

3.3.2 Gap Damper Properties

The gap damper models considered in the parametric study and the equal energy concept were introduced in the previous section. Using the equal energy concept, the properties of the elements in the gap damper system were calibrated. The energy present in the bilinear isolator from $1.0*D_{MCE}$ to $1.375*D_{MCE}$ is referred to as the reference level of energy dissipation (ED_{PMCE}). The

amount of energy dissipated (ED_{PMCE}) in one complete cycle from -1.375*D_{MCE} to 1.375*D_{MCE} is a function of the characteristic strength of the isolator (Q_d) and D_{MCE}, as shown in Equation 3-5:

$$\mathbf{2 * ED_{PMCE} = 4Q_d(1.375D_{MCE} - D_{MCE}) = 1.5Q_dD_{MCE}} \qquad \textbf{Equation (3-5)}$$

The energy dissipated by the gap damper device from 0.6*D_{MCE} to 1.0*D_{MCE} is ED_{DAMPER}. Properties of the dissipative device depend on the type of energy dissipation, shown in Figure 3-9 for a hysteretic and viscous device.

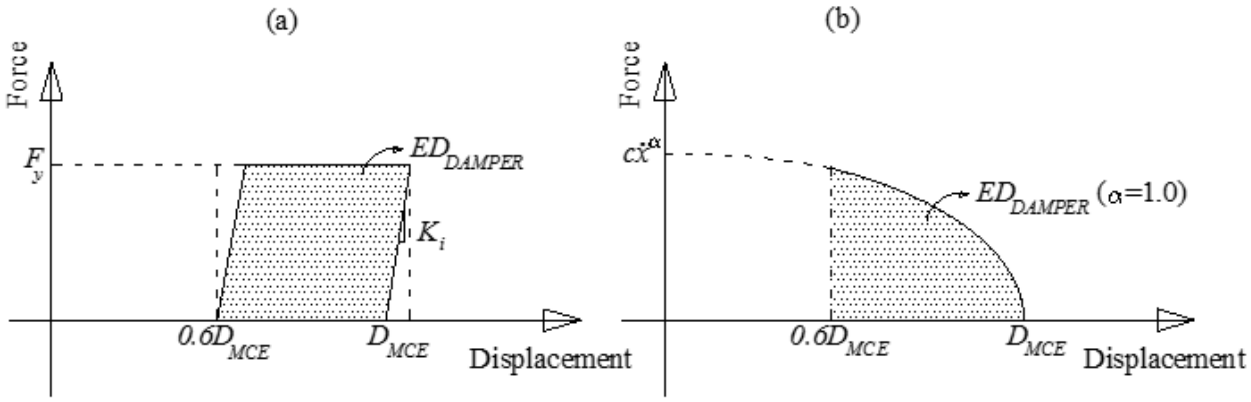

Figure 3-9. Supplemental Energy Dissipation for a) Hysteretic Element and b) Viscous Element

The energy present in a full gap damper cycle from -1.0*D_{MCE} to 1.0*D_{MCE} for the elastic-perfectly plastic hysteretic device can be defined using Equation 3-6:

$$\mathbf{2 * ED_{DAMPER} = 2F_y\left((1.0D_{MCE} - 0.6D_{MCE}) - \frac{F_y}{K_i}\right)} \qquad \textbf{Equation (3-6)}$$

where K_i is the initial stiffness and F_y is the yield force of the hysteretic material. The performance of the hysteretic gap damper was found to be insensitive to the initial stiffness K_i, and was given a value equivalent to the initial stiffness of the isolation system. Equating the energy present in Equation 3-5 (ED_{PMCE}) to the energy in Equation 3-6 (ED_{DAMPER}), and solving for the yield force of the hysteretic element produces Equation 3-7:

$$F_y = \frac{0.4K_i D_{MCE} \pm \sqrt{(0.4K_i D_{MCE})^2 - (4(0.75)Q_d K_i D_{MCE})}}{2} \quad \textbf{Equation (3-7)}$$

which completes the configuration of the properties for the hysteretic gap damper.

Calibration of the viscous gap damper device first requires the definition of viscous damping which is velocity-dependent and can be expressed as:

$$F = c * sgn(\dot{u})|\dot{u}|^{\alpha} \quad \textbf{Equation (3-8)}$$

where c is the damping constant, $\dot{u}$ is the velocity in the dashpot, and α is the damping coefficient, initial taken as 1 for a linear viscous damper. Assuming harmonic motion at a resonant frequency, the energy dissipated by a viscous gap damper device in a full cycle from -1.0*D_{MCE} to 1.0*D_{MCE} is found in Equation 3-9:

$$2 * ED_{DAMPER} = 2 * c * w_n{}^{\alpha} \int_{0.6D_{MCE}}^{D_{MCE}} \sqrt{(D_{MCE}{}^2 - u^2)^{\alpha}}\, du \quad \textbf{Equation (3-9)}$$

where w_n is the natural frequency of the isolation system and u is the displacement. Equating the energy present in Equation 3-5 (ED_{PMCE}) to the energy in Equation 3-9 (ED_{DAMPER}), and solving for the damping constant of the hysteretic element produces:

$$c = \frac{0.75Q_d D_{MCE}}{w_n{}^{\alpha} \int_{0.6D_{MCE}}^{D_{MCE}} \sqrt{(D_{MCE}{}^2 - u^2)^{\alpha}}\, du} \quad \textbf{Equation (3-10)}$$

which completes the configuration of the properties for the viscous gap damper. For a linear viscous model, Equation 3-10 can be simplified to:

$$c = \frac{0.3535Q_d}{w_n D_{MCE}} \quad \textbf{Equation (3-11)}$$

The three other models considered in the parametric study involved a hybrid configuration, as described earlier. The calibration of the gap damper properties was similar to the previous systems with a differing portions ED_{PMCE} dissipated by the hysteretic and/or viscous devices. Table 3-2 outlines the properties of the hybrid systems with an explanation of the portion of

ED_{PMCE} dissipated by each element and the initial activation threshold. These hybrid properties were optimized prior to being included in the parametric study.

Table 3-2. Hybrid Gap Damper Parameters

Hybrid Gap Damper	Portion of energy dissipation by viscous component	Portion of energy dissipation by hysteretic component	Initial gap for viscous component	Initial gap for spring or hysteretic component
Kelvin	75%	25%	$0.6 \cdot D_{MCE}$	$0.6 \cdot D_{MCE}$
Two-Phase Viscoelastic	100%	NA	$0.6 \cdot D_{MCE}$	$0.8 \cdot D_{MCE}$
Two-Phase Viscoplastic	70%	30%	$0.6 \cdot D_{MCE}$	$0.8 \cdot D_{MCE}$

3.3.3 Performance Index

As alluded to previously, beneficial reductions in base-level displacements are accompanied by increased acceleration in the superstructure. As the amount of energy dissipated by the gap damper system increases, the acceleration in the superstructure is expected to increase. The optimal value of energy dissipation in the gap damper may not be equivalent to ED_{PMCE}. In order to investigate this phenonmenon, a new variable was added to the parametric study that normalized the energy dissipation level (EDL):

$$\mathbf{EDL} = \frac{\mathbf{ED_{DAMPER}}}{\mathbf{ED_{PMCE}}} \qquad \textbf{Equation (3-12)}$$

where a number less than 1 would indicate that the gap damper energy dissipation is less than the over-gap energy dissipation of the isolator from $1.0*D_{MCE}$ to $1.375*D_{MCE}$ (ED_{PMCE}) and vice versa. The smaller the EDL, the less likely the gap damper is able to control isolator displacements to meet the desired target of the study. On the contrary, as the EDL increases, the gap damper is able to control the isolator displacements but with consequential acceleration spikes in the superstructure. EDLs evaluated in the parametric study ranged from 0.5-2.25.

In order to identify systems that performed the best in the parametric study, a performance index was created that weighs both displacement at the base level and acceleration in the superstructure. The reduction in displacement necessary for the success of the gap damper device is from $1.375*D_{MCE}$ to the moat wall location of $1.1*D_{MCE}$, meaning there is a target reduction of $0.275*D_{MCE}$. Variation of gap damper response is potentially sensitive to individual ground motion content. Introducing a statistical aspect to the study, the 84th percentile (median plus one standard deviation) displacement (D_{84th}) of the suite of ground motions was used for the overall displacement level of the gap damper system. This means the achieved reduction can be defined as $1.375*D_{MCE} - D_{84th}$. The performance index (PI_D) developed for the displacement response in the gap damper is defined in Equation 3-13:

$$\mathbf{PI_D = 1 + \frac{Target\ Reduction - Achieved\ Reduction}{Target\ Reduction} = 1 + \frac{D_{84th} - 1.1D_{MCE}}{0.275D_{MCE}}} \qquad \textbf{Equation (3-13)}$$

where a value of 1.0 indicates that the displacement objective has been met. Values less than 1.0 are possible if the system exceeds the target reduction and values up to 2.0 are possible if the gap damper has no effect on the displacement of the system. Figure 3-10 illustrates the range of PI_D vs. EDL for individual ground motions with the 84th percentile line used for analysis of the system. The plot clearly indicates the spread of the gap damper performance across ground motions.

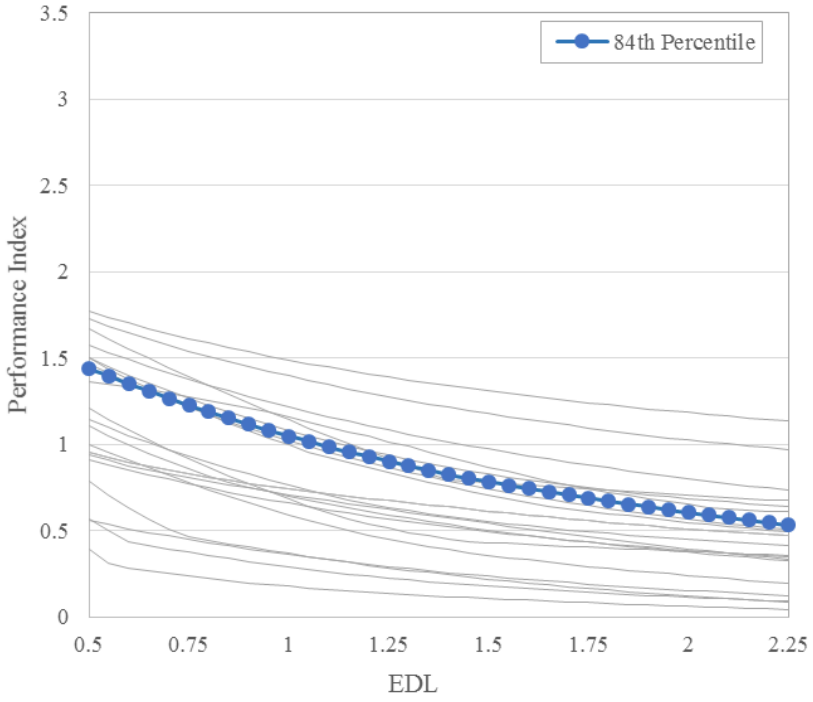

Figure 3-10. PI_D vs. EDL (T_M = 2.36 seconds, ξ_M = 20%)

For the acceleration performance objective, the target acceleration of the gap system was defined as 3 times the median roof acceleration for a reference base isolated system subjected to a suite of design level ground motions ($3*A_{DM}$). The acceleration performance index is defined in Equation 3-14:

$$\mathbf{PI_A = \frac{Achieved\ Acc}{Target\ Acc} = \frac{A_{GD}}{3A_{DM}}} \qquad \textbf{Equation (3-14)}$$

where A_{GD} is the median acceleration present in the gap damper superstructure subjected to a suite of ground motions. Similar to the displacement performance, a PI_A less than 1.0 means that the system has met the acceleration objective. Figure 3-11 illustrates the range of PI_D vs. EDL for individual ground motions with the average line used for analysis of the system. For this particular system (T_M = 2.36 seconds, ξ_M = 20%), the median roof acceleration (A_{DM}) for the suite of design motions was 0.225g,k therefore a performance index of 1.0 would indicate a gap damper system with a median roof acceleration (A_{GD}) of 0.675g, or 3 times A_{DM}.

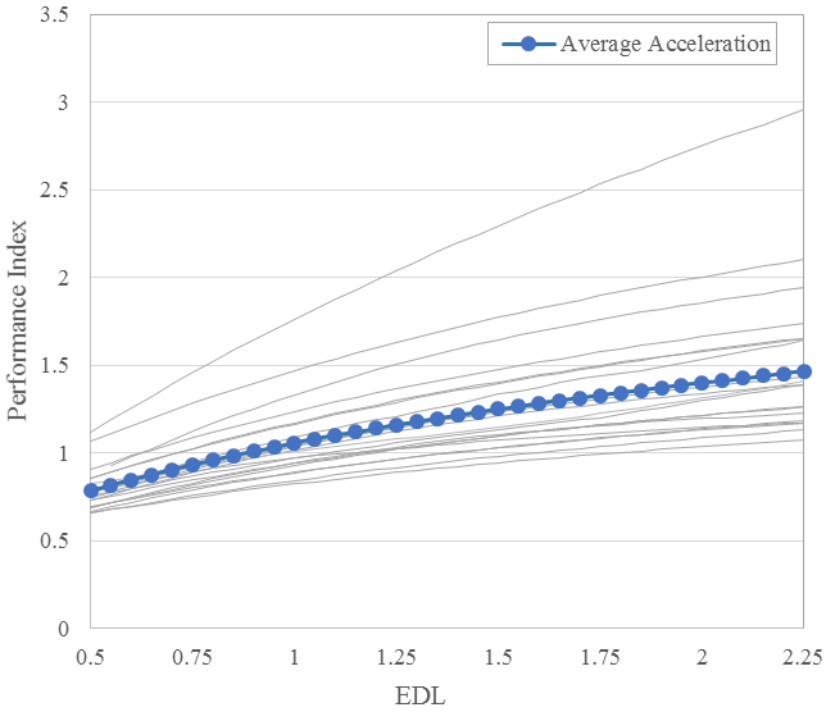

Figure 3-11. PI_D vs. EDL (T_M = 2.36 seconds, ξ_M = 20%)

The overall performance index (PI) is a combination of PI_D and PI_A, with the larger index controlling:

$$\mathbf{PI = max(PI_D, PI_A)} \qquad \textbf{Equation (3-15)}$$

Figure 3-12 illustrates the range of PI vs. EDL for individual ground motions with the overall system performance index used for analysis of the system. The resulting performance index is a piecewise line with the maximum index, either from displacement or acceleration, controlling the function. The displacement line controls the left-hand portion of the curve while the acceleration line controls the right-hand portion of the curve. The EDL associated with the minimum PI would be considered the dissipation level "optimal" for design of the gap damper system, which occurs when the displacement curve and acceleration curve intersect. Although this is the minimum value for the suite of motions, it is not necessarily optimal for an individual ground motion, as evident in Figure 3-12 which shows the spread of the data.

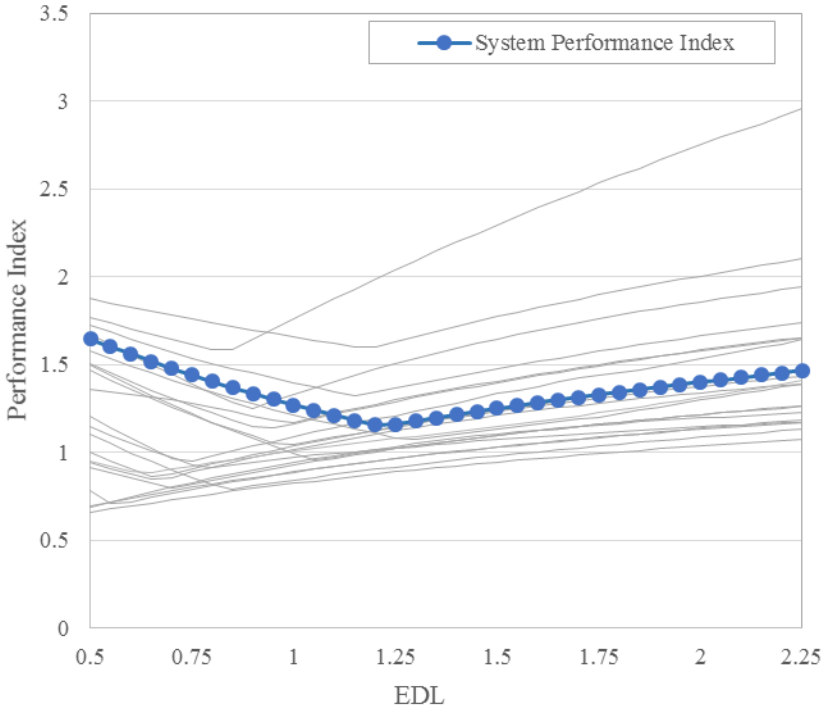

Figure 3-12. PI vs. EDL (T_M = 2.36 seconds, ξ_M = 20%)

3.3.4 Results

With the gap damper properties and the evaluation criteria established, the systems could be effectively compared in a parametric study. For any device utilizing a viscous element, the possibility of linear or nonlinear damping must be considered. Figure 3-13 illustrates the PI vs. EDL curves for differing damping exponents (α) for a system (T_M = 3.0 sec, ξ_M = 15%). The optimum PI does not change much based on the damping coefficient, although the optimum EDL value decreases as the damping coefficient increases. Without a large difference in optimal performance, a linear viscous damper (α = 1) was chosen for the parametric study.

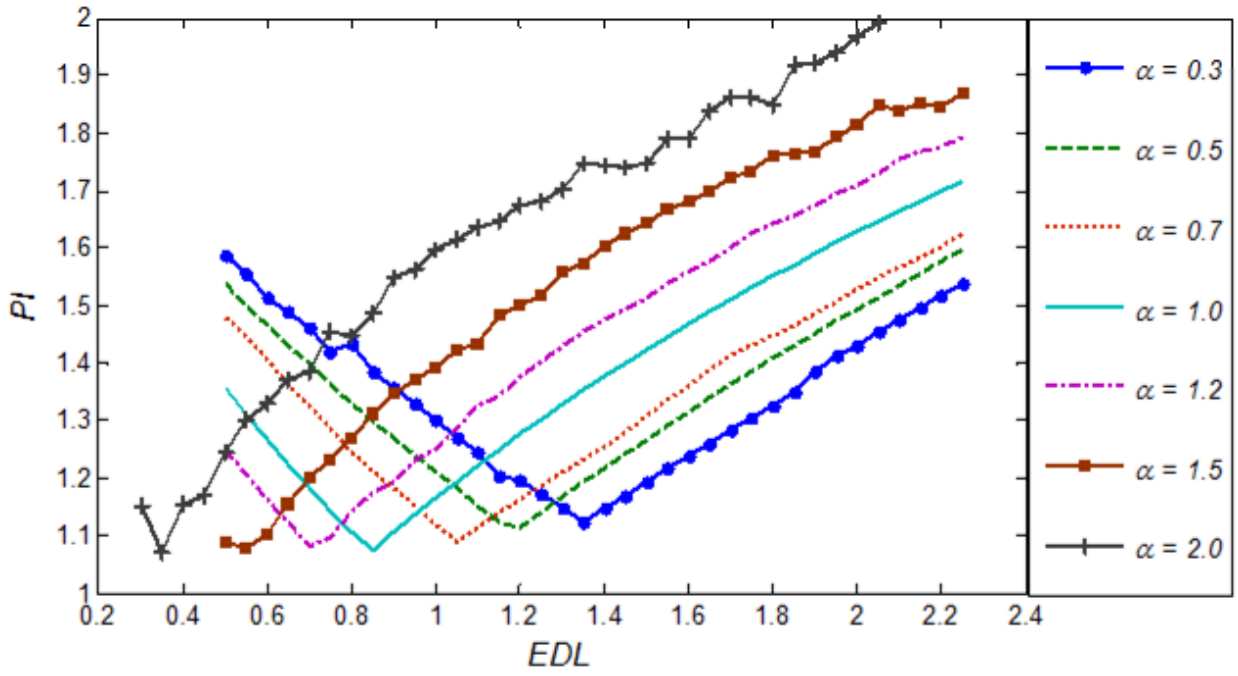

Figure 3-13. Performance Index vs. Equivalent Dissipation Level for Varying Damping Coefficients (T_M = 3.0 sec, ξ = 15%)

For the parametric study, these overall PI vs EDL lines were used to compare the five potential models. Figure 3-14 shows a comparison of the results for the models for T_M = 3.0 sec, ξ_M = 15%, with the hysteretic model clearly showing the worst performance with a minimum PI of approximately 1.35, while PIs for the other systems ranged from 1.0 to 1.1. None of the systems were able to meet the desired performance objective of PI < 1.0. The hysteretic gap damper performs very poorly from both a displacement and acceleration perspective.

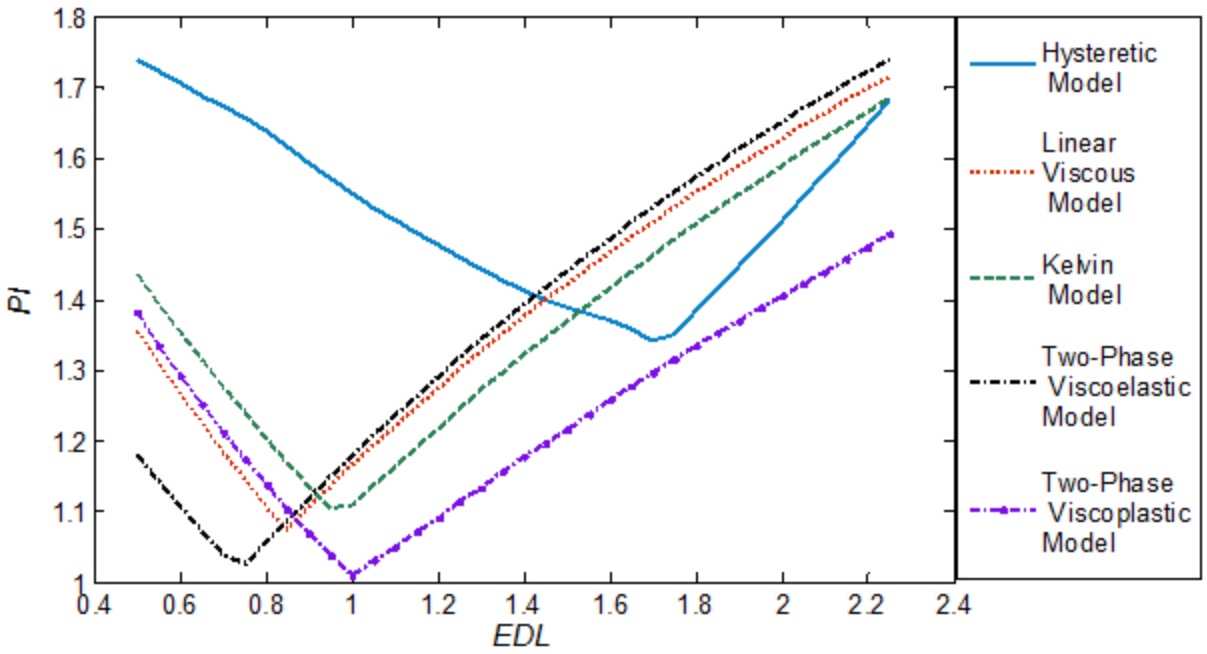

Figure 3-14. Performance Index vs. Equivalent Dissipation Level for the Systems Considered (T_N = 3.0 sec, ξ = 15%)

Gap damper systems utilizing a viscous damper show more promising results, with the two-phase hybrid models exhibiting the best overall behavior. Activation of the viscous elements is often accompanied by a large acceleration spike in the superstructure, as evident in the time history plots shown in Figure 3-15. If a portion of the energy is also dissipated by a hysteretic device, the acceleration at activation is decreased and the displacement objective can still be maintained. The second phase of the hybrid models (>0.8*D_{MCE}) provides beneficial supplemental energy dissipation, as the velocity-sensitive viscous devices provide less energy dissipation towards the maximum displacement demands. Since the elastic and hysteretic devices present in the second phase are not viscous and the amount of energy is smaller relative to the viscous device, sharp acceleration spikes are not present in the superstructure upon activation. Figure 3-15 clearly shows that the two-phase viscoplastic device is the only system able to meet both the acceleration and displacement objectives. The figure also demonstrates that there is only one acceleration spike

per half-cycle evident in the two-phase systems upon the activation of the viscous device. The second phase provides the beneficial energy dissipation without another spike.

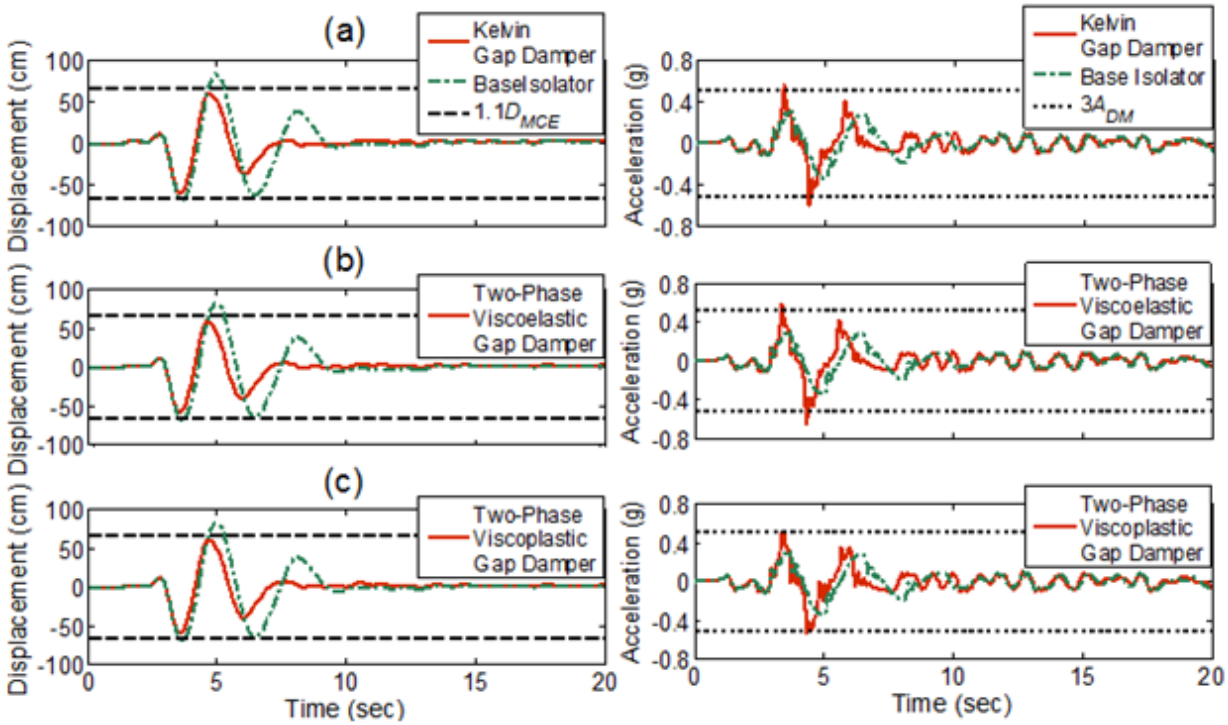

Figure 3-15. Isolator Displacement and Roof Acceleration History Comparison Subjected to the 1992 Erzincan, Turkey Ground Motion for a) Kelvin Gap Damper b) Two-Phase Viscoelastic Gap Damper, and c) Two-Phase Viscoplastic Gap Damper

A more visual representation of the performance of the systems in presented in Figure 3-16, which is a scatter plot showing the performance of the systems for each individual ground motion. These plots are representative of the systems at their optimal EDL with the large marker indicating the overall performance. The hysteretic gap damper system is clearly not able to control acceleration in the superstructure. Although the models containing viscous elements show promising overall results, there is a large variation in the acceleration control. The hysteretic and Kelvin models were dismissed from the parametric study because systems that activate hysteretic elements at the initial onset of supplemental damping ($0.6*D_{MCE}$) experience difficulties in controlling accelerations in the superstructure.

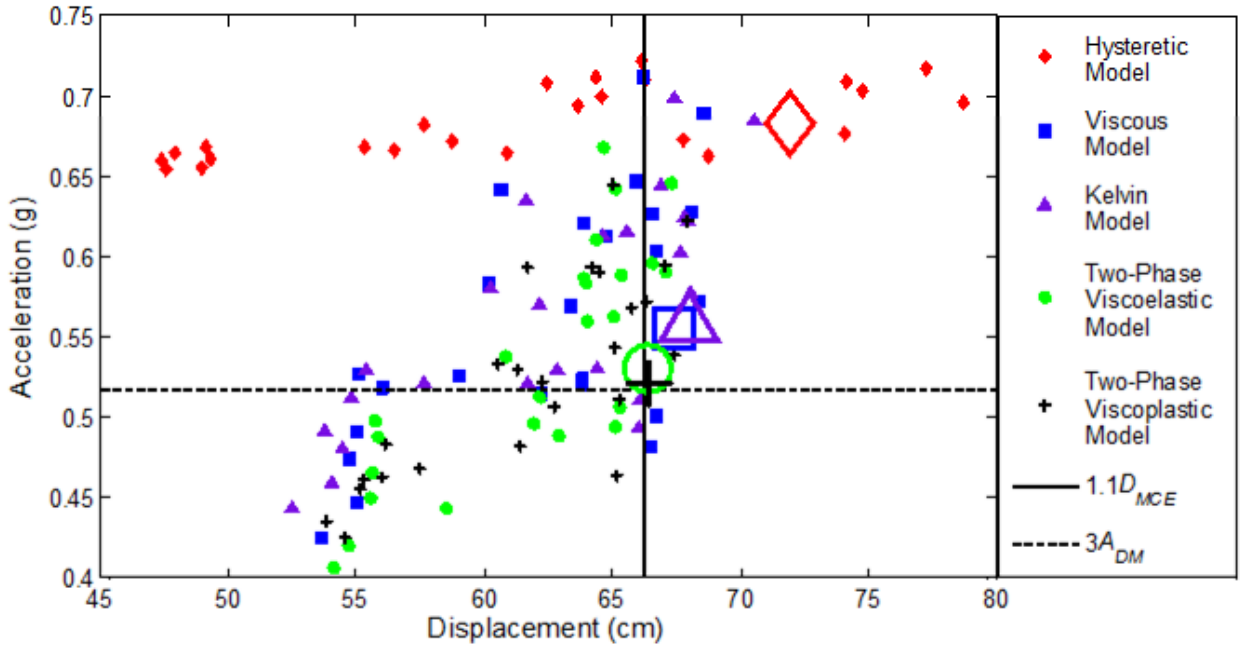

Figure 3-16. Scatter Plot Comparing Individual Ground Motions (T_N = 3.0 sec, ξ = 15%)

For the parametric study, PI curves were used to compare results from models with various natural periods (T_M = 2.5 seconds, 3.0 seconds, 3.5 seconds, and 4.0 seconds) and damping ratios (ξ_M = 10%, 15% and 25%). Figure 3-17 shows a comparison of results of each isolator damping (ξ_M) level for each isolator natural period for a viscous gap damper. Clear trends are noticed in the plot, with the optimal performance index increasing slightly as the natural period of the system increases, suggesting that the gap damper systems are more effective for lower natural periods. This trend is a function of the acceleration performance metric (PI_A), which utilizes the acceleration in the design motions ($3A_{DM}$). As the natural period lengthens, the isolation system becomes more effective and the acceleration in the design motions decreases, creating a more stringent requirement for the gap damper system which is directly compared to target acceleration ($3A_{DM}$).

Another observation evident in Figure 3-17 is that as damping in the isolation system (ξ_M) increases, the optimum EDL decreases. This suggests that less energy dissipation is required of the gap damper as the energy dissipation capacity of the isolation system increases.

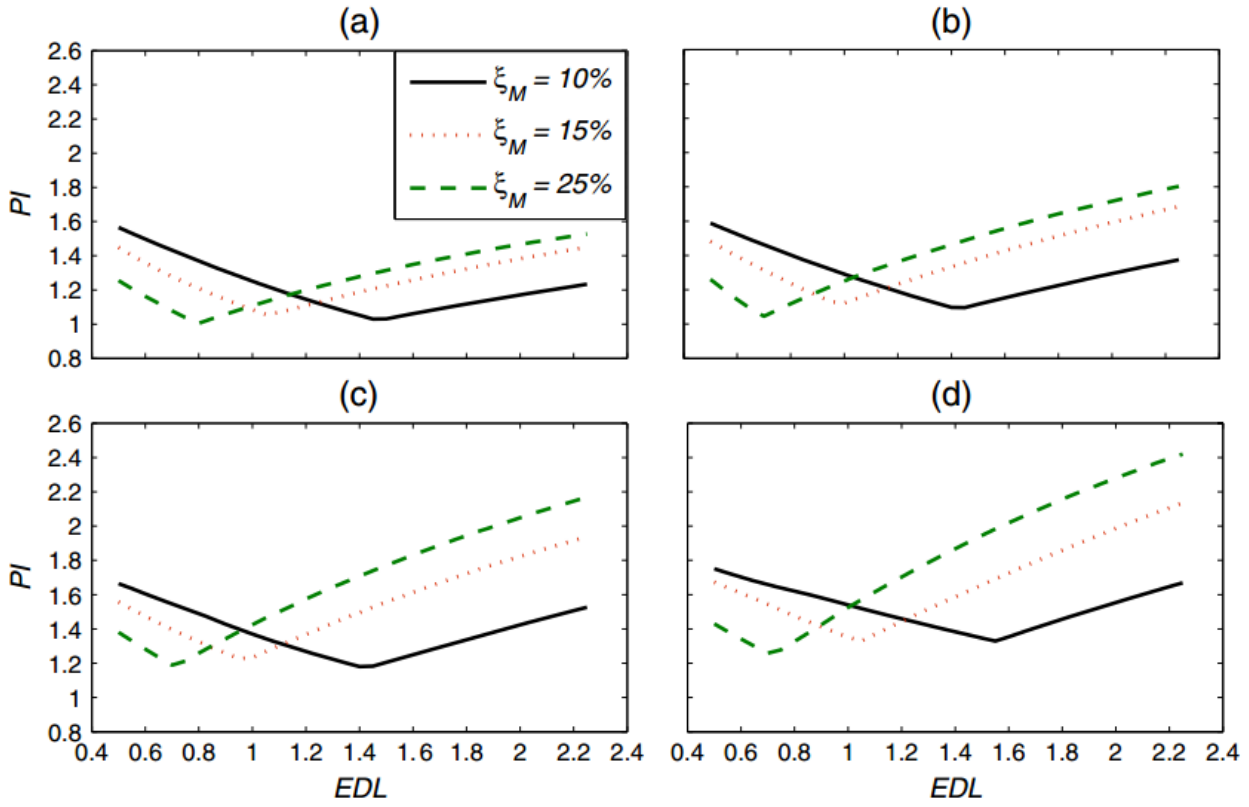

Figure 3-17. Performance Index vs. Equivalent Dissipation Level for a) T_M = 2.5 sec b) T_M = 3.0 sec c) T_M = 3.5 sec d) T_M = 4.0 sec Viscous Gap Damper

These trends hold true for the all of the remaining gap damper systems, as is evident in Figure 3-18. The optimal performance index increases as the natural period of the system increases. PI also tends to decrease as the damping in the isolator increases. Meeting the performance objective (PI<1) is only consistently achieved in the gap damper systems with a natural period of 2.5 seconds and is achieved in a few systems in which there is a natural period of 3.0 seconds accompanied by a larger amount of damping in the isolation system.

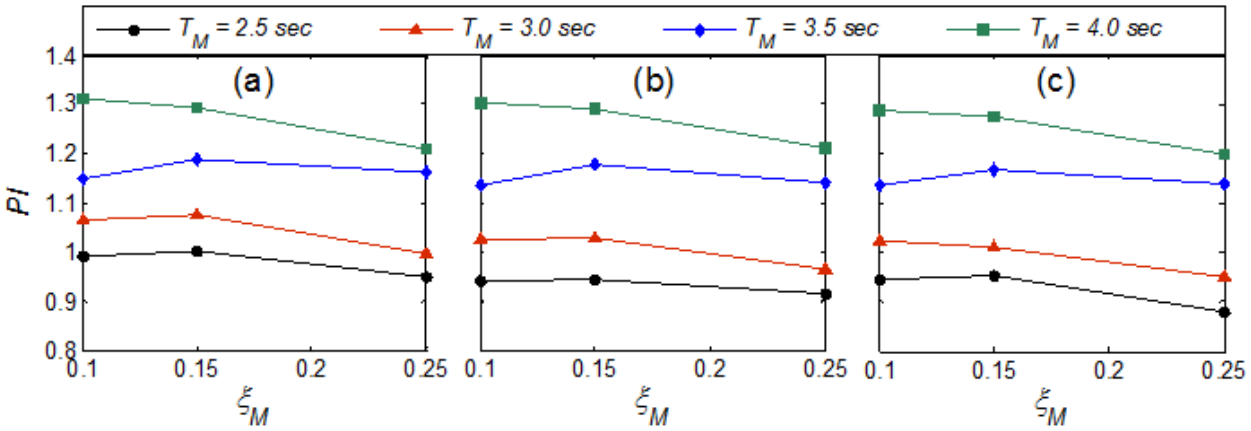

Figure 3-18. Performance Index vs. Damping Ratio for a) Viscous Gap Damper b) Two-Phase Viscoelastic Gap Damper, and c) Two-Phase Viscoplastic Gap Damper

3.3.5 EDL Design Values

Prior to the completion of the parametric study, further examination of the EDL values was necessary to determine the adequacy for a broad design approach. Although clear trends were noticed in the parametric study, various aspects of the study were tied very closely to the parameters of the single-degree-of-freedom superstructure system. EDL values used in design should be relatively consistent regardless of the ground motion suite, gap damper system formulation, and superstructure characteristics. This section evaluates the robustness of the EDL values for the pure viscous gap damper system in regards to differing parameters.

3.3.5.1 Ground Motion Suite Comparison

Previous analysis suggested that the optimal EDL may be sensitive to the ground motions chosen; Figure 3-12 illustrates the spread of performance versus EDL values for individual ground motions. A new suite of ground motions were added to the analysis, taken from the FEMA P-695 report *"Quantification of Building Seismic Performance Factors"* (Applied Technology Council,

2009). The 16 motions chosen were from a set of near-source motions, half containing velocity pulses and half without velocity pulses. Selected motions are summarized in Table 3-3.

Table 3-3. FEMA P695 Ground Motion Selection.

GM #	NGA	Earthquake	Year	Station	Magnitude	Distance (km)	PGA (g)
1	0181	Imperial Valley-06, USA	1979	El Centro Array #6	6.5	27.5	0.43
2	0182	Imperial Valley-06, USA	1979	El Centro Array #7	6.5	27.6	0.42
3	0292	Irpinia, Italy-01	1980	Sturno	6.9	30.4	0.29
4	0879	Landers, USA	1992	Lucerne	7.3	44.0	0.72
5	0828	Cape Mendocino, USA	1992	Petrolia	7.0	4.5	0.62
6	1063	Northridge-01, USA	1994	Rinaldi Receiving Station	6.7	10.9	0.63
7	1086	Northridge-01, USA	1994	Sylmar - Olive View	6.7	16.8	0.70
8	1503	Chi-Chi, Taiwan	1999	TCU065	7.6	26.7	0.66
9	1529	Chi-Chi, Taiwan	1999	TCU102	7.6	45.6	0.24
10	1605	Duzce, Turkey	1999	Duzce	7.1	1.6	0.43
11	0126	Gazli, USSR	1976	Karakyr	6.8	12.8	0.64
12	1048	Northridge-01	1994	Northridge - Saticoy	6.7	3.4	0.41
13	1176	Kocaeli, Turkey	1999	Yarimca	7.5	19.3	0.31
14	1504	Chi-Chi, Taiwan	1999	TCU067	7.6	28.7	0.41
15	1517	Chi-Chi, Taiwan	1999	TCU084	7.6	8.9	0.79
16	2114	Denali, USA	2002	TAPS Pump Station #10	7.9	7.0	0.32

Results from two ground motions suites were compared to evaluate their effect on the performance values. Figure 3-19 compares the two suites for a system with a natural period of 2.5 seconds and damping of 10% and a system with natural period of 3.5 seconds and damping of 20%. Both comparisons suggest that the analysis can be sensitive to the ground motion suite

chosen with P695 motions demonstrating the need for larger energy dissipation capacity of the gap damper system. Relative performance of the system was worse with the P695 motions with a higher performance index. Optimal EDL values obtained increased from 1.55 to 1.8 for the 2.5 second system and from 0.9 to 1.2 for the 3.5 second system. The results of this study indicate that the preliminary EDL values obtained may not be sufficient for the generation of EDLs to be used for a practical design procedure. Further analysis was necessary to determine the usefulness of the EDL values.

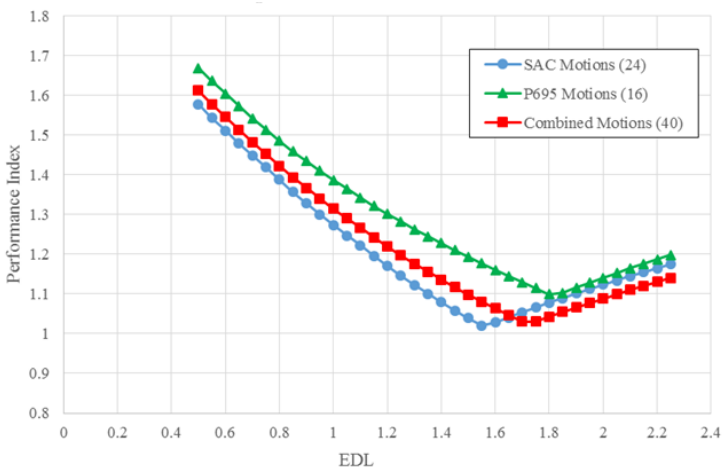

a) $T_N = 2.5$ seconds, Isolator damping = 10%

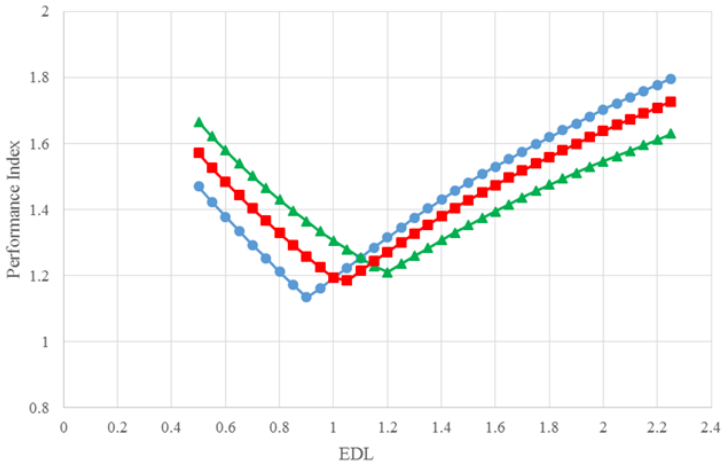

b) $T_N = 3.5$ seconds, Isolator damping = 20%

Figure 3-19. Ground Motion Suite Comparison

3.3.5.2 Superstructure Characteristics

Another potentially influential factor affecting the behavior of the 2-DOF system are the superstructure characteristics. For the parametric study, superstructure properties were held constant with a natural period of 0.5 seconds and a mass ratio M_1/M_2 of 1:4. In the spatial representation of the 2-DOF model, shown in Figure 3-20, the properties altered in the parametric study involved the base-isolation system and gap damper elements, all below the isolation level. Since the total mass ($M_1 + M_2$) remained the same throughout the study, the displacement performance was unlikely to vary with superstructure changes, and primary first mode behavior in the isolation system. However, the fundamental formulation of the acceleration performance index, involving a ratio of roof accelerations, would result in potential changes in EDL curves if the superstructure natural period and mass ratios were changed.

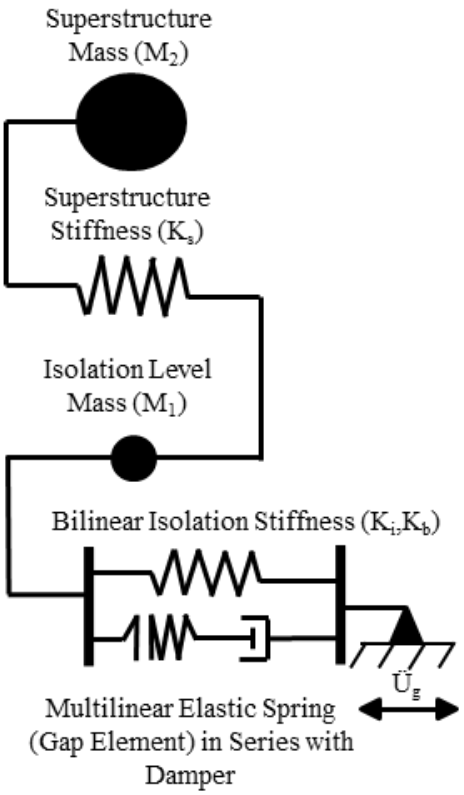

Figure 3-20. 2-DOF System

In order to demonstrate the potential variation in EDL curves due to superstructure variation, curves were developed for a system ($T_M = 2.36$ sec, $\xi_M = 20\%$) with a mass ratio (M_1:M_2) ranging from 1:1 to 1:5. Figure 3-21a compares the curves for the varying mass ratios while maintaining the same superstructure natural period. The displacement controlled portion of the curve remains unchanged but the acceleration controlled curve significantly changes the location of the intersection of the two lines. The acceleration performance index is a ratio of the roof acceleration with the gap damper to system to three times the median design level acceleration. As the mass of the roof increases, the design level acceleration also increases, potentially decreasing the ratio. Note that that the 1:1 mass ratio system had lower values for the performance index than the other ratios.

Another comparison, made in Figure 3-21b, evaluates the same isolated systems and mass ratios but adjusts the natural period of the superstructure. Assuming mass ratios of 1:1 to 1:5 roughly correlate with one to five-story structures, approximate natural periods were found using Section 12.8.2.1 of *ASCE/SEI 7-10* assuming a regularly constructed steel braced frame (ASCE/SEI, 2010). Once again, the displacement portion of the EDL curve is relatively consistent regardless of the superstructure characteristics. The acceleration controlled portion of the curve showed an opposite trend of the previous comparison, with the 1:1 ratio system now exhibiting the highest performance index. When a more representative natural period is associated with the superstructure, the gap damper superstructure acceleration largely increases, increasing the ratio associated with the acceleration performance index. The results of these two comparisons suggest that the superstructure characteristics are an important consideration in the generation of EDL values for design if accelerations are a concern.

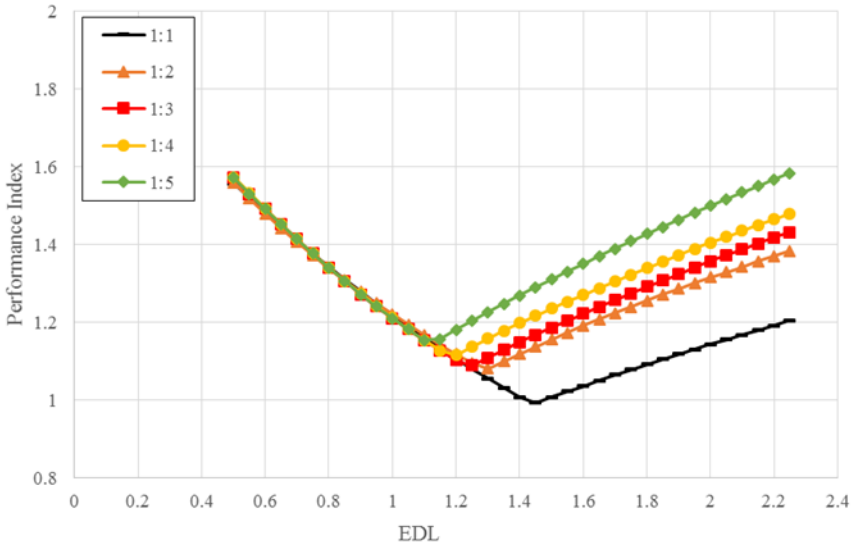

a) Same superstructure natural period (0.5 seconds)

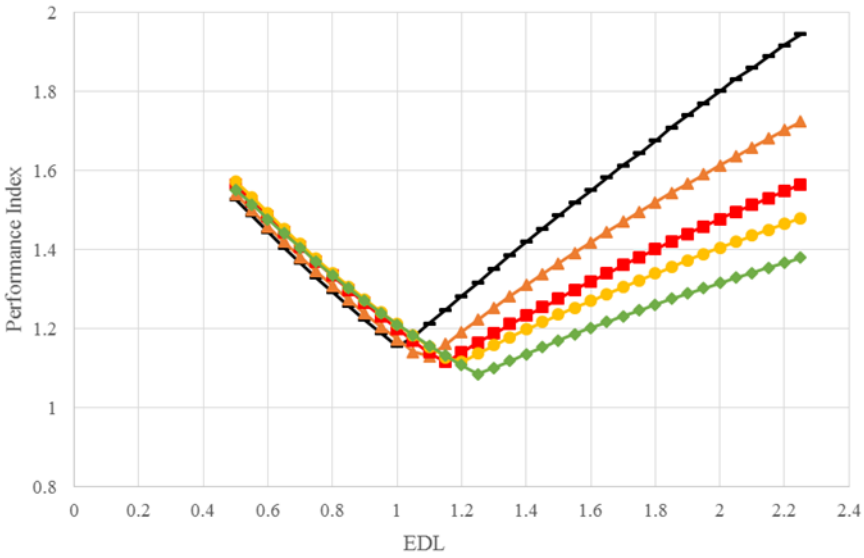

b) Adjusted superstructure natural period

Figure 3-21. Mass Ratio Comparison

3.3.5.3 Target Displacement Reduction

An important variable that was consistent across the initial EDL parametric study was the target displacement reduction of 25%. The preliminary constraints of the study required a reduction from a displacement demand of $1.375*D_{MCE}$ to $1.1*D_{MCE}$. The 25% reduction may not be desirable if

the designer has different objectives for the system. For this reason, differing displacement reduction objectives were compared for the same isolation system ($T_M = 2.36$ sec, $\xi_M = 20\%$). All ground motions were scaled to the target displacement associated with the reduction objective. Results of the study, shown in Figure 3-22, suggest that the target displacement reduction has a large influence on EDL curves. The larger the displacement reduction required, the larger the performance index, suggesting worse overall performance. This indicates that the displacement reduction objectives should be considered in the development of EDL design values.

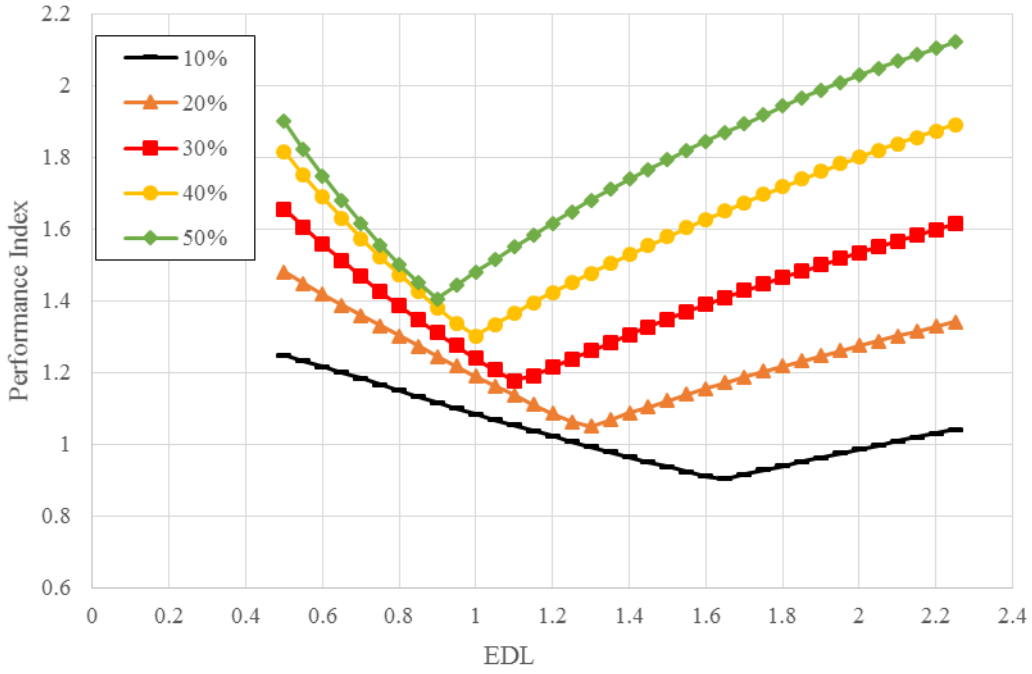

Figure 3-22. Target Displacement Reduction

3.3.5.4 Multi-Degree of Freedom Study

Another limitation of the preliminary study was that the superstructure was modeled as a single-degree-of-freedom (SDOF) system. With base-isolator behavior primarily occurring in the first mode for a one-dimensional system, a SDOF approximation is normally sufficient. The addition of the gap damper system adds complexity to the system with the activation of supplemental

energy dissipation at the base of the structure, potentially exciting other modes of vibration that would be unable to be captured with a SDOF superstructure. With the potential for higher mode behavior, a multi-degree-of-freedom study was also conducted to evaluate the effect on EDL curves. Although the analysis was completed with zero-length elements, the spatial representation of the system is presented in Figure 3-23, with masses added for each story. The total mass remained the same with mass evenly distributed between floors. The stiffness was modified between the floors to ensure that natural periods matched the approximate periods from Section 12.8.2.1 of *ASCE/SEI 7-10*. Although this is not an equivalent representation of the SDOF system, this is a more accurate representation of a multi-story structure.

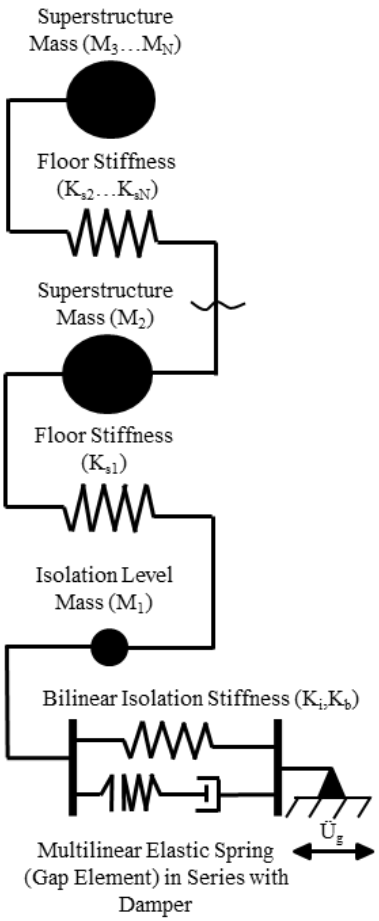

Figure 3-23. MDOF Model

Figure 3-24 compares EDL curves between the SDOF and MDOF superstructures for two to five story structures with the same isolation system (T_M = 2.36 sec, ξ_M = 20%). The MDOF superstructure utilized accelerations at the roof level for the calculation of the acceleration performance index. The SDOF and MDOF system curves differ greatly due to the fundamental formulation of the acceleration performance index. The displacement controlled portion of the curve is similar for both systems while the acceleration controlled curve governs the selection of the minimum EDL.

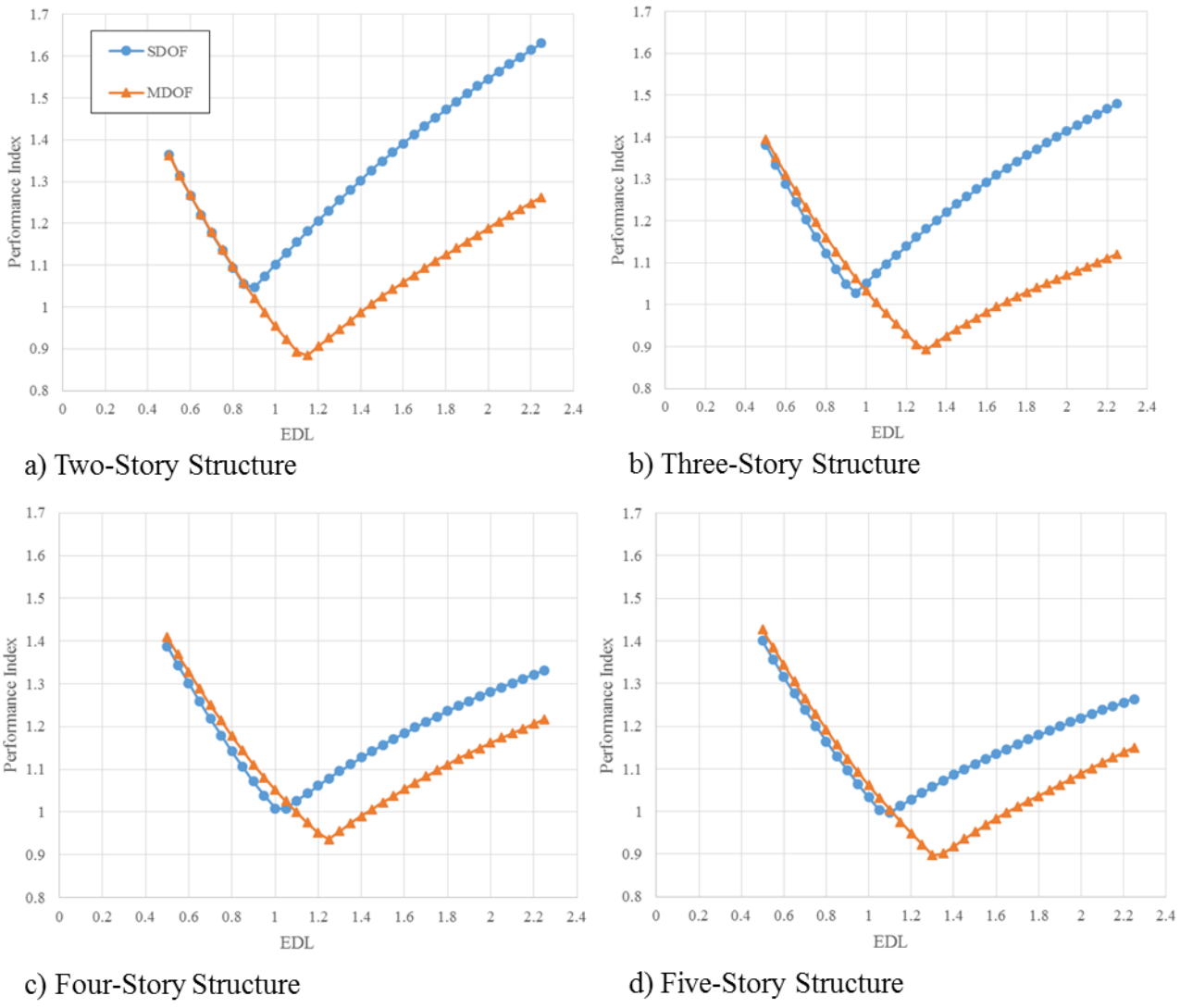

Figure 3-24. SDOF vs MDOF Comparison

EDL curves were also generated for each floor of the MDOF structure, as shown in Figure 3-25. Design level accelerations without the gap damper system are highest on the base and roof levels. The acceleration performance index, defined as the gap damper acceleration divided by three times the design level acceleration, would inherently be lower at the roof level, due to the larger design level accelerations in the denominator. For the base level, high frequency acceleration spikes exist at the activation of the gap damper system, explaining the large performance index values at the base level. Although the EDL curves suggest that the best performance is present at the roof level, this is not necessarily accurate, given the formulation of the acceleration performance index.

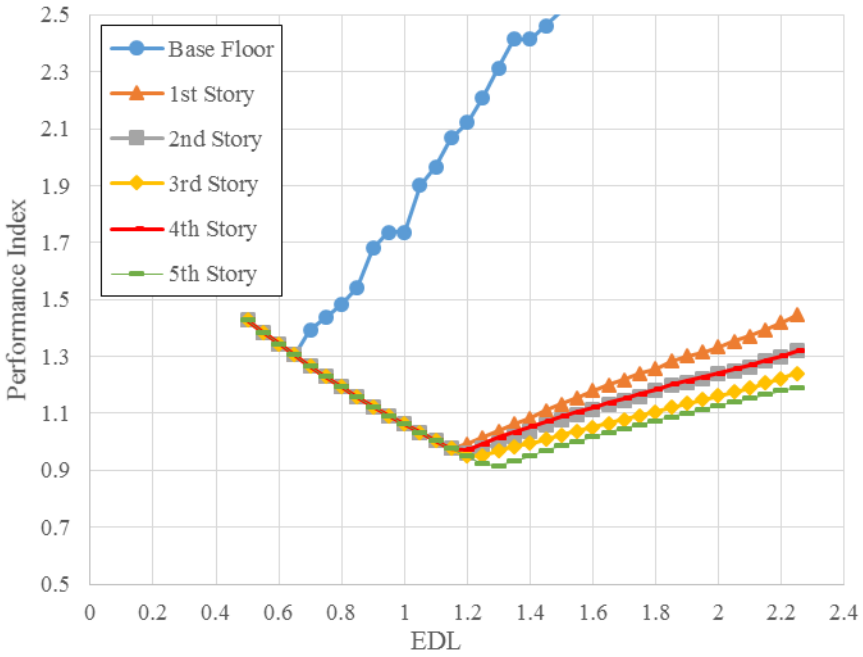

Figure 3-25. EDL Curve Floor Comparison

An additional comparison was made to evaluate the optimum EDL values for the SDOF and MDOF superstructures. For this analysis, the 24 SAC motions and 16 FEMA P695 ground motions were combined to create a larger suite of 40 ground motions. EDL curves were generated for the SDOF and MDOF superstructures for 16 different isolation systems with natural periods

of 2.5 seconds to 4.0 seconds and isolator damping of 10% to 25% of critical damping. Since the primary goal of the gap damper system is the reduction of displacement, EDLs for the percentage of the 40 ground motions for which the model failed to meet the displacement reduction criteria, resulting in an impact with the moat wall, were also shown. EDLs for systems exhibiting impacts are plotted in Figure 3-26 with the solid and dotted lines. As expected, higher EDL values results in a decrease in moat wall impacts. The values chosen for the design EDLs would be at the lowest point of the EDL curves. These potential design values were compared to the impact percentage at that EDL level in order to identify potential trends. Figure 3-26 demonstrates this comparison for an isolation natural period of 3.5 seconds.

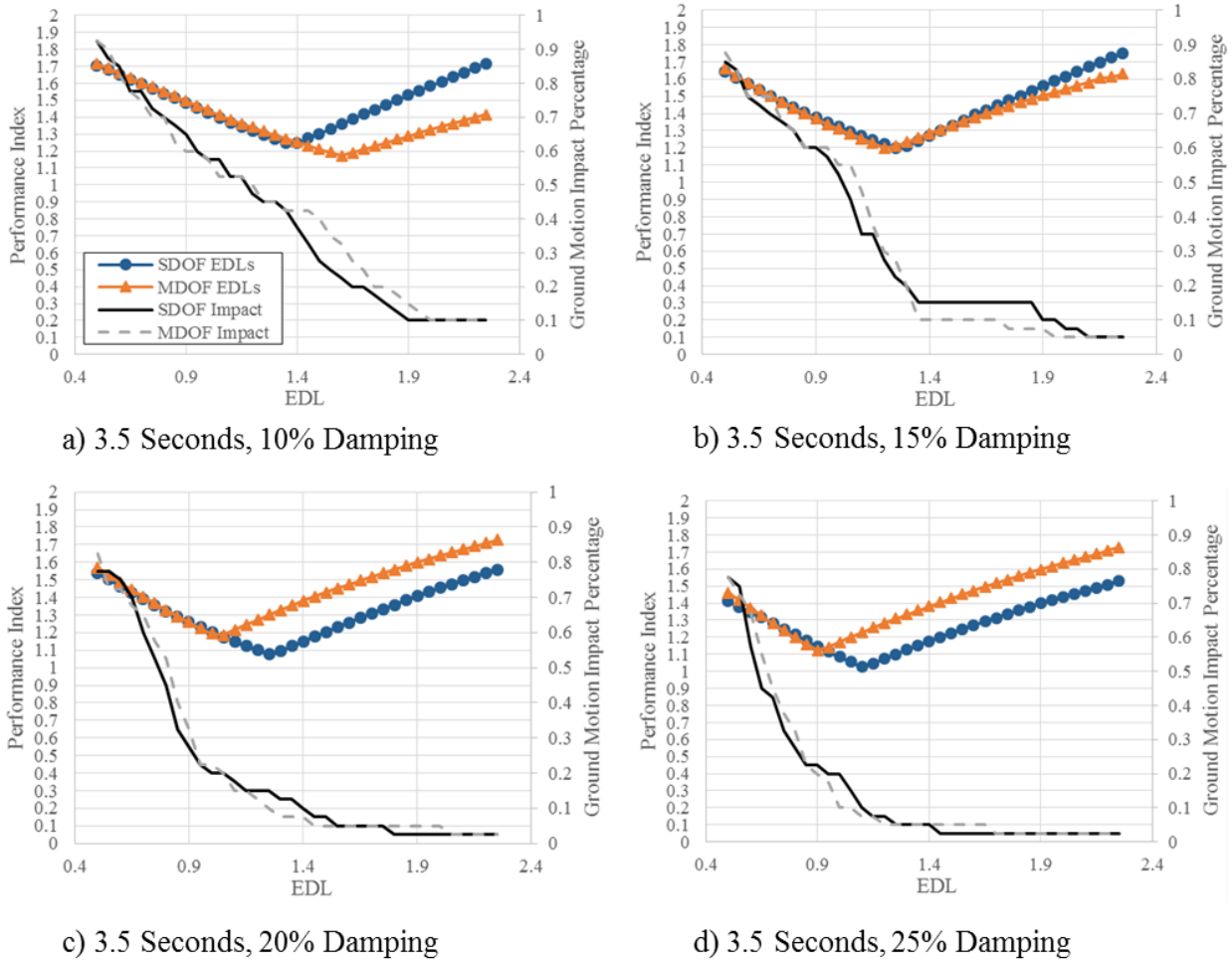

Figure 3-26. EDL Curves and Impact Percentages for 3.5 Second Isolation Period

A summary of this comparison is found in Table 3-4, which associates the design EDL values with the displacement failure rate of the 40 ground motions. Generally speaking, the displacement failure rate increases as the natural period increases. The design EDL also decreases as more damping is added to the system. Beyond these two trends, no clear relationships are evident and the design EDLs do not suggest successful gap damper performance. The acceleration performance index adds complexity to the analysis, resulting in inconsistent performance and difficulties achieving the critical gap damper objective of eliminating moat wall impact.

Table 3-4. Comparison of SDOF and MDOF Superstructure EDLs

Isolation System (Period, Damping)	SDOF Superstructure		MDOF Superstructure	
	Design EDL	Displacement Failure	Design EDL	Displacement Failure
2.5 s, 10%	1.70	22.5%	1.55	30%
2.5 s, 15%	1.30	25%	1.35	27.5%
2.5 s, 20%	1.05	22.5%	1.25	10%
2.5 s, 25%	0.95	10%	1.15	2.5%
3.0 s, 10%	1.65	15%	1.50	32.5%
3.0 s, 15%	1.20	22.5%	1.30	22.5%
3.0 s, 20%	1.00	15%	1.15	15%
3.0 s, 25%	0.90	10%	1.10	10%
3.5 s, 10%	1.60	32.5%	1.40	37.5%
3.5 s, 15%	1.20	30%	1.25	22.5%
3.5 s, 20%	1.05	20%	1.25	15%
3.5 s, 25%	0.90	20%	1.10	10%
4.0 s, 10%	1.75	40%	1.55	52.5%
4.0 s, 15%	1.20	42.5%	1.25	37.5%
4.0 s, 20%	0.95	45%	1.10	22.5%
4.0 s, 25%	0.80	37.5%	1.10	17.5%

3.3.5.5 Suggested EDL Values

Results described in this section clearly demonstrate the potential variability in EDL curves with varying system parameters. Variability was primarily due to the acceleration performance index, which mixes design level accelerations (without a gap damper) and beyond-MCE-level accelerations with a gap damper system. The consequences of this variability could make for a cumbersome EDL selection process when accounting for all structural properties, isolation properties, and design objectives. Rather than over-constraining the design process, elimination of the acceleration performance metric significantly simplifies the selection of the EDLs for design. Since the primary goal of the gap damper system is the reduction of isolation level displacements, the acceleration can be viewed as a "consequential" variable associated with the displacement reduction. The design procedure described in Chapter 6 will address this issue further.

Rather than selecting a design EDL by using the intersection of the displacement sensitive portion of the EDL curve and acceleration-sensitive portion of the EDL curve, a simplified approach was developed in which the EDL values associated with a performance index of 1 on the displacement curve were used for design EDLs. Since the displacement performance index is a function of the mean plus one standard deviation displacement values, this suggests a gap damper displacement success rate of 84%. A sample size of 40 ground motions from the previous analysis introduces an adequate range in ground motions for the calculation of the design EDL values. Design EDL values were generated for 16 isolation systems with natural periods ranging from 2.5 seconds to 4.0 seconds and isolator damping values of 10% to 25% of critical damping for the SDOF superstructure system. In addition, since it was determined that the target displacement reduction may play a role in EDL values, design values were determined for 10%, 20%, 30%, and 40% reductions in displacement. A summary of the design values is found in Figure 3-27, and the range of values is shown in Figure 3-28. Generally, as the displacement reduction requirement

increased, the EDLs increased slightly. The results of this study will be revisited in Chapter 6, which involves the development of practical design guidelines for a gap damper system.

Isolated Natural Period	Isolator Damping 10%	15%	20%	25%
2.5	1.5	1.1	0.8	0.7
3	1.5	1.3	1	0.8
3.5	1.8	1.4	1.1	0.9
4	2.7	1.5	1.1	0.9

a) 10% Displacement Reduction Requirement

Isolated Natural Period	Isolator Damping 10%	15%	20%	25%
2.5	1.7	1.3	1	0.9
3	1.8	1.4	1.1	0.9
3.5	2	1.6	1.3	1
4	2.9	1.8	1.4	1.1

b) 20% Displacement Reduction Requirement

Isolated Natural Period	Isolator Damping 10%	15%	20%	25%
2.5	1.8	1.3	1.1	0.8
3	1.9	1.4	1.2	0.9
3.5	2.2	1.7	1.4	1.1
4	2.9	2	1.5	1.1

c) 30% Displacement Reduction Requirement

Isolated Natural Period	Isolator Damping 10%	15%	20%	25%
2.5	1.8	1.4	1.1	0.9
3	2	1.5	1.2	0.9
3.5	2.2	1.7	1.4	1.1
4	2.9	2	1.5	1.2

d) 40% Displacement Reduction Requirement

Figure 3-27. Design EDL Values

Isolated Natural Period	Isolator Damping 10%	15%	20%	25%
2.5	1.5-1.8	1.1-1.4	0.8-1.1	0.7-0.9
3	1.5-2.0	1.3-1.5	1.0-1.2	0.8-0.9
3.5	1.8-2.2	1.4-1.7	1.1-1.4	0.9-1.1
4	2.7-2.9	1.5-2.0	1.1-1.5	0.9-1.2

Figure 3-28. Design EDL Range

3.3.6 Parametric Study Conclusions

The purpose of this section was to introduce the parametric study. Details of the model, ground motions, the calibration of gap damper properties, and the development of performance metrics were all presented. Overall, the parametric study was successful at identifying some of the better-performing systems and results suggested that the viscous device and two-phase viscoplastic device offer the best overall performance. Devices involving hysteretic elements at the onset of supplemental damping were often unable to meet acceleration criteria. General trends were noticed for the systems, including better performance as the natural period of the isolation system decreases and damping in the isolation system increases.

In addition to the parametric study, a detailed evaluation of the sensitivity of the SDOF model was presented. Differing ground motion parameters and superstructure properties were modeled to determine their effect on the selection of the EDLs for design. The results of the study indicated that elimination of the acceleration performance index in choosing a design EDL was necessary to ensure a consistent performance that would achieve the desired displacement reduction. Using the recommendations from the parametric study, the next step in the development of the gap damper device was to develop a practical implementation of the theoretical systems.

3.4 Conclusions

This chapter introduced the gap damper concept and demonstrated the possibilities available for a gap damper system. A large parametric study compared various systems and identified the better performing systems using a performance index that was developed to compare systems based on both isolation level displacement and superstructure accelerations. The results of the study indicated that the viscous device and two-phase viscoplastic device provided the best overall performance and would be suitable for practical implementation.

Chapter 4. Experimental Evaluation of a Gap Damper System

4.1 Introduction

Chapter 3 introduced the concept of a gap damper device to mitigate displacements in extreme earthquakes. Using the results of the parametric study, Chapter 4 introduces the practical development of the device, design, and fabrication of a viscous and two-stage viscoplastic device for experimental evaluation in Auburn University's Structural Research Laboratory. Multiple gap damper arrangements are presented with a qualitative analysis of the design options. A final design is chosen that meets the desired performance objectives of the system for development into a prototype system. This chapter provides details on the development of the prototype with experimental results. The specifics in the design of the device are outlined with design details and a finite element study developed to assess the complex behavior of the impacting elements. In addition, the chapter covers the testing details for the device including the device qualification, experimental setup, instrumentation, and load cases. A comprehensive analysis of the data is included in order to assess the feasibility and reliability of a gap damper system for use in a shake table test. Recommendations are made based on the results of the study. Details of this study are outlined in three publications, *"Design and testing of a gap damper device to mitigate rare earthquake pounding response in base-isolated buildings"* (Rawlinson T. , Marshall, Ryan, & Zargar, 2014), "*Development and experimental evaluation of a passive gap damper device to prevent pounding in base-isolated structures"* (Rawlinson T. , Marshall, Ryan, & Zargar, 2015),

and "*Exploring the gap damper concept to control seismic isolation displacement demands"* (Zargar, Ryan, Rawlinson, & Marshall, 2012)

4.2 Practical Implementation

Using the results of the parametric study, the next step was in the development of a practical gap damper device for implementation in an experimental setting. The device development process was a progression of ideas, incorporating industry advice and practical experience. The two prototype systems are based on the viscous gap damper system and the two-phase viscoplastic device. The following section details the design performance objectives and a qualitative assessment of the gap damper options.

4.2.1 Performance Objectives

Once the most effective method of energy dissipation was established in the parametric study, the next step is to implement a practical design that can capture the desired gap damper behavior in addition to meeting other practical performance objectives. The device demanded simplicity, feasibility, economy, and reliability to be an effective option in building design and construction. It was important to define these objectives prior to the development of the device so that a meaningful comparison between design options could be made.

Bi-directional behavior is a very important aspect of the development. The gap damper device should respond reliably in each horizontal direction, regardless of the ground motion direction to ensure protection from the collision with the surrounding wall. This requirement provides the most difficult obstacle to this project as it is challenging to configure a series of gap elements to engage the damping phase bi-directionally. Beyond bi-directional behavior, another key issue with the device is reliability. The system is the last line of defense against extreme

ground motions before a detrimental collision with the surrounding moat wall; therefore reliable and predictable performance is crucial to the success of this system. Regardless of the ground motion type or direction, the gap damper system must provide reliable and repeatable behavior throughout the duration of the event. The device must also be simple and practical for construction in order to minimize mistakes in the field implementation and be economically advantageous. Lastly, to minimize the cost of the system, all energy dissipation devices should engage in both forward and reversing directions. Since the energy dissipation devices are the most expensive elements of the system, each damper should be configured to provide as much energy dissipation as possible.

4.2.2 Design Concepts

Using the criteria developed in the previous section, a series of options were considered and qualitatively evaluated for use in the gap damper system. Sketches of a few options were created to visualize the systems in a three-dimensional manner and detect possible weaknesses (Figure 4-1). Although drawn with viscous dampers as the energy dissipation source, the options could be modified to include a plastic device for the two-phase viscoplastic system. All of these devices are located between the base level and the basement, across the isolation interface with attachment to the fixed foundation or moat wall. The over-arching concept involves the attachment of a mechanism to the isolated floor that activates secondary energy dissipation when the relative displacement across the isolation interface reaches a specified magnitude. Potential placement of the devices would be at the perimeter of the building (Figure 4-1b) or in the center of the building (Figure 4-1a, Figure 4-1c, and Figure 4-1d). Although the dampers inherently require minimal maintenance, the inspection of the device may be easier to access in a perimeter device or more efficient if the device is limited to a central location in the middle, depending on the isolation

access. The protruding element at the top of each figure is attached to the base isolated slab of a building while the concrete pedestals or moat wall supporting the gap damper device are attached to the ground. When the relative displacement between the isolated slab and the ground reaches the desired activation displacement, the dampers will dissipate energy and effectively limit base displacements and mitigate moat wall collisions.

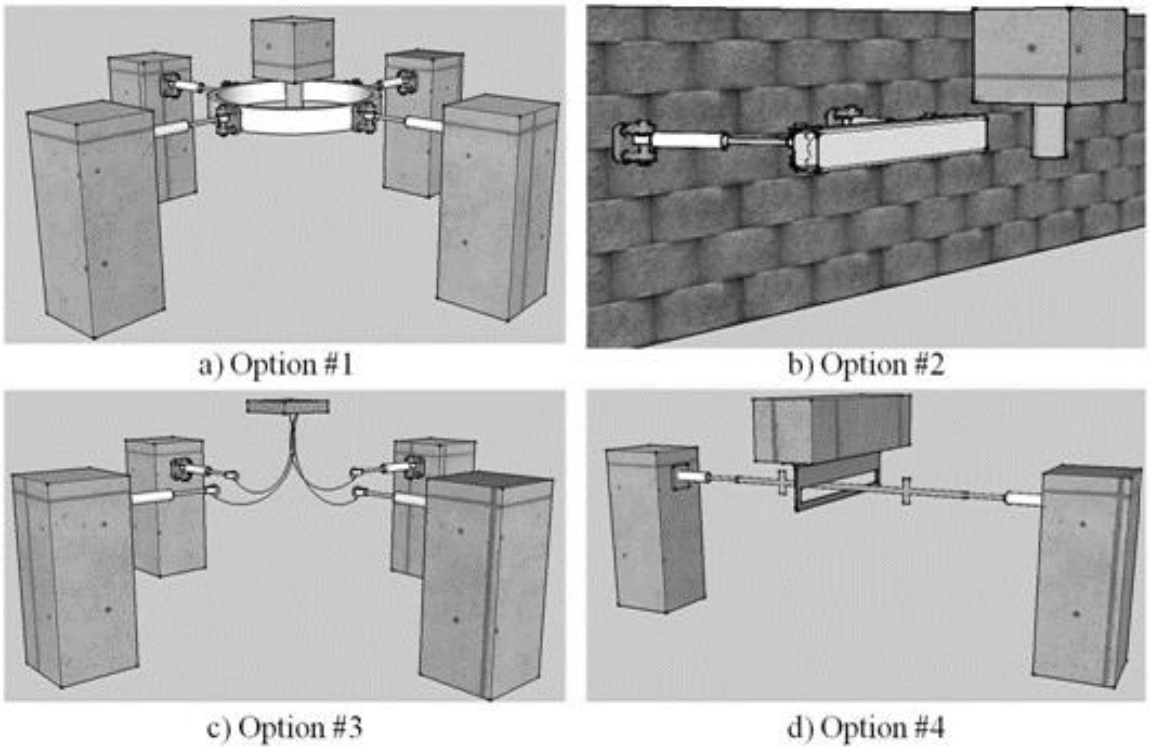

Figure 4-1. Potential Gap Damper Configurations

Option #1 presents a system that relies on a bumper system placed at the desired gap threshold. The protruding tube activates the dampers as the isolated floor approaches the threshold displacement. The benefit of this system is in the ease of energy dissipation activation and fully functional bi-directionality as the system behaves the same regardless of the ground motion direction. Another advantage of the system is the ability to utilize the dampers in both tension and compression, lowering the overall cost and imprint of the system. As one damper is activated in compression, the damper on the opposite side is activated in tension, meaning not only a more

efficient system, but also that the dampers have the ability to dissipate more energy as the base-isolated system reverses and impacts the system in the opposite direction. Option #2 is a simple system that activates supplemental energy around the perimeter of the structure, with dampers attached to the moat wall. Although simple to implement, the system only works in compression; which without re-centering capabilities means the device would only be active for one full impact. Although functional in both directions, one device does not achieve bi-directional functionality and an identical device is required on the transverse moat wall. Option #3 is similar to Option #1 but differs in that the dampers are not activated through impact with a bumper but rather through tension of the wires as the slack is tightened. Although achieving the bi-directionality objective, the dampers are only active in tension and do not have the ability to re-center. Option #4 provides an interesting alternative that utilizes the dampers in tension and compression but requires a larger overall footprint as an identical device would have to be placed in the transverse direction elsewhere in the building to achieve bi-directional functionality. In addition, large friction forces would develop between the activating pegs and slot that would adversely affect the viscous dampers which are restrained from rotation.

Option #1 provided the best opportunity to achieve the desired goals of a gap damper system, and thus was further developed. This design allows one or more gap damper arrangements to be located anywhere under the building, utilizing the dampers in both tension and compression for maximum energy dissipation. Figure 4-2 shows the overall concept of the system with a building layout and detailed drawing of the gap damper system. The system was adapted to include a square bumper system rather than a circular bumper system to prevent early activation of the gap damper system in the event of diagonal movement. In addition, placement of the dampers at the corners of the bumper system provides resistance to rotation due to eccentric impacts. Rather than

suspending the system in the air, the manufacturer of the viscous dampers (Taylor Devices Inc.) suggested they would be more effective if the bumper was allowed to slide on the ground (Personal Communication, June 1st, 2012). The system could be adapted to include a plastic device as well, as detailed in the following chapter.

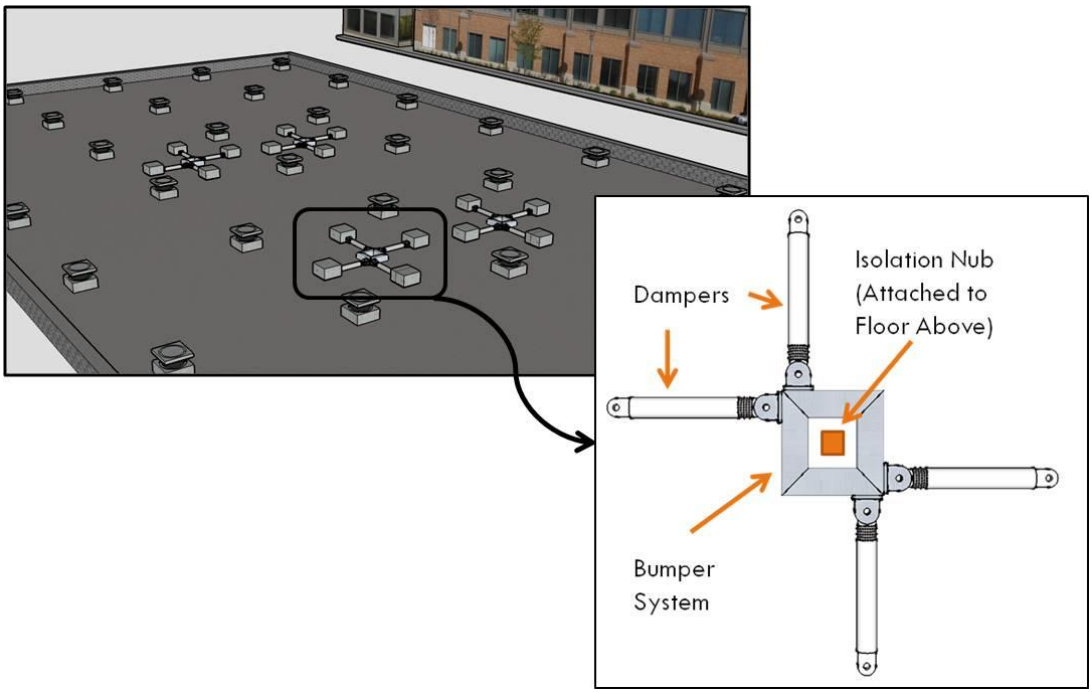

Figure 4-2. Final Design Concept with Gap Damper Detail

4.3 Gap Damper Design Details

The previous chapter introduced some the mathematical basis for the gap damper system, introducing concepts such as the Equivalent Dissipation Level (EDL) and the Performance Index (PI). This section details a prototype gap damper system in the context of the development of an experimental system used for testing at Auburn University and later at UNR's shake table facility.

4.2.1 Test Structure Parameters

The prototypes for the AU testing were designed in correlation with the UNR shake table testing. Seismic hazard, base-isolators, and superstructure details were chosen prior to the design of the

gap damper prototype to ensure the same prototype could be used for both experiments. Isolators chosen for the research were characterized using hysteretic data and a process developed by Ryan, Coria, & Dao (2013) to find isolator stiffness (K_d) and characteristic strength (Q_d). Hysteretic characterization of the isolator is shown in Figure 4-3 with K_d equal to 0.177 kN/mm (1.01 kip/in) and Q_d equal to 8.63 kN (1.94 kip).

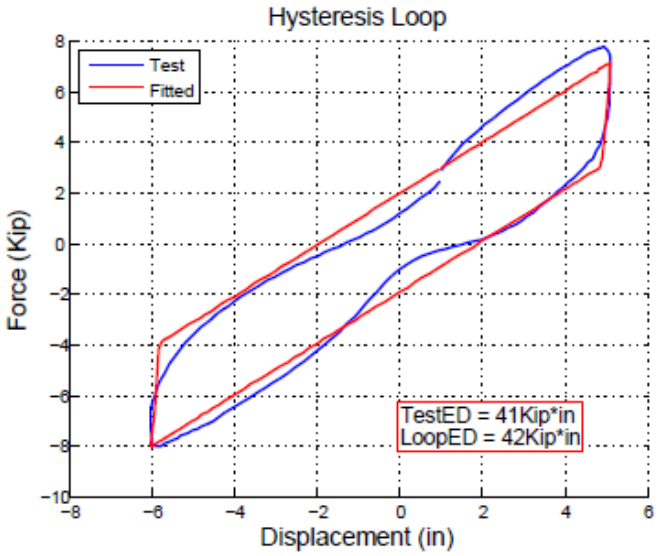

Figure 4-3. Characterization of Isolator Behavior

The three-story base-isolated superstructure was designed at 1/4-scale length, 1/2-scale time, 1/1-scale acceleration and is to remain elastic throughout the testing. The superstructure was designed at UNR and fabricated for the shake table testing at UNR's Network for Earthquake Engineering Simulation (NEES) facility. A moment frame is used in one direction for the ease of placement of the supplementary mass while a braced frame is used in the transverse direction providing a stiffer superstructure in that direction. The completed superstructure with supplementary mass is shown in Figure 4-4.

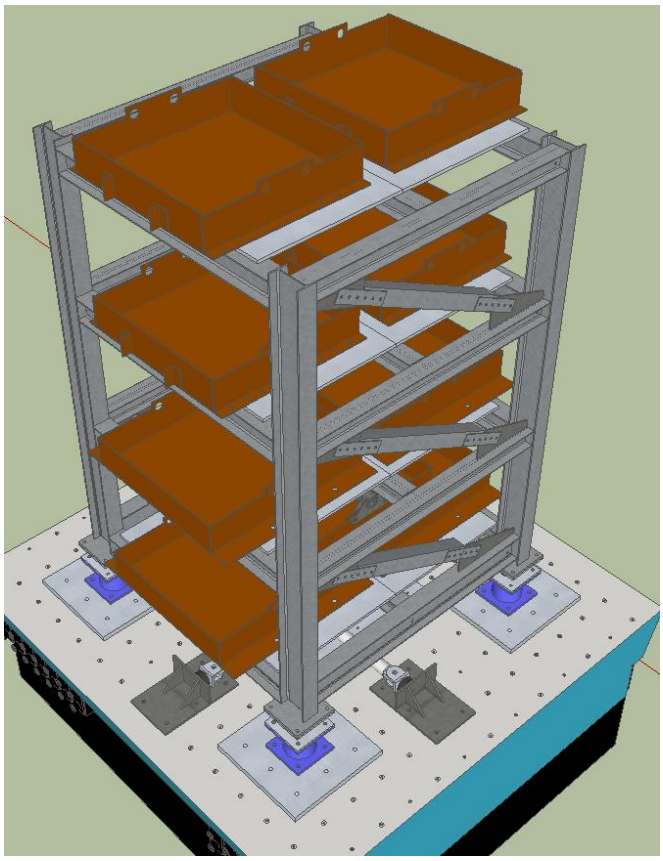

Figure 4-4. UNR Superstructure

The four rubber isolators provide a scaled natural period of 1.18 seconds when carrying 36.29 tonnes (80 kips), including superstructure self-weight and additional supplementary mass. With a S_{M1} value of 1.11g chosen for a seismic hazard, the maximum considered earthquake displacement (D_{MCE}) demand is 0.426 m (16.8 in) or 0.106 m (4.2 in) scaled. Given the mass and isolator properties, the isolators are estimated to provide 20.0% of critical damping for the test structure designed. These values were found by using the nomenclature shown in Figure 4-5 and solving five simultaneous equations shown below.

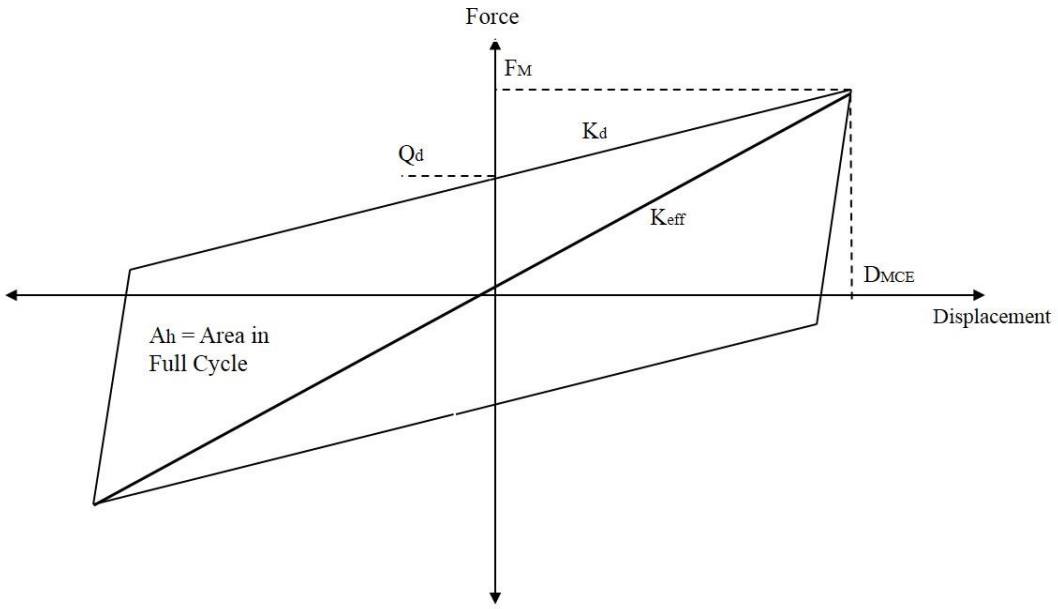

Figure 4-5. Isolator Hysteresis

The ultimate strength (F_M) at the MCE displacement (D_{MCE}) can be defined as:

$$\mathbf{F_M = Q_d + K_d D_{MCE}} \qquad \textbf{Equation (4-1)}$$

Where Q_d is the characteristic strength found in the line fit of hysteretic data and D_{MCE} is found using Equation 4-2:

$$\mathbf{D_{MCE} = \frac{S_{M1}\left(2\pi\sqrt{\frac{M}{N\left(\frac{F_M}{D_{MCE}}\right)}}\right)}{4\pi^2 B_D}} \qquad \textbf{Equation (4-2)}$$

Where S_{M1} is the 1-second spectral acceleration, M is the mass of the superstructure, N is the number of isolators, and B_D is the isolator damping factor defined by Equation 4-3:

$$\mathbf{B_D = \frac{1.65}{2.31 - 0.41\ln(\zeta * 100)}} \qquad \textbf{Equation (4-3)}$$

Where ζ is the damping ratio defined in Equation 4-4:

$$\mathbf{\zeta = \frac{1}{2\pi}\left(\frac{A_h}{\frac{F_M}{D_{MCE}} D_{MCE}^2}\right)} \qquad \textbf{Equation (4-4)}$$

Where A_h is the area enclosed in the hysteresis, defined as:

$$\mathbf{A_h = 4Q_d\left(D_{MCE} - D_y\right)} \qquad \textbf{Equation (4-5)}$$

Where D_y is the yield displacement of the lead plug, assumed as 2.54 mm (0.1 inch). Using the five relationships defined above, appropriate similitude requirements, and solving the equations simultaneously, the isolator damping capacity, MCE displacement, and effective stiffness (K_{eff}) can be found. With the given K_{eff} and mass of the superstructure, the isolated natural period of the structure is 2.36 seconds (1.18 seconds scaled). The parameters of the isolator and superstructure are summarized in Table 4-1. The threshold displacement in which the gap damper system is activated is 0.6*D_{MCE} or 0.064 m (2.5 in).

Table 4-1. Isolator and Superstructure Parameters

Isolator Properties					
Number of Isolators	Diameter (Circular)	Lead Plug Diameter	Damping @ D_{MCE}	Isolator Stiffness (K_d)	Characteristic Strength (Q_d)
4	190.5 mm (7.5 in)	31.75 mm (1.25 in)	20%	0.177 kN/mm (1.01 kip/in)	8.63 kN (1.94 kip)
Building Details					
Scaling	Spectral Acc. (S_{M1})	Weight	Natural Period (Scaled)	D_{MCE} (Scaled)	Threshold Disp. (Scaled)
¼ Length ½ Time $^1/_1$ Acceleration	1.11g	36.29 tonnes (80 kips)	1.18 seconds	0.106 m (4.2 in)	0.064 m (2.5 in)

4.2.2 Viscous Gap Damper Parameters

Reintroducing concepts introduced in Chapter 3, the parameters can be developed for a prototype viscous gap damper system. The equal energy concept that is the theoretical basis of the viscous gap damper system is shown in Figure 4-6 within the context of the prototype parameters.

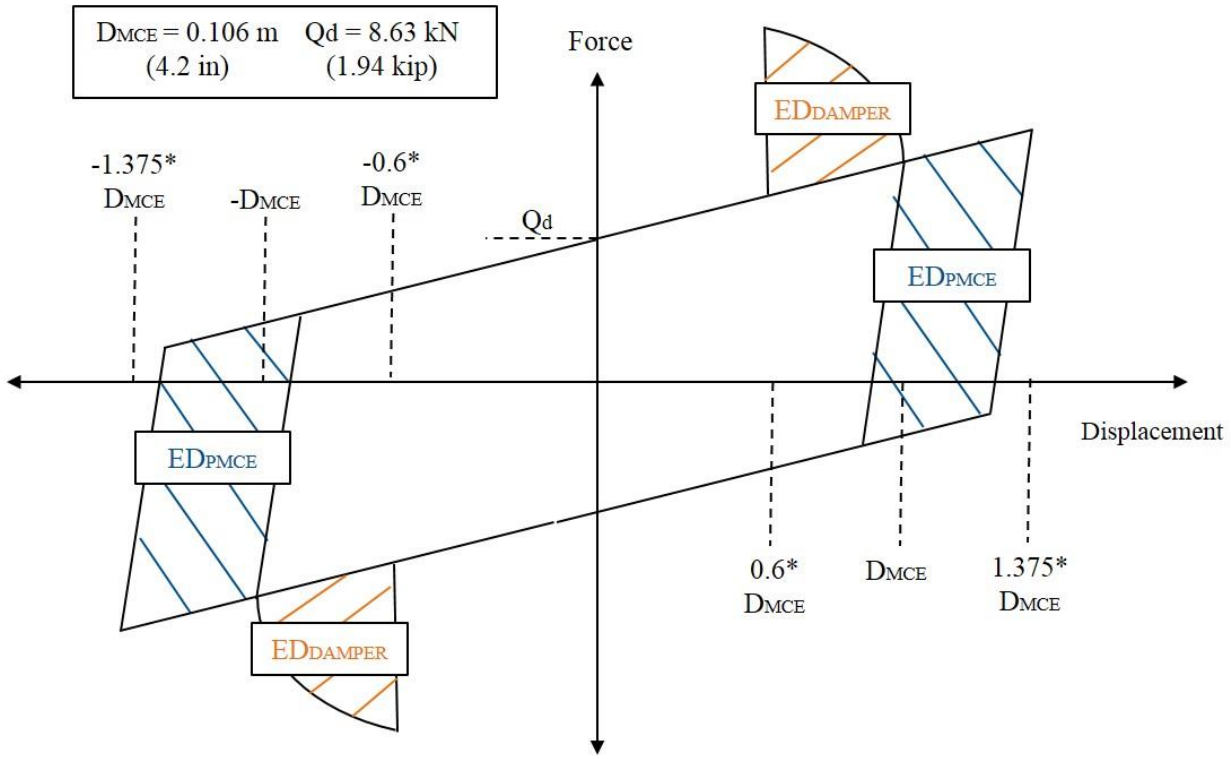

Figure 4-6. Viscous Gap Damper Idealization

The amount of energy dissipated by the gap damper is a function of the energy present in a full isolator cycle from the MCE displacement to the overgap requirement of 1.375*D_{MCE}. Within the context of the prototype system using the system properties from Table 4-1, this energy (ED_{PMCE}), is calculated using Equation 4-6. The energy (ED_{PMCE}) in one full cycle for the 4 isolators (N_{iso}) used in the isolation of the superstructure is 5.489 kN*m (48.888 kip*in).

$$\mathbf{ED_{PMCE} = N_{iso} 1.5 Q_d D_{MCE} = 4(1.5)(8.63)(0.106) = 5.489\ kN * m} \qquad \textbf{Equation (4-6)}$$

Calculating the energy requirement from the gap damper system is a function of the equivalent dissipation level (EDL). Figure 4-7 shows the EDL curves calibrated for the properties of the shake table specimen. The shake table experiment design was completed prior to the sensitivity analysis of the EDL curves, which is the reason for the inclusion of the acceleration performance index. The results of the study indicate that the EDL for the viscous gap damper system should be 0.8 while the EDL for the two-phase viscoplastic device is 1.0.

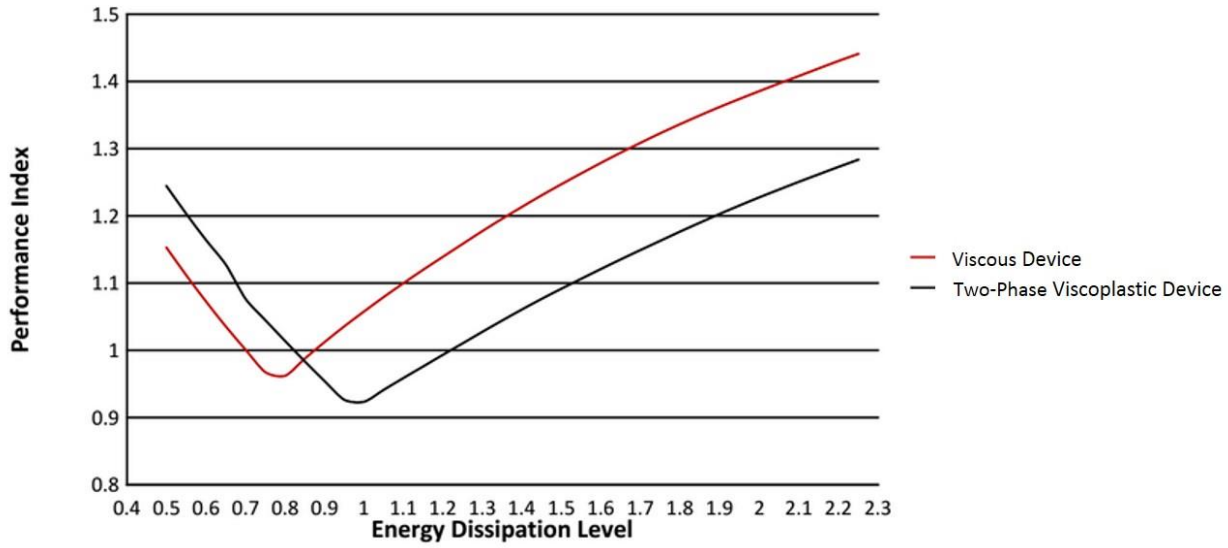

Figure 4-7. EDL Curves Used for Design

Using the EDL value for the viscous gap damper, the amount of energy dissipation required for the viscous dampers can be calculated using Equation 4-7. The amount of energy dissipation required from the dampers is 4.391 kN*m (39.11 kip*in).

$$\mathbf{ED_{DAMPER} = EDL * ED_{PMCE} = 0.8(5.489) = 4.391\ kN(m)} \qquad \textbf{Equation (4-7)}$$

The conceptual viscous gap damper system proposed in Figure 4-2 has two viscous dampers resisting motion in each direction. Activation of the viscous gap damper system would utilize one damper in compression and the opposite damper in tension. When the superstructure reverses direction, the dampers are no longer engaged until the threshold displacement is exceeded in the opposite direction. Although residual displacements would allow earlier activation in the opposite direction, the calibration of the parameters neglected the effect of residual displacements. Since there are two dampers in a given direction of travel, the amount of energy (ED_{DAMPER}) is halved for the calculation of the damping constant (c). As evident in Figure 4-6, the energy dissipation is present from both $0.6*D_{MCE}$ to $1.0*D_{MCE}$ and $-0.6*D_{MCE}$ to $-1.0*D_{MCE}$, indicating that the energy present in the damper equation formulation should be multiplied by a factor of 2. Assuming

harmonic motion at a resonant frequency, the energy dissipated by one damper in a viscous gap damper device in a full cycle from -1.0*D_{MCE} to 1.0*D_{MCE} is found in Equation 4-8. The damping constant is unknown while the natural frequency (w_n) is taken as 5.33 rad/sec and the damping coefficient (α) is equal to 1 when assuming a linear viscous damper.

$$\frac{ED_{DAMPER}}{2} = 2 * c * {w_n}^{\alpha} \int_{0.6D_{MCE}}^{D_{MCE}} \sqrt{({D_{MCE}}^2 - u^2)^{\alpha}}\, du \qquad \textbf{Equation (4-8)}$$

$$\frac{4.391}{2} = 2 * c * 5.333^{1.0} \int_{0.064}^{0.106} \sqrt{(0.106^2 - u^2)^{1.0}}\, du$$

Solving the equation for the damping constant yields 81.91 kN*s/m (0.465 kip*s/in). The damper in the gap damper system is active from 0.6*D_{MCE} to 1.0*D_{MCE} which requires 0.042 m (1.68 in) of stroke. Given a pseudovelocity of 0.565 m/s (22.4 in/s) and the damping constant, a reasonable approximation of the force demand in the dampers can be made using the damping equation. With the demands of the prototype system known, a consultation with Taylor Devices, Inc indicated that a seismic viscous damper with a force capacity of 244.6 kN (55 kip) with ± 76.2 mm (3 in) of stroke was the best option. The details of this damper are found in Figure 4-8. Further details of the viscous gap damper configuration are found in Section 4.2.5.

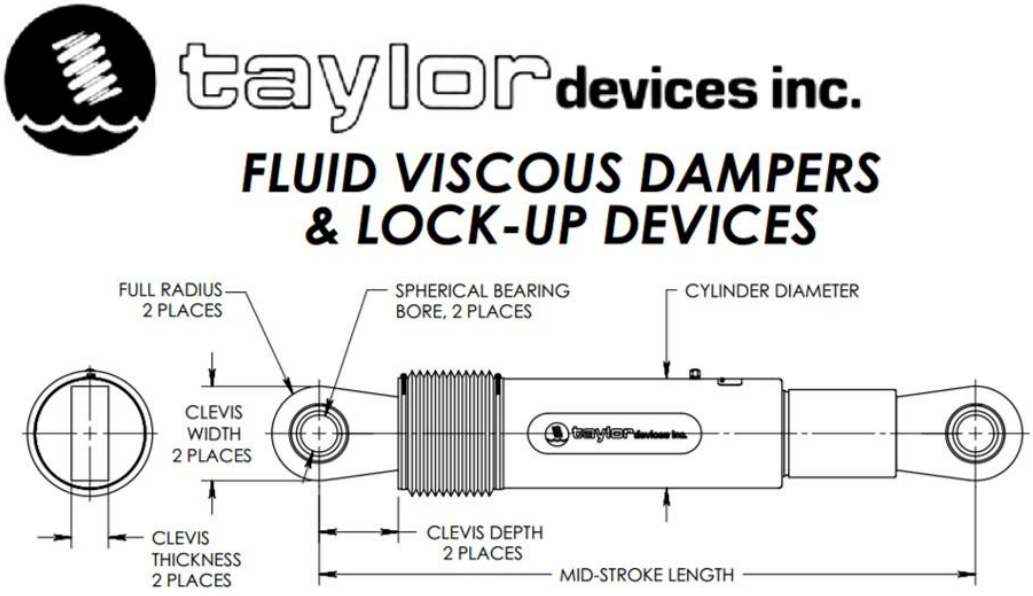

Force	Spherical Bearing Bore Diameter	Mid-Stroke Length	Stroke	Clevis Thickness	Clevis Width	Clevis Depth	Cylinder Diameter	Weight
244.6 kN (55 Kip)	38.1 mm (1.50 in)	866.8 mm (34.13 in)	±76.2 mm (±3.0 in)	41.3 mm (1.63 in)	101.6 mm (4.0 in)	82.6 mm (3.25 in)	114.3 mm (4.5 in)	40.82 kg (90 lbs)

Figure 4-8. Viscous Damper Selection (Taylor Devices Inc., 2012)

4.2.3 Two-Phase Viscoplastic Gap Damper Parameters

Using a similar precedure to the previous section, the parameters can also be developed for a prototype two-phase viscoplastic gap damper system. The equal energy concept that is the theoretical basis of the viscoplastic gap damper system is shown in Figure 4-9 within the context of the prototype parameters. The primary difference between the two prototype systems is the addition of friction device from $0.8*D_{MCE}$ to $1.0*D_{MCE}$, which accomplishes the desired second phase plastic behavior of the system.

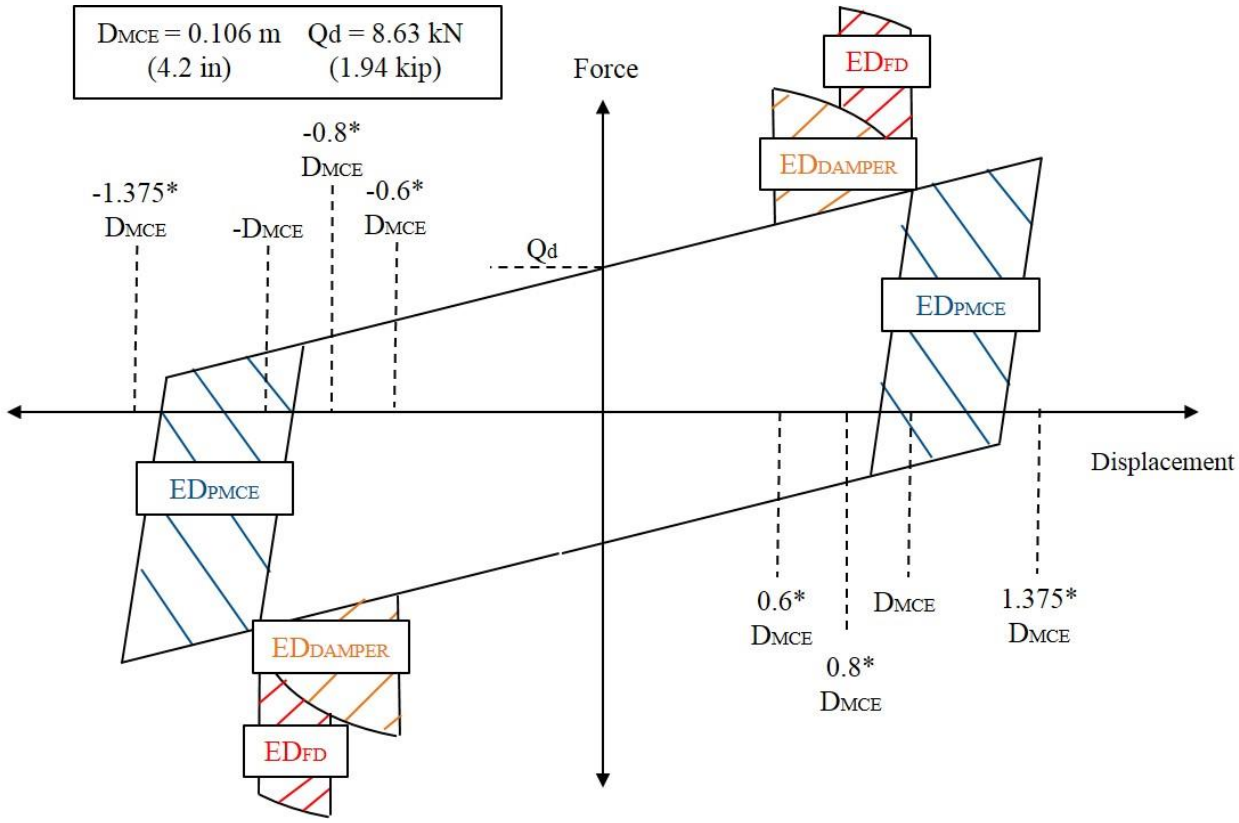

Figure 4-9. Two-Phase Viscoplastic Gap Damper Idealization

The parametric study was insensitive to the activation stiffness of the plastic device, therefore a friction device was chosen as a simple implementation of plastic energy dissipation. The plastic action of the friction device utilized for the two-phase visco-plastic device was achieved using a slotted bolted connection (SBC) shown in Figure 4-10. The SBC used in the gap damper system required two slots; one at the clevis connection to delay the activation until $0.8*D_{MCE}$ and one in the center plate at the bolted connection, which allowed the plates to move

relative to each other, dissipating energy based on the clamping force provided by the bolts. Further details of the friction device can be found in Section 4.2.5.

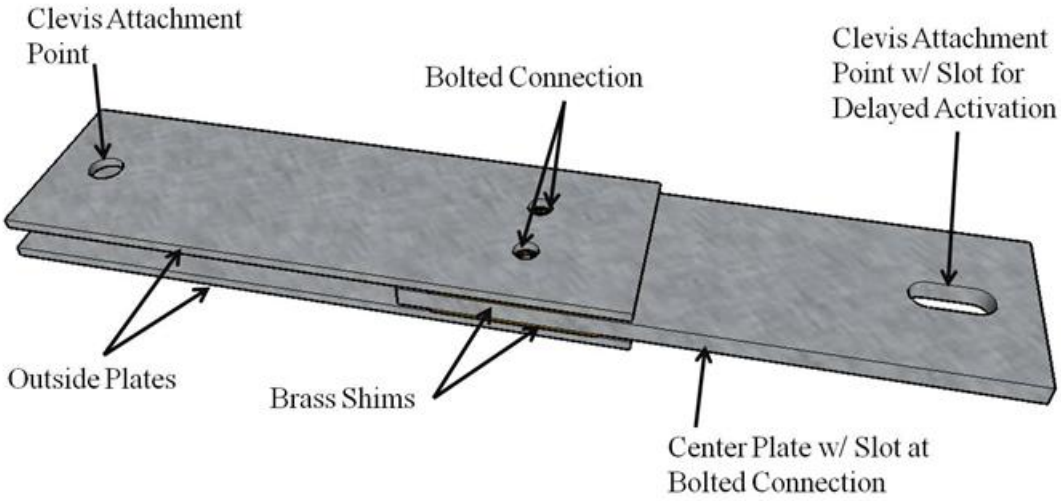

Figure 4-10. Slotted Bolted Friction Device

For the two-stage viscoplastic device, further analysis of the parametric study indicated that 70% of the energy should be dissipated by the viscous dampers and 30% by the friction device. Using results in Figure 4-7, the EDL for the viscoplastic device should be taken as 1.0. Modifying Equation 4-7 to account for the modifications to the energy requirements and EDL:

$$\mathbf{ED_{DAMPER} = 70\% * EDL * ED_{PMCE} = 0.7(1.0)(5.489) = 3.842\ kN * m} \qquad \textbf{Equation (4-9)}$$

ED_{PMCE} remains the same as the number of isolators and the isolator characteristics are unchanged. Modifying Equation 4-8 for the new energy requirement yields a damping constant of 71.67 kN*s/m (0.406 kip*s/in) for the viscous dampers. The stroke requirement of 0.042 m (1.68 in) remains the same.

The energy dissipation requirement of the friction device (ED_{FD}) is defined in Equation 4-10 as 30% of the total energy dissipation requirement or 1.647 kN*m (14.58 kip*in).

$$\mathbf{ED_{FD} = 30\% * EDL * ED_{PMCE} = 0.3(1.0)(5.489) = 1.647\ kN(m)} \qquad \textbf{Equation (4-10)}$$

The parametric study indicated that the friction device should be active from 0.8*D_{MCE} to 1.0*D_{MCE}. Assuming an ideal rectangular plastic hysteresis, the slip force (F_{slip}) of the friction device can be found by:

$$\mathbf{ED_{FD}} = \int_{\mathbf{0.8D_{MCE}}}^{\mathbf{D_{MCE}}} \mathbf{F_{slip}}\,\mathbf{du} \qquad \textbf{Equation (4-11)}$$

$$\mathbf{1.647} = \int_{\mathbf{0.085}}^{\mathbf{0.106}} \mathbf{F_{slip}}\,\mathbf{du}$$

Where the slip force required for the appropriate amount of energy dissipation is 77.69 kN (17.46 kip). This slip force can be obtained by proper tensioning of the bolts in the SBC, detailed in Section 4.4.2. A summary of the gap damper parameters for both systems is presented in Table 4-2. Manufacturer drawings of the viscous dampers are on Appendix Pages A-2 and A-3.

Table 4-2. Summary of Gap Damper Parameters

Viscous Gap Damper Parameters			
Viscous Damper (100% of Energy Dissipated)			
Damping Constant		Stroke Required	
81.91 kN*s/m (0.465 kip*s/in)		±42.67 mm (±1.68 in)	
Two-Phase Viscoplastic Gap Damper			
Viscous Damper (70% of Energy Dissipated)		Friction Device (30% of Energy Dissipated)	
Damping Constant	Stroke Required	Slip Force	Displacement Required
71.67 kN*s/m (0.407 kip*s/in)	42.67 mm (1.68 in)	77.69 kN (17.46 kip)	±0.021 m (±0.84 in)

4.2.4 Finite Element Analysis of Gap Damper Components

Once the gap damper parameters were established, the next step in the development of a prototype device involved the design of the components. Besides the energy dissipation elements, there are

three essential components in a gap damper system, pictured in Figure 4-11. The "isolation nub" is a protruding tube attached to the floor above the isolation level. The isolation nub activates the gap damper system once the threshold displacement is reached. Activation of the gap damper system is accomplished by contacting a bumper system that is composed of tube sections. The bumper system has clevis attachments that are attached to the dampers. A successful component system will fully transfer the load from the superstructure to the supplementary energy dissipation devices.

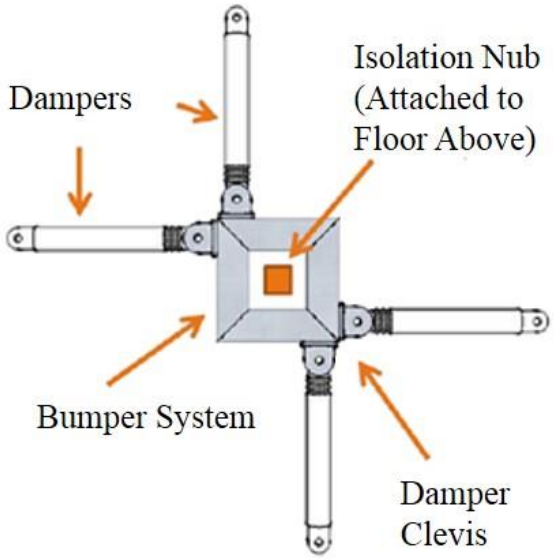

Figure 4-11. Gap Damper Concept

The isolation nub and bumper system were designed using strength limit states in addition to finite element modeling to capture the stress behavior at impact. The bumper system is comprised of 4-152.4x152.4x12.7 mm (6x6x1/2 in) hollow structural steel (HSS) members welded at the diagonals to form the square bumper system shown in Figure 4-11. Collision of the isolation nub with the bumper system activates the secondary energy dissipation, resulting in a large force transfer with localized contact stresses. The isolation nub is the most crucial aspect of the gap damper system because of the large force transfer to the dampers. A finite element study was

completed in Abaqus/Explicit evaluating various shapes and sizes of the contacting elements ensuring adequate force transfer to the dampers (Dassualt Systemes Simulia Corp., 2010). The analysis was completed using 3-D solid, deformable, 8-node elements and dashpot connector sections for the dampers. Analysis was a simplification of the real system involving one collision of the isolation nub with one side of the bumper backed by a damper at each corner (Figure 4-12).

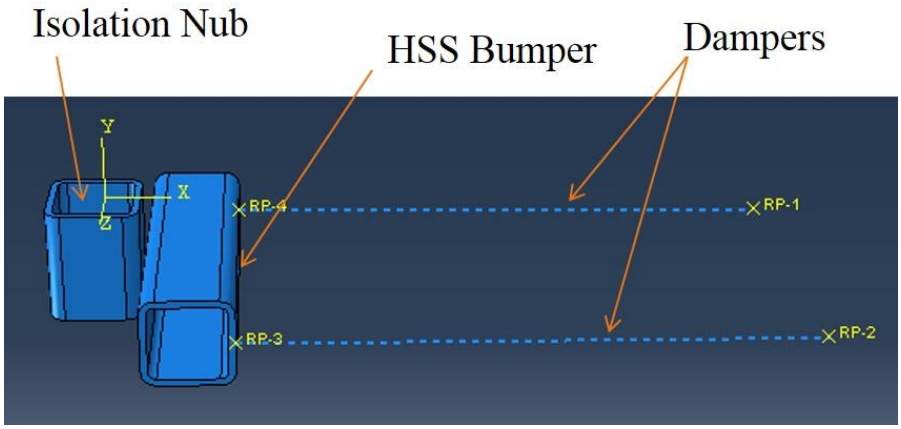

Figure 4-12. Finite Element Model Configuration

The boundary conditions consisted of the isolation nub restrained at the top surface in all directions except the primary direction of movement, with an assigned harmonic velocity in the primary direction. The bumper was restrained from vertical movement at the bottom surface with the dashpots tied to the back surface. A kinematic tie constraint was added at the connection of the dashpots and the bumper system to ensure proper displacement behavior in the dashpots. Force and displacement in the dampers were monitored to ensure the model was functioning properly. The opposite side of the dampers were attached to a reference point. The velocity at contact was 1.016 m/s (40 in/sec), 60% larger than the MCE velocity expected for the system. This value was suggested as an extreme in preliminary modeling of the gap damper system.

Initially, a 177.8x12.7mm (7x1/2in) circular tube (Figure 4-13a) and 152.4x152.4x12.7mm (6x6x1/2in) square tube (Figure 4-13b), with approximately the same section modulus and area,

were compared to evaluate the appropriate cross section for the isolation nub. The figure shows section cuts of the cross-sections to qualitatively evaluate the von Mises stresses present throughout the members. Red areas indicate the higher levels of stress. Based on an assumed yield stress of 289 MPa (42 ksi), the circular cross-section experienced the most yielding in both the isolation nub and bumper system.

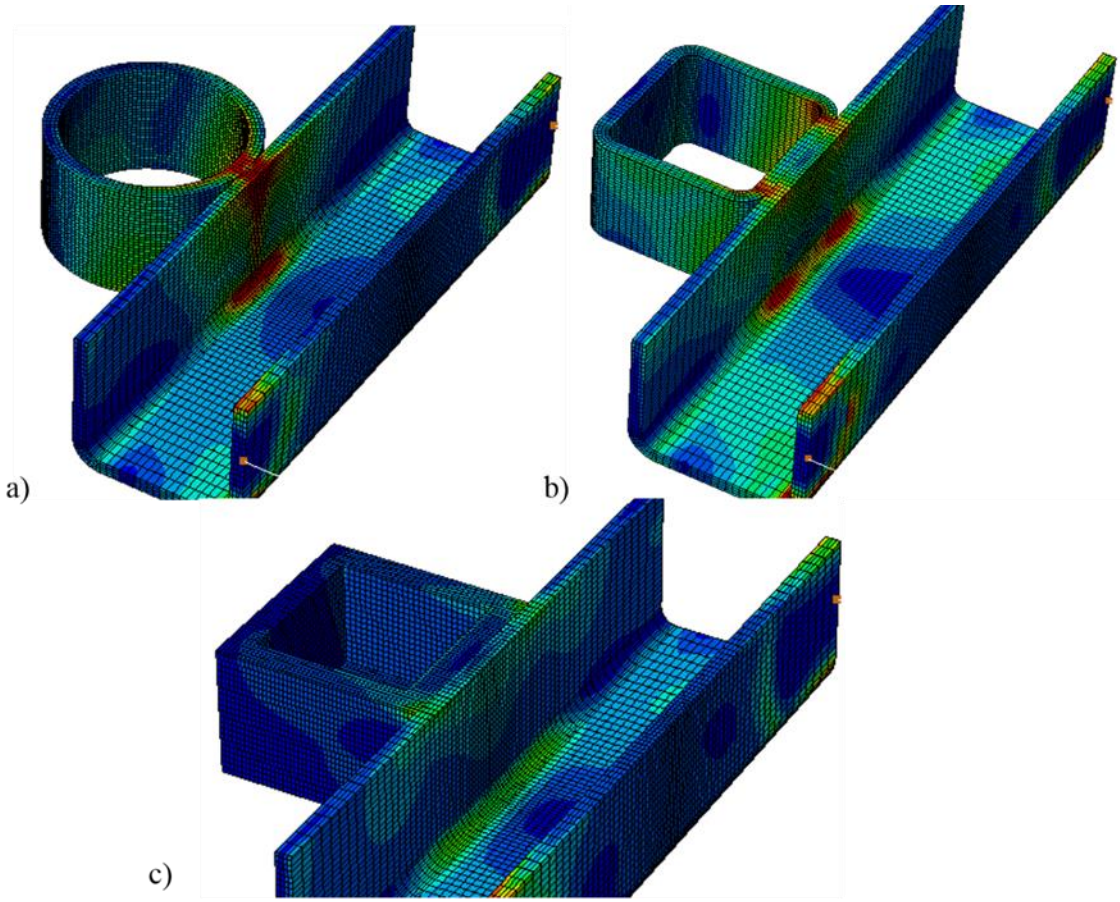

Figure 4-13. Comparison of isolation nub contact with bumper system with different nub cross sections a) 177.8x12.7mm (7x1/2in) circular tube, b) 152.4x152.4x12.7mm (6x6x1/2in) square tube, and c) 152.4x152.4x19mm (6x6x3/4in) built-up section with stiffener.

Various square cross-section geometries were analyzed and a 152.4x152.4x19mm (6x6x3/4in) built-up section was chosen for the final design (Figure 4-14c). A plate was welded to the bottom of the nub to aid in the force transfer and stiffen the nub. In the final design, the peak stress reached a maximum of about 75% of the yield stress and was only present over a small area

of the cross-section. In addition, the plates chosen for design have a strength of 344 MPa (50 ksi), providing more safety. One problem with a square section is angled impact, which does show some localized yielding at the point of contact (Figure 4-14a & Figure 4-14b). The red areas indicate yielding in the isolation nub and bumper. Another scenario evaluated was the possibility of a fabrication error resulting in a slight radius on the impacting plate (Figure 4-14c & Figure 4-14d). This scenario was exaggerated in the analysis to capture the effect of the incidental plate radius. Yielding was found locally in the bumper system upon impact.

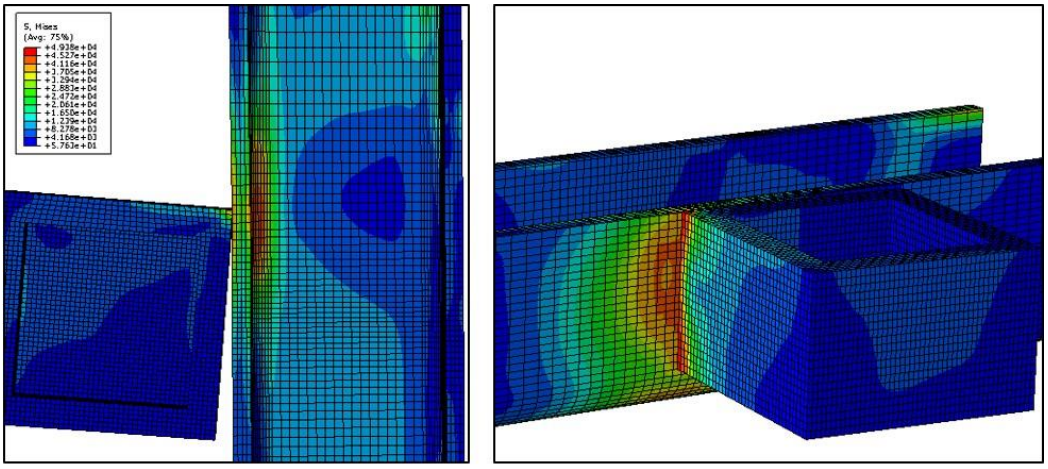

a) Oblique Impact (Top View)

b) Oblique Impact (Side View)

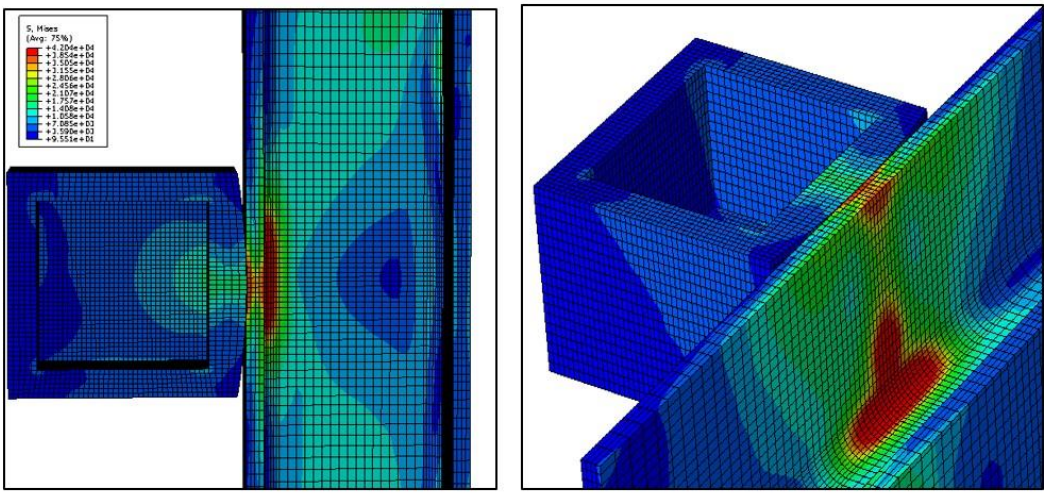

c) Incident Radius (Top View)

d) Incident Radius (Side View)

Figure 4-14. Section Cuts of Oblique and Incidental Radius Impacts

Although there may be localized yielding in the bumper system, this would most likely mean localized small dents that would not be detrimental to the overall system performance. Since the gap damper system is intended for extreme events, some yielding is acceptable but should be minimized if possible.

4.2.5 Design Details

Once the preliminary design was finalized using the results of the finite element analyses, the components of the system could be fabricated. This section overviews the design details with completed drawings in Appendix A. The components were fabricated locally at Davis Machine Works and were assembled in Auburn University's Structural Research Laboratory for testing. A materials list is shown on Page A-6 detailing the material types and sizes necessary for the fabrication of the gap damper prototype. The isolation nub and clevises were fabricated using 1018 cold-formed steel and the bumper system was fabricated using hollow steel sections (HSS tube) of A500 Grade-B steel. All drawings are for reference only and should not be used as construction documents.

As alluded to previously, the bumper system is comprised of 4-152.4x152.4x12.7 mm (6x6x1/2 in) HSS members welded at the diagonals to form the square bumper system shown in Figure 4-15. The gap required before the damper activates is 0.6*DMCE or 64.5 mm (2.5 in). Note that with the 1/4 length scale factor, this corresponds to 254 mm (10 in) at full scale. Full details on the bumper system are found on Page A-7.

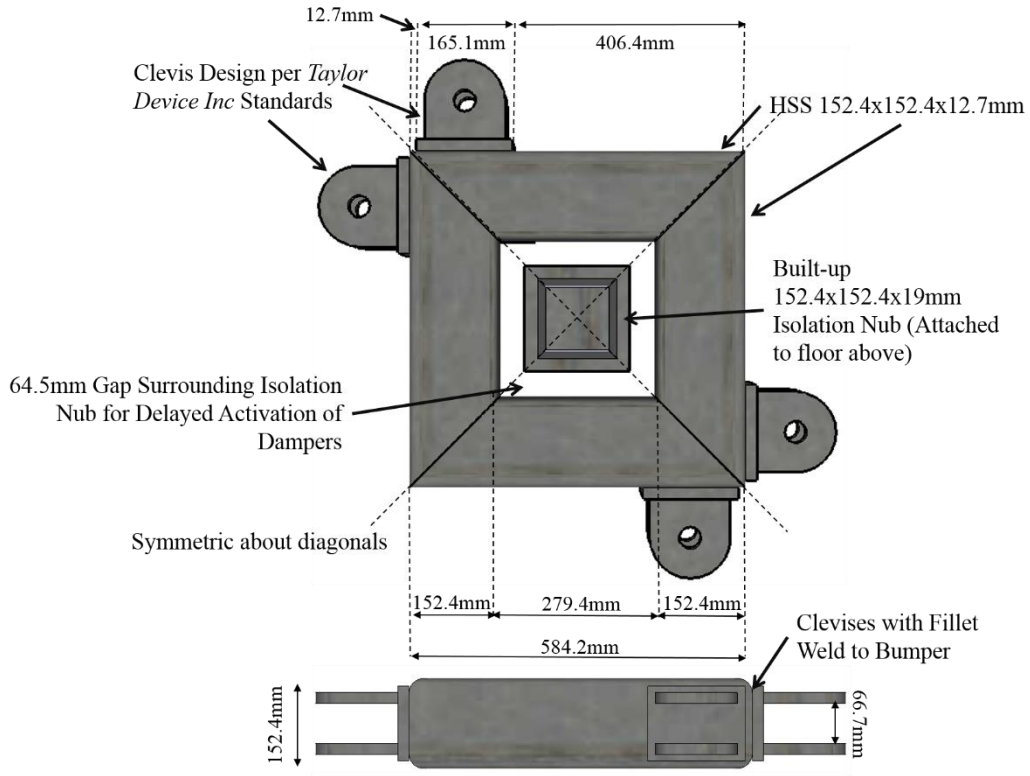

Figure 4-15. Plan View of Bumper System and Isolation Nub for the Viscous Gap Damper Setup

The clevises were designed according to the standards provided by Taylor Devices to ensure adequate connection behavior of the viscous dampers. Clevises are welded to the corners of the bumper system in order to resist eccentric impacts. Typical manufacturer requirements for the clevis attachments are found in *Field Installation Guide Standard #17120* found on Page A-5. Drawings for clevis fabrication for both damper attachments and friction device attachments are found on Pages A-9 and A-10 respectively. The clevis pins used to attach the dampers to the bumper system are made of a high strength 17-4PH stainless steel with a precise tolerance to minimize slop in the connection. The details of the pins and shims used to attach the dampers are found on Page A-4. Figure 4-16 shows the fabricated clevises for the friction device and viscous damper. The friction device clevis had to be fabricated to allow for the delayed activation of the device accomplished with the slot detailed in Figure 4-18. Clevises attached to the side of the

damper opposite of the bumper system were fabricated with a threaded hole for attachment to a load cell.

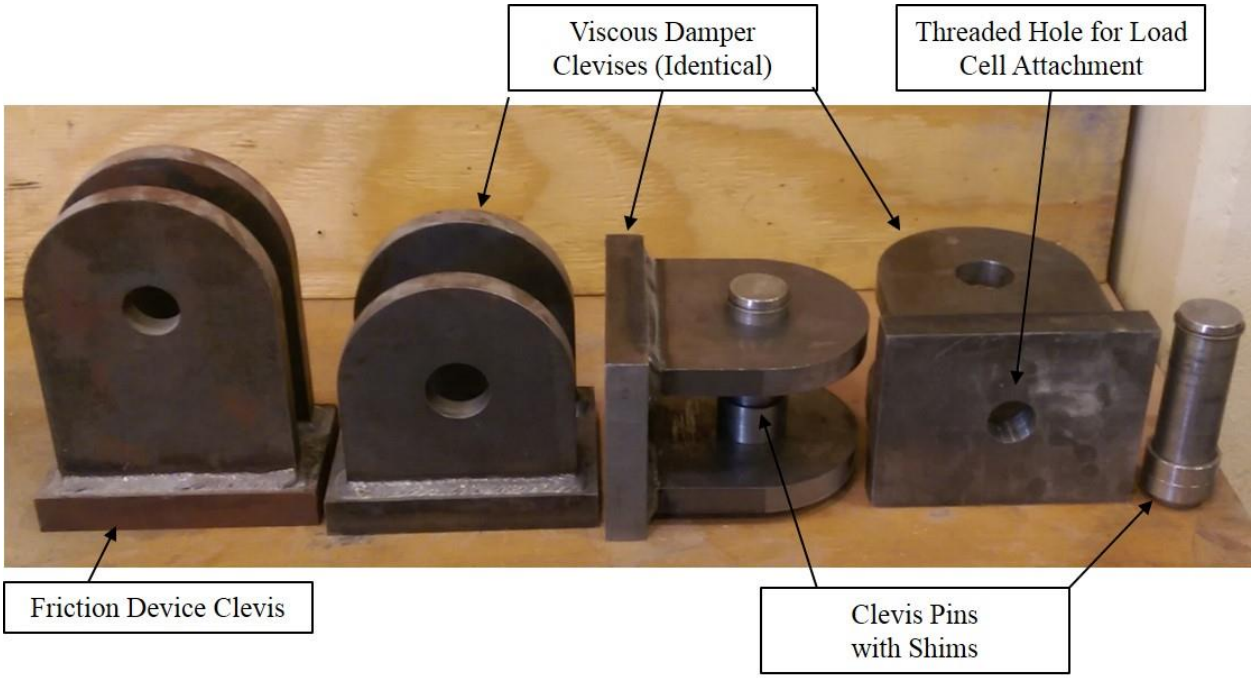

Figure 4-16. Clevis Hardware

In order to incorporate both prototype systems into a single bumper system, a clevis attachment was added to the middle of the bumper system as shown in Figure 4-17. This clevis is used for the connection of the bumper system to the friction device. For the AU testing, only one-directional testing was possible but the response of the dampers transverse to the movement was also captured. The dampers transverse to actuator movement were primarily for stability of the system while the dampers in the direction of movement were responsible for the energy dissipation. Therefore, for the viscous gap damper setup, the two dampers fabricated with the higher damping constant (81.91 kN*s/m (0.465 kip*s/in)) were used in the direction of actuator movement while the dampers with the smaller constant (71.67 kN*s/m (0.406 kip*s/in)) were used in the transverse direction. For the viscoplastic arrangement, the damper locations were switched so that the dampers with the lower damping constant and one friction device were in the direction

of movement to accomplish the necessary plastic energy dissipation. Drawings indicating the clevis layout on the bumper system can be found on Page A-8.

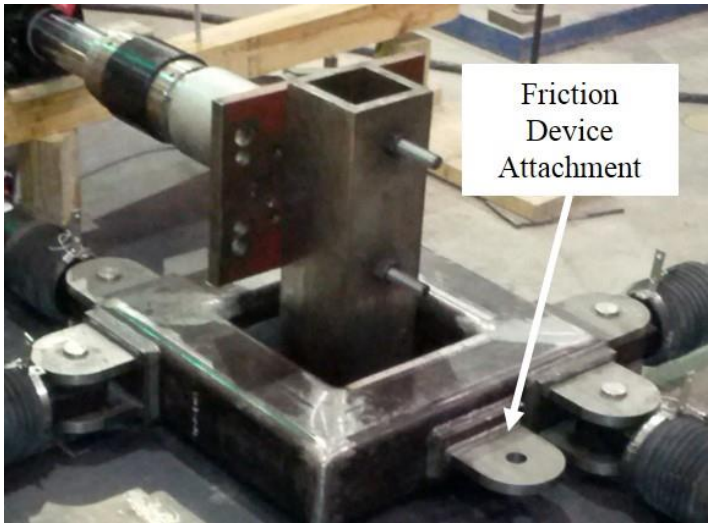

Figure 4-17. Two-Phase Viscoplastic Bumper System

Detail drawings for the friction device are found on Page A-12 with an overview of the system in Figure 4-18. Given the length of the plates in the friction device, stiffeners were added to the top and bottom plates to prevent buckling when the device is in compression. Brass shims were used between the outside steel plates and the center plate to provide a more reliable slip behavior (Grigorian & Popov, 1994). Bolts equipped with strain gages in the center were calibrated so the clamping force on the bolted connection could be controlled, achieving the desired slip force for the testing. Calibration of the friction device using bolt tension and the coefficient of friction can be found in Section 4.4.2.

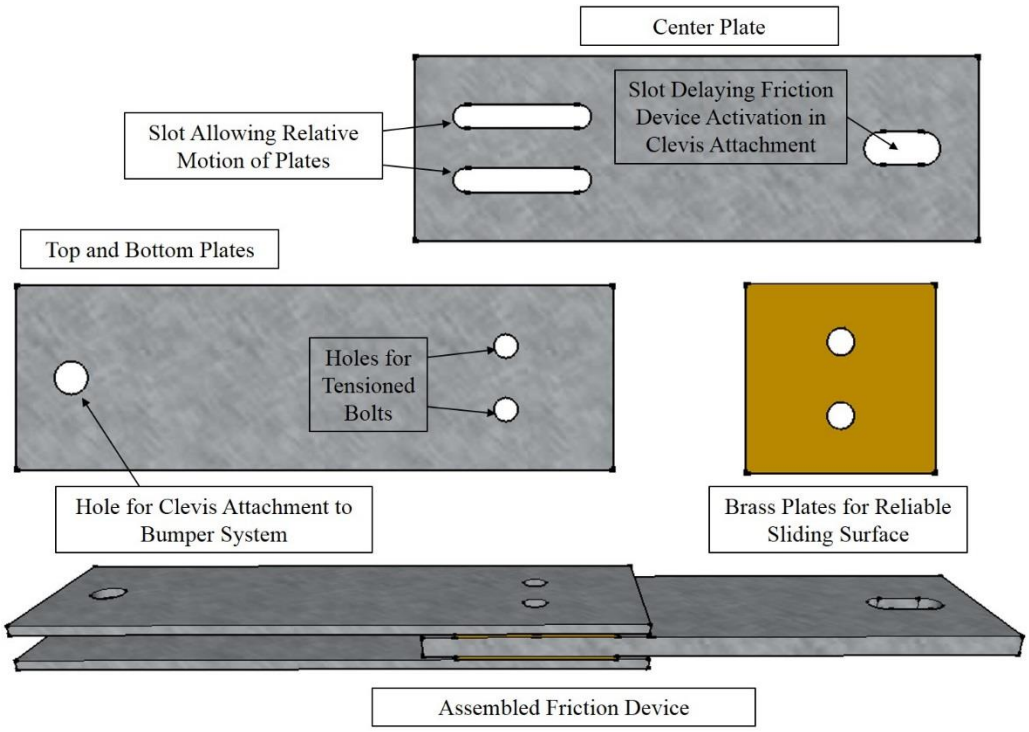

Figure 4-18. Friction Device for Viscoplastic Gap Damper Arrangement

Lastly, drawing details for the isolation nub are on Page A-11. Resulting from the finite element analysis detailed in Section 4.2.4, the square isolation nub was assembled as built-up section using four steel plates. The isolation nub is pictured in Figure 4-19 with holes fabricated for attachment to the actuator plate with thread through-rods. The nub was given a smooth finish in order to reduce contact friction.

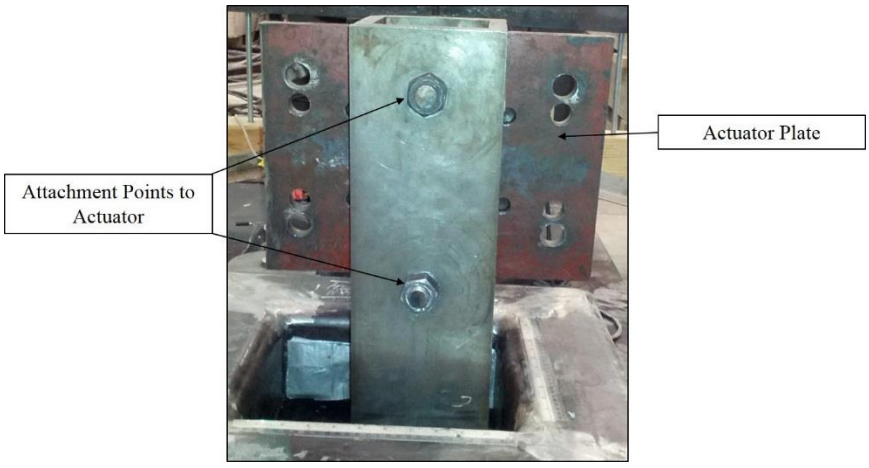

Figure 4-19. Isolation Nub

4.4 Experimental Design

With the design and fabrication completed, the experimental testing began at Auburn University's Structural Research Laboratory. This section covers the experimental design with an overview of the calibration of viscous damper properties and friction device properties, experimental setup for both prototypes, instrumentation details, and the loads cases tested for each system.

4.4.1 Viscous Damper Properties

The viscous dampers were manufactured with a "preload" of approximately 8.9 kN (2 kips) which added a slight static stiffness. This preload delayed the activation of the dampers until the threshold was reached. Typically this is not an issue as the force range for dampers of this size is much higher. Due to laboratory limitations, the velocities expected in the preliminary testing were smaller than 12.7 cm/sec (5 in/sec), meaning the preload could have a significant effect on the behavior of the system and a deviation from linear viscous behavior. To alleviate this concern, damper fluid was bled from the dampers. The manufacturer of the dampers suggested that the properties of the dampers may change slightly with the elimination of the preload. In addition, although the gap damper system utilizes most of the stroke, the forces present in the damper will be much smaller than the capacity of the dampers. In order to accurately evaluate the performance of the gap damper system, the viscous dampers were tested in order to find the properties in the range of experimental values.

For the viscous gap damper prototype, the dampers were laid out in the laboratory according to Figure 4-20. Dampers 2 and 4 were fabricated with a larger damping constant calibrated for the viscous gap damper system while Dampers 1 and 3 were fabricated with the smaller damping constants calibrated from the viscoplastic gap damper system. Since the tests are

uni-directional in nature, the dampers transverse to the actuator movement do not provide much energy dissipation due to small displacement but are able to stabilize the system.

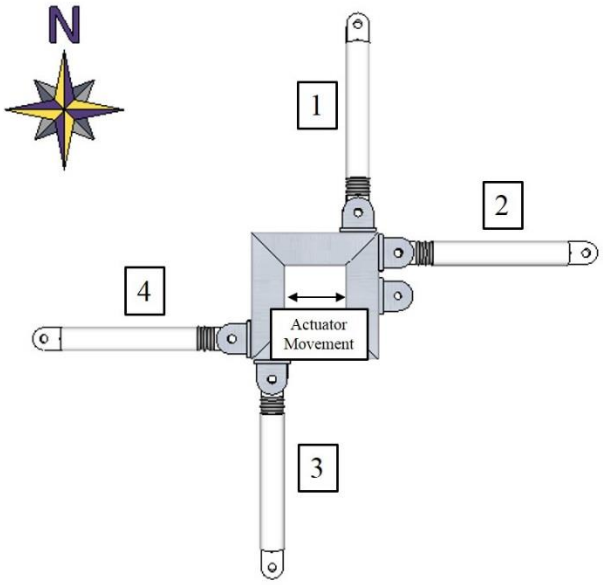

Figure 4-20. Damper Layout and Naming Scheme

In order to find the damper properties, the dampers were attached between a horizontal actuator and reaction block, as shown in Figure 4-21. The dampers were instrumented with a drawstring wire gage attached to the damper and a load cell attached to clevis. More details on the instrumentation is found in Section 4.4.4.

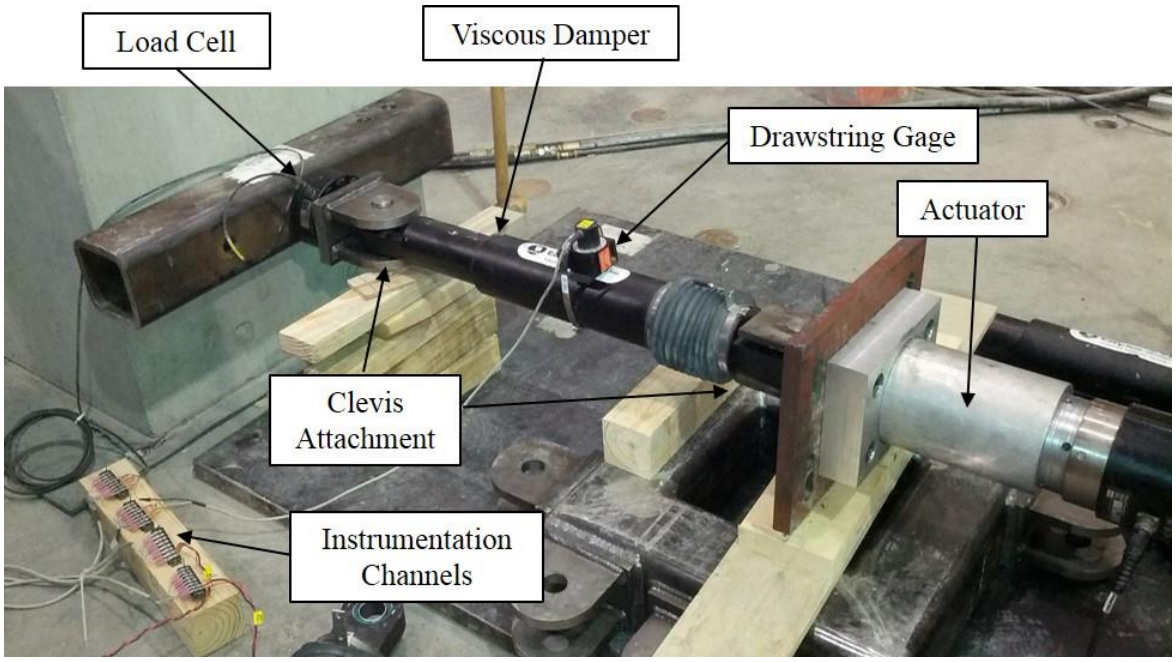

Figure 4-21. Damper Property Test Setup

Each damper was subjected to a sinusoidal 0.3Hz motion over a displacement range of ±44.45 mm (1.75 in). This corresponded to a maximum velocity of 82.45 mm/sec (3.24 in/sec) at mid-stroke. The hysteretic plots and force vs. velocity plots were generated for all four dampers. Velocity values were derived using a moving average filter on the raw displacement data. Some of the data indicated slight nonlinearities around velocities close to zero (max displacement) but the nonlinearities could be due to instrumentation sensitivity or damper nonlinearity. A linear fit for the plots indicated a strong linear relationship between the force and velocity with coefficients of determination (R^2) above 0.97 for all four dampers (Figure 4-22b). Using the damping constant from the linear fit, a fitted hysteresis was compared to the raw data (Figure 4-22a).

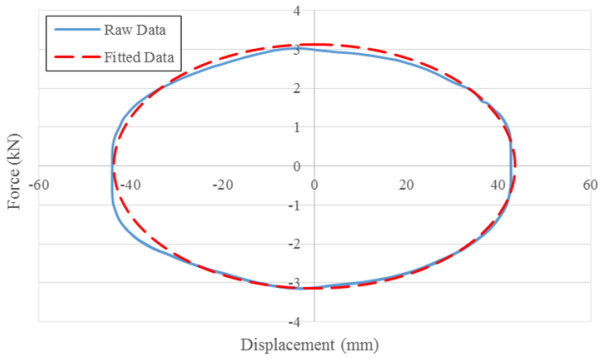

a) Hysteretic Data

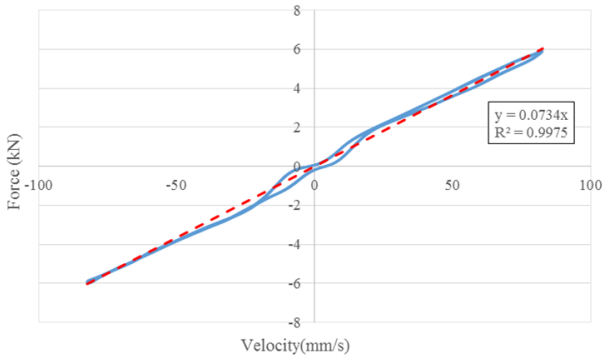

b) Force vs. Velocity Data

Figure 4-22. Damper Properties Calibration for Damper 2

Figure 4-23 shows all four dampers with raw data and calibrated data based on the linear regression. The fitted data agrees well with the raw hysteretic data. With designed damping constants of 81.91 kN*s/m (0.465 kip*s/in) for dampers 2 and 4 and 71.67 kN*s/m (0.407 kip*s/in) for dampers 1 and 3, values were 2%-16% lower than intended. A possible explanation for this range in difference is that the dampers were not bled uniformly leading to varying damper properties. The small force range that the dampers were tested in may have also factored into the varying damper properties. The load cell and damper behavior when subjected to small forces may have skewed the properties since they are both designed for at least a 200 kN capacity. These decreased constants should be considered when evaluating the gap damper systems as the amount of energy dissipation will also decrease.

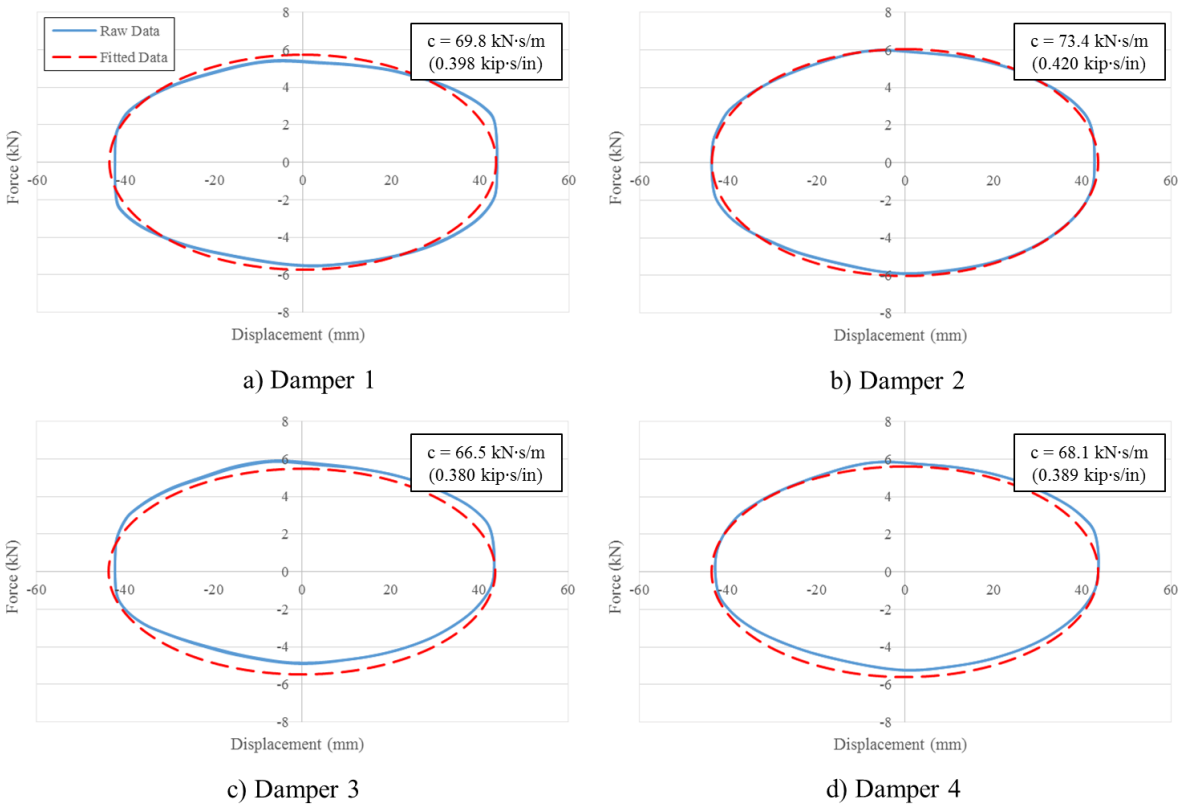

Figure 4-23. Raw Data with Calibrated Fitted Data

4.4.2 Friction Device Properties

The friction device was fabricated in order to achieve the desired objectives of the previous sections. In order to achieve the desired energy dissipation for the two-phase viscoplastic gap damper system, the slip force (F_{slip}) must be known. Using the standard equation for friction behavior found in Equation 4-12, the slip force can be found.

$$\mathbf{F_{slip} = \mu N} \qquad \textbf{Equation (4-12)}$$

Where μ is the coefficient of friction and N is the normal clamping force of the bolts. Although a reasonable approximation of the friction coefficient can be made using published values, slight variations in the surfaces could change the values. Controlling the slip force is crucial to the

success of the viscoplastic device, therefore a calibration of friction device properties was necessary.

In order to find the coefficient of friction for the device, the normal clamping force provided by the bolts must be known. The bolts used for the friction device were a 7/8”-9 A490 structural steel bolts with a small hole drilled in the center. Belleville washers were used in order to maintain a consistent clamping force throughout the duration of motion. Strain gages were epoxied inside the shank of the bolts to capture the strain for a given load. A *Tinius-Olsen* machine was used for the tensile testing of individual bolts as shown in Figure 4-24. The bolts were incrementally loaded up to 111.2 kN (25 kips) in three separate trials and an average force vs. strain plots was generated. Using a linear regression, a direct relationship between the strain and the tension in the bolt could be developed as shown in Figure 4-25. These values were used when tensioning the bolts in the friction device to ensure an accurate clamping force.

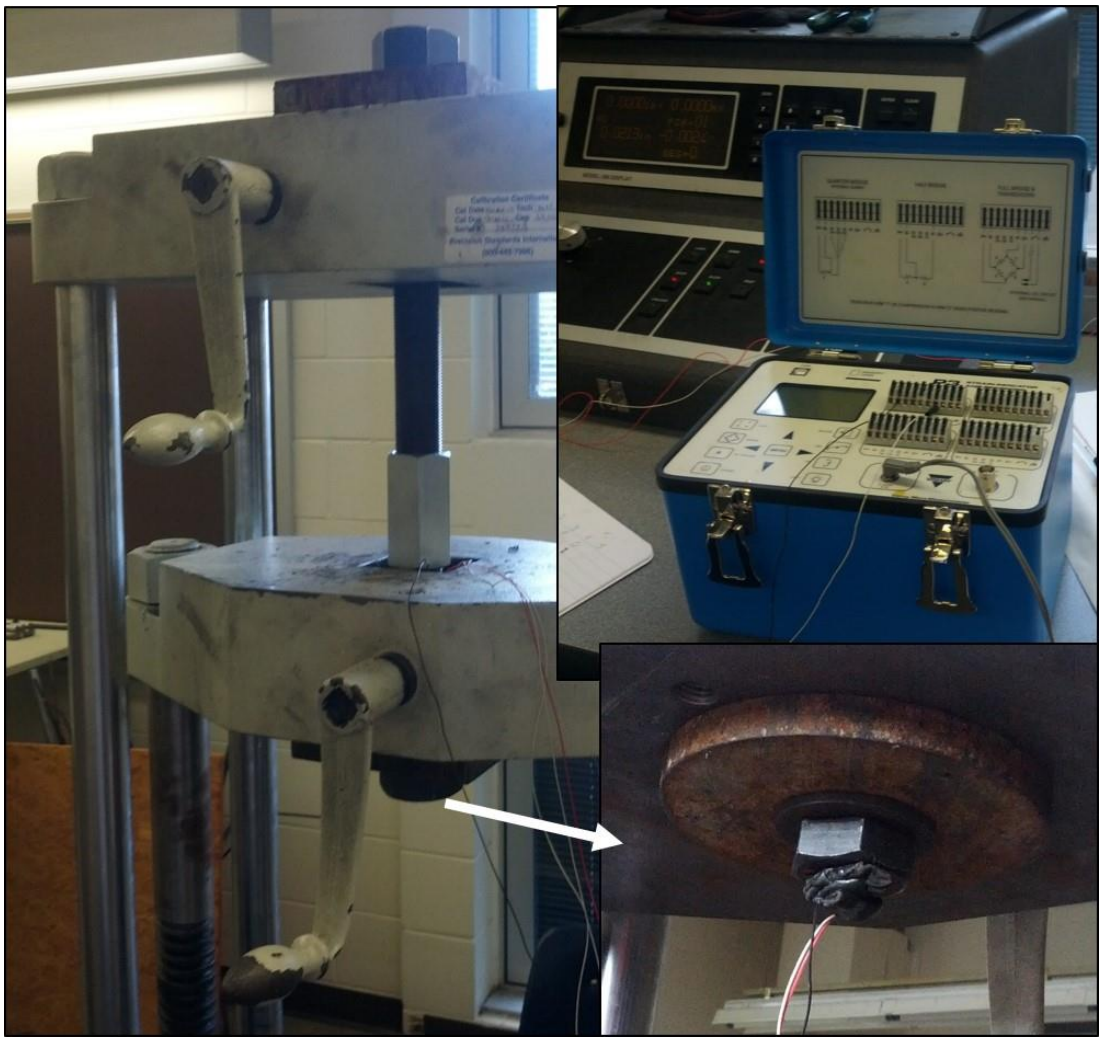

Figure 4-24. Bolt Tension Calibration Setup

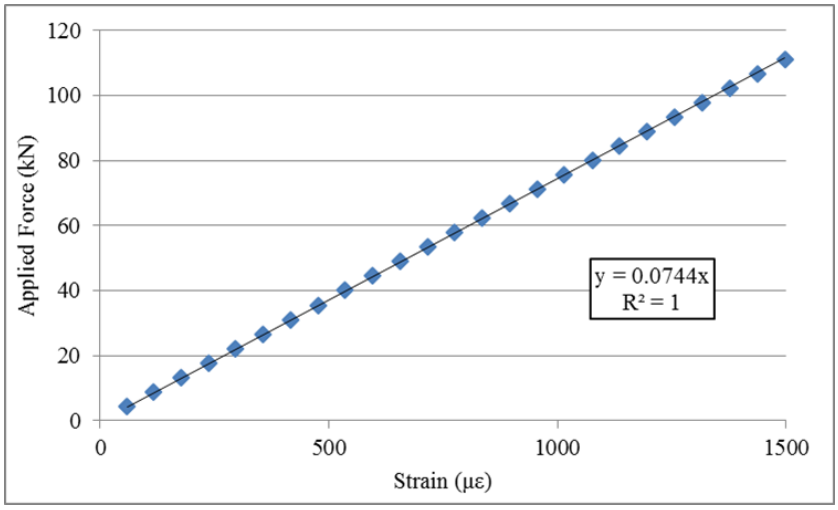

Figure 4-25. Bolt 1 Tension Test

Once the tension values were calibrated, the coefficient of friction could be found by testing the friction device at given levels of bolt tension. Similar to the setup for the calibration of damper properties, the friction device was tested by itself in order to find the as-built properties. The viscoplastic device requires a slip force of 77.7 kN (17.5 kip) for a slip displacement of 21 mm (0.84 in) with a delayed activation of $0.2*D_{MCE}$. An initial guess in bolt tension was made to achieve the desired force. The friction device was subjected to two sinusoidal motions of 0.25 Hz over two different displacement ranges (Figure 4-26a & Figure 4-26b). Slip behavior for both displacement ranges were relatively consistent with a slip force of approximately 60 kN (13.5 kip). The force was maintained throughout the duration of the slip behavior which is a desirable characteristic for consistent energy dissipation. In addition to the 0.25 Hz motions, a 0.5 Hz sinusoidal motion was tried in order to assess the reliability of the slip behavior at larger activation velocities (Figure 4-26c). The slip force for the higher frequency motion was consistently around 70-75 kN (15.7-16.9 kips), which is 15%-25% higher than the slip force for the lower frequency.

Since the initial trials had a slip force under the desired slip force of 77.7 kN (17.5 kip), bolt tension was increased. Two different frequencies were also tried with the higher bolt tension to see if there was a significant effect on slip behavior. The increase in total bolt tension by about 50 kN resulted in a significant increase in slip force that was disproportional to the original bolt tension, as shown in Figure 4-27a & Figure 4-27b. Frequency did not seem to play as large of a role in the slip behavior of the device with the larger bolt tensions.

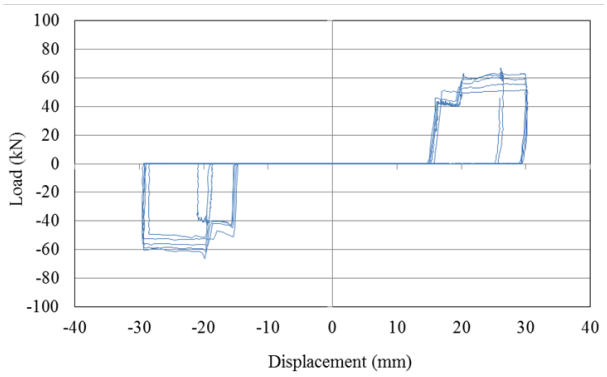

a) 0.25 Hz, +/-31.75mm

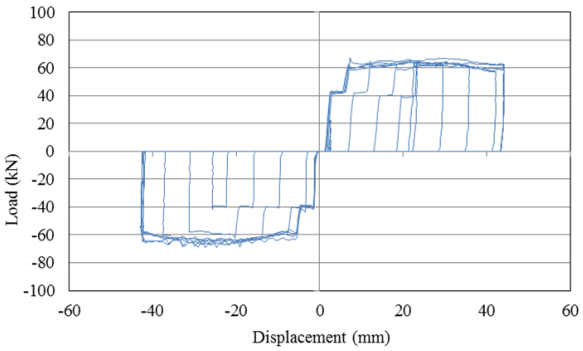

b) 0.25 Hz, +/-45.72mm

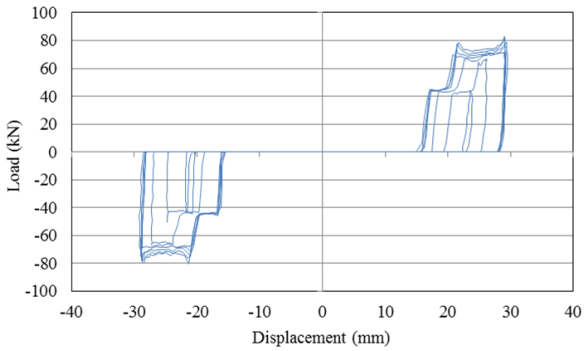

c) 0.5 Hz, +/-31.75mm

Figure 4-26. Friction Device Results (Initial Bolt Tension)

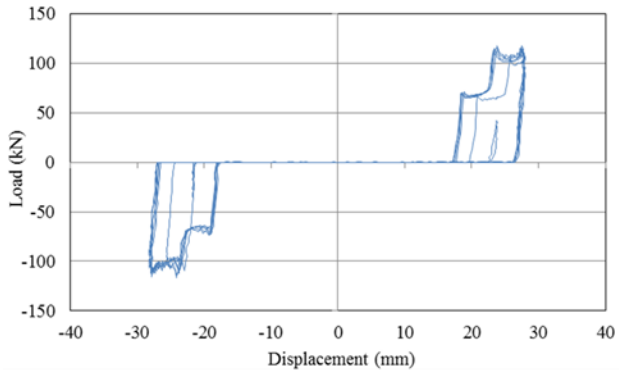

a) 0.25 Hz, +/-31.75mm

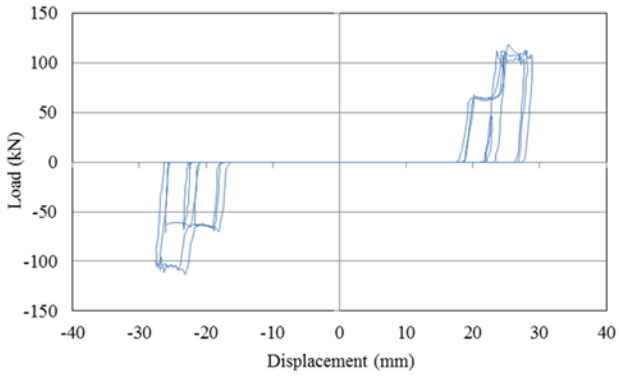

b) 0.5 Hz, +/-31.75mm

Figure 4-27. Friction Device Results (Increased Bolt Tension)

A summary of the friction device results is found in Table 4-3. The calculated coefficient of friction is based on an average bolt tension during the duration of the motion and an average slip force. Coefficients of friction varied largely based on the input motions, indicating a potentially unreliable system.

Table 4-3. Friction Device Calibration

Trial	Average Bolt Tension (kN)	Average Slip Force (kN)	Calculated Coefficient of Friction
0.25 Hz ± 31.75 mm	151	55	0.36
0.25 Hz ± 42.72 mm	153	60	0.39
0.5 Hz ± 31.75 mm	156	70	0.45
0.25 Hz ± 31.75 mm	216	105	0.49
0.5 Hz ± 31.75 mm	198	105	0.53

Another interesting observation in the friction device testing was a two-stage slip behavior with each trail experiencing an initial slip at a lower force and a slip at a higher force. This could be due to slop in the friction device connections, out of plane behavior, and/or imperfections in the sliding surfaces. Deterioration of sliding surfaces could be a significant source of potential error and inconsistent results. Figure 4-28 shows the sliding surfaces at the completion of friction device trials. Significant wearing of the brass shims is evident with gouging of the material creating depressions on the surface. In addition, the material is deposited on the steel surface creating a rough sliding interface. This may explain the increase in the coefficient of friction as the trials were completed. The softer brass shims were replaced between trials of the viscoplastic gap damper but the wear of the steel plates could result in unreliable behavior of the friction device. Recent research involving the use of brake pads, rather than brass shims, indicate a more reliable slip behavior (Golondrino, MacRae, Chase, Rodgers, & Clifton, 2013). Future research into the two-phase system may benefit from the use of different materials but the brass and steel materials were used for the remainder of this research.

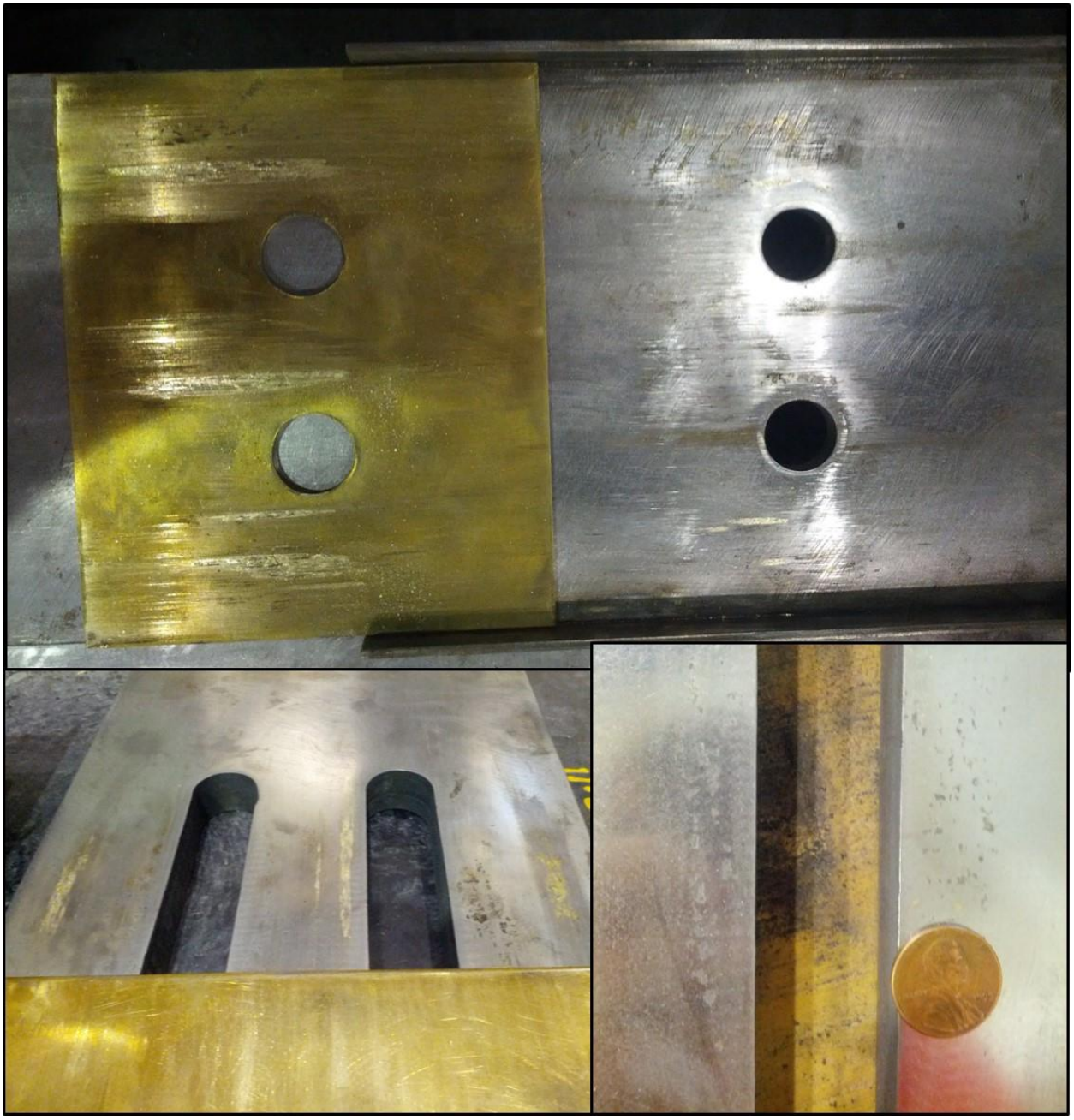

Figure 4-28. Deterioration of Sliding Surfaces

With the unreliable behavior of the friction device, the bolt strain and calculated bolt tension throughout the duration of the motions were evaluated to see if there was erratic fluctuations that may offer insight towards the inconsistent behavior. Figure 4-29 shows the change in bolt behavior for one of the trials. Although the tension does fluctuate, the total bolt

clamping force only varies about +/- 7% throughout the trial. This fluctuation does not seem to be significant enough to explain the variation in results. It was concluded that the unpredictable behavior is most likely due to slip surface material imperfections.

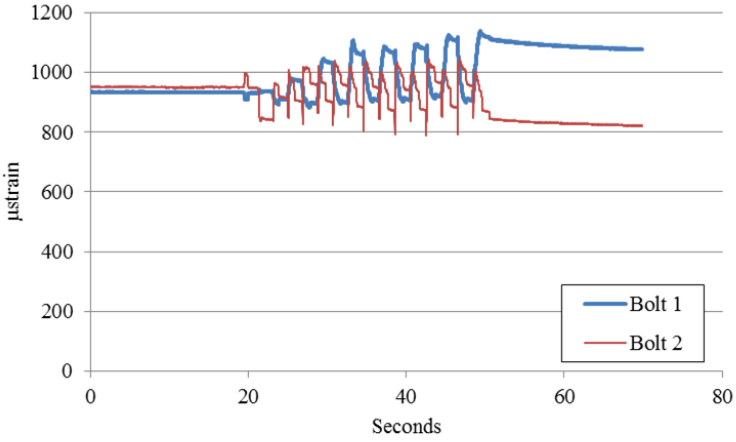

a) Bolt Strain vs. Time

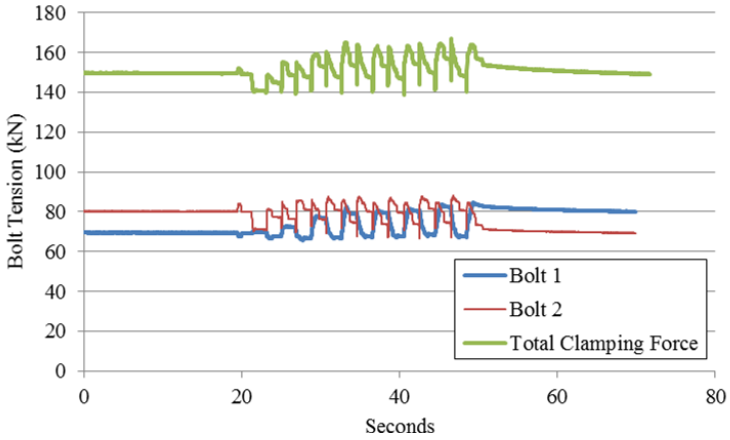

b) Bolt Tension vs. Time

Figure 4-29. Friction Device Bolt Behavior

Given the relative uncertainty of the slip behavior with varying frequencies and bolt tensions, an approximation of the coefficient of friction was necessary for the viscoplastic gap damper device. A coefficient of 0.4 was used in the calculation of bolt tension necessary for the gap damper system.

4.4.3 Experimental Setup

Prior to the setup of the laboratory experiment, 3-dimensional renderings of both gap damper systems were created to ensure the proper placement of the components (Figure 4-30 & Figure 4-31). Relative movement between the isolation nub and bumper system was simulated by attaching the isolation nub to an *MTS 243.35* actuator, with a capacity of 240 kN (54 kips) in tension and 365 kN (82 kips). The stroke capacity of the actuator is 254 mm (10 in). The actuator was attached to a reaction block that was tensioned to the strong floor of the lab. A reaction block on the opposite side was also created for the reaction of the viscous damper and friction device. The isolation nub was affixed to the actuator with the use of two through rods attached to a plate. For the purposes of this experiment, a new actuator head was fabricated that provided a more rigid attachment than the original swivel that experiences slop in the connection with tension/compression load reversals. Figure 4-31 demonstrates the different attachments with the original attachment in the rendering and fabricated attachment in the picture of the lab setup. Detailed drawings of the actuator attachment are found on Page A-14.

Only one-direction testing was possible with this setup but the response of the transverse dampers was also captured during movement. The dampers were attached to the bumper using the pin and clevis connections detailed in Section 4.2.5. The opposite side was attached to a reaction support with a pin and clevis connection as well. All damping devices were attached to a 222 kN (50 kip) tension/compression load cell to capture the load in the devices. In addition, each device was equipped with a drawstring displacement gage in the axial and transverse direction. Pairing the load data with the axial displacement data captured the hysteretic behavior of the gap damper system. The transverse drawstring gages captured the rotational movement of each damper. Axial and transverse gages were used for both setups with the addition of an axial gage for the friction

device on the viscoplastic setup. The transverse movement of the friction device was assumed to be equal to the transverse movement of the parallel damper.

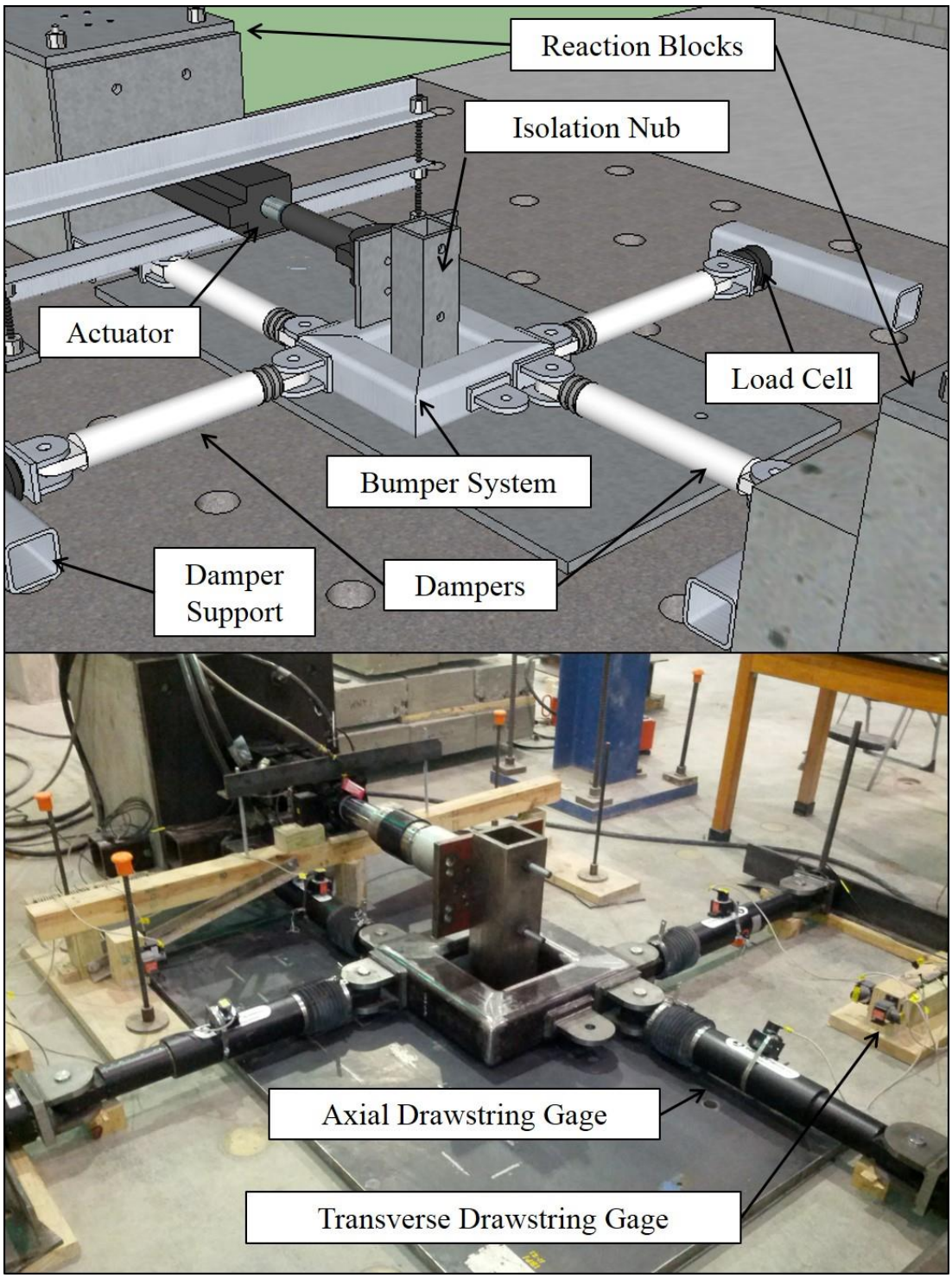

Figure 4-30. 3D Rendering and Photo of Viscous Gap Damper Setup

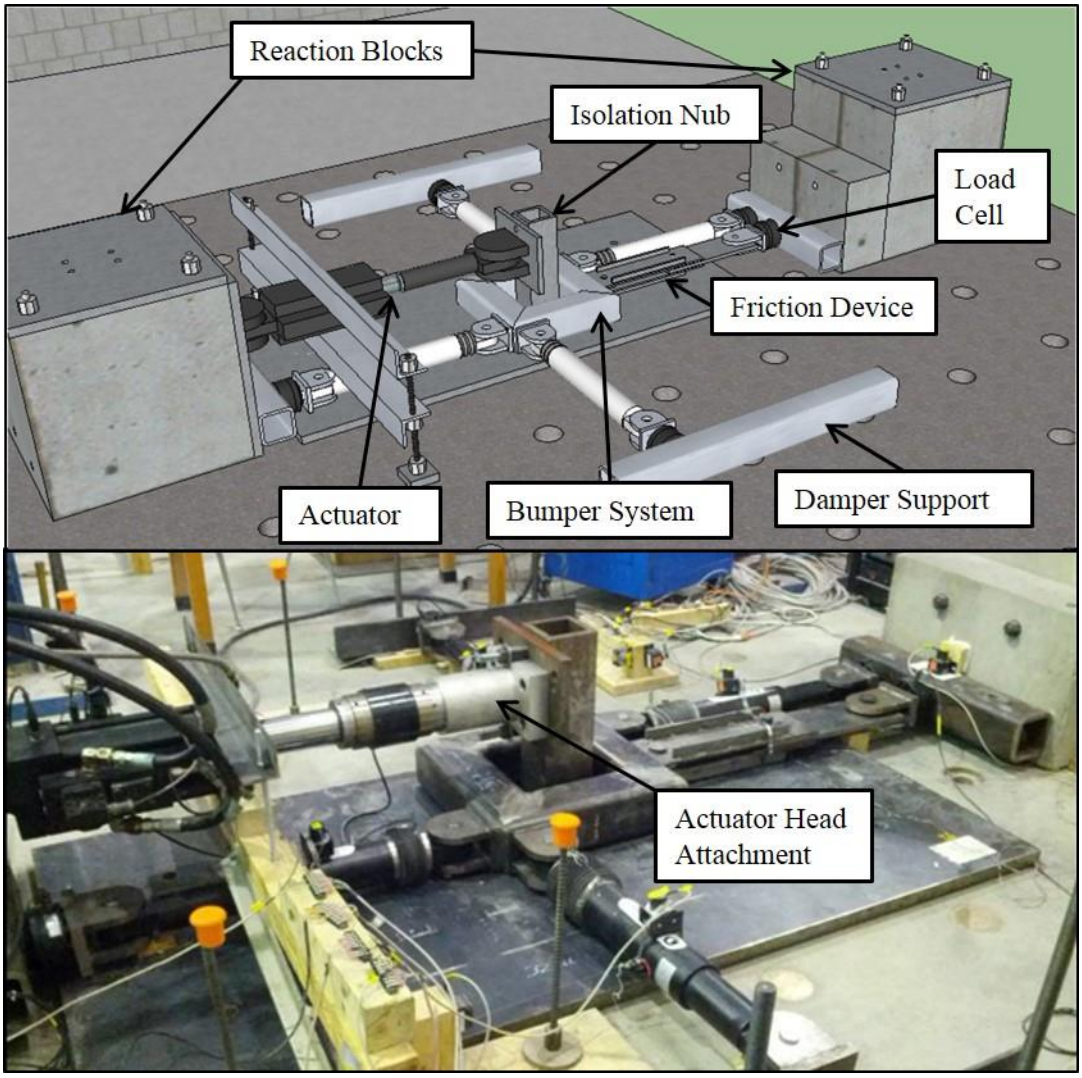

Figure 4-31. 3D Rendering and Photo of Two-Phase Viscoplastic Gap Damper Setup

4.4.4 Instrumentation

Beyond the components and materials necessary for the gap damper prototypes, other important equipment of note necessary for the completion of the experiment included:

- *MTS Systems Corporation (MTS) 243.35* Single Ended Actuator
- *MTS 407* Controller
- *MTS 506* Hydraulic Power Supply

- *MTS 292.14* Hydraulic Service Manifold Model
- *MTS 111.12C-06* Piston Accumulator
- *Pacific Instruments 6000* Data Acquisition System
- *Micro-Epsilon WDS-1000-P60-CR-P* Drawstring Gauges (Stringpots)
- *Load Cell Central LPSW-B-50K* Load Cells
- 32”x32”x32” Reinforced Concrete Reaction Blocks with 1.5” PVC holes at 24” O.C. for anchorage to strong floor
- *Tokyo Sokki Kenkyujo Co., LTD BTM-6C* Bolt Strain Gages
- *Micro-Measurements CEA-06-250UW-350/P2* General Purpose Strain Gages

To assess the performance of the gap damper prototypes, it was important to capture the energy dissipated by the devices. In order to capture the energy, the dissipation devices were equipped with load cells and displacement gages. Figure 4-32 shows the use of drawstring gages (springpots) for the experiment. The axial displacement of the damper was measured by clamping the drawstring gage to the damper or friction device and attaching the drawstring to a fixed point across the displacement interface. In addition to axial displacement, the rotation of the dampers were also measured using drawstring gages. Measuring the rotation is important in understanding the global behavior of the gap damper systems. Attaching the drawstring to a fixed point on the damper, as shown in Figure 4-32, the linear displacement transverse to the primary direction of the damper can be found. Using a fixed reference point at the center of the clevis attached to the load cell and the distance to the attachment point, the rotation of the damper can be found assuming small angles.

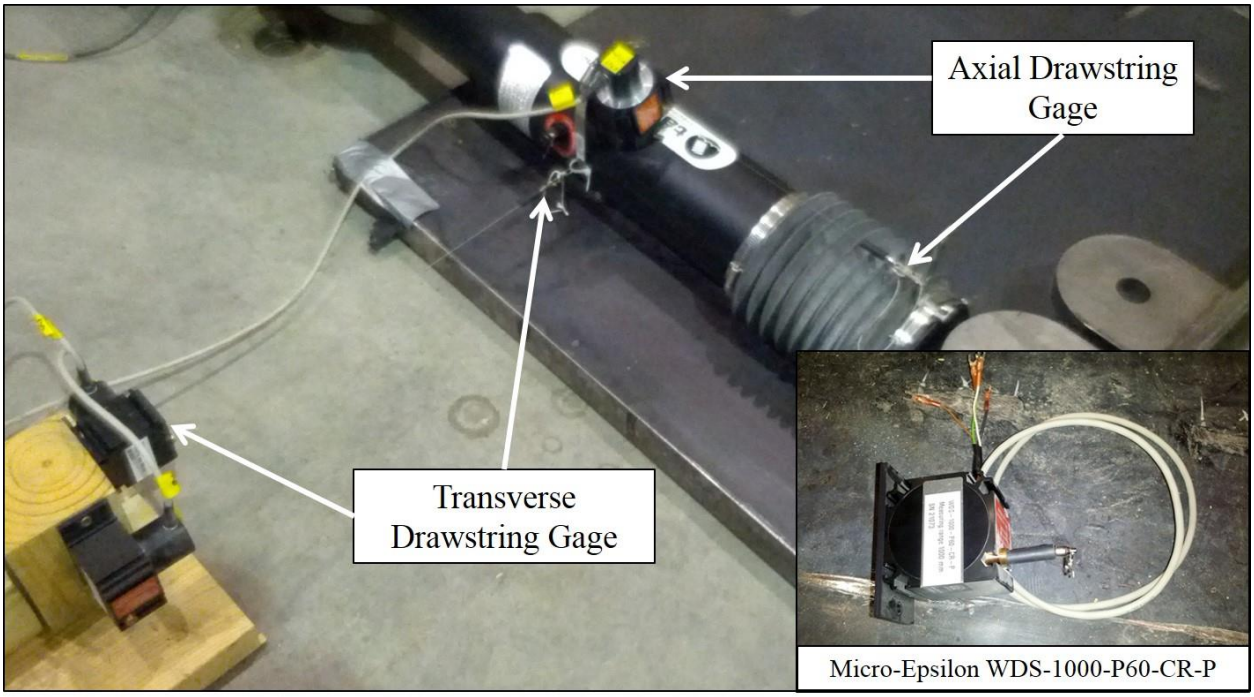

Figure 4-32. Drawstring Gage Arrangement

In addition to the drawstring gages, each damper was equipped with a load cell as pictured in Figure 4-33. The 222 kN (50 kip) tension/compression load cells were attached to the damper or friction device clevis with a threaded rod. The opposite end of the load cell was affixed to an HSS square tube via a threaded rod and nut. Reactions from the load cell arrangement were passed through the HSS member into the reaction block. There were four load cells available for use and therefore a load cell was fabricated and calibrated for use in the viscoplastic gap damper testing which required five load cells. The fabricated load cell was used on a transverse damper that saw very little load during testing.

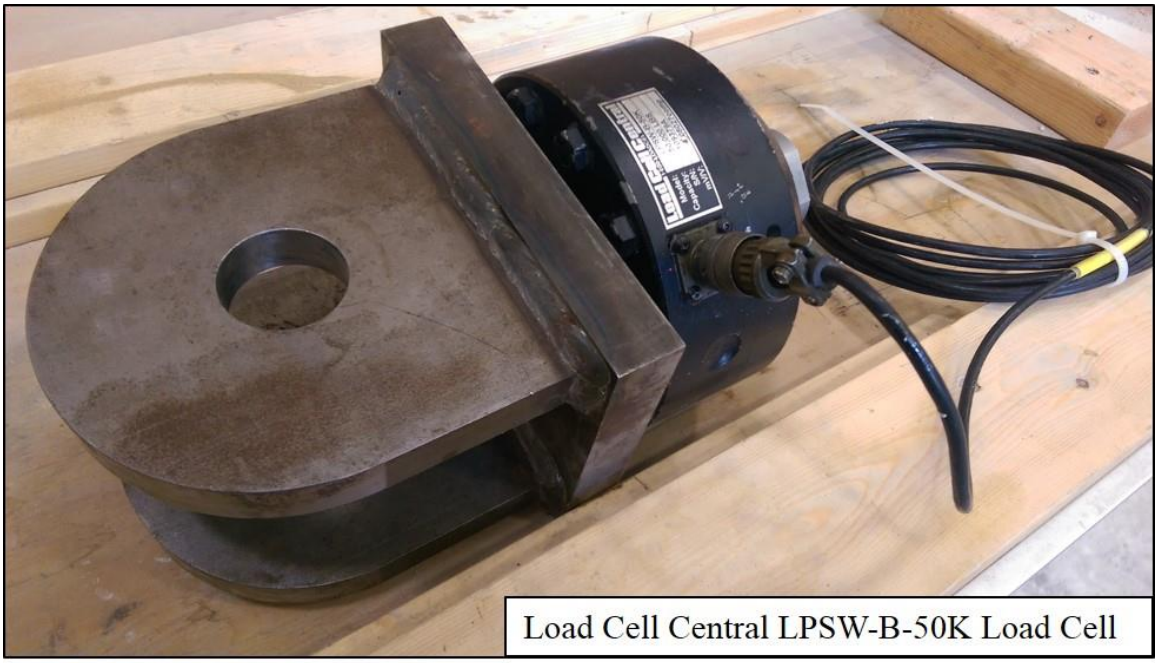

Figure 4-33. Load Cell with Attached Damper Clevis

Instrumentation was wired to terminal blocks according to manufacturer specifications. The channels were connected to a *Pacific 6000* data acquisition system with their proprietary software used for instrumentation calibration and data collection. A total of 16 channels were used for the viscous gap damper setup and 20 channels used for the viscoplastic gap damper setup. The layout of all the experimental instrumentation is found in Figure 4-34 for the viscous gap damper and Figure 4-35 for the viscoplastic gap damper. Each layout has the position, direction, and channel number for the instrument type. Table 4-4 and Table 4-5 provide a reference for each of the instrumentation layouts. Each table has information on the channel number, type of sensor, location, calibration constants, and excitation voltages used for the experiment.

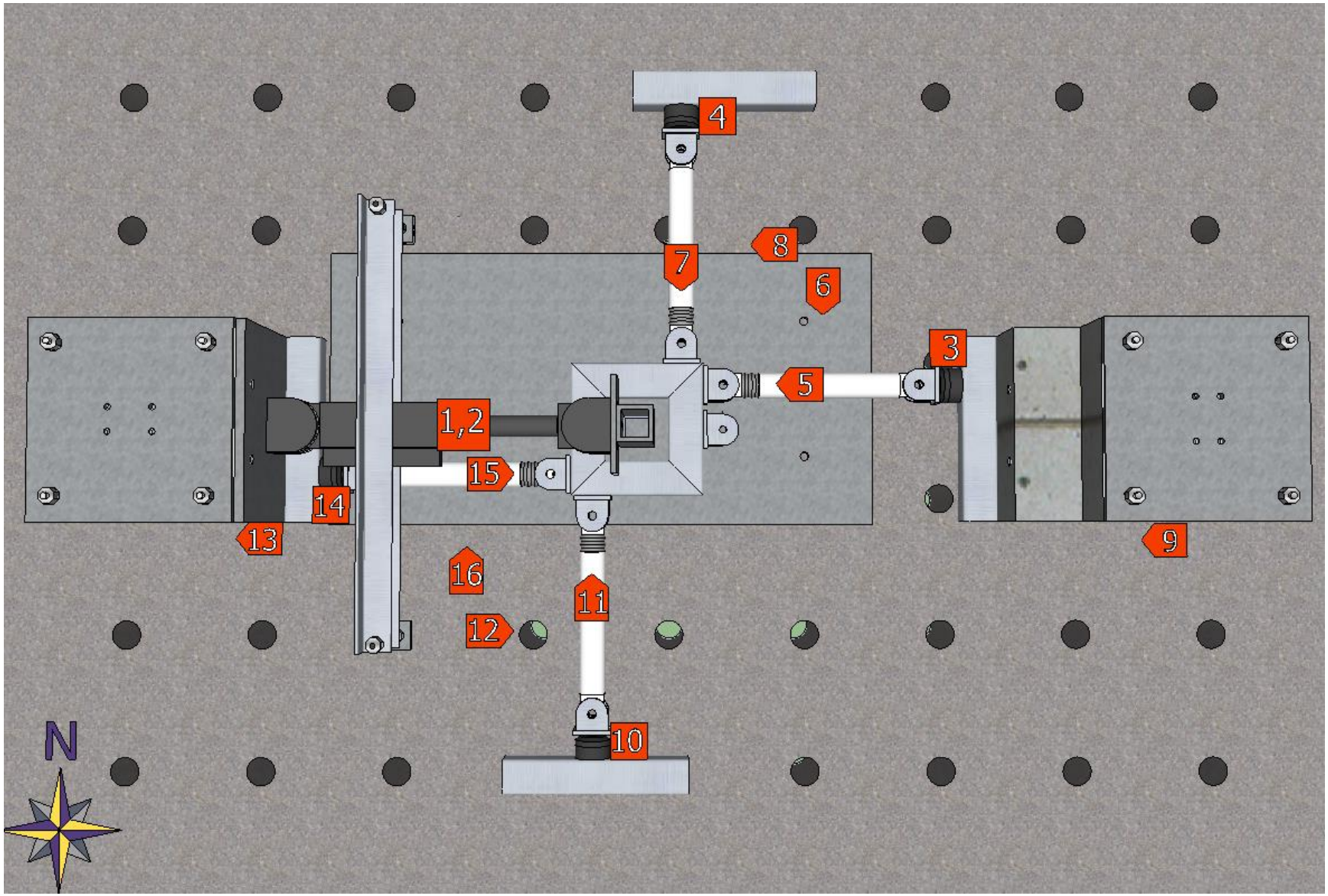

Figure 4-34. Instrumentation Layout for Viscous Gap Damper

Table 4-4. Instrumentation Information for Viscous Gap Damper Setup

Channel Number	Sensor Label	Sensor Type	Comment	Sensor Measurement	Manufacturer Calibration Constant		Excitation Voltage (V)
					Value	Units	
1	Act-LC	Load Cell	Actuator Load Cell	Force	0.1	mV/lb	NA
2	Act-LVDT	LVDT	Actuator LVDT	Displacement	2000	mV/in	NA
3	East-LC	Load Cell	East Damper Load Cell	Force	-4.08801	mV/V/lb	10
4	North-LC	Load Cell	North Damper Load Cell	Force	-4.09464	mV/V/lb	10
5	East-Axial	Stringpot	East Damper Axial Displacement	Displacement	0.969	mV/V/mm	10
6	East-Transverse	Stringpot	East Damper Transverse Displacement	Displacement	0.968	mV/V/mm	10
7	North-Axial	Stringpot	North Damper Axial Displacement	Displacement	0.968	mV/V/mm	10
8	North-Transverse	Stringpot	North Damper Transverse Displacement	Displacement	0.969	mV/V/mm	10
9	East Block	Stringpot	East Reaction Block Displacement	Displacement	0.967	mV/V/mm	10
10	South-LC	Load Cell	South Damper Load Cell	Force	-4.08027	mV/V/lb	10
11	South-Axial	Stringpot	South Damper Axial Displacement	Displacement	0.969	mV/V/mm	10
12	South-Transverse	Stringpot	South Damper Transverse Displacement	Displacement	0.968	mV/V/mm	10
13	West Block	Stringpot	West Reaction Block Displacement	Displacement	0.968	mV/V/mm	10
14	West-LC	Load Cell	West Damper Load Cell	Force	-4.0927	mV/V/lb	10
15	West-Axial	Stringpot	West Damper Axial Displacement	Displacement	0.969	mV/V/mm	10
16	West-Transverse	Stringpot	West Damper Transverse Displacement	Displacement	0.968	mV/V/mm	10

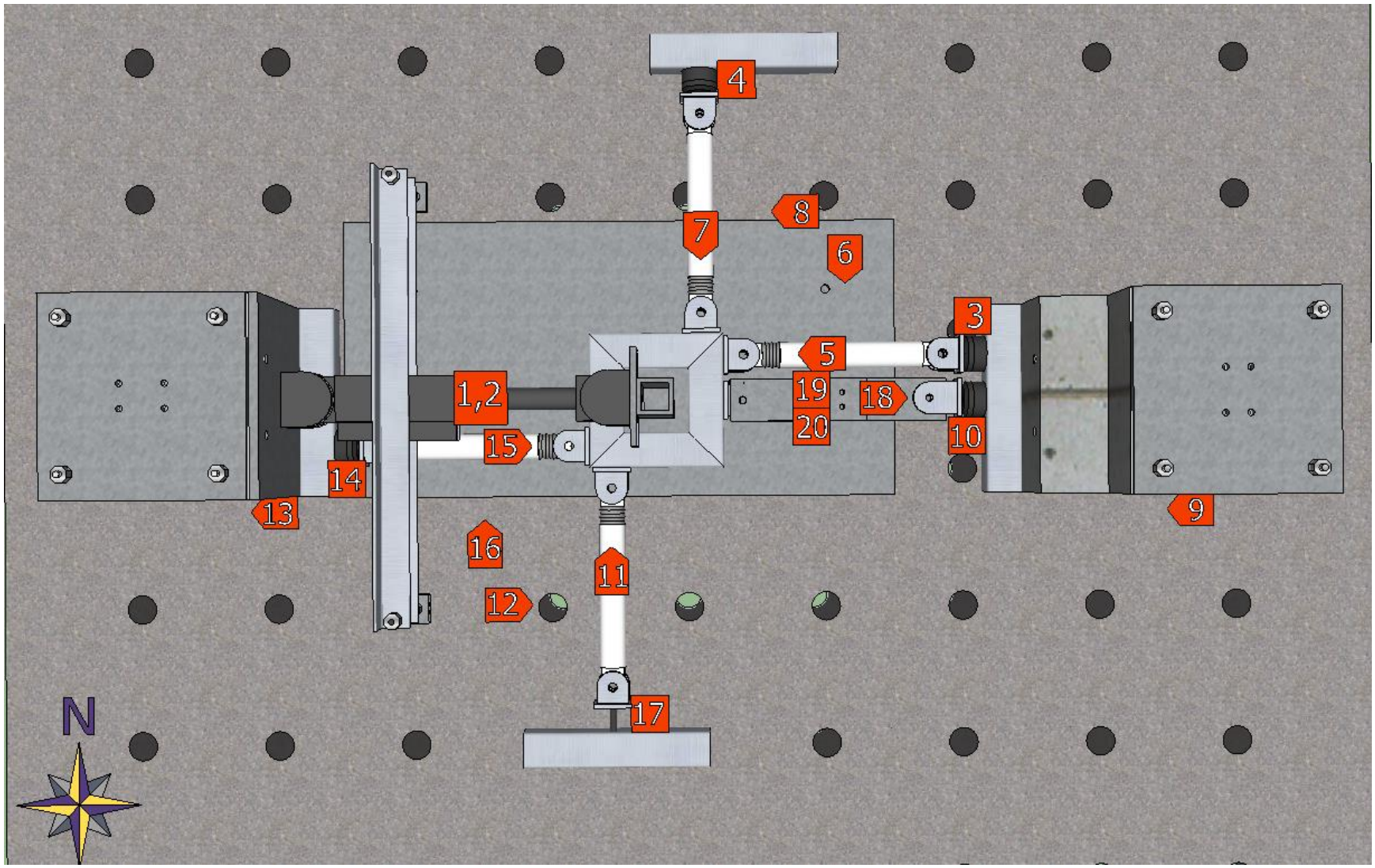

Figure 4-35. Instrumentation Layout for Viscoplastic Gap Damper

Table 4-5. Instrumentation Information for Viscoplastic Gap Damper Setup

Channel Number	Sensor Label	Sensor Type	Comment	Sensor Measurement	Manufacturer Calibration Constant		Excitation Voltage (V)
					Value	Units	
1	Act-LC	Load Cell	Actuator Load Cell	Force	0.1	mV/lb	NA
2	Act-LVDT	LVDT	Actuator LVDT	Displacement	2000	mV/in	NA
3	East-LC	Load Cell	East Damper Load Cell	Force	-4.08801	mV/V/lb	10
4	North-LC	Load Cell	North Damper Load Cell	Force	-4.09464	mV/V/lb	10
5	East-Axial	Stringpot	East Damper Axial Displacement	Displacement	0.969	mV/V/mm	10
6	East-Transverse	Stringpot	East Damper Transverse Displacement	Displacement	0.968	mV/V/mm	10
7	North-Axial	Stringpot	North Damper Axial Displacement	Displacement	0.968	mV/V/mm	10
8	North-Transverse	Stringpot	North Damper Transverse Displacement	Displacement	0.969	mV/V/mm	10
9	East Block	Stringpot	East Reaction Block Displacement	Displacement	0.967	mV/V/mm	10
10	East-FD-LC	Load Cell	East Friction Device Load Cell	Force	-4.08027	mV/V/lb	10
11	South-Axial	Stringpot	South Damper Axial Displacement	Displacement	0.969	mV/V/mm	10
12	South-Transverse	Stringpot	South Damper Transverse Displacement	Displacement	0.968	mV/V/mm	10
13	West Block	Stringpot	West Reaction Block Displacement	Displacement	0.968	mV/V/mm	10
14	West-LC	Load Cell	West Damper Load Cell	Force	-4.0927	mV/V/lb	10
15	West-Axial	Stringpot	West Damper Axial Displacement	Displacement	0.969	mV/V/mm	10
16	West-Transverse	Stringpot	West Damper Transverse Displacement	Displacement	0.968	mV/V/mm	10
17	South-SG-Load Cell	Strain Gage	South Strain Gage Damper Load Cell Full Bridge	Strain	Gage Factor	2.115	5
					Resistance	350	
18	East-Axial-FD	Stringpot	East Friction Device Axial Displacement	Displacement	0.970	mV/V/mm	10
19	Bolt1-SG	Strain Gage	Strain Gage for Bolt 1 Full Bridge	Strain	Gage Factor	2.1	10
					Resistance	120	
20	Bolt2-SG	Strain Gage	Strain Gage for Bolt 2 Full Bridge	Strain	Gage Factor	2.1	10
					Resistance	120	

4.4.5 Load Cases

A total of 24 load cases were tested for the pure viscous device. The input function to the actuator consisted of either a constant velocity triangular function or sine wave. Frequencies of approximately 76.2 mm/s (3 in/sec) and 101 mm/s (4 in/sec) were applied, the higher of which corresponded to the limit of the actuator's pump system. To capture the range in behavior of the system, various geometry setups were implemented. In the concentric setup (Figure 4-36a), the isolation nub was cycled +/- 106.7 mm (4.2 inches) from its original centered position. Eccentric movements, involving an initial isolation nub position of 25.4 or 50.8 mm (1 or 2 in) from center in the direction perpendicular to the stroke (Figure 4-36b), were also simulated. This was meant to capture the gap damper's resistance to eccentric impact. In order to capture the gap damper's response to oblique impacts, movement of a rotated isolation nub was tested. This was done with a concentric rotated setup and eccentric rotated setup, as shown in Figure 4-36c and Figure 4-36d respectively. These tests demonstrated the importance of the dampers transverse to a ground motion for overall stability of the gap damper system due to their increased participation with oblique impacts. A large rotation of 5 degrees was chosen to allow more participation of the transverse dampers. The rotation of the nub was achieved by using 5 degrees shims at the connection of the nub and actuator plate, as shown in Figure 4-37.

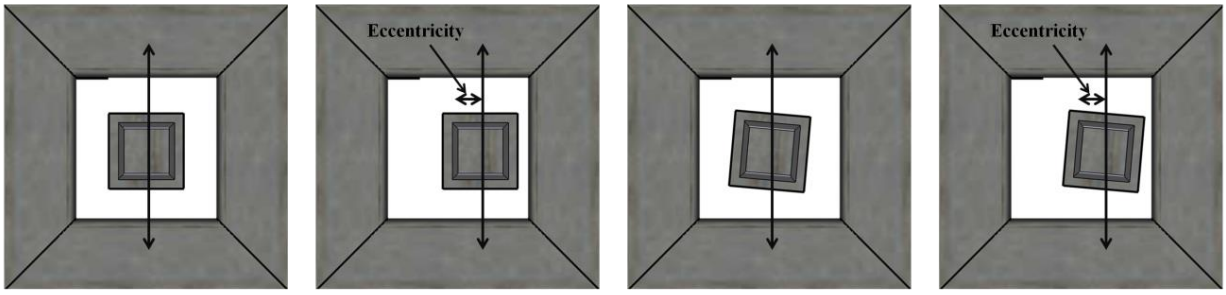

a) Concentric Movement +/- MCE Displacement

b) Eccentric Movement +/- MCE Displacement

c) Rotated Movement +/- MCE Displacement

d) Rotated Movement +/- MCE Displacement with Eccentricity

Figure 4-36. Load Case Arrangements

Figure 4-37. Clockwise Load Case

The load cases run in the viscous gap damper arrangement are summarized in Table 4-6. The system was re-centered in between each load case to eliminate the residual displacements.

Table 4-6. Load Cases for the Viscous Gap Damper

Trial Name	Load Case	Input Frequency (Hz)	Actuator Displacement Range mm (in)	Rotation (5 degrees)*	Eccentricity mm (in)	Wave Form**
E0-0.125Hz-+/-4.2-Sine	1	0.125	+/- 106.7 (4.2)	No	0	Sine
E0-0.2Hz-+/-4.2-Sine	2	0.2	+/- 106.7 (4.2)	No	0	Sine
E0-0.125Hz-+/-4.2-Tri	3	0.125	+/- 106.7 (4.2)	No	0	Tri
E0-0.2Hz-+/-4.2-Tri	4	0.2	+/- 106.7 (4.2)	No	0	Tri
T5CCW-E0-0.125Hz-+/-4.0-Sine	5	0.125	+/- 101.6 (4.0)	CCW	0	Sine
T5CCW-E0-0.2Hz-+/-4.0-Sine	6	0.2	+/- 101.6 (4.0)	CCW	0	Sine
T5CCW-E0-0.125Hz-+/-4.0-Tri	7	0.125	+/- 101.6 (4.0)	CCW	0	Tri
T5CCW-E0-0.2Hz-+/-4.0-Tri	8	0.2	+/- 101.6 (4.0)	CCW	0	Tri
E1-0.125Hz-+/-4.2-Sine	9	0.125	+/- 106.7 (4.2)	No	25.4 (1)	Sine
E1-0.2Hz-+/-4.2-Sine	10	0.2	+/- 106.7 (4.2)	No	25.4 (1)	Sine
E1-0.125Hz-+/-4.2-Tri	11	0.125	+/- 106.7 (4.2)	No	25.4 (1)	Tri
E1-0.2Hz-+/-4.2-Tri	12	0.2	+/- 106.7 (4.2)	No	25.4 (1)	Tri
T5CCW-E1-0.125Hz-+/-4.2-Sine	13	0.125	+/- 106.7 (4.2)	CCW	25.4 (1)	Sine
T5CCW-E1-0.2Hz-+/-4.2-Sine	14	0.2	+/- 106.7 (4.2)	CCW	25.4 (1)	Sine
T5CW-E1-0.125Hz-+/-4.2-Sine	15	0.125	+/- 106.7 (4.2)	CW	25.4 (1)	Sine
T5CW-E1-0.2Hz-+/-4.2-Sine	16	0.2	+/- 106.7 (4.2)	CW	25.4 (1)	Sine
E2-0.125Hz-+/-4.2-Sine	17	0.125	+/- 106.7 (4.2)	No	50.8(2)	Sine
E2-0.2Hz-+/-4.2-Sine	18	0.2	+/- 106.7 (4.2)	No	50.8(2)	Sine
E2-0.125Hz-+/-4.2-Tri	19	0.125	+/- 106.7 (4.2)	No	50.8(2)	Tri
E2-0.2Hz-+/-4.2-Tri	20	0.2	+/- 106.7 (4.2)	No	50.8(2)	Tri
T5CCW-E2-0.125Hz-+/-4.0-Sine	21	0.125	+/- 101.6 (4.0)	CCW	50.8(2)	Sine
T5CCW-E2-0.2Hz-+/-4.0-Sine	22	0.2	+/- 101.6 (4.0)	CCW	50.8(2)	Sine
T5CW-E2-0.125Hz-+/-4.0-Sine	23	0.125	+/- 101.6 (4.0)	CW	50.8(2)	Sine
T5CW-E2-0.2Hz-+/-4.0-Sine	24	0.2	+/- 101.6 (4.0)	CW	50.8(2)	Sine

*CW = Clockwise Rotation, CCW = Counter-Clockwise Rotation (Viewed from above)
**Tri = Constant Velocity

For the viscoplastic gap damper arrangement, calibration of the bolt tension and aggregate wear of the sliding surfaces over the duration of the testing required less load cases. A total of eight load cases were tried for the viscoplastic gap damper system with similar attributes to the viscous load cases. A summary of the viscoplastic gap damper load cases is found in Table 4-7.

Table 4-7. Load Cases for the Viscoplastic Gap Damper

Trial Name	Load Case	Input Frequency (Hz)	Actuator Displacement Range mm (in)	Rotation (5 degrees)*	Eccentricity mm (in)	Wave Form
E0-0.125Hz-+/-4.2-Sine	1	0.125	+/- 106.7 (4.2)	No	0	Sine
E0-0.2Hz-+/-4.2-Sine	2	0.2	+/- 106.7 (4.2)	No	0	Sine
T5CW-E0-0.2Hz-+/-4.0-Sine	3	0.2	+/- 106.7 (4.2)	CW	0	Sine
T5CCW-E0-0.2Hz-+/-4.0-Sine	4	0.2	+/- 106.7 (4.2)	CCW	0	Sine
E2-0.125Hz-+/-4.2-Sine	5	0.125	+/- 106.7 (4.2)	No	50.8(2)	Sine
E2-0.2Hz-+/-4.2-Sine	6	0.2	+/- 106.7 (4.2)	No	50.8(2)	Sine
T5CW-E2-0.2Hz-+/-4.0-Sine	7	0.2	+/- 106.7 (4.2)	CW	50.8(2)	Sine
T5CCW-E2-0.2Hz-+/-4.0-Sine	8	0.2	+/- 106.7 (4.2)	CCW	50.8(2)	Sine

*CW = Clockwise Rotation, CCW = Counter-Clockwise Rotation (Viewed from above)

4.5 Experimental Results

With the gap damper systems in place, instrumentation setup and calibration, and load case protocol established, the testing was completed in May 2013. This section provides an in-depth analysis of the gap damper system behavior. Comparisons are made between different load cases to assess the gap damper's ability to respond to different impact conditions. In addition, comparisons are made between energy dissipation capacity of different loading conditions and comparisons to theoretical values. The data from the experiment are published as *"Component Test of a Gap Damper System to Control Isolator Displacements in Extreme Earthquakes"* in the NEEShub Project Warehouse (Rawlinson T. , Marshall, Ryan, & Zargar, 2014).

4.5.1 Viscous Device

Prior to the analysis of the gap damper performance, the general behavior of the system was evaluated to ensure the system was behaving as anticipated. Numerous plots were generated for each trial to assess the gap damper performance, summarized in Appendix B.

The following plots are presented for two contrasting load cases to compare the differences between gap damper arrangements. The two load cases are Load Case 3 (LC3) (E0-0.125Hz-+/-4.2-Tri) and Load Case 22 (LC22) (T5CCW-E2-0.2Hz-+/-4.0-Sine) chosen due to differences in nub rotation, eccentricity, frequency, and wave form. Figure 4-38 shows the time history plots for the actuator and all four viscous dampers. Actuator input varied between the two load cases with LC3 input as a constant velocity or triangular wave form and LC22 input as a sine wave. The actuator had to ramp up to the desired displacement range and frequency, then complete five cycles before the termination of the trial. As LC22 reached the desired displacement at the input frequency, the actuator struggled to meet the desired input which is why the time history in Figure 4-38b does not look like a sinusoidal wave during full cyclic motion. The east and west dampers are in the direction of the actuator movement and therefore have significantly more participation in the system. Since the dampers are opposing, as one damper contracts, the other one extends. Contraction is defined as negative displacement and extension is defined as positive displacement. When the actuator reverses direction, the dampers are left with residual displacements that are evident in the time histories as plateaus. Since LC3 is a concentric impact without nub rotation, the north and south (transverse) dampers experience very little displacement. The north damper participates slightly in the first impact of the system but this is likely due to a slight misalignment in the setup of the system. Transverse dampers in LC22 have much more participation due to the rotation of the nub. The bumper system has a tendency to align with the angle of the nub, requiring the activation of the transverse dampers until the bumper system reaches an equilibrium point. The transverse dampers are primarily active during the initial rotation of the bumper system.

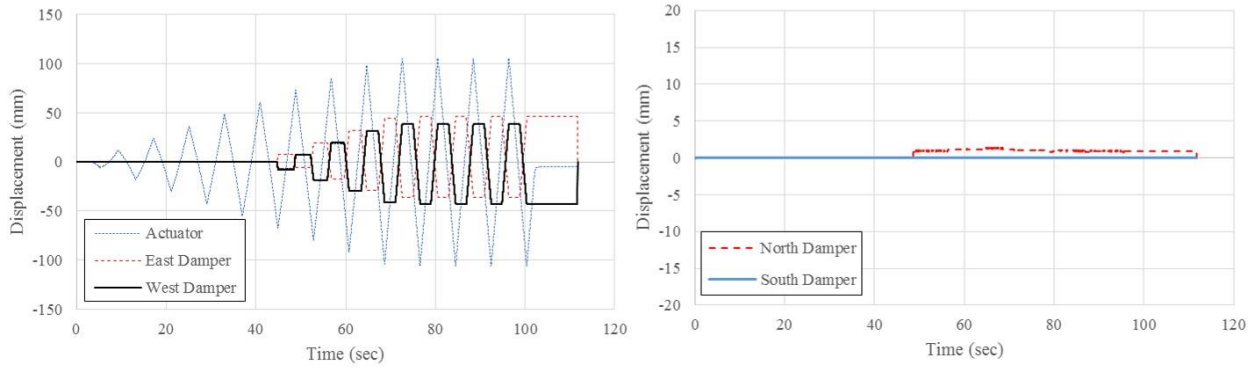

a) Load Case 3

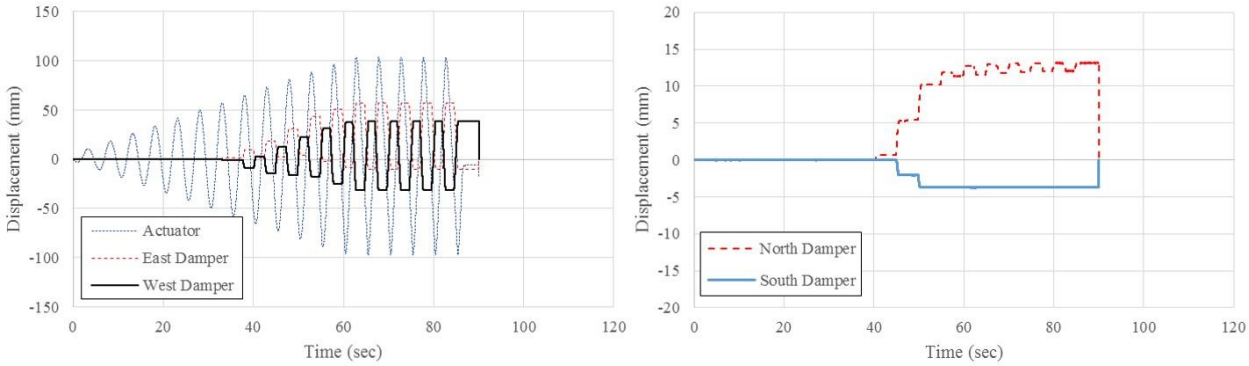

b) Load Case 22

Figure 4-38. Displacement Time Histories for Actuator and Dampers

In addition to the displacement history of the dampers, it was also important to observe the global behavior of the system by looking at the rotation of dampers. Figure 4-39 demonstrates the rotation of LC3 and LC22 for each damper. A positive rotation is representative of a clockwise rotation when viewed from above relative to the damper load cell and clevis attachment. Rotations on the order of 3 degrees for the north and south dampers in LC3 demonstrates the lack of participation of the transverse dampers. The small angles require very little stroke in the dampers with the current geometry of the system. In full scale, beneficial energy dissipation would be more evident in the transverse dampers as the displacements increase and the transverse dampers rotate more. The length of the dampers does not increase proportional to the force capacity which will

result in larger transverse damper rotation and possible contribution to the energy dissipation at the end of the primary damper stroke.

A slight rotation is noticed in east and west dampers for LC3 as the system was not perfectly aligned in the initial state. An exact concentric impact without nub rotation would have very little transverse movement of the east and west dampers. Rotation of the east and west dampers for LC22 was more substantial with a CCW rotation in the first few cycles followed by oscillation around the equilibrium point established once the bumper has fully rotated. The rotated condition of the gap damper system is shown in Figure 4-39 with full actuator extension. East and west dampers have a slight CCW rotation while the north and south dampers have reached full rotation with opposing CCW rotation in the north damper and CW rotation in the south damper.

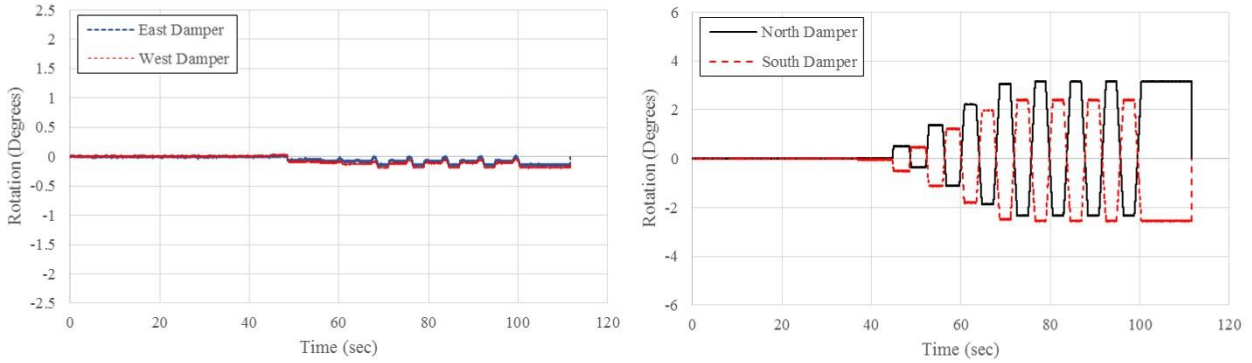

a) Load Case 3

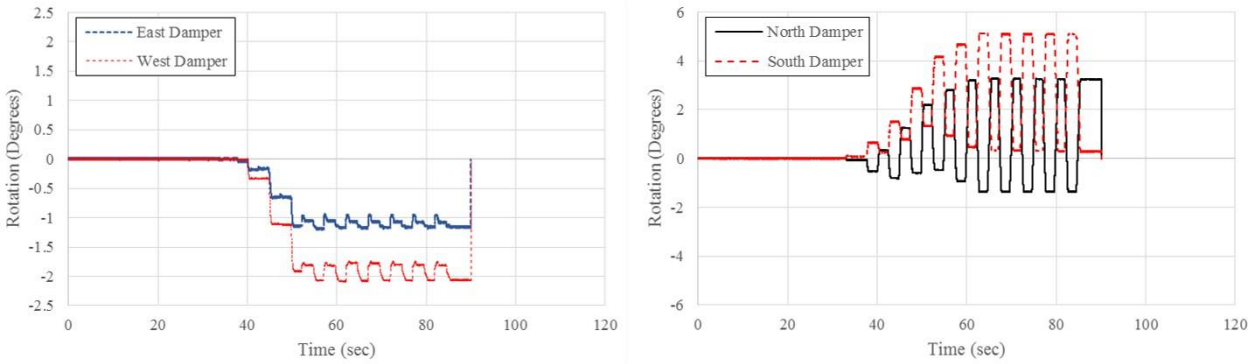

b) Load Case 22

Figure 4-39. Time Histories for Damper Rotation

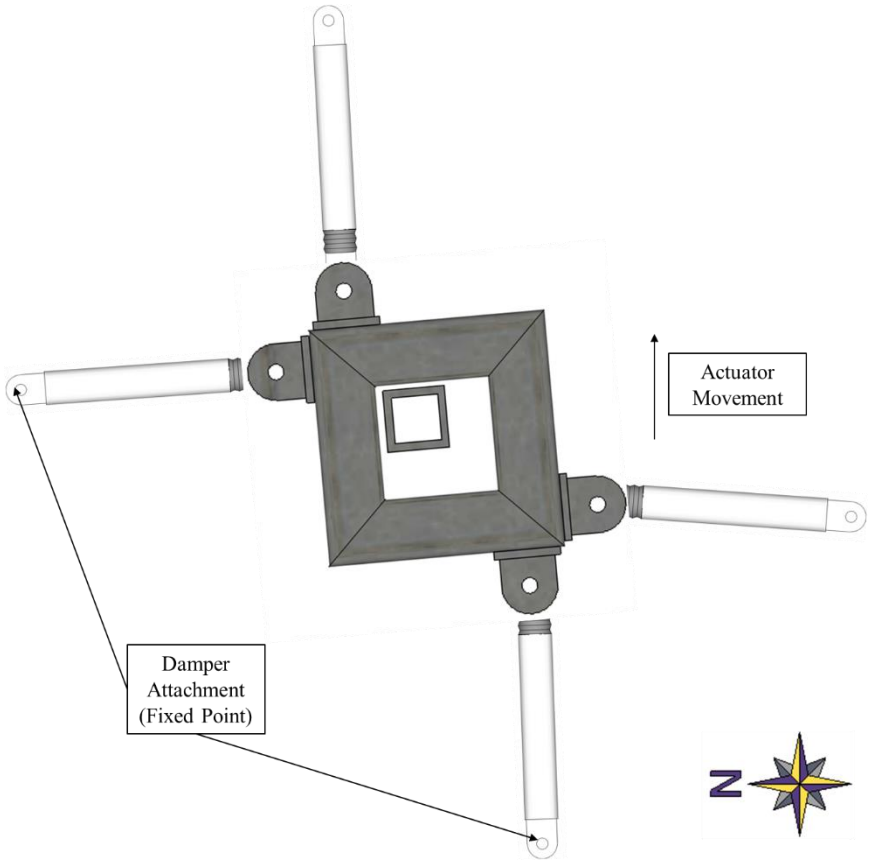

Figure 4-40. Load Case 22 Displaced Condition

In addition to the displacements of the gap damper system, the force in the dampers was also captured using load cells. Figure 4-41 shows the force time history for each damper for LC3 and LC22. As expected, when a primary damper in compression, the opposite damper is in tension, and vice versa. The maximum force in LC22 was greater than the force in LC3 due to higher frequency of the actuator movement. Although the displacement participation was relatively small for the transverse dampers, the force was relatively significant upon activation of the gap damper system with a quick spike. This suggests that although the transverse dampers do not participate much in the overall energy dissipation of the gap damper, reactionary forces assist in the overall stability of the system.

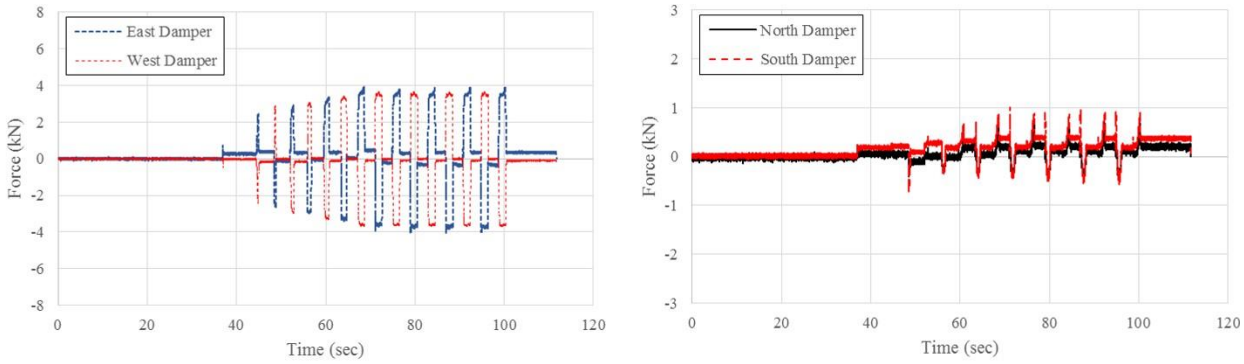

a) Load Case 3

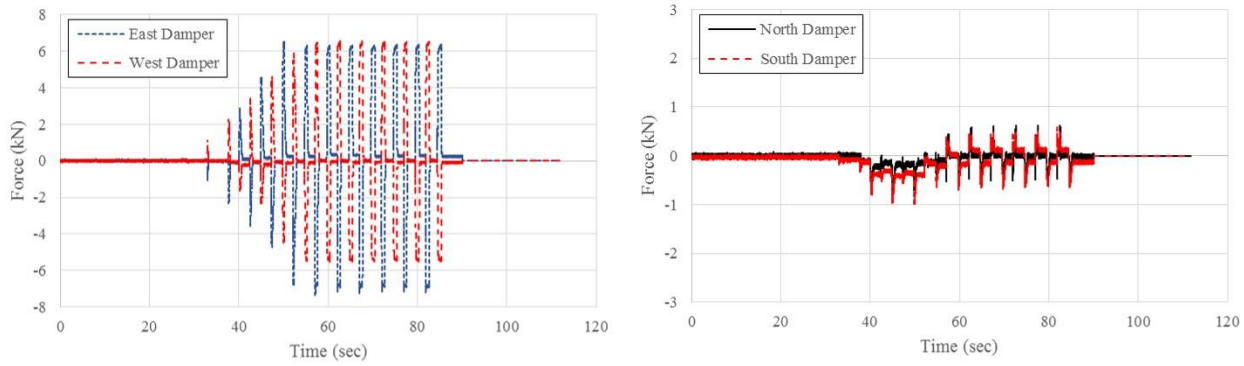

b) Load Case 22

Figure 4-41. Force Time Histories for Dampers

The most significant plot to determine the overall performance of the gap damper is that of the system hysteresis, shown in Figure 4-42. The force in these plots is a summation of the force in each primary damper, with the actuator reaction governing the sign convention. When the actuator is extended, the gap damper is in compression. LC3 yields a hysteretic behavior expected from the system, with a constant force throughout the damper activation due to the constant velocity of the load case. LC22 reaches the desired sine wave behavior for the smaller displacement cycles but became more of a constant velocity behavior for the full cycles due to actuator limitations. The overall force in LC22 is larger than the force in LC3 due to the higher frequency motion of the actuator.

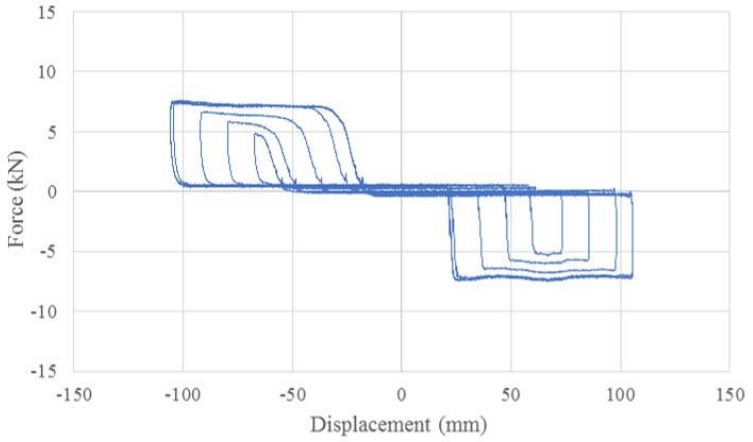

a) Load Case 3

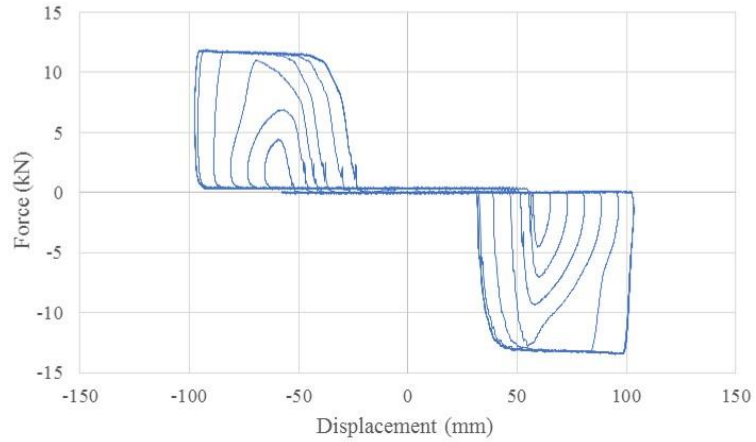

b) Load Case 22

Figure 4-42. System Hysteresis Comparison

The slight slope of the line when the actuator is pulling the gap damper system, rather than abrupt theoretical force increase, is partly a function of the actuator setup. The large eccentricity between the connection of the actuator head and isolation nub impact location results in a slight rotation of the nub, meaning the sudden change in stiffness is not as evident as in the theoretical values. Figure 4-43 illustrates the upward movement of the nub which corresponds with the lifting of the gap damper system on the opposite side. This behavior is only seen in the negative displacement range of the actuator which suggests that an imperfection or misalignment may have contributed to the behavior. Regardless, the tilting of the nub is not expected in the shake table testing due to the rigid connection designed at the nub's interface with the floor above.

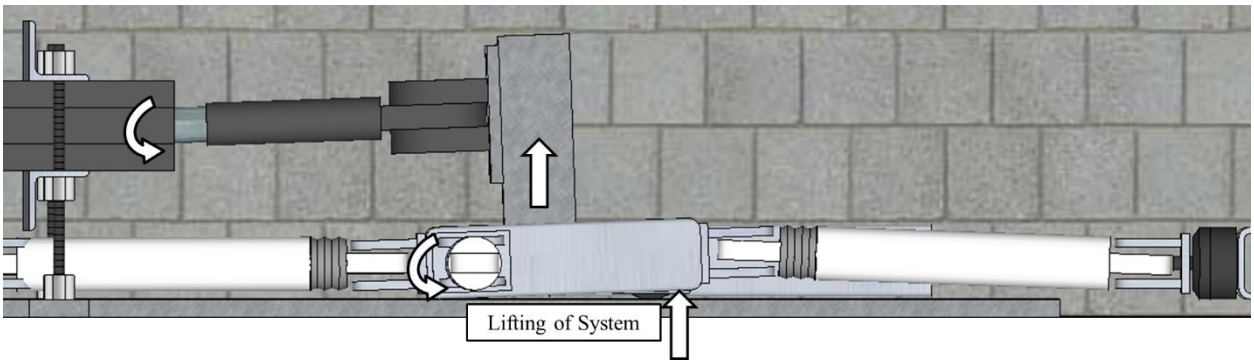

Figure 4-43. System Imperfection (Exaggerated for Demonstration)

Hysteretic plots were generated for each load case with a theoretical curve, as shown in Figure 4-44 for LC1. The theoretical values were based on the velocity in the damper and the nominal damping constant provided by the manufacturer. For LC1, the initial theoretical values indicates that the gap damper system can achieve about 75% of the desired energy dissipation for the system. This shortfall is partly due to the loss of "preload" that was bled out prior to the testing, and thus resulted in slightly altered damper properties. Damper qualification tests, covered in Section 4.4.1, indicate that the damping constants were lower by anywhere from 5-15%. Adjusting the theoretical values to match the damper properties observed in damper qualification tests, the observed data approaches the theoretical values with 89.3% of the theoretical energy dissipation. The close correlation with theoretical values is especially evident in the extension of the actuator but departs from theoretical values in the negative displacement range due to the imperfection in the test setup. All future theoretical values use an adjusted damping constant.

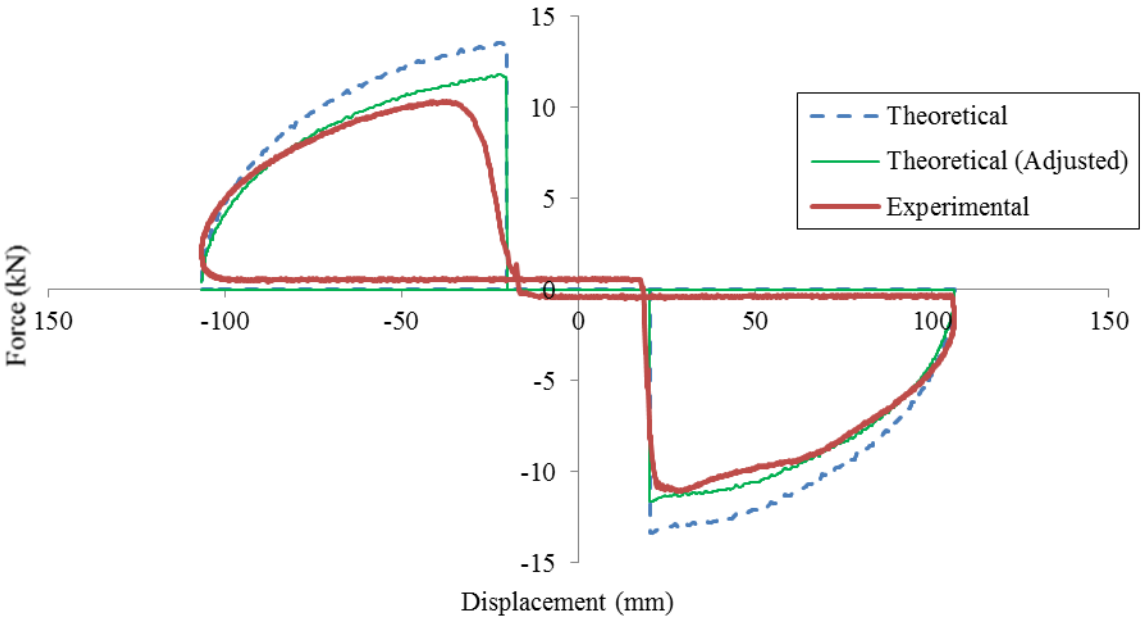

Figure 4-44. Experimental vs. Theoretical (Load Case 1)

Gap damper performance is assessed by comparing the energy dissipation for all 24 load cases, presented in Table 4-8. Energy values are from one complete actuator cycle using the full displacement range and forcing each damper in tension and compression once. The theoretical energy dissipation is based on adjusted theoretical damping constant from damper qualification and damper velocity. The actual energy dissipation is compared to a theoretical energy dissipation to get an overall efficiency of the load case. The efficiency values are normally distributed with a mean of 88.7% and standard deviation of 1.8%. This distribution suggests that the energy dissipation is reliable and repeatable regardless of the load case.

Table 4-8. Experimental Energy Dissipation Results

Load Case	Max Velocity (mm/s)	Displacement Range (mm)	Rotation (5 degrees)	Eccentricity (mm)	Wave Form	Energy Dissipation (J)	Theoretical Energy Dissipation (J)	Efficiency
1	75.9	+/- 106.7	No	0	Sine	1430	1600.9	89.3%
2	87.1	+/- 106.7	No	0	Sine	1914	2178.4	87.9%
3	57.4	+/- 106.7	No	0	Tri	1196	1297.0	92.2%
4	86.9	+/- 106.7	No	0	Tri	1827	2040.2	89.5%
5	68.8	+/- 101.6	Yes	0	Sine	1145	1300.8	88.0%
6	85.6	+/- 101.6	Yes	0	Sine	1681	1937.3	86.8%
7	51.8	+/- 101.6	Yes	0	Tri	1000	1077.8	92.8%
8	81.8	+/- 101.6	Yes	0	Tri	1513	1691.5	89.4%
9	75.9	+/- 106.7	No	25.4	Sine	1385	1545.7	89.6%
10	86.9	+/- 106.7	No	25.4	Sine	1850	2140.3	86.4%
11	56.1	+/- 106.7	No	25.4	Tri	1132	1272.2	89.0%
12	86.4	+/- 106.7	No	25.4	Tri	1786	2005.0	89.1%
13	72.4	+/- 106.7	Yes	25.4	Sine	1347	1509.5	89.2%
14	87.1	+/- 106.7	Yes	25.4	Sine	1817	2100.3	86.5%
15	76.2	+/- 106.7	Yes	25.4	Sine	1377	1491.4	92.3%
16	86.4	+/- 106.7	Yes	25.4	Sine	1699	1927.8	88.1%
17	77.2	+/- 106.7	No	50.8	Sine	1329	1560.0	85.2%
18	87.6	+/- 106.7	No	50.8	Sine	1855	2165.1	85.7%
19	56.1	+/- 106.7	No	50.8	Tri	1142	1279.8	89.2%
20	87.6	+/- 106.7	No	50.8	Tri	1776	2022.1	87.8%
21	72.1	+/- 101.6	Yes	50.8	Sine	1120	1276.0	87.8%
22	89.4	+/- 101.6	Yes	50.8	Sine	1681	1932.6	87.0%
23	70.9	+/- 101.6	Yes	50.8	Sine	1129	1249.3	90.4%
24	86.9	+/- 101.6	Yes	50.8	Sine	1687	1899.2	88.8%
							Mean:	88.7%

The discrepancy in the energy dissipation data between the theoretical and experimental data can be attributed to multiple sources. The seismic dampers are fabricated for a 244.6 kN (55 kip) capacity, yet the loads tested were only a fraction of the capacity, which may have led to inconsistent results. Although there are fairly tight tolerances in the system, there is some give in the connections which may also contribute to the imperfect energy transfer. The majority of the discrepancy is most likely due imperfect test setup that resulted in the lifting of the device upon activation. In addition, a slight slope is also expected due to the compressibility of the fluid in the damper (Taylor & Constantinou, 1998). Although the slight slope and rounded peak force response do not allow full theoretical energy dissipation, this may be beneficial because it will ease the force transition into the superstructure and reduce roof accelerations. The shake table

testing will provide more feedback on the overall efficiencies of the gap damper system. Using this data, adjustments can be made to energy dissipation requirements if needed.

Other meaningful comparisons can be made between load cases to assess the performance of the gap damper system. Figure 4-45 compares load cases 1, 9, and 17, during which the system is subjected to the same max velocity, sinusoidal wave form, and displacement range, but differing eccentricities. A half cycle is used to allow a more precise comparison of the curves. In theory, the summation of the forces in the primary dampers (dampers in the direction of nub travel) should lead to relatively the same hystereses regardless of the contact location along the bumper. This plot demonstrates that this behavior is evident in the gap damper system and that the eccentricity of impact does not affect energy dissipation.

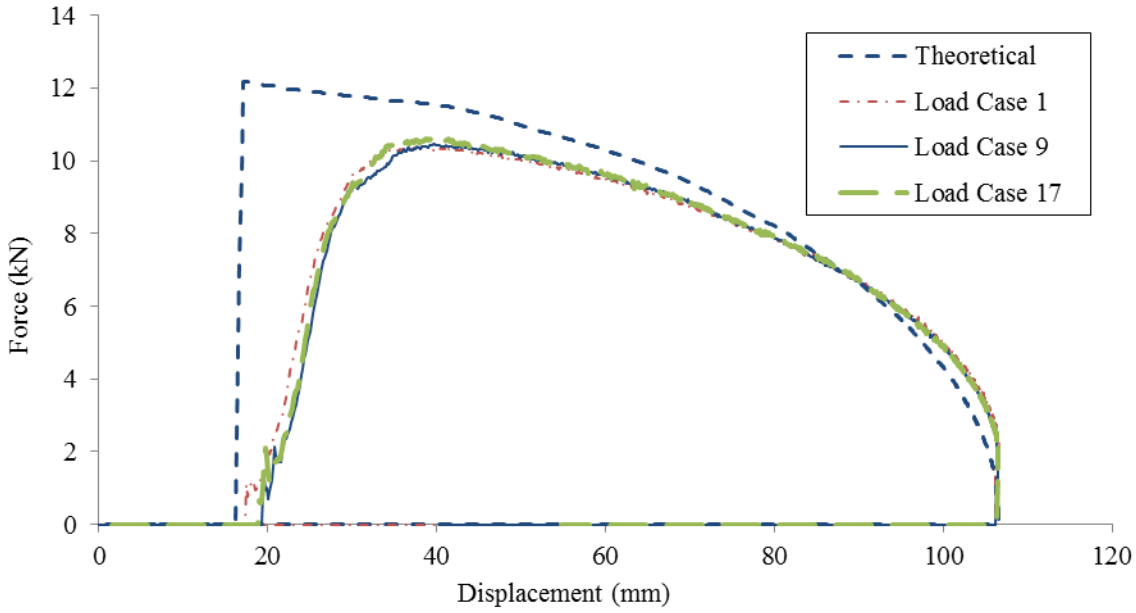

Figure 4-45. Comparison of Load Cases with Varying Eccentricities (Sine Wave)

Figure 4-46 compares load cases 4, 12, and 20, during which the system is subjected to a larger velocity, triangular wave form with the same displacement range, but different

eccentricities. Similar to Figure 4-45, this plot demonstrates similar response regardless of the eccentricity, suggesting that impact eccentricity does not affect the energy dissipation. The hysteresis is square due to the constant velocity of the actuator movement.

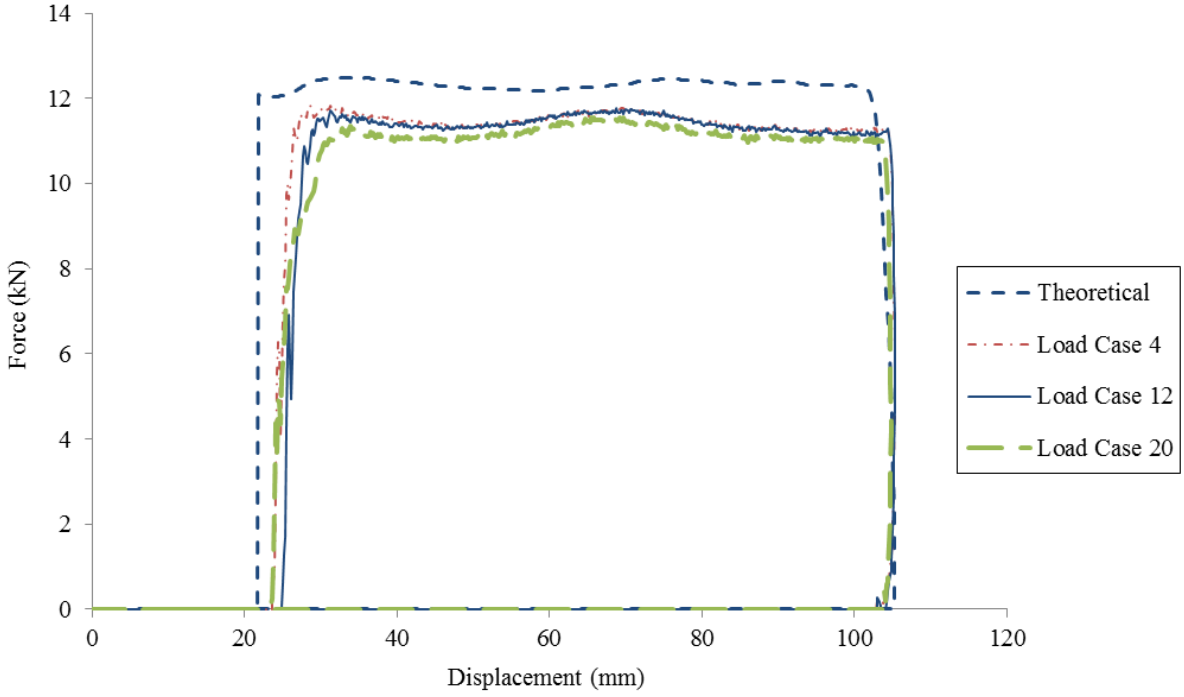

Figure 4-46. Comparison of Load Cases with Varying Eccentricities (Triangular Wave)

Figure 4-47 compares load cases 6, 22, and 24 which involve system setups with similar velocities, displacement range, and all have a nub rotated 5 degrees. Load case 6 is a concentric impact and load cases 22 and 24 involve a 50.4 mm (2 in) eccentric impact. In addition, load cases 6 and 22 are rotated clockwise while load case 24 is rotated counter-clockwise. This comparison is made to further illustrate the repeatable response of the gap damper system regardless of the impact eccentricity or rotation.

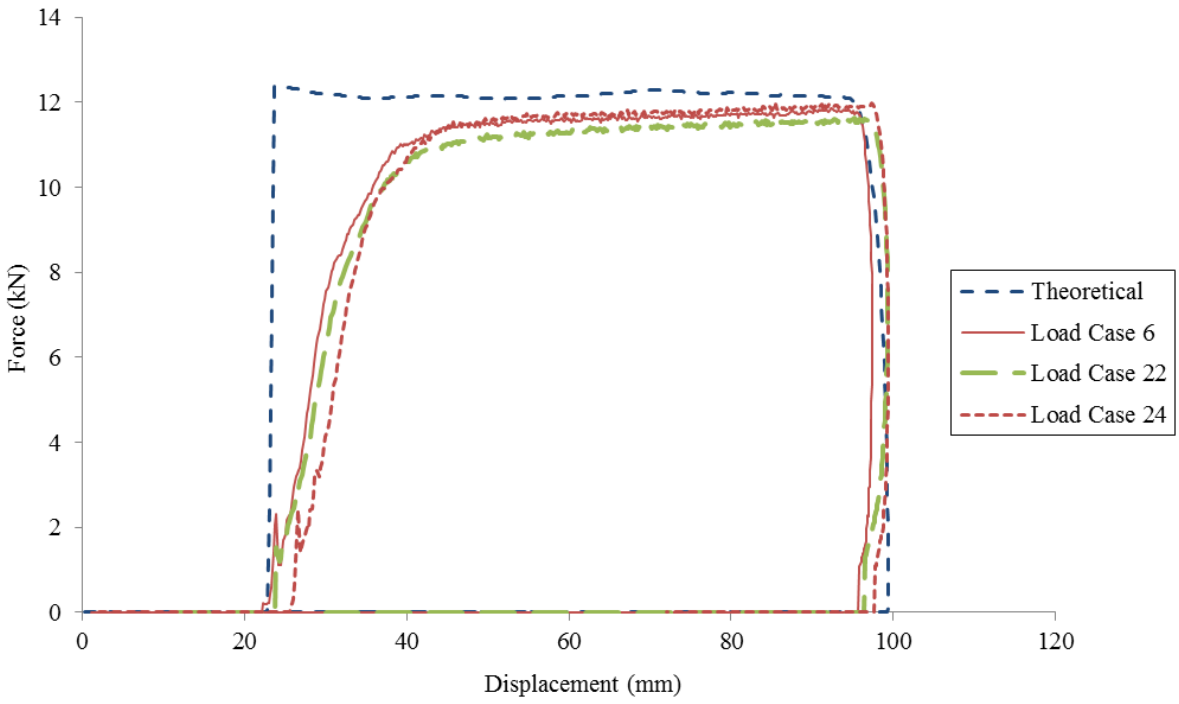

Figure 4-47. Comparison of Load Cases with Varying Eccentricities and Rotations.

The data in Table 4-8 and Figure 4-45-Figure 4-47 are from the final cycles in the actuator motion. During these cycles, the contribution of energy dissipation from the dampers transverse to the direction of motion was negligible, comprising less than a thousandth of the total energy dissipation. For the rotated load cases, the first few cycles in each load case saw more participation from transverse dampers as the bumper became skewed to match the impact angle of the isolation nub. The initial participation of the transverse dampers is evident in Figure 4-48, which shows the force-displacement relationship of the transverse dampers for the first 4 cycles of actuator motion for a concentric impact. In ideal conditions, each transverse damper should participate equally, but this load case shows transverse damper 1 participating more than transverse damper 2. Transverse damper 1 extended out to 25.4 mm (1 in) before the bumper stopped rotating, while the damper on the opposite side only displaced 2.5 mm (0.1 in). Since the dampers cannot be perfectly aligned and the damper properties may vary slightly, the overall system finds a natural pivot point. This

phenomenon should be investigated further in future testing. Load cases without a rotated nub demonstrated displacements on the order of 2.5mm (0.01 in) in the transverse dampers, diminishing the role of dampers and suggesting the bumper system does not rotate unless the nub is also rotated. Although the dampers participated slightly in the system behavior, the velocity in the dampers is very small and they are there primarily for stability with uni-directional movement. With bi-directional movement, the distinction of primary and transverse dampers is dependent on the direction of building motion.

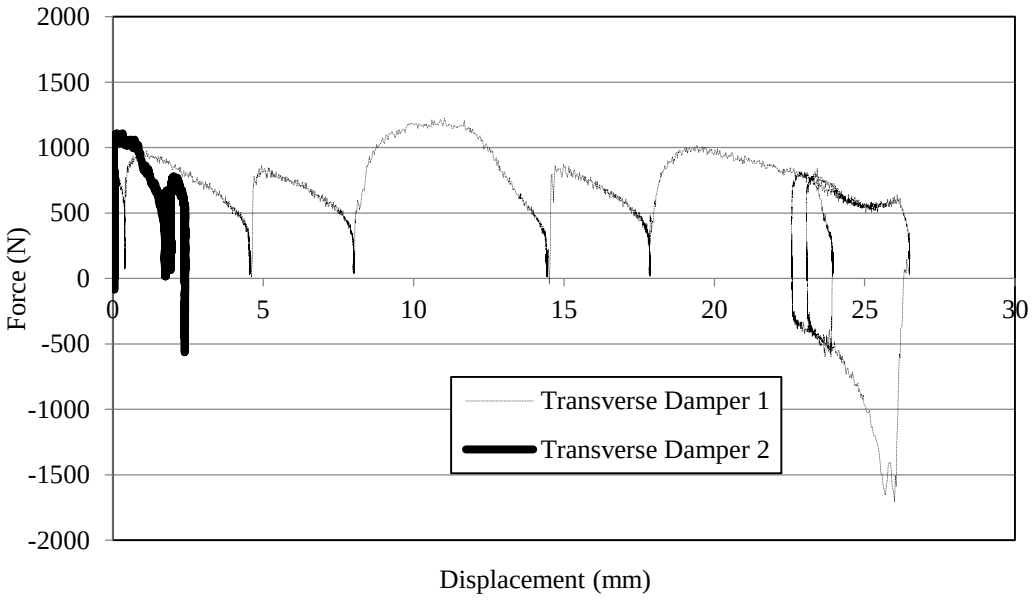

Figure 4-48. Participation of Transverse Dampers in Rotated Impact

The transverse dampers are further analyzed to demonstrate their energy dissipation capabilities. Figure 4-49a illustrates the energy dissipation performance of a concentric impact with no isolation nub rotation (LC2) while Figure 4-49b illustrates the energy dissipation behavior of a concentric impact with a 5 degree rotation of the isolation nub (LC6). The plots represent the cumulative energy dissipation of the gap damper system for the first four cycles of movement, when the transverse dampers were most active. The energy dissipation efficiency for LC 2 was 74.3% at the end of the first four cycles while the efficiency for load case 6 was 71.8%. Generally

speaking, the efficiencies were less in the initial cycles than in the final cycles presented in Table 4-8, which involved the full range of displacement. Transverse energy dissipation for LC2 was 0.005% of the primary direction energy dissipation as opposed to 1.03% for load case 6. Adding the energy from the primary and transverse direction brings the overall energy efficiency to 72.83% for load case 6, similar to the value for LC2. This data provides some insight towards the transverse damper response, but the behavior is not fully understood due to limitations in the data in the early actuator cycles. Overall, with an exaggerated rotation of 5 degrees in the nub, it is likely that the transverse energy dissipation is negligible in most scenarios.

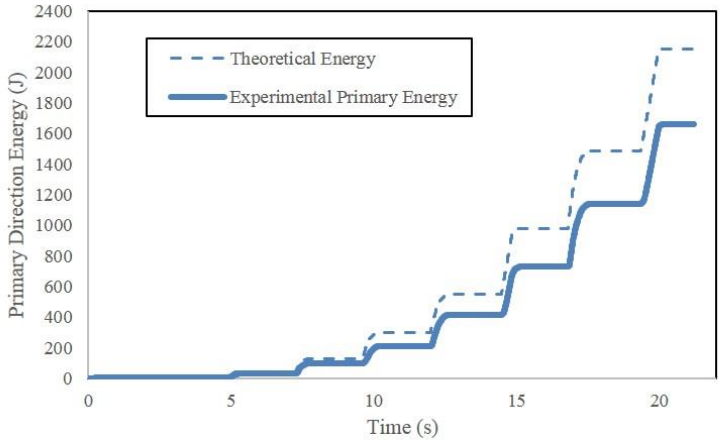

a) Concentric Impact without Rotation

b) Concentric Impact with Rotation

Figure 4-49. Cumulative Energy Dissipation Comparison

The major conclusions of the viscous gap damper testing study are:

- Overall system response is similar to theoretical response, suggesting that the gap damper is capable of achieving the desired behavior.
- Energy dissipation values are shown to be about 85% of the theoretical values consistently across all 24 load cases; which demonstrates the reliability and repeatability of the system.
- The deviation from theoretical response of the gap damper system is attributed to imperfections in the test setup and inherent flexibility and energy losses within the system.
- Load cases involving eccentric impact of the isolation nub were compared in order to illustrate the reliable and consistent energy dissipation capabilities of the system regardless of the impact condition.
- Participation of dampers transverse to the direction of motion was investigated in response to an impact of a rotated structure. The transverse dampers were shown to contribute little energy dissipation in comparison to the primary direction of travel.

Overall, the experimental evaluation of the gap damper device indicates that, given the developed design criteria, the device exhibits the desired performance.

4.5.2 Two-phase Viscoplastic Device

With the completion of the viscous gap damper trials, the friction device was added to the system and the dampers were switched so that the dampers with the smaller damping constant are in the primary direction of actuator movement. Due to the small velocities and small energy dissipation present in the viscous devices, the energy dissipation in the friction device had to be significantly reduced in order to meet the 70% viscous, 30% plastic energy requirement. The friction device

was tested and calibrated at slip forces that correlated with the test structure at UNR, therefore the values estimated for the small slip forces could prove difficult to accomplish. The strains tested in the friction device configuration were on the order of 900 to 1300 microstrain while the slip force for the viscoplastic gap damper called for strains of about 70-80 microstrain to reach a desired slip force of 4.4 kN (1 kip) for the 0.125Hz motions. The strain required for the 0.2Hz motions was about 110-120 microstrain for a desired slip force of 6.7 kN (1.5 kip).

Similar to the viscous gap damper device, numerous plots were generated for each trial to assess the gap damper performance, summarized in Appendix C. Additional plots were added to the analysis to assess the performance of friction device. Since the slip force was an important part of the viscoplastic gap damper behavior, the bolt tension was monitored throughout the duration of the tests. Figure 4-50a shows the bolt tension vs. time for LC1. Total bolt tension was around 10kN at the start of the tests to achieve a slip force around 4-5kN. Tensions varied from 8kN to 16 kN throughout the test, suggesting an unpredictable slip behavior. In addition, the force in the friction device was measured throughout the test, as shown in Figure 4-50b. Slip forces were relatively consistent around 12kN but did not correlate well with the desired slip force of 4-5kN. This behavior suggests that the estimated tension in the bolts may not have been accurate in the lower strain ranges. Deterioration of the sliding surfaces may have also contributed to this poor performance. Finally, Figure 4-50c demonstrates the typical hysteretic behavior of the friction device. The two-stage slip behavior noticed in the friction device property testing of Section 4.4.2 is still present in the viscoplastic testing. The initial slip force seems to correlate better with the desired slip force of the friction device with the final slip force at least twice the expected value.

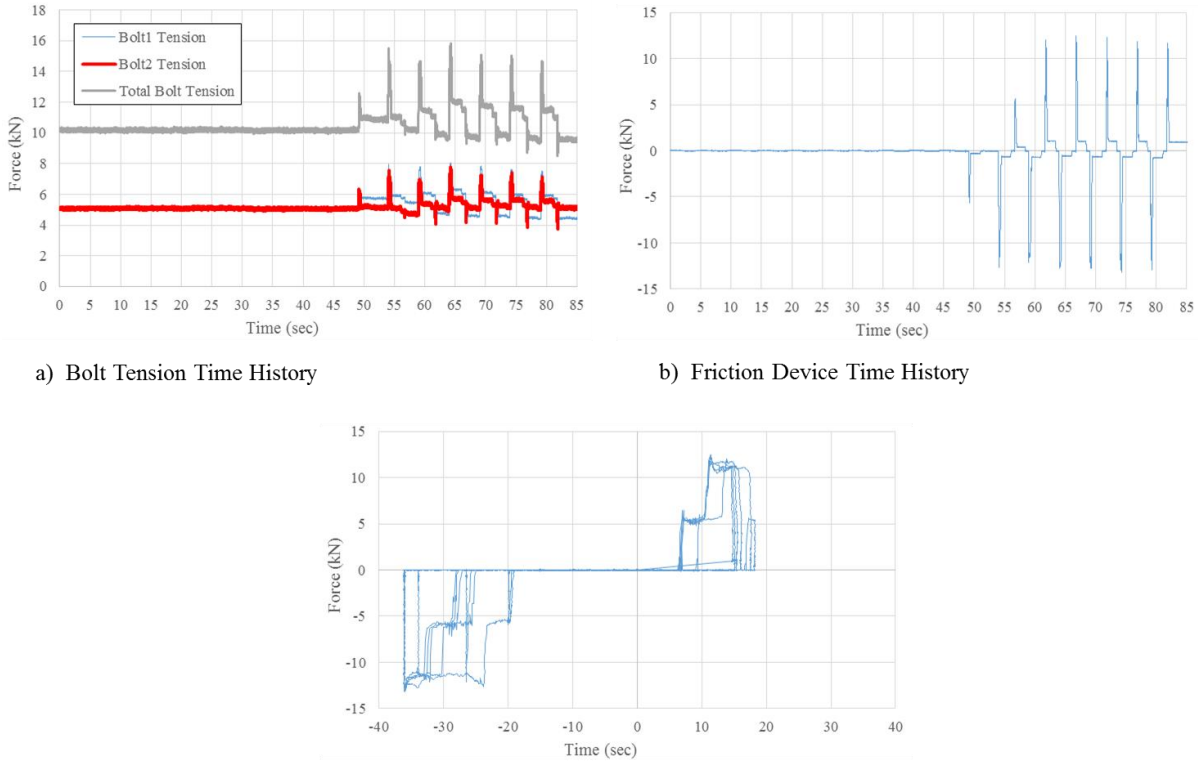

a) Bolt Tension Time History

b) Friction Device Time History

c) Friction Device Hysteresis

Figure 4-50. Friction Device Plots (Load Case 1)

Since the behavior of the viscous gap damper system was defined in the previous section, meaningful comparisons could be made to the viscoplastic device to see if there were differences. For the most part, the overall behavior of the two prototypes was similar. Figure 4-51 compares the rotation of two identical load cases for the viscous gap damper and viscoplastic gap damper to assess the global behavior of the system. Rotations are similar with the exception of the end of the trials where the north and east dampers approach oscillation about a more neutral point near zero degrees. This is due to the placement of the friction device at the center of the bumper system. Since the reaction of the friction device was coincidental with a 90 degree plane and the bumper system is rotated, there is slight perpendicular resultant that pushes the bumper system in the north direction. This decreases the eccentricity for a CCW movement (Figure 4-52) and increases the eccentricity for a CW movement.

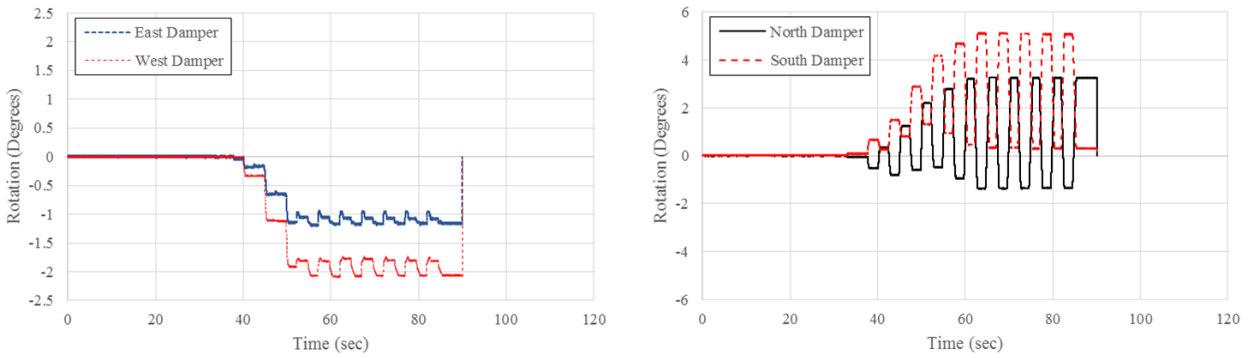

a) Load Case 22 (Viscous Gap Damper)

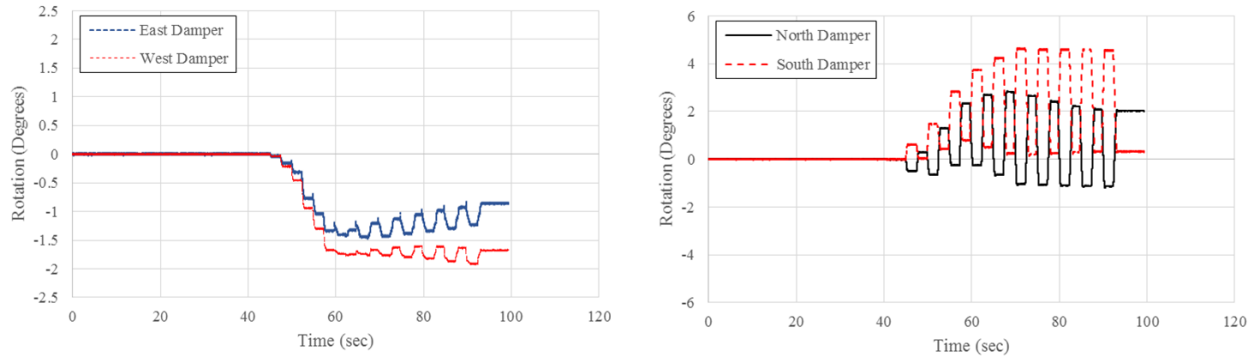

b) Load Case 7 (Viscoplastic Gap Damper)

Figure 4-51. Gap Damper Prototype Rotation (T5CCW-E2-0.2Hz-+/-4.0-Sine)

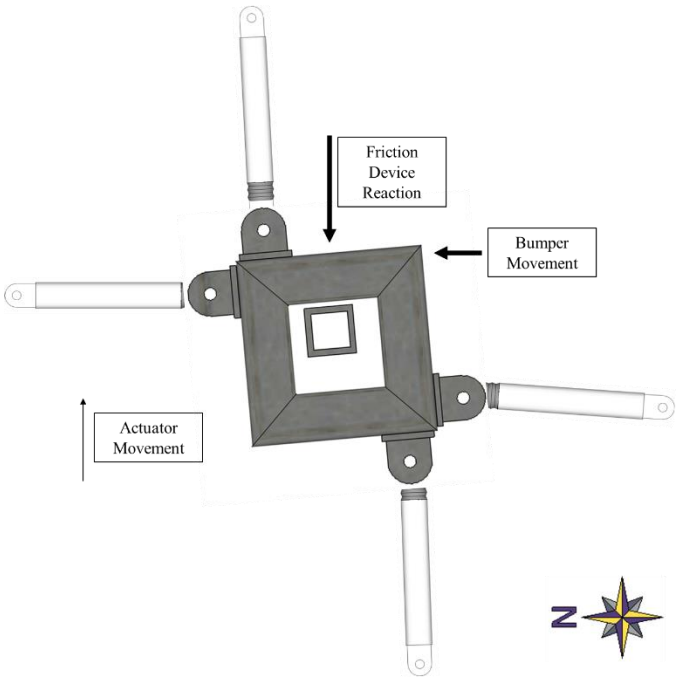

Figure 4-52. Bumper Movement with Eccentric Impact

The lateral movement of the bumper system is evident in the displacement time histories as well, as shown in Figure 4-53. The south damper initially compressed as the bumper rotated counter-clockwise and oscillated about this location. As the bumper system moved to the north, the displacement in the south damper started to approach zero displacement and the north damper was compressed further. Besides the obvious differences in the force characteristics of the system due to the addition of the plastic behavior, this was the only discernable difference noticed in the global behavior of the system. This is likely not to affect the energy dissipation capacity of the viscoplastic system.

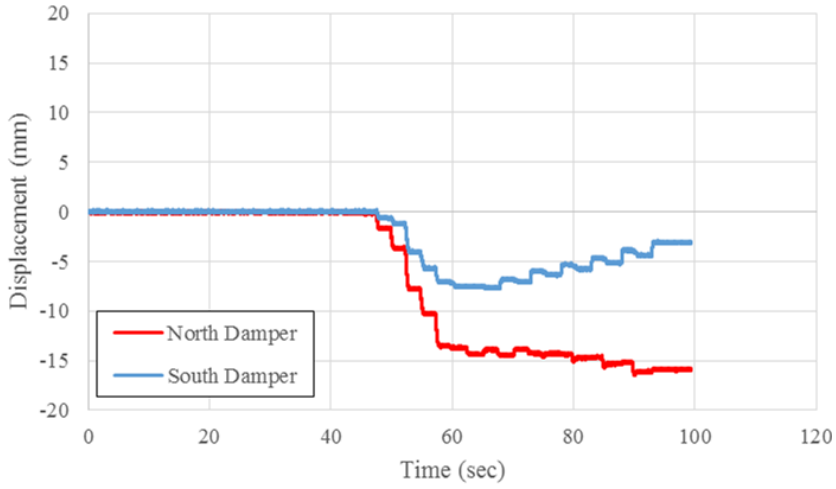

Figure 4-53. Viscoplastic Gap Damper Displacement Time History

Similar to the viscous gap damper device, comparisons were made between the energy dissipation capacities of the different load cases and compared to theoretical values. Although the load cases are intended to reach a desired displacement and frequency, the actuator was not always able to achieve the input. Theoretical values are based on the achieved velocities and displacements, not the input values; therefore, the certain load cases may not be directly comparable even though the input were identical. This is especially true for the higher frequency motions as the actuator was not able to achieve the desired inputs.

Comparisons were first made between the viscous components of the viscoplastic system, as shown in Figure 4-54. Generally speaking the viscous behavior was similar to the viscous gap damper system. The primary difference is the loss of load in the viscous devices at the activation of friction device. For this reason, the overall viscous efficiency was slightly less than the 88.7% observed in the viscous gap damper system.

Table 4-9 summarizes the viscous energy dissipation for all eight load cases. Fairly consistent behavior is observed with an average of 77.0% efficiency when compared to theoretical values. The theoretical values were based on the velocity measured in the dampers and the adjusted damping constants from Section 4.4.1.

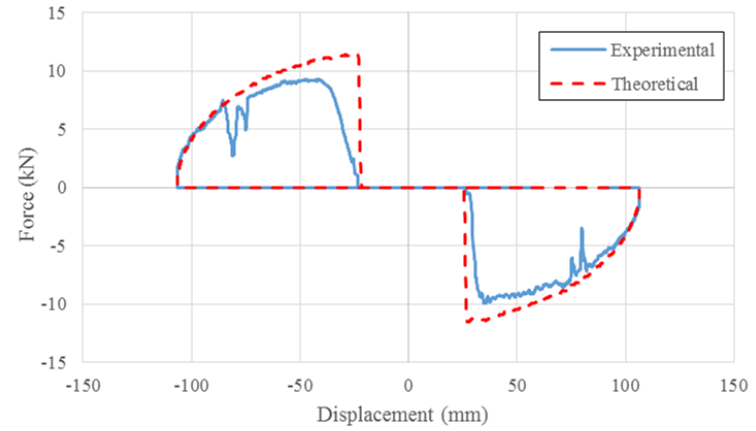

a) Viscous Hysteresis

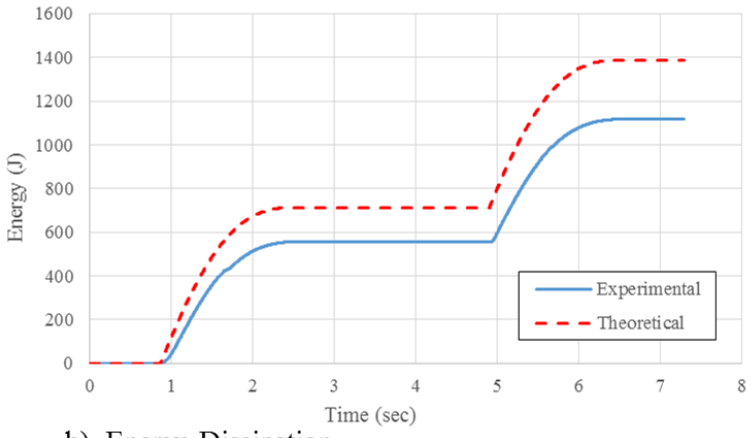

b) Energy Dissipation

Figure 4-54. Viscous Device in Viscoplastic System

Table 4-9. Viscous Energy Dissipation for Viscoplastic Gap Damper

Trial Name	Load Case	Actual Viscous Energy	Theoretical Viscous Energy	Efficiency
E0-0.125Hz-+/-4.2-Sine	1	1122	1393	80.6%
E0-0.2Hz-+/-4.2-Sine	2	1452	1852	78.4%
T5CW-E0-0.2Hz-+/-4.0-Sine	3	1331	1759	75.7%
T5CCW-E0-0.2Hz-+/-4.0-Sine	4	1448	1933	74.9%
E2-0.125Hz-+/-4.2-Sine	5	1096	1395	78.6%
E2-0.2Hz-+/-4.2-Sine	6	1521	1980	76.8%
T5CW-E2-0.2Hz-+/-4.0-Sine	7	1340	1734	77.3%
T5CCW-E2-0.2Hz-+/-4.0-Sine	8	1223	1657	73.8%
			Mean:	77.0%

*CW = Clockwise Rotation, CCW = Counter-Clockwise Rotation (Viewed from above)

A similar comparison was made for the friction device with a large variance in the results. Figure 4-55 compares the experimental plastic behavior and theoretical behavior in LC1. With the slip forces much higher than intended for load case, the experimental energy dissipation was much higher than the desired energy dissipation (156.6%). This is important as too much energy in in the friction device could result in high accelerations in the superstructure. If this behavior was consistent, adjustments could be made to the friction device calibration to solve the problem. Unfortunately, the achieved energy dissipation in the load cases with higher frequencies was often less than the theoretical energy dissipation with no clear pattern of behavior. Table 4-10 summarizes the plastic energy dissipation for all of the load cases with energy efficiencies ranging from 40.4% to 156.6%. Although the average values was 96.9%, the spread of the data is unacceptable for reliable energy dissipation from the friction device. More research is clearly necessary for the success of a friction device in the gap damper system.

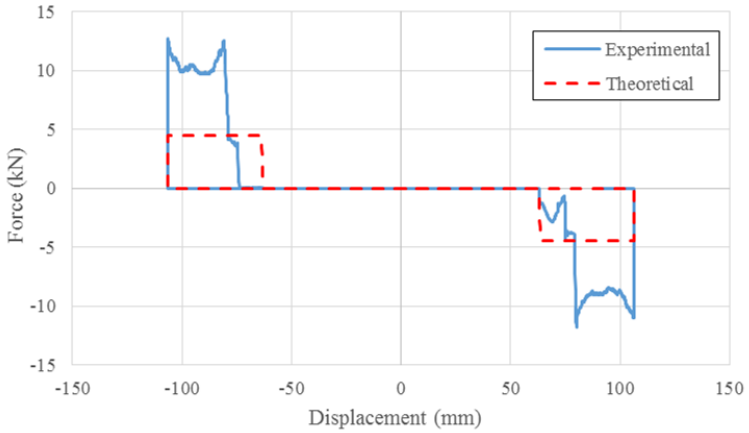

a) Plastic Hysteresis

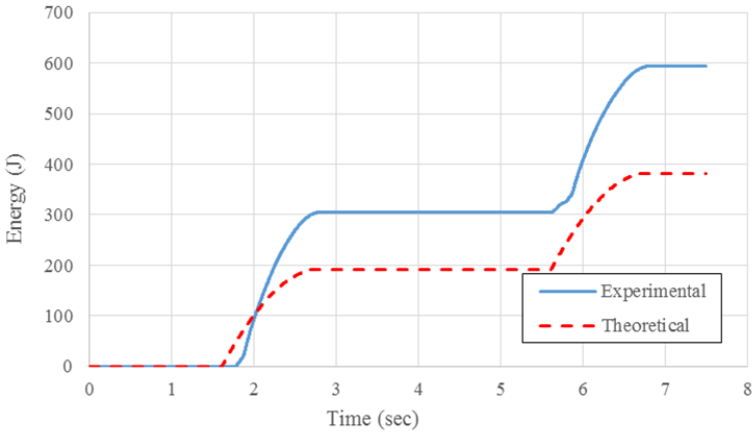

b) Energy Dissipation

Figure 4-55. Plastic Device in Viscoplastic System

Table 4-10. Plastic Energy Dissipation for Viscoplastic Gap Damper

Trial Name	Load Case	Actual Plastic Energy	Theoretical Plastic Energy	Efficiency
E0-0.125Hz-+/-4.2-Sine	1	595	382	156.6%
E0-0.2Hz-+/-4.2-Sine	2	372	500	74.4%
T5CW-E0-0.2Hz-+/-4.0-Sine	3	313	489	64.0%
T5CCW-E0-0.2Hz-+/-4.0-Sine	4	516	524	98.5%
E2-0.125Hz-+/-4.2-Sine	5	596	383	155.8%
E2-0.2Hz-+/-4.2-Sine	6	522	518	100.6%
T5CW-E2-0.2Hz-+/-4.0-Sine	7	350	414	84.5%
T5CCW-E2-0.2Hz-+/-4.0-Sine	8	168	417	40.4%
			Mean:	96.9%

*CW = Clockwise Rotation, CCW = Counter-Clockwise Rotation (Viewed from above)

Combining the two previous plots, a combined system hysteresis can be plotted to assess the overall behavior of the system. Figure 4-56 compares the experimental and theoretical values for LC1. Although the slip force for the friction device was difficult to control, the system hysteresis does resemble the overall behavior desired for the viscoplastic system. For LC1, the shortfall in viscous energy dissipation was actually overcome with the plastic energy dissipation for an overall efficiency of 96.7%. Table 4-11 summarizes the total energy dissipation for the load cases with values varying from 67.1% to 96.7% and an average of 81.3%.

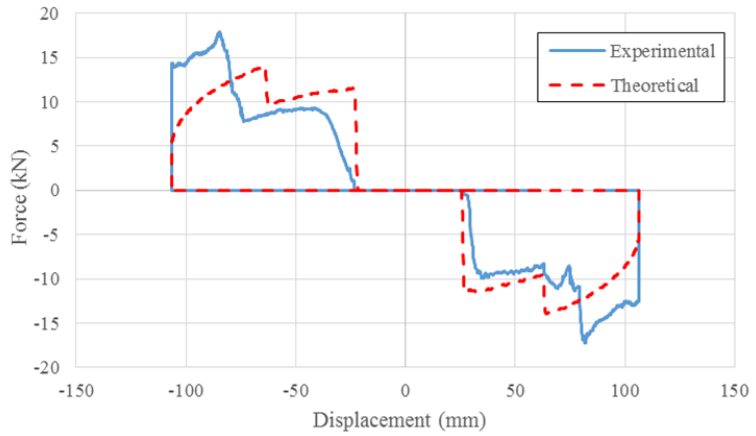

a) Total Hysteresis

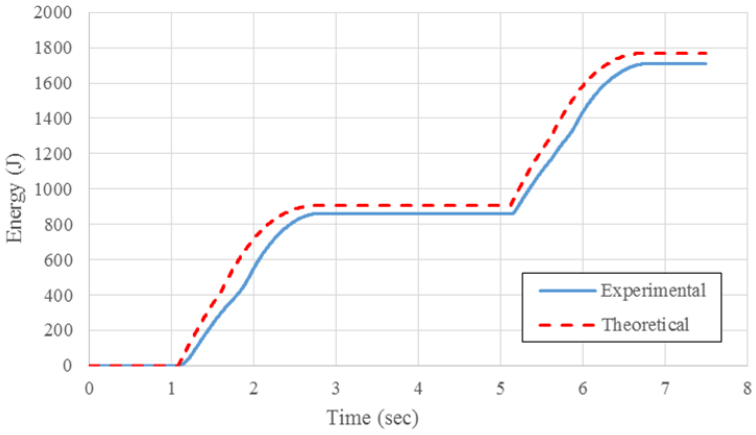

b) Energy Dissipation

Figure 4-56. Total Device Behavior in Viscoplastic System

Table 4-11. Total Energy Dissipation for Viscoplastic Gap Damper

Trial Name	Load Case	Actual Total Energy	Theoretical Total Energy	Efficiency
E0-0.125Hz-+/-4.2-Sine	1	1717	1775	96.7%
E0-0.2Hz-+/-4.2-Sine	2	1824	2352	77.5%
T5CW-E0-0.2Hz-+/-4.0-Sine	3	1644	2248	73.2%
T5CCW-E0-0.2Hz-+/-4.0-Sine	4	1964	2457	79.9%
E2-0.125Hz-+/-4.2-Sine	5	1693	1777	95.3%
E2-0.2Hz-+/-4.2-Sine	6	2043	2498	81.8%
T5CW-E2-0.2Hz-+/-4.0-Sine	7	1691	2148	78.7%
T5CCW-E2-0.2Hz-+/-4.0-Sine	8	1391	2074	67.1%
			Mean:	81.3%

*CW = Clockwise Rotation, CCW = Counter-Clockwise Rotation (Viewed from above)

Overall, the best performance was noticed in the lower frequency motions (LC1 and LC5). Similar to the viscous gap damper comparisons, the two eccentricities were compared to find any noticeable differences in energy dissipation capacity (Figure 4-57). This comparison suggests that, even though the plastic action is not desirable, the eccentricity has little effect on the overall performance of the system.

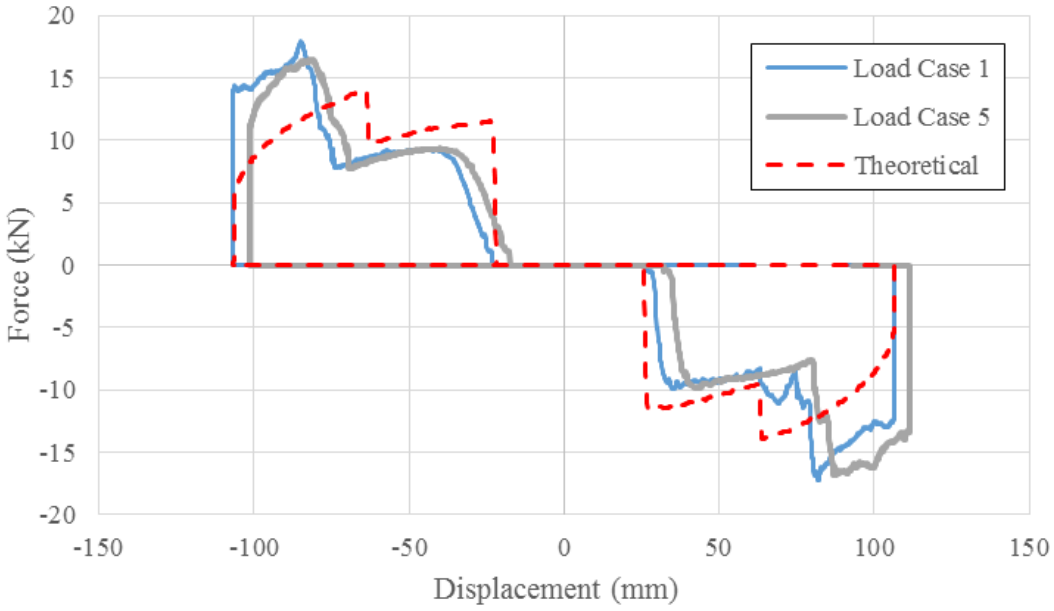

Figure 4-57. Comparison of Eccentricities

The major conclusions of the viscoplastic gap damper testing study are:

- Overall system response is a departure from theoretical response due to difficulties controlling the friction device behavior. Controlling the strain in the bolts at the small amount of tension required in the device may have resulted in the large variance in response.
- Global behavior of the gap damper system is similar to that of the viscous gap damper system with the friction device slightly altering overall behavior.
- Energy dissipation values are shown to be about 77.0% of the theoretical values for the viscous portion of the viscoplastic device with relatively repeatable behavior. Energy dissipation varied largely for the friction device with values ranging from 40.4% to 156.6% of the desired energy dissipation. Overall energy dissipation ranged from 67.1% to 97.6% with an average of 81.3%.
- Although the desired performance of the friction device was not achieved, the general shape of the hysteresis was observed. Eccentric impacts had no observable effect on the energy dissipation capacity of the system.

4.6 Recommendations

At the conclusion of the prototype testing at Auburn University's Structural Research Laboratory, the viscous gap damper system is a clear favorite for the shake table testing. The gap damper system demands reliability and repeatability to be effective system in the mitigation of displacements in extreme events. As the last line of defense against potential collapse of a structure, the behavior needs to be well understood and controlled. The viscoplastic gap damper device, in its current state, does not provide the reliable behavior necessary for the system. Further research into the friction behavior with consideration of other slip surfaces and better control of

bolt tension is necessary for success of the device. For these reasons, and time and resource constraints with the shake table test, the viscous device is the only device considered further in this research.

Observations were made during testing of the viscous gap damper system that may help create a more efficient gap damper system. Figure 4-58 demonstrates three potential design changes that could result in a better load transfer from the nub to the dampers.

1. The shims that were placed between the clevis and the damper allowed some vertical movement of the damper. The rotation of the damper resulted in out of plane forces that may detract from the overall performance. New damper shims were fabricated for the shake table test that eliminated the extra space between the damper attachment and the clevis. Using the new shims and leveling the dampers should result in a better load transfer.
2. The rounded edges of the HSS bumper system may have allowed the bumper system to roll up on the edges. Eliminating the rounded edges and adding a sharp edge should result in a better load transfer.
3. Flexure of the nub may result in an inefficient load transfer into the dampers as the nub and bumper make a flush contact. Nub flexure paired with the rounded edges of the bumper system would result in the tilting of the system. Shortening the distance between the nub connection and bumper would reduce the flexure in the nub. This could be done by shortening the nub and/or raising the bumper system closer to the floor above using a pedestal that the bumper could slide on.

In addition to potential design changes, the shake table testing should also consider the modified damping constants of Section 4.4.1. The dampers may behave differently in the higher

load ranges but if the energy dissipation is less than anticipated, the damper property calibration may provide insight towards the discrepancies.

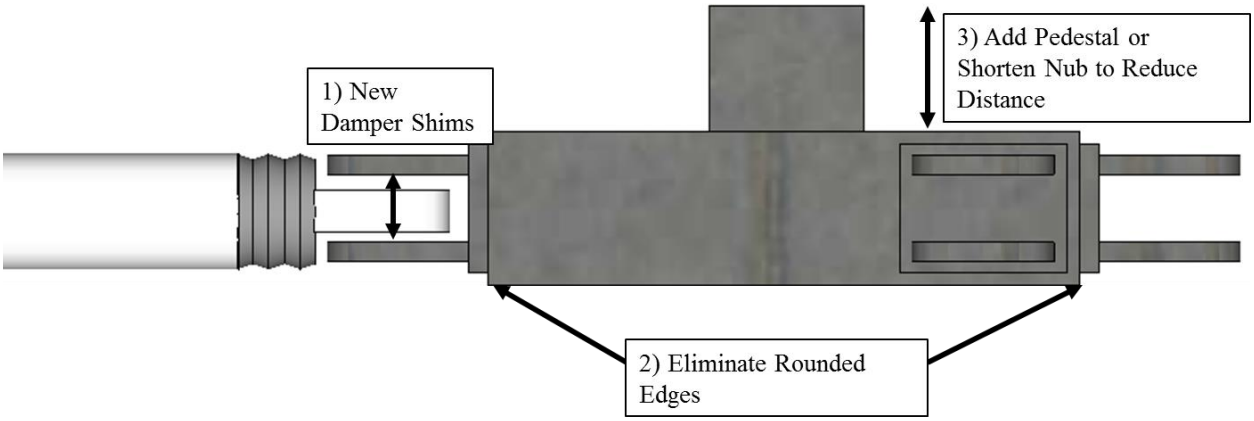

Figure 4-58. Design Recommendations

4.7 Shake Table Experiment

Although a large part of this research endeavor involved the shake table experiment, a full discussion of the experiment and results are not presented within the scope of the this dissertation. A thorough discussion of the shake table specimen design, experimental setup, and experimental results is found in the dissertation entitled "*An Innovative Gap Damper to Control Seismic Isolator Displacements in Extreme Earthquakes*" (Zargar H. , 2015). The behavior of the components of the gap damper system behaved as intended, as is evident in Figure 4-59. For the Loma Prieta excitation, the gap damper clearly engages five times throughout the motion with a similar hysteretic behavior to the component tests presented in Chapter 4. The damper energy dissipation was often less than the theoretical values, indicating an increase in damping constant may be necessary to achieve the proper displacement objectives.

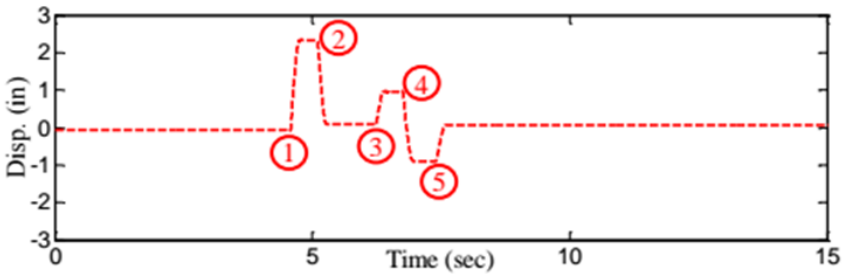

a) East Damper Time History (70% of Loma Prieta Ground Motion)

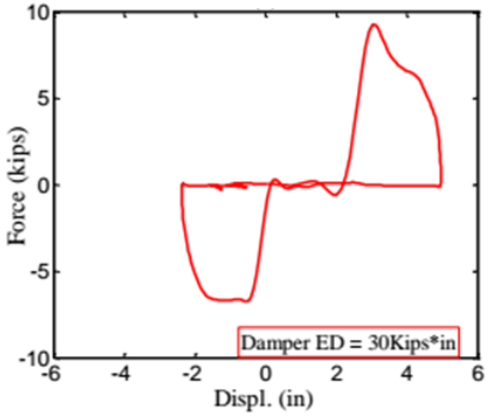

b) East Damper Hysteresis (70% of Loma Prieta Ground Motion)

Figure 4-59. Component Behavior during Shake Table Testing (Hamed)

Overall, the gap damper system did not achieve the desired displacement reduction of 25%, with a maximum reduction of 18% for the unidirectional Loma Prieta motions. Other motions experienced small reductions and some motions actually had an increase in isolator displacement with the gap damper system. Figure 4-60 comparison the displacement response for the system with the gap damper (GD) and without the gap damper (BI) for the unidirectional Loma Prieta excitation. A clear reduction in the displacement is noticed for the gap system when comparing the peak displacement values.

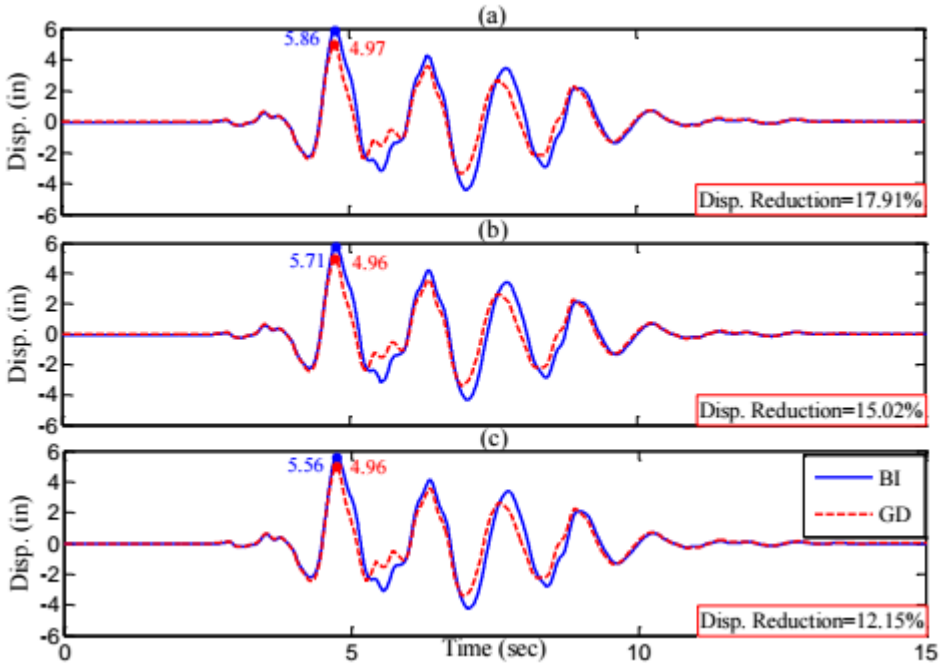

Figure 4-60. Displacement history comparison of a) Southeast bearing b) Average displacement at center and c) Northwest bearing for the Loma Prieta uni-directional ground motion

In addition to the displacement response, comparisons in acceleration response can also be made between the system with and without the gap damper. Figure 4-61 demonstrates the increase in acceleration at each level due to the introduction of the gap damper system for the same Loma Prieta uni-directional ground motion. Increases were highest in the roof and base levels on the order of 2.5 to 3 times the base-isolated system without the gap damper.

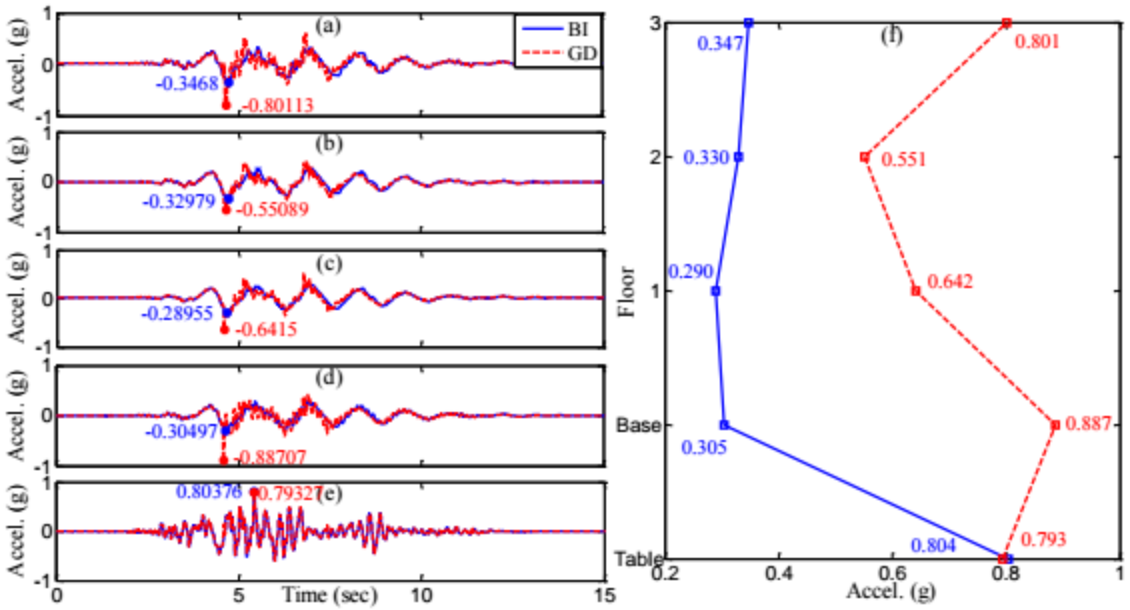

Figure 4-61. Acceleration comparison between a) third floor b) second floor c) first floor d) base floor e) shake table and f) maximum values for the Loma Prieta uni-directional ground motion

Bearing degradation and instability played an important role in the behavior of the test structure. The base-isolated structure was first tested without the gap damper system initial to establish the displacement demand of the desired input motions. The gap damper system was added to the structure and the displacements were compared to evaluate the reduction capacity of the system. The isolator hystereses clearly changed through the duration of the test, suggesting degradation and softening of the isolators. In addition, the impact force created a large overturning moment that caused isolator compression stability issues. The degradation and stability issues make it difficult to quantify the relative performance of the structure. A full scale structure would have more redundancy and larger resistance to overturning. Although the gap damper did not meet the performance objectives, the system was successful at reducing displacement. Further research is necessary to fully validate the system for full scale use.

4.8 Conclusions

Using the results from the parametric study, this chapter thoroughly covered the development of a gap damper system for prototype implementation. Design details and considerations were covered and a final design presented for both a viscous and viscoplastic gap damper. Prior to the experiments, the calibration of the viscous dampers and friction device was completed to ensure they were achieving the desired behavior. An experimental plan including the instrumentation, component layout, and load cases was also overviewed. Testing for the viscous gap damper included 24 load cases while the viscoplastic device had 8 load cases including different eccentric and rotated impacts. Comparisons were made between load cases to assess the energy dissipation capacity of the gap damper system. Reliable and repeatable behavior was found for the viscous gap damper while the viscoplastic system needs more research to be an effective system for consideration. Using the results from this experiment, the next step was to create a finite element model that captures the system behavior. In addition, a shake table test using the gap damper system designed in this chapter will assessed the performance of a gap damper system with the presence of a superstructure. Results were mixed due to confounding variables but displacement reduction was noticed in some instances.

Chapter 5. Finite Element Modeling of a Gap Damper System

5.1 Introduction

After the completion of the experimental work, the global understanding of the system was well established through the analysis of the lab data. The contact of the bumper system with the nub involves a tremendous amount of load transfer from the superstructure into the dampers for the dissipation of energy. Capturing the localized behavior of the gap damper system was not feasible in the experimental study. In addition, the high velocities possible in the shake table testing were not achieved due to limitations with the lab equipment. For these reasons, the addition of a finite element model to the study is beneficial to the research effort. In order to develop an effective model, a coarse mesh was developed to capture global behavior of the system and compare to the experimental data. Once the calibration of the model was achieved, a fine mesh could be used to capture any local behavior of interest. In addition, a fully calibrated model could be used to investigate any modifications to the design.

5.2 Model Details

The analysis required a large displacement, dynamic, nonlinear, and contact formulation to achieve the desired results with Abaqus/Explicit chosen to model the system (Dassualt Systemes Simulia Corp., 2010). The finite element model is an idealized model of the experimental setup, not accounting for potential imperfections.

The layout of the system, shown in Figure 5-1a, consists of the nub, bumper system, and viscous dashpots to represent the dampers. Components of the gap damper system were imported from a 3-D AutoCAD model to ensure the proper geometry. Given the oblique nature of some of the system components, use of partitions was necessary to ensure a uniform mesh with appropriate element shapes and sizes. The mesh was verified to ensure a proper formulation. A coarse mesh, shown in Figure 5-1b, was developed to calibrate the system with the experimental values. The elements were three-dimensional, first order, and hexahedral with reduced-integration. The materials used for the nub and the bumper system were a bilinear elastic-plastic relationship with a yield stress of 50 ksi and 42 ksi respectively, and strain hardening in the plastic range.

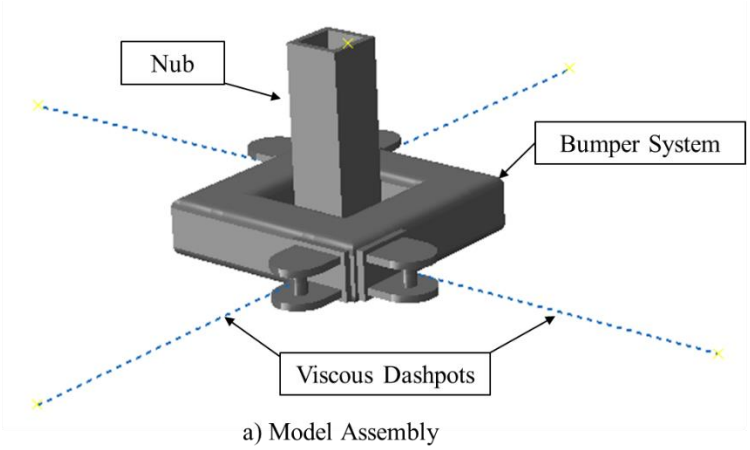

a) Model Assembly

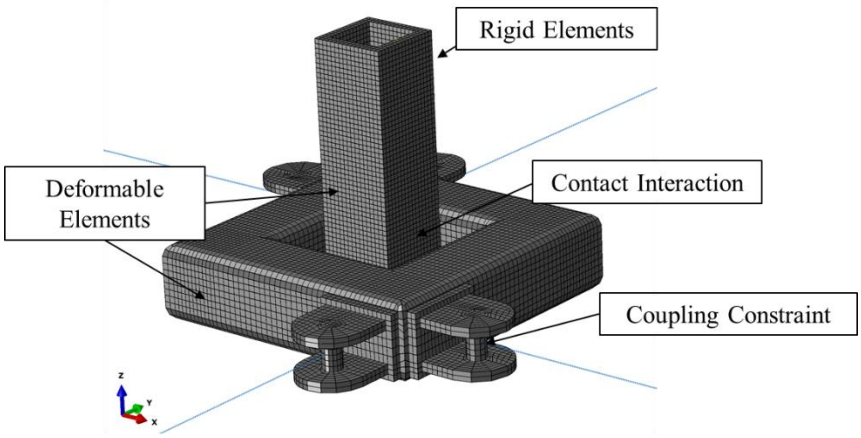

b) Coarse Mesh Model

Figure 5-1. Finite Element Model of Viscous Gap Damper System

The nub was split into two sections, the top half consisting of rigid elements and the bottom half made up of deformable elements. Rigid body motion was introduced to the system to by assigning the simulated actuator movement to the reference point tied to the rigid portion of the nub. Nub movement was in the form of sinusoidal or constant velocity inputs (sawtooth wave) matching the load case velocity. The deformable portion of the nub was tied to the rigid body and was therefore driven into the bumper system with the rigid body motion. Boundary conditions were assigned to the rigid nub reference point, allowing movement in the x-y plane but restricting all rotations and vertical movement along the z-axis (see Figure 5-1b for reference). These modeling conditions were set to simulate the rigid attachment to the floor above the gap damper system with a small amount of the nub component allowed to deform.

A general contact formulation was used that enforced a "hard" contact to eliminate penetration of the slave surface. The hard contact formulation enforces direct coupling of the node displacements and shows good agreement with the Hertzian contact solution (Konter, 2005). The nub was defined as the slave surface as the component with the finer mesh that was the "contacting" surface. The bumper was the master surface or contacted surface. Separation of the surfaces was allowed after contact.

The bumper system was entirely meshed with deformable elements. Boundary conditions were defined at the bottom of the bumper system to allow the system to slide in the x-y plane but not move along the z-axis (gravity direction). The dampers were modeled as simple linear dashpots with the damping properties obtained in the lab testing in Section 4.4.1. Connection points for the dampers were the middle of the pin element and a reference point 866.8 mm (34.125 in) along the axis of concern. The length corresponded with the length of the viscous dampers at mid-stroke. Dashpot elements were pure axial connector elements that were allowed to rotate but

only experienced axial deformations. The connection of the dashpot to the pin of the bumper system was enforced with a kinematic coupling constraint that paired the movement of the entire pin with the dashpot to avoid localized stresses at the connection point.

5.3 Results

Displacement output for nodes on the nub and bumper system were chosen to ensure the system was behaving as desired. Figure 5-2 shows the displacement time history for the nub and the primary dampers for LC1 (E0-0.125Hz-+/-4.2-Sine). The nub was subjected to one and a half cycles so that the last cycle could be compared to final cycles of the experimental data that had residual displacements from early cycles. Overall, behavior was as expected with the sinusoidal movement of the nub and delayed activation of the dampers until 63.5 mm (2.5 in) due to the presence of the gap. The dampers are active until the peak actuator movement and then stationary as the actuator switches directions.

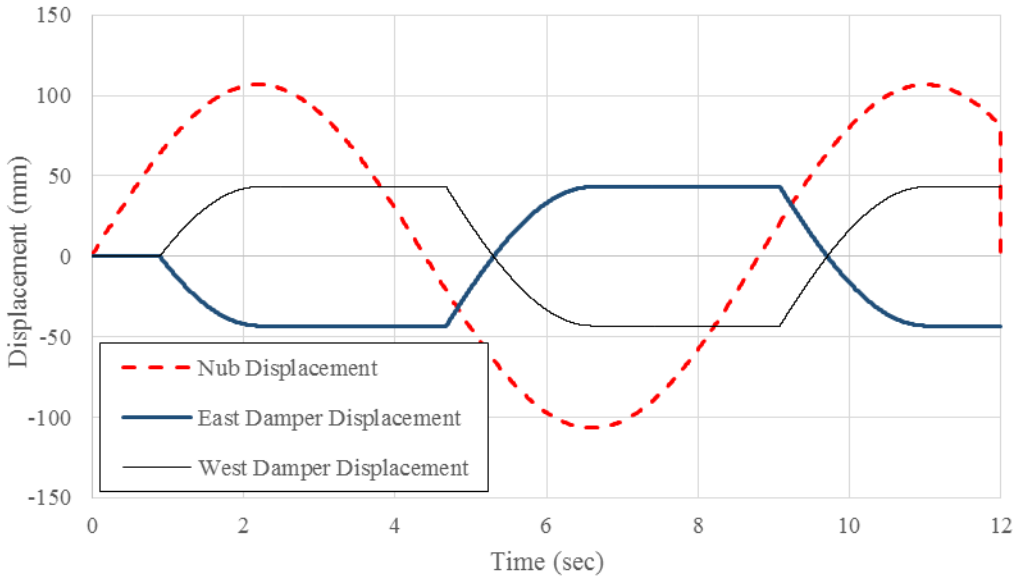

Figure 5-2. Time History for LC1 (E0-0.125Hz-+/-4.2-Sine)

Global behavior was checked to ensure the movement of the system was proper. Figure 5-3 shows the displaced condition corresponding with Figure 5-2, as the actuator reaches maximum displacement in the east direction. The east damper has compressed and the west damper is extended. Lateral dampers have rotated as expected as well.

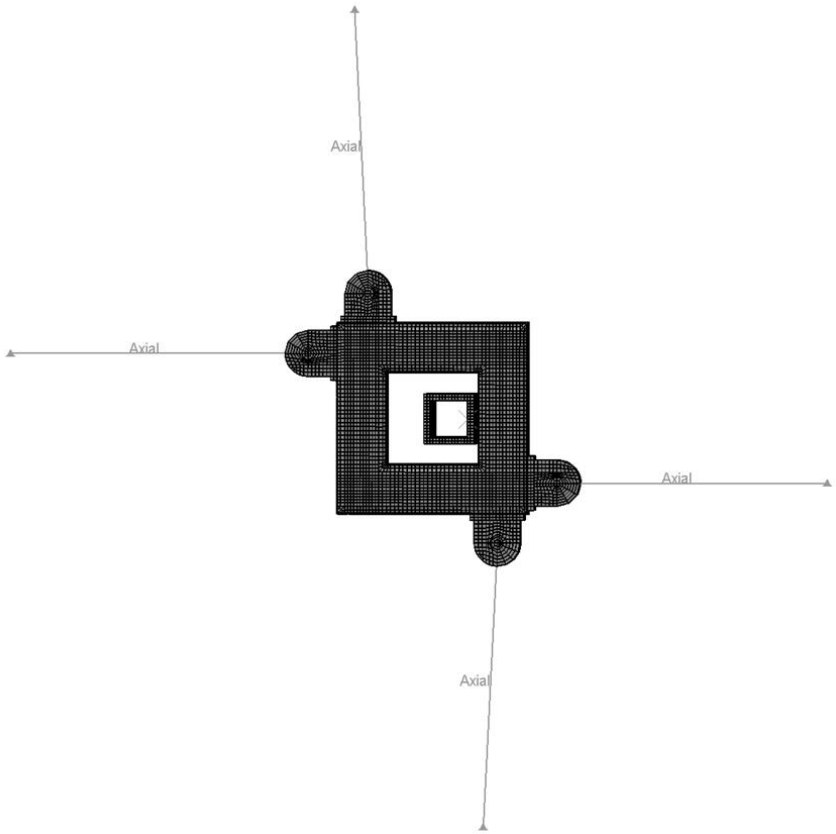

Figure 5-3. Displaced Condition of Finite Element Model for LC1

In addition to displacement checks, energy checks were also done to ensure the model was sufficient. Figure 5-4a shows the cumulative viscous energy in the model, with the expected behavior evident as the energy has the sinusoidal relationship expected when the dampers are active and no viscous energy when the gap damper is stationary. Figure 5-4b shows the kinetic energy time history of the model. The model matches well with the velocity of the nub system. Lastly, the cumulative artificial energy was compared to internal energy to ensure the values were

not excessive, as shown in Figure 5-4c. Artificial energy of around 15% of internal energy indicates excessive hourglass control of the reduced elements (Dassualt Systemes Simulia Corp., 2010). This implies that the local solution in the contact region may not be accurate which is expected in a coarse mesh. Since the global solution and behavior of the gap damper system is correct, the artificial energy is not a problem for the coarse mesh simulations. Further analyses with finer meshes should consider the portion of artificial energy in order to ensure an accurate solution.

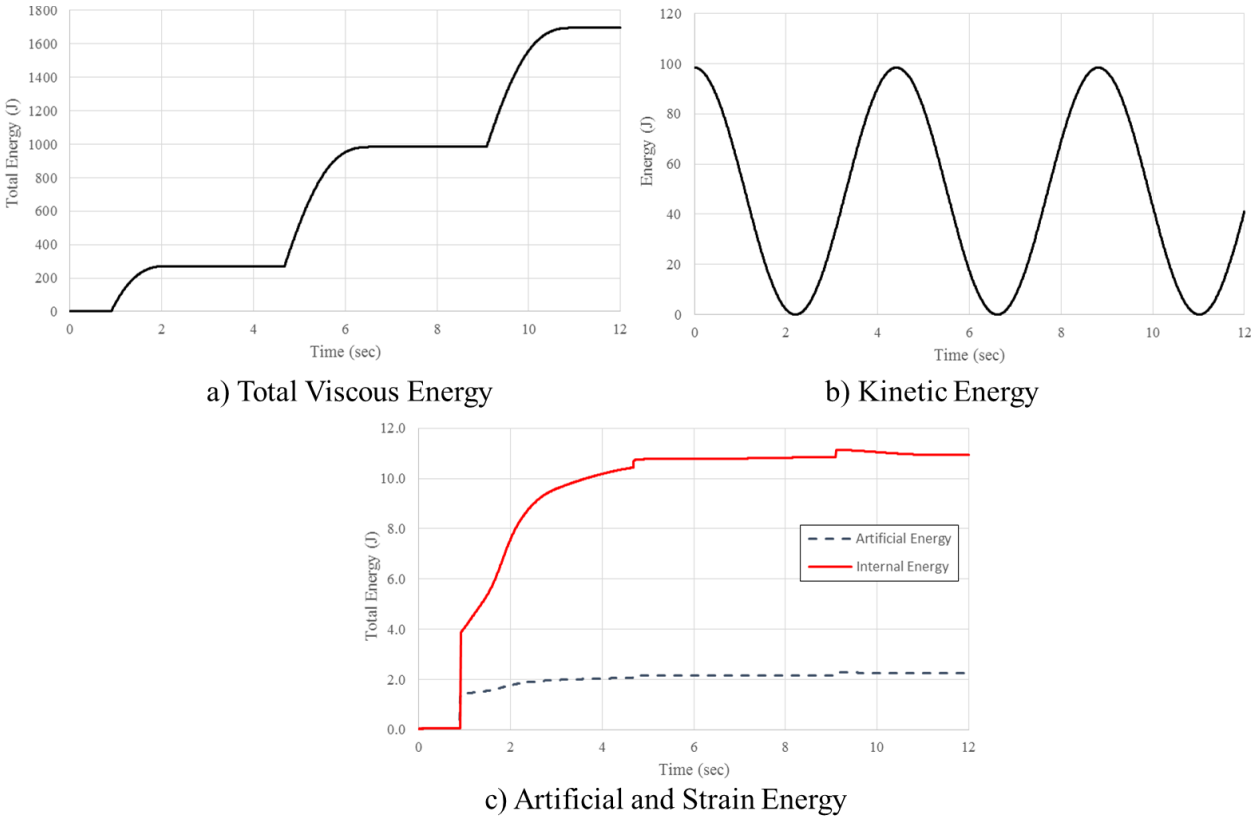

a) Total Viscous Energy

b) Kinetic Energy

c) Artificial and Strain Energy

Figure 5-4. Energy Comparison for LC1

5.4 Coarse Mesh Analyses

With the verification of expected global behavior of the system, the results from the coarse finite element models are compared to various experimental values to ensure accuracy. The load cases

of concern, shown in Figure 5-5, encompass the different types of impact conditions possible with the gap damper system. The actuator displacement data from the experiment was input as the displacement controlled boundary condition for the nub to allow a direct comparison to experiment. Data from the experiment were taken as a full actuator cycle in the third (of five) full cycles in the load case. Velocity and damper force values were filtered using a 25 Hz Butterworth filter. Damping constants used in the dashpots were from the damper calibration in Section 4.2.2.

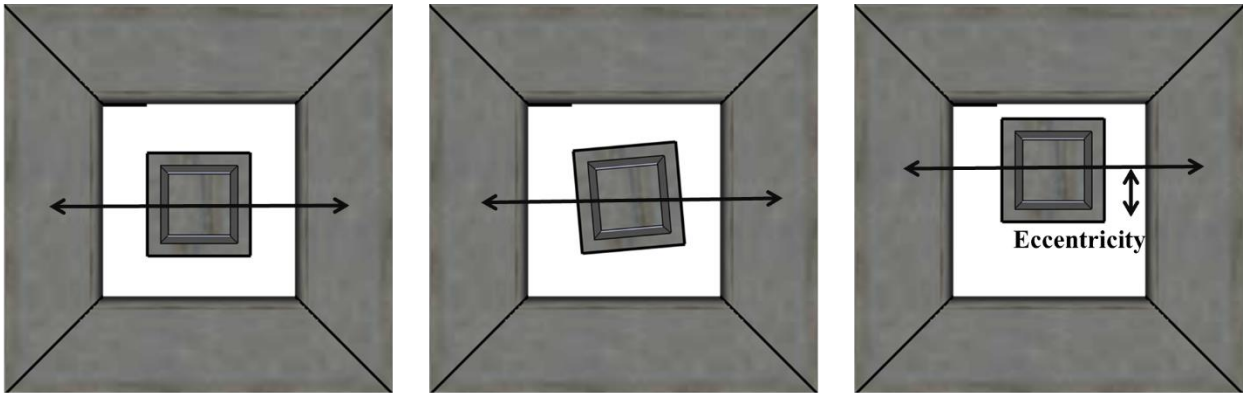

a) LC1 Concentric Movement b) LC5 Rotated Movement c) LC17 Eccentric Movement

Figure 5-5. Load Cases Evaluated

A comparison between experimental and finite element data for LC1 is found is shown in Figure 5-6. The two parameters compared are the displacement time histories and force time histories for the primary dampers (east and west) in the direction of the actuator movement. The load case was a sinusoidal motion with a maximum displacement of ±106.7 mm (4.2 in) with a 63.5 mm (2.5 in) gap delaying the activation of the bumper system. Delaying the activation of the dampers, would require a stroke of 43.2 mm (1.7 in) in each damper for a uniform impact condition. The displacement data from the experiment matches very closely with the model with slight variations in peak displacements. This is likely due to imperfections in the test setup, instrumentation, and residual displacements from previous actuator cycles. Figure 5-6b shows the force comparison between the experiment and model. The experimental values match well with

the model, with the exception of the east damper when pulled in tension. This is due to the phenomenon explained previously in Figure 4-43 in which a test imperfection lifted the bumper system near the connection of the east damper to the bumper system. The lifting of the system did not allow the full transfer of load into the damper upon impact, explaining the shortfall in experimental force and slight slope of the curve upon activation (approximately 2.25 seconds). When the actuator was extending and impacting the bumper system (6.0 seconds), the force transfer was better and the experimental values matched well with the model.

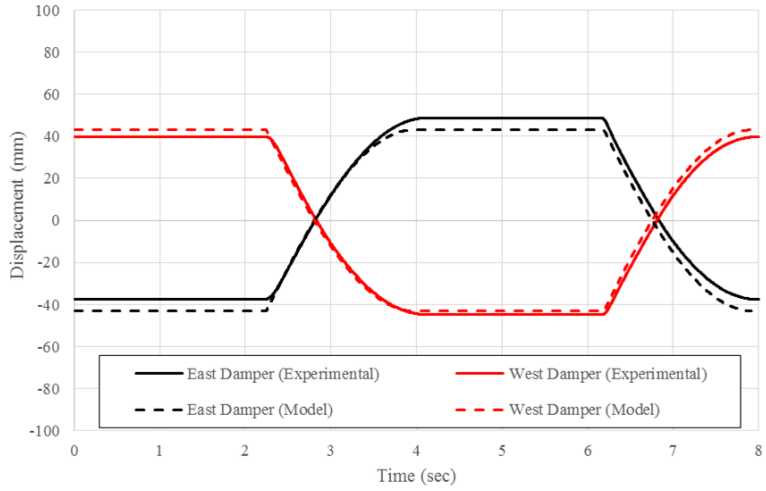

a) Displacement Comparison

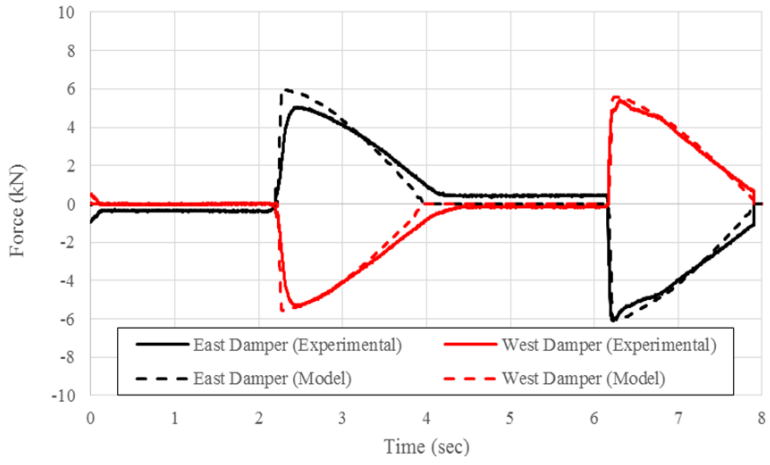

b) Force Comparison

Figure 5-6. Load Case 1 Comparison to Model

Similar to LC1, data for LC17 was compared to the finite element model. The primary difference in the two load cases is the eccentric impact present in LC17. Theoretically, the two systems should behave the same as no rotation is evident in the system and the load cases have the same sinusoidal input. The displacement history in Figure 5-7a agrees very well with the model data with some slight discrepancies. Figure 5-7b illustrates the force time history comparison, which shows some discrepancies in comparison to the model. In addition to the disjoint in the force due to the lifting of the bumper system, the experimental force in the west damper does not match well with the model values, with force values consistently less than the model predicts. Given that the displacement time history, and therefore velocity time history, agrees well with the model, the disjoint in the force values is unexpected. Possible explanations for the difference could be slop in the connection to the load cell or instrumentation error.

Overall, the model behavior demonstrates an accurate portrayal of the gap damper system with test setup imperfections accounting for discrepancies. If necessary, the imperfection of the test setup could be simulated using a rotational spring at the top of the rigid portion of the nub rather than the currently used rigid rotational constraint. Contact elements would also have to be implemented at the bottom surface of the bumper to allow the lifting of the system. Since the imperfection will not be present in the final configuration of the gap damper system in a real structure, this analysis is not necessary unless the shake table experiment indicates otherwise.

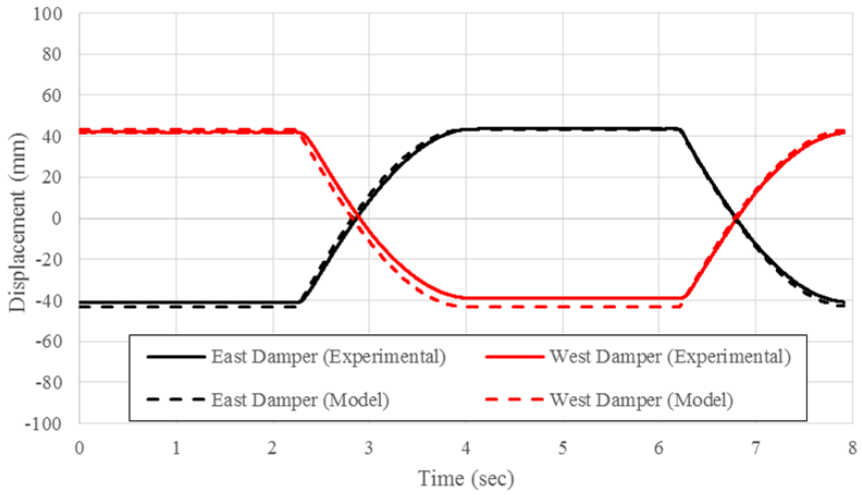

a) Displacement Comparison

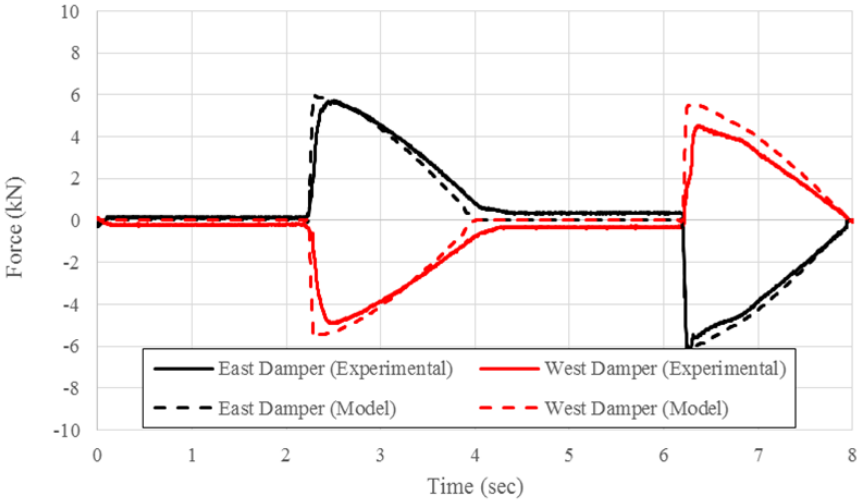

b) Force Comparison

Figure 5-7. Load Case 17 Comparison to Model

In addition to the primary dampers, the data from the lateral dampers were also compared to the model. The lateral dampers have very little participation in the load cases without a nub rotation, such as LC1 and LC17. Figure 5-8 shows the force time history comparison for LC1 between the lab data and model data. Even though the participation of the lateral dampers is very small in comparison to the primary dampers, the general shape of the curves are very similar. The magnitude of the forces in the lateral dampers are much higher than the model predicts which is likely due to a slight static stiffness. In addition, the accuracy of the load cell in the small load

range with the self-weight of the dampers possible influencing response could provide another source of error. The accurate shape of the lateral dampers is indicative of correct model behavior.

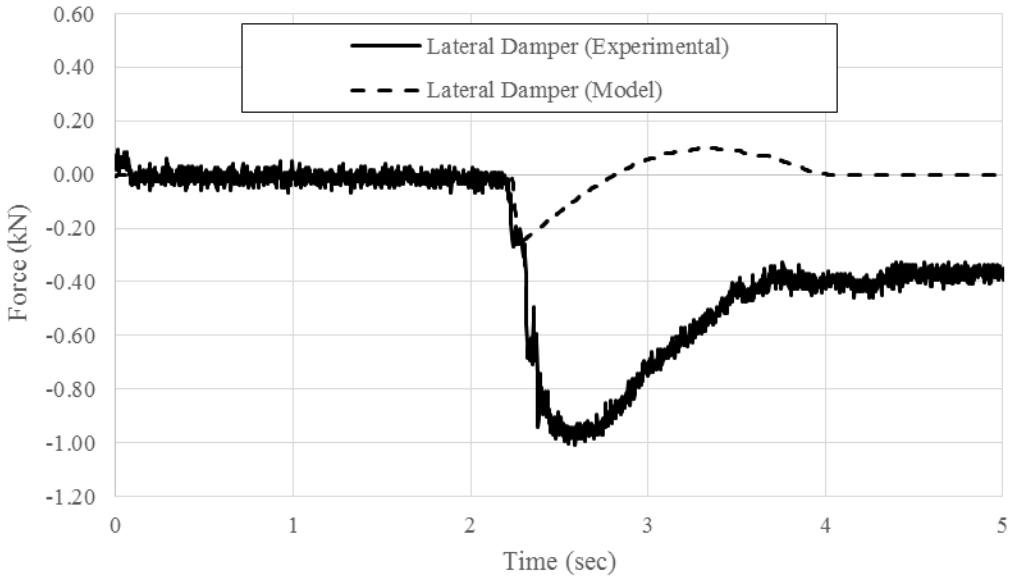

Figure 5-8. Lateral Damper Comparison (LC1)

In the previous analyses of the rotated impacts, it was difficult to capture the behavior of the lateral dampers. The actuator had to ramp up to the intended velocity and the bumper system slowly rotated to match the impact angle of the nub after a couple cycles. The sequence of motion typical of the gap damper is shown in Figure 5-9 which is representative of the concentric motion of LC5 with a rotated nub. At about 75 mm/sec (3 in/sec) and a maximum displacement range of ±106.7 mm (4.2 in), three impacts occurred before the bumper system fully aligned with the rotation of the nub. The gap damper system would oscillate about this rotated bumper system position for the remaining motion.

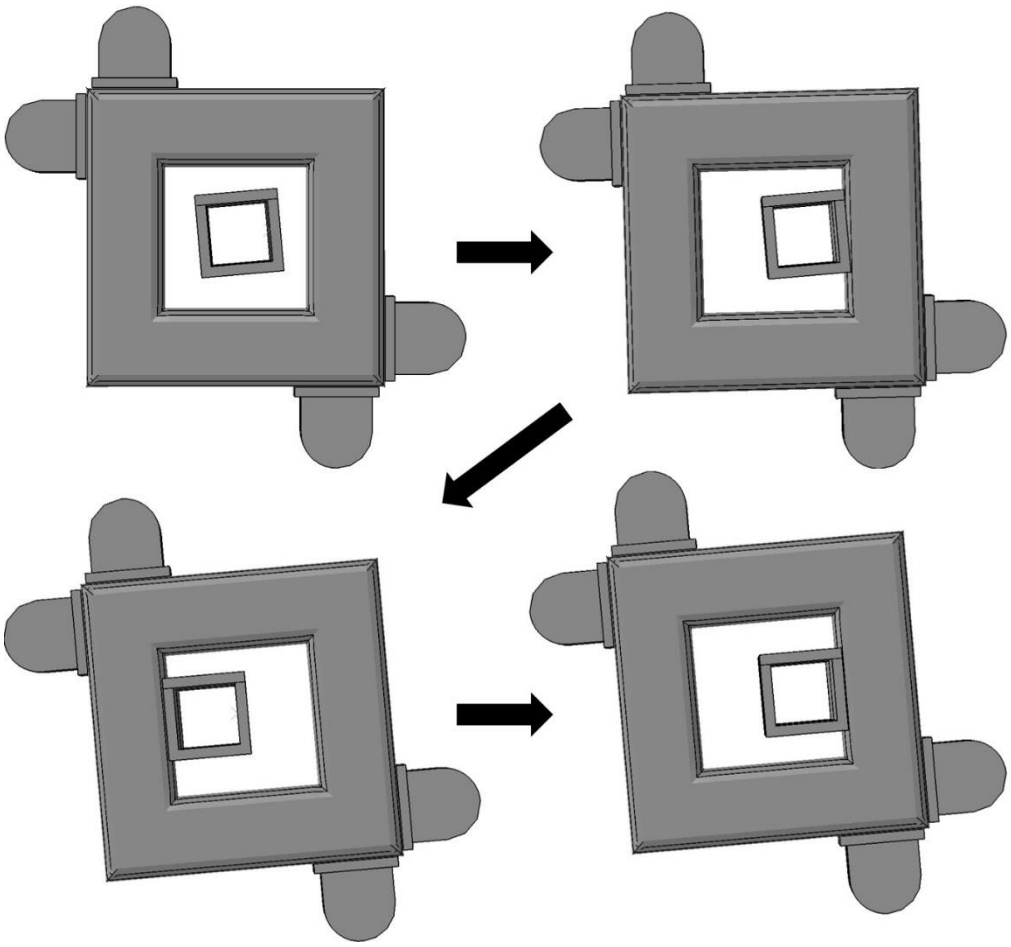

Figure 5-9. Rotation Sequence

With an accurate model capturing the behavior of the system, the participation of the lateral dampers can be further investigated for high speed collisions. To accomplish this task, the nub was assigned a constant velocity of 1.016 m/s (40 in/sec) for 0.1 seconds and positioned close to the bumper system (Figure 5-10). At the conclusion of 4 inches of nub travel, the bumper system was still not flush with the nub rotation Figure 5-10b and Figure 5-10c. This suggests that the lateral dampers had a contribution in resisting the rotation. The velocity at the end of nub movement in the direction of travel is evident in Figure 5-10b. This figure indicates a velocity (red) higher than the nub velocity in the primary damper closest to the impact point (on the right side) and a velocity (orange) lower than the impact velocity in the primary damper furthest from

the impact point (left side). This could potentially effect the overall energy dissipation capacity of the system.

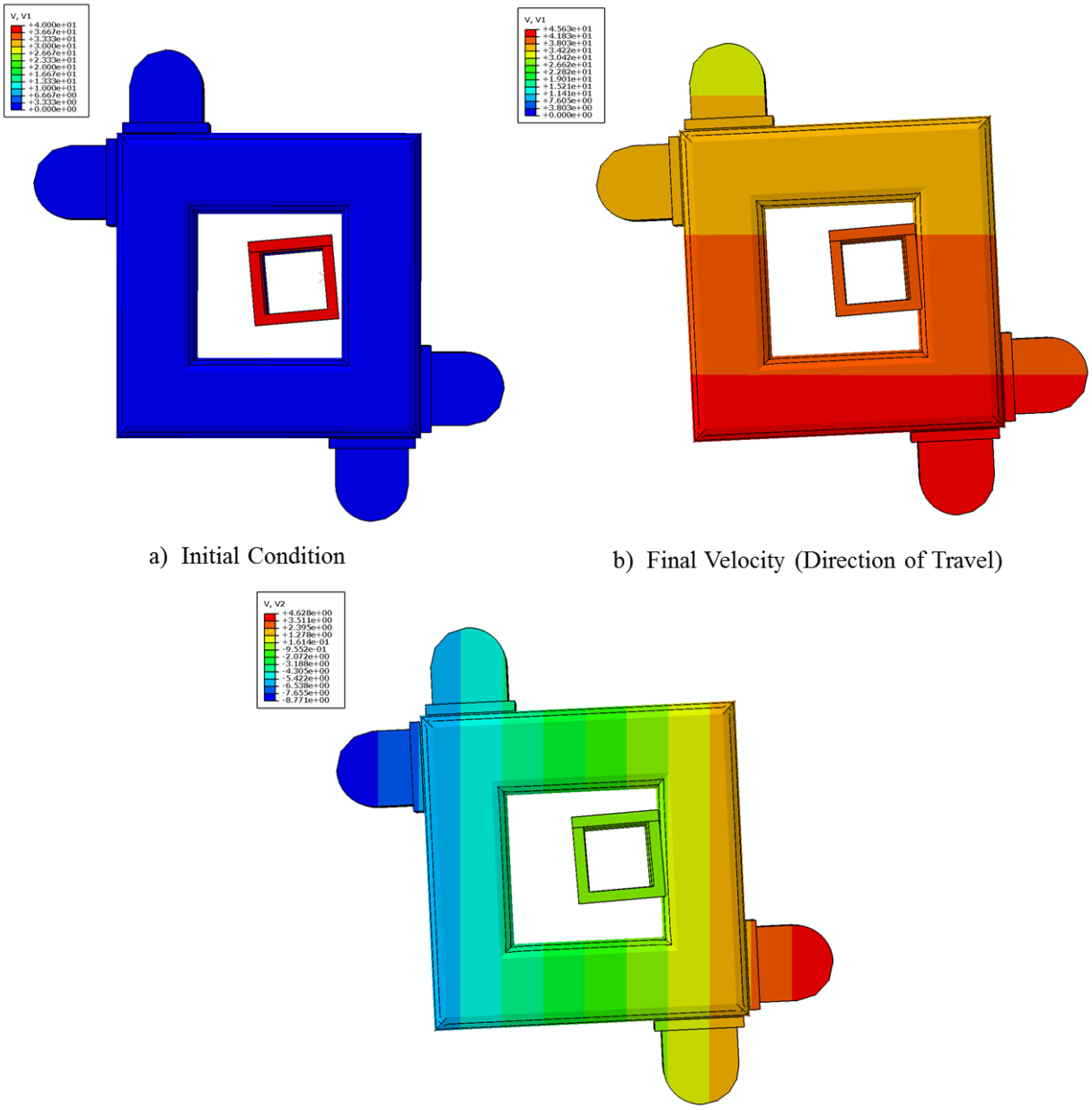

a) Initial Condition

b) Final Velocity (Direction of Travel)

c) Final Velocity (Transverse to Direction of Travel)

Figure 5-10. High Speed Collision with Rotated Impact

In addition to the velocity in the primary direction, velocity transverse to the movement was also investigated, as shown in Figure 5-10c. Velocities (yellow) in this direction indicate the

amount of participation for the lateral damper closest to the impact location (bottom) is less than the velocity (light blue) in the lateral damper further away from the impact location (top). This shows that the top damper is participating more in the response of the system.

With the non-uniform response of the dampers in the rotated impact, it was important to investigate the amount of energy dissipation present in the system in comparison to a non-rotated system. For an effective gap damper system, energy dissipation should be relatively the same regardless of the impact condition. In order to make this comparison, a system without rotation of the nub was also modelled with an assigned constant velocity of 1.016 m/s (40 in/sec) for 0.1 seconds. The energy dissipation time histories for this system are shown in Figure 5-11. Results are as expected with the primary dampers participating equally and the lateral dampers showing very little participation relative to the primary energy dissipation. Energy dissipation is also symmetric as expected with a concentric impact. The total energy dissipation for the system, shown in Figure 5-11c, reaches 14.3 kJ over 0.1 seconds with the linear relationship expected with the constant velocity of the nub.

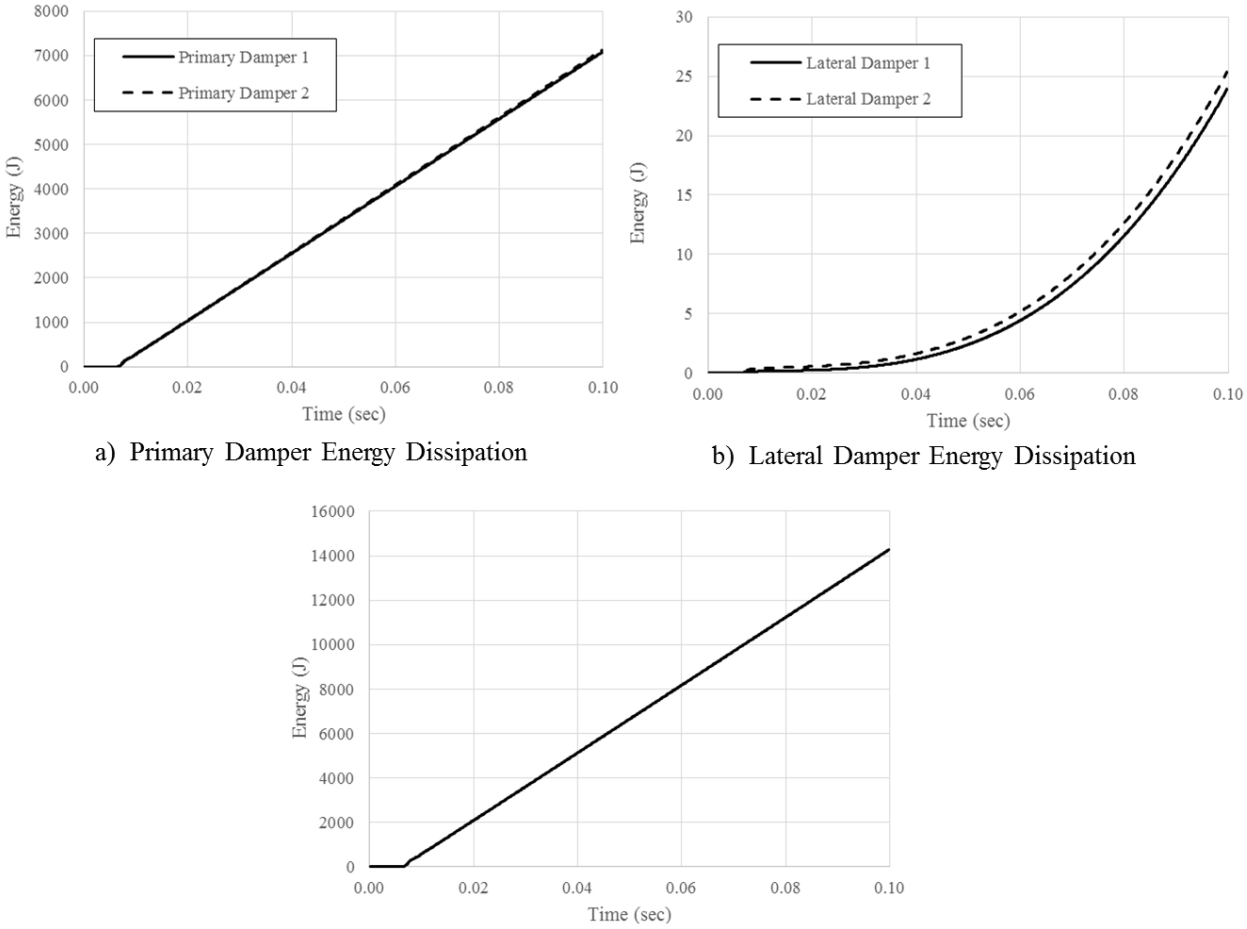

a) Primary Damper Energy Dissipation

b) Lateral Damper Energy Dissipation

c) Total Damper Energy Dissipation

Figure 5-11. Concentric Impact Energy Dissipation

In comparison, Figure 5-12 shows the energy dissipation characteristics of the system with the rotated nub. With this system, it is clear that primary damper 1 (right), is dissipating more energy than primary damper 2 (left). Relative to the concentric impact, the energy dissipation in primary damper 1 for rotated impact is higher than concentric impact while primary damper 2 is lower. For the lateral dampers, shown in Figure 5-12b, overall participation is much higher than in the concentric impact. Even with the higher participation, energy dissipation is still minimal in the lateral dampers relative to the primary dampers. The lateral damper closest to the impact point (bottom) participates less than the opposite lateral damper. The total energy dissipation for the system, shown in Figure 5-12c, reaches 13.7 kJ over 0.1 seconds. Total energy dissipated in

rotated impact is about 96% on the concentric impact indicating that a rotated impact does have a slight impact on the energy dissipation capacity of the system. Given a 5 degree impact is an extreme condition, the gap damper system still behaves as desired for rotated impacts and is able to dissipate a significant amount of energy.

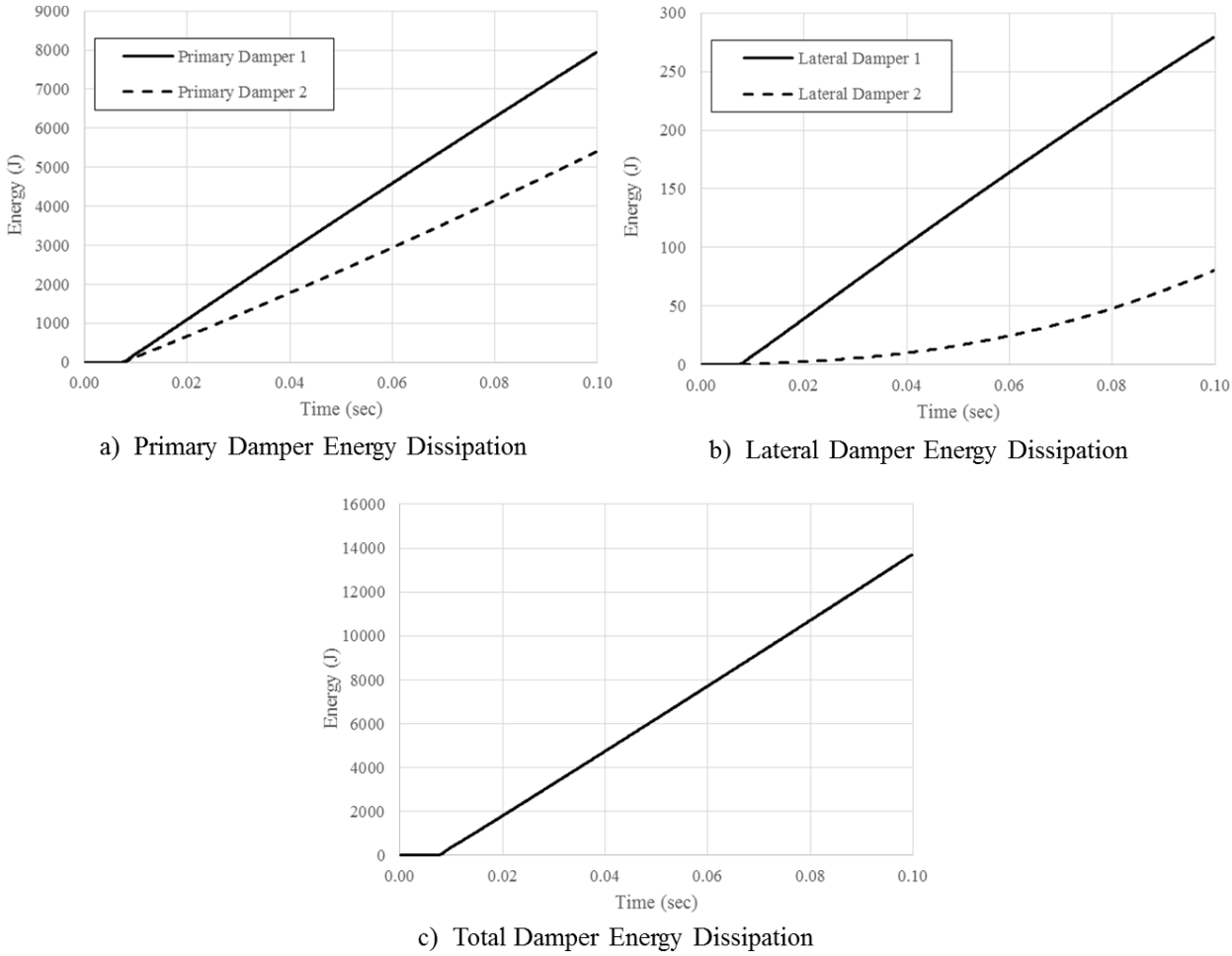

a) Primary Damper Energy Dissipation

b) Lateral Damper Energy Dissipation

c) Total Damper Energy Dissipation

Figure 5-12. Rotated Impact Energy Dissipation

Another concept of interest with the gap damper system is the contribution from the lateral dampers in full scale. As the stroke required in the dampers increases in full scale, the dampers will not be proportionally longer. This could potentially mean the lateral dampers have increased participation towards the end of the stroke as an increasing portion of displacement component is in the direction of motion. In order to capture the increased participation of the lateral dampers,

gap damper motion was simulated out to 0.508 m (20 in), corresponding to a 30 degree rotation in the lateral dampers (Figure 5-13a). As the rotation in the dampers increases, the energy dissipation in the lateral dampers does increase substantially when the dampers are in the 20 to 30 degree range. However, even with the increased rotation, the energy dissipated at 30 degrees is only 8% of the energy dissipated in the primary damper. Given that a 30 degree rotation is an extreme value beyond expected design values, the contribution of lateral damper energy can be ignored in future analyses.

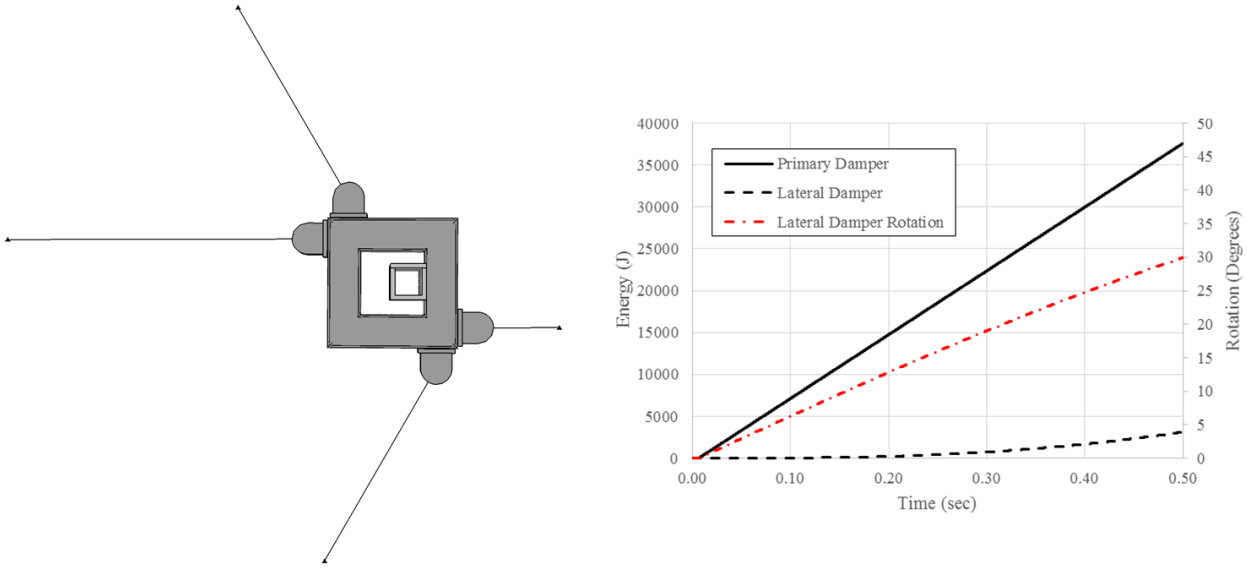

a) Displaced Condition (30 Degrees)

b) Final Velocity (Direction of Travel)

Figure 5-13. Lateral Damper Contribution

5.5 Fine Mesh Analysis

The coarse mesh allowed many useful conclusions to be drawn based on the global behavior of the system. With the global behavior verified in the previous section, analysis of a fine mesh can provide a better localized analysis of gap damper behavior. While the preliminary analysis was completed with different nub shapes and sizes Section 4.2.4, a fine mesh analysis of the as-built condition of the gap damper system was necessary to ensure the design of the device is sufficient.

The fine mesh was setup similarly to the coarse mesh with a refinement of the mesh for the deformable portion of the nub and contact area of bumper system, as shown in Figure 5-14. The mesh was refined until the model approached a constant solution. In addition, one key difference in the fine mesh is the use of full integration for the elements close to contact area in order to reduce artificial energy in the system. A constant velocity of 1.016 m/s (40 in/sec) was assigned to the reference point associated with the rigid portion of the nub part. The velocity is 60% over the design velocity of 0.635 m/s (25 in/sec). Model behavior was captured for the initial activation of the system, associated with the first 6.35 mm (0.25 in) of damper stroke. Two systems were compared for the fine mesh models, a concentric flush contact condition and a rotated impact involving a corner impact condition, the most critical contact condition for the gap damper system.

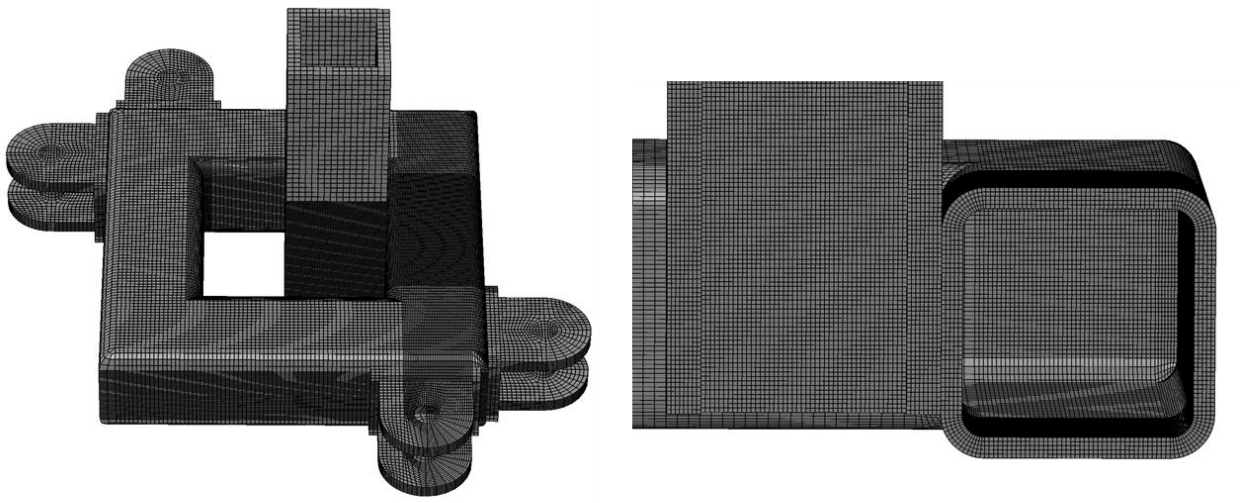

a) Fine mesh model b) Section cut in contact area

Figure 5-14. Fine Mesh Overview

Figure 5-15 and Figure 5-16 show the stress distribution for the concentric and rotated impact respectively. All stresses in the figures are in ksi with a yield stress of 344.7 MPa (50 ksi) in the nub and 289.6 MPa (42 ksi) in the bumper system. Stresses below 68 MPa (10 ksi) were eliminated from the figures for clarity. The nub stresses in the concentric impact condition (Figure

5-15a) were primarily at the top of the contact surface with the bumper and at the interface with the rigid portion of the nub. Small portions of the nub experienced high stresses in the range 206.8 MPa to 275.8 MPa (30 to 40 ksi) with a very small area experiencing stresses larger than 275.8 MPa (40 ksi). Figure 5-15b shows the stresses on the bumper system with the elimination of the nub. Stresses in the range 206.8 MPa to 275.8 MPa (30 to 40 ksi) are more widespread with small areas (yellow) suggesting localized yielding at the corner of the nub impact location.

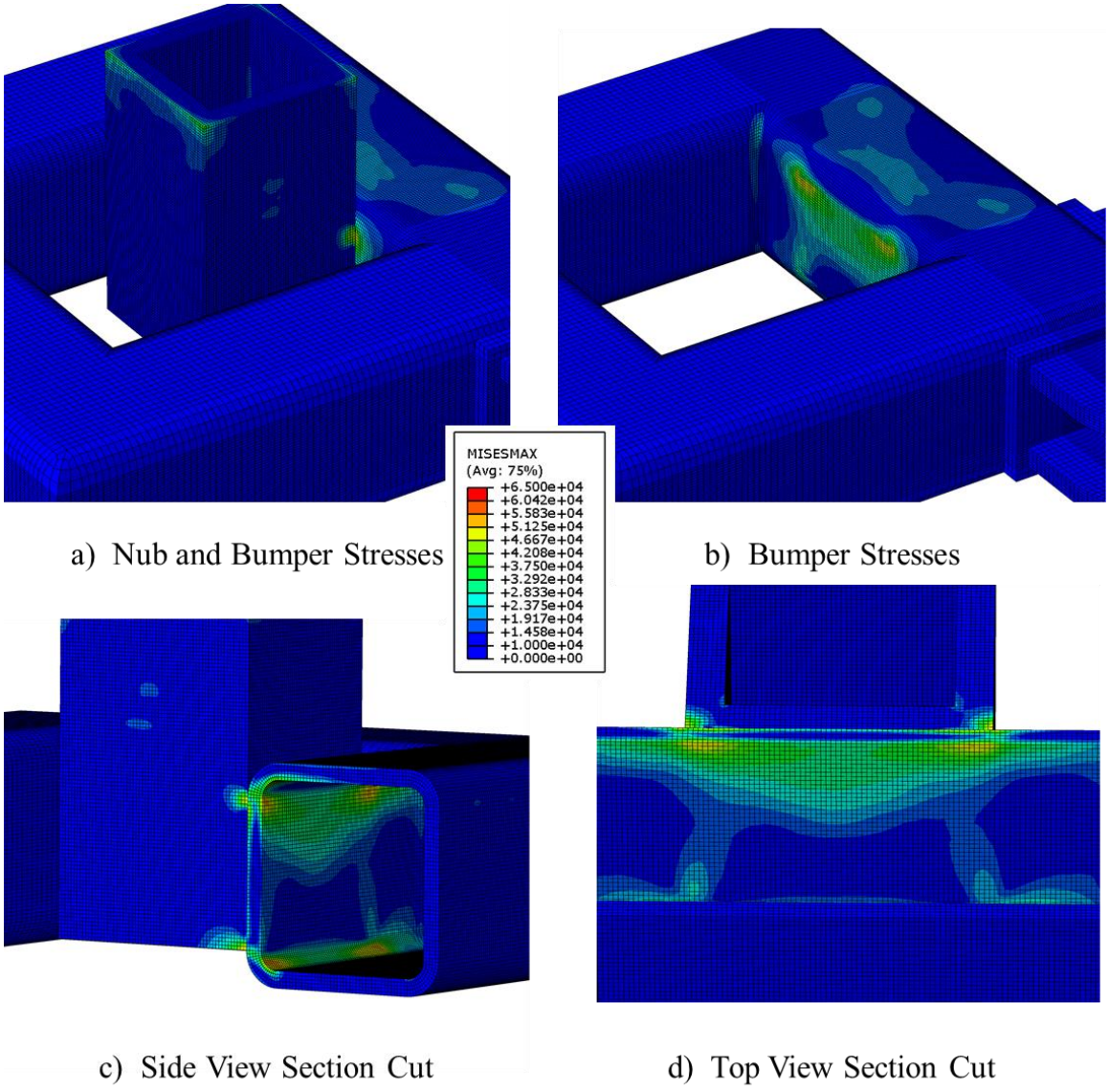

Figure 5-15. Concentric Impact

Figure 5-15c and Figure 5-15d are section cuts in areas of interest, showing the widespread stress distribution in the bumper system. Views of the inside of bumper system show areas of highly localized stresses beyond the yield capacity with high stresses through the thickness. The nub stresses are not as prevalent through the thickness, most likely due to the larger thickness. Since the gap damper system is intended for rare events and the finite model has a level of conservatism with the high impact velocity, some yielding is acceptable and not likely to affect the global behavior of the system.

Figure 5-16 shows a similar comparison with a nub rotated 5 degrees for impact with the bumper system. Similarly to the concentric impact analysis, Figure 5-16a shows the stress distribution of the nub and bumper. As expected, the corner impacting the bumper system experiences large stresses, indicating localized yielding in the nub. Figure 5-16d shows that this localized yielding is not present throughout the thickness of the nub, suggesting the overall integrity of the nub system would be maintained. Figure 5-16b shows the stress distribution on the bumper system, only present near the impact location. High stresses through the thickness of the bumper system, as shown in Figure 5-16c and Figure 5-16d indicate that some yielding may be present in the bumper system, likely causing indentations at the contact point. Similar to the concentric impact, this localized yielding is not likely to affect the global behavior of the gap damper system. Further analysis of the localized yielding could be done with mesh refinement in the region of concern.

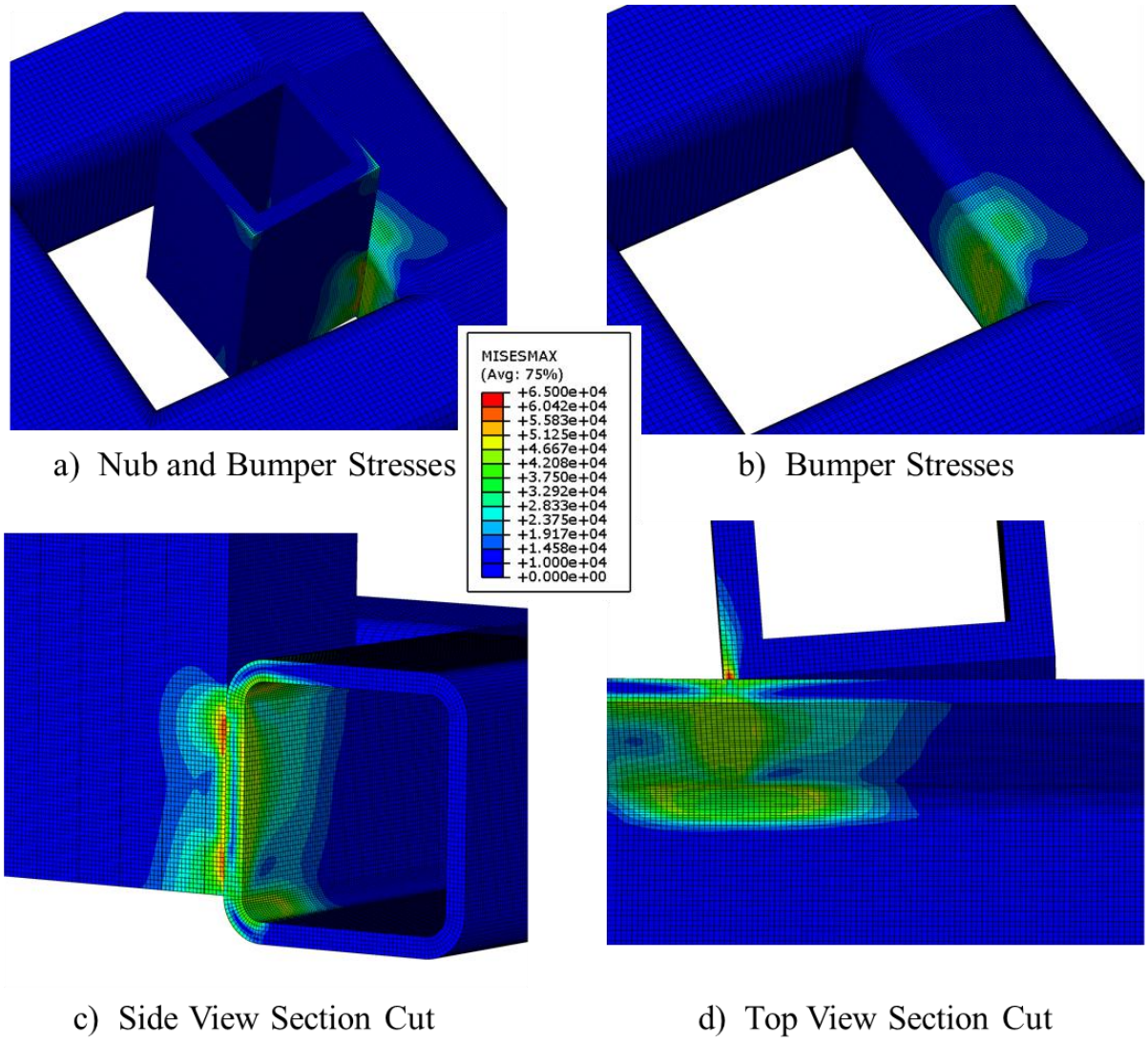

Figure 5-16. Rotated Impact

Further analysis is shown Figure 5-17, comparing the contact area and contact force for the two impact conditions. The data was filtered with a high frequency Butterworth filter. As expected, the contact area for the rotated impact condition is smaller than the concentric impact condition. Contact force approaches the same values corresponding with the cumulative force expected in the dampers at the given impact velocity. With similar contact forces traveling through a smaller contact area in the rotated impact, the higher stress concentrations are inherent in the system.

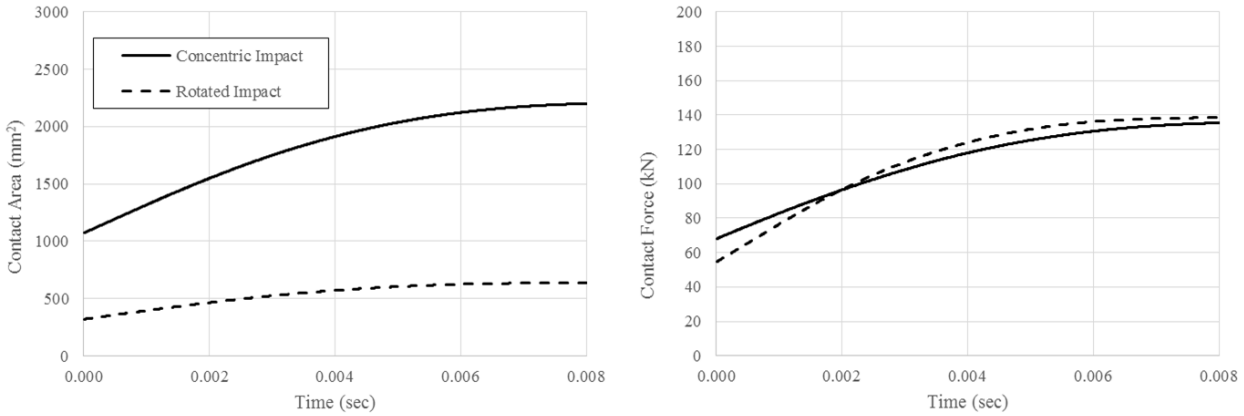

a) Contact Area b) Contact Force

Figure 5-17. Comparison of Contact Conditions between Concentric and Rotated Impact

Lastly, the energy dissipation of the two impact conditions were compared for the nub and the impacted portion of the bumper system. Internal energy (E_I) in the system is defined within the context of this model is shown in Equation 5-1:

$$\mathbf{E_I = E_E + E_P + E_A} \qquad \textbf{Equation (5-1)}$$

Where E_E is elastic strain energy, E_P is plastic strain energy, and E_A is artificial strain energy which is zero due to the use of fully integrated elements (Dassualt Systemes Simulia Corp., 2010). Figure 5-18. Comparison of Energy Dissipation for Different Impact Conditions shows the energy dissipation of the two impact conditions with the portions of the elastic and plastic strain energy present in the internal energy of the system. Similarly to the contact comparison, these plots were also filtered using a high frequency Butterworth filter. Overall, the rotated impact (Figure 5-18b) shows significantly more energy dissipation than the concentric impact (Figure 5-18a). In addition, the portion of plastic energy in the rotated impact condition is significantly more than concentric impact condition. This suggests that the rotated impact is more critical to the gap damper system.

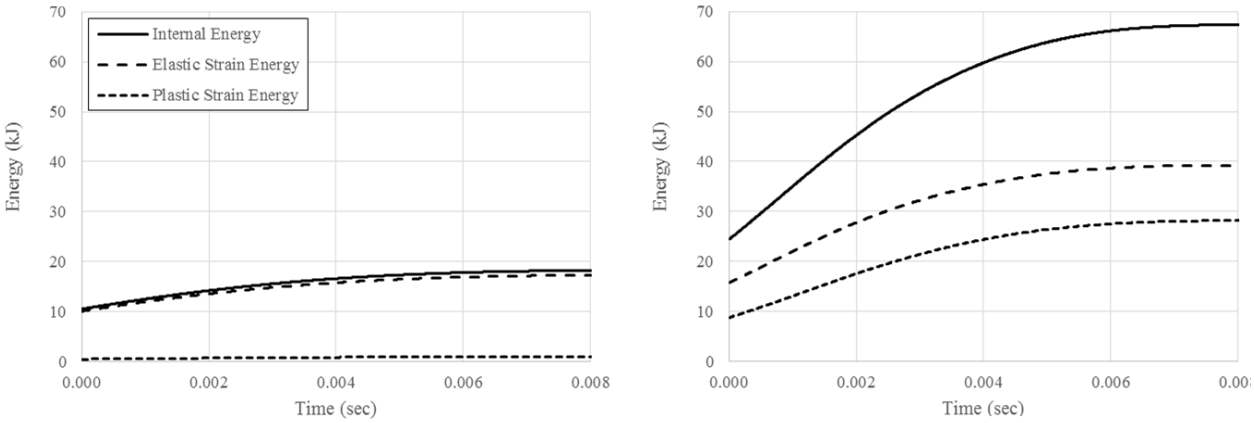

a) Concentric Impact b) Rotated Impact

Figure 5-18. Comparison of Energy Dissipation for Different Impact Conditions

5.6 Conclusions

This chapter details the finite element work completed for the project in order to develop a further understanding of the gap damper system behavior. A coarse mesh was initially used to assess global behavior of the system. Models were compared to experimental load cases showing good agreement with results. A calibrated model meant that other parameters of interest, such as lateral damper participation, could be evaluated using the coarse model. Further analysis was completed with a fine mesh in order to assess the behavior of the system when subjected to high speed impacts. Overall, the gap damper systems exhibited satisfactory behavior that indicates the device will behave as intended. Special attention should be given to gap damper systems that may involve rotated impacts as they may cause localized areas of yielding. Rounding the edges of the nub may also help to ease the local stresses evident in these impacts.

Chapter 6. Development of a Performance-Based Design Criteria

6.1 Introduction

Although seismically isolated structures perform very well during design level earthquakes, during maximum considered earthquakes, these structures can experience very large displacement demands leading to pounding between the structure and the surrounding moat wall. Recent studies on pounding show this phenomenon can introduce very large demands to the superstructure and possible system collapse. In order to limit displacement of seismically isolated structures during a maximum considered earthquake (MCE) and prevent pounding, a passive control device was developed to provide supplemental damping to these structures when specific threshold displacement demands are reached.

In this chapter, this displacement restraint system (gap damper) and its design procedure as backup system will be introduced. The chapter starts by reviewing design requirements for seismically isolated structures. Then gap damper system objectives and components design are presented. At the end of this chapter, a case study of a base isolated structure with the proposed gap damper system is presented. This numerical example which uses the NEES TIPS building (NEESTIPS, 2009) has been modeled in both *OpenSees* and *SAP2000*. The two models are compared to evaluate the suitability of the gap damper modeling process. Using the design procedure developed for the gap damper system, its effectiveness in limiting isolated structure displacement demands will be investigated.

6.2 Gap Damper Design Procedure

6.2.1 Gap Damper as Displacement Restraint System

The proposed displacement restraint system, henceforth known as the "gap damper", limits displacement of seismically isolated structures during a MCE. The main function of the gap damper system is to act as a backup system when a specified displacement threshold demand is reached in the system. Section 6.2.1 summarizes the new procedure to design seismically isolated structures including the design spectrum (Section 6.2.2), isolation system properties (Section 6.2.3), and the selection of ground motions (Section 6.2.4). Then, the general concept of a gap damper and system objectives are introduced in Section 6.2.5. In Section 6.2.6, the gap damper system design procedure is presented. Sections 6.2.7 and 6.2.8 will illustrate further the required analysis to evaluate gap damper performance and general comments on detailing of gap damper systems.

6.2.2 Design Spectrum

Seismically isolated structures that do not require using site-specific ground motion procedures (Chapter 21 of ASCE 7-10 (ASCE/SEI, 2010)) shall be analyzed using a MCE response spectrum. The MCE spectral response acceleration parameters S_{MS} and S_{M1} shall be determined based on following criteria:

1. Location of the site of interest to determine mapped acceleration parameters (S_S and S_1).
2. Site class to determine the site coefficients (F_a and F_v).

The S_{MS} and S_{M1} adjusted for site class effects shall be determined by:

$$S_{MS} = F_a \cdot S_S \qquad \textbf{Equation (6-1)}$$

$$S_{M1} = F_v \cdot S_M \qquad \textbf{Equation (6-2)}$$

where S_S and S_1 shall be determined using Figures 22-1, 22-3, 22-5 and 22-6 and Figures 22-2, 22-4, 22-5 and 22-6, respectively in ASCE 7-10 (ASCE/SEI, Minimum Design Loads for Buildings and Other Structures: ASCE Standard 7-10, 2010). Site coefficients F_a and F_v are defined in Tables 11.4-1 and 11.4-2, respectively (ASCE/SEI, 2010). The MCE response spectrum curve shall be developed as shown in Figure 6-1. The MCE spectral response acceleration, S_a, shall be taken as:

$$
\begin{aligned}
S_a &= S_{MS}\left(0.4 + 0.6\frac{T}{T_0}\right) && T < T_0 \\
S_a &= S_{MS} && T_0 \le T < T_S \\
S_a &= \frac{S_{M1}}{T} && T_S \le T < T_L \\
S_a &= \frac{S_{M1} \cdot T_L}{T^2} && T \ge T_L
\end{aligned}
\qquad \textbf{Equation (6-3)}
$$

where equations for T_0 and T_S are presented in Figure 6-1. The long-period transition period T_L shall be determined using Figures 22-12 to 22-16 of ASCE 7-10 (ASCE/SEI, Minimum Design Loads for Buildings and Other Structures: ASCE Standard 7-10, 2010).

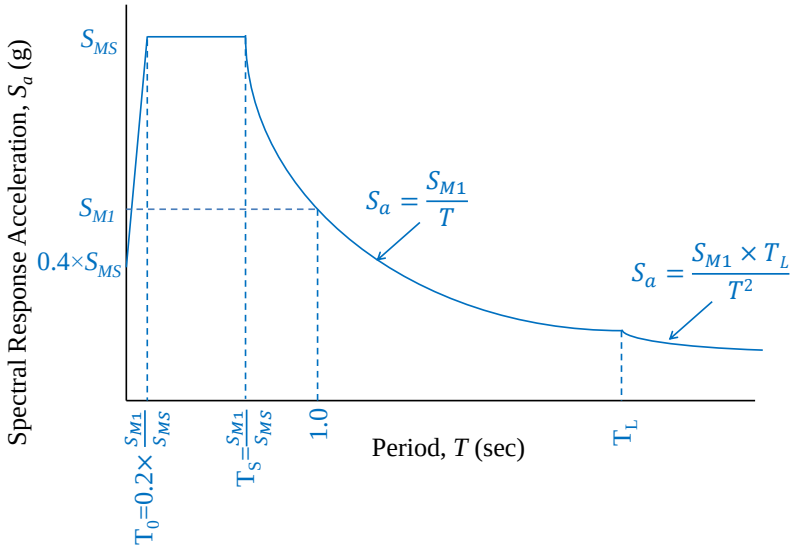

Figure 6-1. MCE Response Spectrum

6.2.3 Isolation System Properties

In this section, isolation system properties at maximum displacement D_M, measured at the isolation system center of rigidity in the direction under consideration, are presented. These properties generally are based on average nominal properties measured over three cycles of prototype testing. Also, a mathematical model of upper-bound and lower-bound force displacement behavior of each isolation system shall be developed. Upper-bound and lower-bound properties of the isolation system shall be determined using property modification factors. Here, the following isolation system properties shall be computed independently for upper-bound and lower-bound properties: the isolation effective stiffness, K_M, the effective damping ratio, β_M, the maximum displacement in system, D_M, the effective period of system, T_M, and total maximum displacement, D_{TM}. Maximum and minimum property modification factors (λ) shall be applied to determine upper-bound and lower-bound properties of the isolation system, respectively. These modification factors shall be used to account for the variation in all isolation component properties as specified in following equations:

$$\lambda_{\max} = (1 + (0.75 \cdot (\lambda_{(ae,\max)} - 1))) \cdot \lambda_{(test,\max)} \cdot \lambda_{(spec,\max)} \geq 1.8 \qquad \textbf{Equation (6-4)}$$

$$\lambda_{\min} = (1 + (0.75 \cdot (\lambda_{(ae,\min)} - 1))) \cdot \lambda_{(test,\min)} \cdot \lambda_{(spec,\min)} \leq 0.6 \qquad \textbf{Equation (6-5)}$$

where $\lambda_{(ae,max)}$ and $\lambda_{(ae,min)}$ are maximum and minimum property modification factors, respectively, used to account for aging effects and environmental exposure. $\lambda_{(test,max)}$ and $\lambda_{(test,min)}$ are maximum and minimum property modification factors, respectively, used to account for the effects of heating, rate of loading and scragging. $\lambda_{(spec,max)}$ and $\lambda_{(spec,min)}$ are maximum and minimum property modification factors, respectively, used to account for permissible manufacturing variation.

Here, required equations to determine isolation system properties are provided. Appropriate modification factors shall be used to find nominal upper-bound and lower bound

isolation properties. The effective stiffness of the isolation system K_M at D_M shall be determined using:

$$K_M = \frac{\sum |F_M^+| + \sum |F_M^-|}{2D_M} \qquad \textbf{Equation (6-6)}$$

where $\sum F_M^+$ and $\sum F_M^-$ are sum of the absolute value of force in isolation units at a positive and negative displacement equal to D_M, respectively. Effective damping ratio in the isolation system, β_M, shall be determined by the following equation:

$$\beta_M = \frac{\sum E_M}{2\pi K_M D_M^2} \qquad \textbf{Equation (6-7)}$$

where $\sum E_M$ is total energy dissipated in the isolation system during a full cycle at the displacement D_M. The effective period, T_M, in isolation system at the displacement D_M shall be computed by:

$$T_M = 2\pi \sqrt{\frac{W}{gK_M}} \qquad \textbf{Equation (6-8)}$$

where W is the effective seismic weight of the structure above isolation level and g is acceleration due to gravity. The maximum displacement at the center of rigidity of isolation system in the direction under consideration, D_M, shall be computed by:

$$D_M = \frac{gS_{M1}T_M}{4\pi^2 B_M} \qquad \textbf{Equation (6-9)}$$

where B_M is numerical coefficient based on effective damping ratio, β_M, and provided in Table 17.5-1 of ASCE 7-10 (ASCE/SEI, Minimum Design Loads for Buildings and Other Structures: ASCE Standard 7-10, 2010). The total maximum displacement, D_{TM} shall include additional displacement due to actual and accidental torsion. The total maximum displacement, D_{TM}, shall be computed by:

$$D_{TM} = D_M \left[1 + \left(\frac{y}{P_T^2} \right) \frac{12e}{b^2 + d^2} \right] \geq 1.1 \cdot D_M \qquad \textbf{Equation (6-10)}$$

where y is the distance between the isolation system center of rigidity and the location of interest measured perpendicular to the direction of seismic loading. The parameter e is actual eccentricity measured in plan between the structure center of mass and the center of rigidity plus accidental eccentricity, taken as 5 percent of the longest plan dimension perpendicular to the direction of seismic loading. Parameters b and d are the shortest and longest plan dimensions of the structure, respectively. The parameter P_T shall be computed by using following equation:

$$P_T = \frac{1}{r_I} \sqrt{\frac{\sum_{i=1}^{N} (x_i^2 + y_i^2)}{N}} \qquad \textbf{Equation (6-11)}$$

where x_i and y_i are horizontal distances from the center of mass to the i^{th} isolator unit in the two horizontal axes of the isolation system. Parameter N is the number of isolators and r_I is the isolation system radius of gyration which is equal to $(b^2+d^2)^{1/2}/12$.

6.2.4 Ground Motion Selection and Scaling

Where response history analysis procedures are used to design seismically isolated structures, at least seven pairs of horizontal acceleration components shall be selected and scaled (using amplitude or spectral matching) from individual MCE recorded motions. These motions shall have magnitudes, fault distance and source mechanisms that are consistent with those that control the MCE. Simulated ground motions are also permitted for use in case a sufficient number of recorded ground motion pairs are not available.

To scale selected ground motions, first, the 5 percent-damped response spectra of the scaled components shall be determined. Then, SRSS (a square root of the sum of the squares) spectrum

of each pair of horizontal ground motion components shall be constructed by taking the SRSS of the previously defined components spectra. Finally, each pair of motions shall be scaled such that in the period range from $0.75 \cdot T_{M,upper}$ and $1.25 \cdot T_{M,lower}$, determined using upper bound and lower bound isolation properties respectively, the average of all horizontal component pairs SRSS spectrum does not fall below the corresponding ordinate of the MCE response spectrum shown in Figure 6-1.

6.2.5 Gap Damper System Objectives

This section introduces various objectives for designing a gap damper system. Here, considering the displacement restraint system's potential in limiting seismically isolated structures displacement demands, the following performance targets are introduced:

1. As explained previously, the primary function of a gap damper system as backup system is to prevent pounding between isolated structures and surrounding moat wall. According to recent modifications in ASCE 7, a minimum gap of D_{TM} (total maximum displacement) between isolation level and surrounding moat wall shall be provided in seismically isolated structures (ASCE/SEI, 2014). Therefore, the gap damper system shall, at a minimum, limit isolated structure displacement demands to less than D_{TM} during maximum considered earthquakes (MCE).
2. For seismically isolated structure design procedure, required gap between isolation level and surrounding moat wall can be reduced from total maximum displacement D_{TM} to smaller displacement demands D'_{TM} ($D'_{TM} < D_{TM}$), if gap damper system has been designed to reduce displacement demands to less than D'_{TM}. This objective is suitable for isolated structures with large torsional effects, which increase total maximum displacement demands (D_{TM}) and consequently the required distance between the structure and the moat

wall. Numerical studies on gap damper system performance indicated that using gap damper system can reduce the torsional effects in seismically isolated structures. This objective is also suitable where providing a large gap between isolated structures and the surrounding moat wall is not possible due to geometric limitations. Where providing gap distance equal to D_{TM} is feasible, the designer can decrease the risk of pounding between seismically isolated structures and surrounding moat wall by setting larger objectives for gap damper system.

3. The gap damper system can also be designed to limit displacement demands in seismically isolated structures to less than maximum displacement, D_M. Reducing the overall displacement of the system is useful in relaxing requirements for non-structural elements that have to accommodate large relative displacements between the structure and the ground.
4. Where seismically isolated structures are needed to accommodate ground motions larger than MCE motions, the gap damper system can be designed to reduce displacement demands to less than moat wall gap distance.
5. Lastly, the gap damper system can be designed for use in the retrofit of existing seismically isolated structures. Change in seismic hazard, isolation system displacement demand, or a desired increase in structural reliability are all potential reasons for a gap damper retrofit.

Where gap damper system is designed to restrain displacement demands in seismically isolated structures to less than D_{TM}, following criteria shall be satisfied:

a. Nonlinear characteristics of the isolation system and the superstructure shall be considered according to dynamic analysis requirements of Section 17.6 (ASCE/SEI, 2014).

b. The ultimate capacity of the isolation system and structural elements below the isolation system shall surpass their strength and displacement demands during MCE (ASCE/SEI, 2014).

c. The superstructure shall be checked for stability and ductility demands during MCE (ASCE/SEI, 2014).

d. The displacement restraint system shall not become effective at a displacement less than $0.6 \cdot D_{TM}$ (ASCE/SEI, 2014).

Prior to selecting the appropriate design objective for gap damper system, the designer shall determine the ultimate displacement demands in seismically isolated structures. The designer shall select and scale suite of ground motions (consisting of at least seven pairs of motions) and apply them to the seismically isolated structure. The selection and scaling process of these ground motions are based on the magnitude and extent of demands (MCE or beyond MCE) that the designer expects for the seismically isolated structure. The average of peak displacement demands under applied ground motions will determine the displacement demands in the seismically isolated structures or D_{DEMAND}. Based on the gap damper design objective the designer selects, the gap damper target displacement reduction can be determined. In this document, the gap damper system objective is set to limit displacement demands in seismically isolated structures to maximum displacement, D_M. However the gap damper system will typically be considered successful as long as it prevents pounding in the structure, depending on the design objectives. Here, the gap damper target displacement reduction, D_{TR}, can be determined by using:

$$D_{TR} = D_{DEMAND} - D_M \qquad \textbf{Equation (6-12)}$$

After D_{TR} is determined, target displacement reduction percentage or $\%D_{TR}$ can be computed by using:

$$\%D_{TR} = 100 \cdot \left(\frac{D_{TR}}{D_{DEMAND}} \right) \qquad \textbf{Equation (6-13)}$$

Once target reduction and reduction percentage are determined for the gap damper system, components can be designed using procedure presented in Section 6.2.6.

6.2.6 Design of Gap Damper System Components

The theoretical derivation of the gap damper system involves the equal energy concept, shown in Figure 6-2. Parameters of the dampers are calibrated to a reference level of energy dissipation (ED_{ISO}), which is the theoretical energy dissipated by the isolation system as it moves from D_M to the displacement demand of the system, D_{Demand}, for a full cycle. Energy dissipated by the gap damper (ED_{GD}) activates at a threshold displacement of 0.6 times the total maximum displacement (D_{TM}) and is active until reaching D_M. The primary objective of the gap damper is to limit the base displacement to be less than the moat wall clearance, located at D_{TM}, which is a minimum of 1.1 times D_M according to Section 17.5.3.5 (ASCE/SEI, Minimum Design Loads for Buildings and Other Structures: ASCE Standard 7-10, 2010).

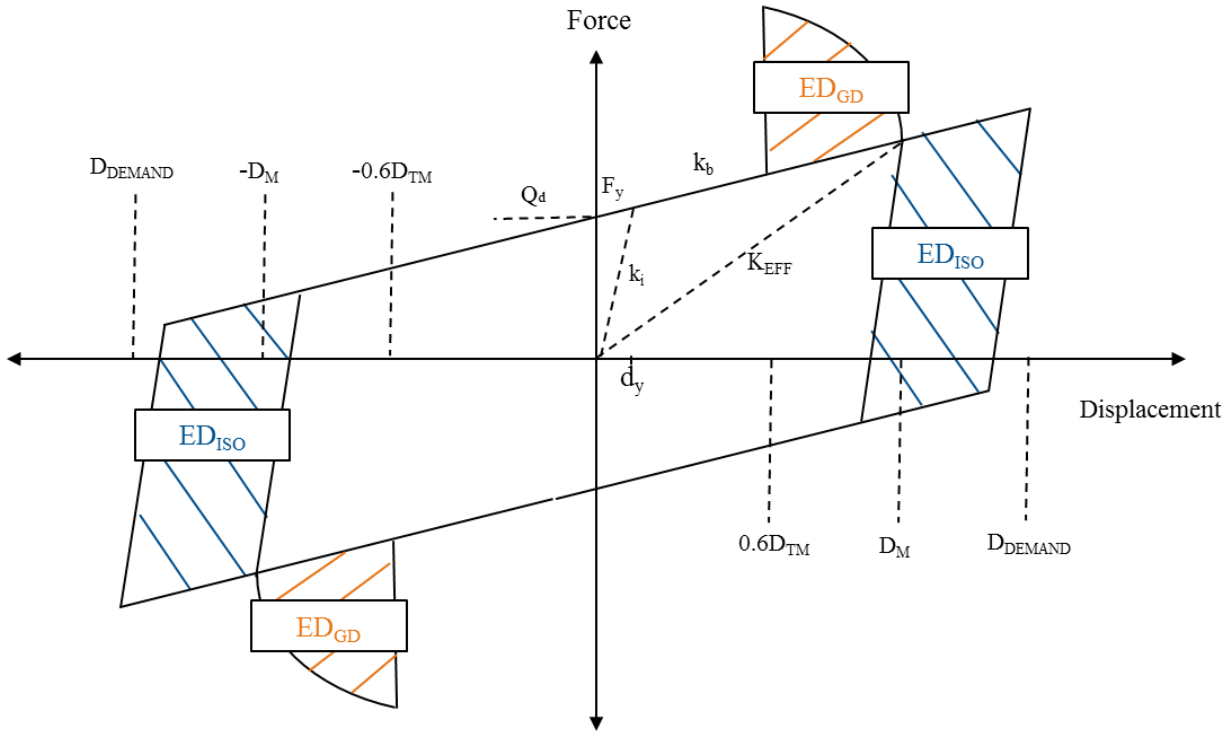

Figure 6-2 Equal Energy Concept

A direct ratio of ED_{GD} to ED_{ISO} does not necessarily achieve the desired system objectives. For this reason, a normalized energy dissipation level is introduced:

$$EDL = \frac{ED_{GD}}{ED_{ISO}} \qquad \textbf{Equation (6-14)}$$

where a number greater (or less) than unity indicates the gap damper possesses a higher (or lower) energy dissipation capacity than that calibrated to reduce the isolator displacement from the D_{Demand} to D_M. EDL values were optimized via parametric study to ensure targeted displacement reduction in the 84th percentile (median plus one standard deviation) of ground motion displacement demands (Section 3.3.5.5). EDLs are largely a function of the fundamental period of vibration, damping capacity of the isolators, and the target displacement reduction. Design values are given in Figure 6-3, with natural period (T_N) corresponding to the first mode of vibration and effective damping (β_{eff}) defined according to Section 17.8-2 (ASCE/SEI, 2010). Values can

be linearly interpolated between values in the tables. Values can be interpolated for natural period and effective damping values not given within a table, but can also be interpolated target reduction values parameters if the design parameters are not presented in the design tables.

T_N (seconds)	β_{eff} 10%	15%	20%	25%
2.5	1.5	1.1	0.8	0.7
3	1.5	1.3	1	0.8
3.5	1.8	1.4	1.1	0.9
4	2.7	1.5	1.1	0.9

a) 10% Target Displacement Reduction

T_N (seconds)	β_{eff} 10%	15%	20%	25%
2.5	1.7	1.3	1	0.9
3	1.8	1.4	1.1	0.9
3.5	2	1.6	1.3	1
4	2.9	1.8	1.4	1.1

b) 20% Target Displacement Reduction

T_N (seconds)	β_{eff} 10%	15%	20%	25%
2.5	1.8	1.3	1.1	0.8
3	1.9	1.4	1.2	0.9
3.5	2.2	1.7	1.4	1.1
4	2.9	2	1.5	1.1

c) 30% Target Displacement Reduction

T_N (seconds)	β_{eff} 10%	15%	20%	25%
2.5	1.8	1.4	1.1	0.9
3	2	1.5	1.2	0.9
3.5	2.2	1.7	1.4	1.1
4	2.9	2	1.5	1.2

d) 40% Target Displacement Reduction

Figure 6-3. EDL Design Values

Fundamentally, if the isolator properties, target displacement reduction (D_{TR}), and EDLs are known, the energy dissipation requirement of the gap damper system can be found by rearranging Equation 6-14 and adding a modification factor (M):

$$ED_{GD} = M \cdot EDL\left(ED_{ISO}\right) \qquad \textbf{Equation (6-15)}$$

where a modification factor of 1.0 is used for the initial analysis. Adjustment of the modification factor up (or down) may be necessary if the design does not achieve the desired displacement

reduction objective (or too much displacement reduction). Energy dissipated by a full isolator cycle (ED_{ISO}) can be defined as:

$$ED_{ISO} = \sum_{n=1}^{N_{ISO}} 4Q_{ISO}\left(D_{TR}\right) \qquad \textbf{Equation (6-16)}$$

where N_{ISO} is the number of isolators and Q_{ISO} is the characteristic strength of the isolator. This summation accounts for potential variation in isolator energy dissipation capacity throughout the isolation system.

Using the elliptical hysteresis equation for a linear viscous damper assuming harmonic motion and that the forcing and natural period are equivalent, ED_{GD} is defined by:

$$ED_{GD} = 4N_{GD}\, w_n c \int_{0.6D_{TM}}^{D_M} \sqrt{D_M{}^2 - x^2}\, dx \qquad \textbf{Equation (6-17)}$$

where the constant *"4"* is a function of a gap damper system having two dampers in a direction of movement. In addition, N_{GD} is the number of gap damper systems, w_n is the effective frequency of the isolated structure, and c is the damping constant required in each damper in the system.

Utilizing Equation 6-15, Equation 6-16, and Equation 6-17, the damping constant required for individual dampers is given by:

$$c = EDL \frac{M \sum_{n=1}^{N_{ISO}} 4Q_{ISO}\left(D_{TR}\right)}{N_{GD}\, w_n \int_{0.6D_{TM}}^{D_M} \sqrt{D_M{}^2 - x^2}\, dx} \qquad \textbf{Equation (6-18)}$$

The threshold displacement (or gap) between the nub element and bumper system is defined as:

$$Gap = 0.6 \cdot D_{TM} \qquad \textbf{Equation (6-19)}$$

which is governed by the working version of Section 17.2.4.5 of ASCE 7-16, stating that a displacement restraint system may not become active until 60% of maximum total displacement (ASCE/SEI, 2014). In a building design, the dampers should be active until contact with the moat

wall if the energy dissipation was not sufficient to limit the displacement enough to avoid impact. Therefore, the minimum stroke required in the damper is given by:

$$Stroke_{REQUIRED} = \pm\left(1.1D_{TM} - 0.6D_{TM}\right) \qquad \textbf{Equation (6-20)}$$

which ensures reserve capacity beyond the moat wall location, typically at D_{TM}.

When considering the number of gap damper systems, economy is likely the most important factor as long as performance is not sacrificed. Due to detailing requirements and economies of scale, fewer gap damper systems are typically more desirable. Using more gap damper systems may be preferable to reduce the localized force demands on the isolation system. The number of systems used beneath a structure should be chosen based on the objective of the designer but should be a minimum of two in order to reduce the possibility of eccentricity upon activation of the dampers.

In addition, placement of the gap damper systems should be relatively equidistant from the center of mass as to not induce torsional response upon activation of an eccentric system. Gap damper systems can provide a reduction in torsional response in comparison to a traditionally base-isolated structure by placing them towards the perimeter of the structure. Geometric constraints should be considered to ensure the movement of the dampers and components are not impeded by other elements in the isolation interface. Placement should also consider access for inspection of the components over the life of the structure.

For preliminary sizing of the viscous dampers, the force capacity of the damper can be reasonably estimated as:

$$Force = c \cdot S_v \qquad \textbf{Equation (6-21)}$$

where c is the damping constant found in Equation 6-18 and S_v is the spectral velocity of the system. With a known force demand, stroke requirement, and damping constant, a damper can be

chosen for the system. Another important consideration, in the selection of the damper is efficiency of the damper as the specified energy dissipation may not be fully realized. Close communication with the damper manufacturer is necessary to ensure the damper will achieve the desired design objectives. After the completion of the gap damper preliminary sizing, analysis of the structure proceeds per typical base-isolation design procedure with a few additional considerations.

6.2.7 Analysis Recommendations

The analysis of the structure should be completed in accordance to the *Dynamic Analysis Procedures* of ASCE 7-16 Section 17.6, considering nonlinear characteristics of the isolation system and the superstructure (ASCE/SEI, 2014). Modeling recommendations for the inclusion of a gap damper system in a base-isolated structure are found in Section 6.3.2 and Section 6.3.3. Preliminary analysis of the structure should consider the displacement reduction achieved by the system in comparison to the target identified in the design objectives. If the gap damper falls short of the design objectives (or displacement exceeds the desired reduction), the modification factor (M) in Equation 6-15 should be adjusted up (or down) accordingly. Iteration may be necessary to achieve the desired design objectives.

Careful consideration should be given to increases in the modification factor as increased energy dissipation in the gap damper system will have an effect on the superstructure behavior. In addition to the displacement demands, the adequacy of structural design should also be examined. Structural members will likely see an increase in demand due to the activation of the gap damper system. Story accelerations, member forces, story drifts, and other performance metrics should all be considered in the analysis of the superstructure in accordance with design requirements. Superstructure stability and demand of the structural and non-structural elements below the

isolation system should be checked for adequacy. In addition to analysis considerations, the final design of the gap damper components should consider the *Detailing Recommendations* of Section 6.2.8.

6.2.8 Detailing Recommendations

The detailing of the gap damper system components is subject to designer discretion. All elements should meet minimum strength and limit state requirements without a fundamental deviation from gap damper formulation. Figure 6-4 overviews the important design considerations when detailing gap damper components, including:

1. Placement of the damper clevis connections in adjacent corners to resist rotation of the bumper system due to eccentric impact.
2. Smooth, non-corrosive finish on contacting surfaces to minimize friction.
3. Adequate force transfer from the damper into the foundation considering force demands from dynamic analyses.
4. Rounded edges on the nub to minimize local stress concentrations upon impact.
5. Clevis, pin, and shim requirements per damper manufacturer specifications and recommendations.
6. Connection of the nub to the superstructure considering the large force demands from the dampers in the dynamic analysis.
7. Minimization of the length of the nub to increase rigidity. Consideration shall be given to the vertical displacement of the nub element at large displacements.
8. Sliding interface between bumper system and ground shall be clear of any mechanisms that may restrict movement.

9. Outside corners of the bumper system shall be 90 degrees or employ a design that discourages the rotation of the bumper system due to eccentric impact of the nub relative to line of damper action. See Figure 6-4 for details.

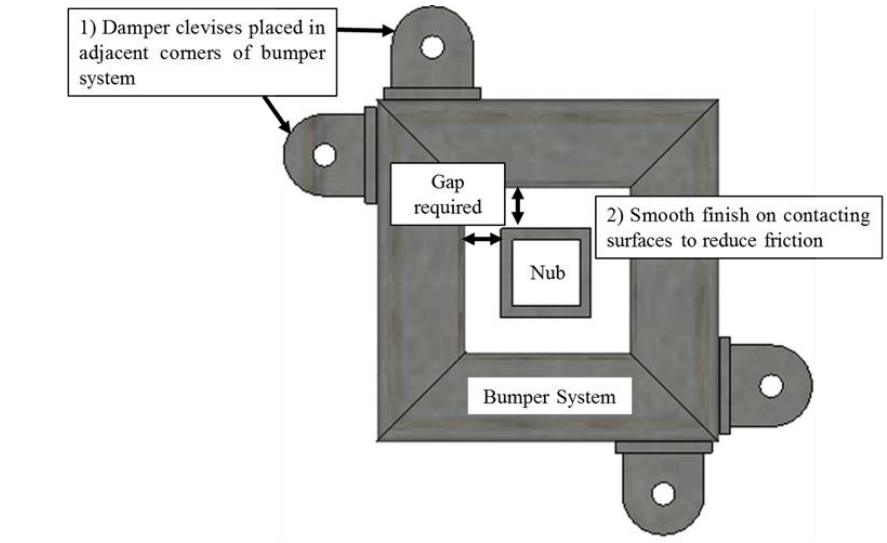

a) Gap Damper Components (Plan View)

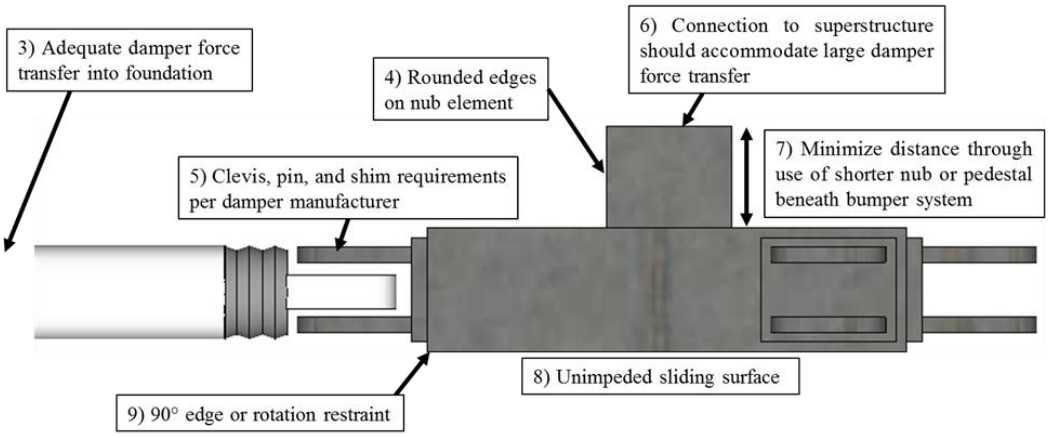

b) Gap Damper Components (Elevation View)

Figure 6-4. Design Considerations

6.3 Gap Damper Case Study

This section utilizes the developed design methodology in a practical building design. The case study involves the design of a three-story structure with a gap damper system implemented as a back-up system. An overview of the case study structural details is presented in Section 6.3.1. Three-dimensional models are developed in *OpenSees* and *SAP2000* for comparison purposes with modeling assumptions for both analyses in Sections 6.3.2 and 6.3.3 respectively. Details on ground motion scaling (Section 6.3.4) and gap damper component design (Section 6.3.5) are also demonstrated. The results of the preliminary analysis (Section 6.3.6) are discussed with a comparison of the two modeling procedures in Section 6.3.7 and overall behavior of the gap damper system evaluated in Section 6.3.8.

6.3.1 Case Study Structure

The case study structure is a three-story, minimally code-compliant three-story braced-frame office building designed by Forell/Elsesser Engineers, Inc. of San Francisco. The case study structure has been implemented successfully in previous research involving the comparative assessment of base-isolated structures (Erduran, Dao, & Ryan, 2011). Full details on the design assumptions are covered within the scope of the previous research but are summarized as follows:

- Location
    - Los Angeles, CA (Latitude: 34.50N, Longitude 118.2 W)
    - Stiff soil (site class D with shear wave velocity of 180 to 360 m/s)
    - Spectral values S_s = 2.2g and S_1 = 0.74g
- Building Characteristics
    - Three-story, steel braced-frame structure modified from the SAC Steel Project (Federal Emergency Management Agency, 2000)

- Designed with *Equivalent Lateral Force* provisions of ASCE 7-05 (ASCE/SEI, 2005). Other design provisions include IBC 2006 (International Code Council, 2006) and AISC 341-05 (ANSI/AISC, 2005).
- Ordinary concentrically braced-frame with R = 1 and drift limit of 1.5%
- Occupancy category II with an importance factor of I = 1
- Floor weights for the base floor, first floor, second floor, and roof are 7064 kN (1588 kip), 7464 kN (1678 kip), 7464 kN (1678 kip), and 7500 kN (1686 kip) respectively. The center of mass was moved 5% of each plan dimension to account for accidental torsion as required by ASCE 7-05 Provision 12.8.4.2 (ASCE/SEI, 2005).
- Plan dimensions of 55 m x 36.6 m (180 ft x 120 ft) with story heights of 4.57 m (15 ft). Bay dimensions are 9.15 m x 9.15 m (30 ft x 30 ft). See Figure 6-5 and Figure 6-6 for layout details.

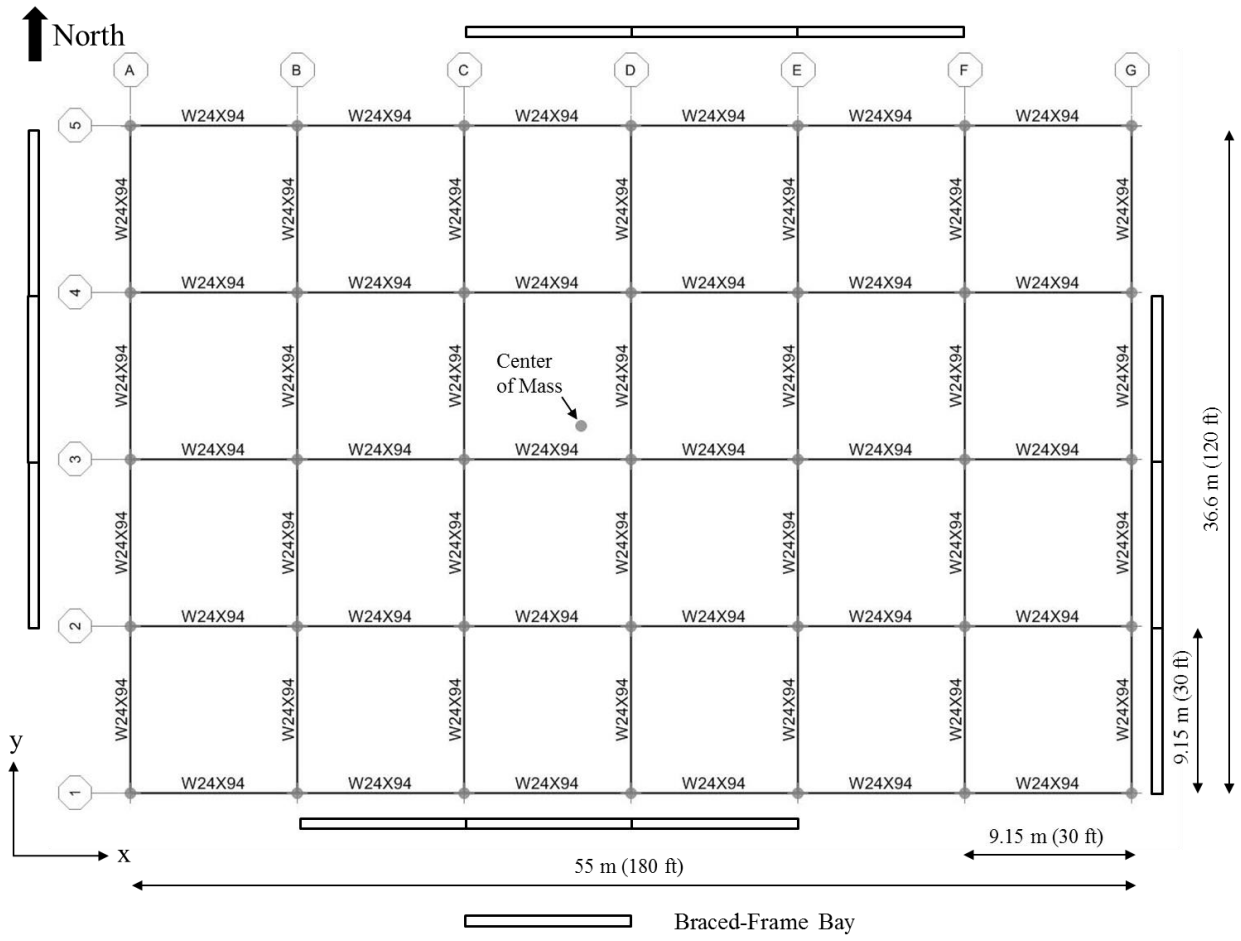

Figure 6-5. Base Floor Plan View

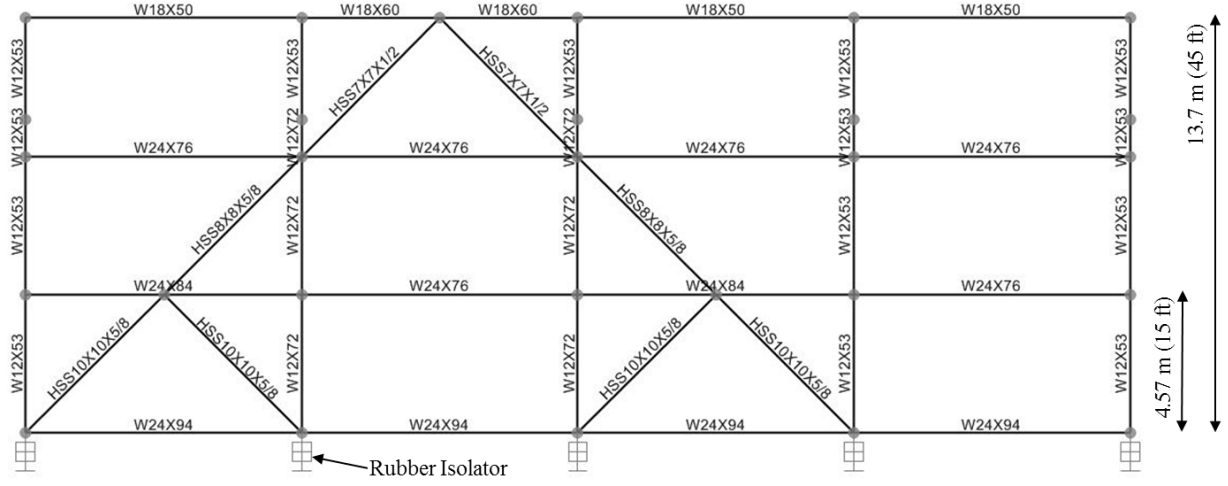

Figure 6-6. Elevation View (Column Line G)

- Isolation Characteristics
  - Elastomeric isolators, with hysteretic behavior summarized in Figure 6-7, are placed under each column (35 total) with properties calibrated to meet the target values for the system:

    Target MCE values: T_M = 3.10 Seconds, β_M = 15.0%

$$D_M = \frac{gS_{M1}T_M}{4\pi^2 B_M} = 0.622m(24.5in) \quad \textbf{Equation (6-22)}$$

    Total maximum displacement:

$$D_{TM} = 1.1D_M = 0.684m(27.0in) \quad \textbf{Equation (6-23)}$$

  - The effective secant stiffness (K_M) of each isolator is found using the target period (T_M), total mass (M), and number of isolators (N_{ISO}) in the structure:

$$K_M = \frac{M\left(\frac{2\pi}{T_M}\right)^2}{N_{ISO}} = 380.5\frac{kN}{m}\left(2.17\frac{kip}{in}\right) \quad \textbf{Equation (6-24)}$$

    With characteristic strength (Q) defined as:

$$Q = \frac{\pi K_M \beta_M D_M^2}{2(D_M - D_y)} = 56.7kN(12.7kip) \quad \textbf{Equation (6-25)}$$

    where damping ratio (β_M) = 15% and yield displacement (D_y) = 1 cm (0.39 in). Post-yield stiffness (k_b) and initial stiffness (k_i) are then solved according to Equations 6-26 & 6-27 respectively:

$$k_b = \frac{K_M D_M - Q}{D_M} = 289.4\frac{kN}{m}\left(1.65\frac{kip}{in}\right) \quad \textbf{Equation (6-26)}$$

$$k_i = k_b + \frac{Q}{D_y} = 5966.9\frac{kN}{m}\left(34.1\frac{kip}{in}\right) \quad \textbf{Equation (6-27)}$$

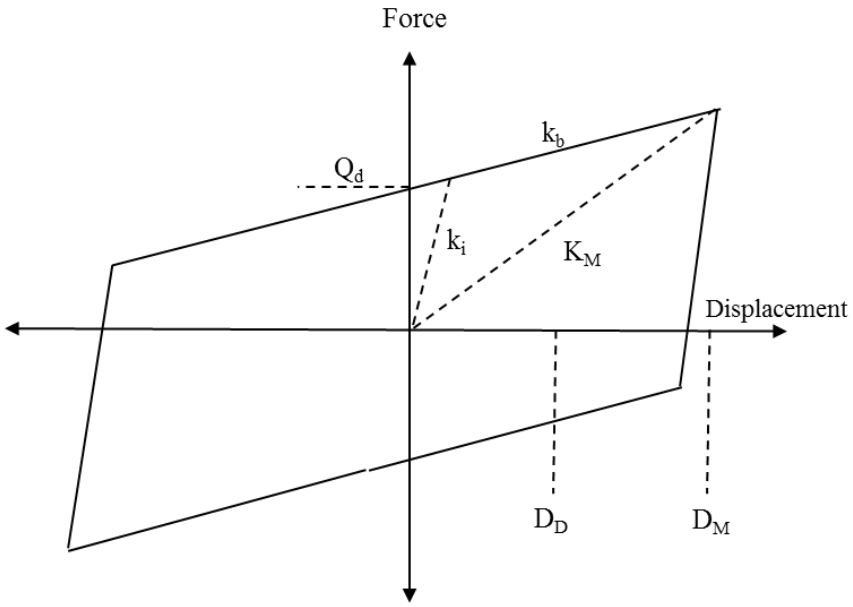

Figure 6-7. Isolator Hysteresis

A summary of isolation system properties for the case study building is found in Table 6-1.

Table 6-1. Isolation System Properties

System Properties	
Maximum Values	Design Values
T_M = 3.10 Seconds	T_D = 2.79 Seconds
β_M = 15.0%	β_D = 23.6%
D_M = 0.622 m (24.5 in)	D_D = 0.315 m (12.4 in)
D_{TM} = 0.684 m (27.0 in)	
Isolator Properties	
Characteristic Strength (Q)	56.7 kN (12.7 kip)
Effective Stiffness (K_M)	380.5 kN/m (2.17 kip/in)
Initial Stiffness (k_i)	5967 kN/m (34.1 kip/in)
Secondary Stiffness (k_b)	289.4 kN/m (1.65 kip/in)

6.3.2 Modeling Procedure (OpenSees)

The base isolated building for gap damper case study was built in both *OpenSees* and *Sap2000* for verification of gap damper system performance. In this section, modeling assumptions used in building the base-isolated *OpenSees* structure are summarized. These assumptions are primarily discussed in an article by Erduran, Dao, & Ryan (2011) which investigated the response of low-

rise conventional and base-isolated structures subject to several suites representing the seismic hazard for different return period earthquakes or different frequency of occurrence.

The 3D *OpenSees* model uses lumped mass for each story and shifts the center of mass 5% of each plan dimension to account for accidental torsion. Rigid diaphragm constraints were assigned to reduce the effect of local modes on the overall response of the superstructure. Viscous damping in the superstructure elements was set proportional to the tangent stiffness of these elements to model the energy dissipation characteristics of the superstructure. This does not include the isolator or gap damper elements. The factor assigned to tangent stiffness matrix (a_1) was derived by assigning damping ratio (ξ) of 2.5% to the first fundamental mode of superstructure according to:

$$a_1 = \frac{2 \cdot \xi}{\omega} = \frac{2 \cdot 0.025}{\frac{2\pi}{0.43}} = 0.0037 \qquad \textbf{Equation (6-28)}$$

where the first mode of the fixed-based building is a coupled lateral torsional mode with a period of 0.43 seconds. The damping matrix was assigned using the Rayleigh damping command in *OpenSees*. All superstructure frame members were designed to remain elastic during simulations due to the response modification factor, R_I, equal to 1.0 in the steel ordinary concentrically braced frame.

The elastomeric bearing element with the Bouc-Wen material was used to model seismic isolators. This bilinear lateral force-deformation model captures the bidirectional coupling effects in isolators. Due to differing vertical force-deformation behavior of isolators in tension and compression, the element stiffness in the axial direction was defined independently for tension and compression. Here, the compressive stiffness of the isolators was computed by assuming a vertical

frequency of 10 Hz, while tensile stiffness was assumed to be 1% of the value of the compressive stiffness.

The *OpenSees* gap damper model was built by utilizing linear truss elements with viscous energy dissipation capacity. Elements were assembled in series with zero-length elastic, perfectly-plastic gap elements. Figure 6-8 illustrates the bidirectional gap damper model with two dampers in each direction connected to the isolation nub, which was connected to bottom of a girder in the base floor. The node that represented this connection was considered as part of a rigid diaphragm constraint in the base floor.

As shown in Figure 6-8, each damper was modeled in series with two parallel gap elements representing the gap in positive and negative displacements in that specific direction. The initial gap distance was assigned equal to $0.6 \cdot D_{TM}$ (Equation 6-18). The yield strength of the gap element was assigned a very high value to prevent the gap element from developing nonlinear properties. The transition stiffness of the gap elements was critical in evaluating gap damper response and will be discussed in more detail in Section 6.3.5.

The damping coefficient of viscous dampers was derived by the following equation:

$$C_{DAMPER} = \frac{c \cdot L \quad (TrussLength)}{1 \quad (TrussArea)} \qquad \textbf{Equation (6-29)}$$

where c is damping coefficient of viscous damper derived from Equation 6-18. L is the length of the truss element, and a value of *1* is the truss element area.

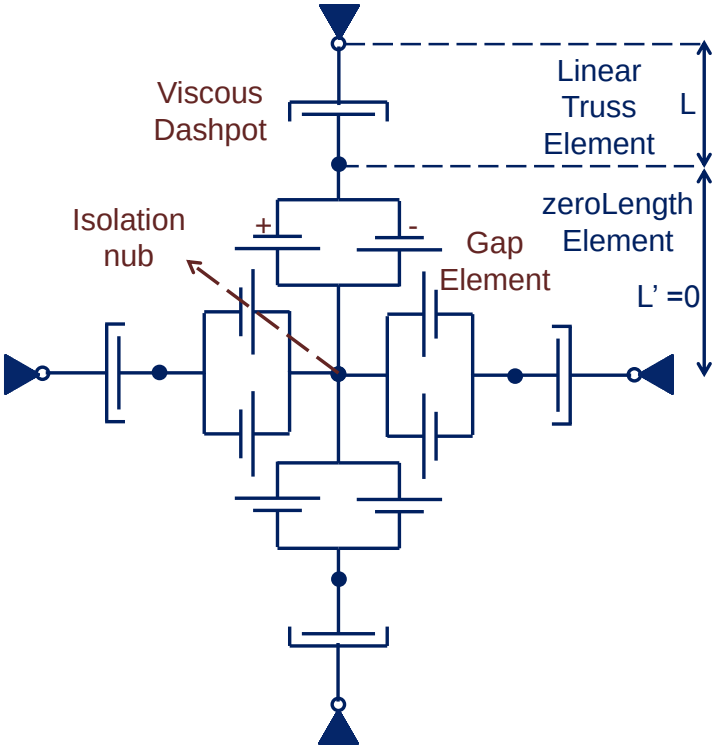

Figure 6-8. Bidirectional Gap Damper Model

6.3.3 Modeling Procedure (SAP2000)

In addition to the detailed *OpenSees* model, a simplified model was created in *SAP2000* to provide an additional implementation method (Computers & Structures, Inc., 2014). The three-dimensional modeling approach has special considerations for the isolated structure and gap damper system to ensure proper behavior within the *SAP2000* framework. Figure 6-9 shows the modeled structure using the *"Rubber Isolator"* link elements under each column. The axial (*U1*), translational (*U2*), and translational (*U3*), properties are defined as derived in Section 6.3.1. An additional level is added beneath the base floor for the inclusion of the gap damper system. The lumped floor mass was moved to an eccentric location on the floor and a rotational inertia was added to account for the accidental torsion as required by ASCE 7-05 Provision 12.8.4.2 (ASCE/SEI, 2005). Each floor mass was tied to all floor joints through the use of a diaphragm constraint for computational efficiency.

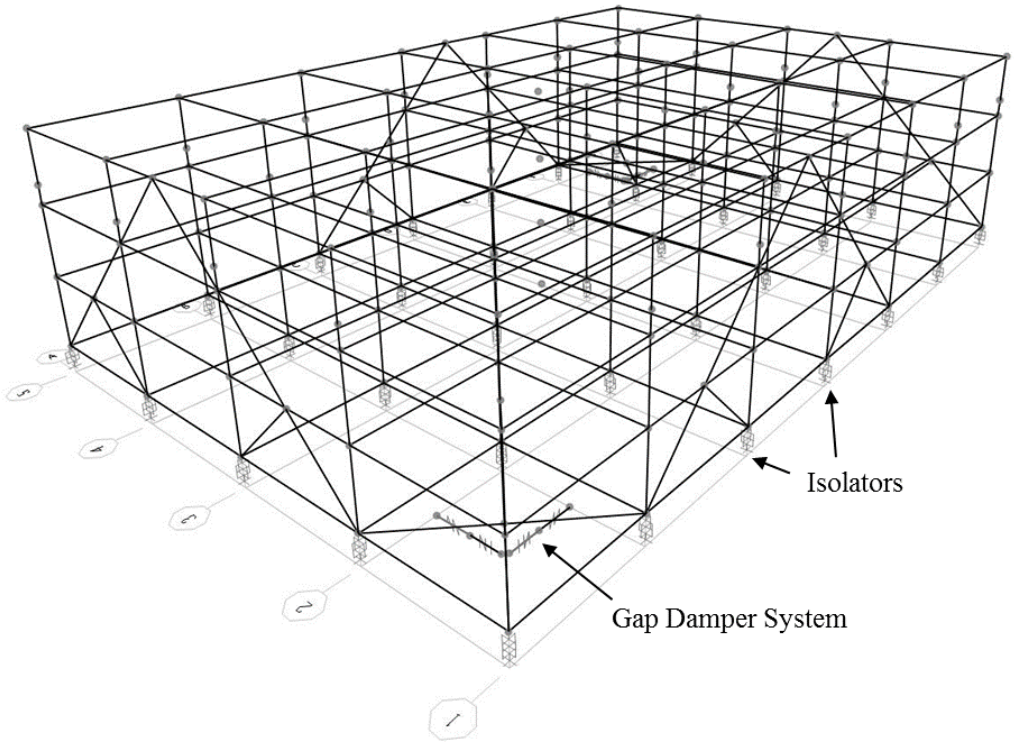

Figure 6-9. Three-Dimensional SAP2000 Model

The analysis of the structure was completed using fast nonlinear analysis (FNA) (Wilson, 2002). Sarlis and Constantinou (2010) recommend the use of FNA over direct integration procedures for the modeling of base-isolated structures due to increased accuracy and computational efficiency. Effective FNA analyses must be primarily linear-elastic and limit nonlinear behavior to a limited number of link elements (Computers & Structures, Inc., 2014). In addition, the proper implementation of FNA should carefully consider the number of Ritz vectors modes for an accurate dynamic analysis. The number of Ritz vectors is typically taken as 3 times the number of isolators plus lumped masses (Sarlis & Constantinou, 2010). Inherent damping of a structure should also be carefully considered with FNA in *SAP2000* as excessive damping is possible due to inclusion of the isolated periods in the Rayleigh damping formulation. Sarlis & Constantinou (2010) recommend the use of Rayleigh damping with overrides, shown in Figure 6-10. Setting damping to zero in the modes associated with the isolation level and assigning 2.5%

Rayleigh damping (associated with the first superstructure frequency) for the mixed isolation and superstructure modes eliminates issues with damping leakage. For a three-dimensional, three-story structure with diaphragm constraints, there are three isolation modes and nine mixed modes. The gap damper elements are independent of this damping formulation.

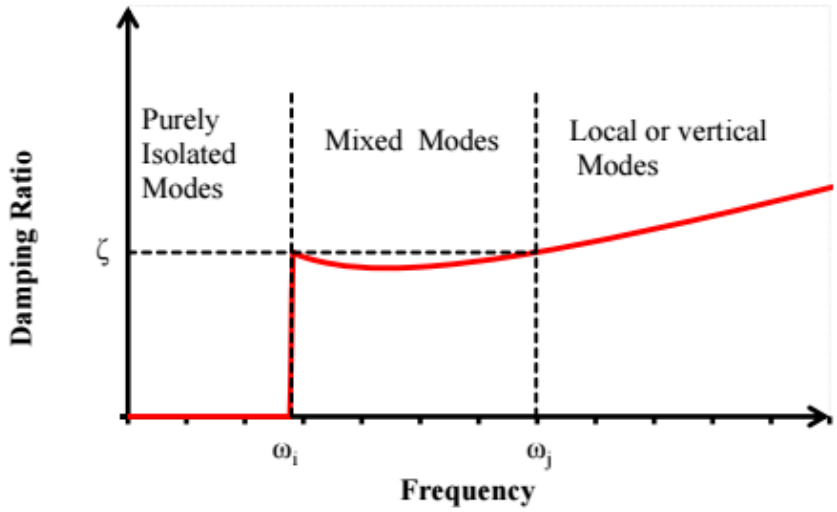

Figure 6-10. Rayleigh Damping with Overrides (Sarlis & Constantinou, 2010)

The modeling of the gap damper system requires a combination of nonlinear link elements to achieve appropriate behavior (Figure 6-11). The simplified model of the gap damper system neglects the explicit modeling of the structural elements such as the nub and bumper system. These elements are designed separately using demands from the dynamic analyses. Although a gap damper system has two dampers in each translational direction, the nonlinear behavior is combined into one series element in order to reduce nonlinear link elements in the FNA.

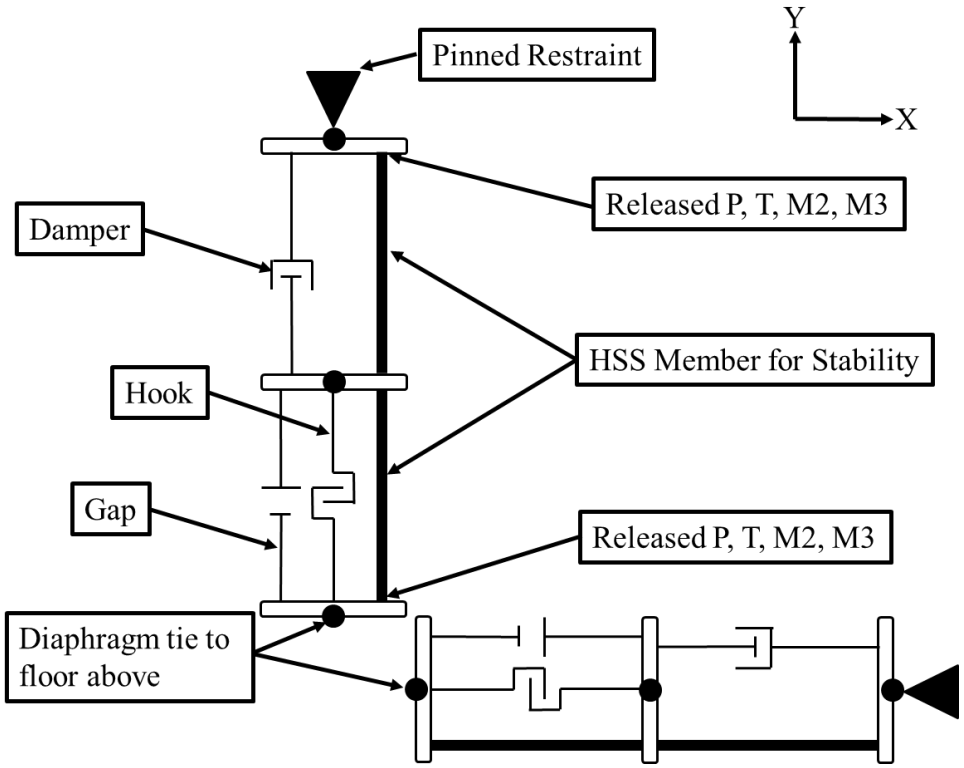

Figure 6-11. Simplified Gap Damper Model (Plan View)

Gap/hook elements are used to model inactive portion of the gap damper system prior to activation of the dampers. The *U1* direction is assigned an "Open" value equal to the gap required for the system and the stiffness value is assigned an appropriately large stiffness, discussed in detail below. The damper element is created using a linear link element in the *U1* direction with a damping value equal to two times the damping constant configured from the gap damper property calculations. A slight mass and effective stiffness is added to the link element degrees of freedom for computational stability and proper participation in the dynamic analysis (Computers & Structures, Inc., 2014). Each translational direction has 3 joints for the connectivity of the link elements (Figure 6-11). A flexural member is added in parallel to the gap damper series system to prevent bifurcation of the link elements at the middle joint. The flexural member requires axial and flexural releases at the end joints to ensure proper behavior of the system.

In order to eliminate issues with the dynamic analysis, the two translational gap damper elements (x and y direction) should be treated as separate series elements. The joint associated with the connectivity of the structure should be tied with a diaphragm constraint to the floor above. The joint associated with the connectivity to the ground should be restrained with a pinned connection in all three translational degrees of freedom. The total length of the gap damper element should be sufficiently long enough so that the angle of rotation if the series element is less than 10 degrees when the system has reached D_{MCE} in the perpendicular direction. The simplified gap damper model utilizes small rotation assumptions to accomplish the complex bi-directional behavior. In addition to these modeling considerations, the stiffness of the gap element also has a tremendous influence on the superstructure behavior. A full analysis of gap damper activation stiffness is presented in Section 6.3.5 *"Gap Damper Properties"*.

6.3.4 Ground Motion Selection

A suite of twenty ground motions were selected and scaled for this case study by using motions provided in recent study by Cutfield, Ryan, & Ma (2015). Here, the ground motions with a hazard level of 1/2475 years were selected. These motions were selected based on their spectral closeness of fit to a conditional mean spectrum at period of 3.0 sec (first isolation period) and over a period range of 1.425 sec ($0.5 \cdot T_D$) to 3.875 sec ($1.25 \cdot T_M$). Scale factors for these motions were found to be between 0.7 and 2.9.

The motions were applied to the base-isolated building of the case study and the peak displacement demands at center and corners of building were determined. Based on peak displacement demands, they were categorized into two subsets of seven motions. The first subset, 20% target reduction motions (%D_{TR} = 20%), imposed average resultant displacement demands, D_{DEMAND} = 0.77 m (30.3 in) in the *OpenSees* model and 0.8 m (31.5 in) in the *SAP2000* model.

These demands are approximately 20% larger than isolation system maximum displacement, D_M (0.622 m or 24.5 in). The second subset, 40% target reduction motions (%D_{TR} = 40%), imposed average resultant displacement demands, D_{DEMAND} = 1.09 m (42.91 in) in the *OpenSees* model and 1.11 m (43.7 in) in the *SAP2000* model. These demands are approximately 40% larger than isolation system maximum displacement, D_M (0.622 m or 24.5 in). Table 6-2 presents the two motion subsets along with their essential characteristics including earthquake, station, magnitude, closest distance to fault rupture, and applied scale factors. The structural response of case study building subjected to the two suite of motions is discussed in Sections 6.3.6 and 6.3.7. Once the percent target reduction was determined for the two sets of motions, the design objective was defined as reducing the displacement of the system below D_{TM}, as to avoid contact with the moat wall. This objective does not necessarily coincide with a 20% or 40% reduction in displacement but design EDL values for the 20% and 40% target reduction should be used due to subtleties in the derivation of the EDL behavior of a unidirectional system. Once the design objectives were established, the gap damper system components properties were calibrated using the design procedure.

Table 6-2. Selected Ground Motions Suite and Characteristics

20% Target Reduction						
GM #	NGA	Earthquake	Station	Magnitude	Distance (km)	Scale Factor
20-1	NGA 2509	Chi-Chi, Taiwan-03, 1999	CHY104	6.2	35	2.83
20-2	NGA 292	Irpinia, Italy-01, 1980	Sturno	6.9	10.8	1.62
20-3	NGA 821	Erzican, Turkey, 1992	Erzincan	6.69	4.4	1.15
20-4	NGA 2114	Denali, Alaska, 2002	TAPS Pump Station #10	7.9	2.7	1.1
20-5	NGA 1533	Chi-Chi, Taiwan, 1999	TCU106	7.62	15	2.03
20-6	NGA 1534	Chi-Chi, Taiwan, 1999	TCU107	7.62	16	2.02
20-7	NGA 1492	Chi-Chi, Taiwan, 1999	TCU052	7.62	0.7	0.75
40% Target Reduction						
GM #	NGA	Earthquake	Station	Magnitude	Distance (km)	Scale Factor
40-1	NGA 316	Westmoreland, USA, 1981	Parachute Test Site	5.10	16.7	2.54
40-2	NGA 170	Imperial Valley-06, USA, 1979	EC County Center FF	6.53	7.3	2.09
40-3	NGA 183	Imperial Valley-06, USA, 1979	El Centro Array #8	6.53	3.9	2.26
40-4	NGA 143	Tabas, Iran, 1978	Tabas	7.35	2.0	1.15
40-5	NGA 1176	Kocaeli, Turkey, 1999	Yarimca	7.51	4.8	1.43
40-6	NGA 1194	Chi-Chi, Taiwan, 1999	CHY025	7.62	19.1	2.24
40-7	NGA 1535	Chi-Chi, Taiwan, 1999	TCU109	7.62	13.1	1.6
	NGA 0723	Superstition Hills, USA, 1987		6.54	0.95	0.46

6.3.5 Gap Damper Properties

With the design of the isolators completed and design objectives evident from the ground motion scaling, properties of the gap damper system are developed. The case study structure utilizes two gap damper systems in opposite corners of the structure in order to minimize torsional motion, as shown Figure 6-12 with the cross bracing indicative of the location. The nub is attached at the intersection of the cross bracing due to the geometric layout considerations of the gap damper system.

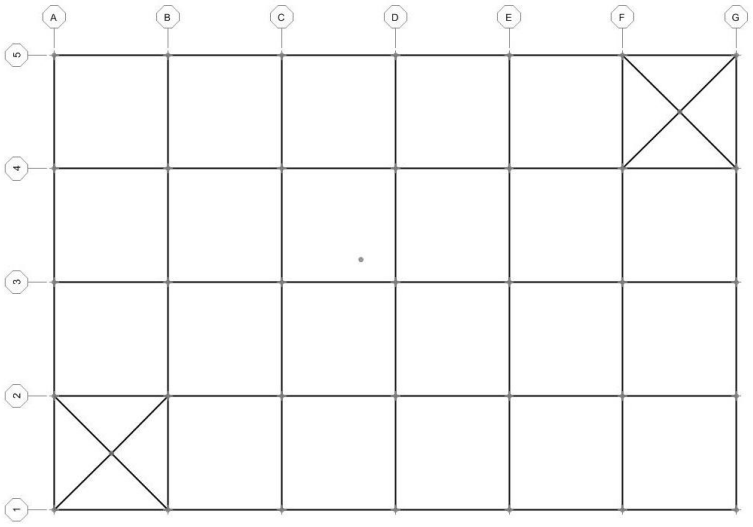

Figure 6-12. Gap Damper Location

Utilizing the fundamental gap damper equations from Section 6.2.6, the properties of the case study gap damper system are derived as follows with representative calculations for the 20% target displacement reduction:

- Energy dissipation:

  Energy dissipated by the 35 isolators beyond D_M:

$$ED_{ISO} = \sum_{n=1}^{N_{ISO}} 4Q_{ISO}\left(D_{TR}\right) \qquad \textbf{Equation (6-30)}$$

$$ED_{ISO} = 35 \cdot 4 \cdot 56.7(0.2 0.622) = 987.5kN \cdot m(8736kip \cdot in)$$

Energy dissipated by the two gap damper systems from $0.6D_{TM}$ to D_M:

$$ED_{GD} = 4N_{GD}w_n c\int_{0.6D_{TM}}^{D_M}\sqrt{D_M{}^2 - x^2}\,dx \qquad \textbf{Equation (6-31)}$$

$$ED_{GD} = 4\cdot 2\cdot 2.027\cdot c\int_{0.6*0.684}^{0.622}\sqrt{0.622^2 - x^2}\,dx = 1.112ckN\cdot m(1721.7ckip\cdot in)$$

- Component design:

  The fundamental gap damper energy equation of Equation 6-15 is rearranged and solved for the damping constant, assuming *M = 1.0* for preliminary design and an EDL of 1.5:

$$EDL = \left(\frac{M\cdot ED_{ISO}}{ED_{GD}}\right) \qquad \textbf{Equation (6-32)}$$

$$c = 1.5\frac{1.0\cdot 987.5}{1.112} = 1333kN\frac{s}{m}\left(7.61kip\frac{s}{in}\right)$$

  where the EDL value used for preliminary design is interpolated using values in Figure 6-13, with a natural period (T_N) corresponding to the first mode of vibration (3.25 seconds) and effective damping value (β_{eff}), associated with the target calibration value of 15%.

T_N (seconds)	β_{eff} 10%	15%	20%	25%
2.5	1.5	1.1	0.8	0.7
3	1.5	1.3	1	0.8
3.5	1.8	1.4	1.1	0.9
4	2.7	1.5	1.1	0.9

a) 10% Target Displacement Reduction

T_N (seconds)	β_{eff} 10%	15%	20%	25%
2.5	1.7	1.3	1	0.9
3	1.8	1.4	1.1	0.9
3.5	2	1.6	1.3	1
4	2.9	1.8	1.4	1.1

b) 20% Target Displacement Reduction

T_N (seconds)	β_{eff} 10%	15%	20%	25%
2.5	1.8	1.3	1.1	0.8
3	1.9	1.4	1.2	0.9
3.5	2.2	1.7	1.4	1.1
4	2.9	2	1.5	1.1

c) 30% Target Displacement Reduction

T_N (seconds)	β_{eff} 10%	15%	20%	25%
2.5	1.8	1.4	1.1	0.9
3	2	1.5	1.2	0.9
3.5	2.2	1.7	1.4	1.1
4	2.9	2	1.5	1.2

d) 40% Target Displacement Reduction

Figure 6-13. EDL Selection

Estimating damper demands for preliminary sizing using Equations 6-33 and 6-34:

Force demand estimate:

$$Force = cS_v = cw_n D_M \qquad \textbf{Equation (6-33)}$$

$$Force = 1333 \cdot 2.027 \cdot 0.622 = 1680 kN (380 kip)$$

Stroke required in damper:

$$Stroke_{REQUIRED} = \pm(1.1 D_{TM} - 0.6 D_{TM}) \qquad \textbf{Equation (6-34)}$$

$$Stroke_{REQUIRED} = 1.1(0.684) - 0.6(0.684) = \pm 0.342 m (13.5 in)$$

Displacement threshold (gap) required in the design of the bumper system is defined by:

$$Gap = 0.6(D_{TM}) \qquad \textbf{Equation (6-35)}$$

$$Gap = 0.6(0.684) = 0.410 m (16.2 in)$$

The 40% target displacement reduction values would follow the same process with differing EDL and D_{TR}. Gap damper properties for the preliminary analysis of the system are summarized in Table 6-3. Using the derived properties and damper manufacturer information available from T*aylor Devices Inc.*, a seismic damper is chosen for design that has a force capacity of 2000 kN (450 kip) and a stroke capacity of ±13. (Taylor Devices Inc., 2015) . A damper of this capacity and stroke would be approximately 2.75 m (9 feet) in length and require large clevis connections. The bumper system and nub would have to be designed to accommodate the large force transfer to the superstructure from the damper forces. The gap between the nub and bumper system should be equal to the derived threshold displacement of $0.6 \cdot D_{TM}$ or 0.41 m (16.25 in). The layout of the system is shown in Figure 6-14.

Table 6-3. Gap Damper Values for Preliminary Analysis

Energy Dissipation		
Property	20% Target Reduction	40% Target Reduction
Isolator Energy (ED_{ISO})	988 kN·m (8736 kip·in)	1974 kN·m (17470 kip·in)
Gap Damper Energy (ED_{GD})	1481 kN·m (13104 kip·in)	3159 kN·m (27950 kip·in)
Energy Dissipation Level (EDL)	1.5	1.6
Modification Factor (M)	1.0	1.0
Component Design Values		
Property	20% Target Reduction	40% Target Reduction
Damping Constant (c)	1333 kN(sec/m) (7.61 kip(sec/in))	2843 kN(sec/m) (16.24 kip(sec/in))
Threshold Displacement (Gap)	0.411 m (16.2 in)	0.411 m (16.2 in)
Stroke Required	±0.342 m (13.5 in)	±0.342 m (13.5 in)
Damper Force	1680 kN (380 kip)	3585 kN (805 kip)

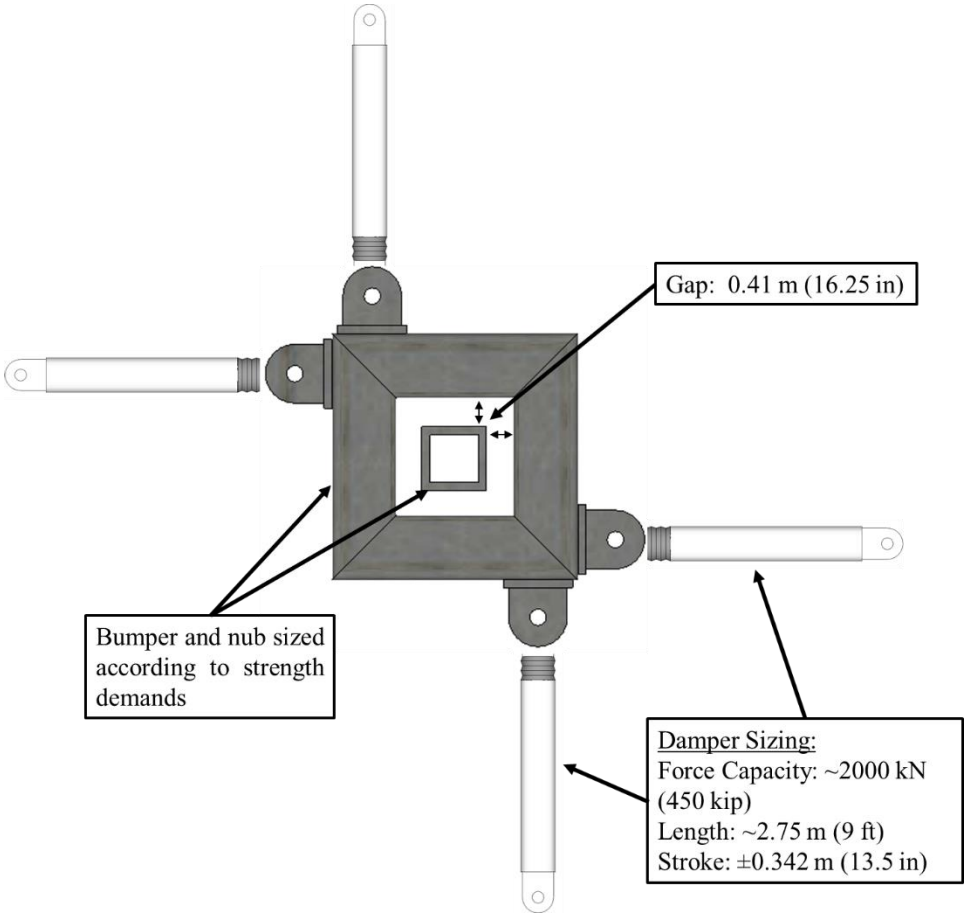

Figure 6-14. Gap Damper Design for the 20% Target Displacement Reduction

The transitional stiffness of the gap/hook elements is a very important consideration in the proper modeling of the gap damper system for appropriate superstructure response. Transitional stiffness is the stiffness present with a gap element closure, transferring the force to the damping elements. A gap damper sensitivity analysis evaluates isolation level displacements and roof accelerations with varying gap stiffness values utilizing the three-dimensional *SAP2000* model for the 7 ground motions associated with 40% displacement reduction objective. Gap stiffness is varied from 437.8 kN/cm (250 kip/in) to 17512.7 kN/cm (10000 kip/in) with the response of the base-isolated structure without a gap damper system (BI) presented for reference. Figure 6-15 indicates that the isolator displacements are relatively insensitive to the gap stiffness although smaller stiffnesses tend to yield slightly higher displacements. Figure 6-16a shows that the peak

roof acceleration ranges from 0.53g for the 437.8 kN/cm (250 kip/in) stiffness and 1.03g for the 17512.7 kN/cm (10000 kip/in), suggesting the predicted acceleration is extremely sensitive to gap stiffness values. Figure 6-16b makes the same comparison with accelerations that are filtered using a 25 Hz filter to eliminate the high frequency peaks that may not be a realistic representation of building behavior. Although the filtering is effective at reducing the high accelerations associated with the higher gap stiffness, the variability in predicted roof acceleration is still large.

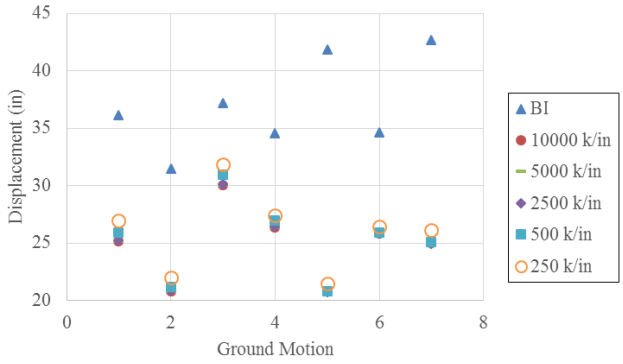

Figure 6-15. Gap Element Displacement Sensitivity Analysis

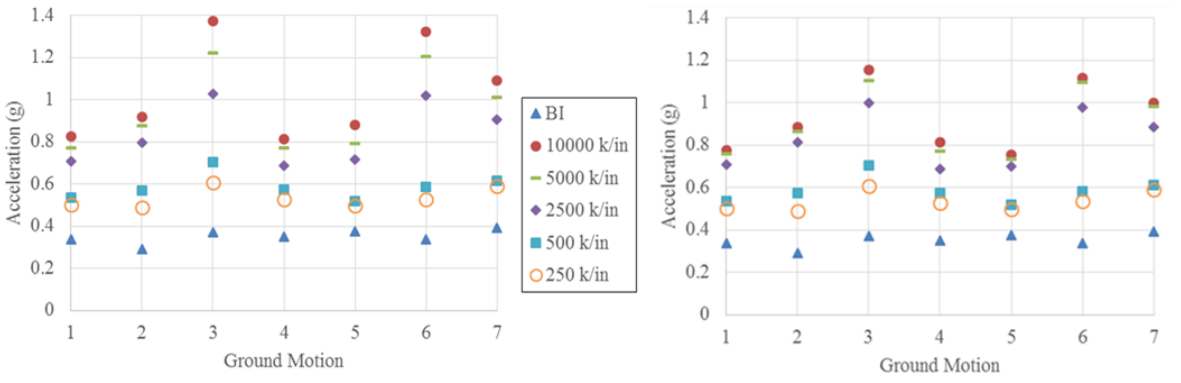

a) Roof acceleration at the center of building (unfiltered)

b) Roof acceleration at the center of building (25 Hz filter)

Figure 6-16. Gap Element Acceleration Sensitivity Analysis

The variability of acceleration response requires a reasonable approximation of the gap stiffness for effective modeling of the system. True gap stiffness is a function of the flexibility of the structural elements associated with the gap damper system, connection between the damper and structural elements, and the compressibility of the damper fluid. Taylor & Constantinou

(1998) introduce the concept of a "rise deflection," which is the distance required to reach the full damper force. With an assumption of 5% volumetric compression, the rise deflection is reasonably approximated as 0.05 multiplied by the total damper stroke. The gap damper system requires the damper to be at mid-stroke prior to first impact which leads to a rise deflection of 0.05 times the total damper stroke capacity divided by two. Using the spectral velocity (S_v) associated with the effective period and damping constant (c) required for the system, the damper force

$$k_{GAP} = 0.75\frac{c \cdot S_V}{0.05\left(\frac{Stroke}{2}\right)} \qquad \textbf{Equation (6-36)}$$

with a 0.75 adjustment factor added to account for the other contributions to flexibility in the system. If quantifiable by the designer, the stiffness may be adjusted as necessary. For the case study building, gap stiffness values are 1621 kN/cm (925 kip/in) for the 20% displacement reduction system and 3458 kN/cm (1975 kip/in) for the 40% displacement reduction system.

6.3.6 Preliminary Analysis

Preliminary models were analyzed in *OpenSees* and *SAP2000* to determine the demands with and without the gap damper system. The primary design objective of the case study is to reduce the displacement demand from the peak value observed with the base isolation system alone (D_{DEMAND}) to a total displacement less than the moat wall location (D_{TM} = 68.4 cm). The 20% target reduction system successfully reduces displacements to below D_{TM} in 5 of 7 ground motions. Conversely, the 40% target reduction system is unable to reduce average displacement below the moat wall location for both analyses (Table 6-5).

Table 6-4 and 6-5 present peak isolator displacement demands (resultant direction) for the case study models without and with a gap damper system, respectively. According to The primary

design objective of the case study is to reduce the displacement demand from the peak value observed with the base isolation system alone (D_{DEMAND}) to a total displacement less than the moat wall location (D_{TM} = 68.4 cm). The 20% target reduction system successfully reduces displacements to below D_{TM} in 5 of 7 ground motions. Conversely, the 40% target reduction system is unable to reduce average displacement below the moat wall location for both analyses (Table 6-5).

Table 6-4, displacement demands predicted by *SAP2000* model exceed those of *OpenSees* models by about 4% for 20% target reduction motions and 2% for 40% target reduction motions. In Section 6.3.7, a comparison between *OpenSees* and *SAP2000* models response is presented in more detail.

The primary design objective of the case study is to reduce the displacement demand from the peak value observed with the base isolation system alone (D_{DEMAND}) to a total displacement less than the moat wall location (D_{TM} = 68.4 cm). The 20% target reduction system successfully reduces displacements to below D_{TM} in 5 of 7 ground motions. Conversely, the 40% target reduction system is unable to reduce average displacement below the moat wall location for both analyses (Table 6-5).

Table 6-4. Peak Displacement Demands at Isolation Level in Base Isolated Case Study

Displacement (cm) (D_M = 62.2, D_{TM} = 68.4)				
	20% Target Reduction		40% Target Reduction	
GM	OpenSees	SAP2000	OpenSees	SAP2000
1	75.7	82.3	101.0	99.9
2	82.1	80.4	94.2	96.9
3	77.0	80.5	94.3	100.3
4	79.6	80.1	123.0	123.2
5	71.9	76.6	134.2	138.7
6	74.0	76.8	102.5	104.7
7	78.5	83.9	113.6	113.5
Average:	**77.0**	**80.1**	**109.0**	**111.0**

Table 6-5. Peak Displacement Demands at Isolation Level in Base Isolated with Gap Damper Case Study

Displacement (cm) (D_M = 62.2, D_{TM} = 68.4)				
	20% Target Reduction		40% Target Reduction	
GM	OpenSees	SAP2000	OpenSees	SAP2000
1	64.5	65.0	71.9	69.2
2	74.0	69.0	61.2	56.9
3	64.6	64.9	77.3	79.1
4	73.6	72.3	73.7	70.5
5	61.7	59.9	66.5	66.6
6	67.4	64.1	76.1	70.5
7	64.4	63.1	69.7	67.5
Average:	**67.2**	**65.4**	**70.9**	**68.6**

With the failure to meet the design objective for the 40% target reduction objective, the gap damper properties are reevaluated using a modification factor of 1.25 in Equation 6-33. The factor increases the energy dissipation required, and subsequently the damping constant, in the gap damper system by 25%. **Error! Not a valid bookmark self-reference.** shows iterated energy values were able to reduce the average displacement close to D_{TM} with mixed results depending on the ground motion. Further analysis of the 40% target reduction system is found in Section 6.3.9. Final design values used for the case study gap damper systems are found in Table 6-7.

Table 6-6. Peak Displacement Demands at Isolation Level in Base Isolated with Gap Damper Case Study with Design Iteration

Displacement (cm) (D_M = 62.2, D_{TM} = 68.4)				
	20% Target Reduction		40% Target Reduction (Modified Values)	
GM	OpenSees	SAP2000	OpenSees	SAP2000
1	64.5	65.0	69.4	67.3
2	74.0	69.0	58.6	55.0
3	64.6	64.9	75.1	77.0
4	73.6	72.3	71.7	69.2
5	61.7	59.9	65.9	63.8
6	67.4	64.1	72.4	67.7
7	64.4	63.1	67.7	65.7
Average:	**67.2**	**65.4**	**68.7**	**66.5**

Table 6-7. Final Case Study Gap Damper Properties

Energy Dissipation		
Property	20% Target Reduction	40% Target Reduction (Modified Values)
Isolator Energy (ED_{ISO})	988 kN·m (8736 kip·in)	1974 kN·m (17470 kip·in)
Gap Damper Energy (ED_{GD})	1481 kN·m (13104 kip·in)	3948 kN·m (27950 kip·in)
Energy Dissipation Level (EDL)	1.5	1.6
Modification Factor (M)	1.0	1.25
Component Design Values		
Property	20% Target Reduction	40% Target Reduction (Modified Values)
Damping Constant (c)	1333 kN(sec/m) (7.61 kip(sec/in)	3551 kN(sec/m) (20.29 kip(sec/in))
Threshold Displacement (Gap)	0.411 m (16.2 in)	0.411 m (16.2 in)
Stroke Required	±0.342 m (13.5 in)	±0.342 m (13.5 in)
Damper Force	1680 kN (380 kip)	4480 kN (1000 kip)

6.3.7 Comparison of Results

In Section 6.3.6, the isolator displacement demands for the case study building with and without the gap damper system were summarized. According to these results, *SAP2000* and *OpenSees* models predicted displacement demands in close agreement. Generally, the displacement demand predicted by *SAP2000* was slightly higher than *OpenSees* for base-isolation alone and slightly lower than OpenSees for the system with a gap damper, suggesting a higher overall displacement reduction for the *SAP2000* model. In this section, *SAP2000* and *OpenSees* models response including displacement and acceleration demands subject to some of applied motions will be compared to evaluate the suitability of the models for modeling the gap damper behavior.

Table 6-8 provides the periods of the first six modes of vibration for the base-isolated building modeled in *OpenSees* and *SAP2000*. Both models predict the fundamental first mode period of about 3.25 sec. The first three modes are isolation modes (including lateral bidirectional and coupled lateral torsional) and the second three modes are mixed isolation and structural modes. Comparison between the first six modal periods suggests the two models are in close agreement

Table 6-8. First Six Modal Periods of the Case Study Structure

Software	SAP2000	OpenSees
Isolation Modes		
1	3.254	3.252
2	3.146	3.146
3	2.617	2.609
Mixed Modes		
4	0.268	0.267
5	0.266	0.263
6	0.184	0.187

As previously explained, *SAP2000* and *OpenSees* models predict slightly different displacement demands in the isolation level. Displacement demands were higher in the *SAP2000* model due to the Rayleigh damping overrides in the isolation modes. Table 6-9 compares displacement demands in the isolated building with gap damper system based on analysis with finalized design values (Table 6-7). The percent variation in *OpenSees* and *SAP2000* models predicted displacement varies from 0.4% to 6.7% for 20% target reduction motions versus 2.5% to 6.5% for 40% target reduction motions. The average variation is 2.5% and 3.2% for 20% and 40% target reduction motions, respectively, which verifies agreement between the two models in predicting displacement demands.

Table 6-9. Peak Displacement Demands Predicted by *SAP2000* and *OpenSees* Models

Max Displacement Resultant (cm)		
	20% Target Reduction Motions	40% Target Reduction Motions

GM	SAP2000	OpenSees	Percent Difference	SAP2000	OpenSees	Percent Difference
1	65.0	64.5	0.7%	67.3	69.4	-3.0%
2	69.0	74.0	-6.7%	55.0	58.6	-6.2%
3	64.9	64.6	0.4%	77.0	75.1	2.5%
4	72.3	73.6	-1.9%	69.2	71.7	-3.5%
5	59.9	61.7	-3.0%	63.8	65.9	-3.2%
6	64.1	67.4	-5.0%	67.7	72.4	-6.5%
7	63.1	64.4	-2.0%	65.7	67.7	-2.9%
Average:	**65.4**	**67.2**	**-2.5%**	**66.5**	**68.7**	**-3.2%**

A numerical example is described by Figure 6-17 and Figure 6-18, comparing the response between the *OpenSees* and *SAP2000* models. Figure 6-17 illustrates the displacement demand history where recorded floors displacements in the y-direction are plotted for GM20-5 (Chi-Chi, Taiwan TCU 106). This specific motion and direction was selected due to multiple gap damper activations throughout the duration of the motion, requiring strong agreement between the two models to capture similar behavior. Figure 6-17 (a), (b), (c) and (d) compares y-direction displacement demands at the center of the building at the roof, second, first and base floors, respectively. Figure 6-17 (e) illustrates the displacement profile which was plotted for maximum absolute displacement demands in y-direction in each floor. Although displacement demands between these two models are very close, displacement response in seismically isolated structures is mainly a function of isolation properties. Acceleration response is more closely tied to superstructure properties and modeling, providing more opportunity for discrepancies between the two models.

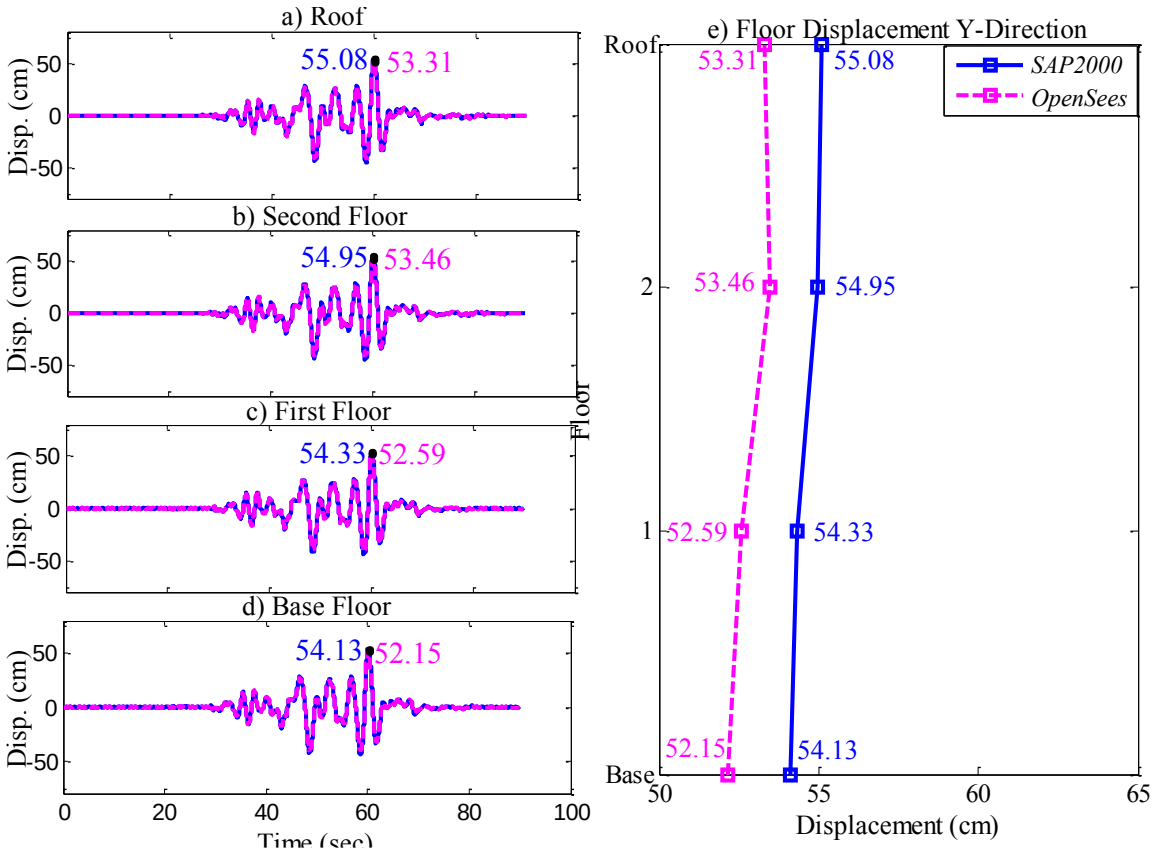

Figure 6-17. Displacement history of building center in Y-direction in: (a) roof, (b) second floor, (c) first floor and (d) base floor; and (e) plot of maximum displacement profile subject to GM20-5 (Chi-Chi, Taiwan TCU 106)

Figure 6-18 illustrates the displacement and force history across the damper aligned in the y-direction in the southwest portion of the structure (plan view), subjected to GM20-5. The damper was activated at 48.6 sec for the first time (Figure 6-18 (a)). Due to a larger displacement demand, the displacement across the damper (3.6 cm) in the *SAP2000* model is more considerable than the displacement across the damper in the *OpenSees* model (0.8 cm). The damper activated for a second time in the same positive y-direction in both models, but again with different amplitude values. Upon damper activation at 59.7 sec, which corresponds to occurrence of the largest displacement amplitudes in the motion, the displacement demands across the damper were very close in the two models (16.5 cm in the *OpenSees* model versus 17.6 cm in *SAP2000*, corresponding to a 6.7% difference). The maximum force across the damper also occurred at 59.7

sec and was equal to 2553 kN for the *SAP2000* model in comparison to 2249 kN for *OpenSees* model (13.5% difference). The larger displacement demands in the *SAP2000* model led to higher velocity demands, which increases force demands in velocity dependent dampers.

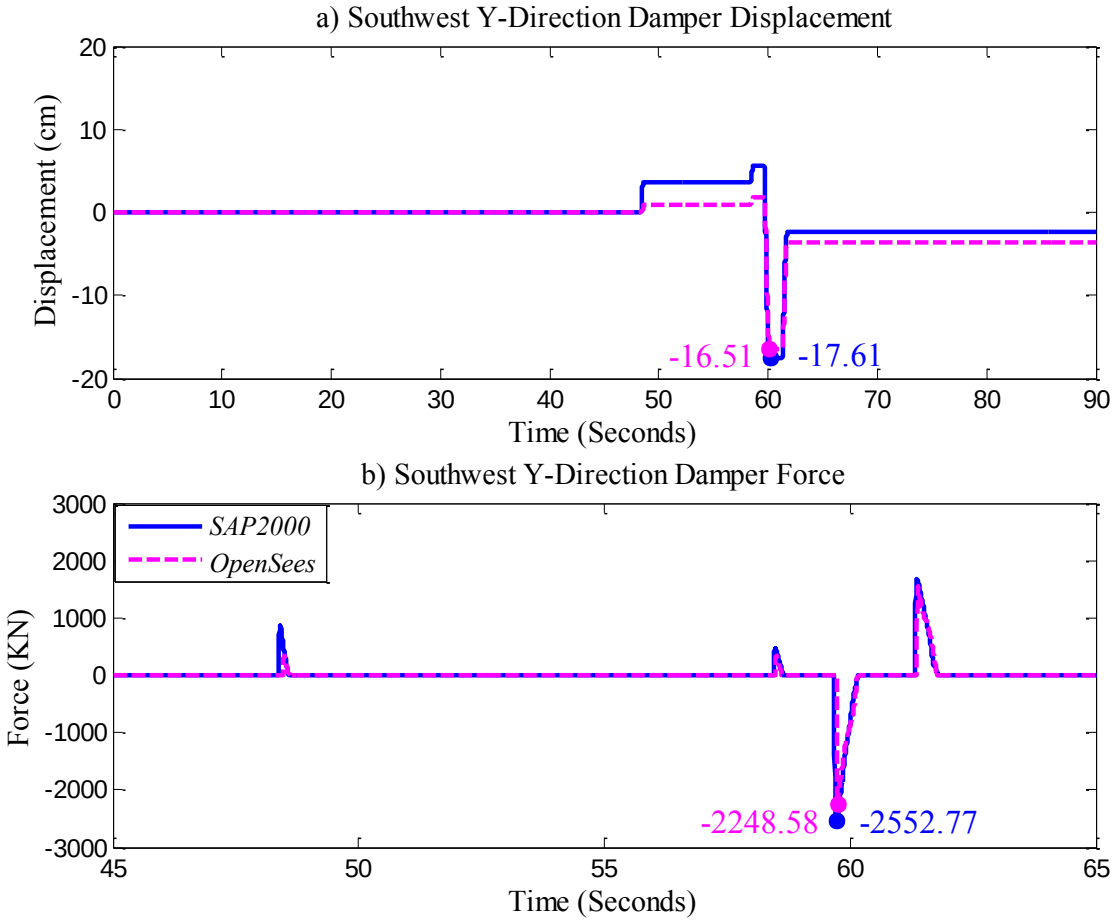

Figure 6-18. History of (a) damper displacement and (b) force across the damper in Y-direction in southwest gap damper system during GM20-5 (Chi-Chi, Taiwan TCU 106)

Contrary to the similarity in displacement demands between two models, acceleration demands are less consistent in the two models. **Error! Not a valid bookmark self-reference.** and Table 6-11 present resultant acceleration demands at the roof for models with and without the gap damper system. While the *OpenSees* model predicts overall higher roof acceleration demands in the base-isolated building in comparison to the *SAP2000* model (9.3% larger for 20% motions), the *SAP2000* model predicts higher accelerations in the base-isolated building with the gap damper

system in comparison to the *OpenSees* model (31.4% for the 40% motions). This acceleration mismatch is mainly due to difference is superstructure damping between the two programs.

Table 6-10. Comparison Between Predicted Roof Acceleration Demands in *SAP2000* and *OpenSees* Models in Base-Isolated Building

Max Total Acceleration Resultant (g)						
	20% Target Reduction Motions			40% Target Reduction Motions		
GM	SAP2000	OpenSees	Percent Difference	SAP2000	OpenSees	Percent Difference
1	0.28	0.31	-10.3%	0.39	0.39	-1.9%
2	0.30	0.35	-12.2%	0.38	0.38	-1.7%
3	0.27	0.36	-23.2%	0.38	0.39	-2.0%
4	0.33	0.34	-3.2%	0.44	0.42	4.5%
5	0.28	0.27	5.0%	0.44	0.45	-0.7%
6	0.32	0.35	-8.6%	0.42	0.40	4.3%
7	0.32	0.35	-9.0%	0.42	0.46	-8.9%
Average:	**0.30**	**0.33**	**-9.3%**	**0.41**	**0.41**	**-1.0%**

Table 6-11. Comparison Between Predicted Roof Acceleration Demands in *SAP2000* and *OpenSees* Models in Base Isolated Building with Gap Damper System

Max Acceleration Resultant (g)						
	20% Target Reduction Motions			40% Target Reduction Motions		
GM	SAP2000	OpenSees	Percent Difference	SAP2000	OpenSees	Percent Difference
1	0.68	0.61	-3.0%	1.11	0.76	46.9%
2	0.51	0.57	-6.2%	1.12	0.88	28.0%
3	0.76	0.65	2.5%	1.10	0.84	29.8%
4	0.57	0.52	-3.5%	1.08	0.85	27.6%
5	0.49	0.42	-3.2%	0.96	0.82	17.8%
6	0.48	0.40	-6.5%	1.19	1.06	12.4%
7	0.64	0.59	-2.9%	1.69	1.08	57.2%

Average:	**0.59**	**0.54**	**-3.2%**	**1.18**	**0.90**	**31.4%**

Roof acceleration demands in the x-direction for two models are investigated in both the base-isolated and base-isolated with gap damper configurations subjected to GM40-7 (Chi-Chi, Taiwan TCU 109). This motion was selected due to the large discrepancy between results in two models. Figure 6-19 and Figure 6-20 compare different floors acceleration demands at the center of building in x-direction. For both configurations, the *OpenSees* model predicted larger acceleration in the base floor compared to the *SAP2000* model. The main reason for this discrepancy in the base floor is that the *OpenSees* model accounts for out-of-plane slab stiffness by using composite beam-slab section properties to improve the model rigidity against local isolator uplift. This assumption in *OpenSees* increased the rigidity of the base floor compared to the *SAP2000* model and was the source of larger base floor accelerations in the *OpenSees* model. For the base-isolated building configuration, acceleration matched closely in other floors, while models including the gap damper system had a large discrepancy in acceleration values. The maximum acceleration profile presented in Figure 6-20 (f), verifies the different trends for the models including the gap damper system.

Another source of discrepancy in floor acceleration demands was the approach used to model the gap damper system in two programs. Although similar properties were used to model gap damper system (damping coefficient and gap element stiffness), the isolation nub was modeled dissimilarly. In the *SAP2000* model, the nub was modeled by a joint tied with a diaphragm constraint to the base floor. In *OpenSees* model, the nub was modeled using an actual structural member, which provided more flexibility in the gap damper system in comparison to *SAP2000* model, reducing acceleration demand.

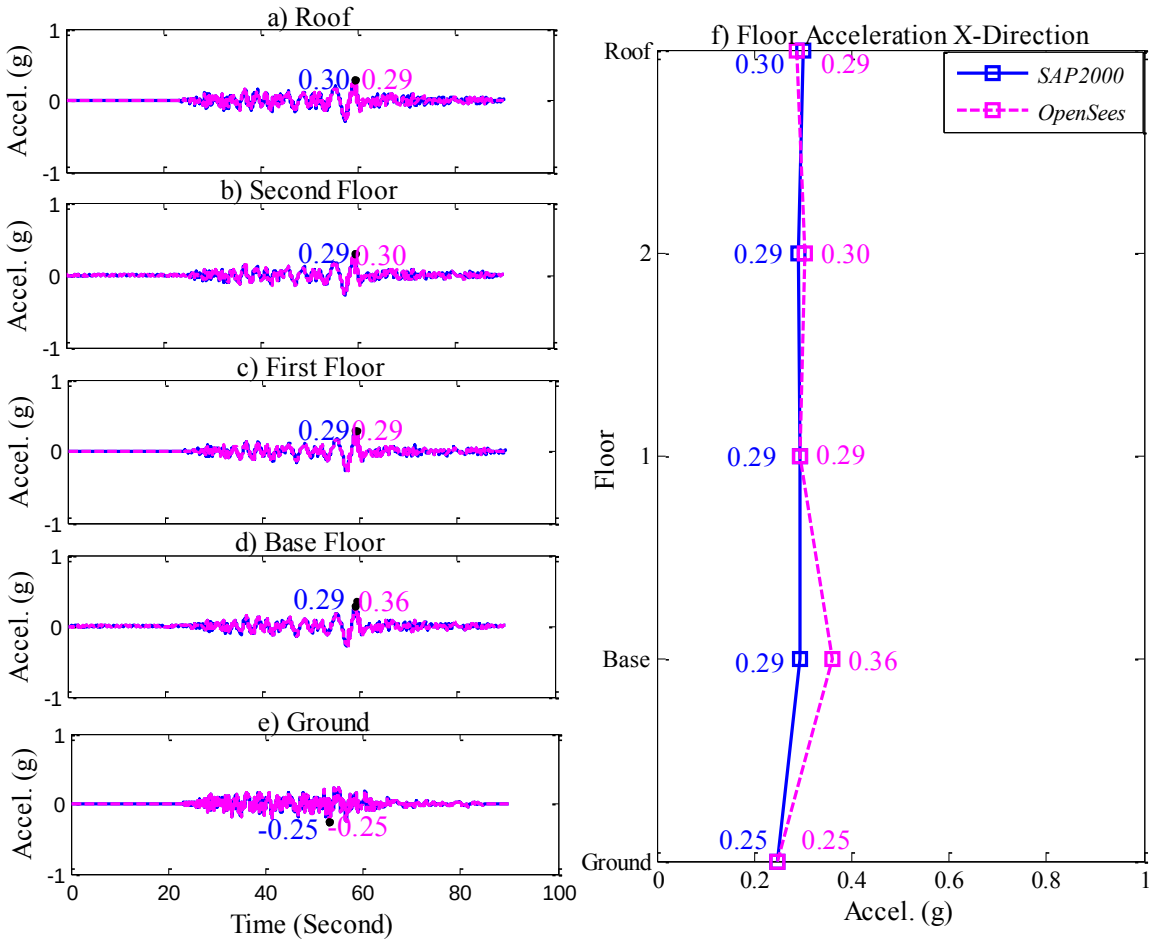

Figure 6-19. Acceleration history of building center in the x-direction for the (a) roof, (b) second floor, (c) first floor and (d) base floor; and (e) plot of maximum acceleration profile subject to GM40-7 (Chi-Chi, Taiwan TCU 109) base-isolated building

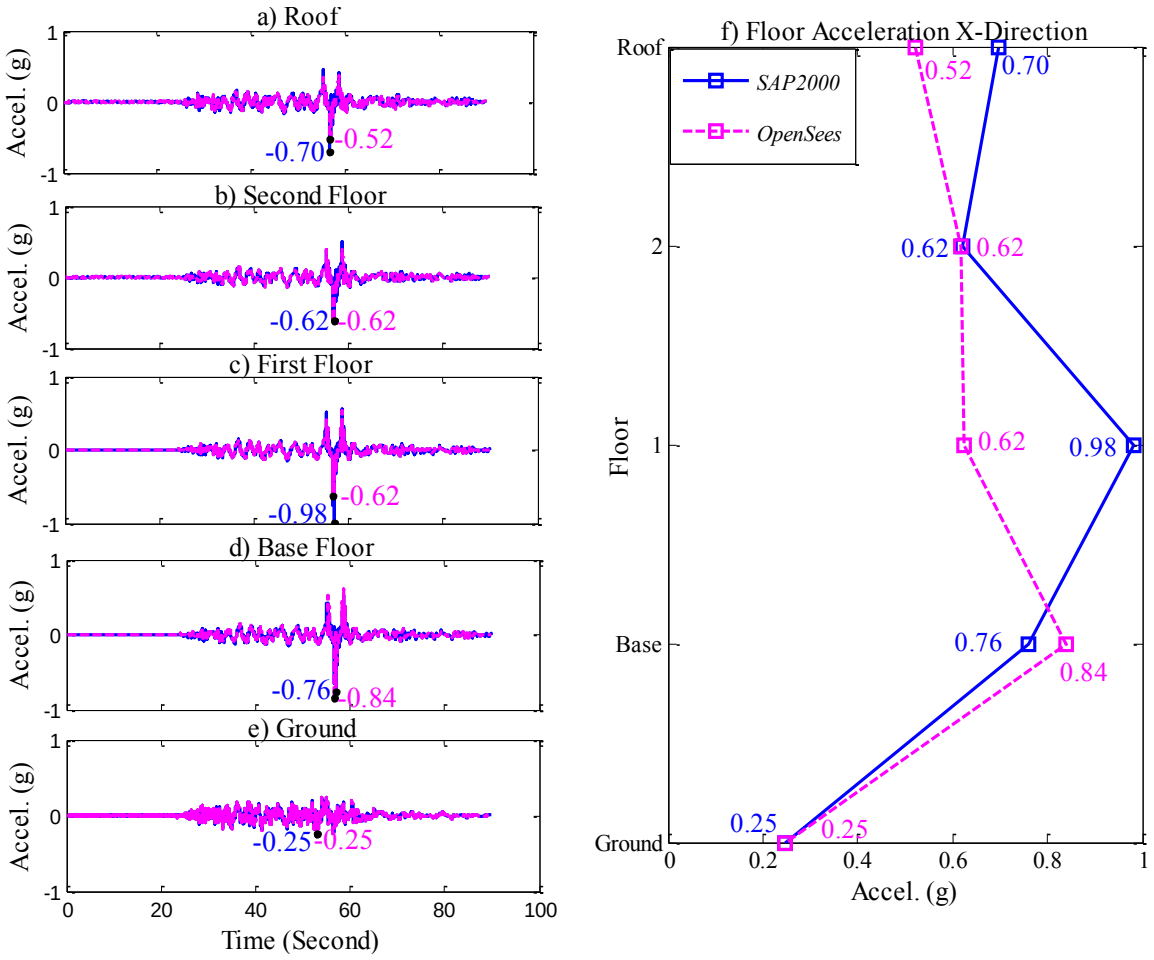

Figure 6-20. Acceleration history of building center in x-direction for the (a) roof, (b) second floor, (c) first floor and (d) base floor; and (e) plot of maximum acceleration profile subject to GM40-7 (Chi-Chi, Taiwan TCU 109) base-isolated building with gap damper

To further investigate acceleration response of the two models subjected to GM40-7, different floor acceleration spectra are presented in Figure 6-21. Comparison between the acceleration spectra in different floors indicated spectral acceleration discrepancy was mainly significant in the high frequency range corresponding to the higher superstructure modes. The activation of the gap damper system excites the higher modes due to the large force imparted at the base of the structure. Floor spectral acceleration matched very well in the lower modes since the overall behavior of model is a function of base isolators in these modes.

Higher spectral acceleration amplitudes were observed for the *SAP2000* model in comparison to the *OpenSees* model with the exception of the base floor. The main reason for different floor acceleration spectra for the two models can be investigated by looking at modeling of damping in the superstructure. The *OpenSees* model uses tangent stiffness proportional damping calibrated to 2.5% damping at first superstructure mode (fixed-base configuration). *SAP2000* uses Rayleigh damping with overrides in the isolation frequencies and 2.5% damping assigned to frequencies corresponding to mixed isolation and superstructure modes.

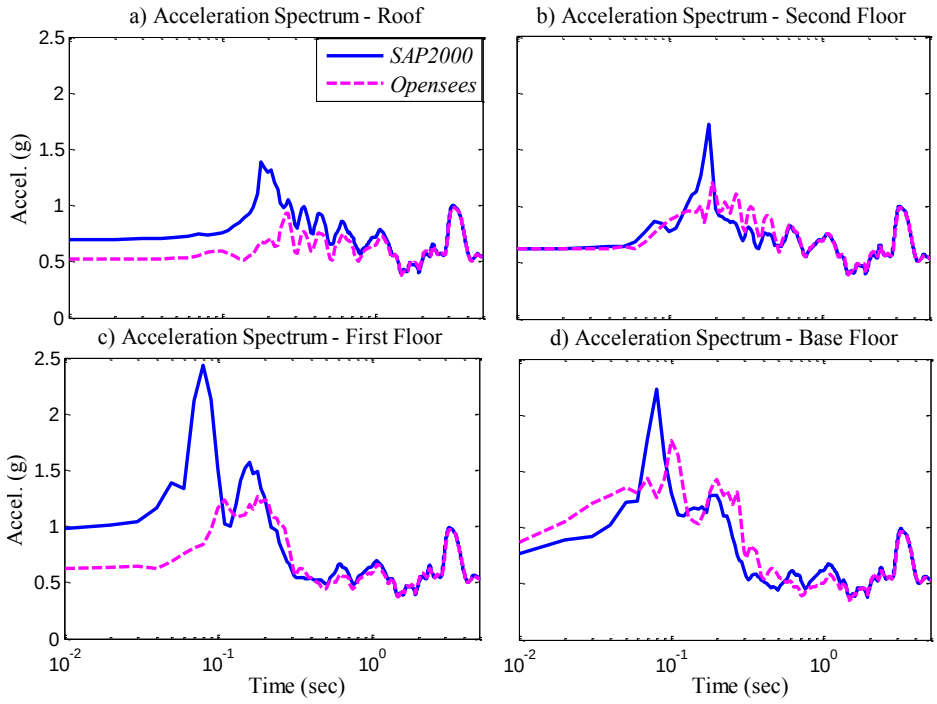

Figure 6-21. Floor acceleration (x-direction) response spectrum for the (a) roof, (b) second, (c) first and (d) base floors during GM40-7 (Chi-Chi, Taiwan TCU 109)

6.3.8 Gap Damper Performance

This next section demonstrates the performance of the gap damper system in comparison to design objectives. The primary objective for the case study building involves reducing the maximum displacement resultant (square root sum of squares) to less than D_{TM} to eliminate the possibility of moat wall impacts. This displacement objective should be achieved while minimizing

superstructure accelerations. The two ground motions suites (20% and 40% larger than D_M) are compared to evaluate the ability of the gap damper system to reduce displacement at varying intensity. The overall system hysteresis for the isolation level of a system with and without a gap damper system for GM 40-1 (Figure 6-22). The system hysteresis consists of the energy from the 35 isolators and energy contribution from the dampers for the gap damper system. The figure clearly illustrates the fundamental energy concept with a reduction in overall displacement in the gap damper configuration due to the added energy dissipation in the gap damper. The closely-spaced negative force peaks in the damper hysteresis are due to the torsion of the structure which activates the two gap damper systems at different times.

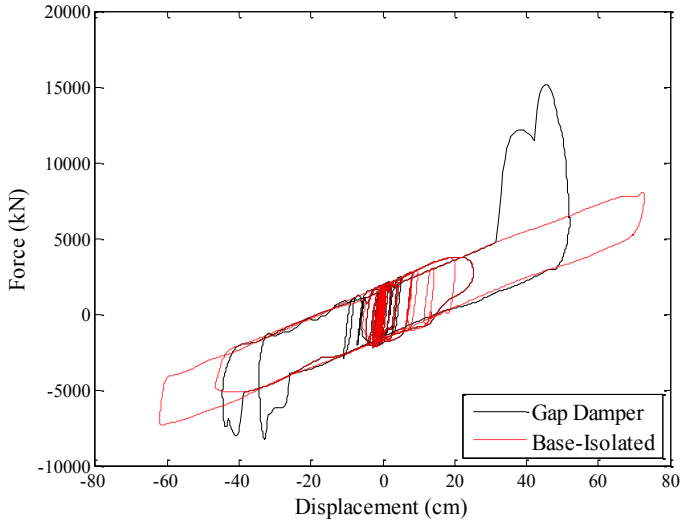

Figure 6-22. System Hysteresis X-Direction (GM40-1)

Figure 6-22 and Figure 6-23 further demonstrate the effectiveness of the gap damper system in reducing isolator displacements. Displacement plots for each floor (Figure 6-23a-Figure 6-23d) show the displacement reduction possible using a gap damper system. In addition, the data in Figure 6-24 represents the displacement traces in the four corners and center isolators for GM40-5. The moat wall is represented with a dashed black line and located at D_{TM} (68.4 cm). The isolation system displacement demand far exceeds the moat wall displacement in the configuration

without the gap damper system, while the isolator displacement is reduced below the moat wall displacement at all four corners when the gap damper is included. This indicates that the gap damper system has mitigated moat wall impact for this particular ground motion.

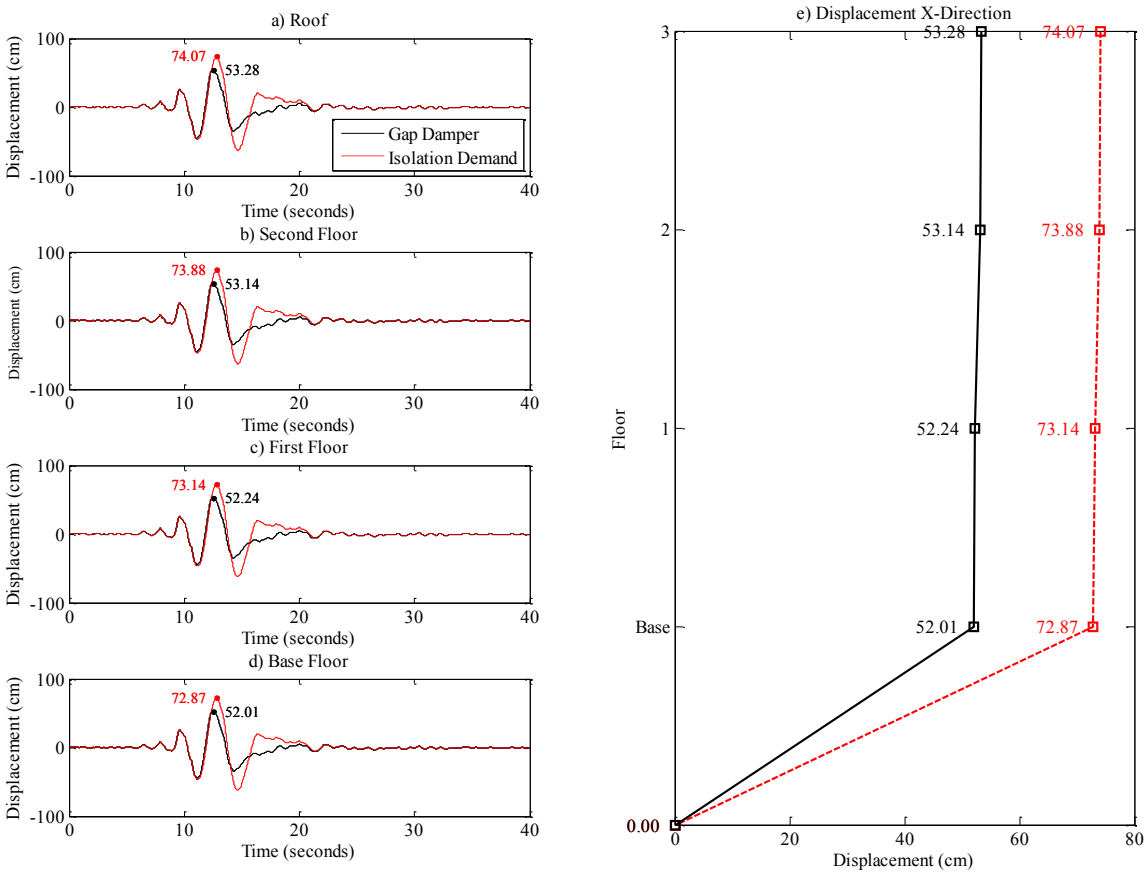

Figure 6-23. Displacement Comparison for a) Roof, b) Second Floor, c) First Floor d) Base Floor, and e) Maximum Values for GM 40-1

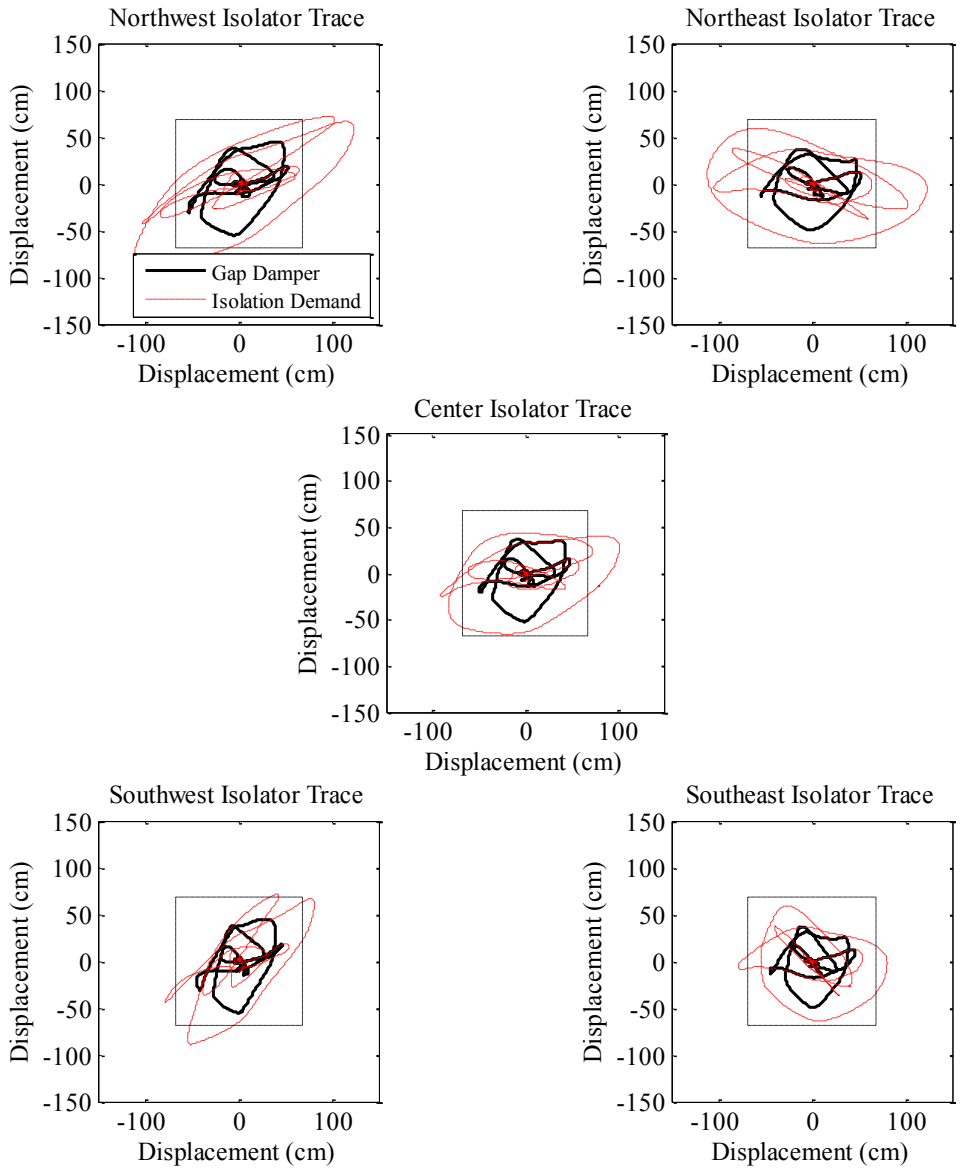

Figure 6-24. Isolator Displacement Trace for GM40-5

Gap damper displacement reduction is summarized in Table 6-12, which includes base-isolation displacement demands (BI), gap damper displacement demands (GD), and the reduction for the system. Results are also compared for the two models in *OpenSees* and *SAP2000*. Generally speaking the BI displacements are slightly higher and GD displacements are slightly lower for the *SAP2000* models, suggesting a larger overall reduction in comparison to the *OpenSees* models. For the 20% ground motion suite, 5 of 7 ground motions are able to reduce displacement to less than D_{TM} (68.4 cm). The same two ground motions (GM20-2 and GM20-4)

failed to meet the design objective for both models, with GM20-4 experiencing very little displacement reduction. GM20-7 experienced the most reduction in displacement with 25% reduction for the *SAP2000* model and 18% reduction for the *OpenSees* model.

Table 6-12. Gap Damper Displacement Reduction Summary

Resultant Displacement (cm)								
20% Target Reduction Motions								
	SAP2000				OpenSees			
GM	BI	GD	Reduction	Percent Reduction	BI	GD	Reduction	Percent Reduction
1	82.3	65.0	17.3	21%	75.7	64.5	11.2	15%
2	80.4	69.0	11.4	14%	82.1	74.0	8.1	10%
3	80.5	64.9	15.6	19%	77.0	64.6	12.4	16%
4	80.1	72.3	7.8	10%	79.6	73.6	6.0	8%
5	76.6	59.9	16.7	22%	71.9	61.7	10.2	14%
6	76.8	64.1	12.7	17%	74.0	67.4	6.6	9%
7	83.9	63.1	20.8	25%	78.5	64.4	14.1	18%
Avg:	**80.1**	**65.4**	**14.7**	**18%**	**77.0**	**67.2**	**9.8**	**13%**
40% Target Reduction Motions								
	SAP2000				OpenSees			
GM	BI	GD	Reduction	Percent Reduction	BI	GD	Reduction	Percent Reduction
1	99.9	67.3	32.6	33%	101.0	69.4	31.6	31%
2	96.9	55.0	41.9	43%	94.2	58.6	35.6	38%
3	100.3	77.0	23.3	23%	94.3	75.1	19.2	20%
4	123.2	69.2	54.0	44%	123.0	71.7	51.3	42%
5	138.7	63.8	74.9	54%	134.2	65.9	68.3	51%
6	104.7	67.7	37.0	35%	102.5	72.4	30.1	29%
7	113.5	65.7	47.8	42%	113.6	67.7	45.9	40%
Avg:	**111.0**	**66.5**	**44.5**	**40%**	**109.0**	**68.7**	**40.3**	**37%**

The 40% ground motion suite produced mixed results wherein the design objective was achieved during 5 of 7 ground motions in *SAP2000* model and 3 of 7 ground motions in the

OpenSees model. The average displacement reduction approached desired reduction of 40% but the spread of performance across the ground motion suite was large. The data for both ground motion suites is shown graphically in Figure 6-25. The agreement between the models is evident with a larger reduction noticed in *SAP2000* models.

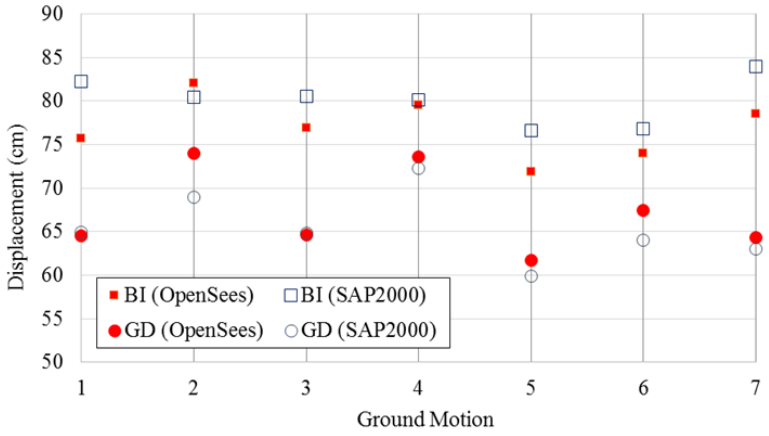

a) Max Displacement Resultant for 20% Target Reduction

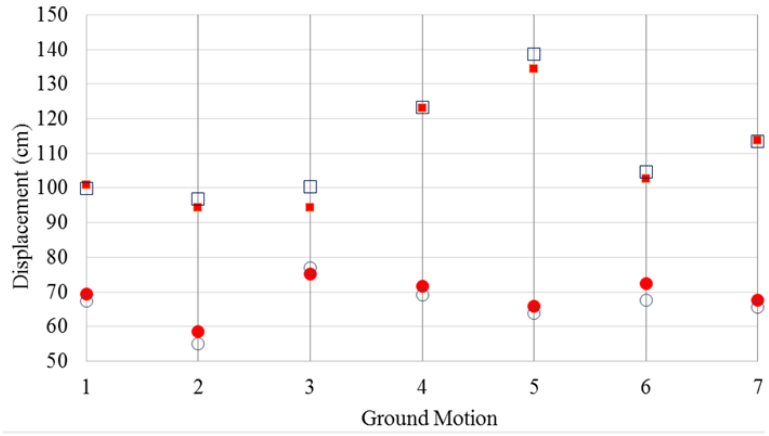

b) Max Displacement Resultant for 40% Target Reduction

Figure 6-25. Displacement Reduction for Ground Motion Suites

Noticeable differences in displacement reduction is evident in Figure 6-25b for ground motions 40-3 and 40-5, with a reduction of about 20 cm (7.9 in) and 70 cm (27.5 in) respectively. Displacement reduction required in GM40-5 is much larger than the reduction required in GM40-3, yet met the displacement objective while GM40-3 failed to meet the displacement objective. Figure 6-26 shows the isolator trace for the four corners and center isolator with the moat wall

placement at D_{TM} (68.4 cm) represented by the dotted black line. Although the displacement resultant of 76.0 cm exceeds the design objective, the maximum x or y-direction displacement of the isolators with the gap damper system does not exceed the moat wall location. The ground motion is primarily bidirectional, with the maximum isolator demands observed in the diagonal direction. The moat wall is placed a perpendicular distance D_{TM} all around the structure base walls, so that the distance to the corner is actually $1.41D_{TM}$. This suggests that the design objective may be too stringent when accounting for bidirectional movement. Design objectives could be relaxed in a design situations if the site characteristics and fault motion is well known.

In addition, Figure 6-27 compares the ground motion velocity and damper displacement histories for GM40-5 and GM40-3 using the *SAP2000* model. The histories are shown in the direction of the largest damper participation, which is the x-direction for GM40-5 and y-direction for GM40-3. Maximum velocity is higher for GM40-3, allowing the dampers to provide more beneficial energy dissipation. The activation of the dampers for GM40-3 correspond well with velocity spikes in the ground motion. Damper displacement is higher in GM40-3 since the gap damper system was unable to control displacement as well as GM40-5.

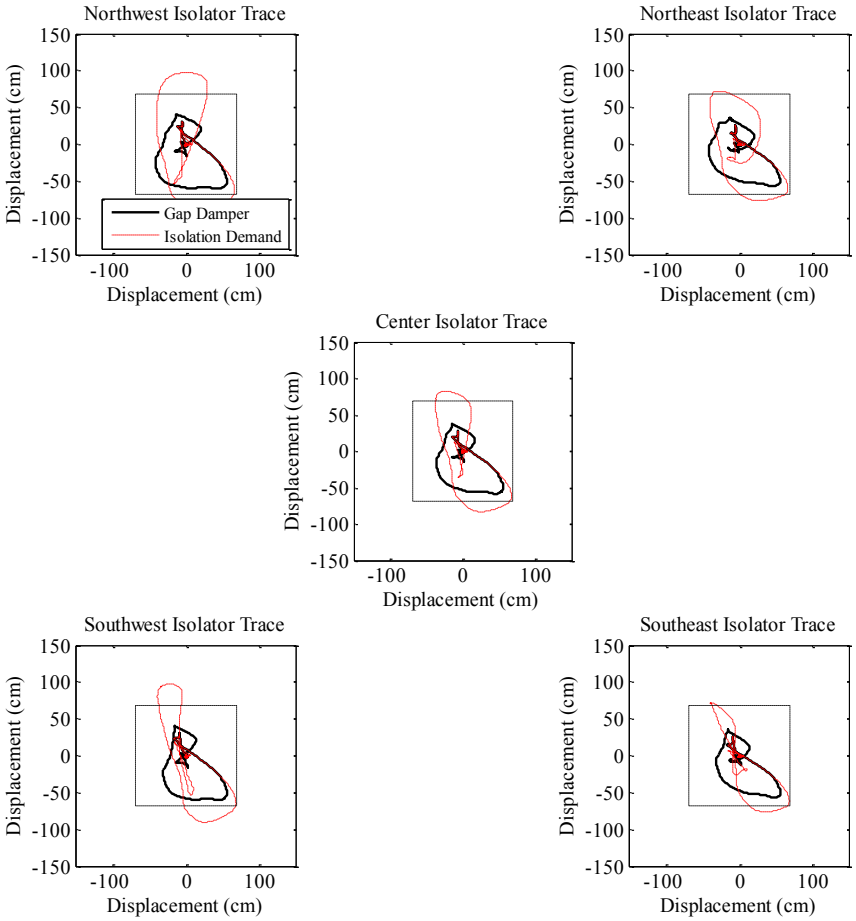

Figure 6-26. Isolator Displacement Trace for GM40-3 (*SAP2000*)

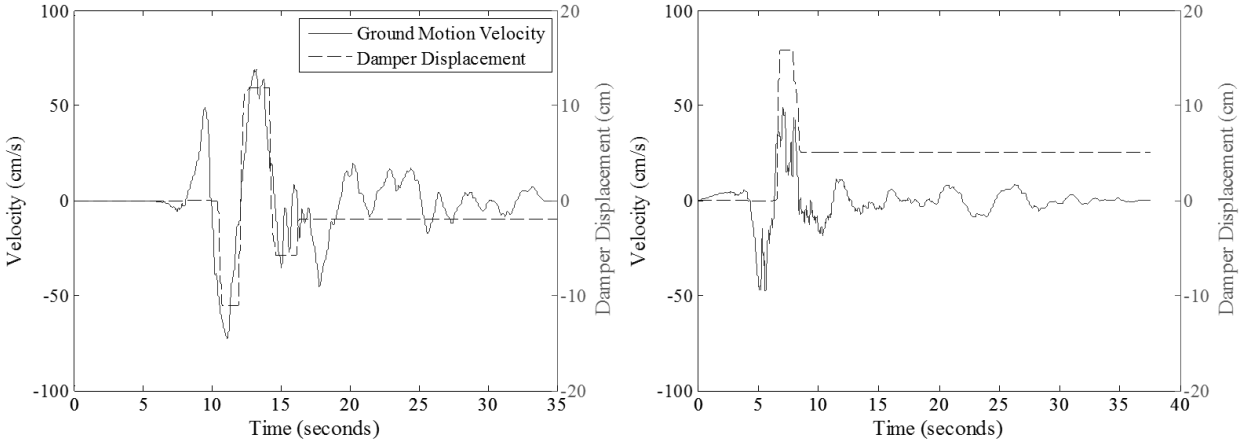

a) Ground motion velocity and damper engagement for GM 40-5

b) Ground motion velocity and damper engagement for GM 40-3

Figure 6-27. Input Velocity and Damper Displacement Time History (*SAP2000*)

Previous analyses have demonstrated the trade-off between displacement reduction and acceleration increase in the superstructure. Table 6-1 summarizes the maximum resultant roof acceleration values for the *SAP2000* and *OpenSees* models for both ground motion subsets. Acceleration increases were more evident in the *SAP2000* due to modeling assumptions discussed in Section **Error! Reference source not found.**. In addition to Table 6-13, a graphical representation of the data in Figure 6-28 clearly shows the increase in acceleration response in response to different ground motions.

Table 6-13. Gap Damper Roof Acceleration Summary

Roof Resultant Total Acceleration (g)						
20% Target Reduction Motions						
	SAP2000			OpenSees		
GM	BI	GD	AccGD / AccBI	BI	GD	AccGD / AccBI
1	0.28	0.68	2.43	0.31	0.61	1.97
2	0.30	0.51	1.68	0.35	0.57	1.63
3	0.27	0.76	2.76	0.36	0.65	1.81
4	0.33	0.57	1.74	0.34	0.52	1.55
5	0.28	0.49	1.75	0.27	0.42	1.58
6	0.32	0.48	1.49	0.35	0.40	1.15
7	0.32	0.64	2.02	0.35	0.59	1.70
Avg:	**0.30**	**0.59**	**1.96**	**0.33**	**0.54**	**1.62**
40% Target Reduction Motions						
	SAP2000			OpenSees		
GM	BI	GD	AccGD / AccBI	BI	GD	AccGD / AccBI
1	0.39	1.11	2.87	0.39	0.76	1.92
2	0.38	1.12	3.00	0.38	0.88	2.30
3	0.38	1.10	2.86	0.39	0.84	2.16
4	0.44	1.08	2.48	0.42	0.85	2.03
5	0.44	0.96	2.16	0.45	0.82	1.82
6	0.42	1.19	2.86	0.40	1.06	2.65

7	0.42	1.69	4.02	0.46	1.08	2.33
Avg:	**0.41**	**1.18**	**2.88**	**0.41**	**0.90**	**2.17**

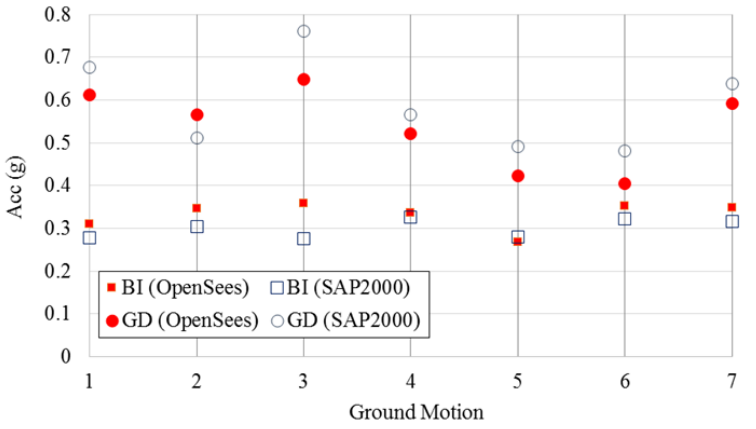

a) Max Acceleration Resultant for 20% Target Reduction

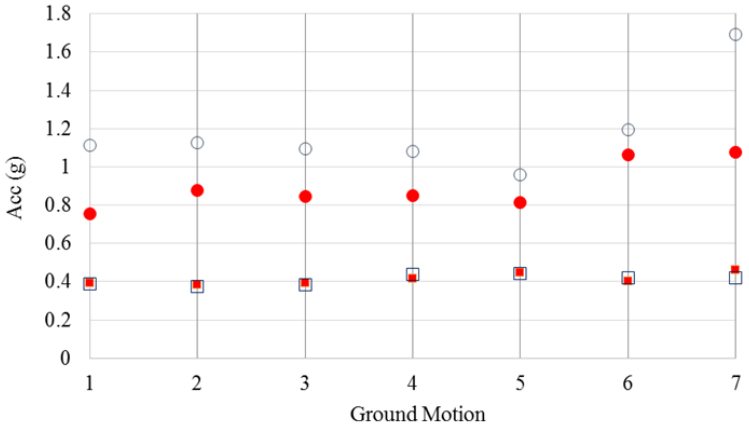

b) Max Acceleration Resultant for 40% Target Reduction

Figure 6-28. Acceleration Response for Ground Motion Suites

The 20% ground motion suite had a slight increase in roof acceleration, with the base-isolated model without the gap damper averaging around 0.3g and the models with the gap damper ranging from 0.5g-0.7g. Introducing the large amount of energy dissipation at the base inevitably increases roof accelerations. If these accelerations are manageable, such as the accelerations noticed in the 20% ground motions, the structure meets the isolation level displacement design objectives while maintaining acceptable superstructure acceleration response.

The 40% ground motion suite had very high acceleration response in the roof of the superstructure. Acceleration demand ranged from 0.4g for the base-isolated structure to more than 1.0g for a few ground motions with the gap damper system. The large amount of energy required for the 40% ground motions requires large damper forces and subsequent increases in floor accelerations. These large acceleration values, paired with the moderate displacement reduction, suggest the gap damper can be successful for a large displacement reduction objective but may require further superstructure response considerations to ensure protection from collapse. Acceleration was shown to be largely influenced by the stiffness during activation of the gap damper system in Section 6.3.5. Large transitional gap damper stiffness values were used for the case study which may have inflated acceleration values in the roof.

Higher accelerations in the structure lead to increased demand in structural members. This is evident in Figure 6-29, which compares filtered (25 Hz Butterworth) brace forces in the base-isolated systems for GM 40-7. Table 6-14 summarizes the maximum force demand (as a percentage of capacity) in tension and compression for the braces located in the top story. The 40% target reduction systems experienced a large increase in brace forces, as expected with the large increase in accelerations. The 20% target reduction systems also experienced an increase in force demand in the braces but would not require a design iteration to remain elastic. These values are generated from the *SAP2000* model, which idealizes the force transfer from the gap damper system to the structure with a rigid body constraint and modeled the superstructure elastically, inflating these maximum values. Due to uncertainty in modeling, accounting for force acceleration spikes in design requires conservatism in the sizing of structural members. If the design objective requires the superstructure to remain elastic, braces would have to be increased in size to accommodate the large force spikes due to the activation of the gap damper system.

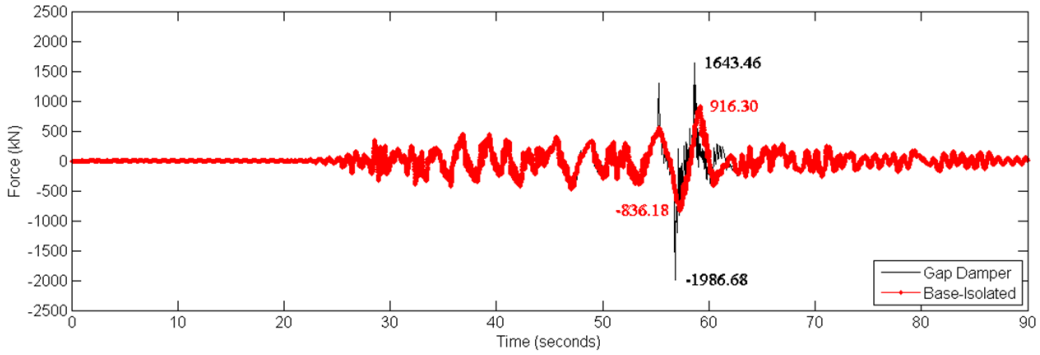

a) Top brace force comparison for GM 40-7

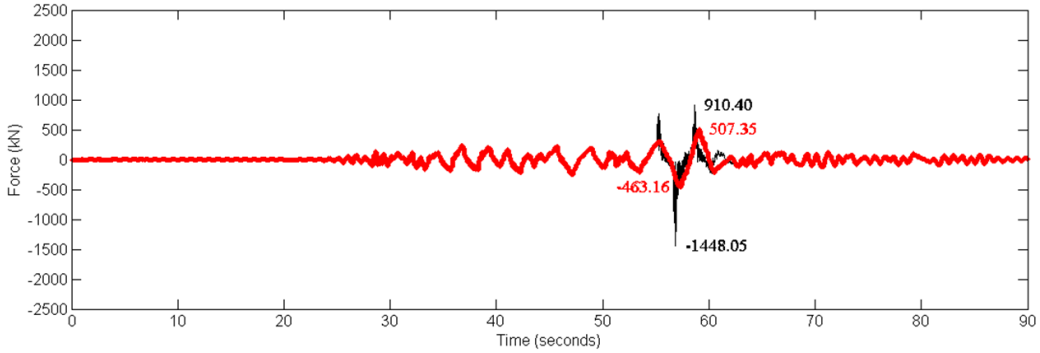

b) Bottom brace force comparison for GM 40-7

Figure 6-29. Brace Force Comparison for GM 40-7 (*SAP2000*)

Table 6-14. Gap Damper Force Demand in Top Brace of Superstructure (SAP2000 Model)

	20% Target Reduction			
	Top Brace (Tension Capacity = 1680 kN, Compression Capacity = 1580 kN)			
GM	X-Direction (Ten.)	X-Direction (Comp.)	Y-Direction (Ten.)	Y-Direction (Comp.)
1	26%	27%	69%	90%
2	55%	68%	52%	53%
3	26%	23%	106%	93%
4	84%	56%	66%	80%
5	36%	43%	50%	73%
6	79%	83%	35%	37%
7	29%	39%	97%	82%
	40% Target Reduction			
GM	X-Direction (Ten.)	X-Direction (Comp.)	Y-Direction (Ten.)	Y-Direction (Comp.)
1	64%	157%	121%	140%
2	63%	81%	103%	152%
3	145%	151%	189%	111%
4	69%	96%	88%	175%
5	143%	124%	151%	127%
6	37%	40%	121%	204%
7	98%	126%	100%	232%

*Highlight indicates exceeded capacity

In addition to brace force, the story drifts were also evaluated for the case study structure. Figure 6-30 shows the elastic drifts for GM20-7 using *SAP2000*, chosen as the largest superstructure demands in the braces, which remained elastic throughout the ground motion. Although drift increases are evident with the gap damper system, values are far from controlling the design of the superstructure with story drifts less that 0.3%. Controlling superstructure drift increases with an isolated moment frame structure, rather than a braced frame, may present more of a design issue with the inherent flexibility of the system.

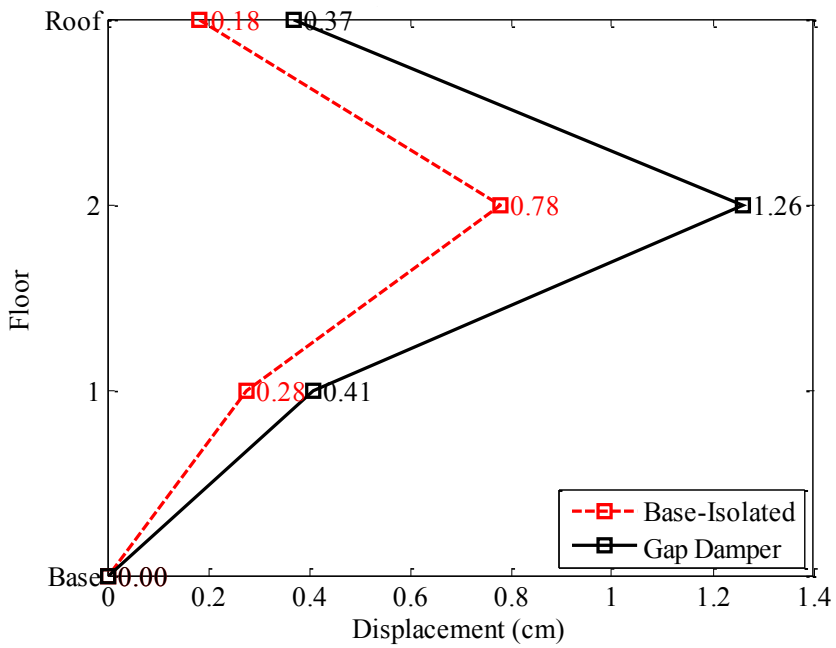

Figure 6-30. Story Drift for GM20-7 (*SAP2000*)

In summary, the case study buildings provide useful insight towards the behavior and performance of the gap damper system. Final case study displacement and acceleration response for the *SAP2000* and *OpenSees* models are found in Table 6-15, clearly demonstrating the trade-off between displacement reduction and increases in roof acceleration. The gap damper system is clearly beneficial at reducing the displacement in the structure but the accelerations can increase significantly depending on the ground motion and the displacement reduction required. The trade-off for the 20% target reduction systems may be acceptable since accelerations are reasonable and the likelihood of moat wall impact is decreased.

Table 6-15. Case Study Summary

20% Target Reduction Motions				
	SAP2000		OpenSees	
GM	Percent Reduction	AccGD / AccBI	Percent Reduction	AccGD / AccBI
1	21%	2.43	15%	1.97
2	14%	1.68	10%	1.63
3	19%	2.76	16%	1.81
4	10%	1.74	8%	1.55
5	22%	1.75	14%	1.58
6	17%	1.49	9%	1.15
7	25%	2.02	18%	1.70
Avg:	**18%**	**1.96**	**13%**	**1.62**
40% Target Reduction Motions				
	SAP2000		OpenSees	
GM	Percent Reduction	AccGD / AccBI	Percent Reduction	AccGD / AccBI
1	33%	2.87	31%	1.92
2	43%	3.00	38%	2.30
3	23%	2.86	20%	2.16
4	44%	2.48	42%	2.03
5	54%	2.16	51%	1.82
6	35%	2.86	29%	2.65
7	42%	4.02	40%	2.33
Avg:	**40%**	**2.88**	**37%**	**2.17**

6.4 Conclusions

This chapter overviewed a displacement restraint system, or "gap damper", which serves as a backup system to limit displacement demands in seismically isolated structures during extreme ground motions. The gap damper system can be designed to satisfy multiple displacement reduction objectives selected by the designer but is envisioned primarily to reduce displacements

to less than the moat wall distance to avoid impacts. The chapter provides design equations and commentary to assist in the design of gap damper system components. In addition to the design of the gap damper components, analysis considerations and gap damper detailing recommendations are provided to assist the designer.

Using the proposed design procedure, a three-story isolated building was designed for a case study comparison. The building was modeled in both *OpenSees* and *SAP2000* to evaluate the suitability of the gap damper modeling procedure across two modeling environments. Two suites of seven ground motion pairs were selected with two different target displacement reductions of 20% and 40% for the gap damper system design. The design objective for the case study structures was to reduce the displacement to less than the moat wall placement of $1.1D_M$ (D_{TM}). Based on the target reduction specified for the gap damper system, the damping coefficients, were calibrated using the equal energy dissipation concept (Figure 6-2) and utilizing EDLs calibrated from a previous parametric study (Figure 6-3). Preliminary results indicated the gap damper system performed satisfactorily for 20% target reduction motions suite where displacement demands in isolation level were limited to less than D_{TM}=68.4 cm. Displacement demands for 40% target reduction motions suite were higher than total maximum displacement of isolated structure, indicating pounding was possible. In order to reduce the possibility of pounding in the 40% target reduction motions, a design iteration with an adjustment factor of 1.25 was applied to the energy equations, increasing dampers sizes.

Comparison of case study responses in *SAP2000* and *OpenSees* models indicated agreement of between the two models in predicting displacement demands in both base-isolated and gap damper configurations However, significant differences in superstructure floor acceleration were observed, especially in the configuration with gap damper system. The

discrepancy can be attributed to a number of modeling assumptions and differences between the two analyses.

In addition to the comparison between models, the overall gap damper system performance was evaluated by comparing response between the base-isolated and gap damper buildings. Comparison of the results indicate that, by adding a gap damper system, desired displacement reduction in a seismically isolated structure can be achieved, with the trade-off of increased superstructure acceleration demands. Results for the 20% target reduction models clearly indicate the potential benefits of the gap damper system with a large displacement reduction and slight trade-off in superstructure acceleration. Preliminary evaluation of the brace forces indicated that the existing braces are adequate and would not require design iteration. On the contrary, the 40% target reduction ground motions indicated rather poor performance, even with the increase in energy dissipation from the design iteration. Displacement reduction was moderately successful but varied across ground motions. Superstructure acceleration demands increased by a factor of 2.2 (*OpenSees*) and 2.9 (*SAP2000*), respectively, when compared to the base-isolated configuration. The increase in superstructure demands led to brace demands exceeding capacity, which may require a design iteration depending on the design objective. Results of the 40% target reduction systems also indicated that the design objective may be too stringent when considering ground motions that are primarily bi-directional due to increased distance between the moat wall and structure with diagonal movement. Design objectives may be relaxed if the ground motion characteristics are well known.

Overall, the gap damper system is shown to be effective at achieving displacement reduction. A moat wall impact could have detrimental effects on the superstructure and should be avoided if possible. The gap damper system provides a useful mitigation technique while allowing

traditional base-isolated behavior for more frequent ground motions. Further research is necessary to examine the trade-off between the displacement of the isolation system versus the acceleration of the superstructure. Acceleration increase is likely less detrimental than a moat wall impact, while the gap damper consistently demonstrates displacement reduction capability, suggesting the system is an improvement on the state-of-the-art.

Chapter 7. Conclusions and Recommendations for Future Work

7.1 Summary

The goal of this research was to fully develop a novel gap damper system for the protection of base-isolated structures in extreme seismic events. This research endeavor is a collaborative effort between researchers at the University of Nevada-Reno and Auburn University. Work completed at Auburn University is primarily summarized within the scope of the dissertation with collaborative work presented to provide contextual background.

A literature review offers insight towards the state-of-the-art in base-isolation research. The history, application, and types of base-isolation were outlined along with important fundamental concepts of isolation systems. The literature illustrates the advancement of base-isolation technologies, clearly demonstrating the benefits through analytical, experimental, and observational research. While promising, base-isolation systems still require research advancements to be a viable design option for widespread use. Concerns with large displacement demands in the isolation level in extreme earthquakes are a prohibitive barrier to base-isolation adoption in vital facilities. Numerous solutions have been offered to reduce displacement demand through the use of supplemental energy dissipation with mixed results, often introducing additional demands in the superstructure.

A performance-based gap damper concept is able to meet the objectives of more frequent ground motions while also protecting the structure in extreme events. The idea utilizes traditional

base-isolated behavior for small to moderate events and activates a secondary system to limit displacements in extreme events, all through passive mechanisms. The theoretical basis for the gap damper system involves the equal displacement principle, which takes a portion of the energy dissipated by isolators in extreme grounds motions and dissipates the energy with supplemental energy dissipation earlier in the motion. A large parametric study compared various energy dissipation techniques and identified the better performing systems using a performance index that was developed to compare systems based on both isolation level displacement and superstructure accelerations. The results of the study indicated that the viscous device and two-phase viscoplastic device provided the best overall performance and would be suitable for practical implementation. This study was furthered by identifying sensitivity of the results to aspects of the parameters, such as ground motion suites, displacement demands, and superstructure modeling assumptions. The results of the study indicated the elimination of the acceleration performance index was necessary to ensure a consistent performance that would achieve the desired displacement reduction.

Using the results of the parametric study, the next task was to develop a prototype for testing at Auburn University. Multiple gap damper arrangements were presented with a qualitative analysis of each presented. A final design was chosen that met the desired performance objectives of the system and was developed into a prototype system. Design details and considerations were covered and a final design presented for both a viscous and viscoplastic gap damper. Prior to the experiments, the calibration of the viscous dampers and friction device was completed to ensure they were achieving the desired behavior. An experimental plan including the instrumentation, component layout, and load cases was also overviewed. Testing for the viscous gap damper included 24 load cases while the viscoplastic device had 8 load cases including different eccentric and rotated impacts. Comparisons were made between load cases to assess the energy dissipation

capacity of the gap damper system. Reliable and repeatable behavior was found for the viscous gap damper while the viscoplastic system needs more research to be an effective system for consideration.

Using the results from this experiment, the next step was the creation of a finite element model that captures the system behavior. The primary goal of the finite element analyses was to evaluate aspects of the system that were not able to be captured in a lab environment. A coarse mesh was initially used to assess global behavior of the system and calibrate the model. Models were compared to experimental load cases showing good agreement with results. A calibrated model meant that other parameters of interest, such as lateral damper participation, could be evaluated using the coarse model. Further analysis was completed with a fine mesh in order to assess the behavior of the system when subjected to high speed impacts. Overall, the gap damper systems exhibited satisfactory behavior that indicates the device will behave as intended. Special attention should be given to gap damper systems that may involve rotated impacts as they may cause localized areas of yielding. Rounding the edges of the nub may also help to ease the local stresses evident in these impacts.

Shake table testing was completed at the University of Nevada-Reno using the gap damper design developed at Auburn University. Although not covered within the scope of this dissertation, a brief summary is given for the experiments. From a design perspective, the gap damper components behaved as intended, accommodating a range of ground motions and bi-directional impacts. The reduction in displacement was not as high as the intended due to a number of confounding variables.

With the completion of the parametric development and experimental aspects of the project, the last step was to develop a practical performance-based design approach using the gap

damper system. The design procedure is a blend of the fundamental derivation of the models from the parametric study and results from the experiments. Design values and suggested details are presented to provide assistance in the practical design of gap damper components within a structure. In addition, analytical models were developed using a three-dimensional case study structure. Results from modeling the system in *OpenSees* and *SAP2000* were compared and practical modeling techniques were presented to assist designers. The results from the two models were compared to assess the overall performance of the gap damper system and the applicability of the practical design procedure.

7.2 Conclusions

Given a summary of the scope of the work, overall conclusions of the work include but are not limited to:

7.2.1 Parametric Study

- The parametric study identified a pure viscous and two-phase viscoplastic as the most viable systems at balancing displacement reductions and limiting acceleration demands in the superstructure.
- Results of the parametric study are highly dependent of the assumptions of the study. The ground motion suite, target displacement reduction, and superstructure modeling (SDOF vs MDOF) all had a significant influence of the derivation of energy requirements. The acceleration performance, although important in the analysis of gap damper objectives, was eliminated to reduce the number of variables in the study. Rather than over-constraining the design process, elimination of the acceleration performance metric significantly simplifies the selection of the EDLs for design. Since the primary goal of the gap damper system is the

reduction of isolation level displacements, the acceleration can be viewed as a "consequential" variable associated with the displacement reduction.

7.2.2 Component Testing

- The development of a practical gap damper device demanded simplicity, feasibility, economy, and reliability to be an effective option in building design and construction. Key consideration was given to these objectives when choosing final design. The ability to accommodate bi-directional behavior is the most difficult design obstacle when choosing a practical design.
- Overall system response of the viscous device is similar to theoretical response, suggesting that the gap damper is capable of achieving the desired behavior.
- Energy dissipation values for the viscous device are shown to be about 85% of the theoretical values consistently across all 24 load cases; which demonstrates the reliability and repeatability of the system.
- Overall system response of the two-phase viscoplastic device is a departure from theoretical response due to difficulties controlling the friction device behavior. Controlling the strain in the bolts at the small amount of tension required in the device may have resulted in the large variance in response.
- Energy dissipation values for the two-phase viscoplastic device is shown to be about 77.0% of the theoretical values for the viscous portion of the viscoplastic device with relatively repeatable behavior. Energy dissipation varied largely for the friction device with values ranging from 40.4% to 156.6% of the desired energy dissipation. Overall energy dissipation ranged from 67.1% to 97.6% with an average of 81.3%.

- The deviation from theoretical viscous response of the gap damper system is attributed to imperfections in the test setup and inherent flexibility and energy losses within the system.
- Load cases involving eccentric impact of the isolation nub illustrate the reliable and consistent energy dissipation capabilities of the system regardless of the impact condition.
- Participation of dampers transverse to the direction of motion was investigated in response to an impact of a rotated structure. The transverse dampers were shown to contribute little energy dissipation in comparison to the primary direction of travel.
- The viscous device is the only recommended device for practical implementation with the current state of the research.

7.2.3 Shake Table Study

Although not fully covered within the scope of this study, a few important conclusions are highlighted:

- Displacement reduction was noticed at the isolation interface but not at the level targeted by the study. Acceleration increases were observed in the superstructure in the order of 2 to 3 times the base-isolated structure without a gap damper system.
- Bearing degradation and instability played an important role in the behavior of the test structure. The base-isolated structure was first tested without the gap damper system initial to establish the displacement demand of the desired input motions. The gap damper system was added to the structure and the displacements were compared to evaluate the reduction capacity of the system. The isolator hystereses clearly changed through the duration of the test, suggesting degradation and softening of the isolators. In addition, the impact force created a large overturning moment that caused isolator compression stability issues. The degradation

and stability issues make it difficult to quantify the relative performance of the structure. A full scale structure would have more redundancy and larger resistance to overturning.

- Although the gap damper did not meet the performance objectives, the system was successful at reducing displacements. Further research is necessary to fully validate the system for full scale use.

7.2.4 Finite Element Analysis

- Finite element models show good agreement with global behavior evident from gap damper component studies.
- A coarse mesh model demonstrated the lack of energy dissipation provided by dampers transverse to the direction of movement. Even at a large angle of 30 degrees, the energy dissipated is only 8% of the energy dissipated in the primary damper.
- Special attention should be given to gap damper systems that may involve rotated impacts as they may cause localized areas of yielding. Rounding the edges of the nub may help to ease the local stresses evident in these impacts.

7.2.5 Design Procedure and Case Study

- The design procedure provides designers with a basis for gap damper design with component sizing and design recommendations based of the results of the parametric study and component experiments.
- Comparison of case study responses in *SAP2000* and *OpenSees* models indicated good agreement between the two models in predicting displacement demands in both base-isolated and gap damper configurations. The percent difference between *OpenSees* and *SAP2000* models varies from 0.4% to 6.7% for 20% target reduction motions versus range of 2.5% to

6.5% for 40% target reduction motions. The average percent difference is 2.5% and 3.2% for 20% and 40% target reduction motions, respectively.

- Acceleration comparison in superstructure floors, especially in the configuration with gap damper system, showed significant differences in response. Although the modal behavior was in close agreement for the primary modes of vibration, superstructure acceleration response differed with larger acceleration demands in *SAP2000* compared to *OpenSees*. The discrepancy can be attributed to a number of modeling assumptions and differences between the two analyses.
- Results for the 20% target reduction models clearly indicate the potential benefits of the gap damper system with a large displacement reduction and slight trade-off in superstructure acceleration. Preliminary evaluation of the brace forces indicated that the existing braces are adequate and would not require design iteration.
- The 40% target reduction ground motions indicated rather poor performance, even with the increase in energy dissipation from the design iteration. Displacement reduction was moderately successful but varied across ground motions. Superstructure acceleration demands increased by a factor of 2.2 (*OpenSees*) and 2.9 (*SAP2000*), respectively, when compared to the base-isolated configuration. The increase in superstructure demands led to brace demands exceeding capacity, which would require a design iteration to increase structural member sizes.
- Results of the 40% target reduction systems also indicated that the design objective may be too stringent when considering ground motions that are primarily bi-directional due to increased distance between the moat wall and structure with diagonal movement. Design objectives may be relaxed is the ground motion characteristics are well known.

Overall, the gap damper system is shown to be effective at achieving displacement reduction. A moat wall impact could have detrimental effects on the superstructure and should be avoided if possible. The gap damper system provides a useful mitigation technique while allowing traditional base-isolated behavior for more frequent ground motions. Further research is necessary to examine the trade-off between the displacement of the isolation system versus the acceleration of the superstructure. If acceleration increase can be shown to be less detrimental than a moat wall impact, while the gap damper reduces the displacement appropriately, then the system is an improvement on the state-of-the-art.

7.3 Recommendations for Future Work

The future research involving the gap damper system should expand upon some of the concepts developed within the scope of this dissertation. Research is an evolution of ideas, requiring thorough validation before an idea can become a practical option in design. The following are ideas that could further gap damper research:

- The fundamental formulation of the gap damper system involved lead-core rubber isolators. The concept should be extended to include other forms of base-isolation, such as friction isolation, by reformulating the energy derivations.
- Design EDL values were developed for using a simplified unidirectional model. Using a large ground motion suite, EDLs could be developed using the case study building and accounting for bi-direction movement.
- The component testing saw difficulty in the control of the slip force in the friction device. The parametric study indicated that the two-phase viscoplastic device was the best arrangement for the reduction of displacements while minimizing superstructure accelerations. Further

research into the friction device could provide a better performing, more reliable option for the gap damper system.

- Further research with the finite element model could evaluate differing impact conditions to assess the best option for the gap damper contacting elements.
- High accelerations were observed in the superstructure upon activation of supplemental energy dissipation. This acceleration was observed to be largely sensitive to the transition stiffness of the gap element. Incorporation of a transition mechanism that eases the force transmission could be reduce the superstructure accelerations and still provide the beneficial displacement reduction. This could be accomplished at the connection of the damper through the use of a viscoelastic sandwich damper or using other innovative solutions.
- Furthering the previous recommendation, research into the high frequency acceleration spikes present upon activation of the dampers could provide valuable insight towards the realistic effects in the superstructure. A further understanding of the actual effects of the gap damper activation could further validate the system as a viable design option.
- Preliminary analysis of the case study structure indicates that the gap damper system may be more effective in ground motions with a velocity pulse. Further research into this aspect could identify the gap damper system as a useful mitigation technique for near-source ground motions.
- The primary goal of the gap damper system is to reduce displacements to decrease the probability of a moat wall collision. Incorporating a moat wall into the case study analysis would allow the comparison of superstructure accelerations for a moat wall collision to the accelerations present upon activation of the gap damper system.

- Furthering the previous idea, a cost/benefit analysis, using the Performance Assessment Calculation Tool (PACT), could provide a useful comparison between the gap damper system and typically base-isolated structures (Miranda & Aslani, 2003).
- Activation of the gap damper creates a large overturning moment. The effect of the overturning was not investigated within the scope of this study but could be substantial in taller structures.
- Incorporation of inelastic elements into the superstructure of the model could provide more information on the effect of the activation of the gap damper system on the drifts of the system, especially with more flexible lateral force resisting systems.
- A scaled shake table study with a redundant and stable superstructure would provide more insight towards the effectiveness of the gap damper system.

References

Alehashem, S. M., Keyhani, A., & Pourmohammad, H. (2008). Behavior and Performance of Structures Equipped with ADAS & TADAS Dampers (A Comparison with Conventional Structures). *The 14th World Conference of Earthquake Engineering.* Beijing, China.

Al-Hussaini, T. M., Zayas, V. A., & Constantinou, M. C. (1994). *Seismic Isolation of Multi-Story Frame Structures Using Spherical Sliding Isolation Systems (NCEER-94-0007).* Buffalo, NY: National Center for Earthquake Engineering Research.

Almazan, J. L., de la Llera, J. C., & Inaudi, J. A. (1998). Modelling Aspects of Structures Isolated with the Frictional Pendulum System. *Earthquake Engineering and Structural Dynamics, 27*, 845-867.

Alvandi, S., & Ghassemieh, M. (2014). Application of Shape Memory Alloys in Seismic Isolation: A Review. *Civil Engineering Infrastructures Journal*.

ANSI/AISC. (2005). *Seismic Provisions for Structural Steel Buildings.* Chicago, IL: American Institute of Steel Construction, Inc.

Applied Technology Council. (2009). *Quantification of Building Seismic Performance Factors (FEMA P695).* Washington, D.C.: Federal Emergency Management Agency.

Applied Technology Council. (2012). *Seismic Performance Assessment of Buildings Volume 1 - Methodology.* Washington, D.C.: Federal Emergency Management Agency.

Applied Technology Council. (2012). *Seismic Performance Assessment of Buildings Volume 3 - Performance Assessment Calculation Tool (PACT).* Washington, D.C.: Federal Emergency Management Agency.

Arendt, L. A., Earle, S., & Meyers, R. (2010). Results of a cross-disciplinary survey of isolation systems. *Proceedings of the 9th U.S. National and 10th Canadian Conference.* Toronto, Canada.

ASCE. (2004). *Primer on Seismic Isolation.* Reston, VA: American Society of Civil Engineers.

ASCE/SEI. (2005). *Minimum Design Loads for Buildings and Other Structures: ASCE Standard 7-05.* Reston, VA: ASCE Publications.

ASCE/SEI. (2010). *Minimum Design Loads for Buildings and Other Structures: ASCE Standard 7-10.* ASCE Publications.

ASCE/SEI. (2010). *Minimum Design Loads for Buildings and Other Structures: ASCE Standard 7-10.* Reston, VA: ASCE Publications.

ASCE/SEI. (2014). *Minimum Design Loads for Buildings and Other Structures: ASCE Standard 7-16 [Manuscript in Progress]*. Reston, VA.: ASCE Publications.

Asteris, P. G. (2008). On The Structural Analysis and Seismic Protection of Historical Structures. *The Open Construction and Building Technology Journal, 2*, 124-133.

Balendra, T., Yu, C., & Lee, F. L. (2001). An Economical Structural System for Wind and Earthquake Loads. *Engineering Structures, 23*(5), 491-501.

Bertero, R. D., & Bertero, V. V. (2002). Performance-based seismic engineering: the need for a reliable. *Earthquake engineering and structural dynamics, 31*, 627-652. doi:10.1002/eqe.146

Bridgestone Corporation. (2014, August). *Seismic Isolator for Buildings (Products).* Retrieved August 2014, from Bridgestone.com: http://www.bridgestone.com/products/diversified/antiseismic_rubber/product.html

Buchanan, A. H., Bull, D., Dhakal, R., MacRae, G., Palermo, A., & Pampanin, S. (2011). *Base Isolation and Damage-Resistant Technologies for improved Seismic Performance of*

Buildings. Christchurch, New Zealand: University of Canterbury. Retrieved from http://www.scnz.org/content/events/docs/ENG.ACA.0020%20low%20damage.pdf

Buckle, I. G., & Mayes, R. L. (1990). Seismic Isolation: History, Application, and Performance - A World View. *Earthquake Spectra, 6*(2), 161-201.

Chen, P. C., Tsai, K. C., & Lin, P. Y. (2013). Real-time hybrid Testing of a Smart Base Isolation System. *Earthqauke Engineering and Structural Dynamics, 43*(1), 139-158. doi:10.1002/eqe.4290110105

Chiou, N., Daragh, R., Gregor, N., & Silva, W. (2008). NGA Project Strong Motion Database. *Earthquake Spectra, 24*(1), 23-44.

Chopra, A. K. (2012). *Dynamics of Structures - Theory and Applications to Earthquake Engineering* (4th ed.). Upper Saddle River, NJ: Prentice Hall.

Computers & Structures, Inc. (2014). *CSI Analysis Reference Manual (For SAP2000, ETABS, SAFE, and CSiBridge).* Berkeley, California: Computers & Structures, Inc.

Constantinou, A. S., Whittaker, A. S., Kalpakidis, Y., Fenz, D. M., & Warn, G. P. (2007). *Performance of Seismic Isolation Hardware under Service and Seismic Loading (MCEER-07-0012).* Buffalo, NY: MCEER.

Constantinou, M. C., Mokha, A., & Reinhorn, A. M. (1990). Teflon Bearings in Base Isolation II: Modeling. *Journal of Structural Engineering, 116*(2), 455-474.

Cutfield, M. R., Ryan, K. L., Buckle, I., & Ma, Q. T. (2014). *Comparative Life Cycle Analysis of Conventional and Base Isolated Buildings.* NEES Tips No. NEES-2008-0571.

Cutfield, M., Ryan, K. L., & Ma, Q. (2015). Comparative Life Cycle Analysis of Conventional and Base Isolated Buildings [In Press]. *Towards Integrated Seismic Design*.

Dassualt Systemes Simulia Corp. (2010). *ABAQUS: Theory Manual.* Providence, Rhode Island: Hibbitt, Karlsson, & Sorenson, Inc.

Dolce, M., Cardone, D., & Marnetto, R. (2001). SMA Recentering Devices for Seismic Isolation of Civil Structures. *Smart Structures and Materials 2001: Smart Systems for Bridges, Structures, and Highways, 4330.* Newport Beach, CA. doi:10.1117/12.434123

Dolce, M., Cardone, D., & Ponzo, F. C. (2007). Shaking-table Tests on Reincforced Concrete Frames with Different Isolation Systems. *Earthquake Engineering and Structural Dynamics, 36*, 573-596.

Dynamic Isolation Systems. (2014). *Products.* Retrieved August 2014, from Dynamic Isolation Systems: http://www.dis-inc.com/products.html

Erduran, E., Dao, N. D., & Ryan, K. L. (2011). Comparative Response Assessment of Minimally Compliant Low-Rise Converntionall Base-Isolated Steel Frames. *Earthquake Engieering and Structural Dynamics, 40*, 1123-1141.

Federal Emergency Management Agency. (2000). *FEMA 355-C State of the Art Report on Systems Performance of Steel Moment Frames Subjected to Earthquake Ground Shaking.* Washington, DC.

Fenz, D. M., & Constantinou, M. C. (2006). Behaviour of the Double Concave Friction Pensulum Bearing. *Earthquake Engineering and Structural Dynamics, 35*, 1403-1424.

Ghobarah, A. (2001). Performance-based Design in Earthquake Engineering: State of Development. *Engineering Structures*(23), 878-884.

Golondrino, J. C., MacRae, G. A., Chase, J. G., Rodgers, G. W., & Clifton, G. C. (2013). Application of brake pads on asymmetrical friction connection (AFC). *New Zealand Society for Earthquake Engineering*, (p. Paper 88). Wellington, New Zealand.

Grigorian, C. E., & Popov, E. P. (1994). *Energy Dissipation with Slotted Bolted Connections (Report UCB/EERC-94/02).* Berkeley, CA: Earthquake Engieering Research Center.
Hall, J. F., & Ryan, K. L. (2000). Isolated buildings and the 1997 UBC Near-Source Factors. *Earthquake Spectra, 16*(2), 393-411.
Hall, J. F., Heaton, T. H., Halling, M. W., & Wald, D. J. (1995). Near-Source Ground Motion and its Effects on Flexible Buildings. *Earthquake Spectra, 11*(4), 569-605.
Hall, J. F., Heaton, T. H., Halling, M. W., & Wald, D. J. (1995). Near-source ground motions and its effect on flexible buildings. *Earthquake Spectra, 11*, 569-605.
Han, M., Xianhua, L., & Du, H. (2008). Testing Study on Isolating Soft-Collision Limiting Displacement. *The 14th World Conference on Earthquake Engineering.* Beijing, China.
Hussain, S., Lee, D., & Retamal, E. (1998). *Viscous Damping for Base Isolated Structure.* Retrieved from http://taylordevices.com/Tech-Paper-archives/literature-pdf/36-ViscousDamping.pdf
International Code Council. (2006). *2006 International Building Code.* Washington, DC: International Code Council.
Iwan, W. D. (1997). Drift Spectrum: Measure of Demand for Earthquake Ground Motions. *Journal of Structural Engineering, 123*, 397-404.
Jangid, R. S., & Kelly, J. M. (2001). Base Isolation for Near-Fault Motions. *Earthquake Engineering and Structural Dynamics, 30*, 691-707.
Jangid, R. S., & Londhe, Y. B. (1998). Effectiveness of Elliptical Rolling Rods for Base Isolation. *Journal of Structural Engineering, 124*(4), 469-472.
Judd, J. P., & Charney, F. A. (2014). Performance-based design in the Central and Eastern United States. *Structures Congress,* (pp. 2355-2368). doi:10.1061/9780784413357.207
Kani, N., Takayama, M., & Wada, A. (2006). Performance of Seismically Isolated Buildings in Japan (Paper No. 2181). *Proceedings of the 8th U.S. National Conference on Earthquake Engineering.* San Francisco, CA.
Kelly, J. M., & Hodder, S. B. (1982, June). Experimental Study of Lead and Elastomeric Dampers for Base Isolation Systems in Laminated Neoprene Bearings. *Bulletin of the New Zealand National Society for Earthquake Engineering, 15*(2), pp. 53-67.
Kelly, J. M., Beucke, K. E., & Skinner, M. S. (1980). *Experimental Testing of a Friction Damped Aseismic Base Isolation System with Fail-safe Characteristics (UCB/EERC-80/18).* Berkeley, CA: Earthquake Engineering Research Center.
Kim, J., Ryu, J., & Chung, L. (2006). Siesmic Performance of Structures Connected by Viscoelastic Dampers. *Engineering Structures, 28*(2), 183-195.
Kircher, C. A. (2012). Chapter 12: Seismically Isolated Structures. In N. I. Council, *FEMA P-751, NEHRP Recommeded Provisions: Design Examples* (pp. 1-63). Federal Emergency Management Agency.
Konter, A. W. (2005). *Advanced Finite Element Contact Benchmarks.* FENet RTD (Durability & Life Extension), FENet EU Thematic Network (Contract G1RT-CT-2001-05034). FENet.
Kunde, M. C., & Jangid, R. S. (2003). Seismic Behavior of Isolated Bridges: A-State-of-the-Art-Review. *Electronic Journal of Structural Engineering*(3), 140-170.
Lake, G. J., & Lindley, P. B. (1967). *Ozone Attack and Fatigue Life of Rubber.* London, UK: Maclaren and Sons LTD.
Lee, D., & Taylor, D. (2001). Viscous Damper Development and Future Trends. *The Structural Design of Tall Buildings, 10*, 311-320.

Levy, R., Marianchik, E., Rutenberg, A., & Segal, F. (2000). Seismic Design Methology for Friction Damped Braced Frames. *Earthquake Engineering & Structural Dynamics, 29*(11), 1569-1585.

Lin, A. N., & Shenton III, H. W. (1992). Seismic Performance of Fixed-Base and Base-Isolated Steel Frames. *Journal of Engineering Mechanics, 118*, 921-941.

Lin, T.-W., & Hone, C.-C. (1993). Base Isolation by Free Rolling Rods Under Basement. *Earthqauke Engineering & Structural Dynamics, 22*(3), 261-273.

Makris, N., & Chang, S.-P. (2000). Effect of Viscous, Viscoplastic and Friction Damping on the Response of Seismic Isolated Structures. *Earthquake Engineering and Structural Dynamics, 29*, 85-107.

Makris, N., & Deoskar, H. S. (1996). Prediction of Observed Response of Base-Isolated Structure. *Journal of Structural Engineering, 122*, 485-493.

Marshall, J. D. (2008). *Development, Analysis, and Testing of a Hybrid Passive Control Device for Seismic Protection of Framed Structures.* Blacksburg, VA: Ph.D. Dissertation, Virginia Polytechnic Institute and State University.

Marshall, J. D., & Charney, F. A. (2010). A Hybrid Passive Control Device for Steel Structures, I: Development and Analysis. *Journal of Constructional Steel Research, 66*(10), 1278-1286.

Masroor, A., & Mosqueda, G. (2012). Experimental Simulation of Base-Isolated Buildings Pounding Against Moat wall and Effects on Superstructure Response. *Earthquake Engineering and Structural Dynamics, 41*, 2093-2109. doi:10.1002/eqe.2177

Miranda, E., & Aslani, H. (2003). *Probabilistic Response Assessment for Building Specific Loss Estimation (PEER Report 2003/03).* Berkeley, CA: Pacific Earthquake Engineering Research Center.

Miwada, G., Sano, T., Katsumata, H., Takiyama, N., Onishi, Y., & Hayashi, Y. (2012). Experimental Study on Hysteresis Characteristics of the Retaining Wall of the Base-Isolated Building. *Proceedings of the 15th World Conference on Earthquake Engineering.* Lisbon, Portugal.

Mokha, A., Constantinou, M. C., Reinhorn, A. M., & Zayas, V. A. (1991). Experimental Study of Friction-Pendulum Isolation System. *Journal of Structural Engineering, 117*, 1201-1217.

Morgan, T. A., & Mahin, S. A. (2011). *The Use of Base-Isolation Systems to Achieve Complex Seismic Performance Objectives (PEER Report 2011/06).* Berkeley, CA: Pacific Earthquake Engineering Research Center.

Mori Living. (2011, May 24). *Base Isolation Cushions Shaking Caused by Earthquakes.* Retrieved from Mori Living: http://www.moriliving.com/en/diary/10

Motlagh, A. Y., & Saadeghvaziri, M. A. (2001). Nonlinear Seismic Response of Stiffeneing SDOF Systems. *Engineering Structures, 23*, 1269-1280.

Naeim, F., & Kelly, J. M. (1999). *Design of Siesmic Isolated Structures (From Theory to Practice).* New York, NY: John Wiley & Sons, Inc.

Nagarajaiah, S., & Ferrell, K. (1999, September). Stability of Ealstomeric Seismic Isolation Bearings. *Journal of Structural Engineering*, 946-954.

Nagarajaiah, S., & Sahasrabudhe, S. (2006). Seismic Control of Smart Sliding Isolated Buildings Using Variable Stiffness Ssystems: An Experimental and Numerical Study. *Earthquake Engineering and Structural Dynamics, 35*, 177-197.

Nagarajaiah, S., & Sun, X. (2000, October). Response of Base-Isolated USC Hospital Building in Northridge Earthquake. *Journal of Structural Engineering*, 1177-1186.

Nagarajaiah, S., & Sun, X. (2001, September). Base-Isolated FCC Building: Impact Response in Northridge Earthquake. *Journal of Structural Engineering*, 1063-1075.

Nagarajaiah, S., Reinhorn, A. M., & Constantinou, M. C. (1991). Nonlinear Dynamic Analysis of 3-D Base-Isolated Structures. *Journal of Structural Engineering, 117*(7), 2035-2054.

National Institute of Standards and Technology. (1994). *1994 Northridge earthquake performance of structures, lifelines, and fire protection systems.* Gaithersburg, MD: National Institute of Standards and Technology.

NEESTIPS. (2009). *Network for Earthquake Engineering Simulation (NEES): Tools for isolation and protective systems (TIPS).* Retrieved from http://www.neng.usu.edu/cee/faculty/kryan/NEESTIPS/PBEE_study.html

NEHRP. (2009). *NEHRP Recommended Seismic Provisions.* Washington D.C.: Federal Emergency Management Agency of the U.S. Department of Homeland Security.

Nippon Steel & Sumitomo Metal Corporation. (2014, August). *Seismic Isolation U-Shaped Damper.* Retrieved from Nippon Steel & Sumitomo Metal: http://www.nssmc.com/en/product/process/damper.html

Pant, D. R., & Wijeyewickrema, A. C. (2014). Performance of Base-Isolated Reinforced Concrete Buildings Under Bidirectional Seismic Excitation Considering Pounding with Retaining Walls Including Friction Effects. *Earthquake Engineering & Structural Dynamics, 43*, 1521-1541. doi:10.1002/eqe.2409

Paril, S. J., & Reddy, G. R. (2012). State of the Art Review - Base Isolation Systems for Structures. *International Journal of Emerging Technology and Advanced Engineering, 2*(7), 438-453.

Ramallo, J. C., Johnson, E. A., & Spencer Jr., B. F. (2002). "Smart" Base Isolation Systems. *Journal of Engineering Mechanics, 128*(10), 1088-1099.

Rawlinson, T. A., & Marshall, J. D. (2014). Single-Degree-of-Freedom Characterization of Multi-Phase Passive Control Systems. *Journal of Earthquake Engineering, 18*(4).

Rawlinson, T., Marshall, J., Ryan, K., & Zargar, H. (2014). Component Test of a Gap Damper System to Control Isolator Displacements in Extreme Earthquakes. Network for Earthquake Engineering Simulation (NEES)(distributor). *Dataset*. doi:10.4231/D30V89J0P

Rawlinson, T., Marshall, J., Ryan, K., & Zargar, H. (2014). Design and Testing of a Gap Damper Device to Mitigate Rare Earthquake Pounding Response in Base-Isolated Buildings. *Tenth U.S. National Conference on Earthquake Engineering.* Anchorage, AK.

Rawlinson, T., Marshall, J., Ryan, K., & Zargar, H. (2015). Development and experimental evaluation of a passive gap damper device to prevent pounding in base-isolated structures. *Earthquake Engineering and Structural Dynamics*.

Reigles, D. G., & Symans, M. D. (2005). Systematic Performance Evaluation of Smart Seismic Isolation Systems. *Structures Congress 2005* (pp. 1-12). New York, New York: American Society of Civil Engineers. doi:10.1061/40753(171)197

Reinhorn, A. M., Constantinou, M. C., & Li, C. (1995). Use of Supplemental Damping Devices for Seismic Strengthening of Lightly Reinforced Concrete Frames. *National Institute for Standards and Technology Workship.* Gaithersburg, MD.

Roussis, P. C., Constantinou, M. C., Erdik, M., Durukal, E., & Dicleili, M. (2003, July/August). Assessment of Performnace of Seismic Isolation System of Bolu Viaduct. *Journal of Bridge Engineering*, 182-190.

Ryan, K. L., Coria, C. B., & Dao, N. D. (2013). *Large sclae earthquake simulation of a hybrid lead rubber isolation system designed with consideration of nuclear seismicity.* University of Nevada, Reno, Center for Civil Engineering Earthquake Research. Washington, D.C.: U.S. Nuclear Regulatory Commission.

Ryan, K. L., Sayani, P. J., Dao, N. D., Abraik, E., & Baez, Y. M. (2010). Comparative Life Cycle Analysis of Conventional and Base Isolated Buildings. *Proceedings of the 9th U.S. National and 10th Canadian Conference on Earthquake Engineering.* Toronto, CA.

Sabelli, R., Mahin, S., & Chang, C. (2009). Seismic Demands on Steel Braced Frame Buildings with Buckling Restrained Braces. *Engineering Structures, 25*, 655-66.

Sarlis, A. S., & Constantinou, M. C. (2010). *Modeling Triple Friction Pendulum Isolators in Program SAP2000.* Buffalo, New York: State University of New York.

Sasaki, T., Sato, E., Ryan, K. L., Okazaki, T., Mahin, S. A., & Kajiwara, K. (2012). NEES/E-Defense Base-Isolation Tests: Effectiveness of Friction Pendulum and Lead-Rubber Bearing Systems. *Proceedings of the 15th World Conference of Earthquake Engineering.* Lisbon, Portugal.

Sayani, P. J., Erduran, E., & Ryan, K. L. (2011). Comparative Response Assessment of Minimally Compliant Low-Rise Base-Isolated and Conventional Steel Moment Resisting Frame Buildings. *Journal of Structural Engineering, 137*(10), 1118-1131.

SEAOC. (1990). *Recommended lateral force requirements and commentary.* Sacramento, CA: Structural Engineers Association of California.

Shenton III, H. W., & Lin, A. N. (2011). Relative Performance of Fixed-Base and Base-Isolated Concrete Frames. *Journal of Structural Engineering, 119*(10), 2952-2968.

Somerville, P., Smith, N., Puntamurthula, S., & Sun, J. (1997). *Development of Ground Motion Time Histories for Phase 2 of the FEMA/SAC Steel Project.* SAC Joint Venture. Richmond, CA: SAC Background Document SAC/BD-97/04.

Song, G., Ma, N., & Li, H. N. (2006). Applications of Shape Memory Alloys in Civil Structures. *Engineering Structures, 28*, 1266-1274.

Spencer Jr., B. F., & Nagarajaiah, S. (2003). State of the Art of Strucutral Control. *Journal of Structural Engineering, 129*(7).

Spencer Jr., B. F., & Sain, M. K. (1997). Controlling Buildings: A New Frontier in Feedback. *IEEE Control Systems Magazine on Emerging Technology, 17*(6), pp. 19-35.

Stewart, J. P., Conte, J. P., & Aiken, I. D. (1999). Observed Behavior of Seismically Isolated Buildings. *Journal of Structural Engineering, 125*, 955-964.

Symans, M. D., & Kelly, S. W. (1999). Fuzzy Logic Control of Bridge Strucutres Using Intelligent Semi-Active Seismic Isolation Systems. *Earthqauke Engineering and Structural Dynamics, 28*, 37-60.

Taylor Devices Inc. (2012). *Seismic Dampers & Seismic Protection Products*. Retrieved from taylor devices inc.: http://taylordevices.com/pdf/web-damper.PDF

Taylor Devices Inc. (2015). *Fluid Viscous Dampers & Lock-up Devices.* Retrieved from taylordevices.com: http://taylordevices.com/pdf/web-damper.PDF

Taylor, A., & Aiken, I. (2011, March). What's Happened to Seismic Isolation of Buildings in the U.S.? *Structure*, pp. 10-13. Retrieved from http://viewer.zmags.com/publication/ccf9bb78#/ccf9bb78/11

Taylor, D. P., & Constantinou, M. C. (1998). *Developement and Testing of an Improved Fluid Damper Configuration for Structrues having High Rigidity.* Retrieved from taylordevices.com: http://taylordevices.com/Tech-Paper-archives/literature-pdf/52-Development-TestingLit%20.pdf

Taylor, D. P., & Constantinou, M. C. (1998). *Development and Testing of an Improved Fluid Damper Configuration for Structures having High Rigidity.* Retrieved from taylordevices.com: http://taylordevices.com/Tech-Paper-archives/literature-pdf/52-Development-TestingLit%20.pdf

Wang, H. (2009). *A Passive Two-Step Control Fluid Damping Devices for Seismic Protection of Structures.* Ann Arbor, MI: ProQuest Information and Learning Company.

Warn, G. P., & Ryan, K. L. (2012). A Review of Seismic Isolation for Buildings: Historical Development and Research Needs. *Buildings*(2), 300-325. doi:10.3390/buildings2030300

Warn, G. P., & Vu, B. (2012). Exploring the Low Shape Factor Concept to Achieve Three-Dimensional Seismic Isolation. *20th Analysis & Computation Specialty Conference.* Chicago: American Society of Civil Engineers.

Weidlinger, P., & Ettouney, M. (1993). Sequential Coupling: New Structural Connection for Seismic Control. *Jornal of Structural Engineering, 119*(1), 181-201.

Weisman, J., & Warn, G. P. (2012, February). Stability of Elastomeric and Lead-Rubber Seismic Isolation Bearings. *Journal of Structural Engineering*, 215-223.

Wilde, K., Gardoni, P., & Fujino, Y. (2000). Base Isolation System with Shape Memory Alloy Device for Elevated Highway Bridges. *Engineering Structures, 22*(3), 222-229. doi:10.1016/S0141-0296(98)00097-2

Wilson, E. L. (2002). Fast Nonlinear Analysis. In E. L. Wilson, *Three Dimensional Static and Dynamic Analysis of Structures (A Physical Approach with Emphasis on Earthquake Engineering).* Berkeley, California: Computers and Structures, Inc.

Wolff, E. D., & Constantinou, C. M. (2004). *Experimental Study of Seismic Isolation Systems with emphasis on Secondary System Response and Verification of Accuracy of Dynaic Response History Analysis Methods (MCEER-04-0001).* Buffalo, NY: Multidisciplinary Center for Earthquake Engineering Research.

Zargar, H. (2015). *An Innovative Gap Damper to Control Seismic Isolator Displacements in Extreme Earthquakes.* Reno, NV: Ph.D. Dissertation, University of Nevada-Reno.

Zargar, H., Ryan, K. L., & Marshall, J. D. (2013). Feasibility Study of a Gap Damper to Control Seismic Isolator Displacements in Extreme Earthquakes. *Structural Control and Health Monitoring, 20*(8), 1159-1175.

Zargar, H., Ryan, K. L., Rawlinson, T., & Marshall, J. D. (2012). Exploring the Gap Damper Concept to Control Seismic Isolation Displacement Demands. *Proceedings of the Fifthteenth World Conference on Earthquake Engineering.* Lisbon, Portugal.

Zayas, V. A., Low, S. S., & Mahin, S. A. (1987). *The FPS Earthquake Resisting System: Experimental Report (UCB/EERC-87/01).* Berkeley, CA: Earthquake Engineering Research Center.

Appendix A. Gap Damper Design Drawings

This Appendix contains the design drawings for the components of the gap damper system. The order of the drawings are as follows:

A-2 Drawing from Taylor Devices Inc. for the viscous damper (c = 81.91 kN*m/s (0.465 kip*s/in))
(John Metzger, personal communication, August 20, 2012)

A-3 Drawing from Taylor Devices Inc. for the viscous damper (c = 71.67 kN*m/s (0.407 kip*s/in))
(John Metzger, personal communication, August 20, 2012)

A-4 Drawing from Taylor Devices Inc. for damper clevis attachments
(Doug Taylor, personal communication, July 27, 2012)

A-5 Drawing from Taylor Devices Inc. for damper clevis pin
(John Metzger, personal communication, August 20, 2012)

A-6 Materials list for fabrication

A-7 Bumper layout

A-8 Bumper layout with clevises

A-9 Damper clevises

A-10 Friction device clevises

A-11 Isolation nub

A-12 Friction device

A-13 Plate for clevis attachment to actuator

A-14 Actuator head attachment

SPECIFICATIONS:

1.) UNIT TYPE: DOUBLE ACTING FLUID VISCOUS DAMPER.
2.) ALL PARTS THAT SLIDE RELATIVE TO ANY SEALS SHALL BE MADE FROM 17-4PH STAINLESS STEEL.
3.) APPROXIMATE WEIGHT OF THE UNIT = 90 LBS. [41 KG].
4.) UNITS TO BE CONSTRUCTED FROM CORROSION PROTECTED MATERIALS.
5.) OPERATING FLUID IS INERT SILICONE, PER U.S.-FEDERAL STANDARD VV-D-1078.
6.) OPERATING AMBIENT TEMPERATURE RANGE: 32°F TO 120°F [0°C TO 49°C] WITH MINIMAL CHANGE IN PERFORMANCE CHARACTERISTICS.
7.) DAMPER STROKE ±3" [±75 mm] WITH IDENTICAL CHARACTERISTICS IN EITHER DIRECTION OF MOTION.
8.) DAMPING FORCE = 12.4 KIP.
9.) NOMINAL OUTPUT FUNCTION: $F=CV^{\alpha}$

$C = 0.465$ KIP*SEC/IN $\alpha = 1.0$

REVISIONS				
ZONE	REV.	DESCRIPTION	DATE	APPROVED
	A	1.) FUNCTION WAS C=0.552 KIP*SEC/IN.	12/8/20	J.C.M.

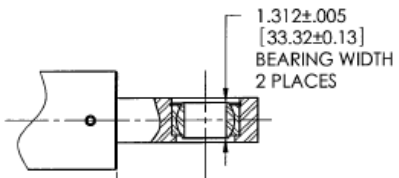

SECTION B-B

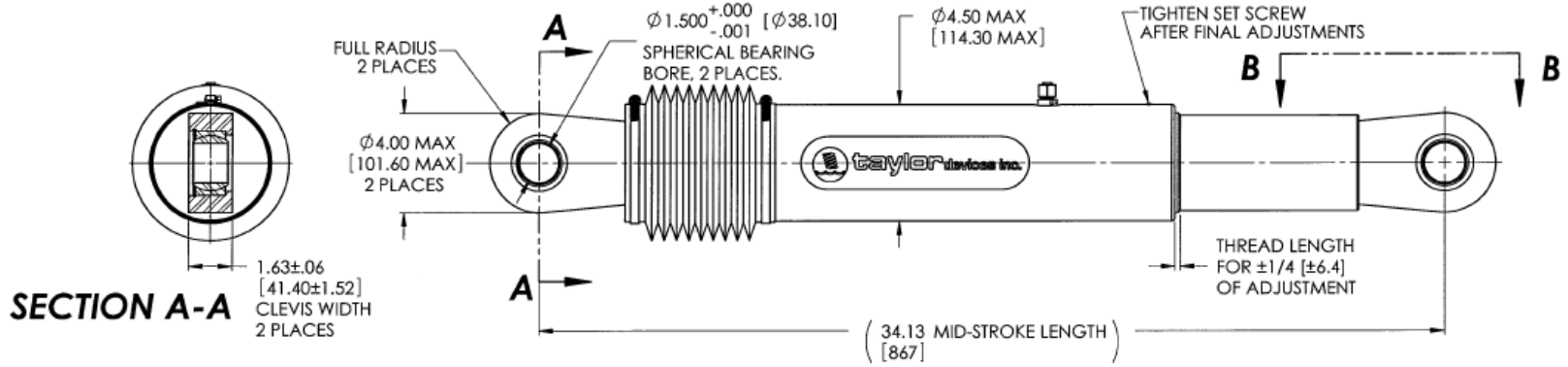

SECTION A-A

1.63±.06
[41.40±1.52]
CLEVIS WIDTH
2 PLACES

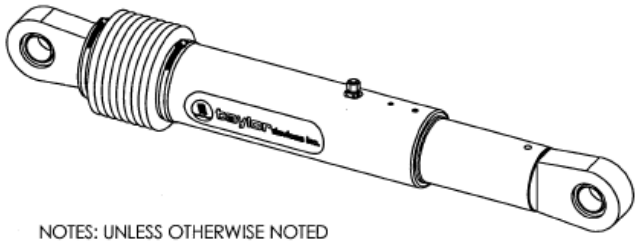

NOTES: UNLESS OTHERWISE NOTED

INCHES
[MILLIMETERS]

UNLESS OTHERWISE SPECIFIED DIMENSIONS ARE IN INCHES. TOLERANCES, ANGLES ±2°
.XX ±.01 .XXX ±.002
.XXXX ±.0002 X/X ±1/16
ALL CORNERS & EDGES TO BE R .01-.02
√ MAX. ALL SURFACES

B/P COPY NO.
B/P SUBJECT TO RECALL:
B/P & SUBJECT MATTER PROPERTY TAYLOR COMPANIES
REPRODUCTION B/P OR SUBJECT MATTER PROHIBITED

PATENTS { PENDING / APPLIED FOR
FORM 5E

STOCK SIZE (REF):
Ø

PREPARED	K.VARNEY	12/8/20
CHECKED		
Q.A.		
MFG APPR.		
ENGINEER	J.C.M.	12/8/20
APPROVED	J.C.M.	12/8/20
MATERIAL:		

taylor devices inc.
NORTH TONAWANDA, NY
PHONE 716-694-0800
FAX 716-695-8015

12.4 KIP FLUID VISCOUS DAMPER
GAP DAMPER PROJECT AUBURN UNIVERSITY

SIZE	CAGE CODE	DRAWING NO:	REV.
B	06742	67DP-19310-01	A

SCALE: 1:4 | WEIGHT: | SHEET 1 OF 1

SPECIFICATIONS:

1.) UNIT TYPE: DOUBLE ACTING FLUID VISCOUS DAMPER.
2.) ALL PARTS THAT SLIDE RELATIVE TO ANY SEALS SHALL BE MADE FROM 17-4PH STAINLESS STEEL.
3.) APPROXIMATE WEIGHT OF THE UNIT = 90 LBS. [41 KG].
4.) UNITS TO BE CONSTRUCTED FROM CORROSION PROTECTED MATERIALS.
5.) OPERATING FLUID IS INERT SILICONE, PER U.S.-FEDERAL STANDARD VV-D-1078.
6.) OPERATING AMBIENT TEMPERATURE RANGE: 32°F TO 120°F [0°C TO 49°C] WITH MINIMAL CHANGE IN PERFORMANCE CHARACTERISTICS.
7.) DAMPER STROKE ±3" [±75 mm] WITH IDENTICAL CHARACTERISTICS IN EITHER DIRECTION OF MOTION.
8.) DAMPING FORCE = 10.5 KIP.
9.) NOMINAL OUTPUT FUNCTION: $F=CV^{\alpha}$

$C = 0.407$ KIP*SEC/IN $\alpha = 1.0$

REVISIONS				
ZONE	REV.	DESCRIPTION	DATE	APPROVED
	A	1.) FUNCTION WAS C=0.468 KIP*SEC/IN.	12/8/20	J.C.M.

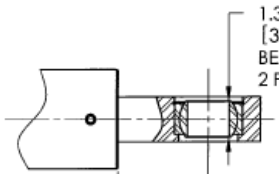

SECTION B-B

3.25±.03
[82.55±0.76]
2 PLACES

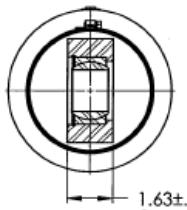

SECTION A-A

1.63±.06
[41.40±1.52]
CLEVIS WIDTH
2 PLACES

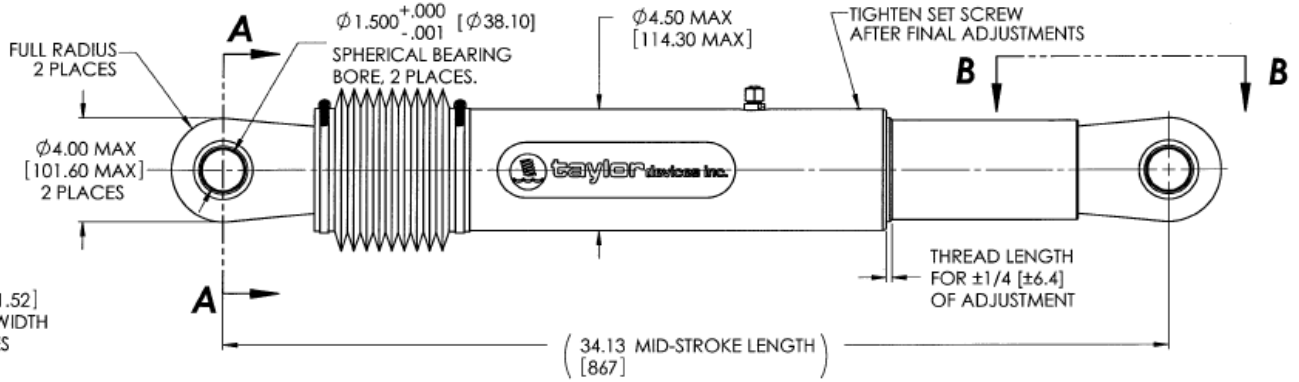

INCHES
[MILLIMETERS]

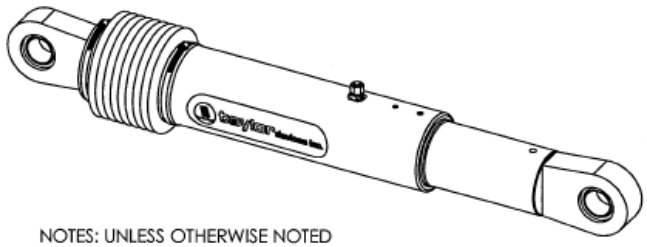

NOTES: UNLESS OTHERWISE NOTED

UNLESS OTHERWISE SPECIFIED DIMENSIONS ARE IN INCHES. TOLERANCES, ANGLES ±2°
XX ±.01 XXX ±.002
XXXX ±.0002 X/X ±1/16
ALL CORNERS & EDGES TO BE R .01-.02
√ MAX. ALL SURFACES

B/P COPY NO.
B/P SUBJECT TO RECALL:
B/P & SUBJECT MATTER PROPERTY TAYLOR COMPANIES
REPRODUCTION B/P OR SUBJECT MATTER PROHIBITED
COPYRIGHT 1956
PATENTS { PENDING / APPLIED FOR } FORM SE

STOCK SIZE (REF):
Ø

PREPARED	K.VARNEY	12/8/20
CHECKED		
Q.A.		
MFG APPR.		
ENGINEER	J.C.M.	12/8/20
APPROVED	J.C.M.	12/8/20

MATERIAL:

taylor devices inc.
NORTH TONAWANDA, NY
PHONE 716-694-0800
FAX 716-695-6015

10.5 KIP FLUID VISCOUS DAMPER
GAP DAMPER PROJECT AUBURN UNIVERSITY

SIZE	CAGE CODE	DRAWING NO:	REV.
B	06742	67DP-19311-01	A

SCALE: 1:4 | WEIGHT: | SHEET 1 OF 1

REVISIONS				
ZONE	REV.	DESCRIPTION	DATE	APPROVED
	A	CORRECTED 17140 PIN HOLE SIZE, UPDATED TANG DIMENSIONS	07/4/3	J.C.M.
	B	ADDED METRIC TOLERANCE TO "H" DIMENSION	08/8/6	D.J.D.H.

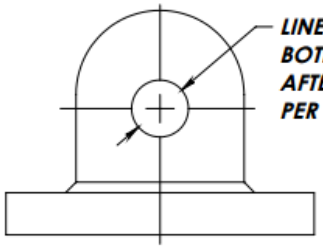

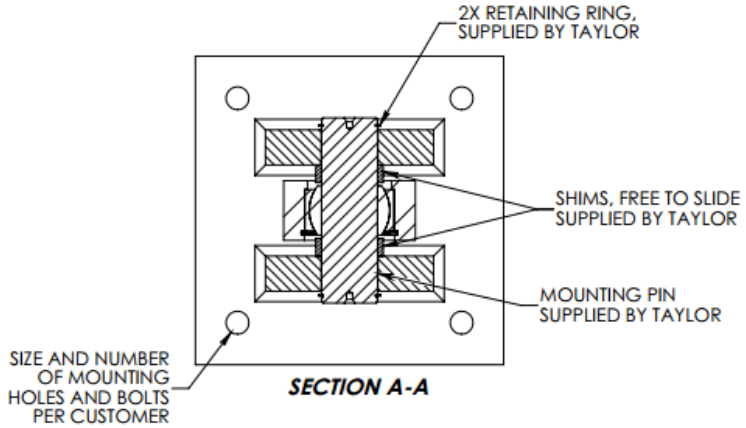

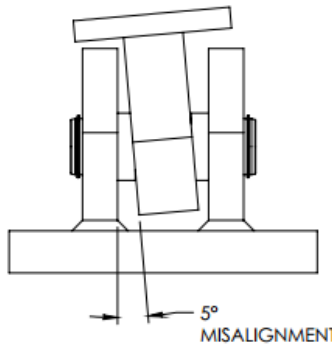

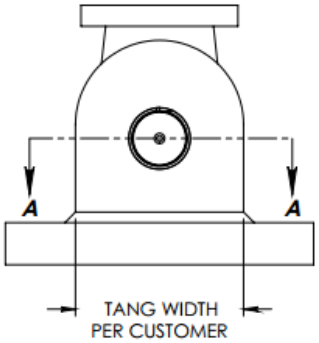

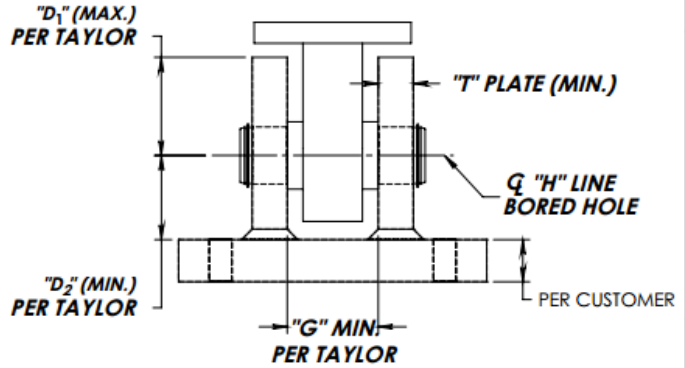

	"G"		"T"		"D1" MAX.		"D2" MIN.		"H" ±.01in./±.25mm	
	INCHES	MM	INCHES	MM	INCHES	MM	INCHES	MM	INCHES	MM
17120	2.63	66.8	0.75	19.1	2.75	69.9	2.75	69.9	1.53	38.9
17130	3.13	79.5	1.00	25.4	3.50	88.9	3.00	76.2	2.03	51.6
17140	3.25	82.6	1.25	31.8	3.75	95.3	3.75	95.3	2.28	57.9
17150	3.75	95.3	1.50	38.1	5.00	127.0	4.50	114.3	2.78	70.6
17160	4.00	101.6	2.00	50.8	5.25	133.4	4.75	120.7	3.03	77.0
17170	4.75	120.7	2.25	57.2	6.50	165.1	5.50	139.7	3.53	89.7
17180	6.00	152.4	3.00	76.2	7.00	177.8	7.00	177.8	4.03	102.4
17190	7.00	177.8	3.50	88.9	8.00	203.2	7.00	177.8	5.03	127.8

THIS IS A TYPICAL INSTALLATION DETAIL FOR A TAYLOR DEVICES UNIT. THIS SHOULD BE USED AS A GUIDELINE FOR CONNECTION DETAILS. DEVIATIONS FROM THE SHOWN CONFIGURATIONS ARE ACCEPTABLE, BUT THE FACTORY SHOULD BE CONSULTED. (COTTER PINS AND WASHERS MAY BE SUBSTITUTED FOR RETAINING RINGS). "SUPPLIED ITEMS" ARE PROVIDED BY TAYLOR DEVICES WITH THE UNITS.

NOTES: UNLESS OTHERWISE NOTED

FOR REFERENCE ONLY

PREPARED	D. HORNE	06/5/10
CHECKED		
Q.A.		
MFG APPR.		
ENGINEER	J.C.M.	07/4/3
APPROVED	J.C.M.	07/4/3
MATERIAL:		

taylor devices inc.
NORTH TONAWANDA, NY
PHONE 716-694-0800
FAX 716-695-6015

FIELD INSTALLATION GUIDE

SIZE	CAGE CODE	DRAWING NO:	REV.
B	06742	PIN AND BRACKET GUIDE	B

SCALE: 1:4 SHEET 1 OF 1

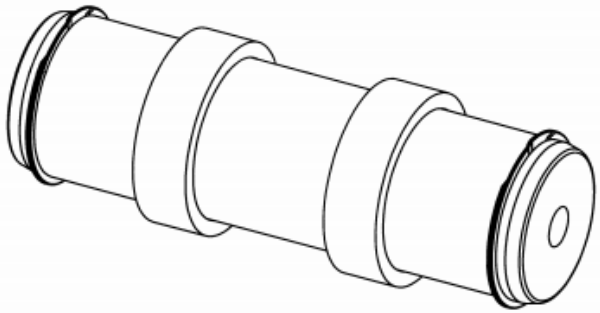

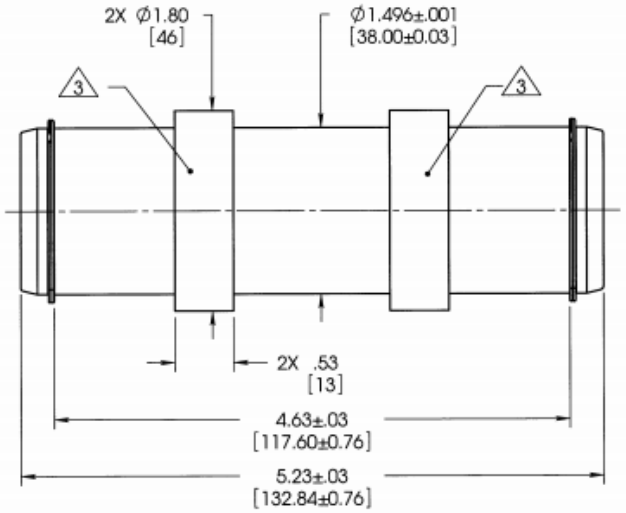

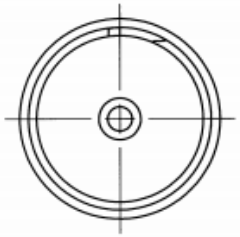

REVISIONS				
ZONE	REV.	DESCRIPTION	DATE	APPROVED

INCHES
(MILLIMETERS)

3 FREE TO SLIDE.

2.) RETAINING RINGS AND SHIMS TO BE STAINLESS STEEL.

1.) PIN TO BE 17-4PH STAINLESS STEEL.

NOTES: UNLESS OTHERWISE NOTED

UNLESS OTHERWISE SPECIFIED DIMENSIONS ARE IN INCHES TOLERANCES ANGLES ±2°
.XX ±.01 .XXX ±.002
.XXXX ±.0002 X/X ±1/16
ALL CORNERS & EDGES TO BE R .01-.02
√ MAX. ALL SURFACES

B/P COPY NO.
B/P SUBJECT TO RECALL:

FORM 5E
PATENTS { PENDING / APPLIED FOR

STOCK SIZE (REF):
Ø

PREPARED	K.VARNEY	08/10/9
CHECKED	Dpth	09/4/14
Q.A.		
MFG APPR.		
ENGINEER	J.C.M.	09/5/14
APPROVED	J.C.M.	09/5/14

MATERIAL:

taylor devices inc.
NORTH TONAWANDA, NY
PHONE 716-694-0800
FAX 716-695-6015

PIN KIT

SIZE	CAGE CODE	DRAWING NO:	REV.
B	06742	67DP-17120-03-1	

SCALE: 1:1 | WEIGHT: 2.88 | SHEET 1 OF 1

Material to be Purchased by Davis		
	Bar Size (in)	Length (ft)
1018 Cold-Formed Steel	$6\frac{1}{2}$x1	3
1018 Cold-Formed Steel	8x$\frac{3}{4}$	3
1018 Cold-Formed Steel	$6\frac{1}{2}$x$\frac{3}{4}$	3
1018 Cold-Formed Steel	6x$\frac{3}{4}$	4
1018 Cold-Formed Steel	$5\frac{1}{2}$x$\frac{3}{4}$	12
1018 Cold-Formed Steel	$4\frac{1}{2}$x$\frac{3}{4}$	4
1018 Cold-Formed Steel	$1\frac{1}{2}$x$\frac{3}{4}$	12
1018 Cold-Formed Steel	8x$\frac{3}{8}$	5

NOTE: ANY QUESTIONS OR CONCERNS CAN BE DIRECTED TO TAYLOR RAWLINSON; AVAILABLE AT TAR629@GMAIL.COM AND (336)314-0193. FEEL FREE TO CONTACT AT ANY TIME.

8" BARS REQUIRE CUT WIDTH FOR $7\frac{1}{4}$" SPECIFIED

Material Locations Provided by AU						
QTY	Material	Item	Sheet	Length (in)	Width (in)	Thickness (in)
3	A500 Steel	HSS 6x6x$\frac{1}{2}$	S1 & S2	~66	6	6
2	A36 Steel	Actuator Plates	S7	16	$11\frac{1}{2}$	1
Purchased by Davis (See above table for purchasing details)						
4	1018 Cold-Formed Steel	Welded Damper Clevis Base Plate	S3	$6\frac{1}{2}$	5	$\frac{3}{4}$
8	1018 Cold-Formed Steel	Welded Damper Clevis Bracket	S3	$5\frac{1}{2}$	$5\frac{1}{2}$	$\frac{3}{4}$
8	1018 Cold-Formed Steel	Threaded Damper Clevis Bracket	S3	$5\frac{1}{2}$	$5\frac{1}{2}$	$\frac{3}{4}$
2	1018 Cold-Formed Steel	Welded Friction Device Clevis Base Plate	S4	$6\frac{1}{2}$	3	$\frac{3}{4}$
2	1018 Cold-Formed Steel	Welded Friction Device Clevis Bracket	S4	$5\frac{1}{2}$	$5\frac{1}{2}$	$\frac{3}{4}$
2	1018 Cold-Formed Steel	Threaded Friction Device Clevis Bracket	S4	$7\frac{1}{2}$	$5\frac{1}{2}$	$\frac{3}{4}$
2	1018 Cold-Formed Steel	Isolation Nub Front and Back	S5	20	6	$\frac{3}{4}$
2	1018 Cold-Formed Steel	Isolation Nub Front and Back	S5	20	$4\frac{1}{2}$	$\frac{3}{4}$
1	1018 Cold-Formed Steel	Isolation Nub Cap Plate	S5	$4\frac{1}{2}$	$4\frac{1}{2}$	$\frac{3}{4}$
1	1018 Cold-Formed Steel	Friction Device Center Plate	S6	$22\frac{3}{16}$	$7\frac{1}{4}$	$\frac{3}{8}$
2	1018 Cold-Formed Steel	Friction Device Side Plates	S6	$23\frac{1}{2}$	$7\frac{1}{4}$	$\frac{3}{8}$
4	1018 Cold-Formed Steel	Friction Device Stiffeners	S6	$17\frac{1}{16}$	$1\frac{1}{2}$	$\frac{3}{8}$
4	1018 Cold-Formed Steel	Threaded Damper Clevis Base Plate	S3	$6\frac{1}{2}$	5	1
1	1018 Cold-Formed Steel	Threaded Friction Device Clevis Base Plate	S4	$6\frac{1}{2}$	4	1

General Notes:

- All steel ordered will be AISI 1018 cold-formed steel (flat bar) or better yield strength
- Use the first table for ordering, the second table indicates the locations and appropriate sheet(s) for the materials
- At least 10% added for cuts/misc
- Ryerson indicated that all bars except the $1\frac{1}{2}$"x$\frac{3}{4}$" can be cut to length.
- Weld material is E-7018

Project Name:
Auburn University Gap Damper Project

Address:
Auburn University
Civil Engineering
238 Harbert

Sheet Name:
Materials

Project Number:

Date: 12/9/2015

Scale: As Noted

Sheet: S0

PRODUCED BY AN AUTODESK EDUCATIONAL PRODUCT

PRODUCED BY AN AUTODESK EDUCATIONAL PRODUCT

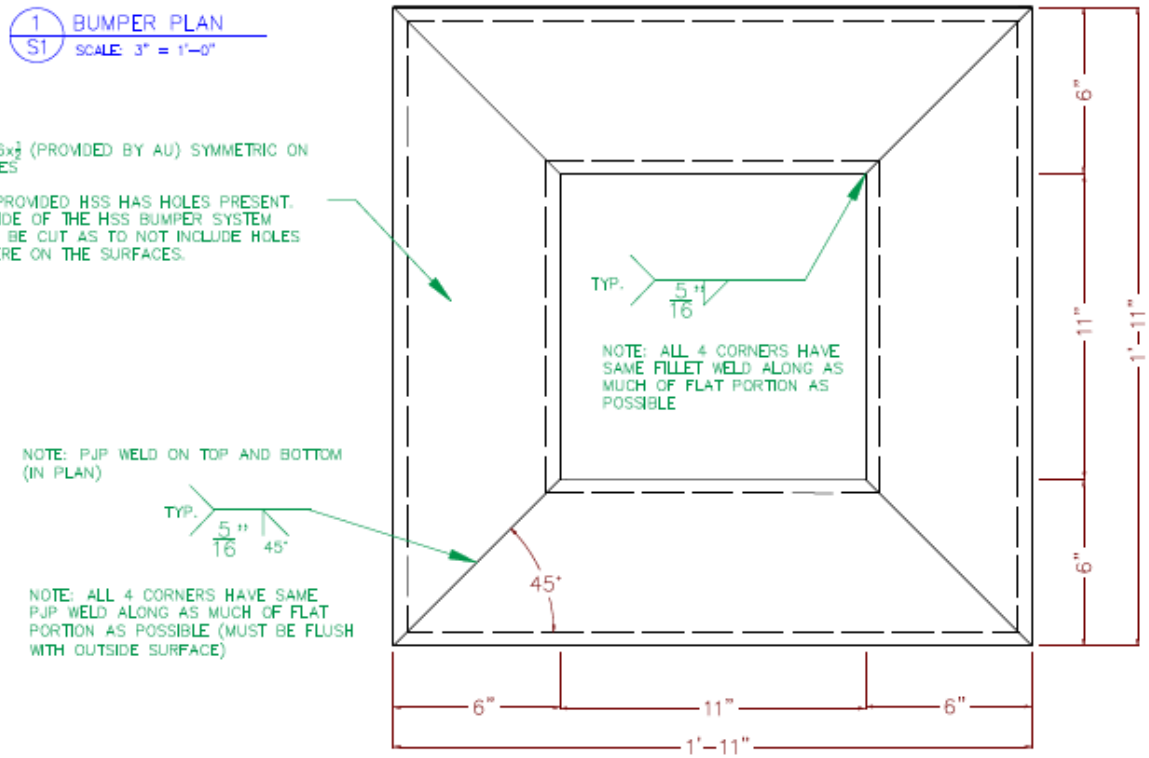

General Notes:

- HSS 6X6X0.5 (A500) will be provided by AU
- Cuts shall be made using solid portion of HSS (avoid using section of HSS with holes already present)
- All scrap HSS should be given back to AU at completion of fabrication
- Tolerances on lengths +/- 1/16 inch
- Weld material is E-7018

Project Name:
Auburn University Gap Damper Project

Address:
Auburn University
Civil Engineering
238 Harbert Center
Auburn, AL 36849

Sheet Name:
Bumper & Clevis Layout

Project Number

Date 12/17/2014

Scale As Noted

Sheet # S1

PRODUCED BY AN AUTODESK EDUCATIONAL PRODUCT

PRODUCED BY AN AUTODESK EDUCATIONAL PRODUCT

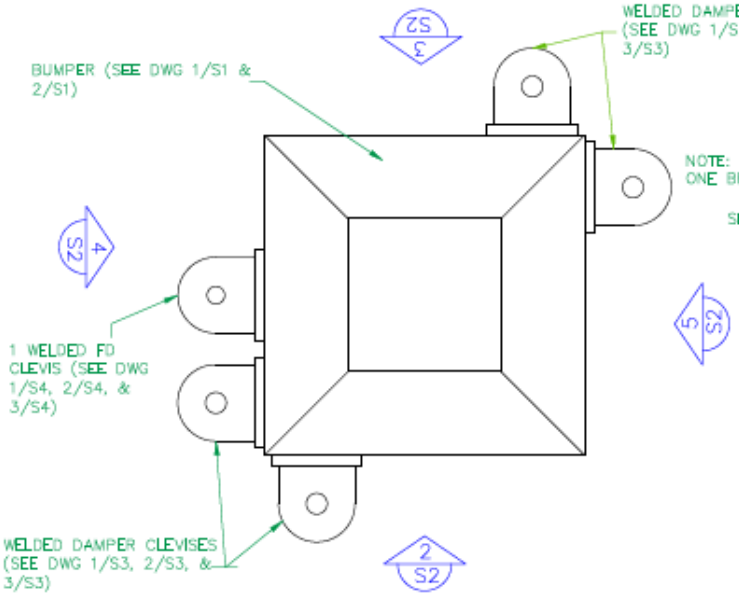

1 S2 BUMPER & CLEVISES PLAN
SCALE: 1-1/2" = 1'-0"

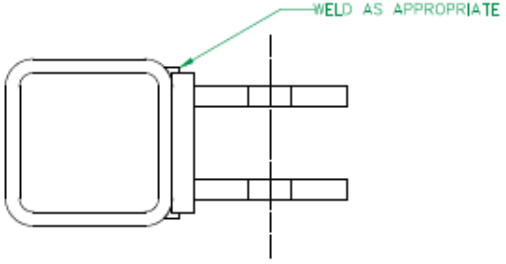

6 S2 PLATE TO HSS WELD DETAIL
SCALE: 3" = 1'-0"

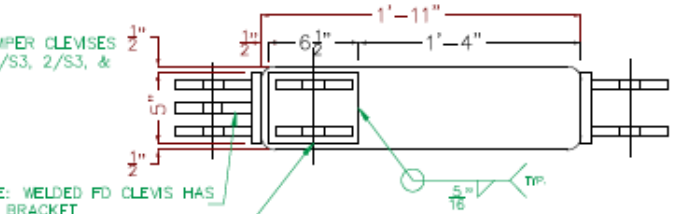

2 S2 BUMPER LAYOUT FRONT
SCALE: 1-1/2" = 1'-0"

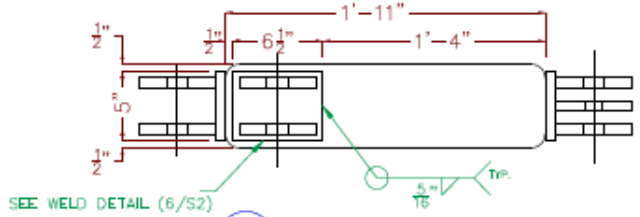

3 S2 BUMPER LAYOUT BACK
SCALE: 1-1/2" = 1'-0"

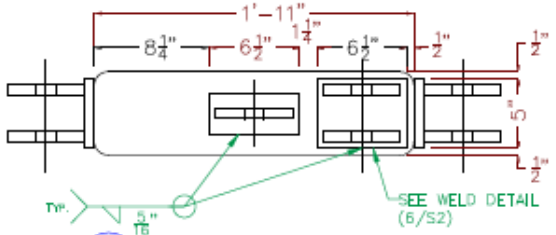

4 S2 BUMPER LAYOUT LEFT SIDE
SCALE: 1-1/2" = 1'-0"

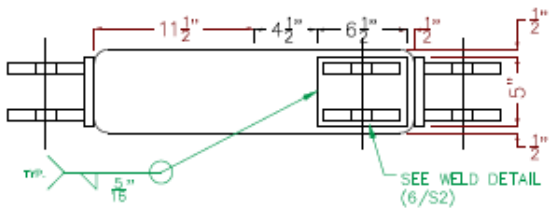

5 S2 BUMPER LAYOUT RIGHT SIDE
SCALE: 1-1/2" = 1'-0"

General Notes:

- This sheet should be used for weld placement of the 4 damper clevises and 1 friction device clevis onto the HSS bumper
- Weld material is E-7018

Project Name:
Auburn University Gap Damper Project

Address:
Auburn University
Civil Engineering
238 Harbert Center
Auburn, AL 36849

Sheet Name:
Bumper & Clevis Layout

Project Number

Sheet
S2

Date
12/7/2012

Scale
As Noted

PRODUCED BY AN AUTODESK EDUCATIONAL PRODUCT

PRODUCED BY AN AUTODESK EDUCATIONAL PRODUCT

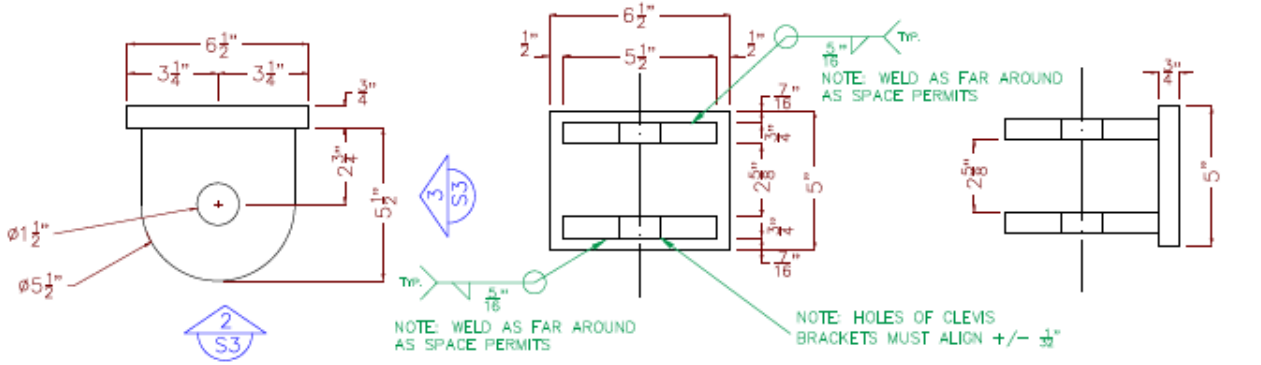

1 S3 WELDED CLEVIS PLAN (QTY 4)
SCALE: 3" = 1'-0"

2 S3 WELDED CLEVIS FRONT
SCALE: 3" = 1'-0"

3 S3 WELDED CLEVIS SIDE
SCALE: 3" = 1'-0"

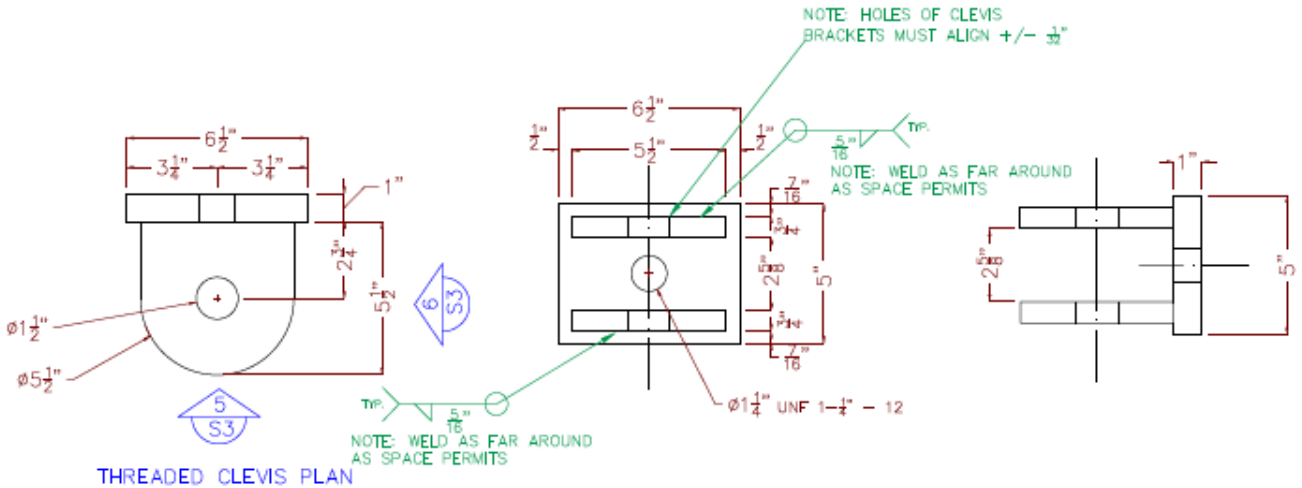

4 S3 THREADED CLEVIS PLAN (QTY 4)
SCALE: 3" = 1'-0"

5 S3 THREADED CLEVIS FRONT
SCALE: 3" = 1'-0"

6 S3 THREADED CLEVIS SIDE
SCALE: 3" = 1'-0"

General Notes:

- Clevises to be fabricated using 50 ksi (A992) steel plates purchased by Davis
- Tolerance on lengths +/- 1/16 inch
- Tolerance on clevis hole alignment +/- 1/32 inch
- Weld material is E-7018

Project Name:
Auburn University Gap Damper Project

Address:
Auburn University
Civil Engineering
238 Harbert Center
Auburn, AL 36849

Sheet Name:
Damper Clevises (Welded and Threaded)

Project Number

Sheet #
S3

Date:
12/19/2012

Scale:
As Noted

PRODUCED BY AN AUTODESK EDUCATIONAL PRODUCT

PRODUCED BY AN AUTODESK EDUCATIONAL PRODUCT

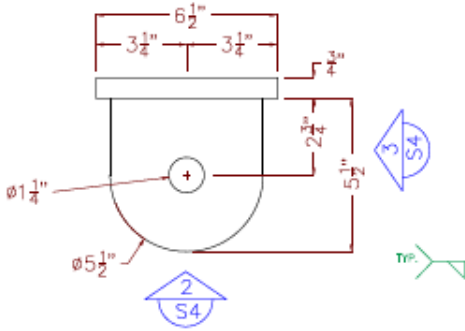

1 S4 WELDED FD CLEVIS PLAN (QTY 2)
SCALE: 3" = 1'-0"

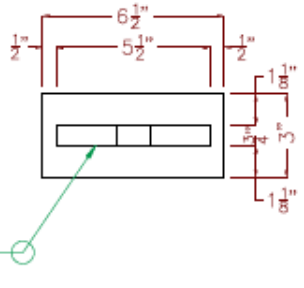

2 S4 WELDED FD CLEVIS FRONT
SCALE: 3" = 1'-0"

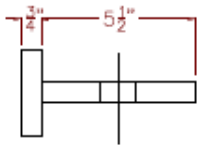

3 S4 WELDED FD CLEVIS SIDE
SCALE: 3" = 1'-0"

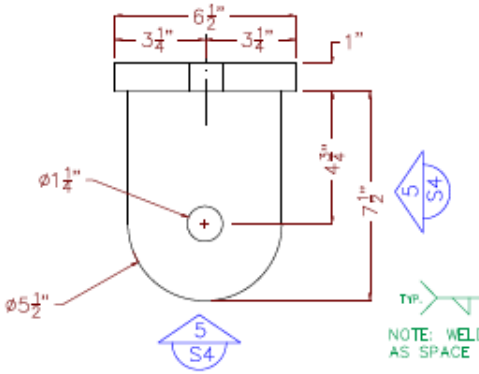

4 S4 THREADED FD CLEVIS PLAN (QTY 1)
SCALE: 3" = 1'-0"

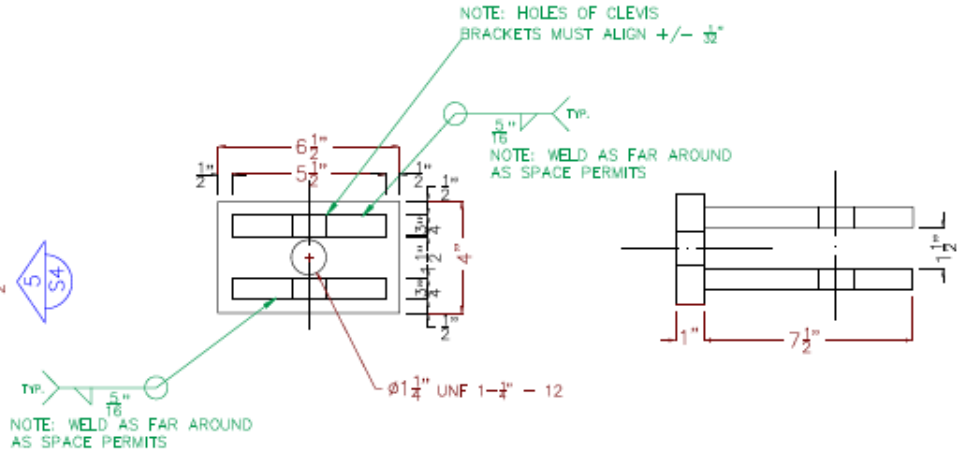

5 S4 THREADED FD CLEVIS FRONT
SCALE: 3" = 1'-0"

6 S4 THREADED FD CLEVIS SIDE
SCALE: 3" = 1'-0"

General Notes:

- Clevises to be fabricated using 50 ksi (A992) steel plates purchased by Davis
- Tolerance on lengths +/- 1/16 inch
- Tolerance on clevis hole alignment +/- 1/32 inch
- Weld material is E-7018

Project Name:
Auburn University Gap Damper Project

Address:
Auburn University
Civil Engineering
238 Harbert Center
Auburn, AL 36849

Sheet Name:
Friction Device Clevises (Welded and Threaded)

Project Number:

Sheet: S4

Date: 12/[illegible]/2018

Scale: As Noted

PRODUCED BY AN AUTODESK EDUCATIONAL PRODUCT

PRODUCED BY AN AUTODESK EDUCATIONAL PRODUCT

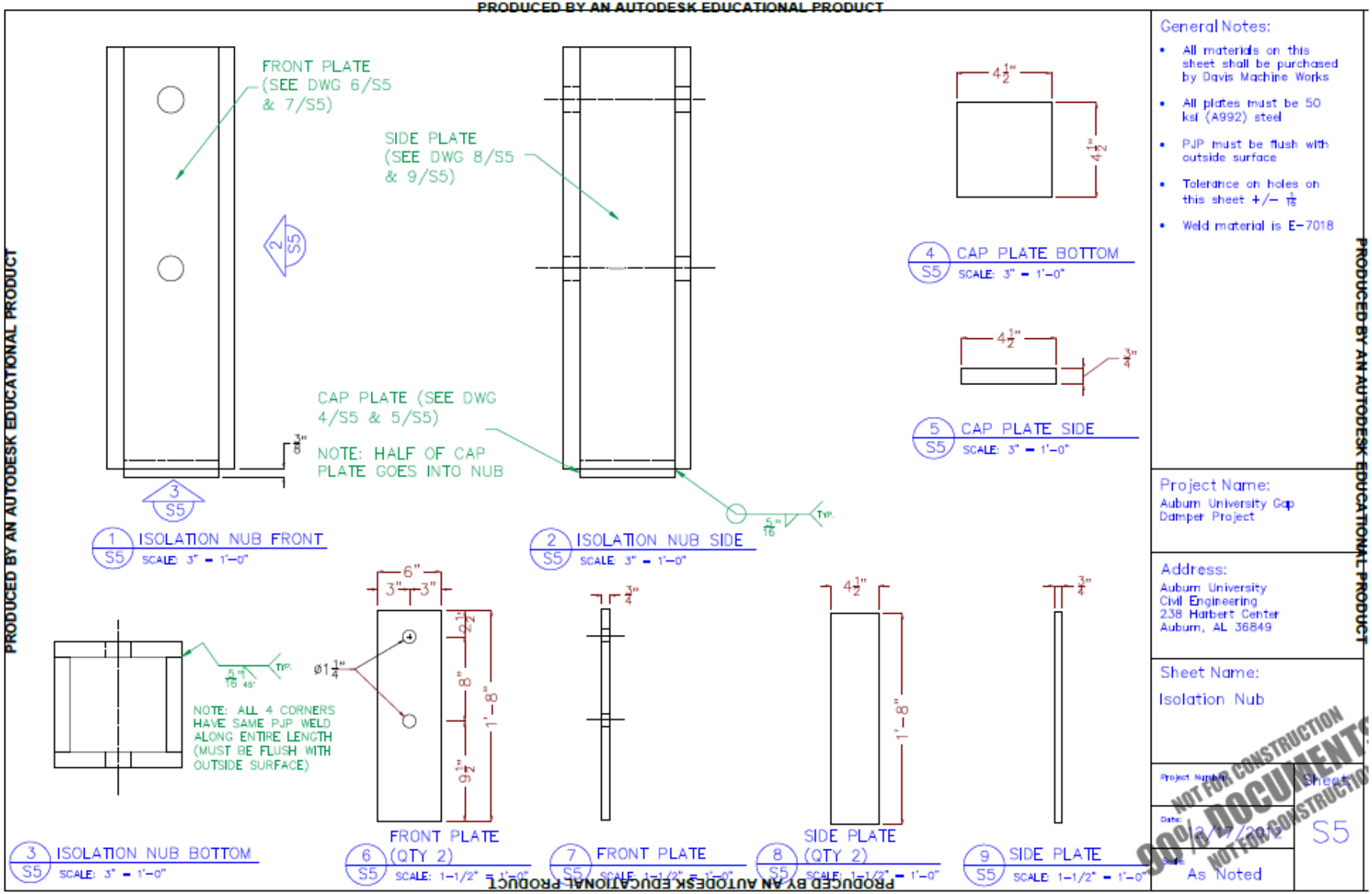

General Notes:

- All materials on this sheet shall be purchased by Davis Machine Works
- All plates must be 50 ksi (A992) steel
- PJP must be flush with outside surface
- Tolerance on holes on this sheet +/- 1/16
- Weld material is E-7018

Project Name:
Auburn University Gap Damper Project

Address:
Auburn University
Civil Engineering
238 Harbert Center
Auburn, AL 36849

Sheet Name:
Isolation Nub

Project Number:

Date: 06/27/2012

Scale: As Noted

Sheet: S5

PRODUCED BY AN AUTODESK EDUCATIONAL PRODUCT

PRODUCED BY AN AUTODESK EDUCATIONAL PRODUCT

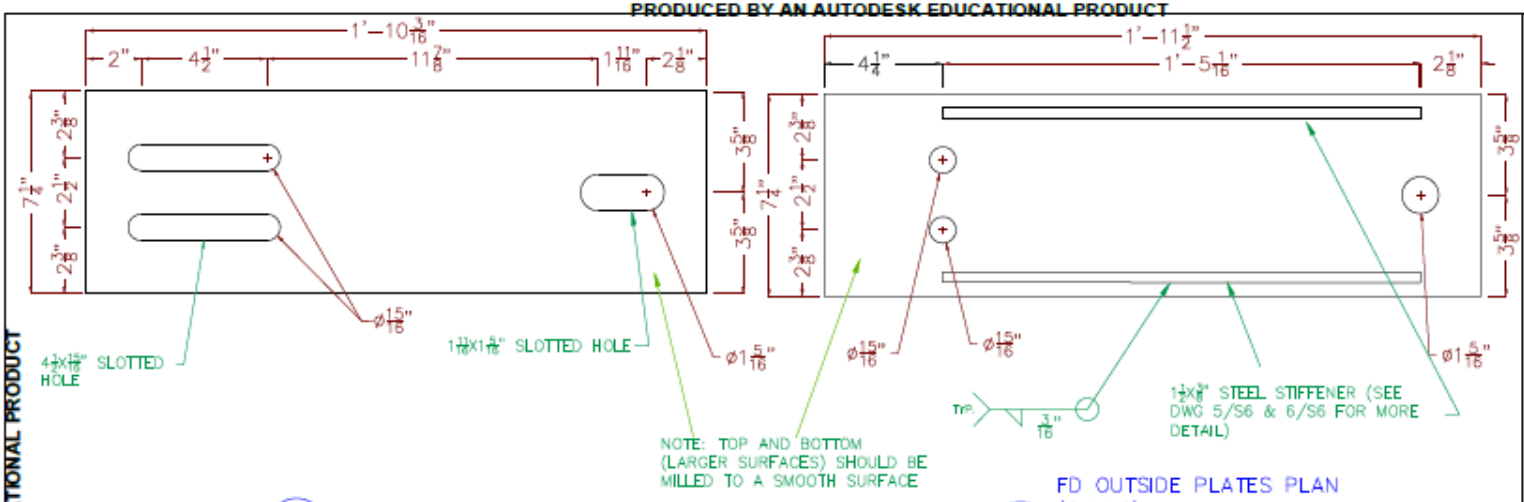

1 / S6 FD CENTER PLATE PLAN
SCALE: 3" = 1'-0"

4 / S6 FD OUTSIDE PLATES PLAN (QTY 2)
SCALE: 3" = 1'-0"

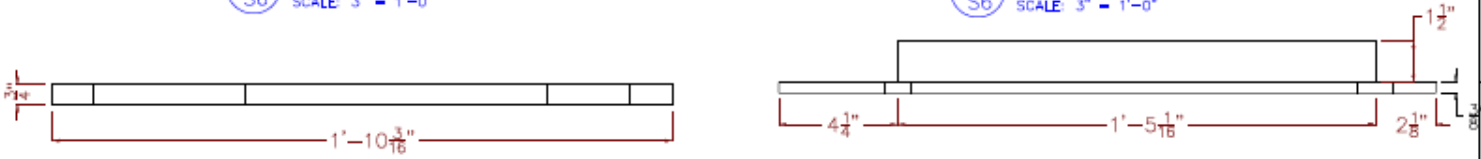

2 / S6 FD CENTER PLATE FRONT
SCALE: 3" = 1'-0"

5 / S6 FD OUTSIDE PLATES FRONT
SCALE: 3" = 1'-0"

3 / S6 FD CENTER PLATE SIDE
SCALE: 3" = 1'-0"

6 / S6 FD OUTSIDE PLATES SIDE
SCALE: 3" = 1'-0"

General Notes:
- All materials on this sheet shall be purchased by Davis Machine Works
- Center plate surfaces must be be smooth
- Tolerance on lengths on this sheet +/- 1/16
- Tolerance on holes on this sheet + 1/16
- Weld material is E-7018

Project Name:
Auburn University Gap Damper Project

Address:
Auburn University
Civil Engineering
238 Harbert Center
Auburn, AL 36849

Sheet Name:
Friction Device

Project Number

Date: FEV17/2012

Scale: As Noted

Sheet: S6

PRODUCED BY AN AUTODESK EDUCATIONAL PRODUCT

PRODUCED BY AN AUTODESK EDUCATIONAL PRODUCT

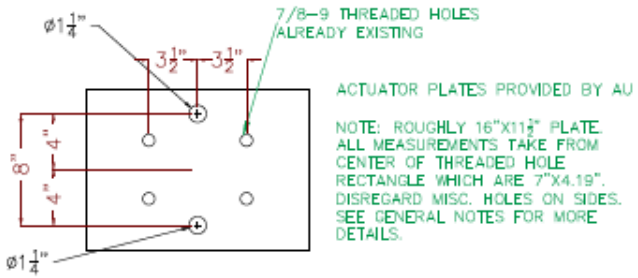

ACTUATOR PLATES PROVIDED BY AU

NOTE: ROUGHLY 16"X11 1/2" PLATE. ALL MEASUREMENTS TAKE FROM CENTER OF THREADED HOLE RECTANGLE WHICH ARE 7"X4.19". DISREGARD MISC. HOLES ON SIDES. SEE GENERAL NOTES FOR MORE DETAILS.

1/S7 ACTUATOR PLATE (1 OF 2)
SCALE: 1–1/2" = 1'–0"

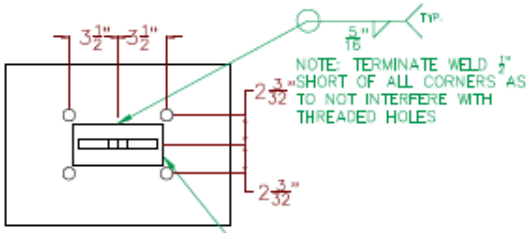

NOTE: TERMINATE WELD 1/2" SHORT OF ALL CORNERS AS TO NOT INTERFERE WITH THREADED HOLES

2/S7 ACTUATOR PLATE FRONT (2 OF 2)
SCALE: 1–1/2" = 1'–0"

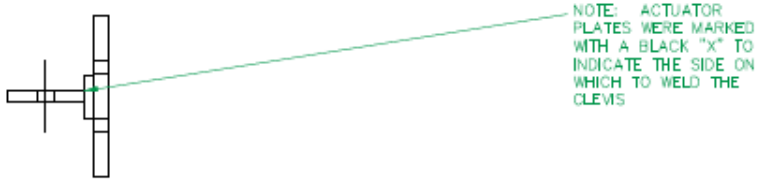

1 WELDED FD CLEVIS (SEE DWG 1/S4, 2/S4, & 3/S4)

NOTE: ACTUATOR PLATES WERE MARKED WITH A BLACK "X" TO INDICATE THE SIDE ON WHICH TO WELD THE CLEVIS

3/S7 ACTUATOR PLATE SIDE (2 OF 2)
SCALE: 1–1/2" = 1'–0"

General Notes:

- HSS will be provided by AU
- Actuator plates will be provided by AU. Plate 1 needs the two holes dimensioned from the center of the threaded hole rectangle already present. Plate 2 needs the Friction Device Welded Clevis (1/S4) welded to the center of the rectangle created by the threaded holes.
- Side to weld the clevis on has been marked with a black "X"
- Tolerance on lengths on this sheet +/– 1/16
- Tolerance on holes on this sheet +/– 1/16
- Weld material is E–7018

Project Name:
Auburn University Gap Damper Project

Address:
Auburn University
Civil Engineering
238 Harbert Center
Auburn, AL 36849

Sheet Name:
Actuator Plates

Project Number

Sheet:
S7

Date:
9/21/2016

Scale:
As Noted

PRODUCED BY AN AUTODESK EDUCATIONAL PRODUCT

PRODUCED BY AN AUTODESK EDUCATIONAL PRODUCT

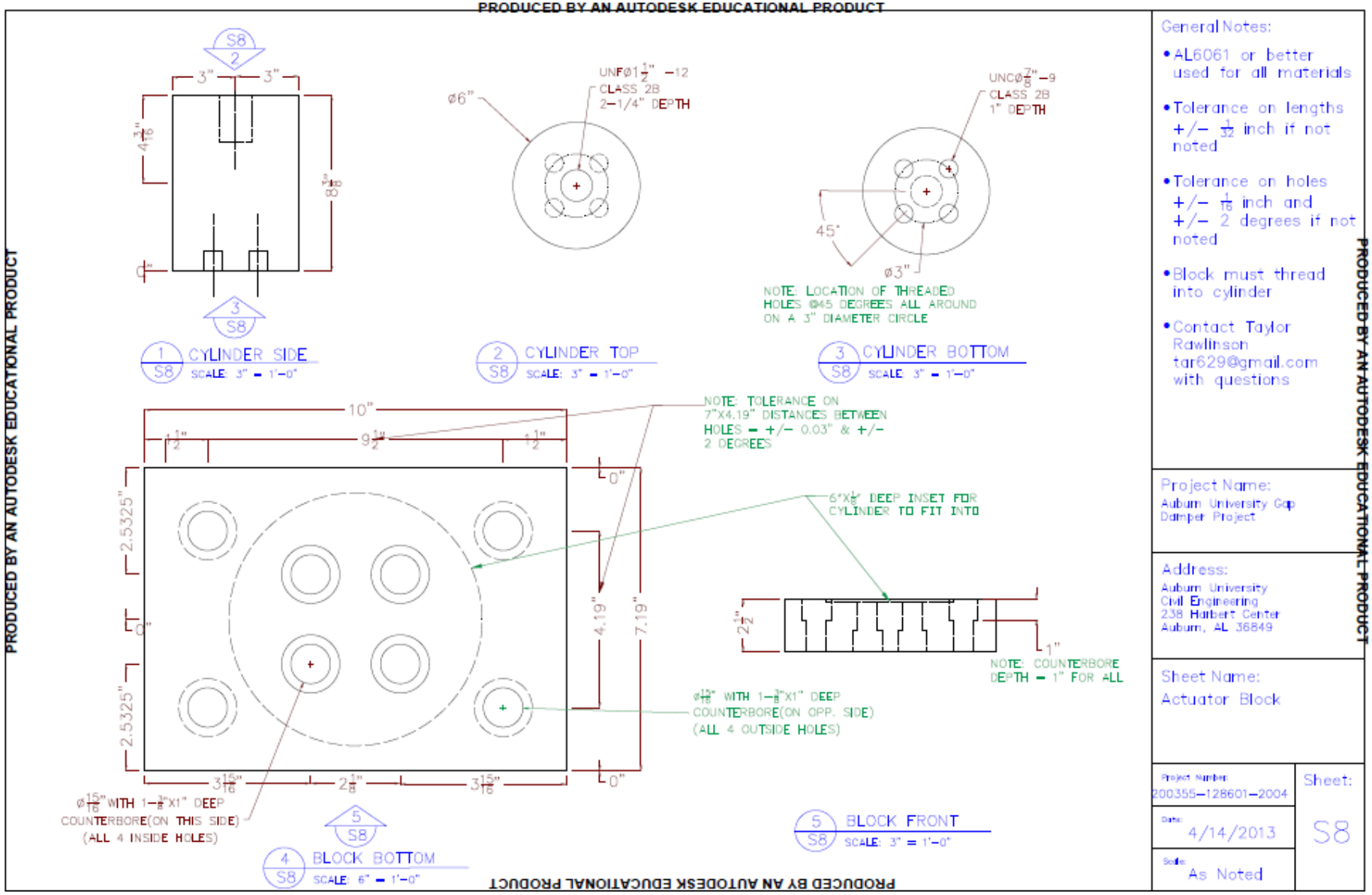

Appendix B. Viscous Gap Damper Trial Results

Table B-1. Load Case Appendix Arrangement

Page	Trial Name	Load Case	Input Frequency (Hz)	Actuator Displacement Range mm (in)	Rotation (5 degrees)*	Eccentricity mm (in)	Wave Form**
B-2	E0-0.125Hz-+/-4.2-Sine	1	0.125	+/- 106.7 (4.2)	No	0	Sine
B-4	E0-0.2Hz-+/-4.2-Sine	2	0.2	+/- 106.7 (4.2)	No	0	Sine
B-6	E0-0.125Hz-+/-4.2-Tri	3	0.125	+/- 106.7 (4.2)	No	0	Tri
B-8	E0-0.2Hz-+/-4.2-Tri	4	0.2	+/- 106.7 (4.2)	No	0	Tri
B-10	T5CCW-E0-0.125Hz-+/-4.0-Sine	5	0.125	+/- 101.6 (4.0)	CCW	0	Sine
B-12	T5CCW-E0-0.2Hz-+/-4.0-Sine	6	0.2	+/- 101.6 (4.0)	CCW	0	Sine
B-14	T5CCW-E0-0.125Hz-+/-4.0-Tri	7	0.125	+/- 101.6 (4.0)	CCW	0	Tri
B-16	T5CCW-E0-0.2Hz-+/-4.0-Tri	8	0.2	+/- 101.6 (4.0)	CCW	0	Tri
B-18	E1-0.125Hz-+/-4.2-Sine	9	0.125	+/- 106.7 (4.2)	No	25.4 (1)	Sine
B-20	E1-0.2Hz-+/-4.2-Sine	10	0.2	+/- 106.7 (4.2)	No	25.4 (1)	Sine
B-22	E1-0.125Hz-+/-4.2-Tri	11	0.125	+/- 106.7 (4.2)	No	25.4 (1)	Tri
B-24	E1-0.2Hz-+/-4.2-Tri	12	0.2	+/- 106.7 (4.2)	No	25.4 (1)	Tri
B-26	T5CCW-E1-0.125Hz-+/-4.2-Sine	13	0.125	+/- 106.7 (4.2)	CCW	25.4 (1)	Sine
B-28	T5CCW-E1-0.2Hz-+/-4.2-Sine	14	0.2	+/- 106.7 (4.2)	CCW	25.4 (1)	Sine
B-30	T5CW-E1-0.125Hz-+/-4.2-Sine	15	0.125	+/- 106.7 (4.2)	CW	25.4 (1)	Sine
B-32	T5CW-E1-0.2Hz-+/-4.2-Sine	16	0.2	+/- 106.7 (4.2)	CW	25.4 (1)	Sine
B-34	E2-0.125Hz-+/-4.2-Sine	17	0.125	+/- 106.7 (4.2)	No	50.8(2)	Sine
B-36	E2-0.2Hz-+/-4.2-Sine	18	0.2	+/- 106.7 (4.2)	No	50.8(2)	Sine
B-38	E2-0.125Hz-+/-4.2-Tri	19	0.125	+/- 106.7 (4.2)	No	50.8(2)	Tri
B-40	E2-0.2Hz-+/-4.2-Tri	20	0.2	+/- 106.7 (4.2)	No	50.8(2)	Tri
B-42	T5CCW-E2-0.125Hz-+/-4.0-Sine	21	0.125	+/- 101.6 (4.0)	CCW	50.8(2)	Sine
B-44	T5CCW-E2-0.2Hz-+/-4.0-Sine	22	0.2	+/- 101.6 (4.0)	CCW	50.8(2)	Sine
B-46	T5CW-E2-0.125Hz-+/-4.0-Sine	23	0.125	+/- 101.6 (4.0)	CW	50.8(2)	Sine
B-48	T5CW-E2-0.2Hz-+/-4.0-Sine	24	0.2	+/- 101.6 (4.0)	CW	50.8(2)	Sine

*CW = Clockwise Rotation, CCW = Counter-Clockwise Rotation (Viewed from above)
**Tri = Constant Velocity

Load Case 1 (E0-0.125Hz-+/-4.2-Sine):

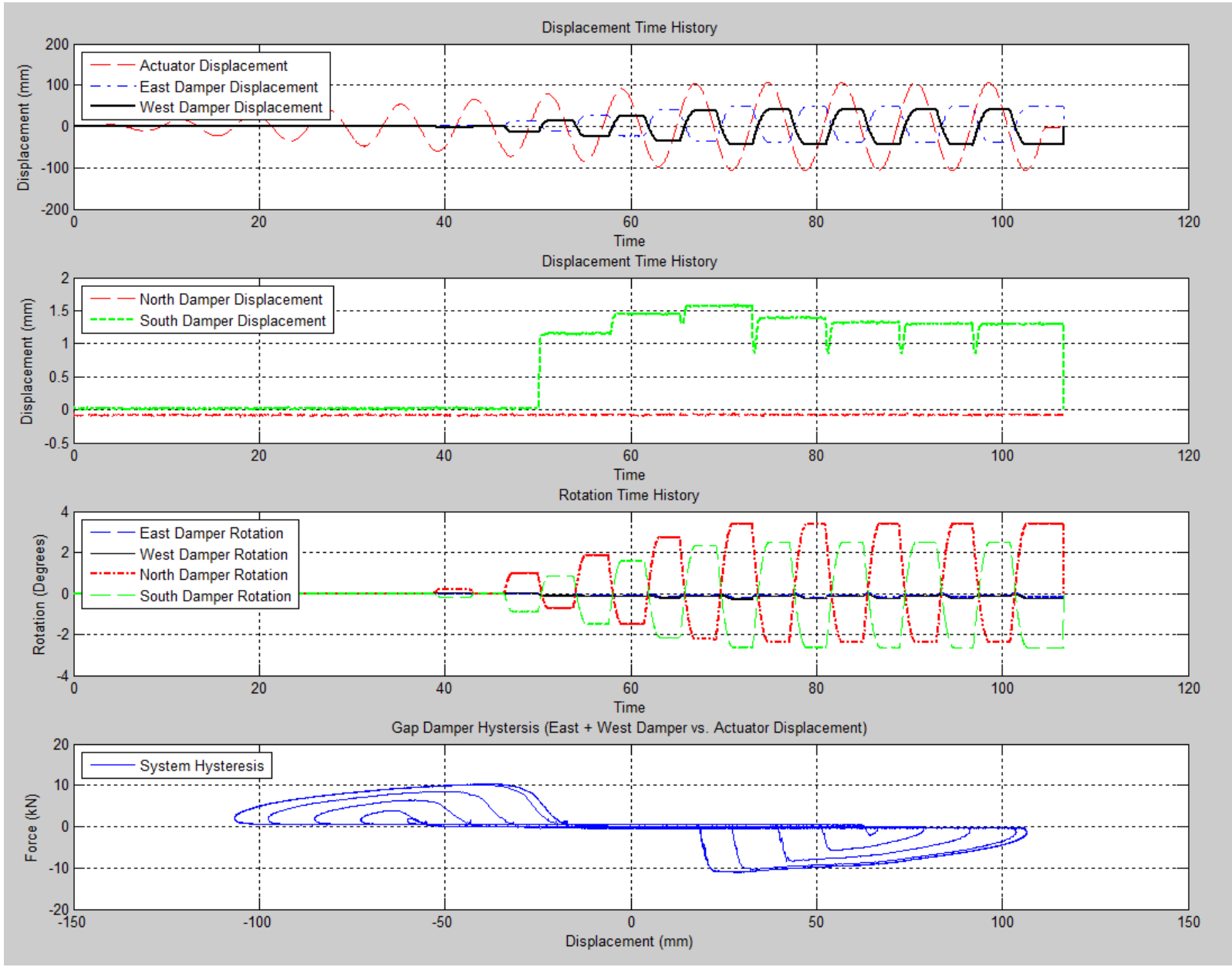

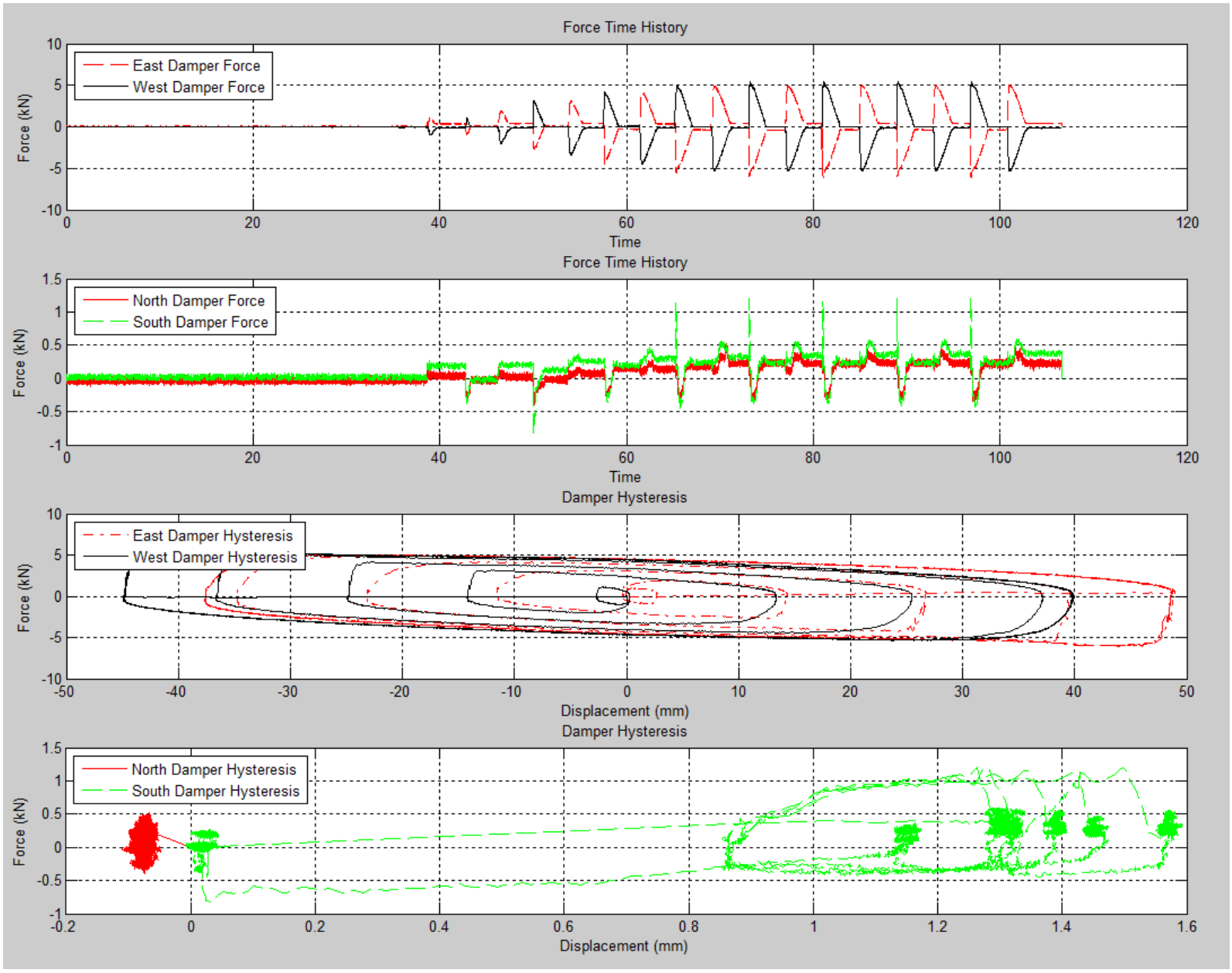
Force Time History
East Damper Force
West Damper Force
Force (kN)
Time
Force Time History
North Damper Force
South Damper Force
Force (kN)
Time
Damper Hysteresis
East Damper Hysteresis
West Damper Hysteresis
Force (kN)
Displacement (mm)
Damper Hysteresis
North Damper Hysteresis
South Damper Hysteresis
Force (kN)
Displacement (mm)

Load Case 2 (E0-0.2Hz-+/-4.2-Sine):

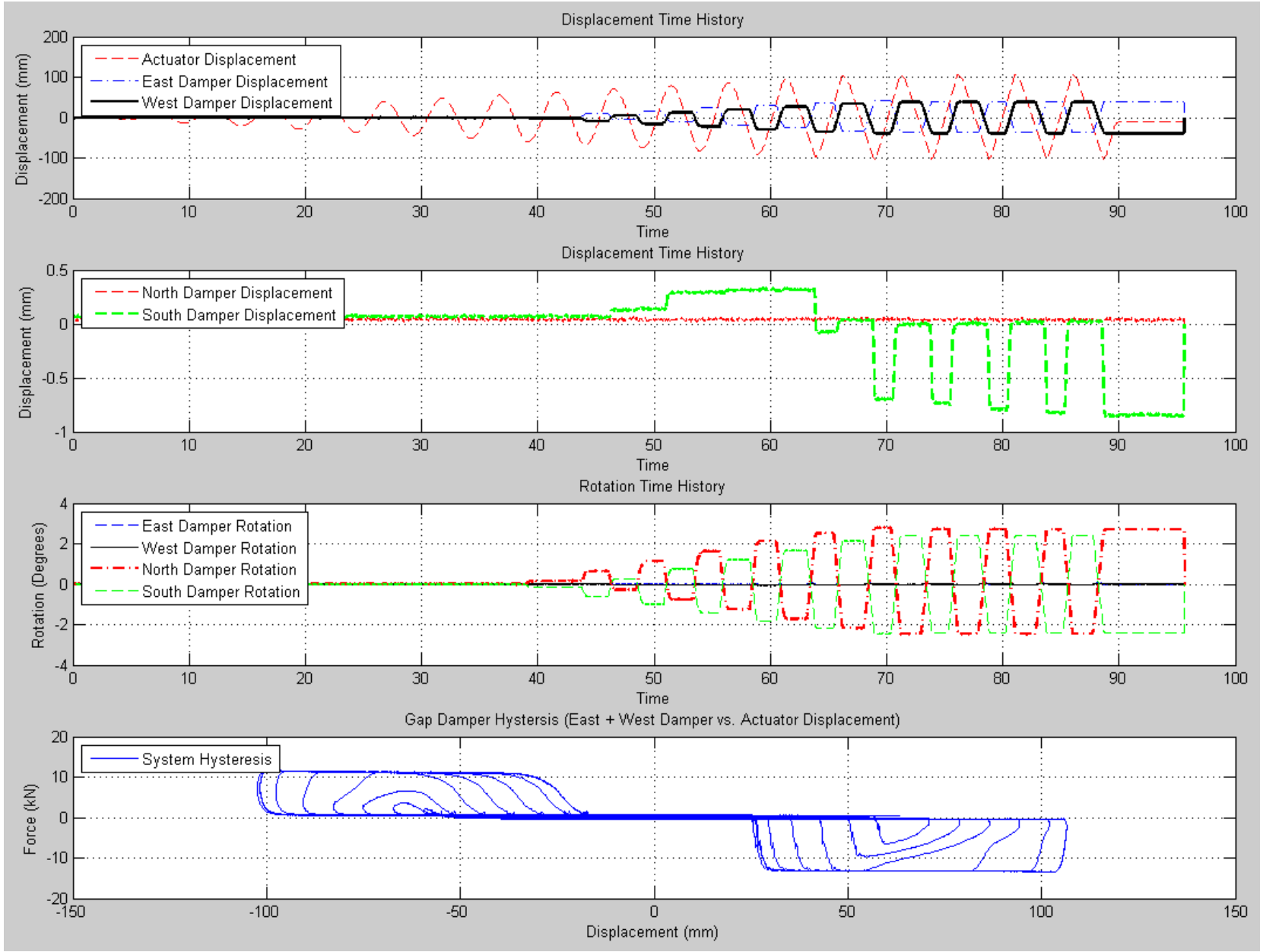

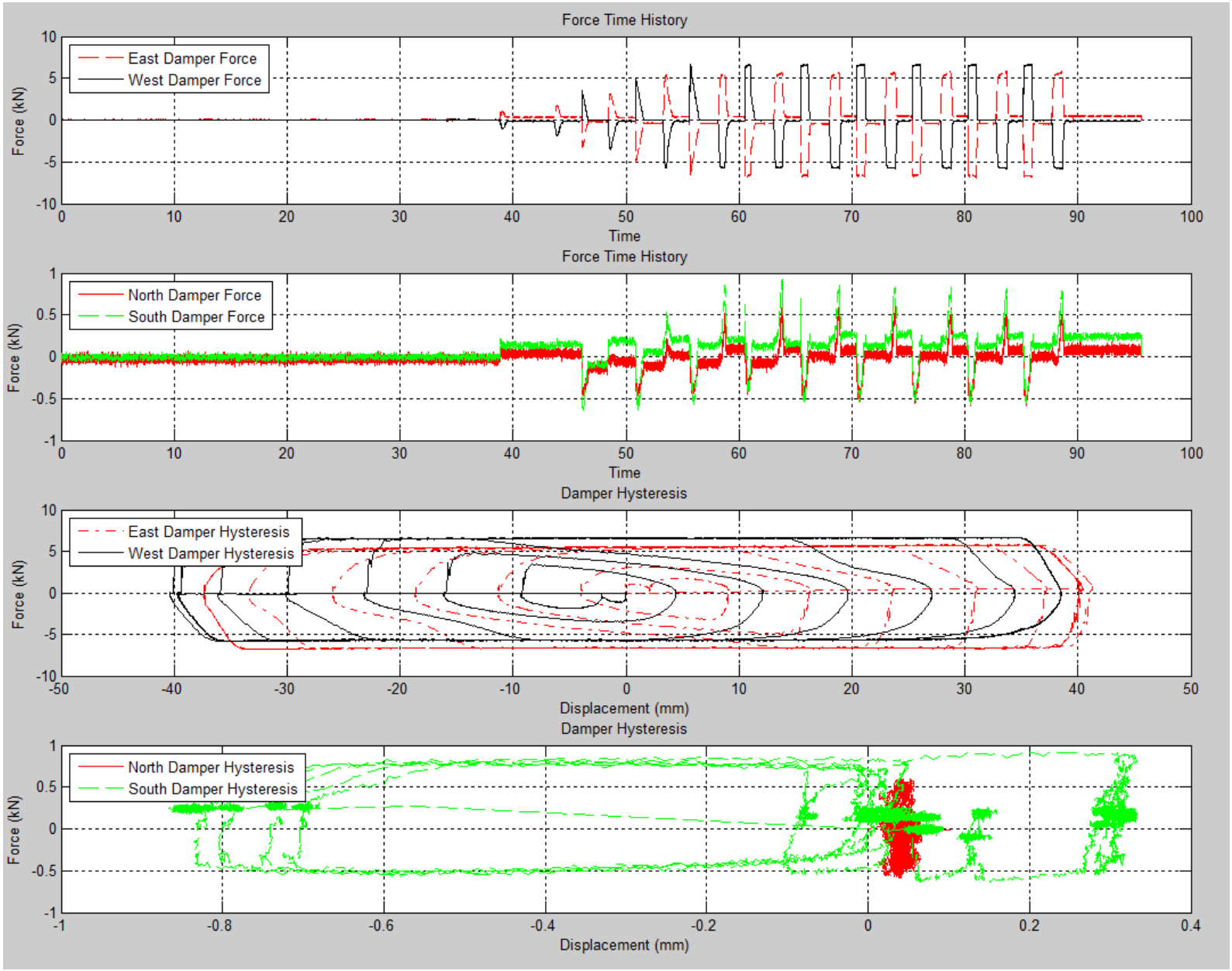
Force Time History
East Damper Force
West Damper Force
Force (kN)
Time
Force Time History
North Damper Force
South Damper Force
Force (kN)
Time
Damper Hysteresis
East Damper Hysteresis
West Damper Hysteresis
Force (kN)
Displacement (mm)
Damper Hysteresis
North Damper Hysteresis
South Damper Hysteresis
Force (kN)
Displacement (mm)

Load Case 3 (E0-0.125Hz-+/-4.2-Tri):

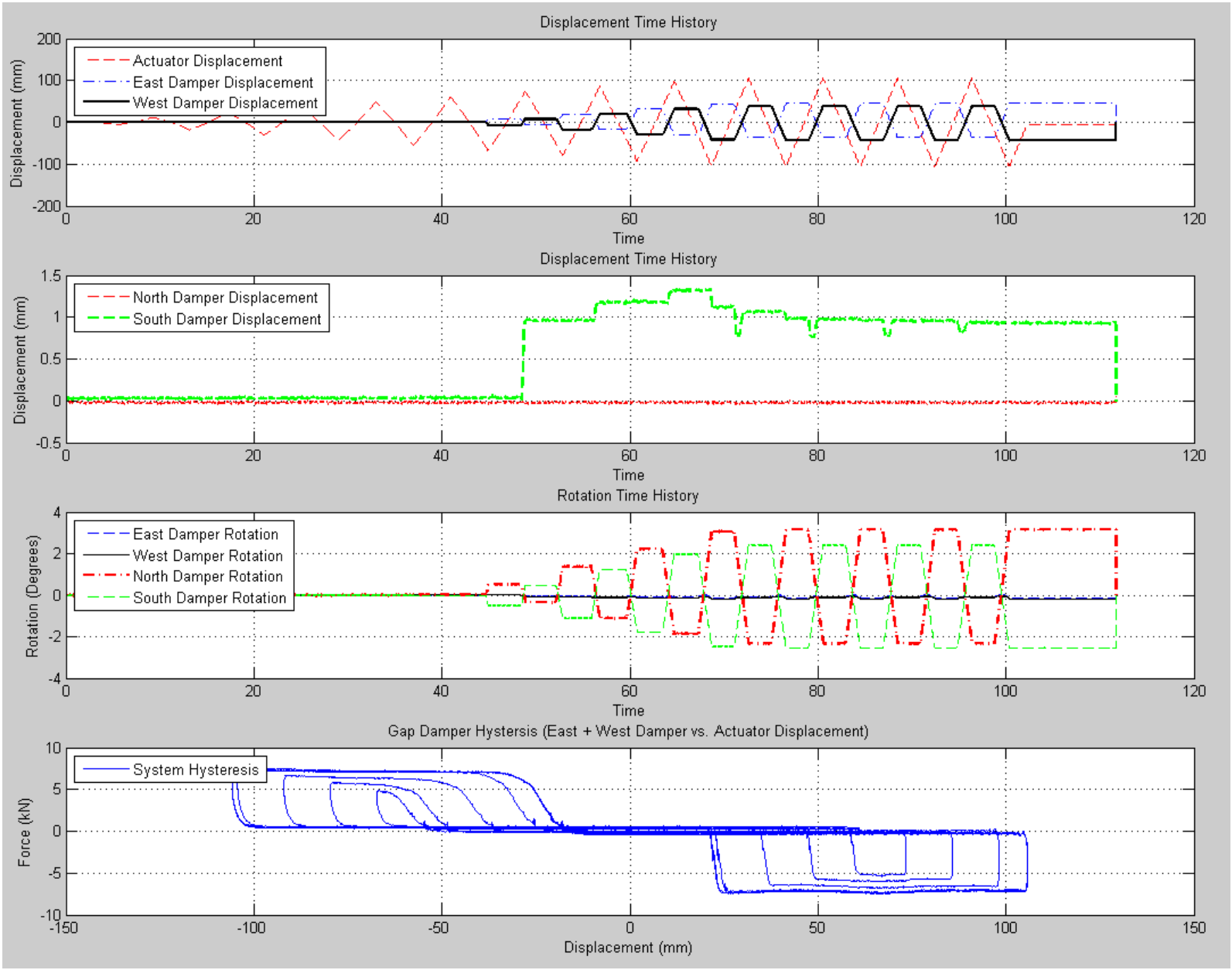

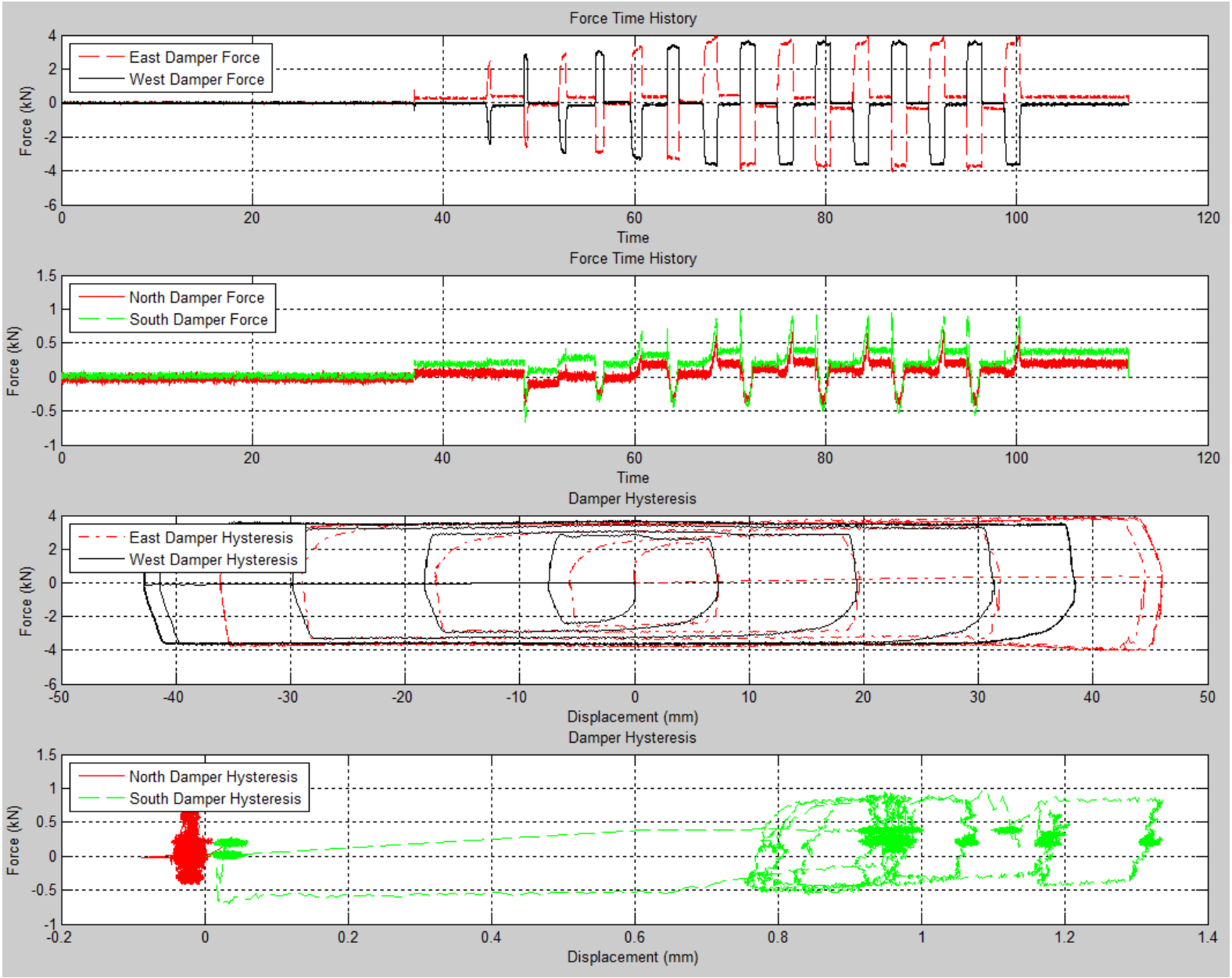
Force Time History
East Damper Force
West Damper Force
Force (kN)
Time
Force Time History
North Damper Force
South Damper Force
Force (kN)
Time
Damper Hysteresis
East Damper Hysteresis
West Damper Hysteresis
Force (kN)
Displacement (mm)
Damper Hysteresis
North Damper Hysteresis
South Damper Hysteresis
Force (kN)
Displacement (mm)

Load Case 4 (E0-0.2Hz-+/-4.2-Tri):

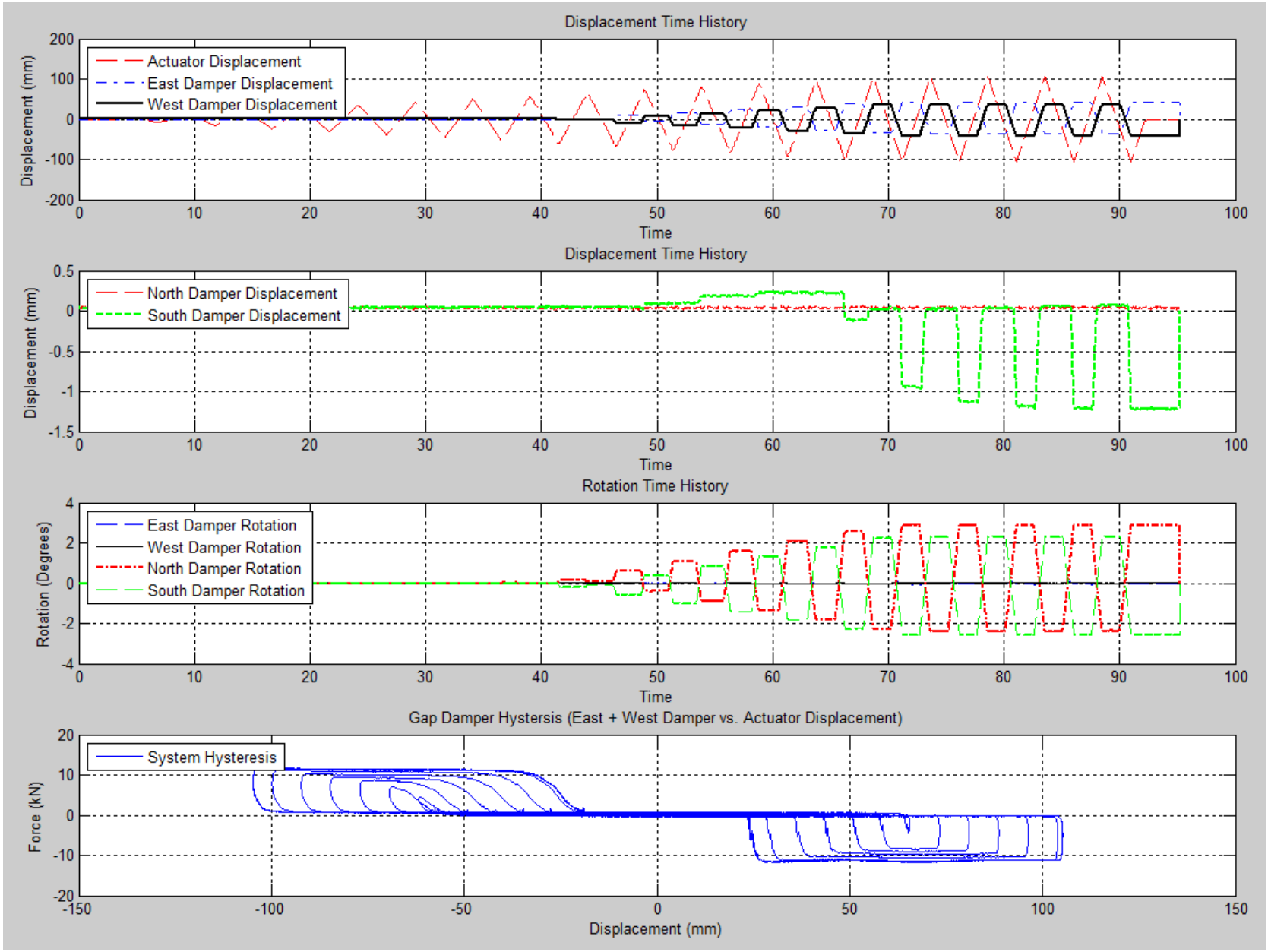

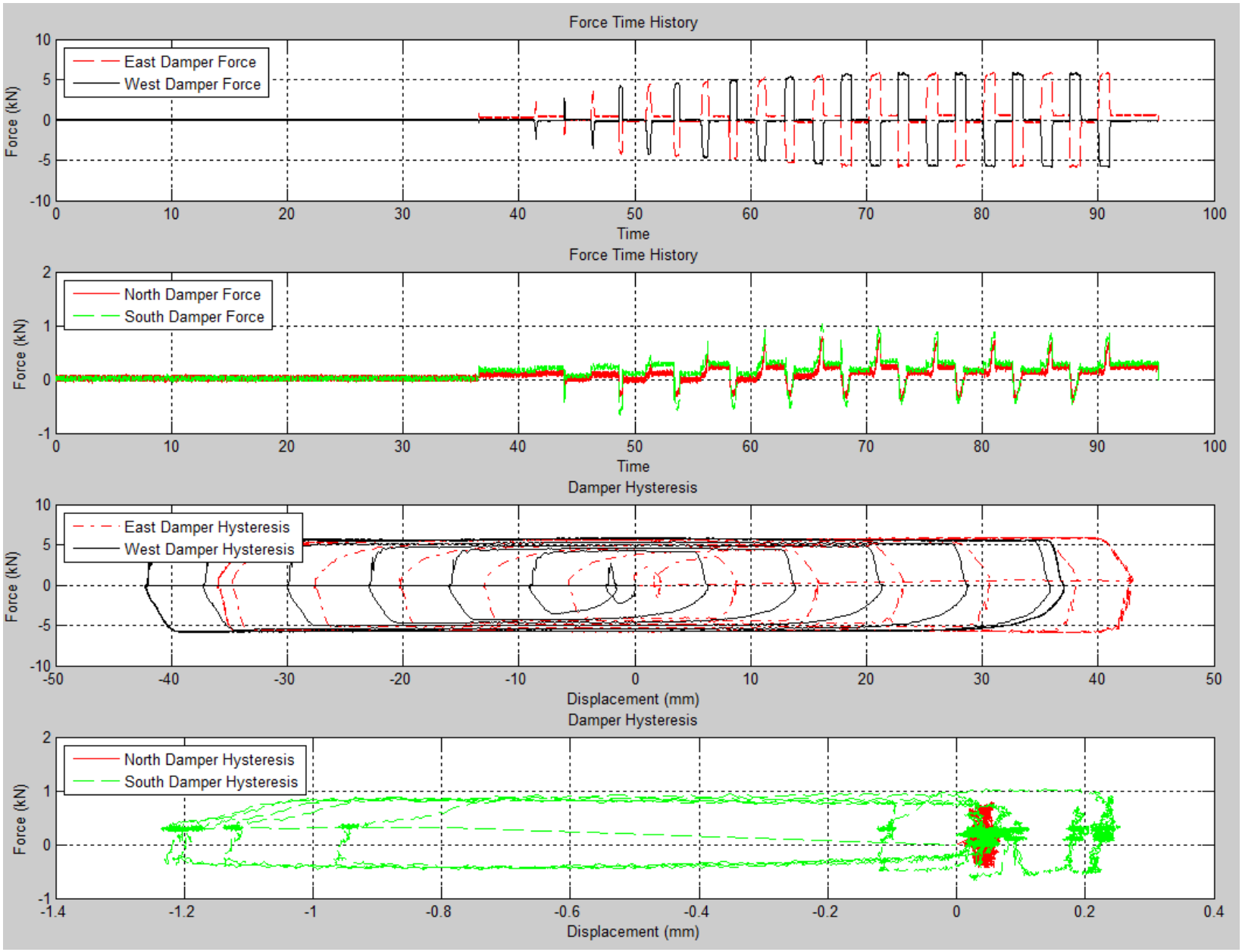
Force Time History
East Damper Force
West Damper Force
Force (kN)
Time
Force Time History
North Damper Force
South Damper Force
Force (kN)
Time
Damper Hysteresis
East Damper Hysteresis
West Damper Hysteresis
Force (kN)
Displacement (mm)
Damper Hysteresis
North Damper Hysteresis
South Damper Hysteresis
Force (kN)
Displacement (mm)

Load Case 5 (T5CCW-E0-0.125Hz-+/-4.0-Sine):

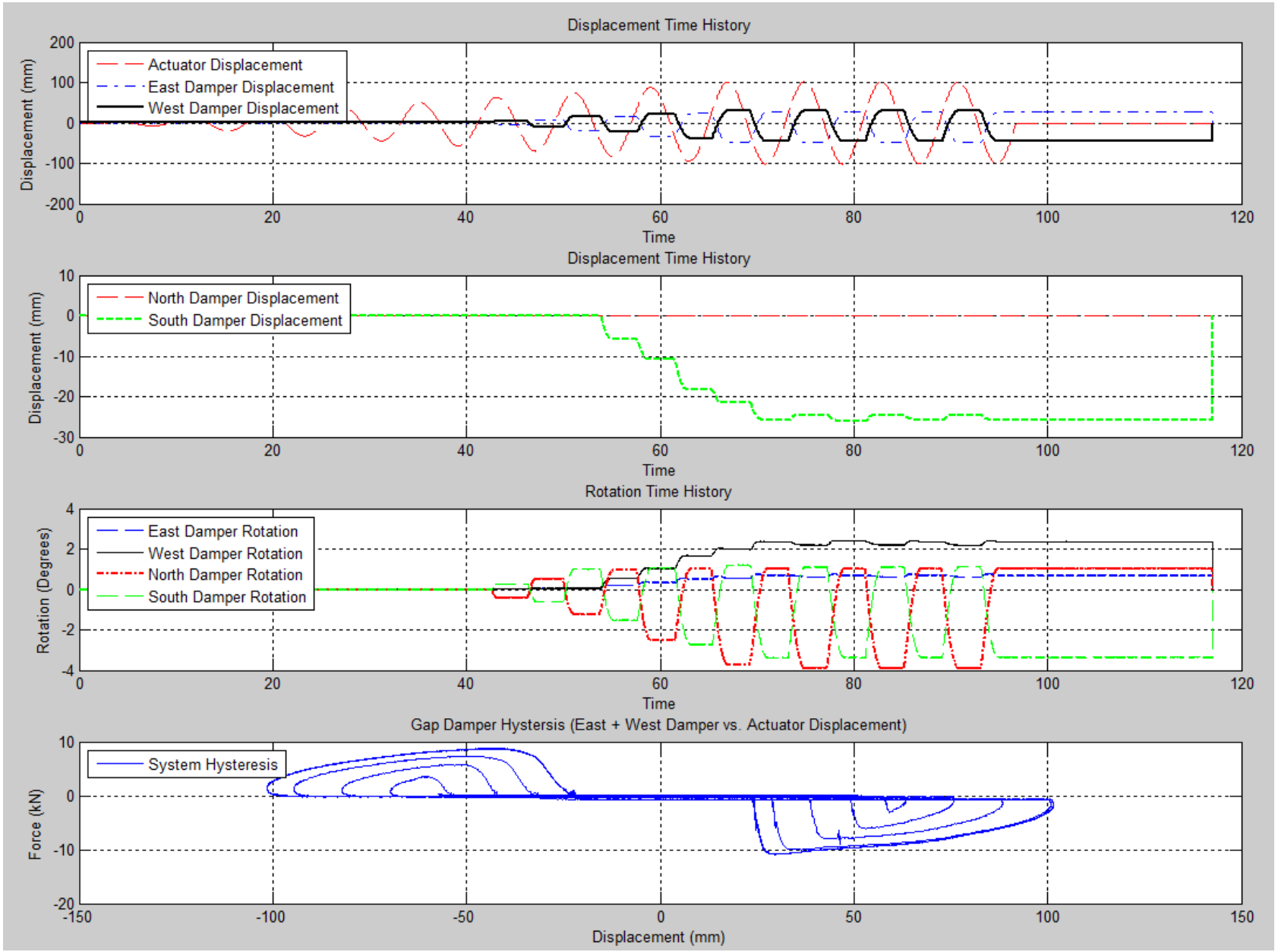

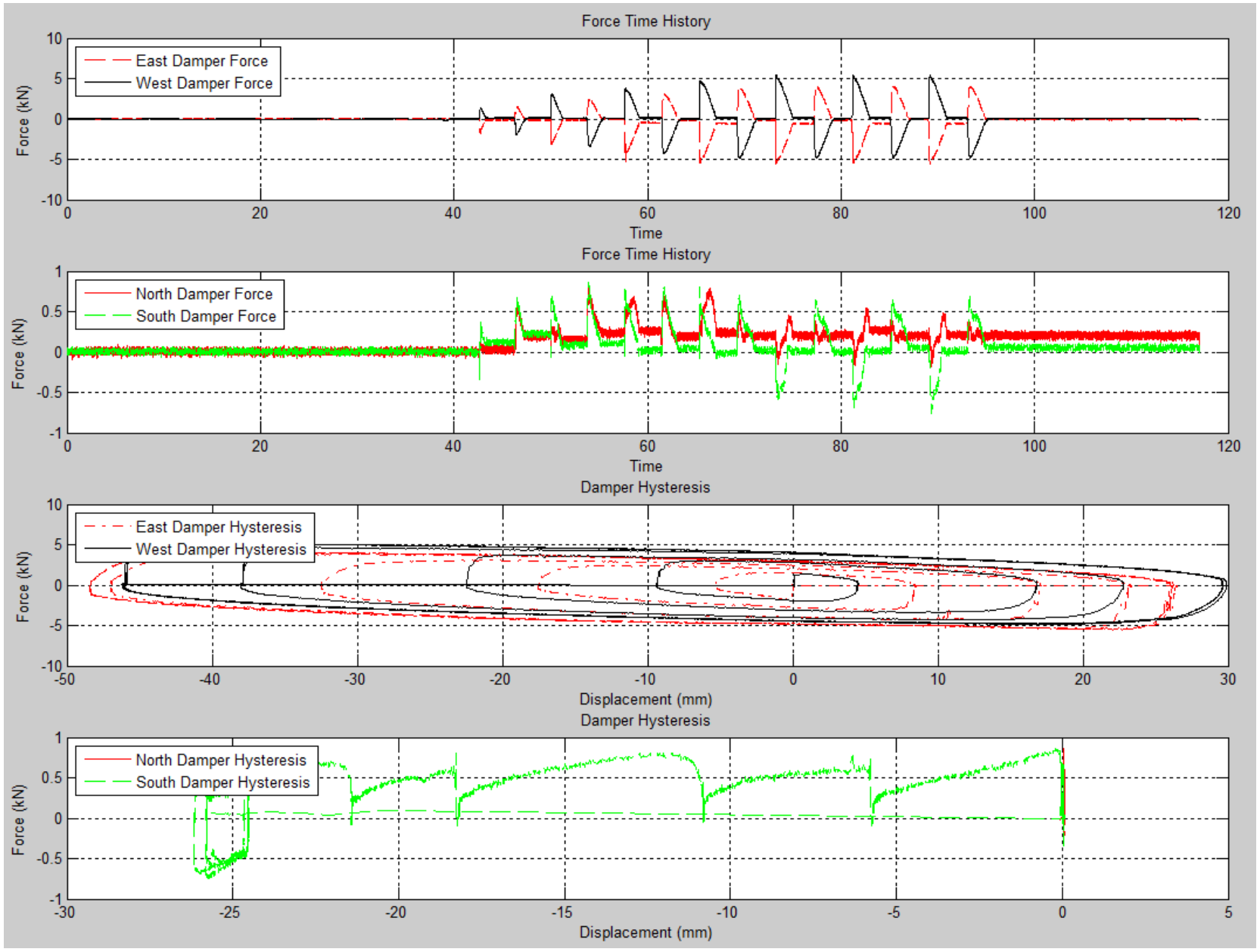
Force Time History
East Damper Force
West Damper Force
Force (kN)
Time
Force Time History
North Damper Force
South Damper Force
Force (kN)
Time
Damper Hysteresis
East Damper Hysteresis
West Damper Hysteresis
Force (kN)
Displacement (mm)
Damper Hysteresis
North Damper Hysteresis
South Damper Hysteresis
Force (kN)
Displacement (mm)

Load Case 6 (T5CCW-E0-0.2Hz-+/-4.0-Sine):

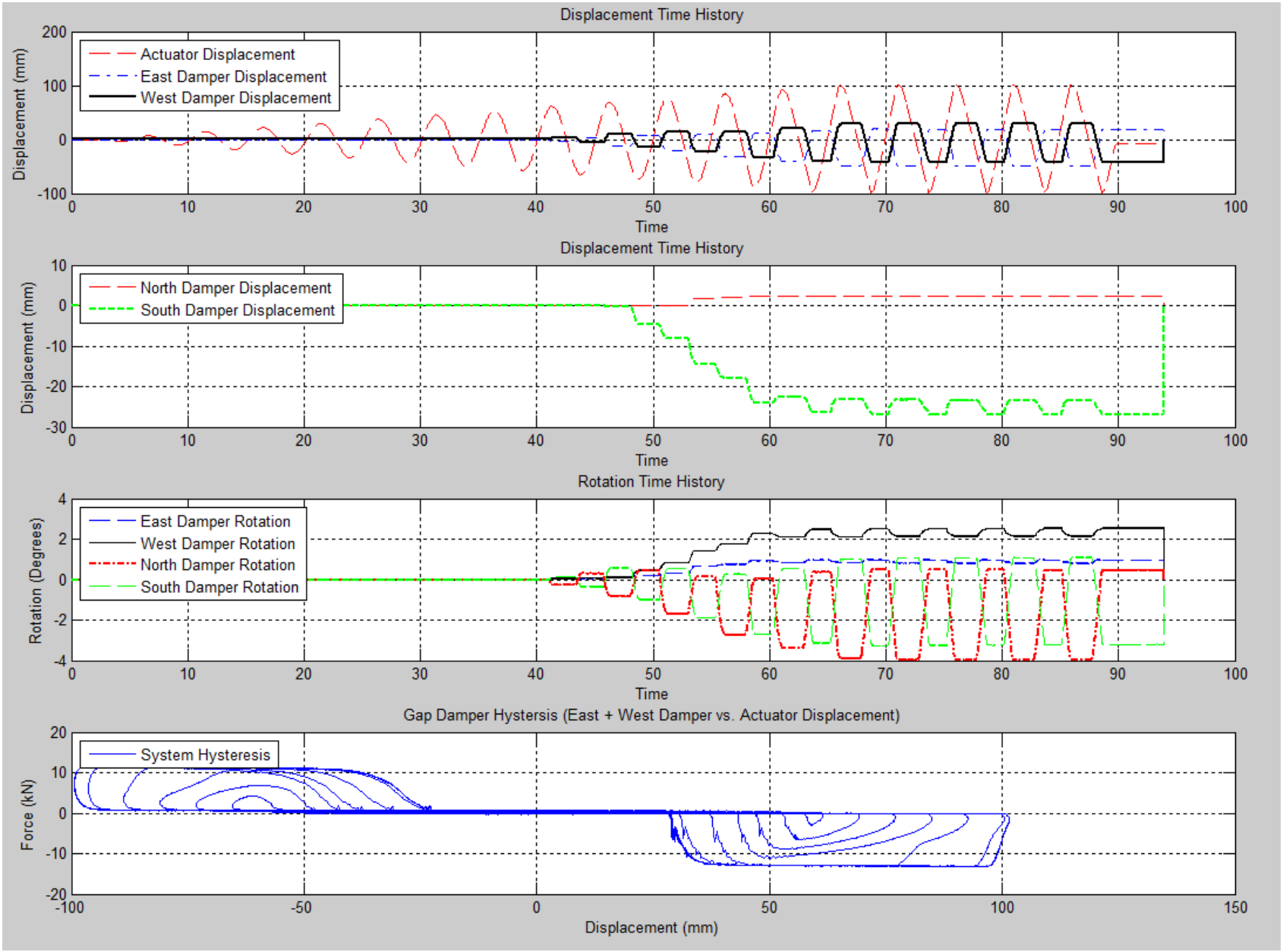

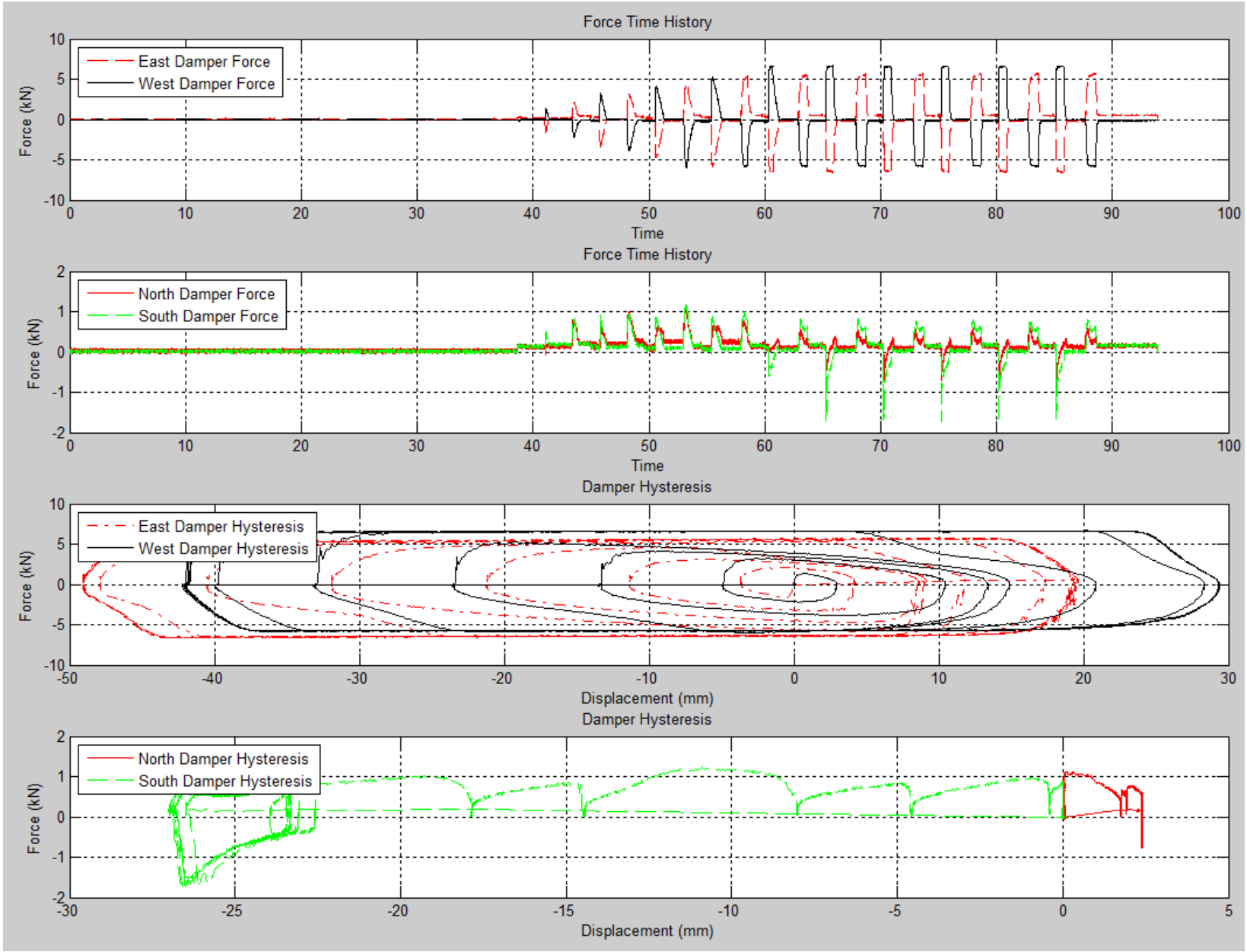
Force Time History
East Damper Force
West Damper Force
Force (kN)
Time
Force Time History
North Damper Force
South Damper Force
Force (kN)
Time
Damper Hysteresis
East Damper Hysteresis
West Damper Hysteresis
Force (kN)
Displacement (mm)
Damper Hysteresis
North Damper Hysteresis
South Damper Hysteresis
Force (kN)
Displacement (mm)

Load Case 7 (T5CW-E0-0.125Hz-+/-4.0-Tri):

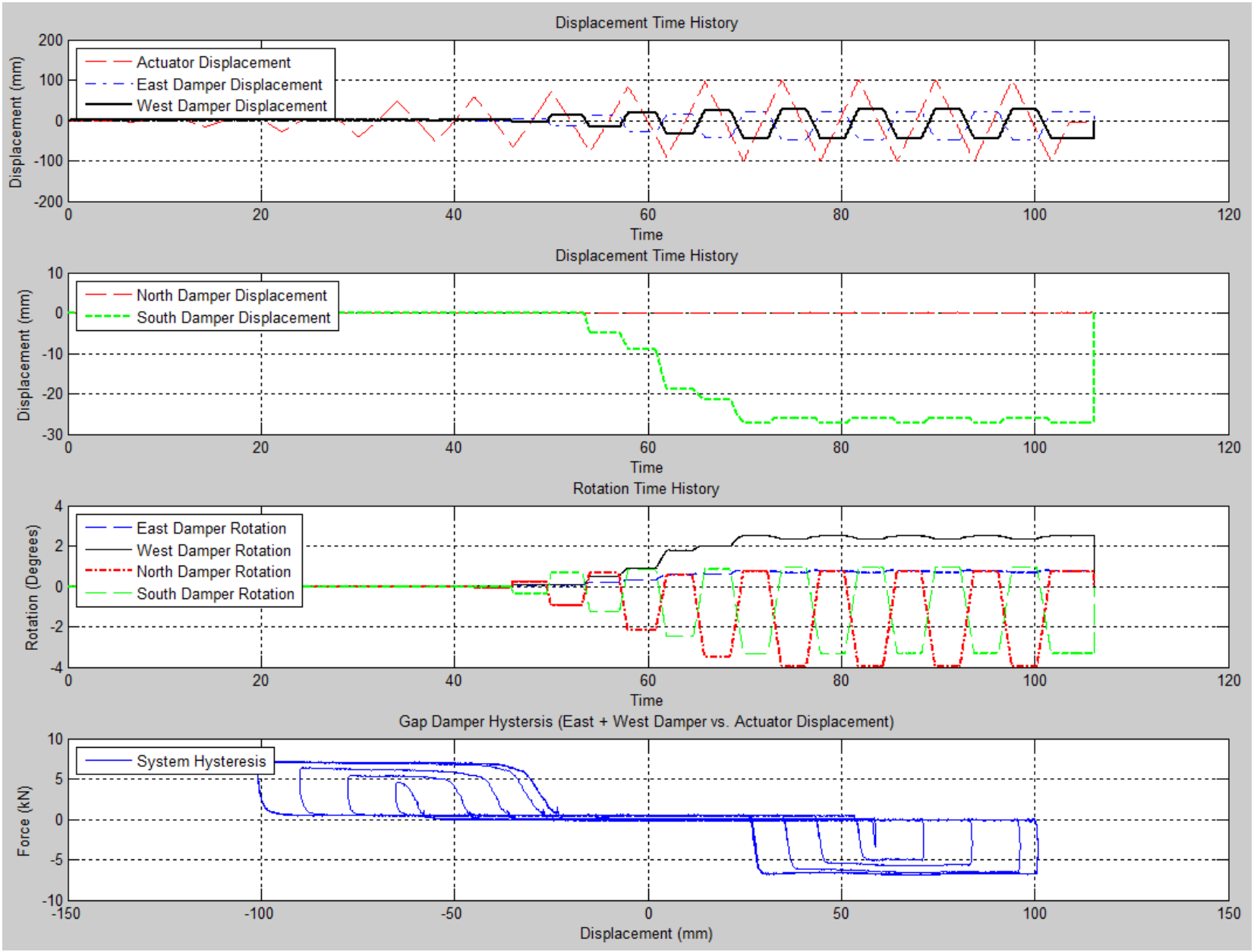

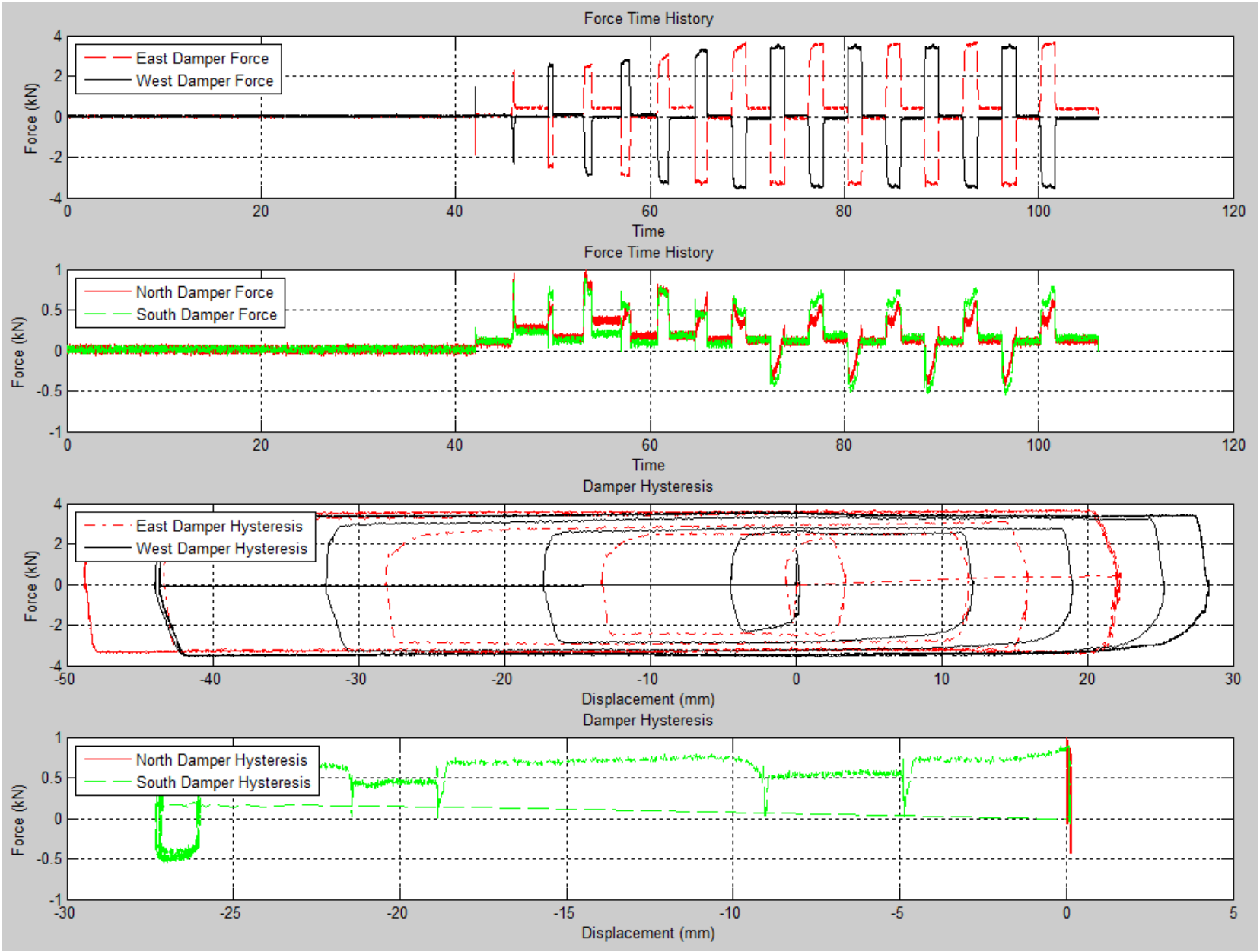
Force Time History
East Damper Force
West Damper Force
Force (kN)
Time
Force Time History
North Damper Force
South Damper Force
Force (kN)
Time
Damper Hysteresis
East Damper Hysteresis
West Damper Hysteresis
Force (kN)
Displacement (mm)
Damper Hysteresis
North Damper Hysteresis
South Damper Hysteresis
Force (kN)
Displacement (mm)

Load Case 8 (T5CW-E0-0.2Hz-+/-4.0-Tri):

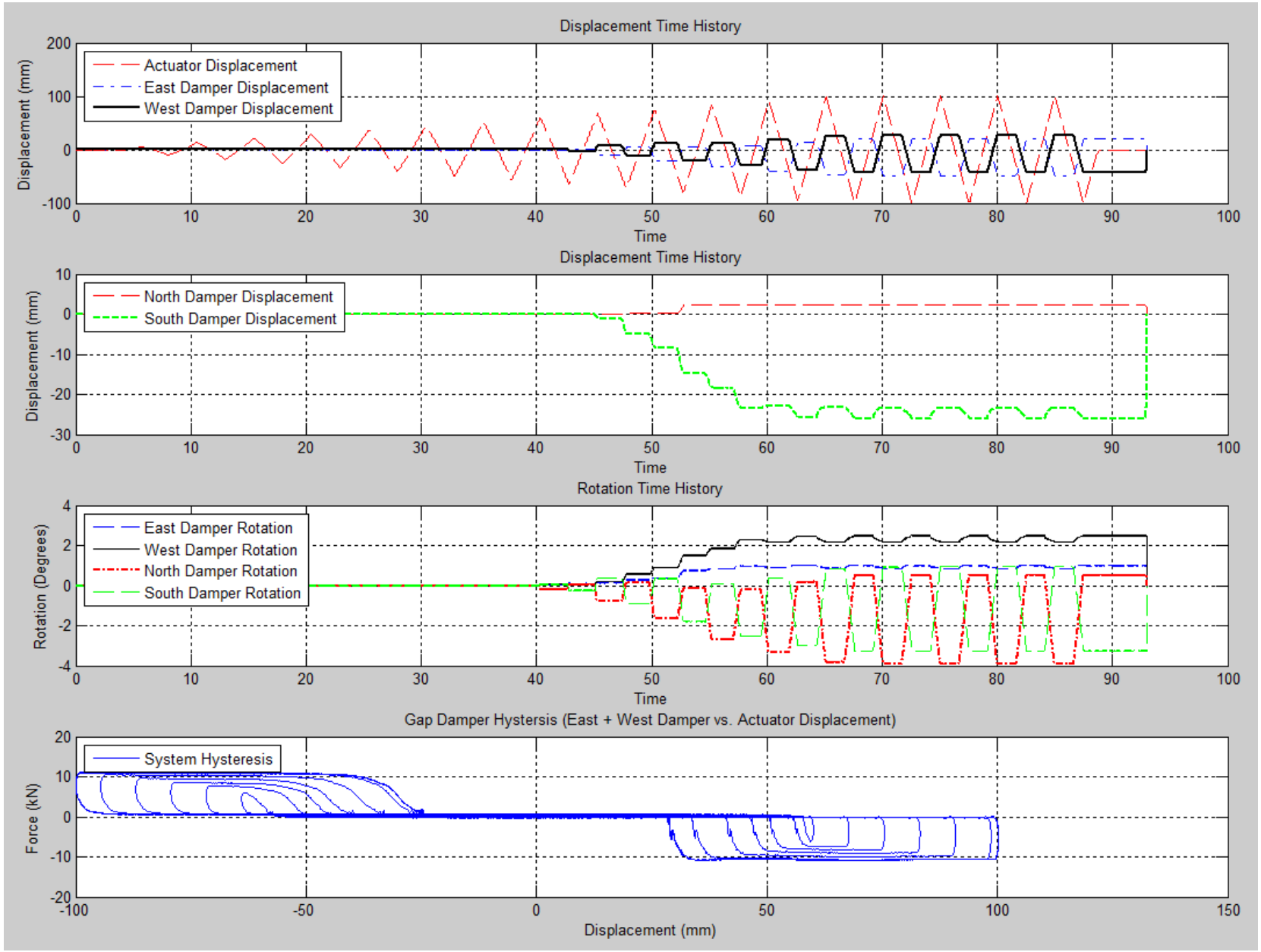

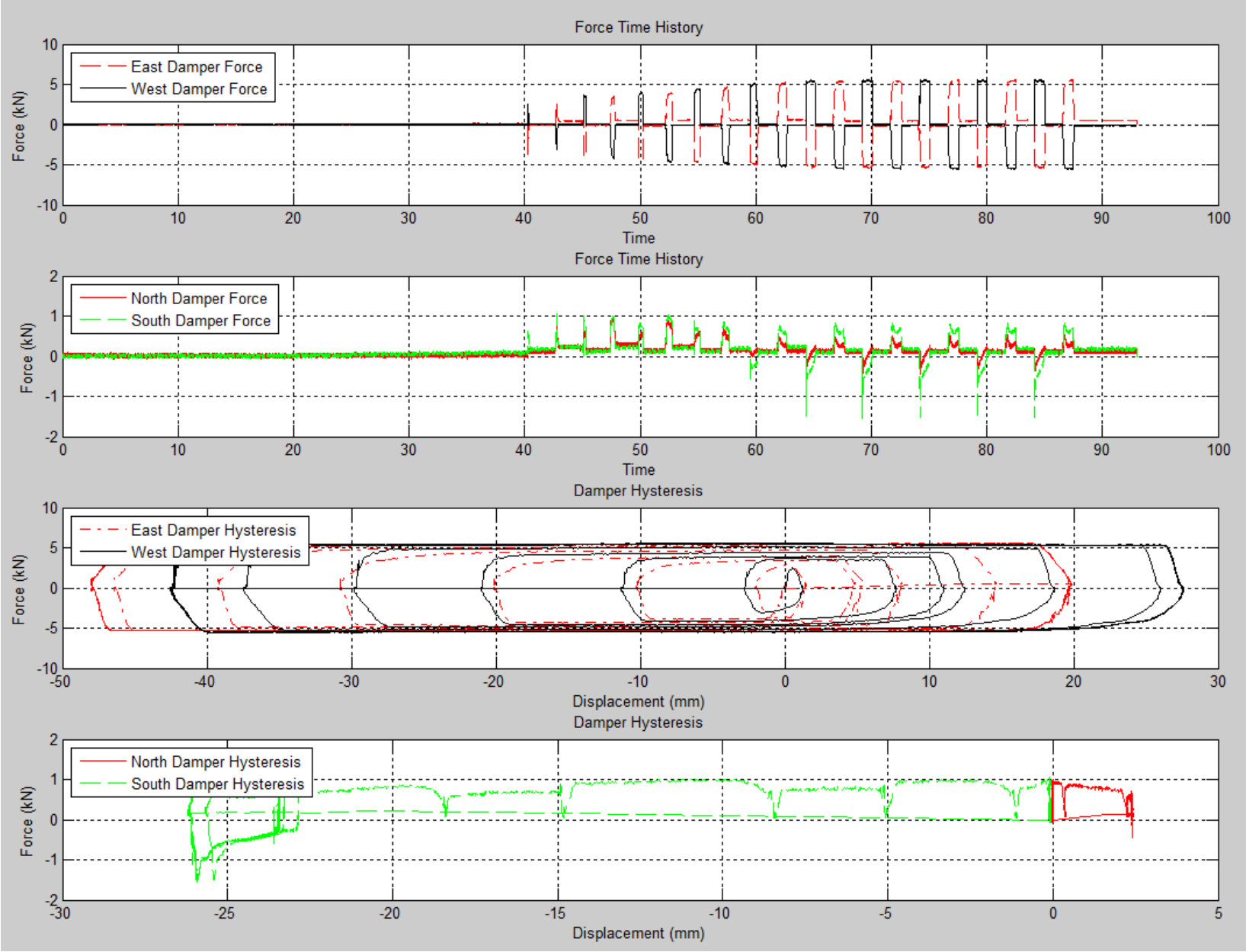
Force Time History
East Damper Force
West Damper Force
Force (kN)
Time
Force Time History
North Damper Force
South Damper Force
Force (kN)
Time
Damper Hysteresis
East Damper Hysteresis
West Damper Hysteresis
Force (kN)
Displacement (mm)
Damper Hysteresis
North Damper Hysteresis
South Damper Hysteresis
Force (kN)
Displacement (mm)

Load Case 9 (E1-0.125Hz-+/-4.2-Sine):

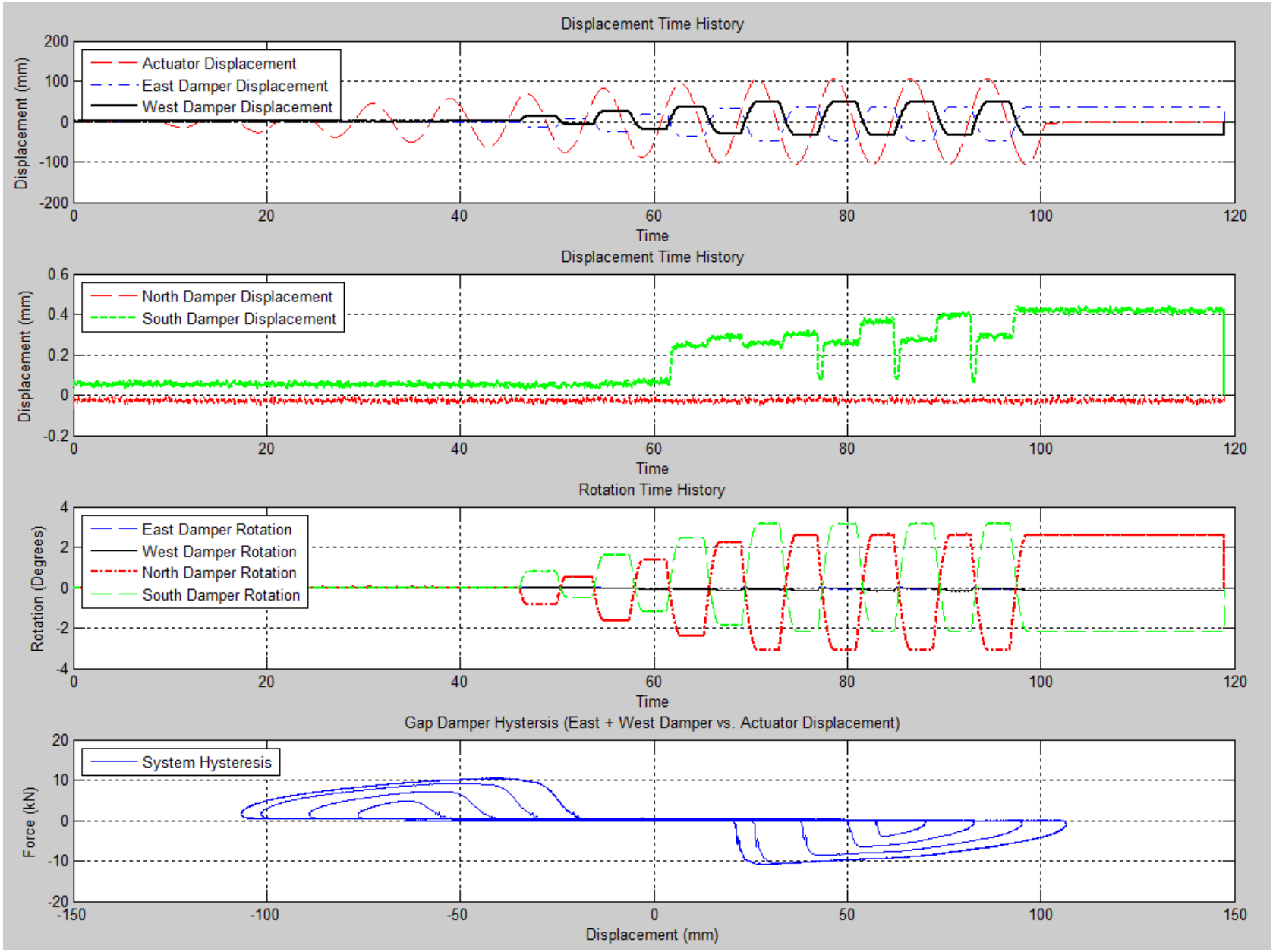

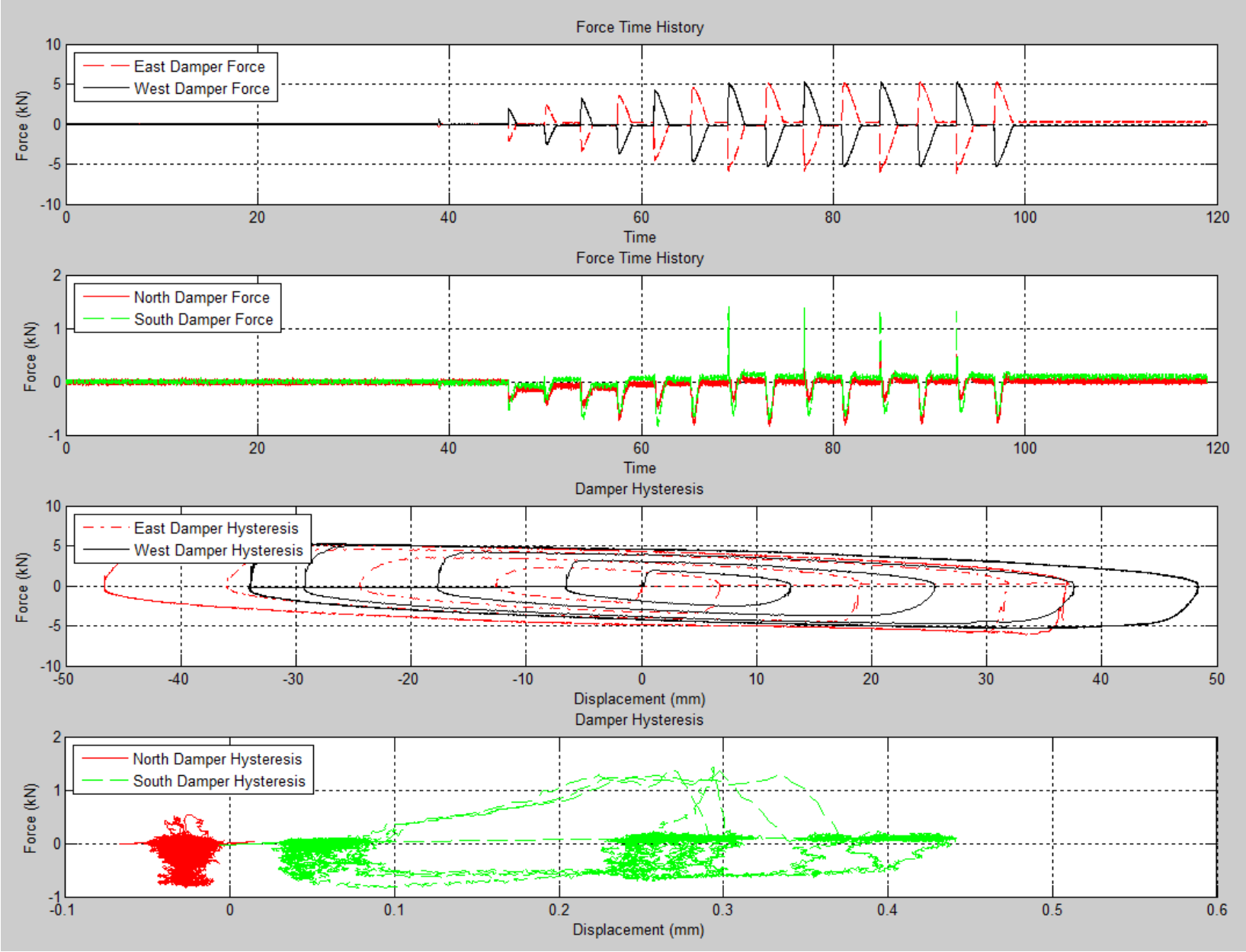
Force Time History
East Damper Force
West Damper Force
Force (kN)
Time
Force Time History
North Damper Force
South Damper Force
Force (kN)
Time
Damper Hysteresis
East Damper Hysteresis
West Damper Hysteresis
Force (kN)
Displacement (mm)
Damper Hysteresis
North Damper Hysteresis
South Damper Hysteresis
Force (kN)
Displacement (mm)

Load Case 10 (E1-0.2Hz-+/-4.2-Sine):

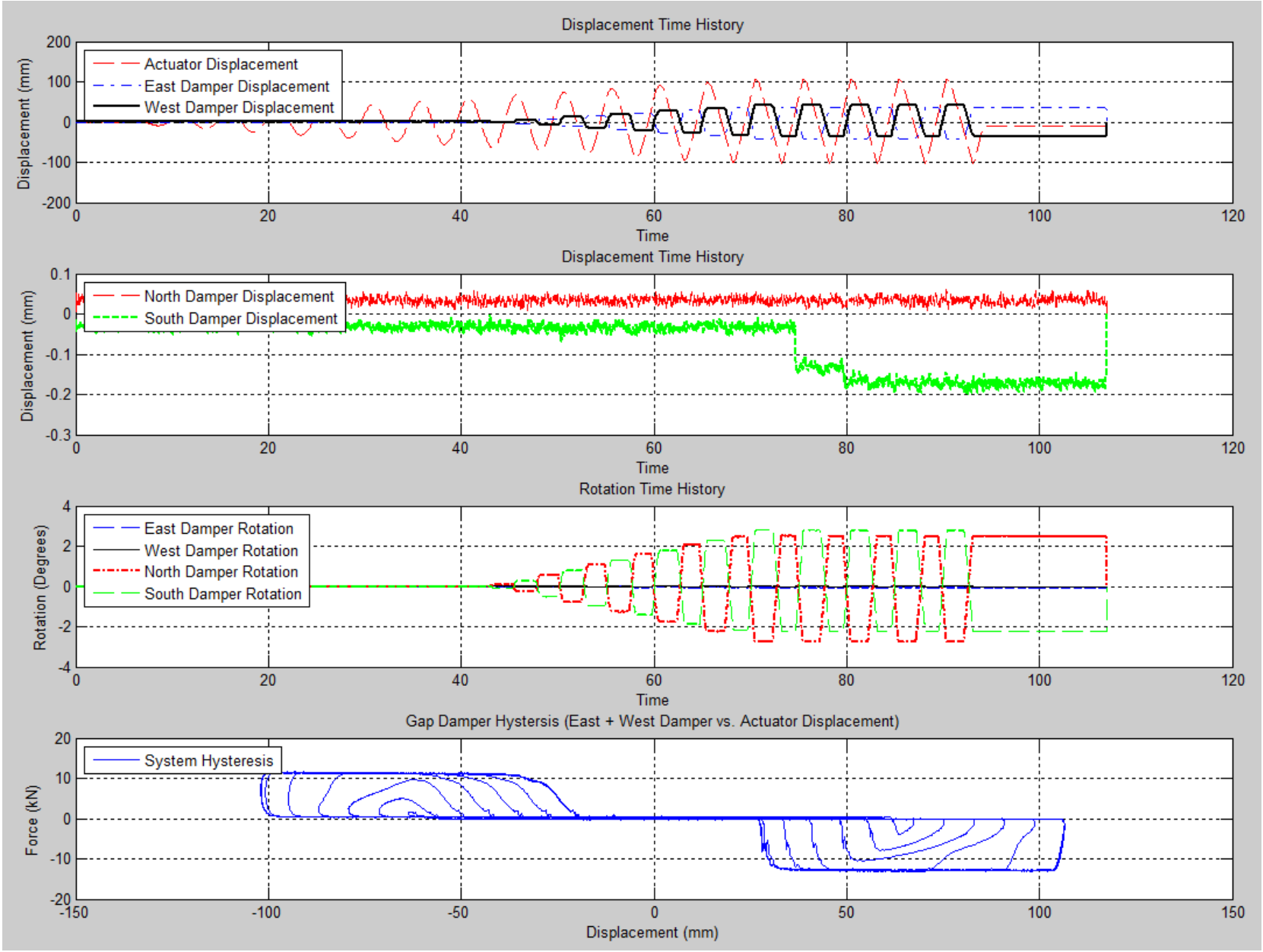

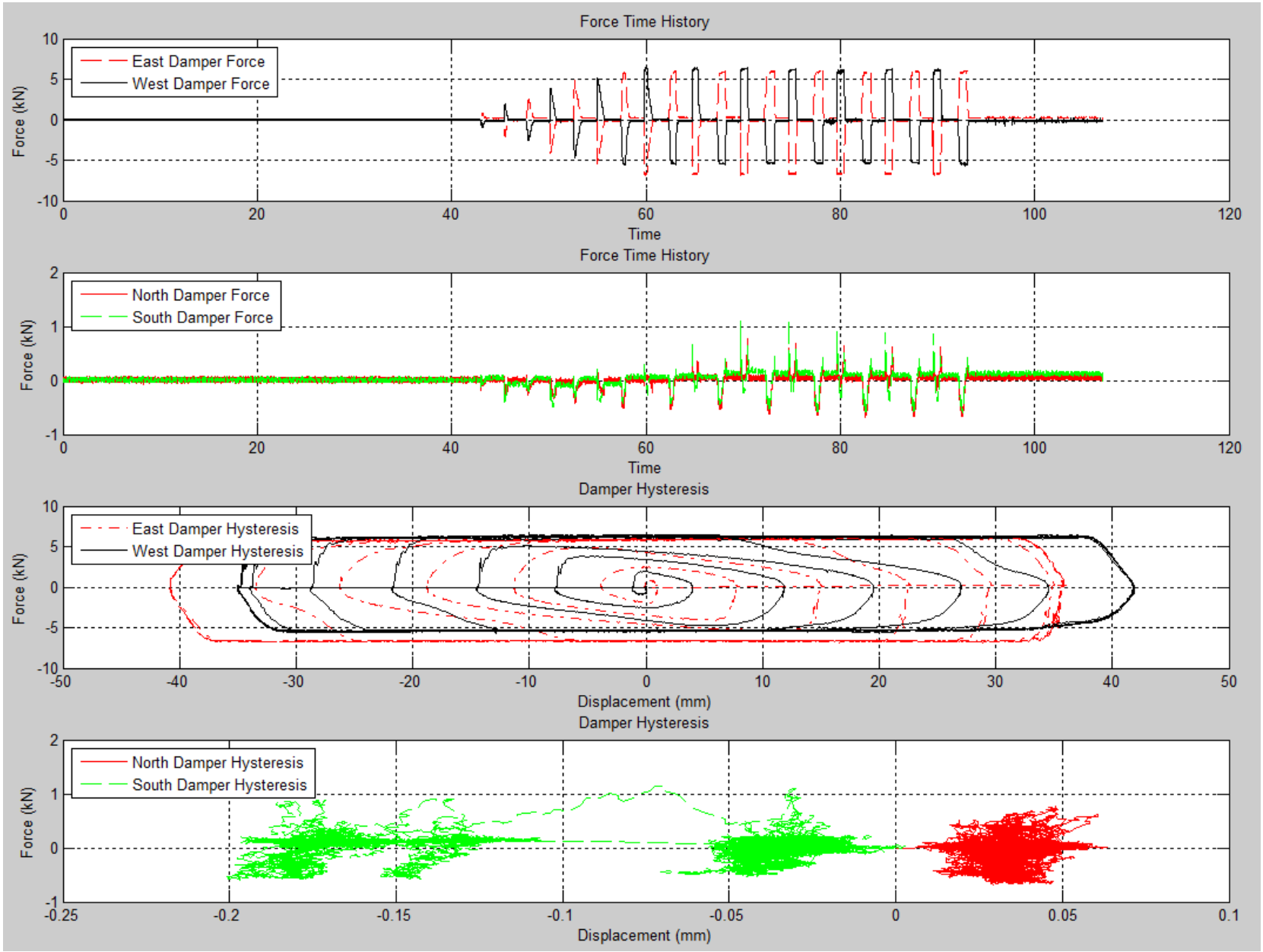
Force Time History
East Damper Force
West Damper Force
Force (kN)
Time
Force Time History
North Damper Force
South Damper Force
Force (kN)
Time
Damper Hysteresis
East Damper Hysteresis
West Damper Hysteresis
Force (kN)
Displacement (mm)
Damper Hysteresis
North Damper Hysteresis
South Damper Hysteresis
Force (kN)
Displacement (mm)

Load Case 11 (E1-0.125Hz-+/-4.2-Tri):

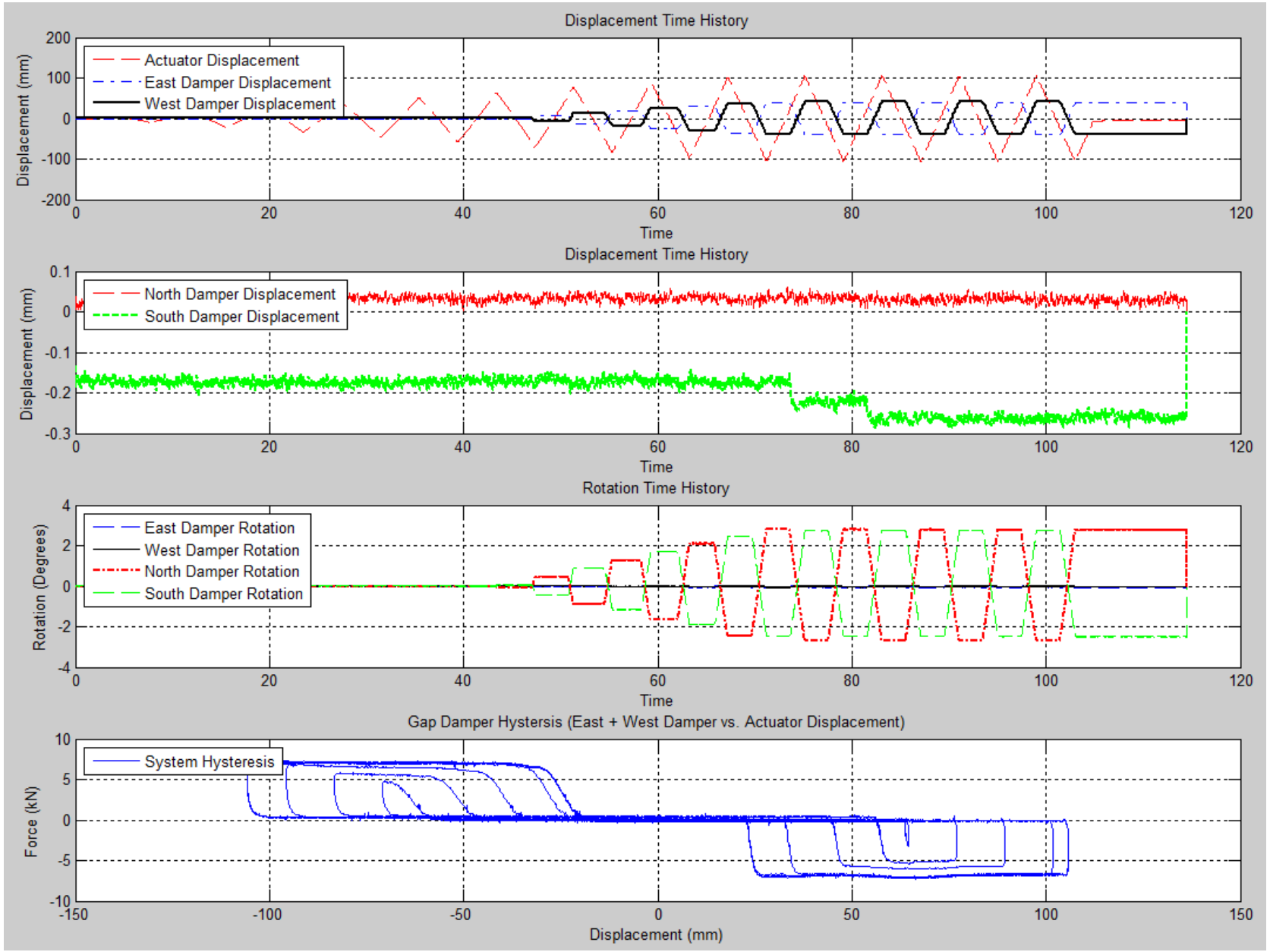

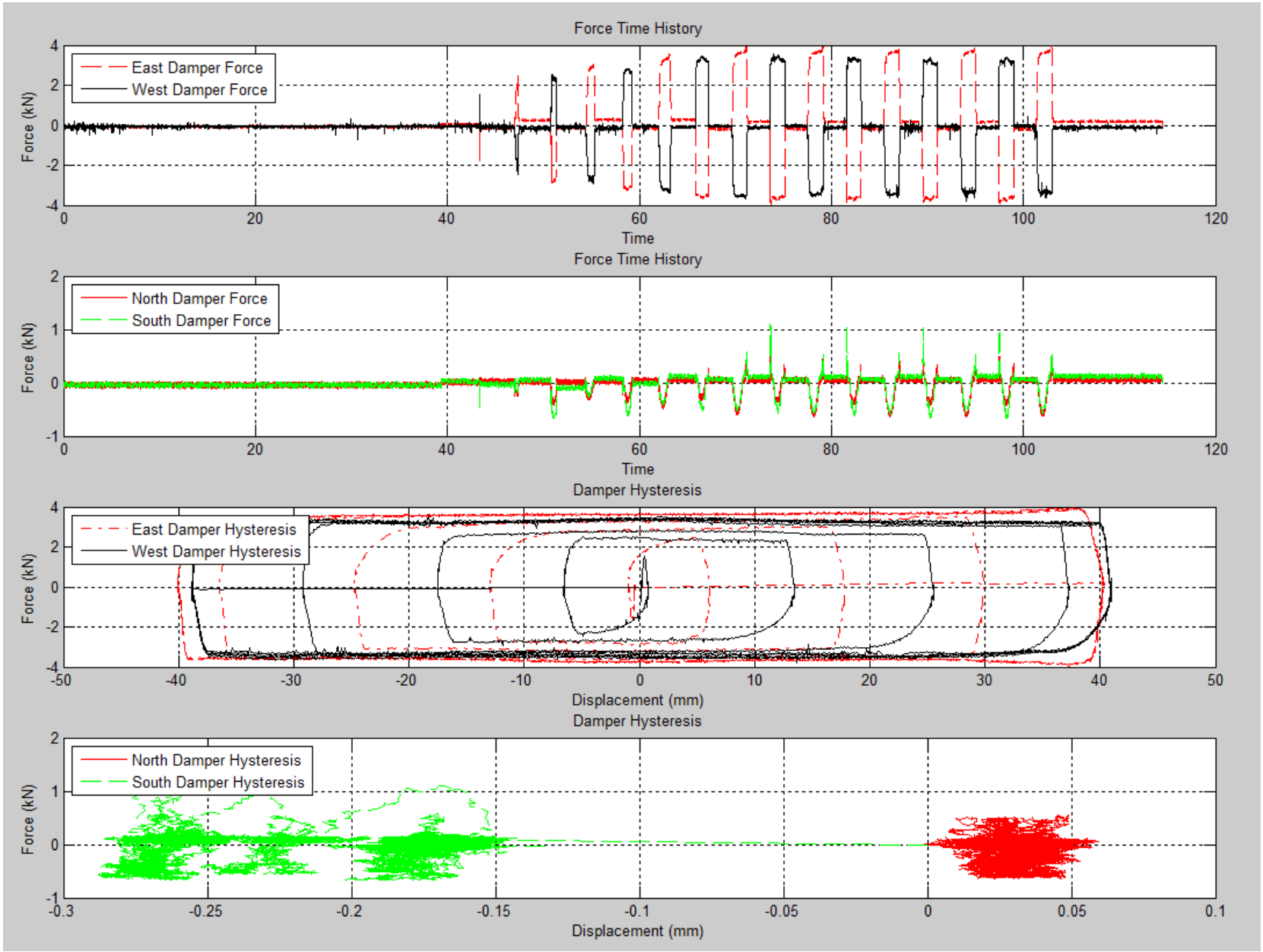
Force Time History
East Damper Force
West Damper Force
Force (kN)
Time
Force Time History
North Damper Force
South Damper Force
Force (kN)
Time
Damper Hysteresis
East Damper Hysteresis
West Damper Hysteresis
Force (kN)
Displacement (mm)
Damper Hysteresis
North Damper Hysteresis
South Damper Hysteresis
Force (kN)
Displacement (mm)

Load Case 12 (E1-0.2Hz-+/-4.2-Tri):

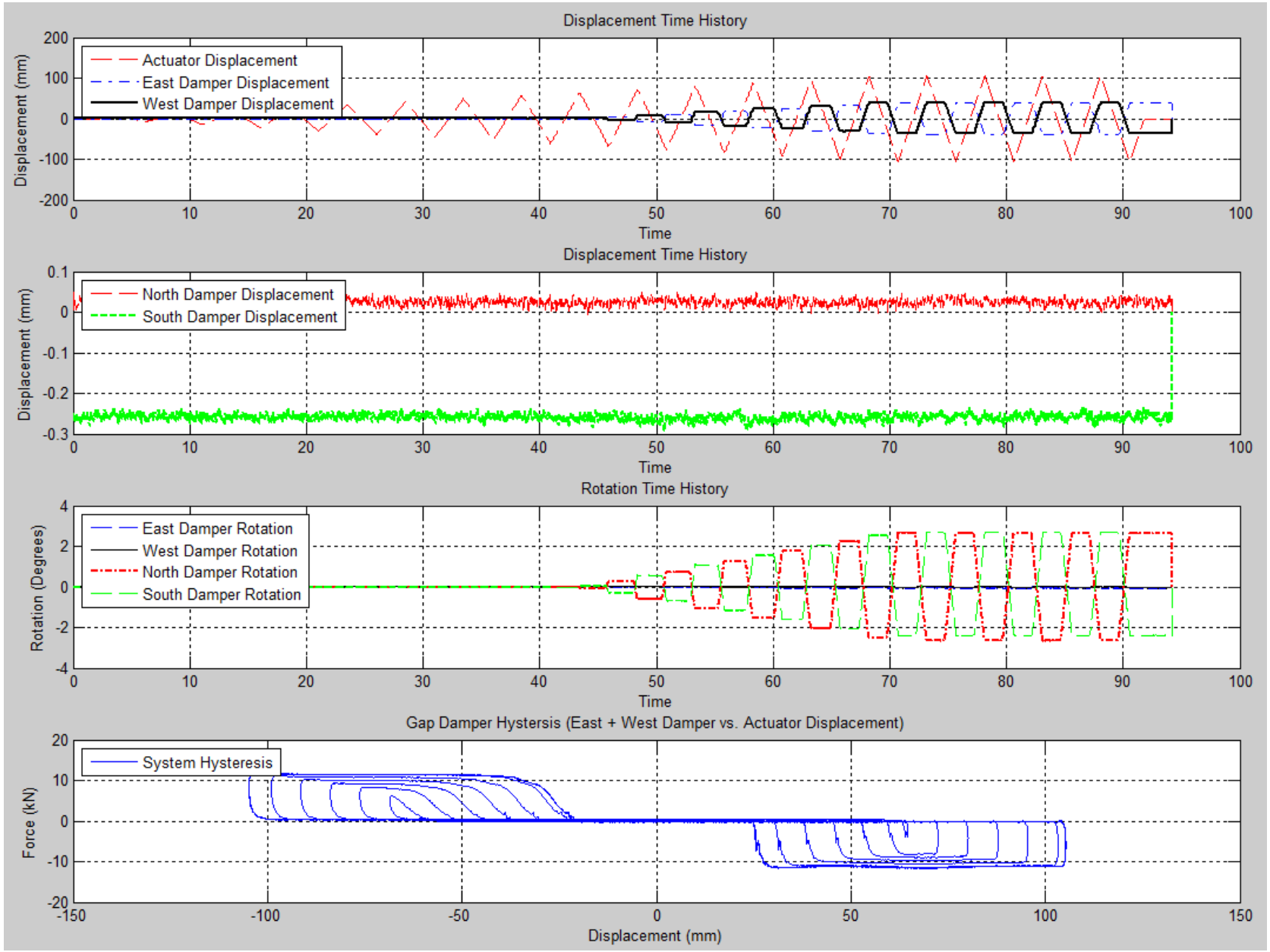

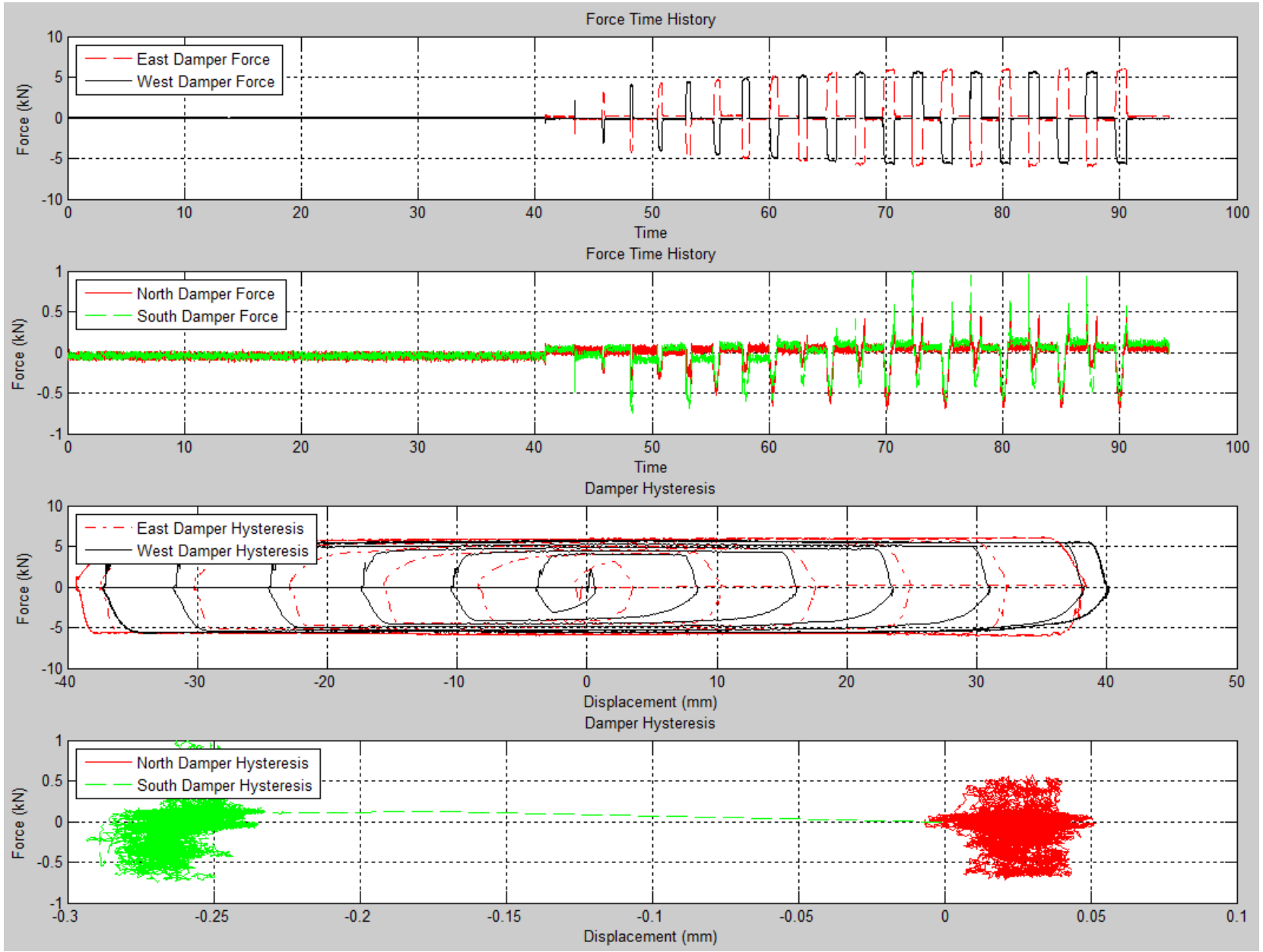
Force Time History
East Damper Force
West Damper Force
Force (kN)
Time
Force Time History
North Damper Force
South Damper Force
Force (kN)
Time
Damper Hysteresis
East Damper Hysteresis
West Damper Hysteresis
Force (kN)
Displacement (mm)
Damper Hysteresis
North Damper Hysteresis
South Damper Hysteresis
Force (kN)
Displacement (mm)

Load Case 13 (T5CCW-E1-0.125Hz-+/-4.2-Sine):

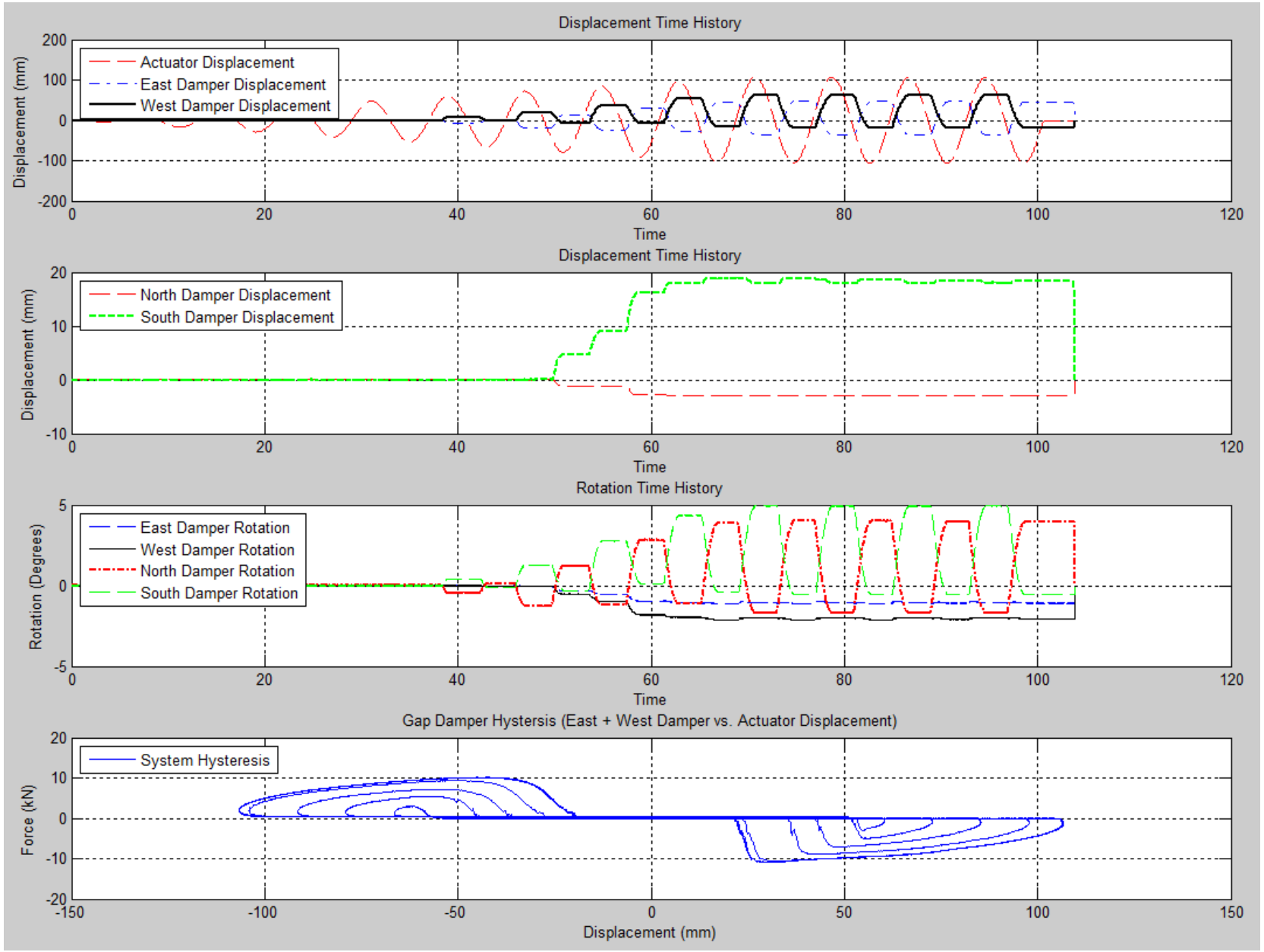

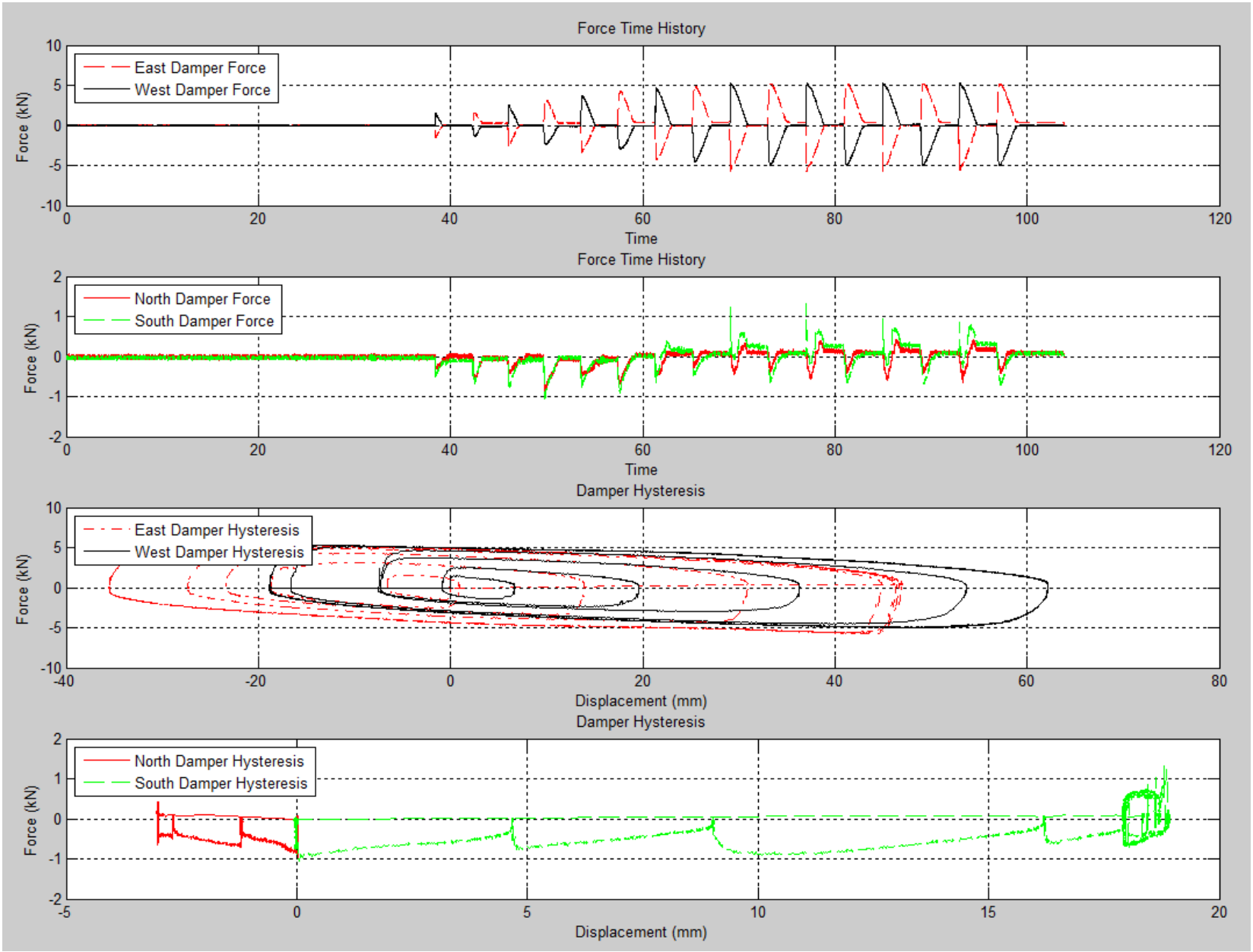
Force Time History
East Damper Force
West Damper Force
Force (kN)
Time
Force Time History
North Damper Force
South Damper Force
Force (kN)
Time
Damper Hysteresis
East Damper Hysteresis
West Damper Hysteresis
Force (kN)
Displacement (mm)
Damper Hysteresis
North Damper Hysteresis
South Damper Hysteresis
Force (kN)
Displacement (mm)

Load Case 14 (T5CCW-E1-0.2Hz-+/-4.2-Sine):

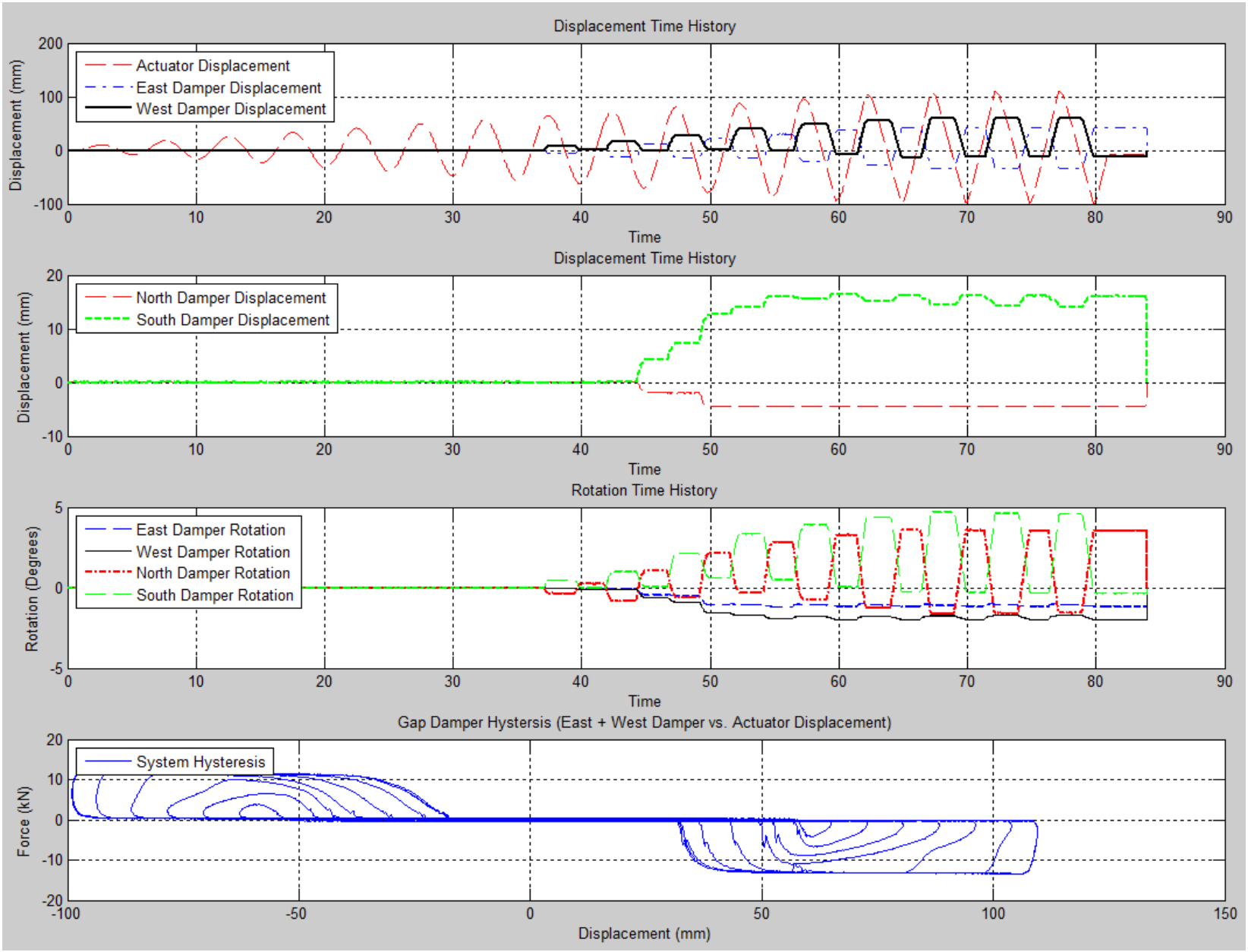

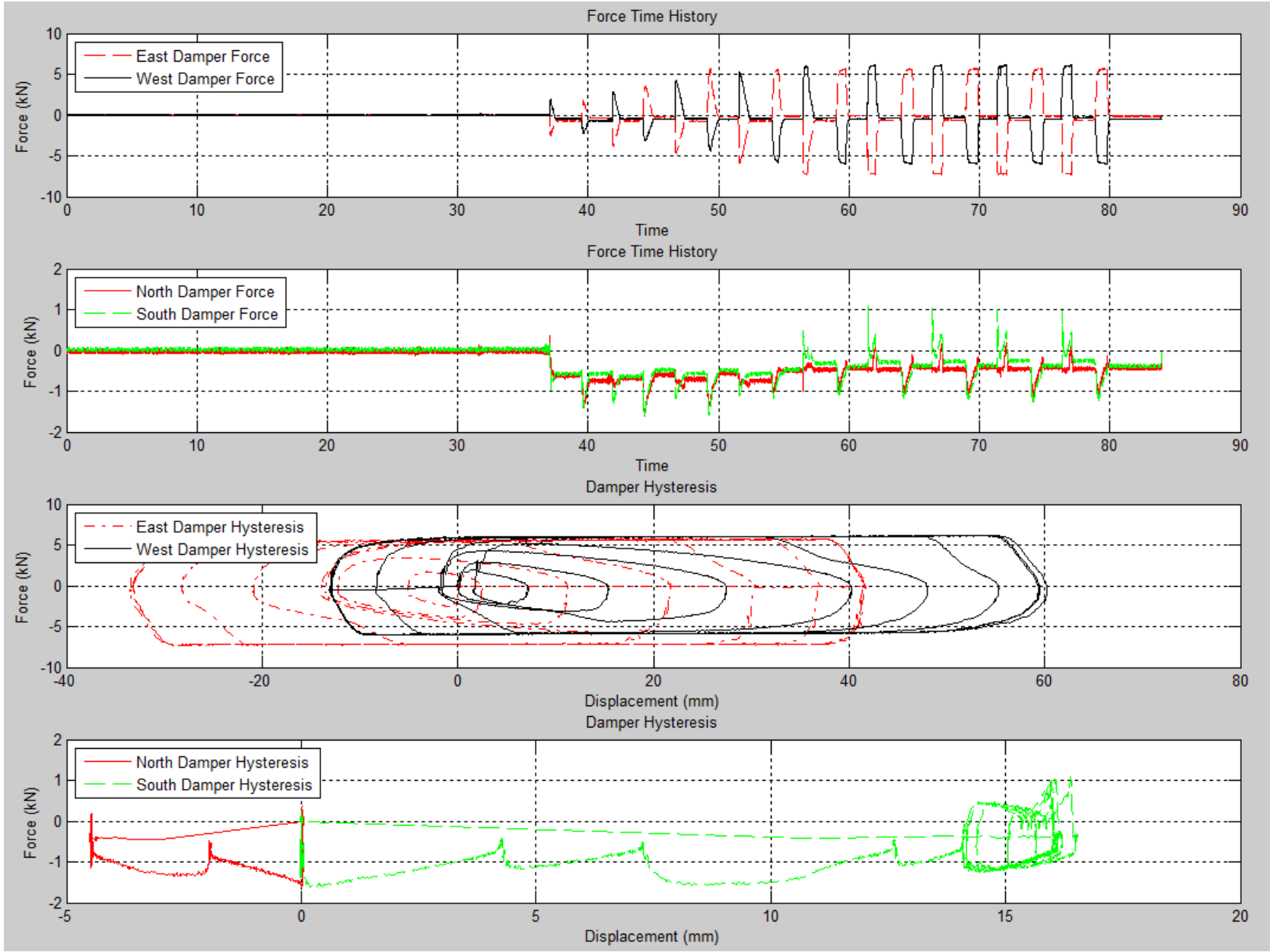
Force Time History
East Damper Force
West Damper Force
Force (kN)
Time
Force Time History
North Damper Force
South Damper Force
Force (kN)
Time
Damper Hysteresis
East Damper Hysteresis
West Damper Hysteresis
Force (kN)
Displacement (mm)
Damper Hysteresis
North Damper Hysteresis
South Damper Hysteresis
Force (kN)
Displacement (mm)

Load Case 15 (T5CW-E1-0.125Hz-+/-4.2-Sine):

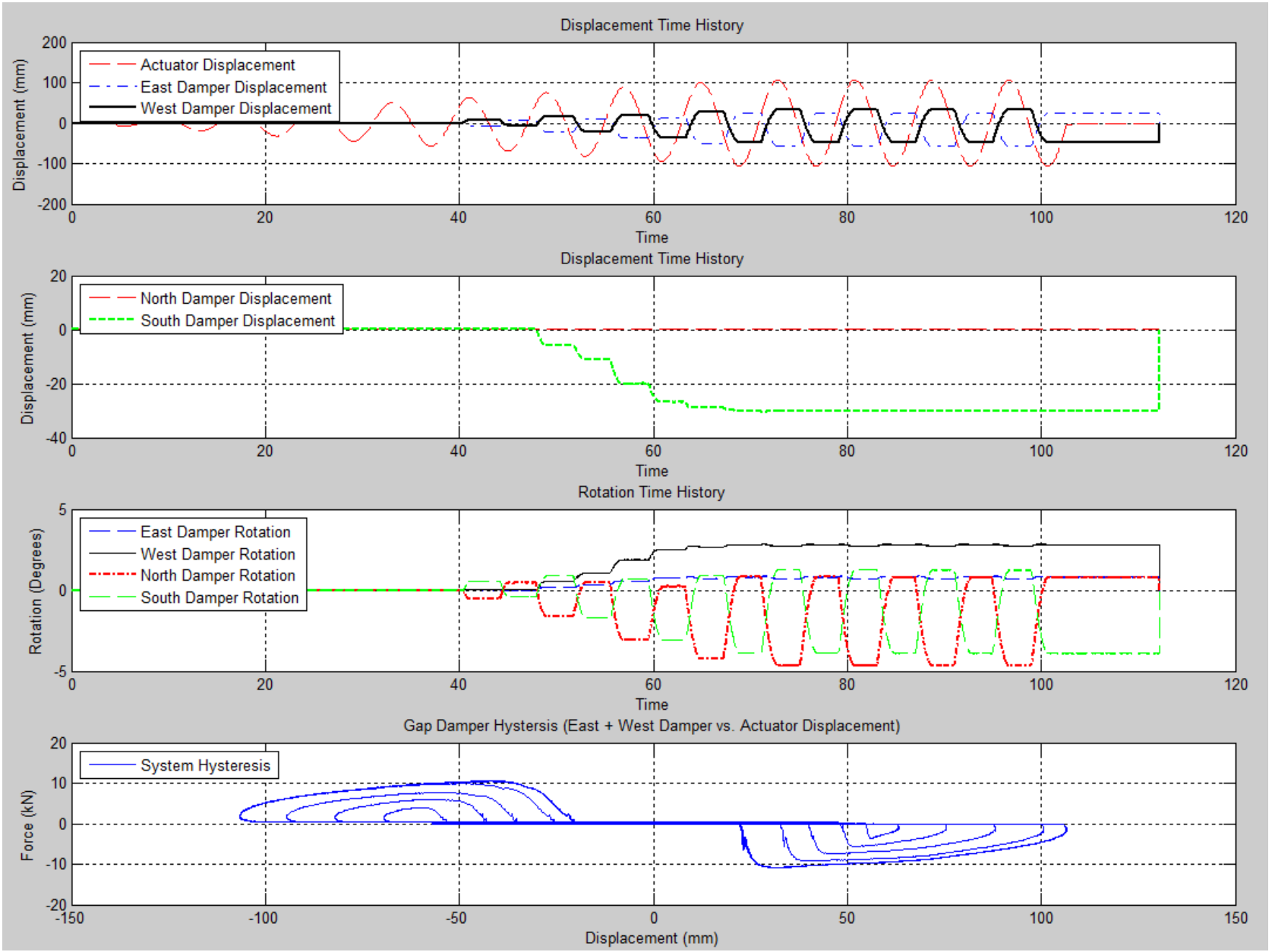

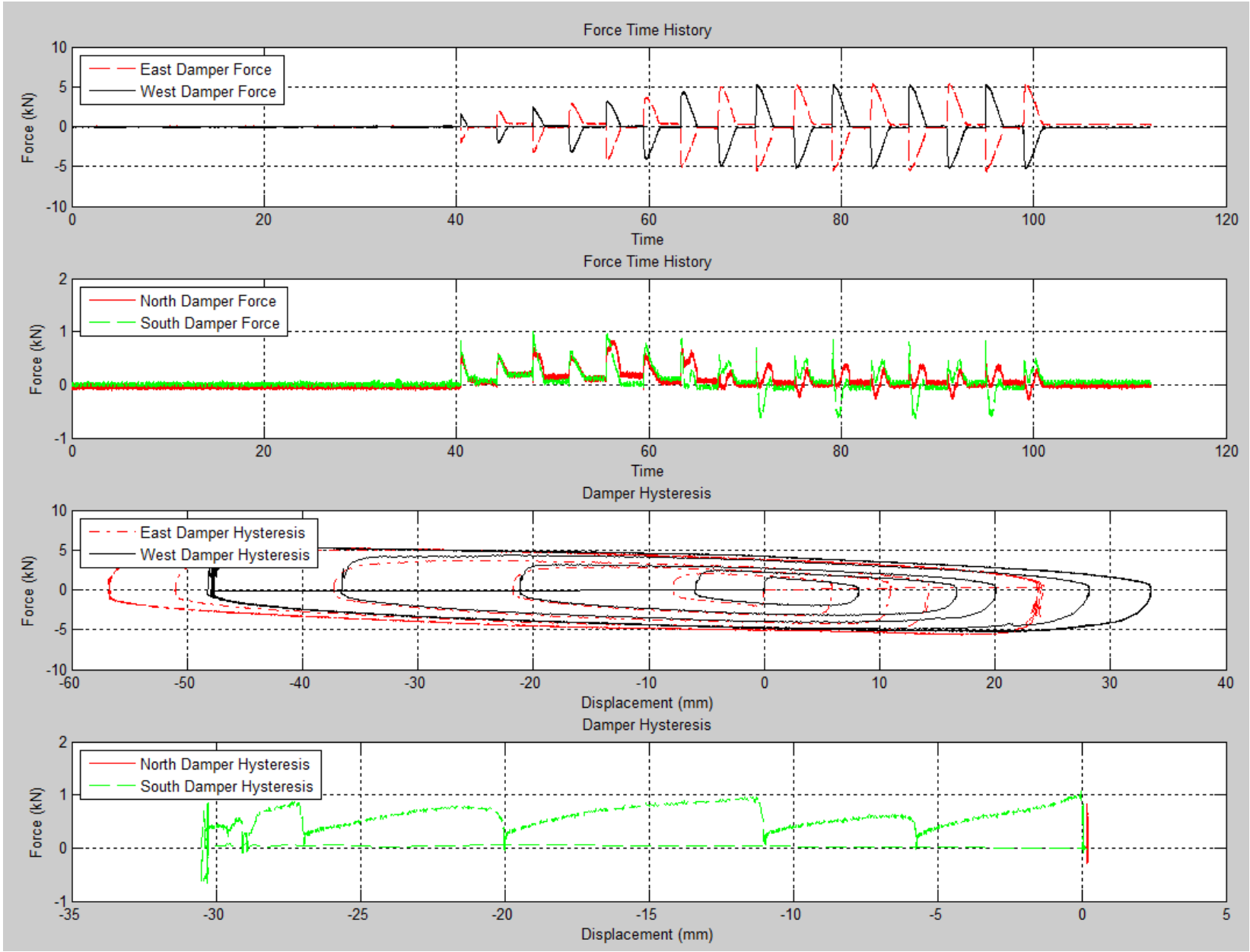
Force Time History
East Damper Force
West Damper Force
Force (kN)
Time
Force Time History
North Damper Force
South Damper Force
Force (kN)
Time
Damper Hysteresis
East Damper Hysteresis
West Damper Hysteresis
Force (kN)
Displacement (mm)
Damper Hysteresis
North Damper Hysteresis
South Damper Hysteresis
Force (kN)
Displacement (mm)

Load Case 16 (T5CW-E1-0.2Hz-+/-4.2-Sine):

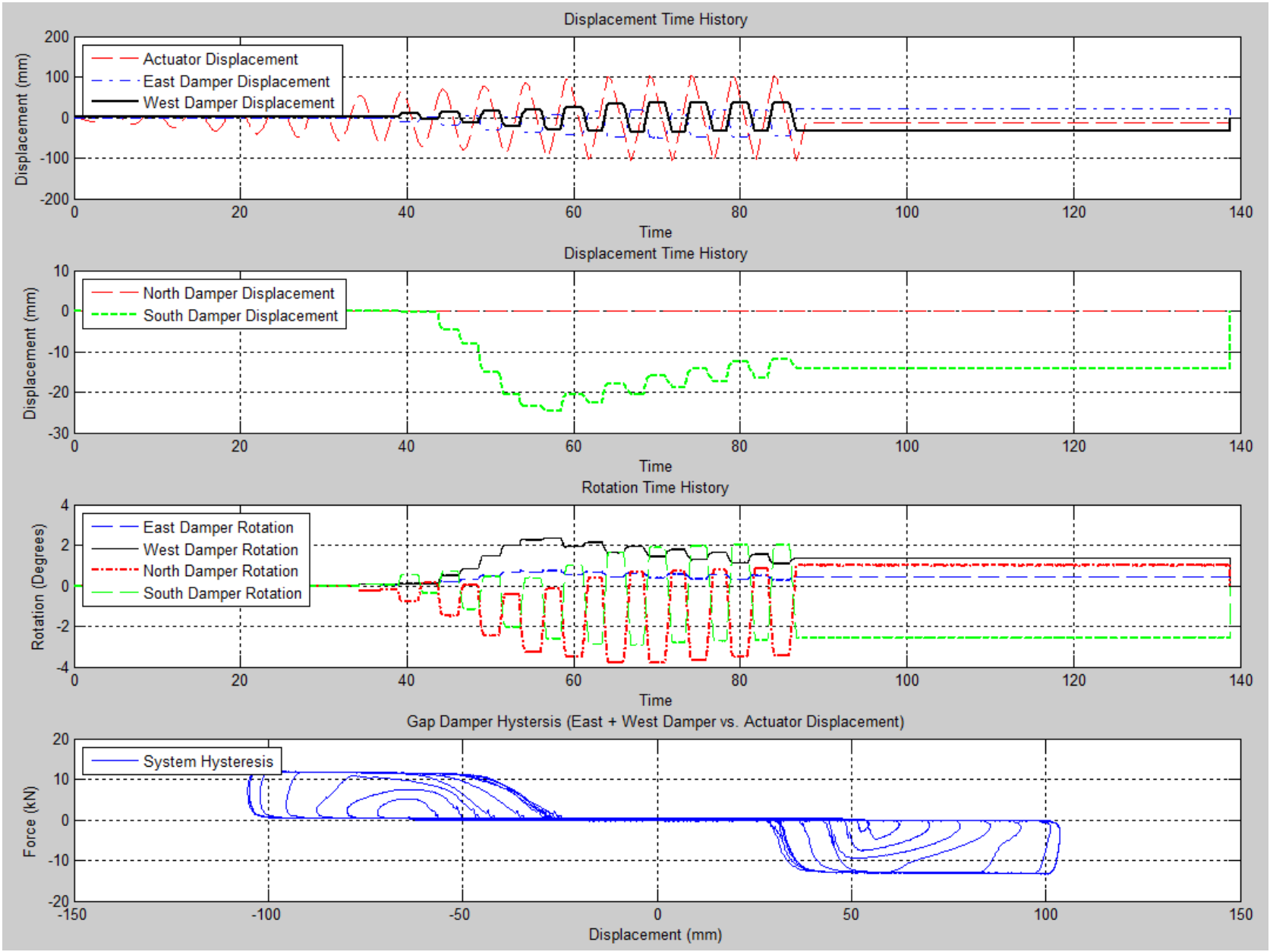

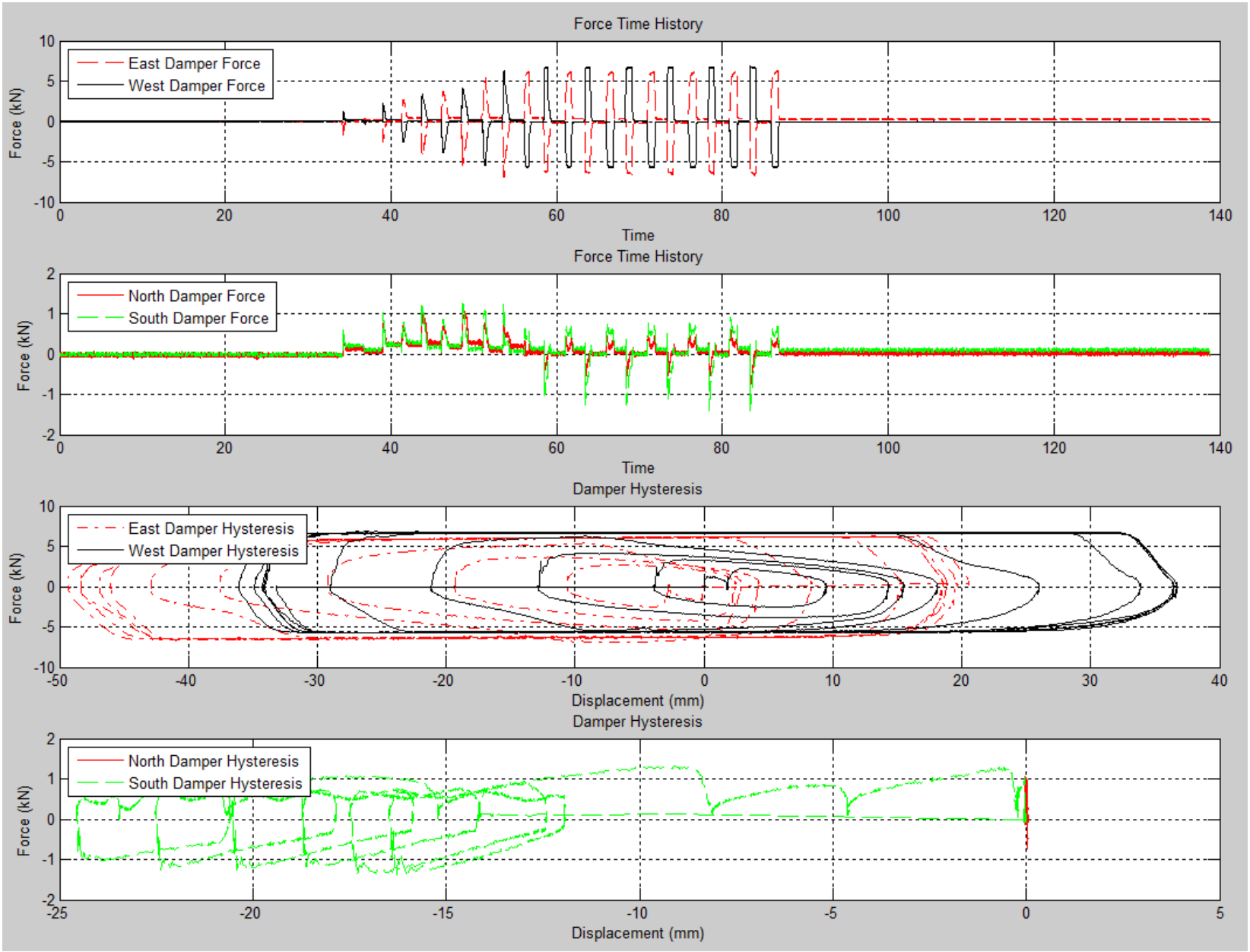
Force Time History
East Damper Force
West Damper Force
Force (kN)
Time
Force Time History
North Damper Force
South Damper Force
Force (kN)
Time
Damper Hysteresis
East Damper Hysteresis
West Damper Hysteresis
Force (kN)
Displacement (mm)
Damper Hysteresis
North Damper Hysteresis
South Damper Hysteresis
Force (kN)
Displacement (mm)

Load Case 17 (E2-0.125Hz-+/-4.2-Sine):

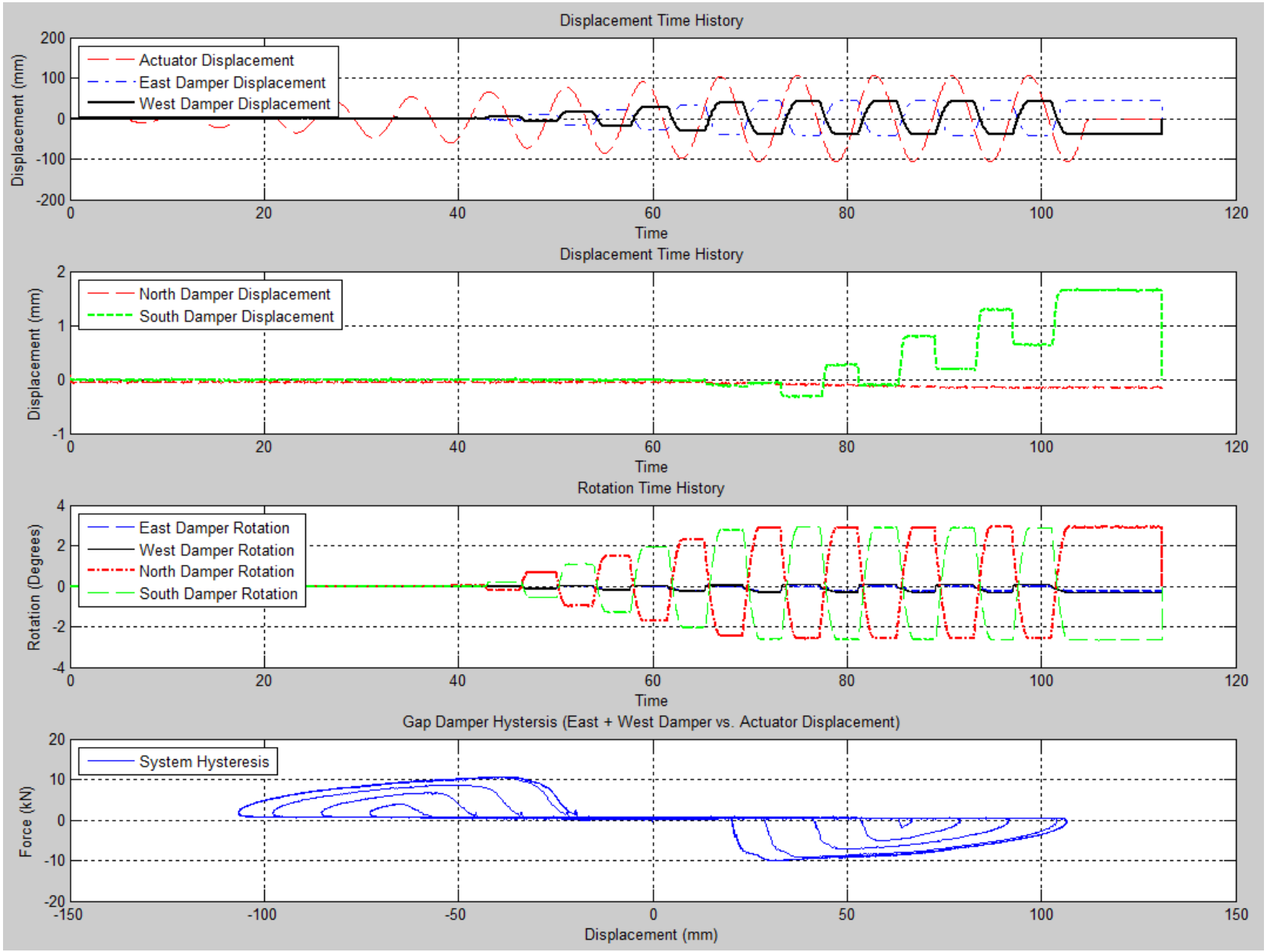

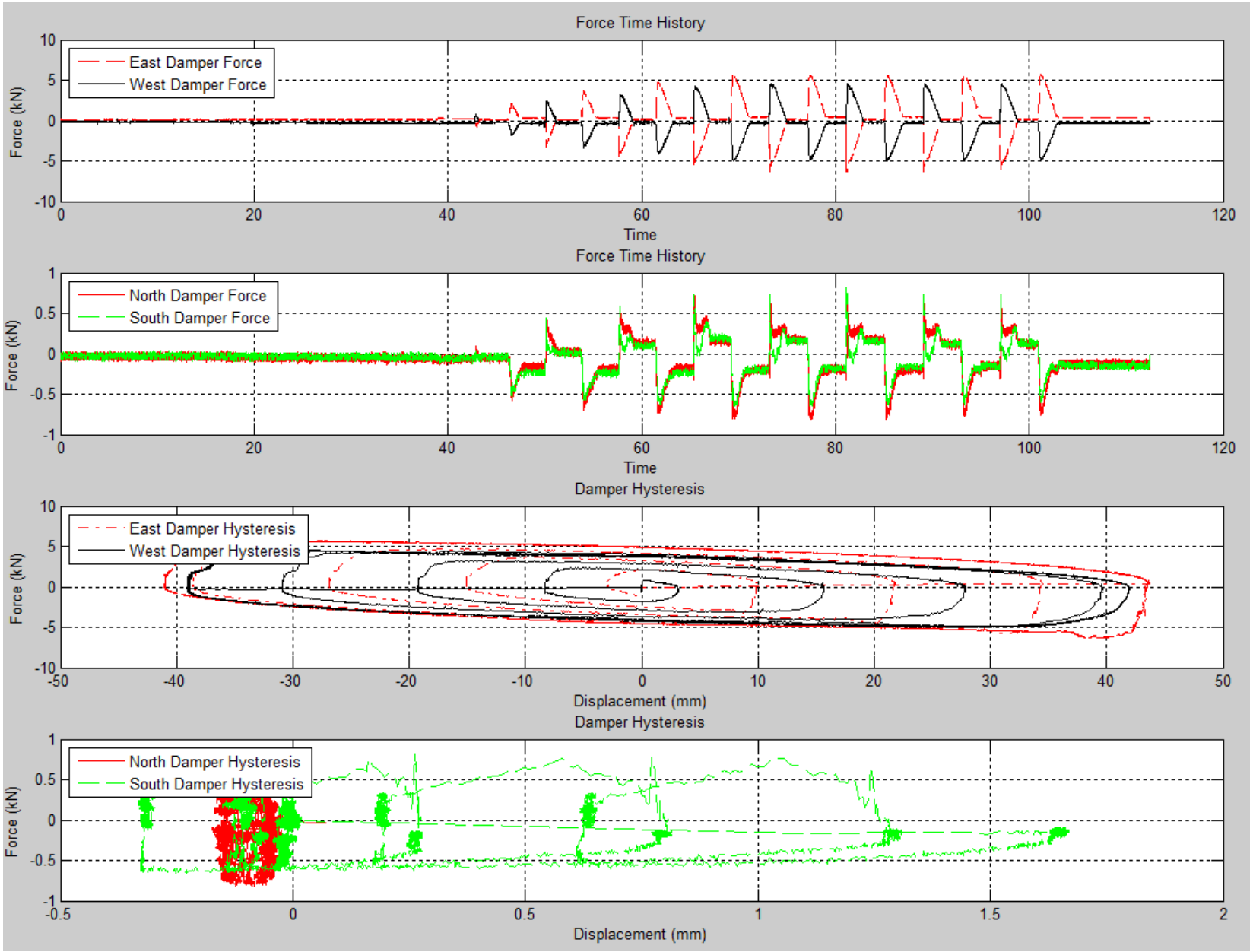
Force Time History
East Damper Force
West Damper Force
Force (kN)
Time
Force Time History
North Damper Force
South Damper Force
Force (kN)
Time
Damper Hysteresis
East Damper Hysteresis
West Damper Hysteresis
Force (kN)
Displacement (mm)
Damper Hysteresis
North Damper Hysteresis
South Damper Hysteresis
Force (kN)
Displacement (mm)

Load Case 18 (E2-0.2Hz-+/-4.2-Sine):

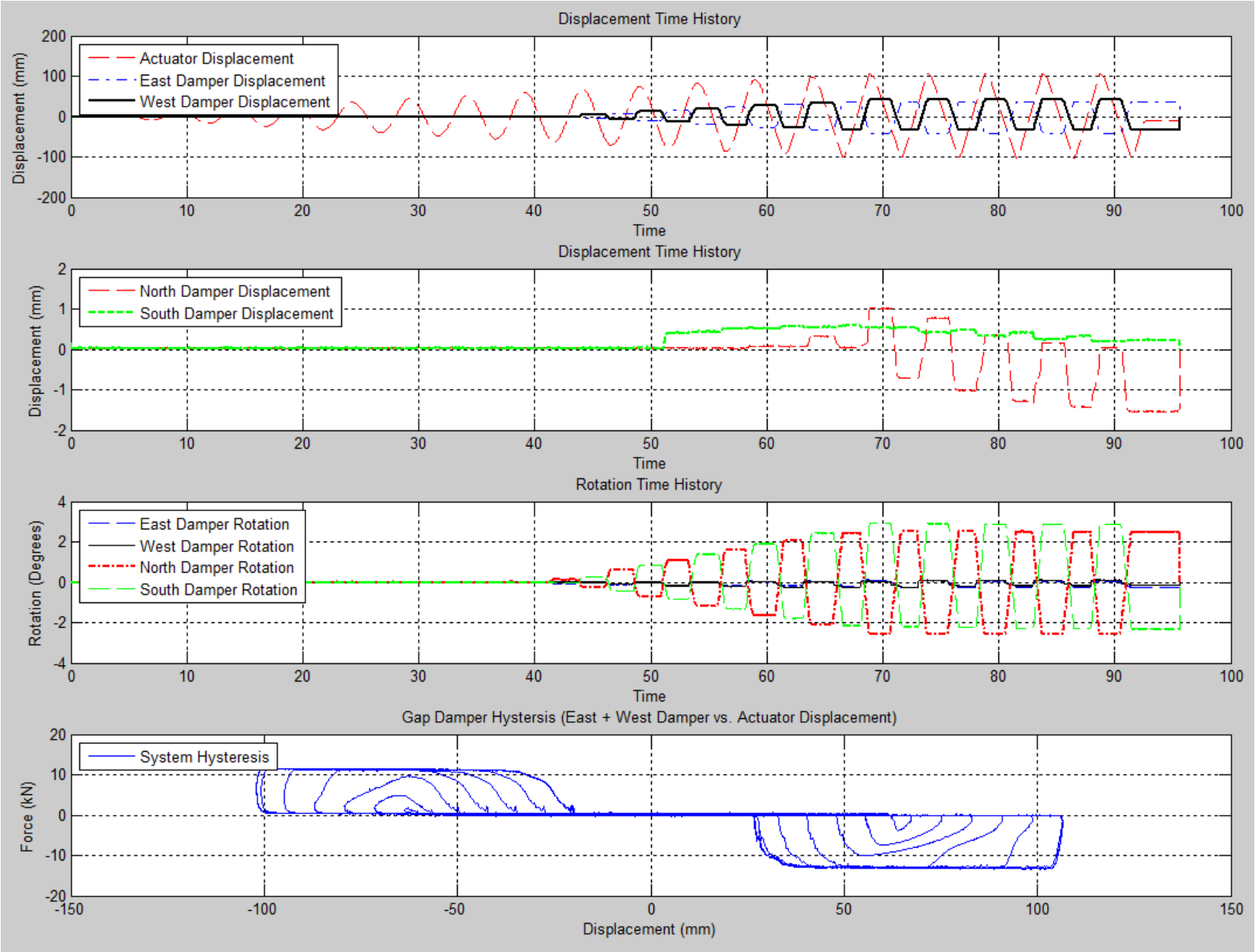

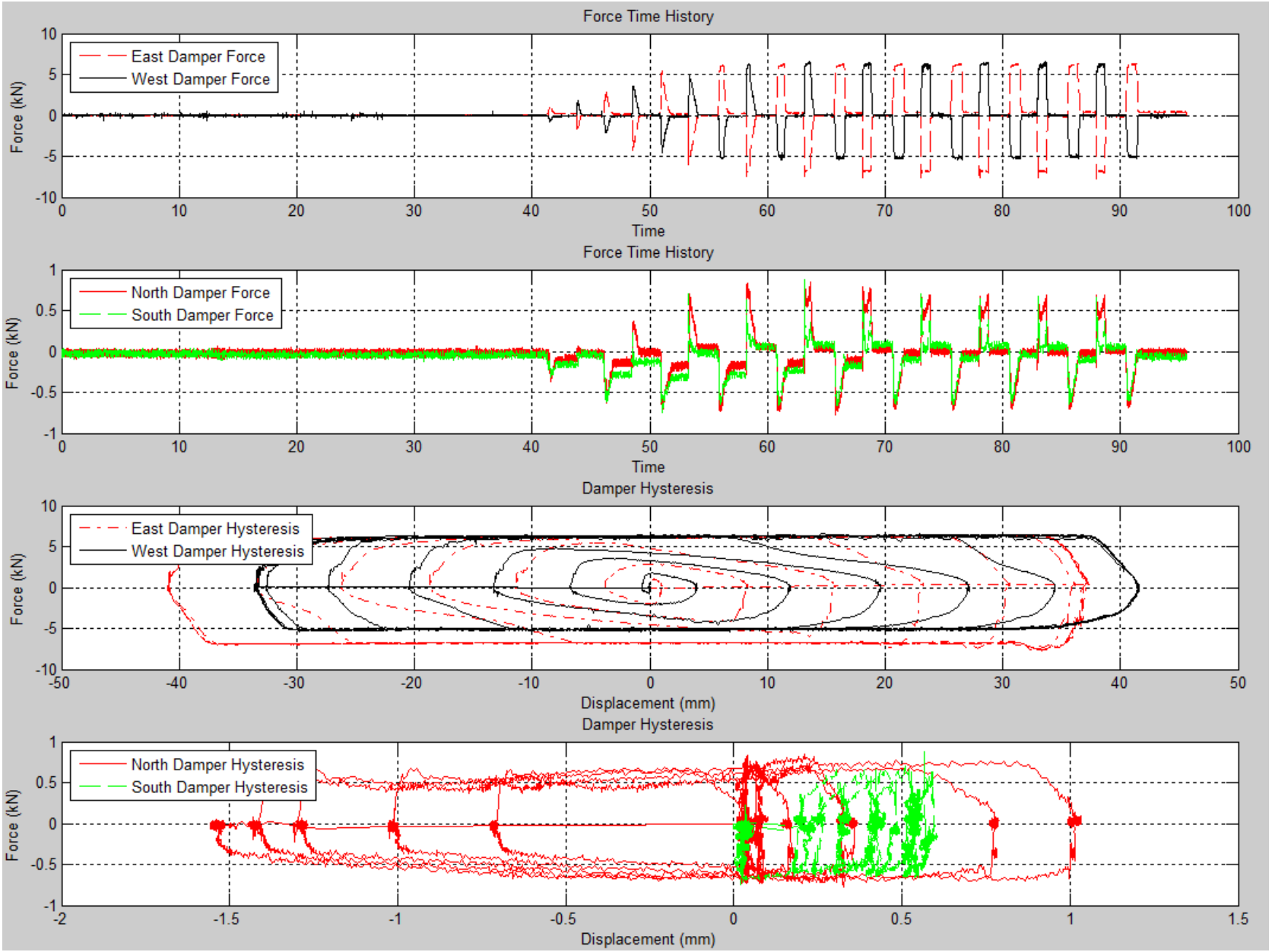
Force Time History
East Damper Force
West Damper Force
Force (kN)
Time
Force Time History
North Damper Force
South Damper Force
Force (kN)
Time
Damper Hysteresis
East Damper Hysteresis
West Damper Hysteresis
Force (kN)
Displacement (mm)
Damper Hysteresis
North Damper Hysteresis
South Damper Hysteresis
Force (kN)
Displacement (mm)

Load Case 19 (E2-0.125Hz-+/-4.2-Tri):

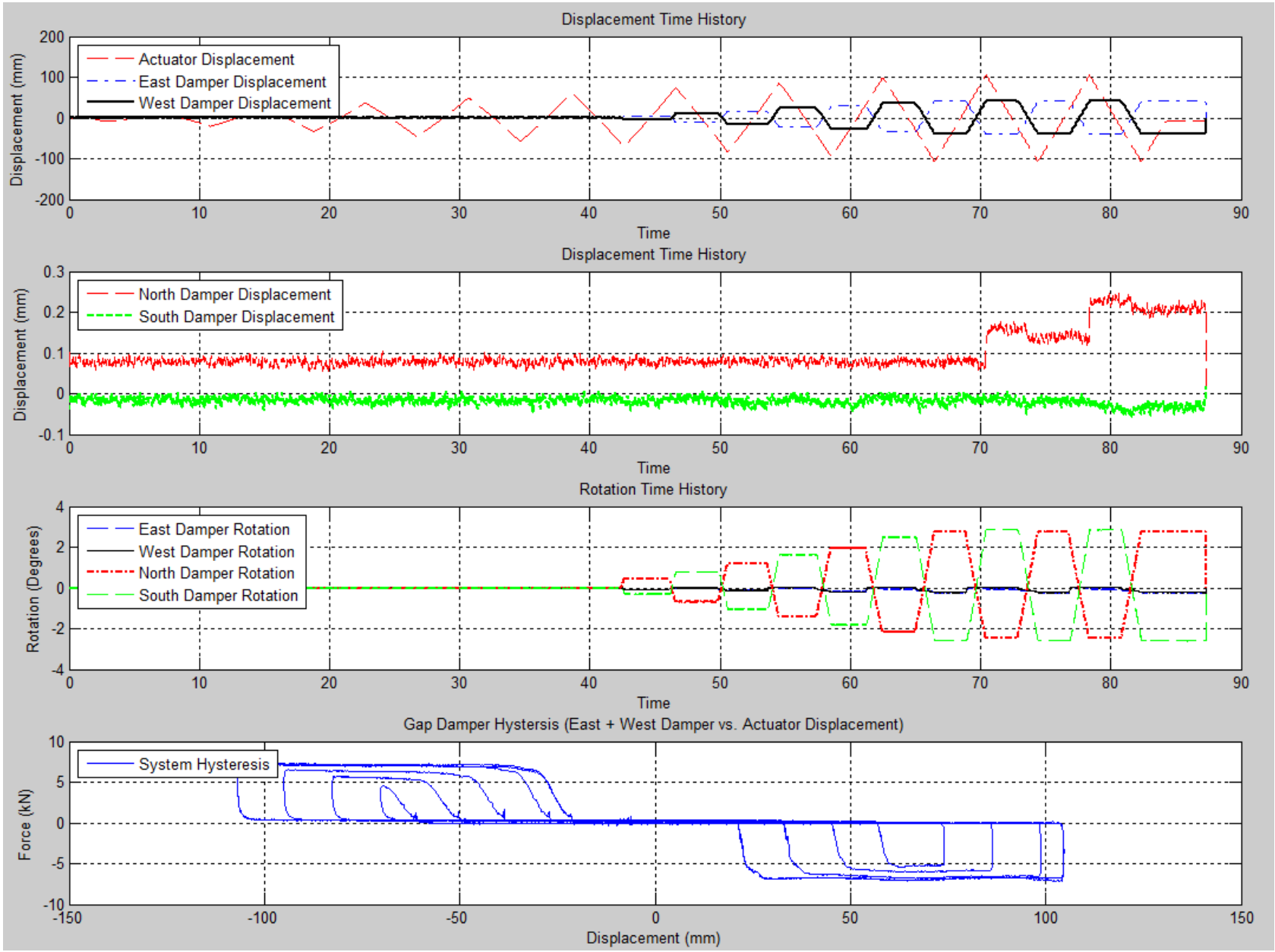

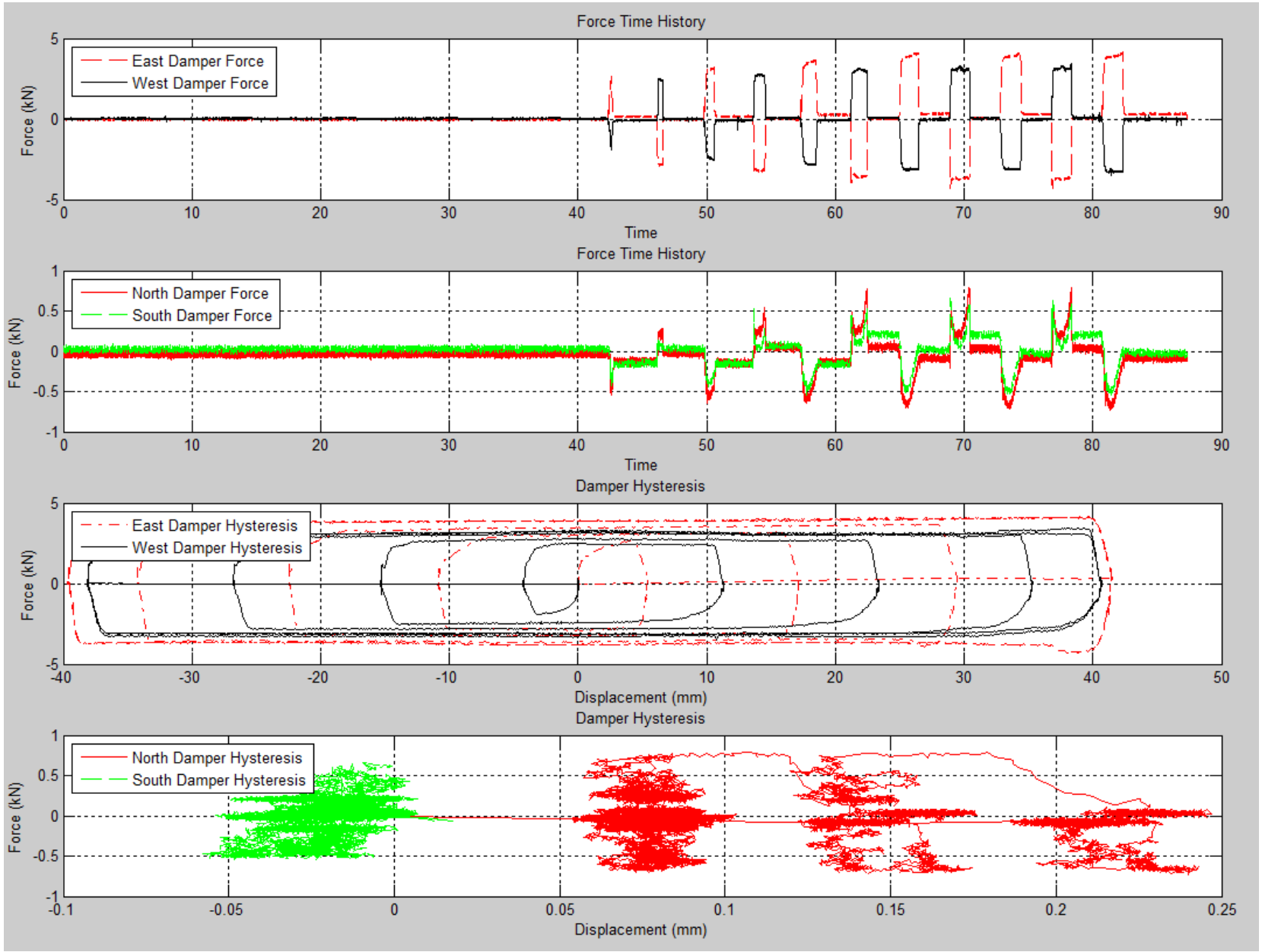
Force Time History
East Damper Force
West Damper Force
Force (kN)
Time
Force Time History
North Damper Force
South Damper Force
Force (kN)
Time
Damper Hysteresis
East Damper Hysteresis
West Damper Hysteresis
Force (kN)
Displacement (mm)
Damper Hysteresis
North Damper Hysteresis
South Damper Hysteresis
Force (kN)
Displacement (mm)

Load Case 20 (E2-0.2Hz-+/-4.2-Tri):

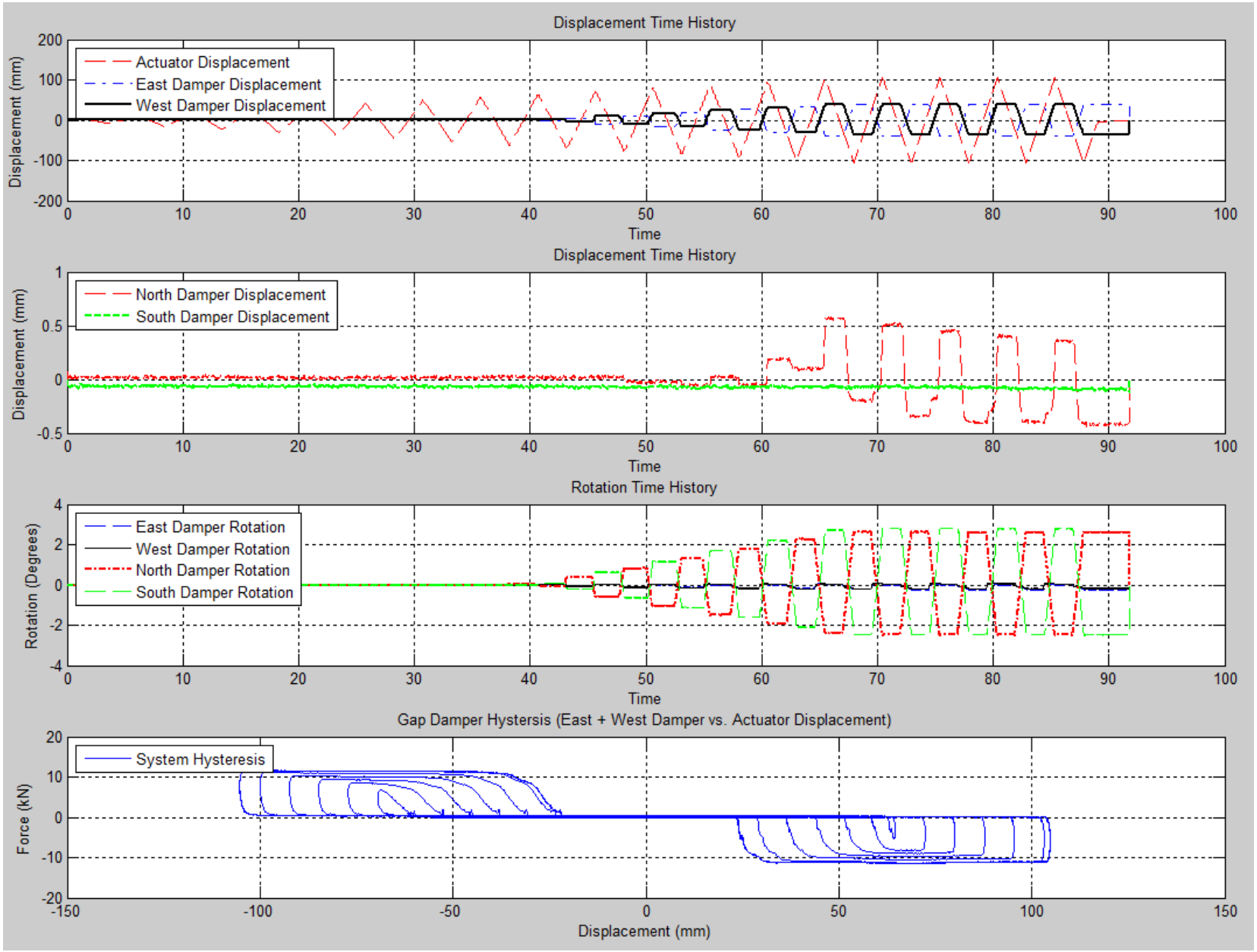

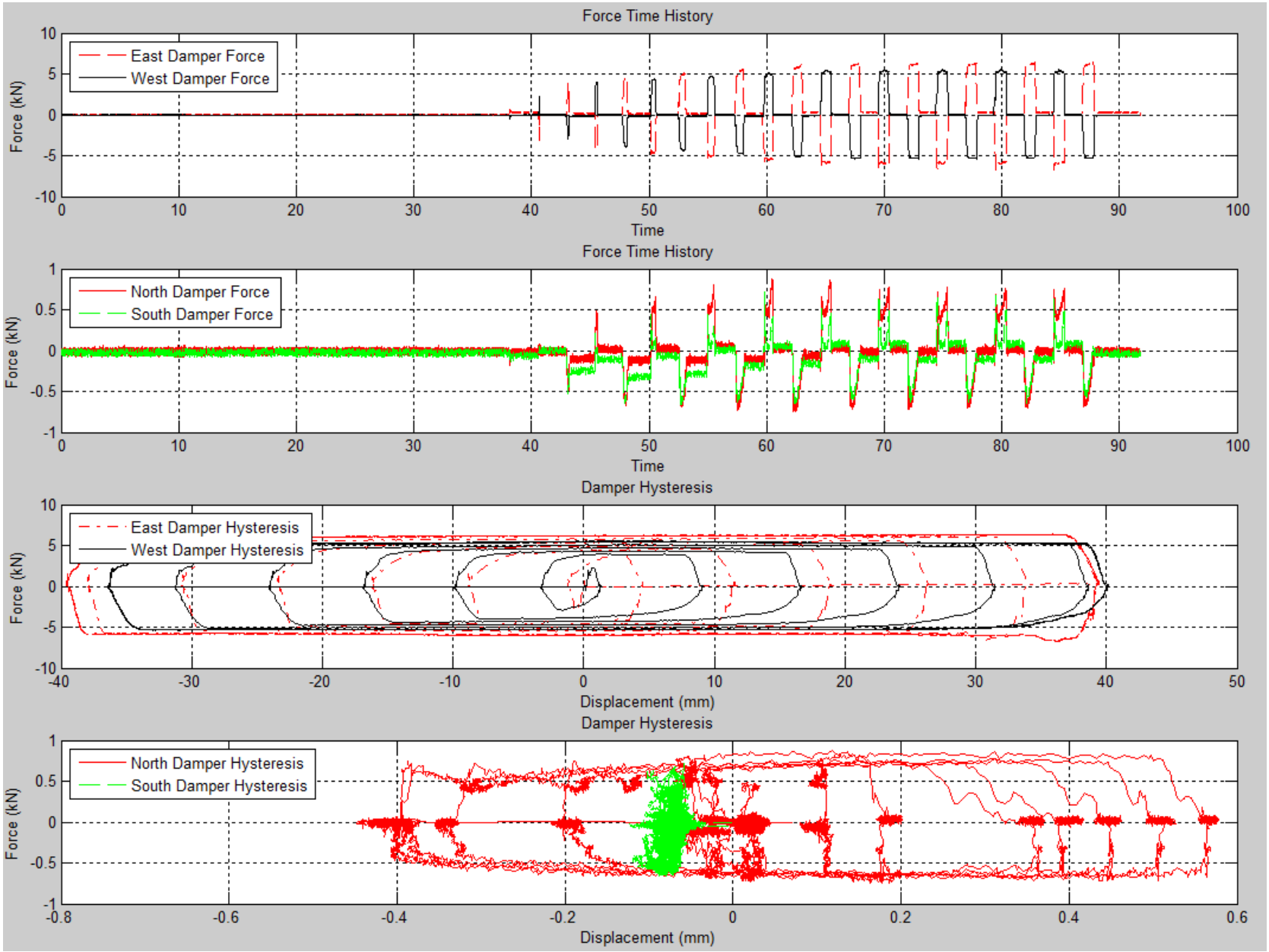
Force Time History
East Damper Force
West Damper Force
Force (kN)
Time
Force Time History
North Damper Force
South Damper Force
Force (kN)
Time
Damper Hysteresis
East Damper Hysteresis
West Damper Hysteresis
Force (kN)
Displacement (mm)
Damper Hysteresis
North Damper Hysteresis
South Damper Hysteresis
Force (kN)
Displacement (mm)

Load Case 21 (T5CCW-E2-0.125Hz-+/-4.0-Sine):

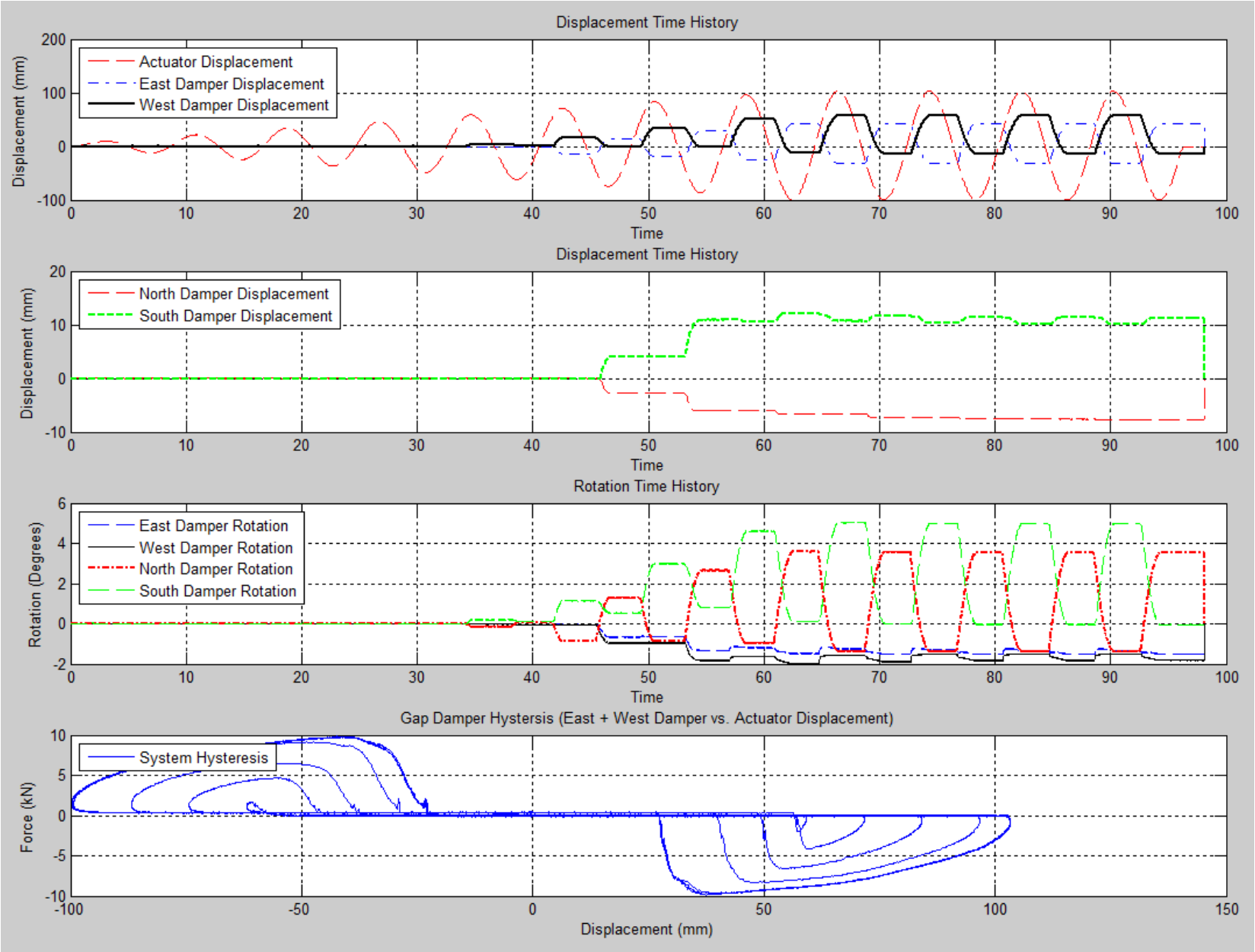

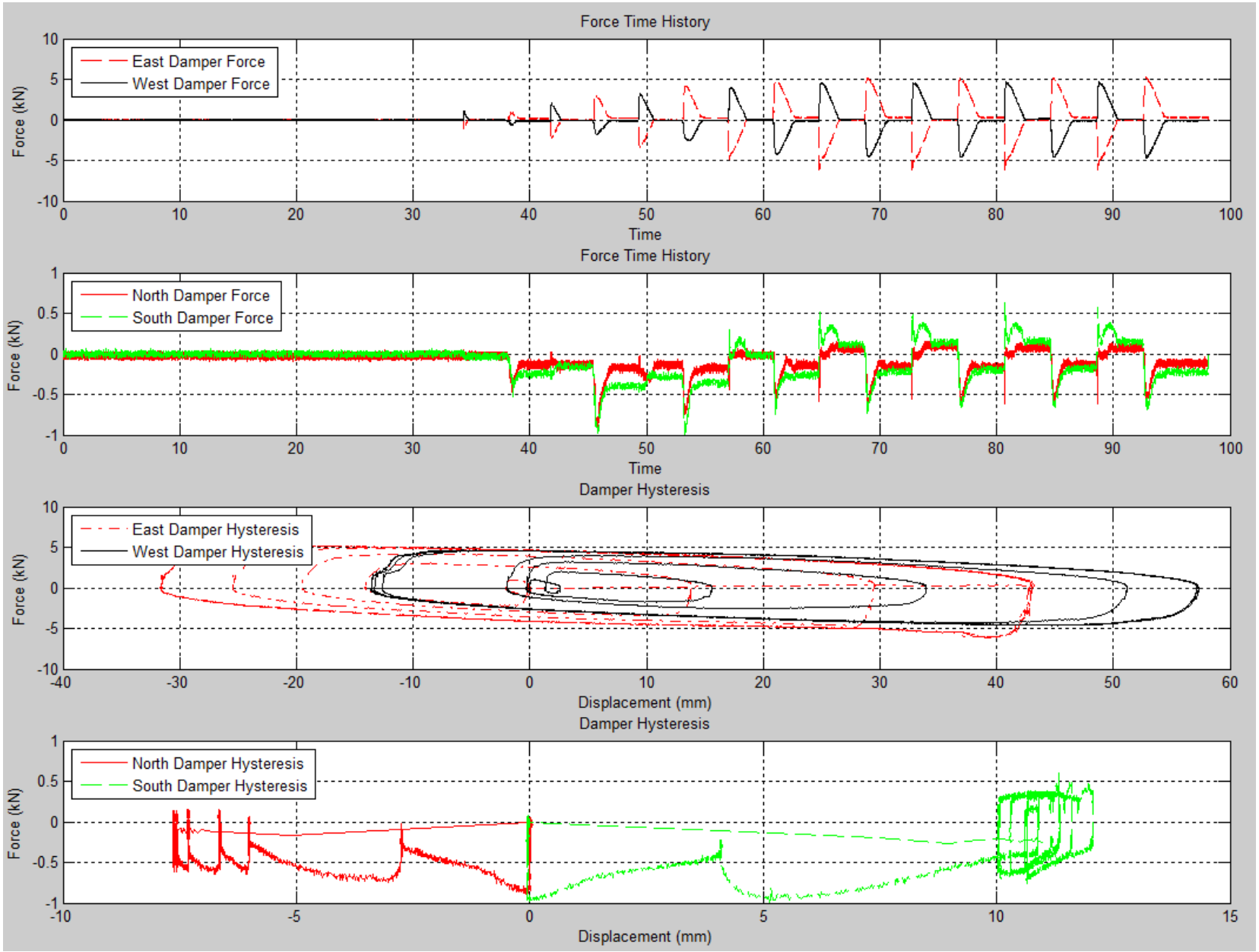
Force Time History
East Damper Force
West Damper Force
Force (kN)
Time
Force Time History
North Damper Force
South Damper Force
Force (kN)
Time
Damper Hysteresis
East Damper Hysteresis
West Damper Hysteresis
Force (kN)
Displacement (mm)
Damper Hysteresis
North Damper Hysteresis
South Damper Hysteresis
Force (kN)
Displacement (mm)

Load Case 22 (T5CCW-E2-0.2Hz-+/-4.0-Sine):

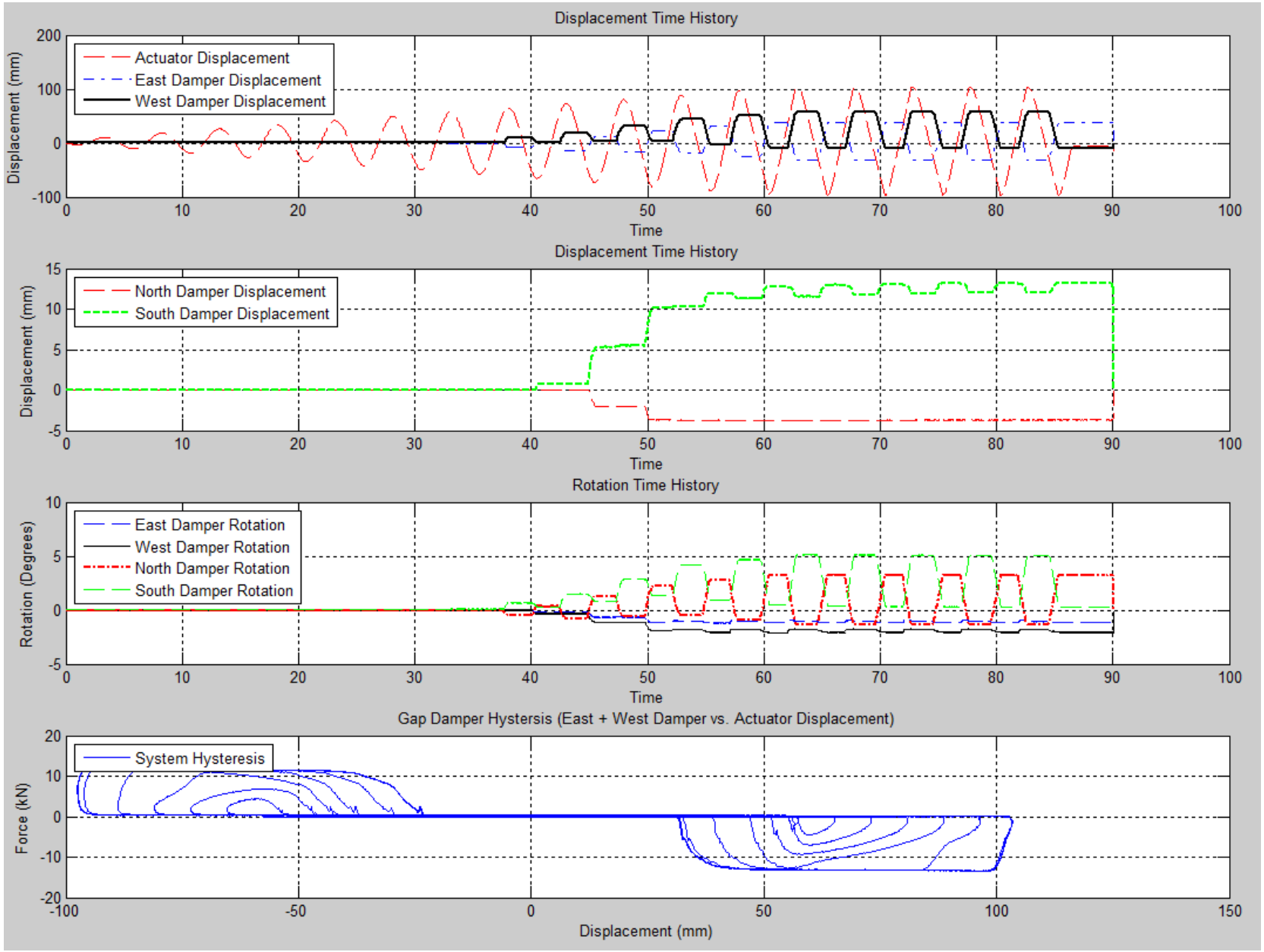

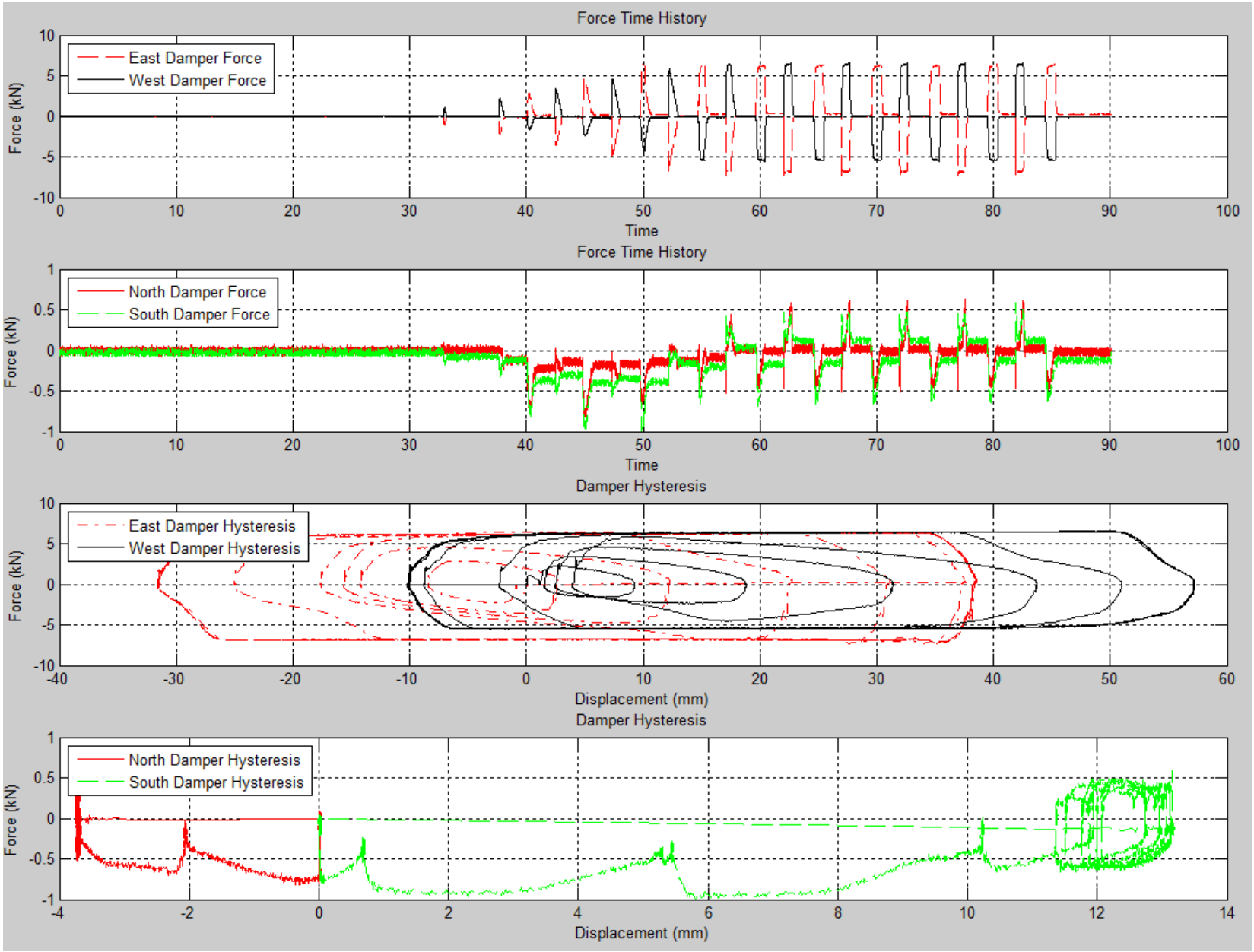
Force Time History
East Damper Force
West Damper Force
Force (kN)
Time
Force Time History
North Damper Force
South Damper Force
Force (kN)
Time
Damper Hysteresis
East Damper Hysteresis
West Damper Hysteresis
Force (kN)
Displacement (mm)
Damper Hysteresis
North Damper Hysteresis
South Damper Hysteresis
Force (kN)
Displacement (mm)

Load Case 23 (T5CW-E2-0.125Hz-+/-4.0-Sine):

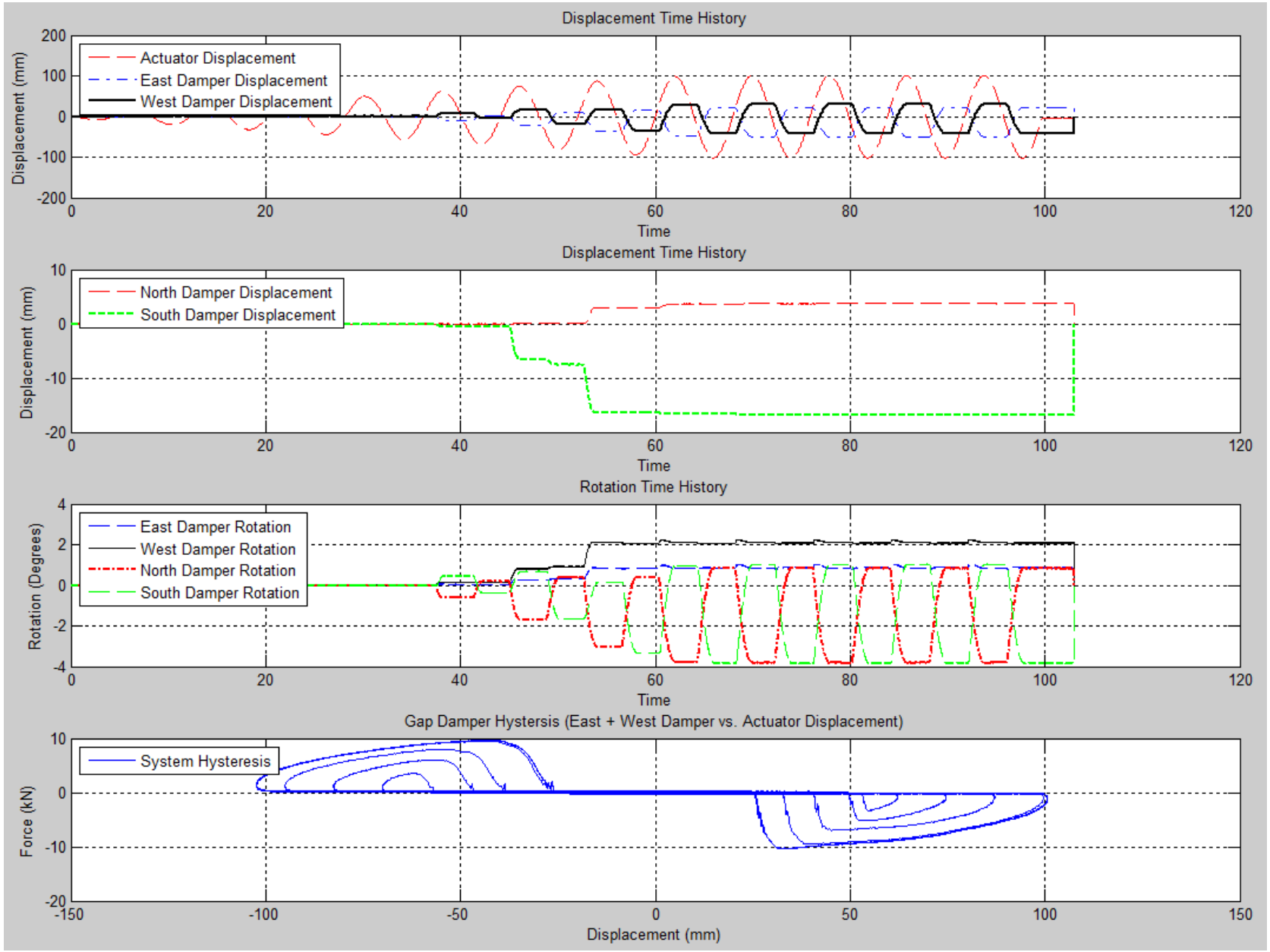

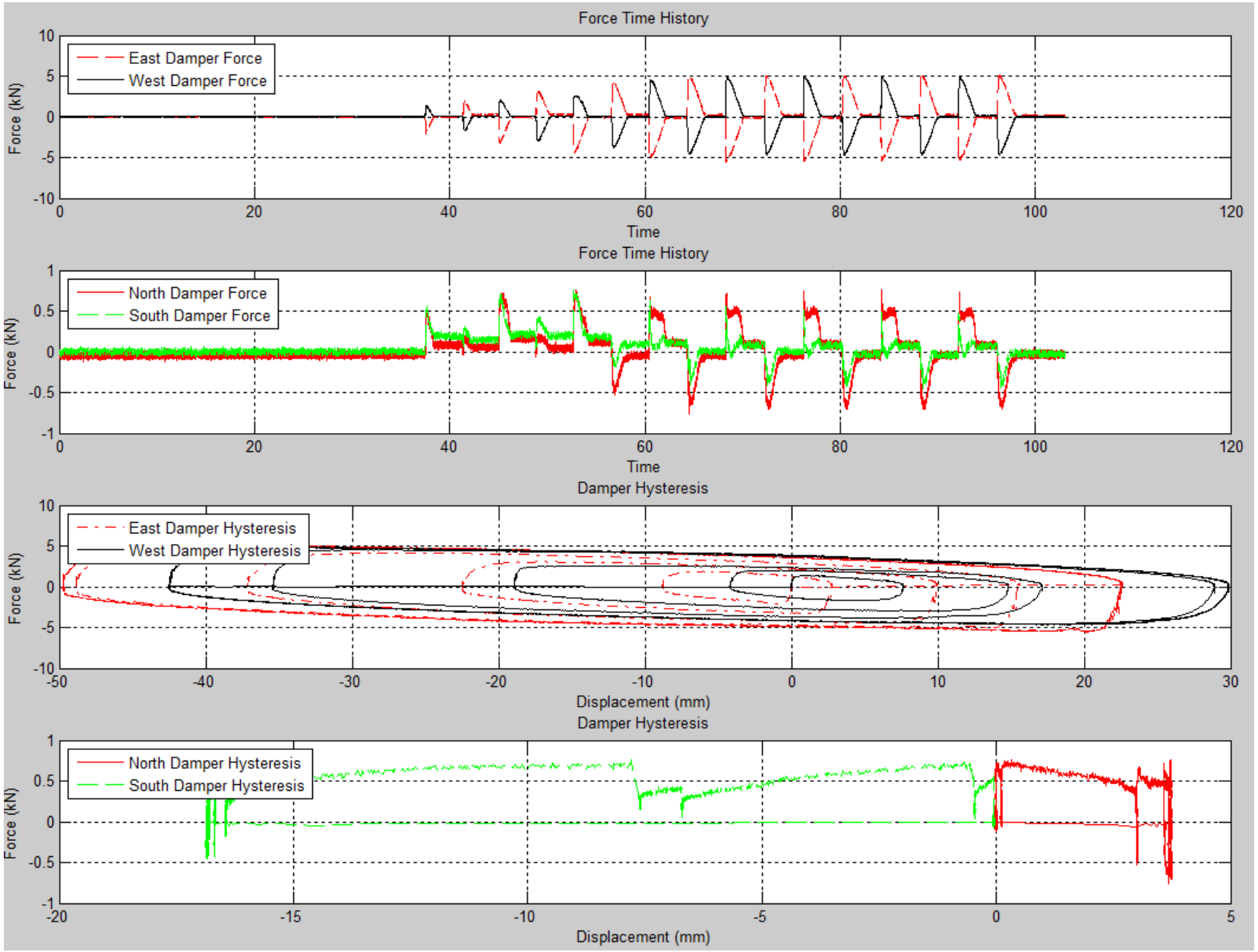
Force Time History
East Damper Force
West Damper Force
Force (kN)
Time
Force Time History
North Damper Force
South Damper Force
Force (kN)
Time
Damper Hysteresis
East Damper Hysteresis
West Damper Hysteresis
Force (kN)
Displacement (mm)
Damper Hysteresis
North Damper Hysteresis
South Damper Hysteresis
Force (kN)
Displacement (mm)

Load Case 24 (T5CW-E2-0.2Hz-+/-4.0-Sine):

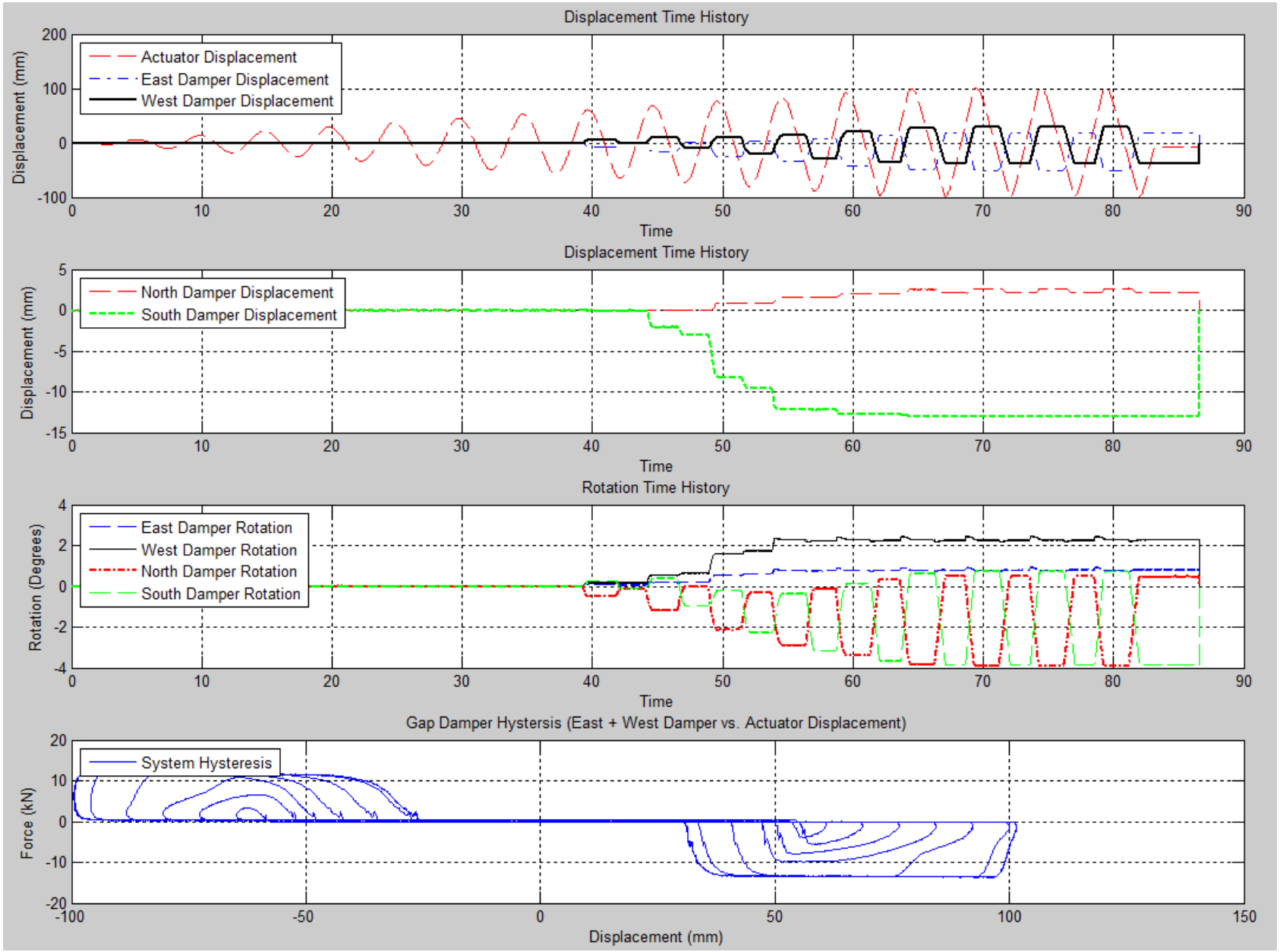

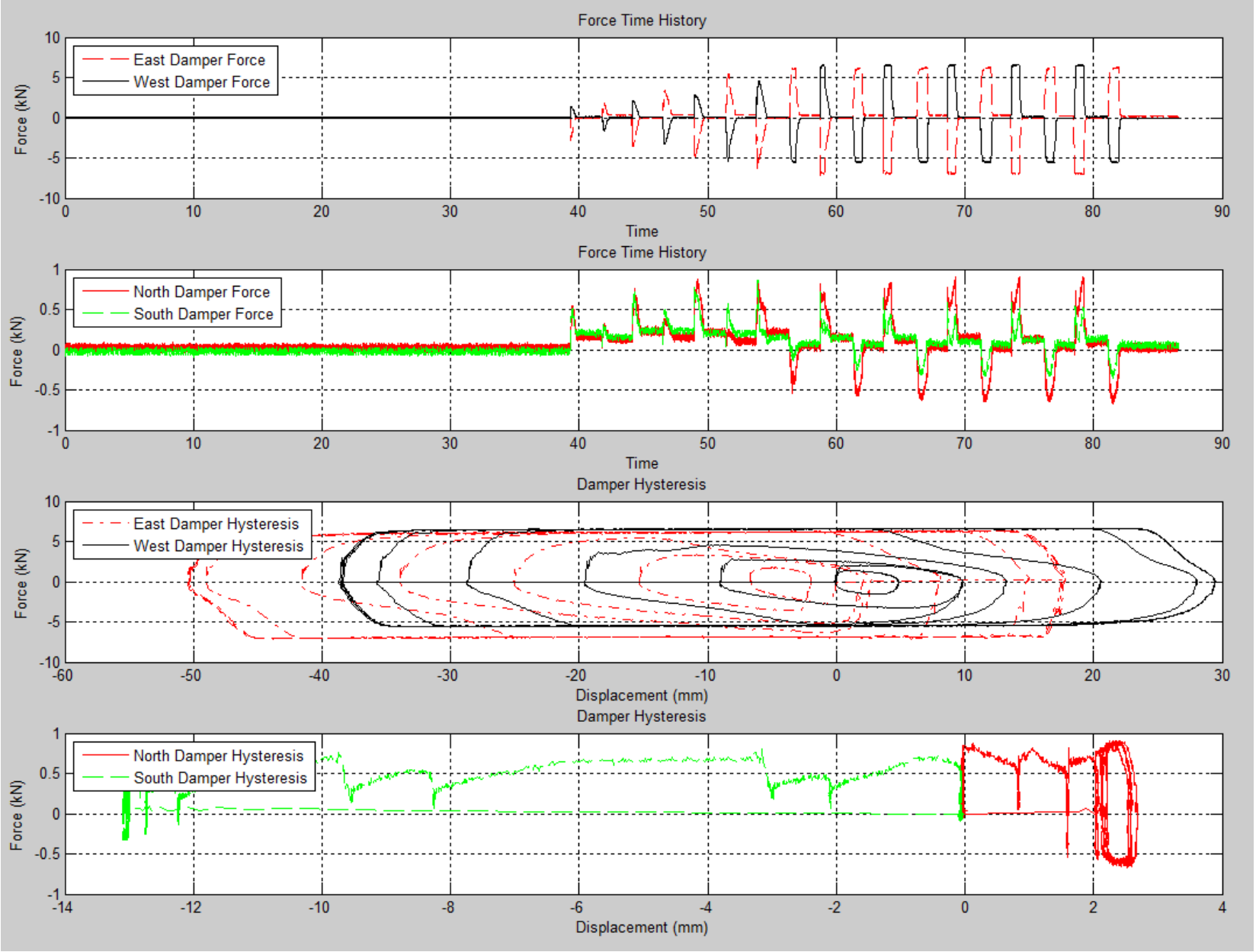
Force Time History
East Damper Force
West Damper Force
Force (kN)
Time
Force Time History
North Damper Force
South Damper Force
Force (kN)
Time
Damper Hysteresis
East Damper Hysteresis
West Damper Hysteresis
Force (kN)
Displacement (mm)
Damper Hysteresis
North Damper Hysteresis
South Damper Hysteresis
Force (kN)
Displacement (mm)

Appendix C. Two-Phase Viscoplastic Gap Damper Trial Results

Table C-1. Load Case Appendix Arrangement

Page	Trial Name	Load Case	Input Frequency (Hz)	Actuator Displacement Range mm (in)	Rotation (5 degrees)*	Eccentricity mm (in)	Wave Form
C-2	E0-0.125Hz-+/-4.2-Sine	1	0.125	+/- 106.7 (4.2)	No	0	Sine
C-5	E0-0.2Hz-+/-4.2-Sine	2	0.2	+/- 106.7 (4.2)	No	0	Sine
C-8	T5CCW-E0-0.2Hz-+/-4.0-Sine	3	0.2	+/- 106.7 (4.2)	CCW	0	Sine
C-11	T5CW-E0-0.2Hz-+/-4.0-Sine	4	0.2	+/- 106.7 (4.2)	CW	0	Sine
C-14	E2-0.125Hz-+/-4.2-Sine	5	0.125	+/- 106.7 (4.2)	No	50.8(2)	Sine
C-17	E2-0.2Hz-+/-4.2-Sine	6	0.2	+/- 106.7 (4.2)	No	50.8(2)	Sine
C-20	T5CCW-E2-0.2Hz-+/-4.0-Sine	7	0.2	+/- 106.7 (4.2)	CCW	50.8(2)	Sine
C-23	T5CW-E2-0.2Hz-+/-4.0-Sine	8	0.2	+/- 106.7 (4.2)	CW	50.8(2)	Sine

*CW = Clockwise Rotation, CCW = Counter-Clockwise Rotation (Viewed from above)

Load Case 1 (E0-0.125Hz-+/-4.2-Sine):

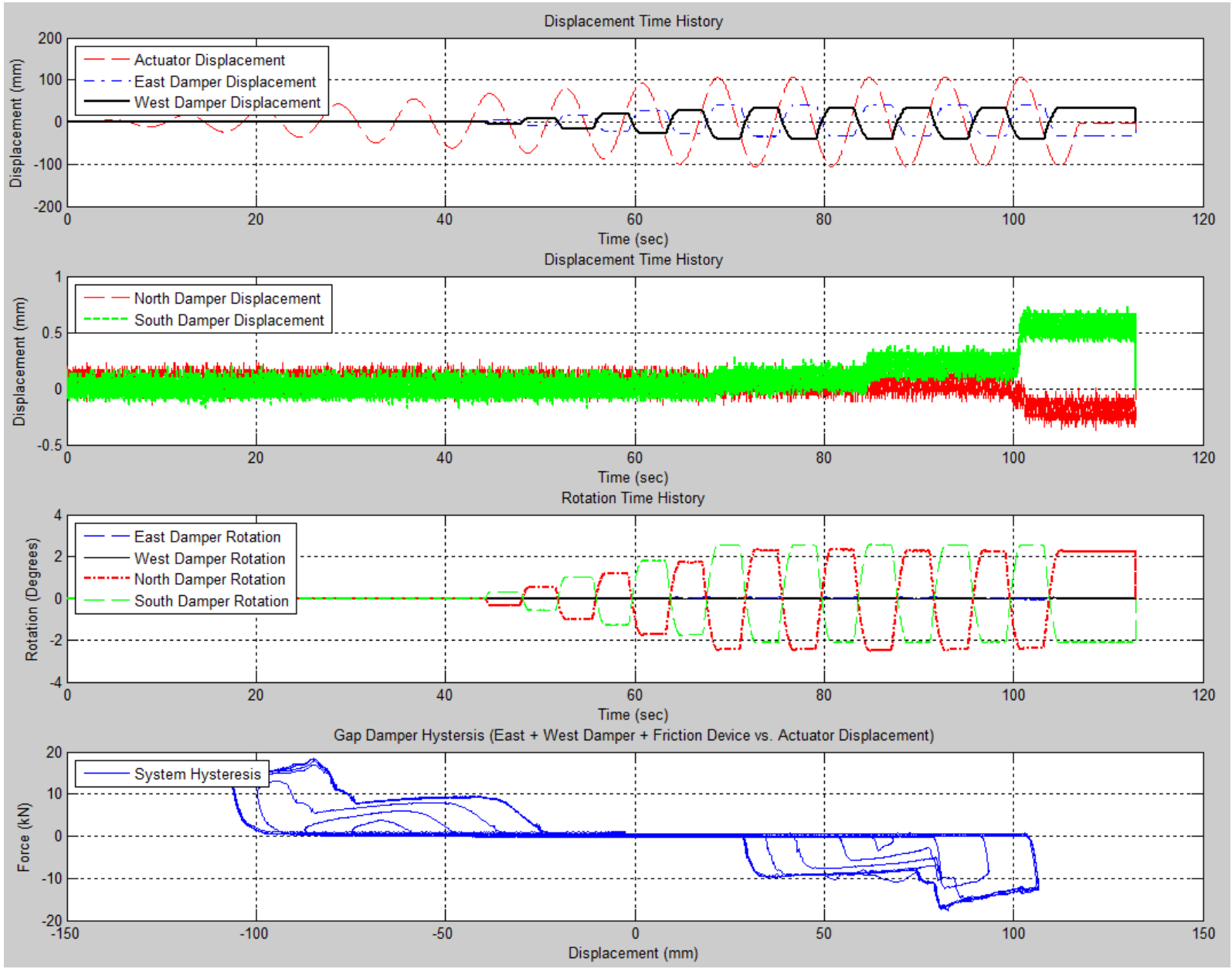

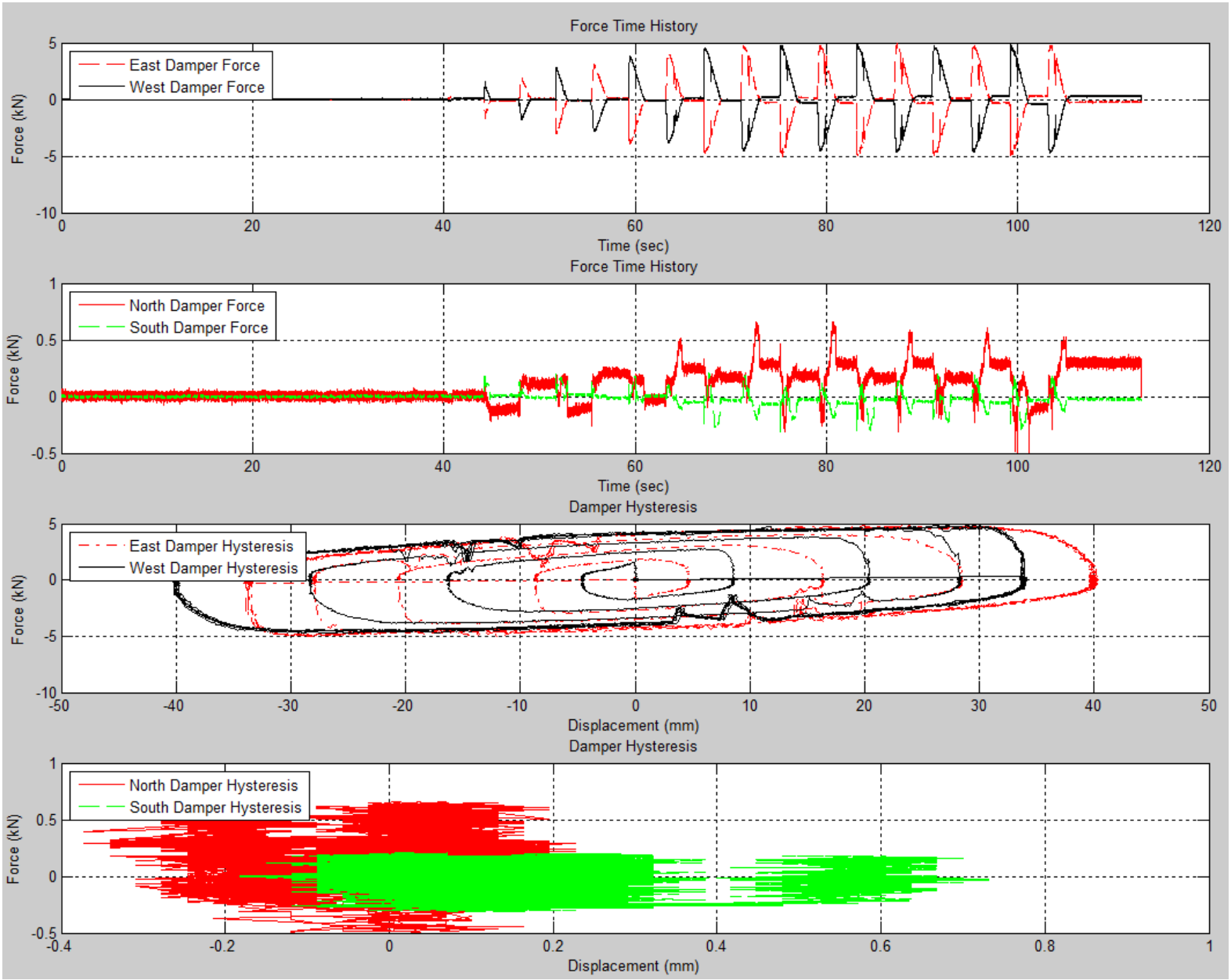
Force Time History
East Damper Force
West Damper Force
Force (kN)
Time (sec)
Force Time History
North Damper Force
South Damper Force
Force (kN)
Time (sec)
Damper Hysteresis
East Damper Hysteresis
West Damper Hysteresis
Force (kN)
Displacement (mm)
Damper Hysteresis
North Damper Hysteresis
South Damper Hysteresis
Force (kN)
Displacement (mm)

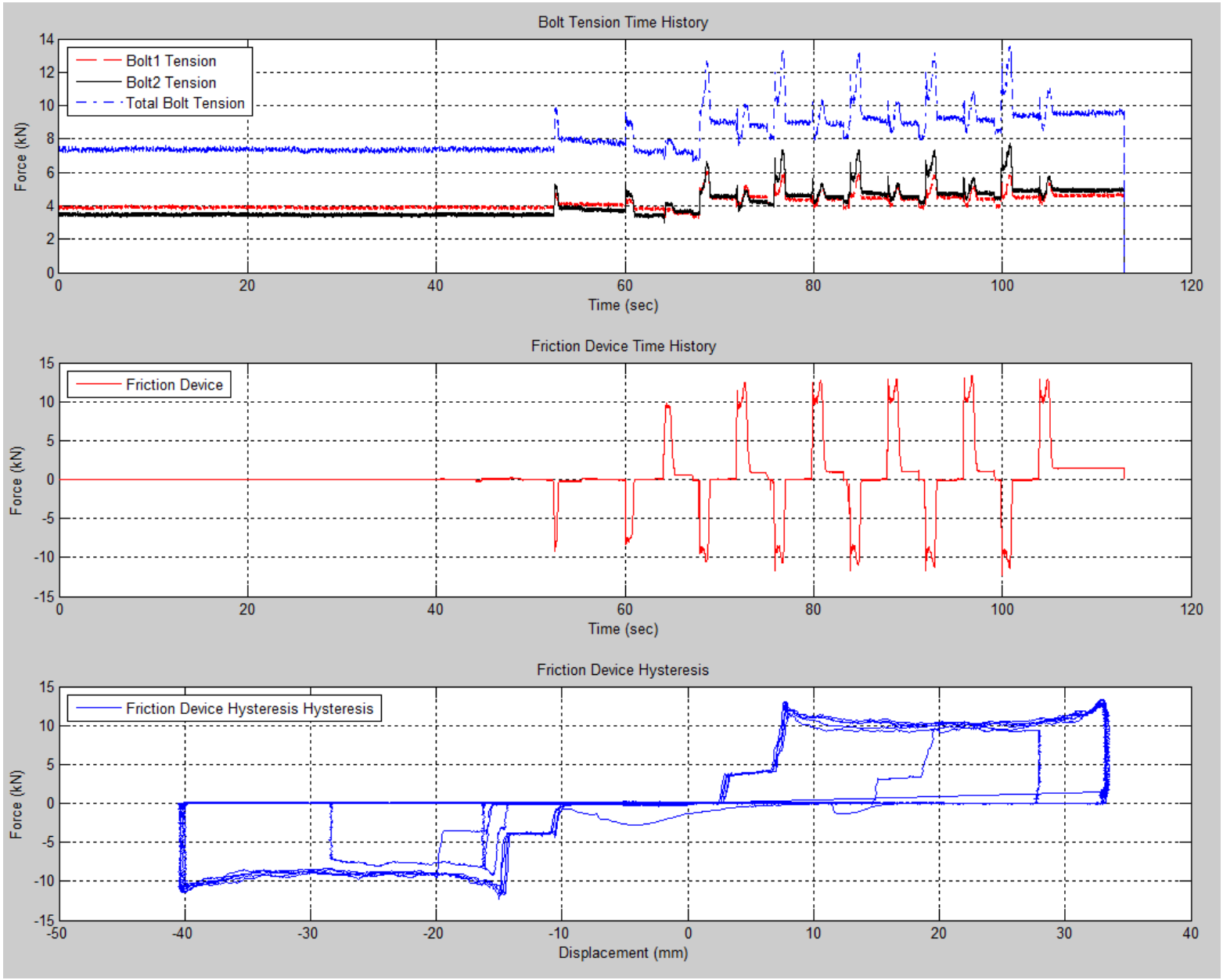
Bolt Tension Time History
Bolt1 Tension
Bolt2 Tension
Total Bolt Tension
Force (kN)
Time (sec)
Friction Device Time History
Friction Device
Force (kN)
Time (sec)
Friction Device Hysteresis
Friction Device Hysteresis Hysteresis
Force (kN)
Displacement (mm)

Load Case 2 (E0-0.2Hz-+/-4.2-Sine):

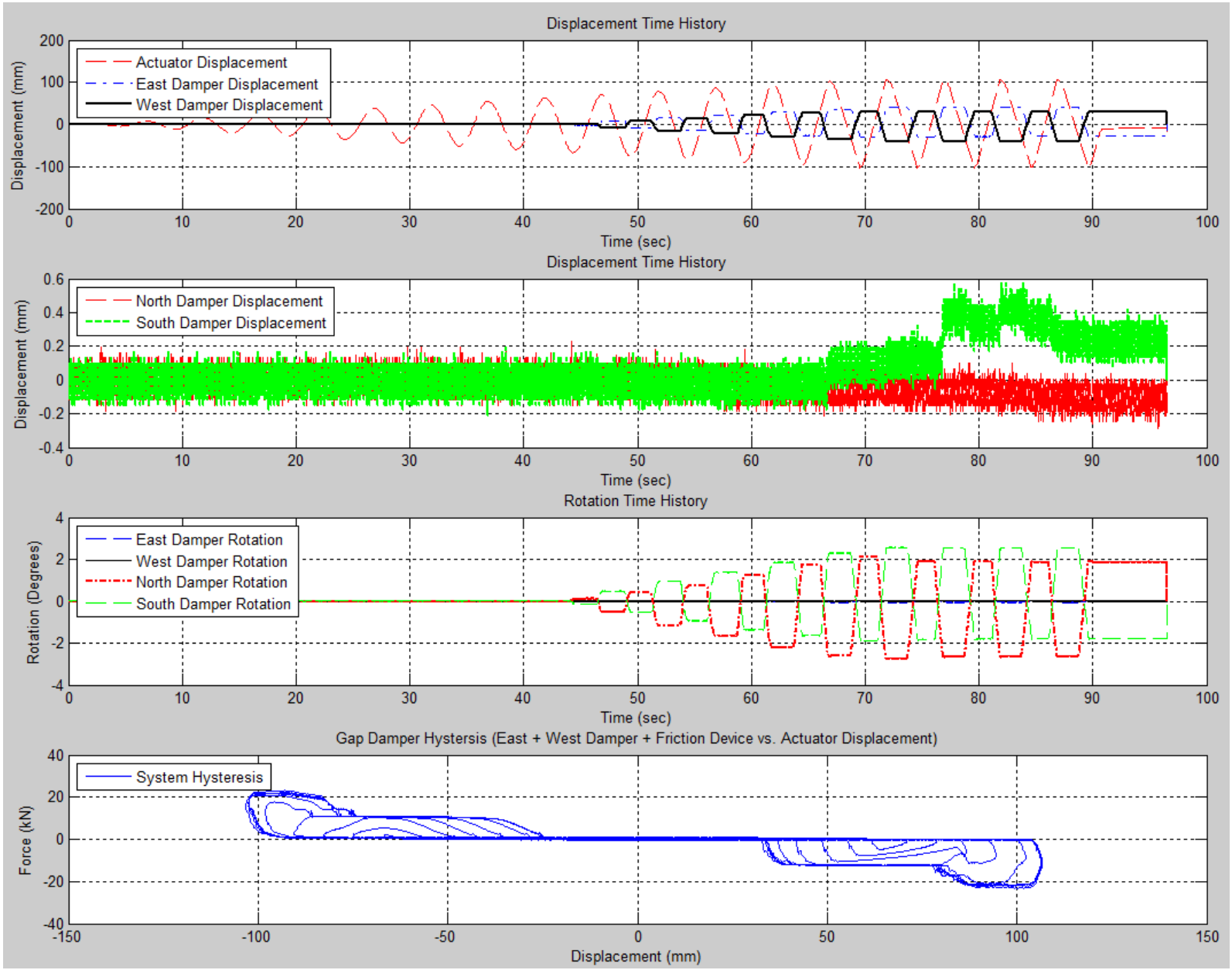

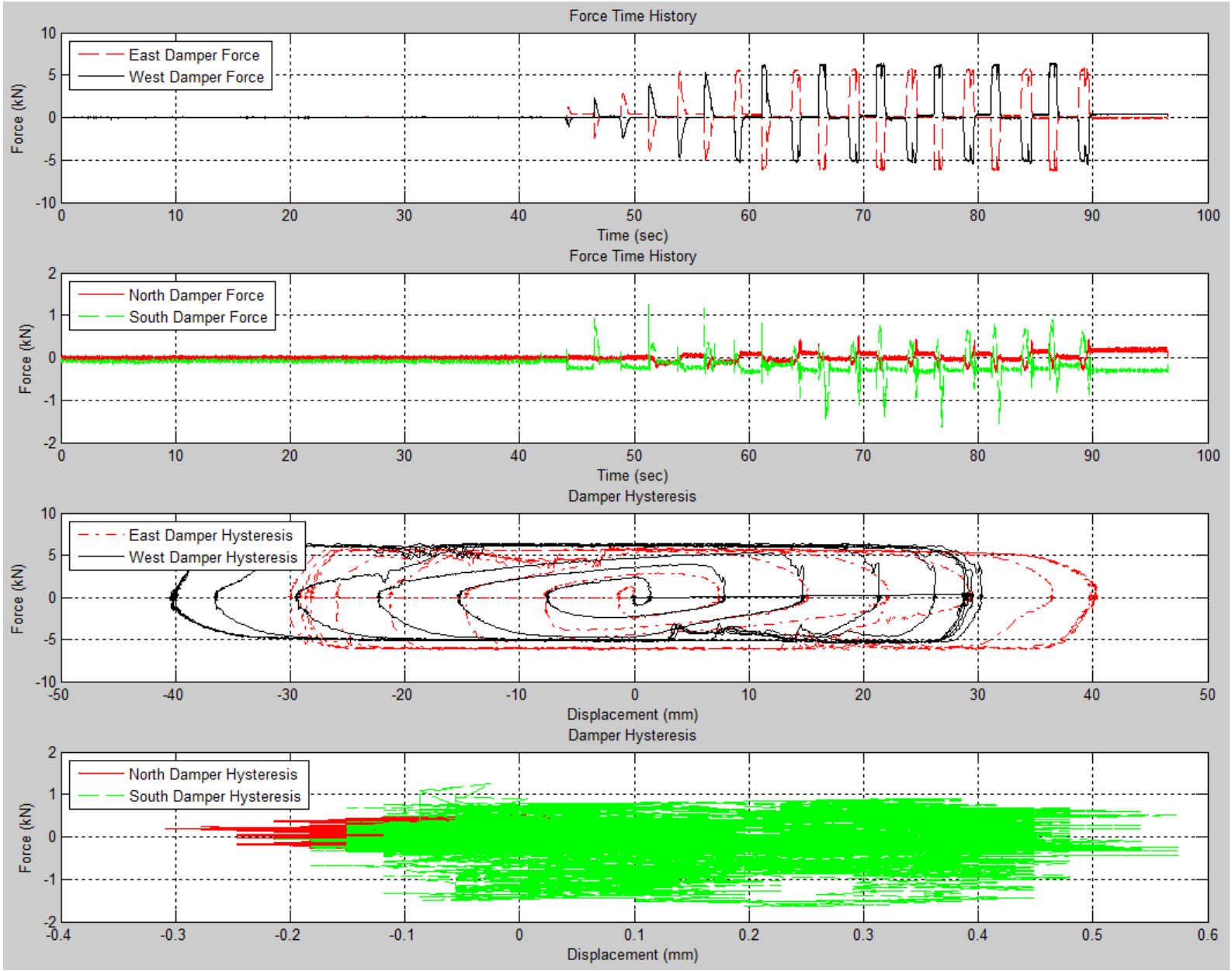
Force Time History
East Damper Force
West Damper Force
Force (kN)
Time (sec)
Force Time History
North Damper Force
South Damper Force
Force (kN)
Time (sec)
Damper Hysteresis
East Damper Hysteresis
West Damper Hysteresis
Force (kN)
Displacement (mm)
Damper Hysteresis
North Damper Hysteresis
South Damper Hysteresis
Force (kN)
Displacement (mm)

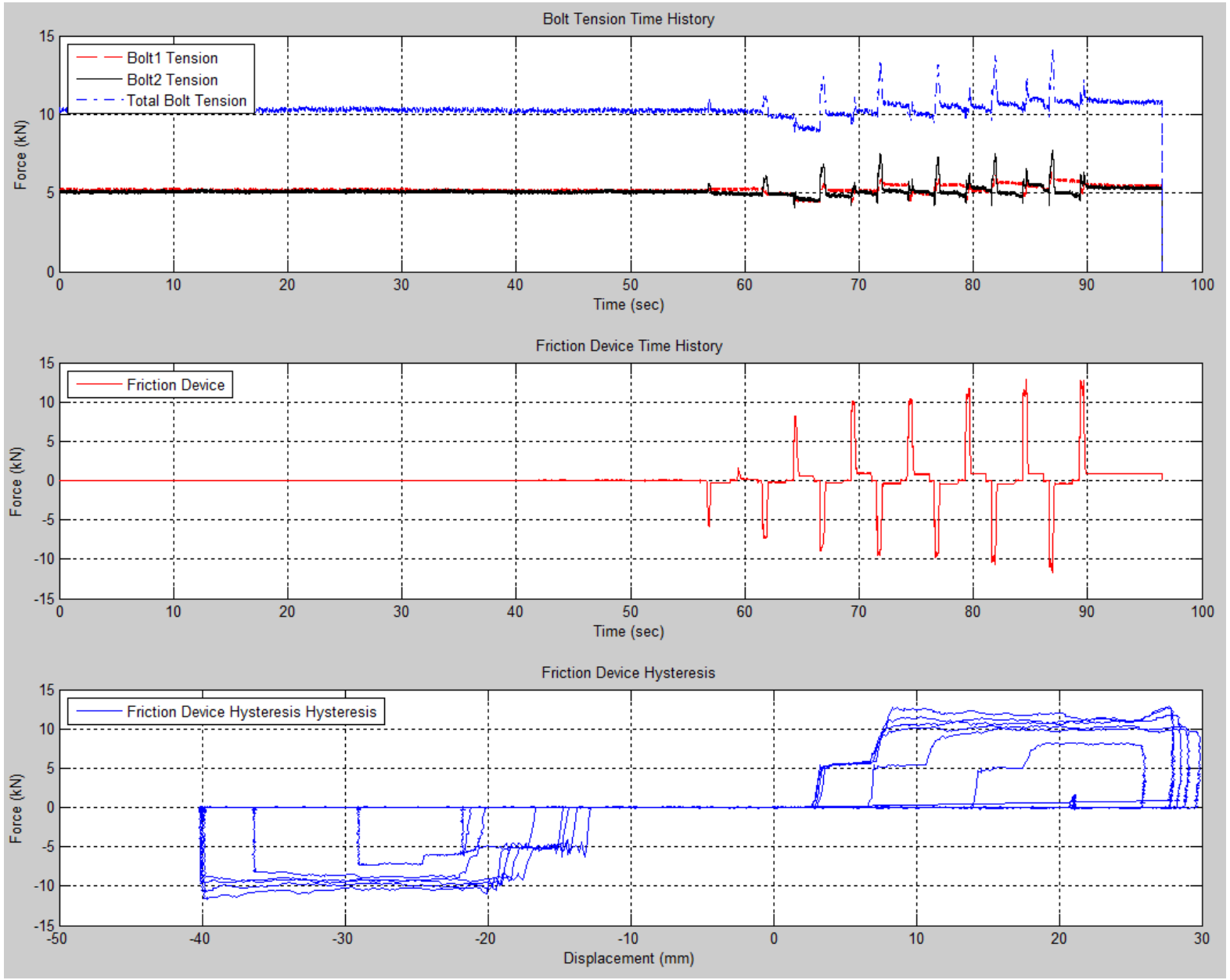
Bolt Tension Time History
Bolt1 Tension
Bolt2 Tension
Total Bolt Tension
Force (kN)
Time (sec)
Friction Device Time History
Friction Device
Force (kN)
Time (sec)
Friction Device Hysteresis
Friction Device Hysteresis Hysteresis
Force (kN)
Displacement (mm)

Load Case 3 (T5CCW-E0-0.2Hz-+/-4.0-Sine):

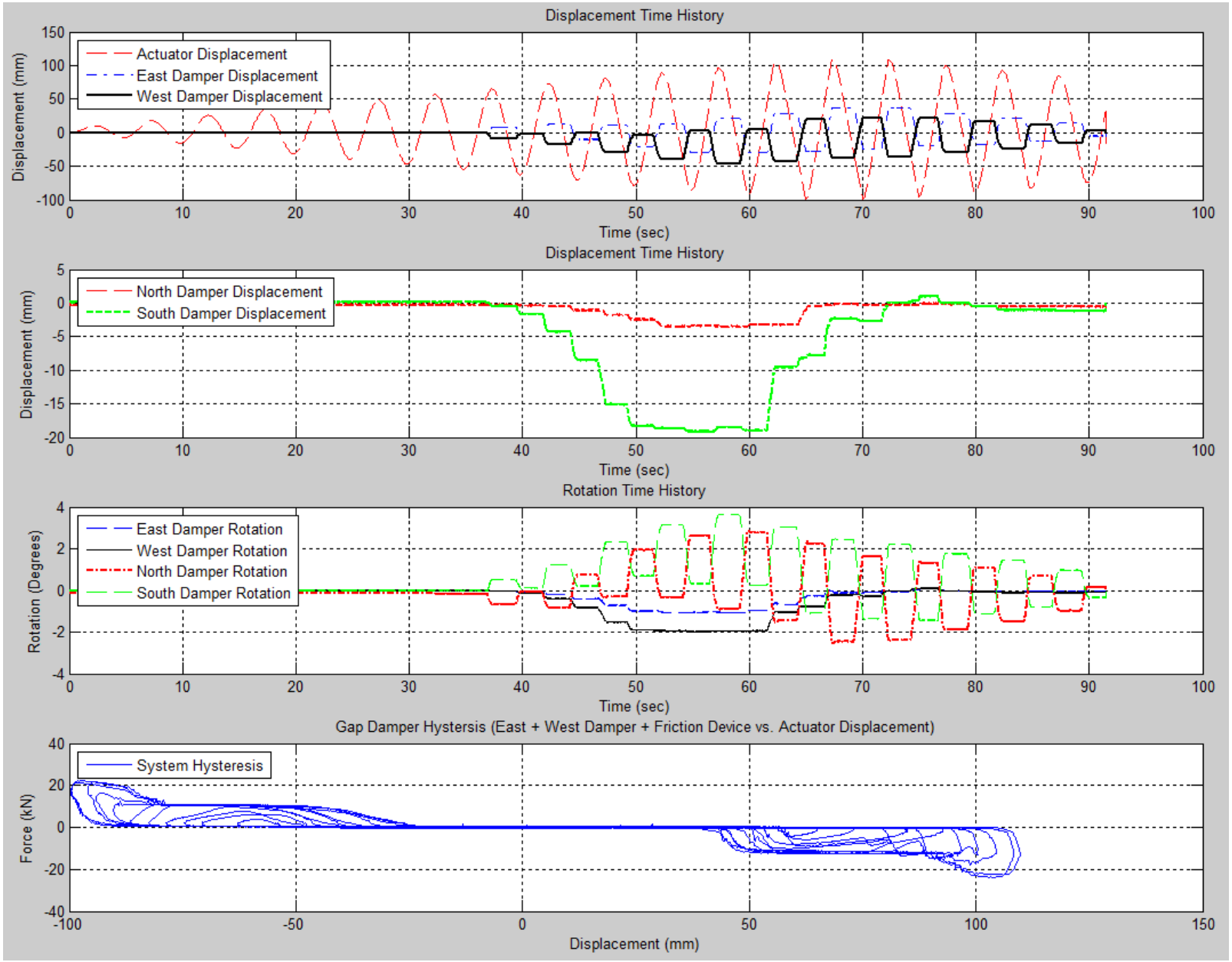

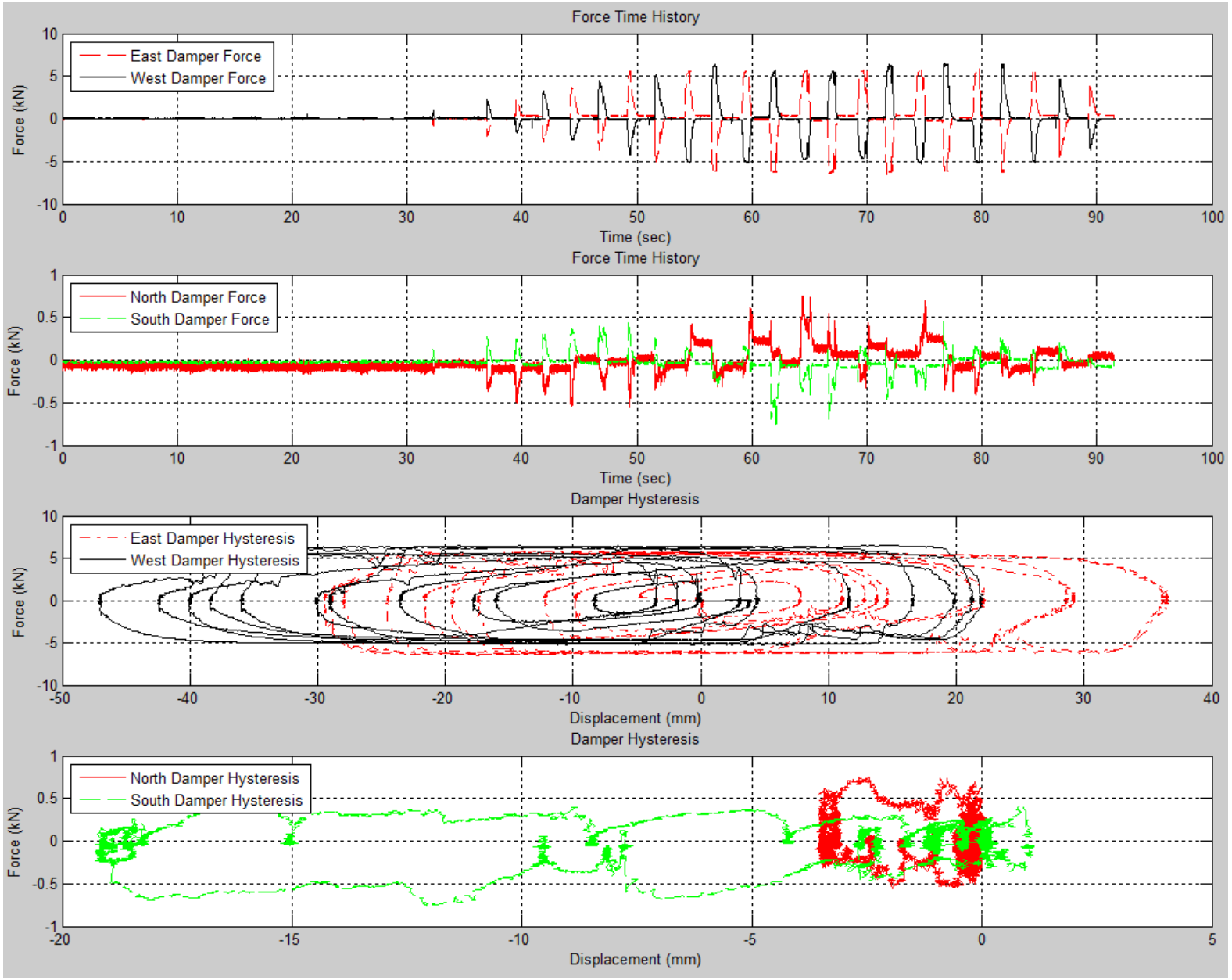
Force Time History
East Damper Force
West Damper Force
Force (kN)
Time (sec)
Force Time History
North Damper Force
South Damper Force
Force (kN)
Time (sec)
Damper Hysteresis
East Damper Hysteresis
West Damper Hysteresis
Force (kN)
Displacement (mm)
Damper Hysteresis
North Damper Hysteresis
South Damper Hysteresis
Force (kN)
Displacement (mm)

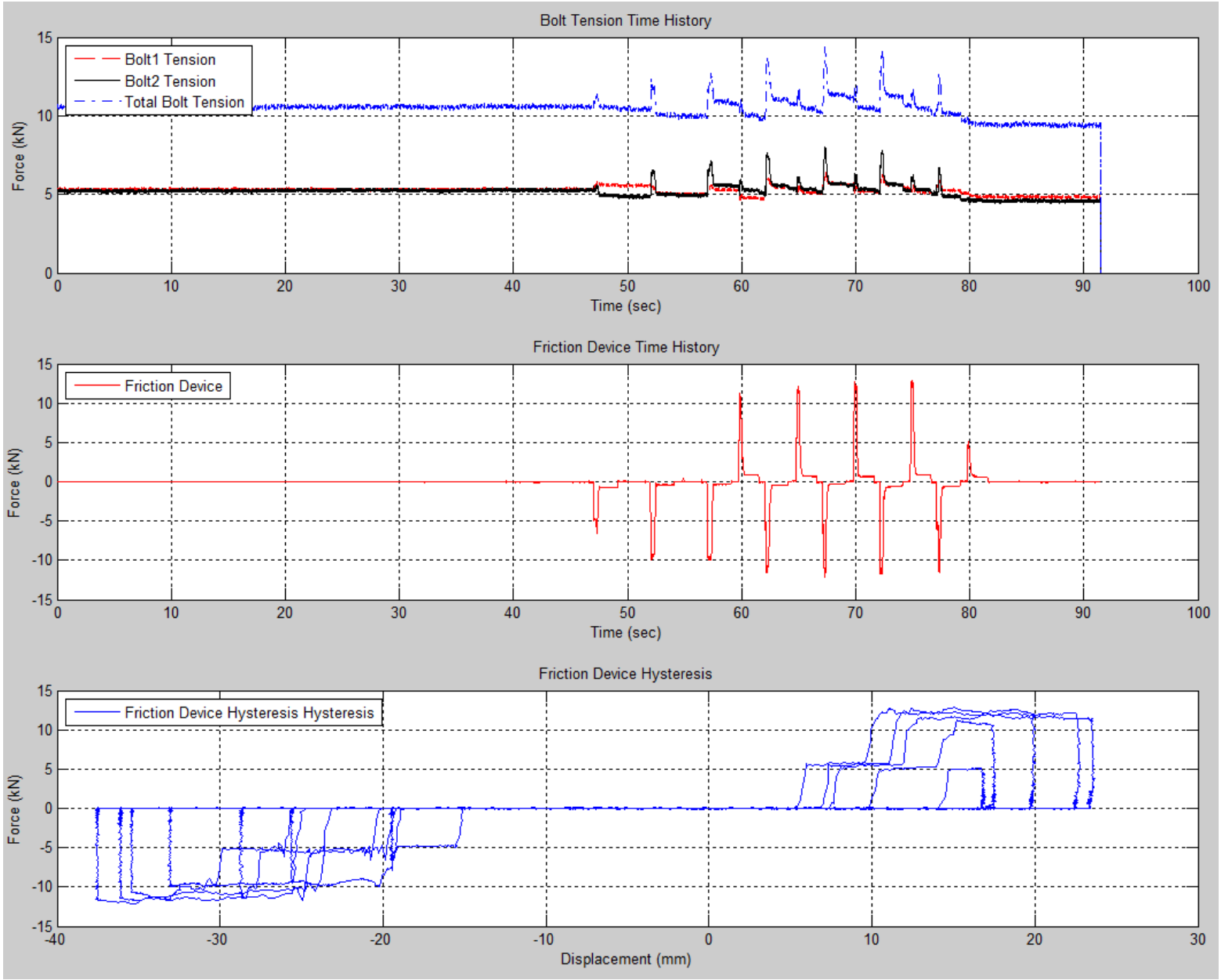
Bolt Tension Time History
Bolt1 Tension
Bolt2 Tension
Total Bolt Tension
Force (kN)
Time (sec)
Friction Device Time History
Friction Device
Force (kN)
Time (sec)
Friction Device Hysteresis
Friction Device Hysteresis Hysteresis
Force (kN)
Displacement (mm)

Load Case 4 (T5CW-E0-0.2Hz-+/-4.0-Sine):

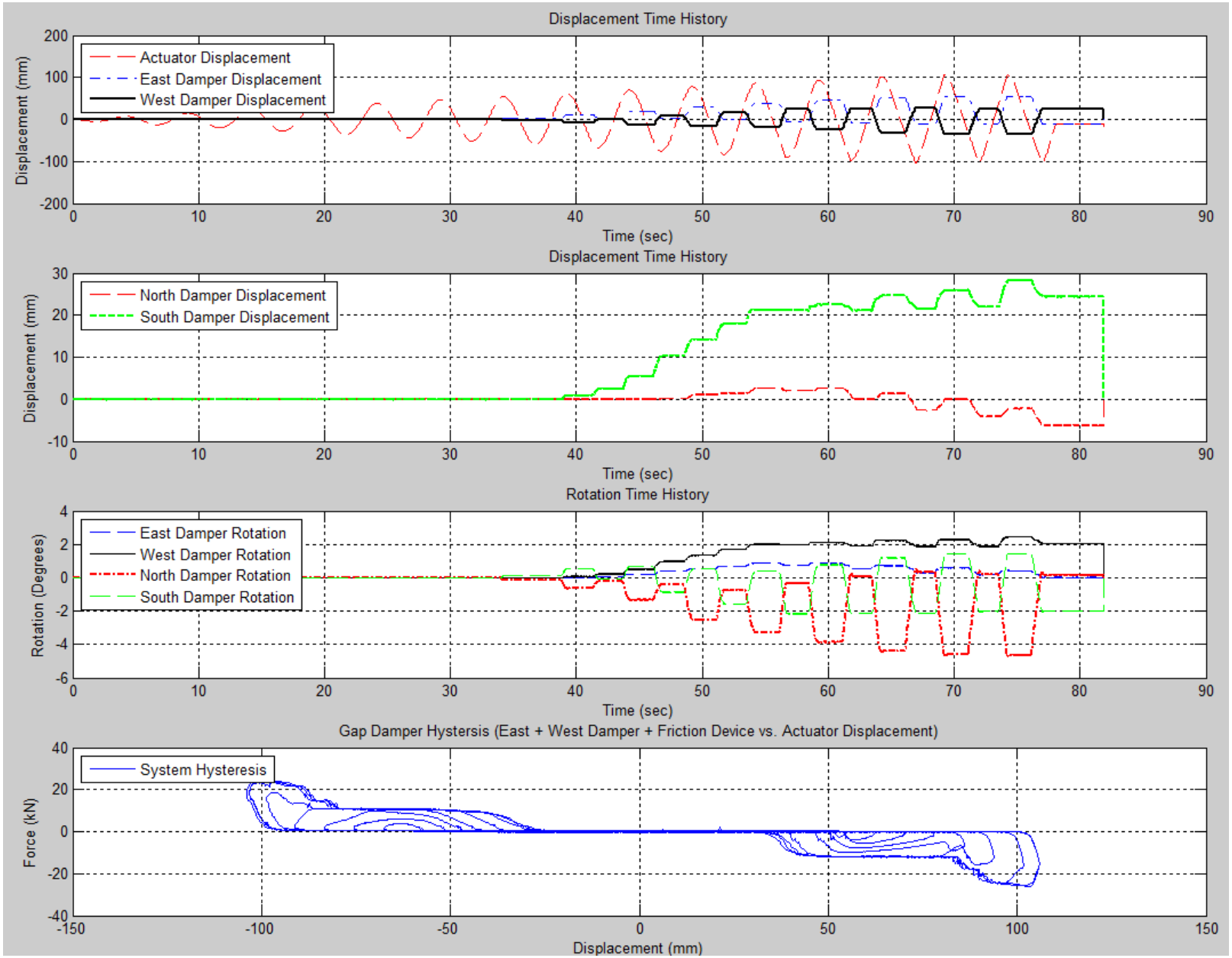

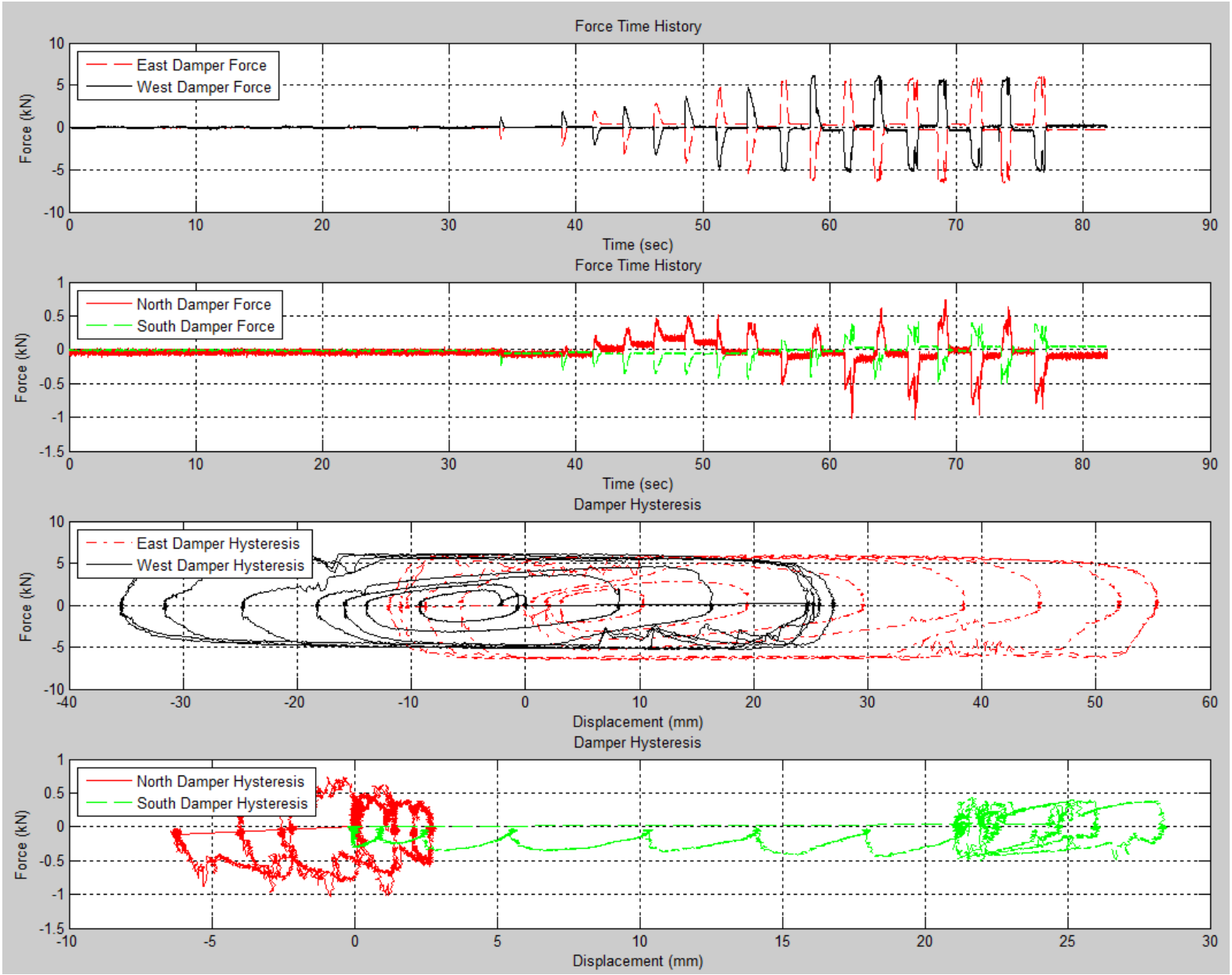
Force Time History
East Damper Force
West Damper Force
Force (kN)
Time (sec)
Force Time History
North Damper Force
South Damper Force
Force (kN)
Time (sec)
Damper Hysteresis
East Damper Hysteresis
West Damper Hysteresis
Force (kN)
Displacement (mm)
Damper Hysteresis
North Damper Hysteresis
South Damper Hysteresis
Force (kN)
Displacement (mm)

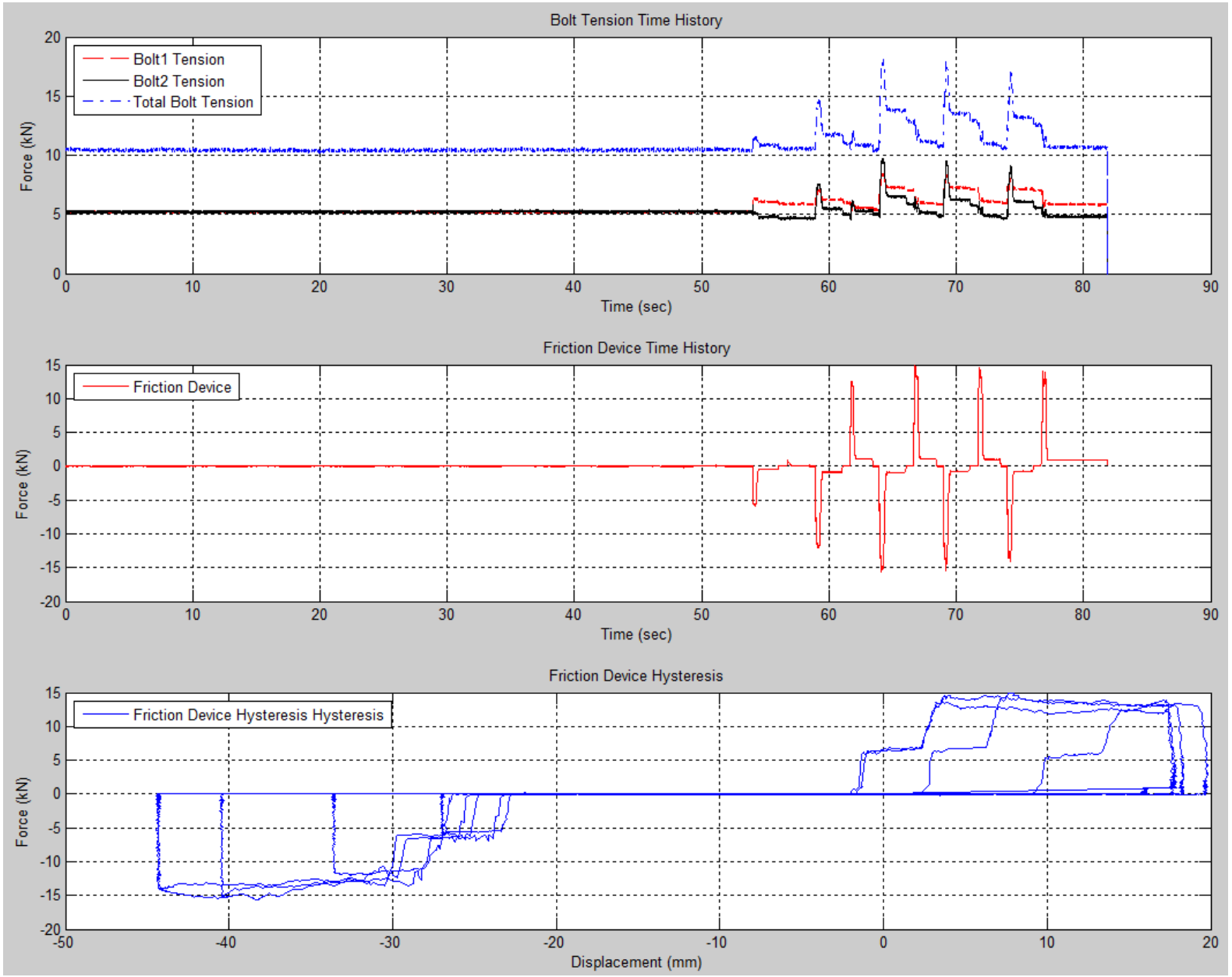
Bolt Tension Time History
Bolt1 Tension
Bolt2 Tension
Total Bolt Tension
Force (kN)
Time (sec)
Friction Device Time History
Friction Device
Force (kN)
Time (sec)
Friction Device Hysteresis
Friction Device Hysteresis Hysteresis
Force (kN)
Displacement (mm)

Load Case 5 (E2-0.125Hz-+/-4.2-Sine):

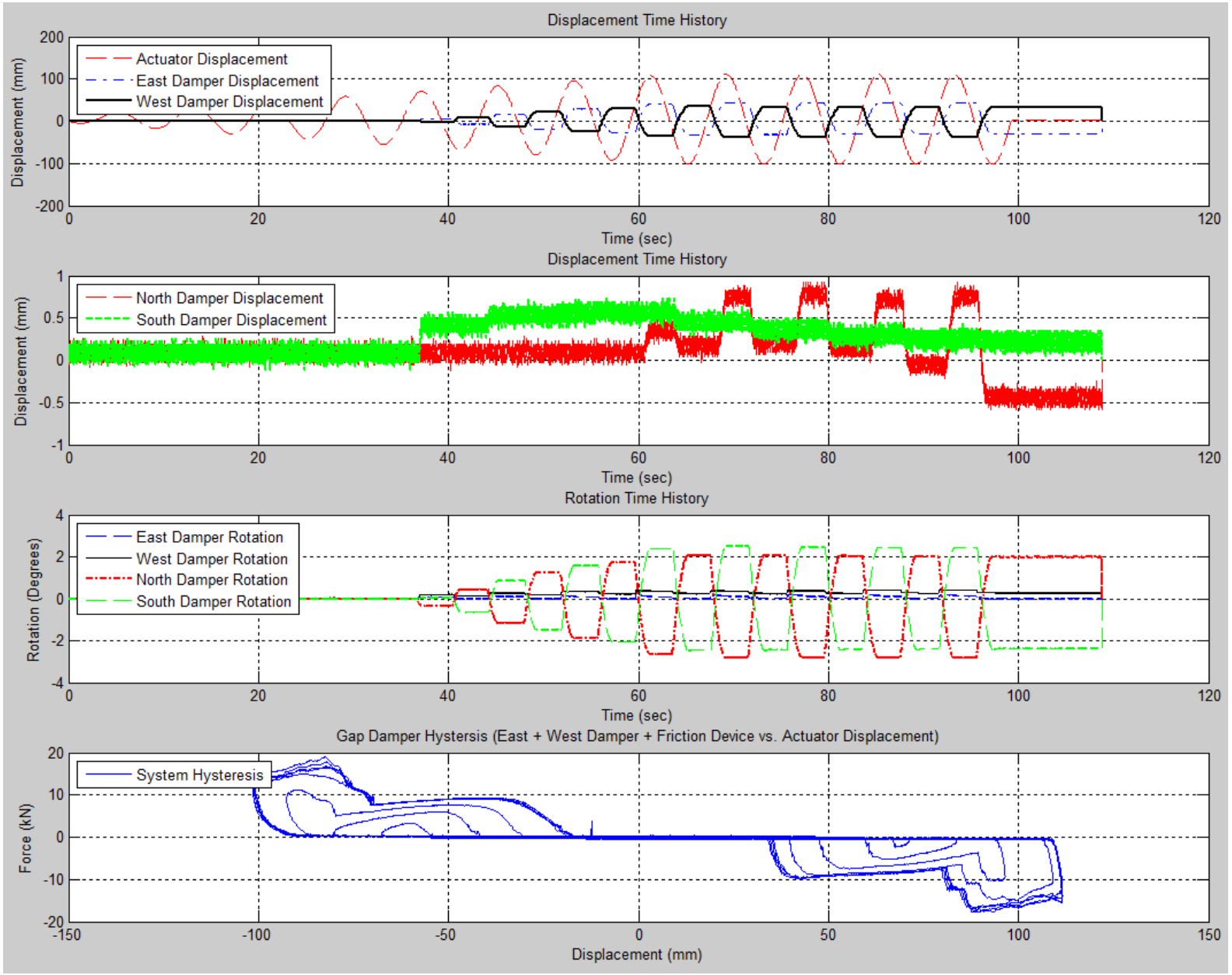

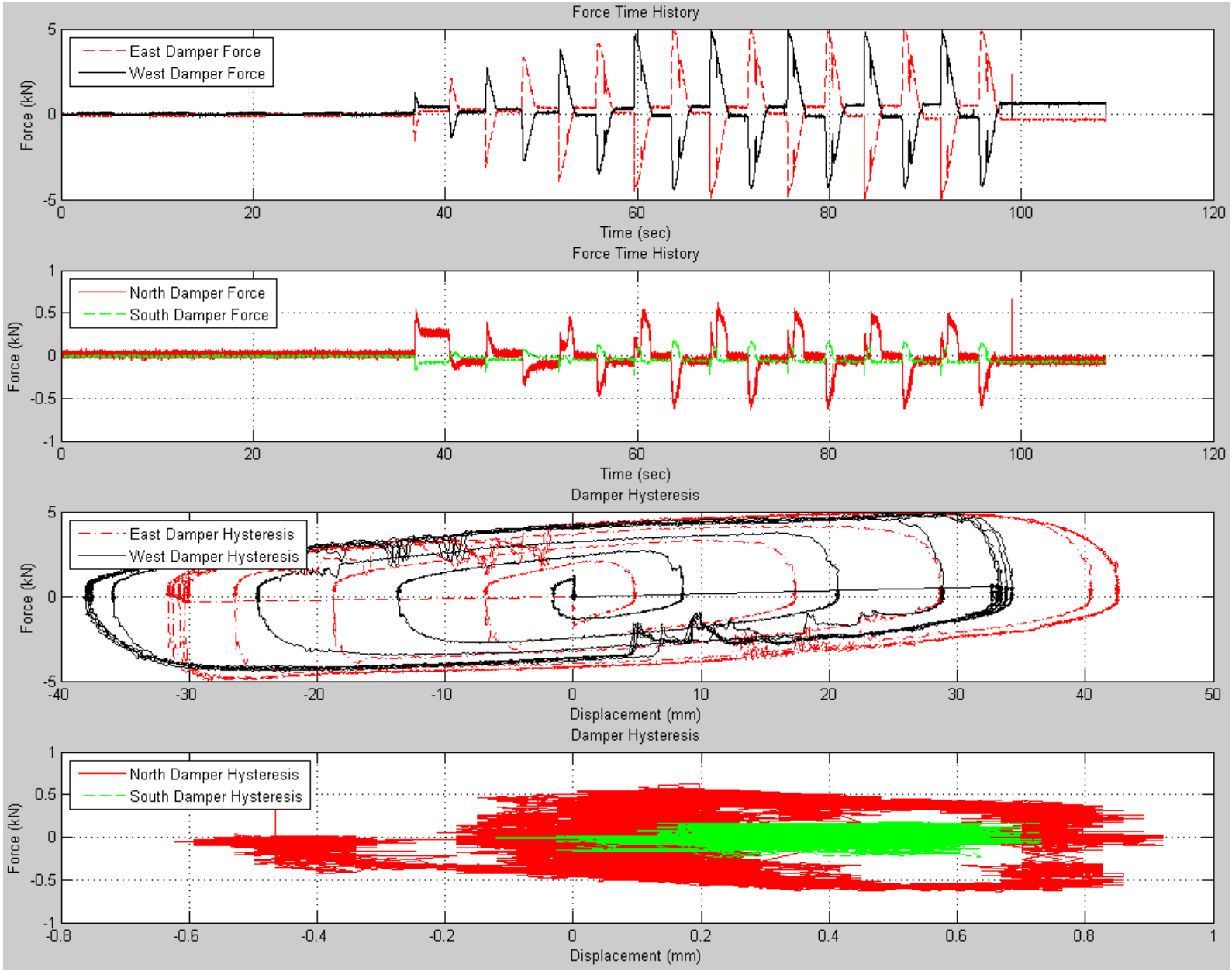
Force Time History
East Damper Force
West Damper Force
Force (kN)
Time (sec)
Force Time History
North Damper Force
South Damper Force
Force (kN)
Time (sec)
Damper Hysteresis
East Damper Hysteresis
West Damper Hysteresis
Force (kN)
Displacement (mm)
Damper Hysteresis
North Damper Hysteresis
South Damper Hysteresis
Force (kN)
Displacement (mm)

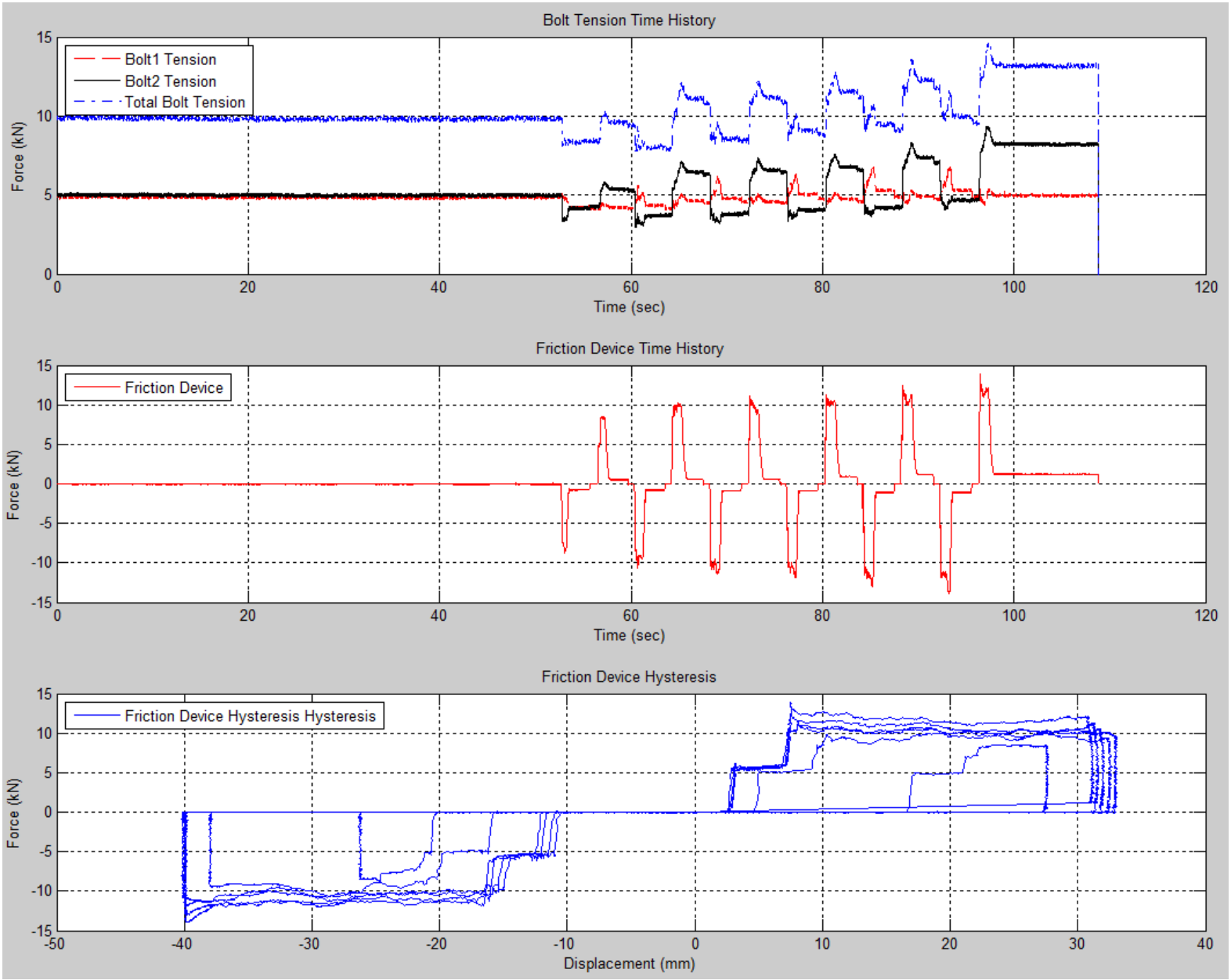
Bolt Tension Time History
Bolt1 Tension
Bolt2 Tension
Total Bolt Tension
Force (kN)
Time (sec)
Friction Device Time History
Friction Device
Force (kN)
Time (sec)
Friction Device Hysteresis
Friction Device Hysteresis Hysteresis
Force (kN)
Displacement (mm)

Load Case 6 (E2-0.2Hz-+/-4.2-Sine):

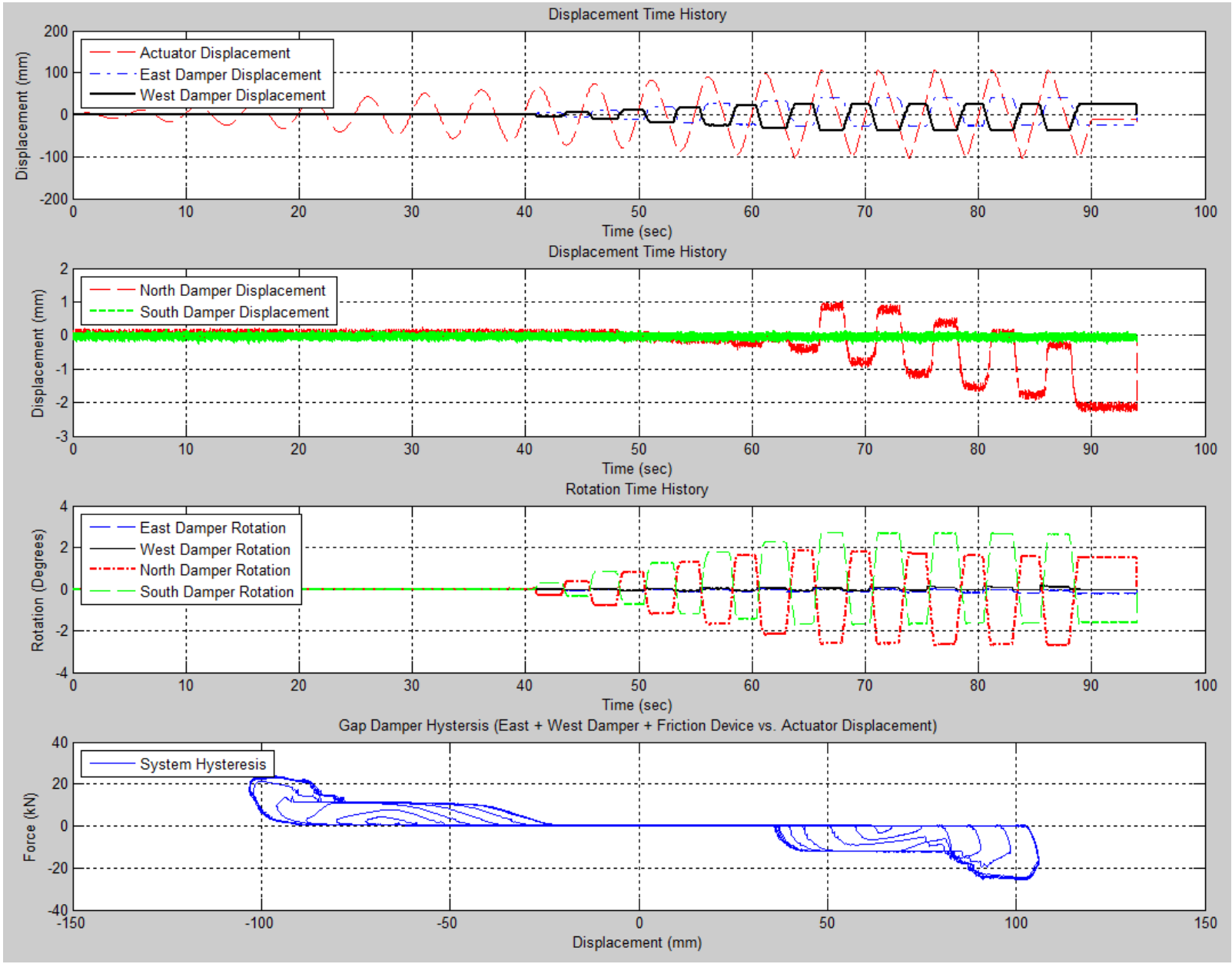

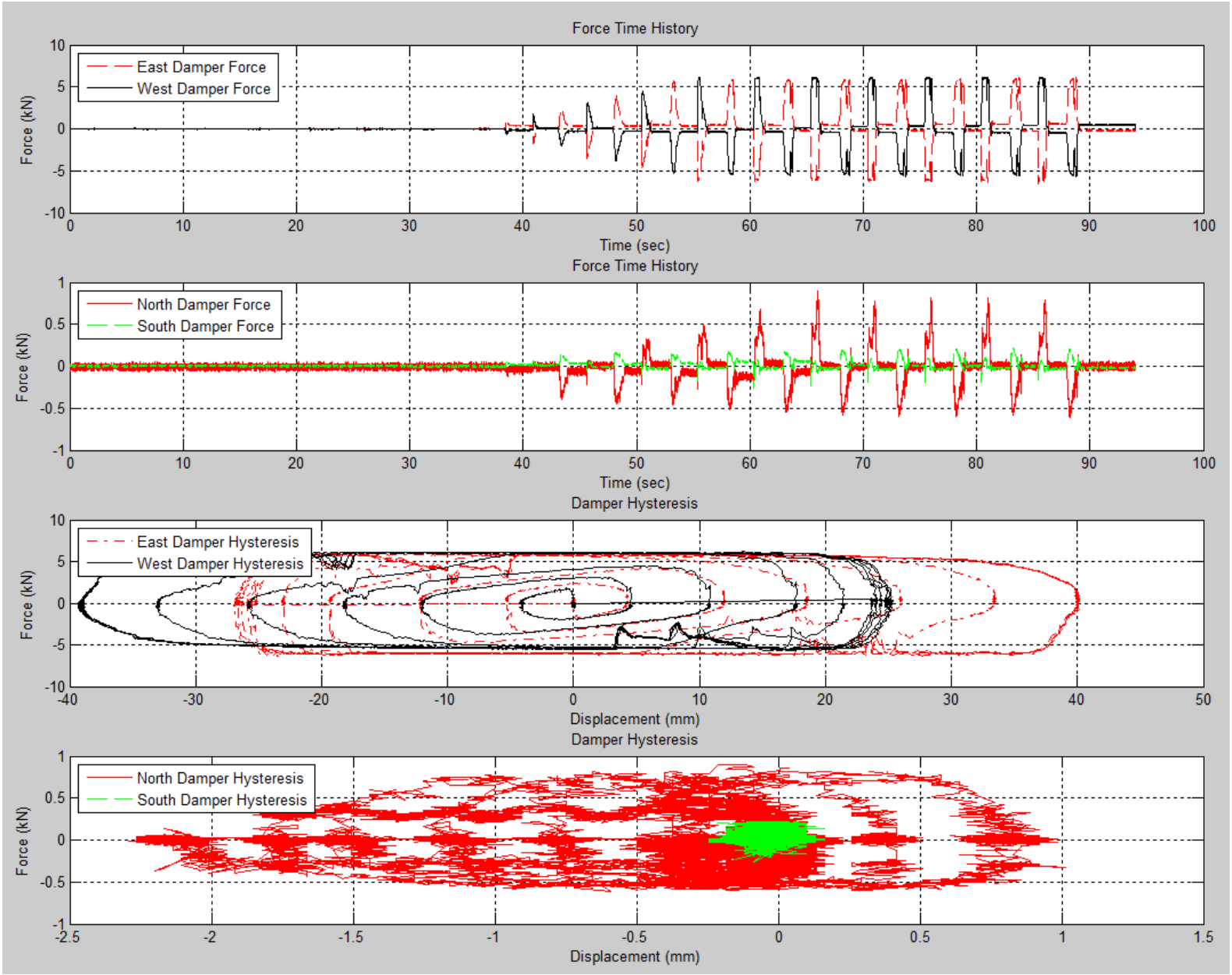
Force Time History
East Damper Force
West Damper Force
Force (kN)
Time (sec)
Force Time History
North Damper Force
South Damper Force
Force (kN)
Time (sec)
Damper Hysteresis
East Damper Hysteresis
West Damper Hysteresis
Force (kN)
Displacement (mm)
Damper Hysteresis
North Damper Hysteresis
South Damper Hysteresis
Force (kN)
Displacement (mm)

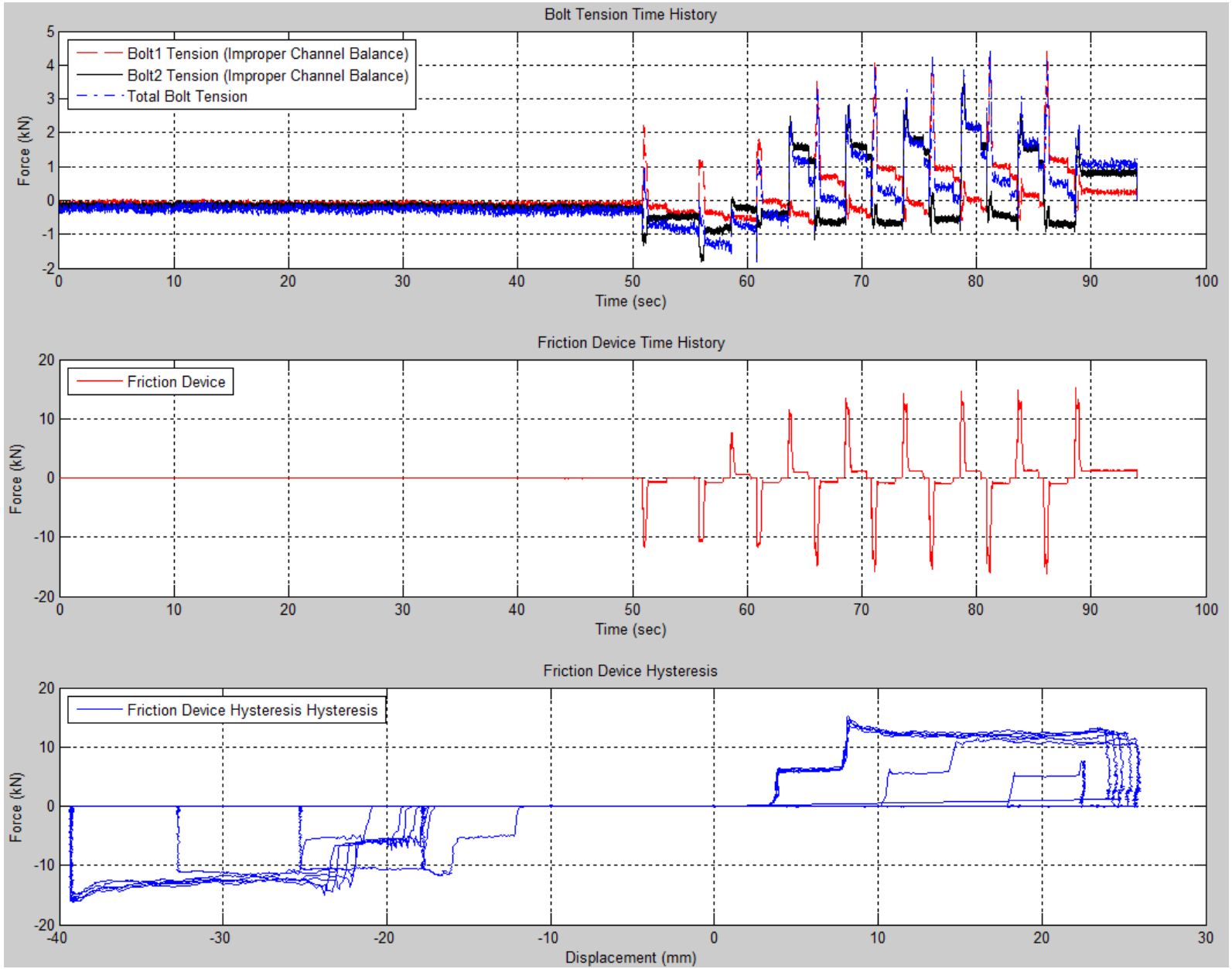
Bolt Tension Time History
Bolt1 Tension (Improper Channel Balance)
Bolt2 Tension (Improper Channel Balance)
Total Bolt Tension
Force (kN)
Time (sec)
Friction Device Time History
Friction Device
Force (kN)
Time (sec)
Friction Device Hysteresis
Friction Device Hysteresis Hysteresis
Force (kN)
Displacement (mm)

Load Case 7 (T5CCW-E2-0.2Hz-+/-4.0-Sine):

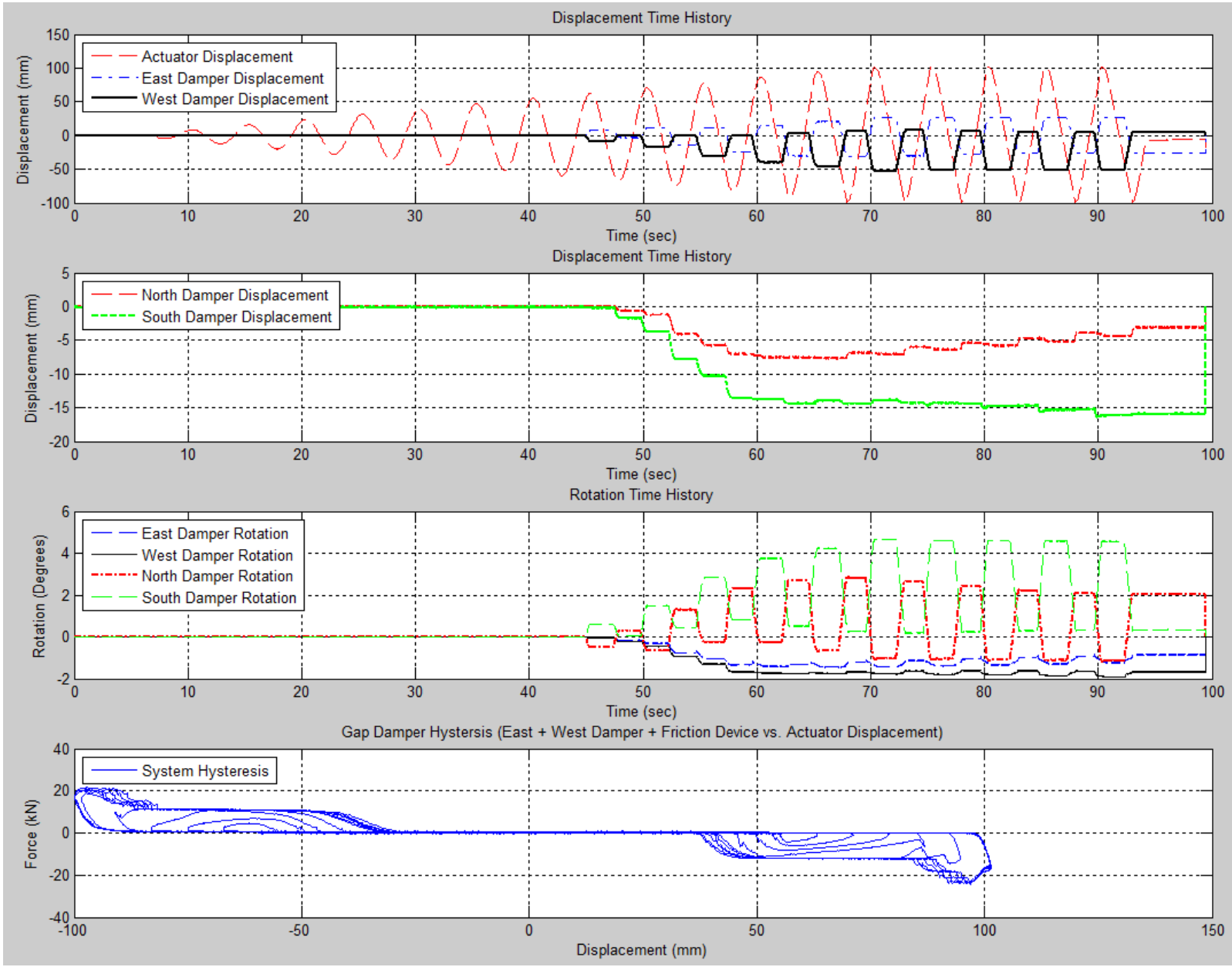

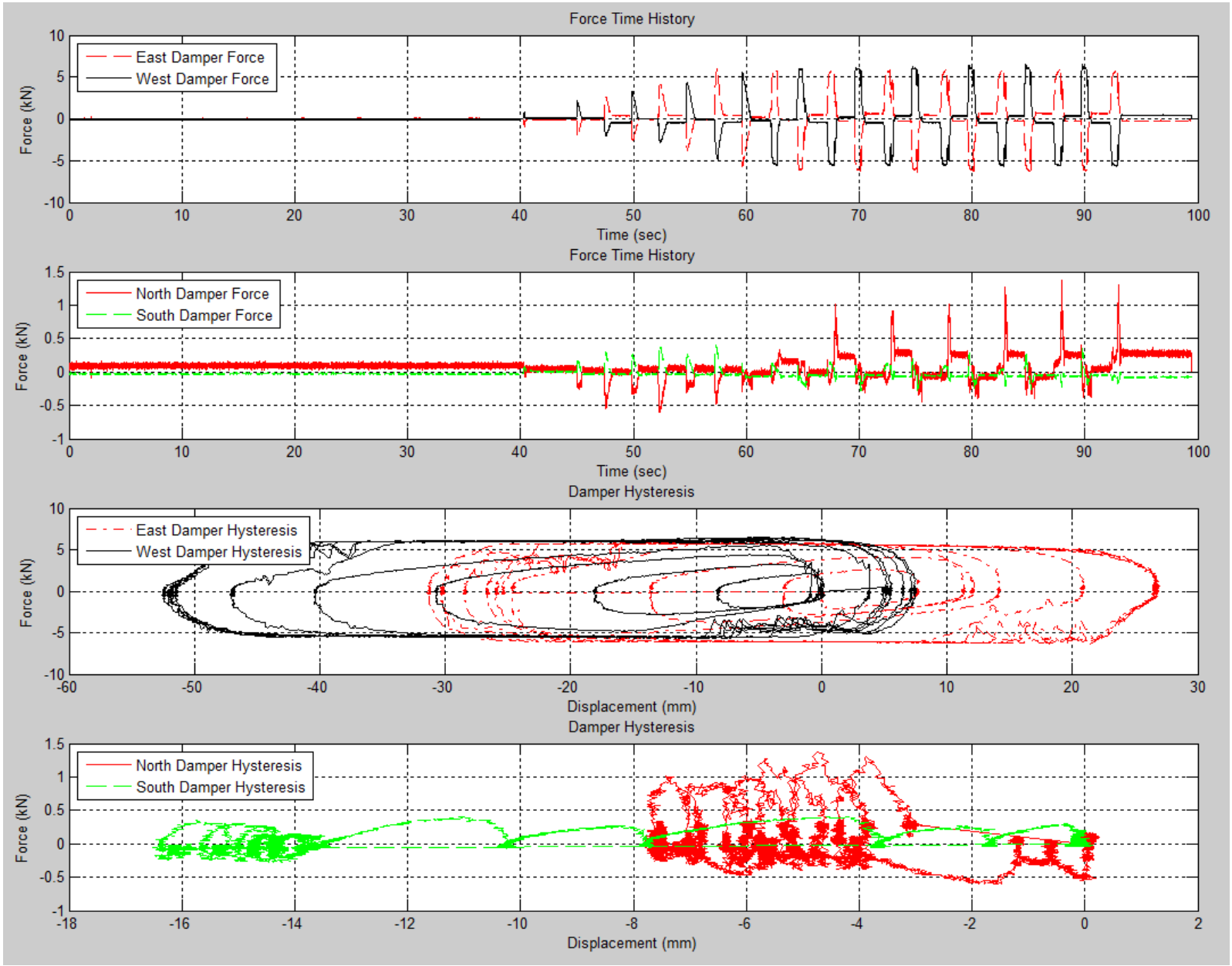
Force Time History
East Damper Force
West Damper Force
Force (kN)
Time (sec)
Force Time History
North Damper Force
South Damper Force
Force (kN)
Time (sec)
Damper Hysteresis
East Damper Hysteresis
West Damper Hysteresis
Force (kN)
Displacement (mm)
Damper Hysteresis
North Damper Hysteresis
South Damper Hysteresis
Force (kN)
Displacement (mm)

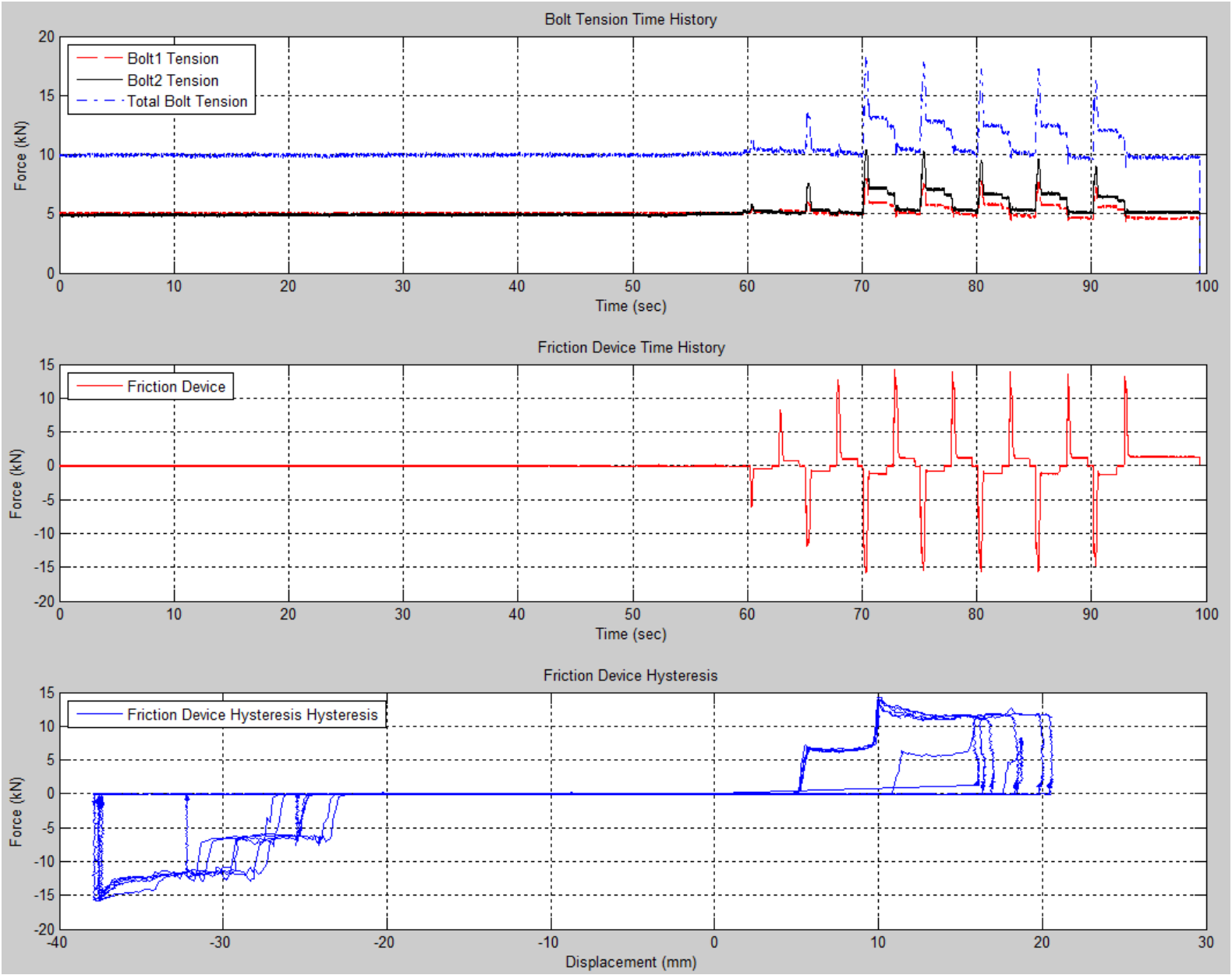
Bolt Tension Time History
Bolt1 Tension
Bolt2 Tension
Total Bolt Tension
Force (kN)
Time (sec)
Friction Device Time History
Friction Device
Force (kN)
Time (sec)
Friction Device Hysteresis
Friction Device Hysteresis Hysteresis
Force (kN)
Displacement (mm)

Load Case 8 (T5CW-E2-0.2Hz-+/-4.0-Sine):

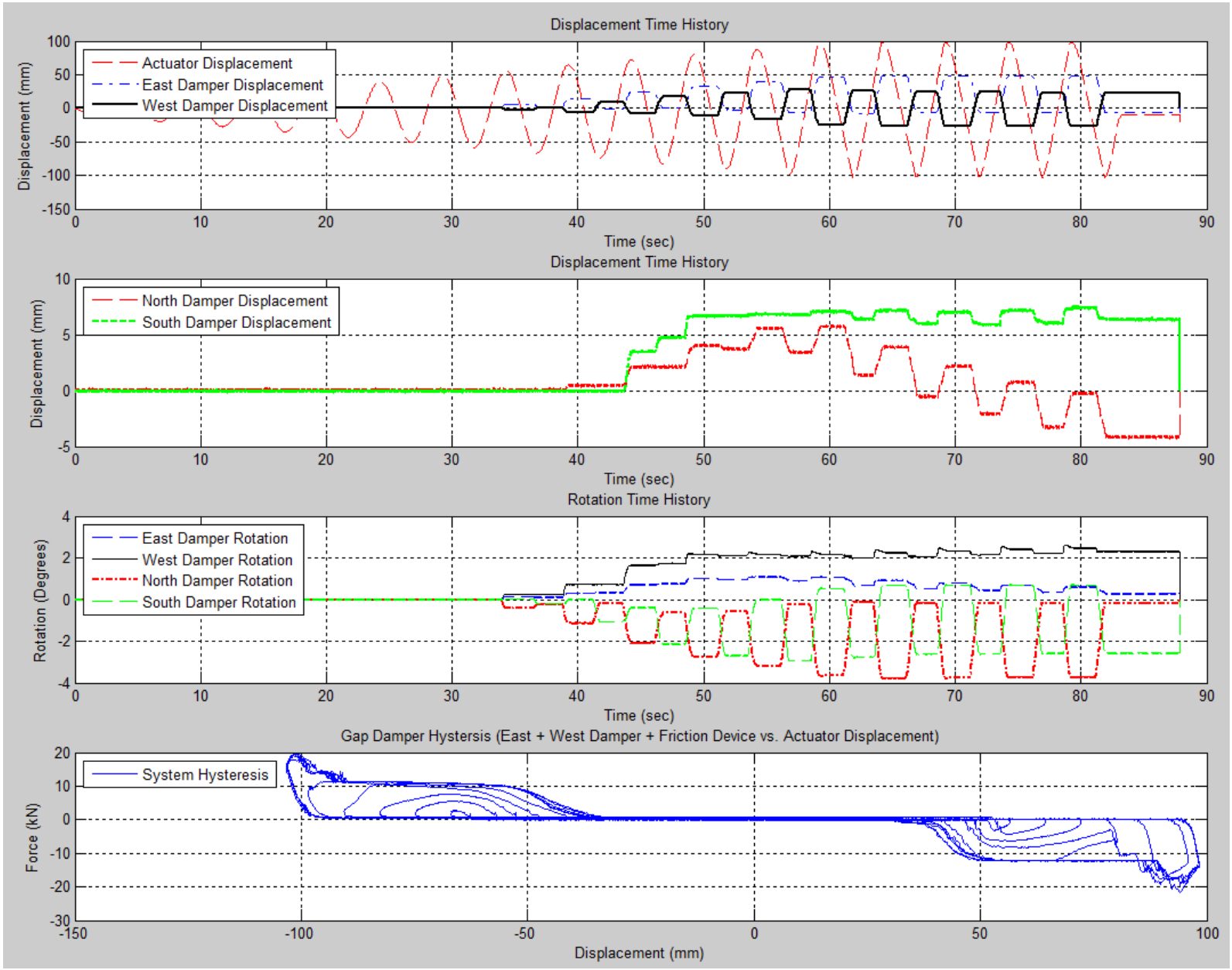

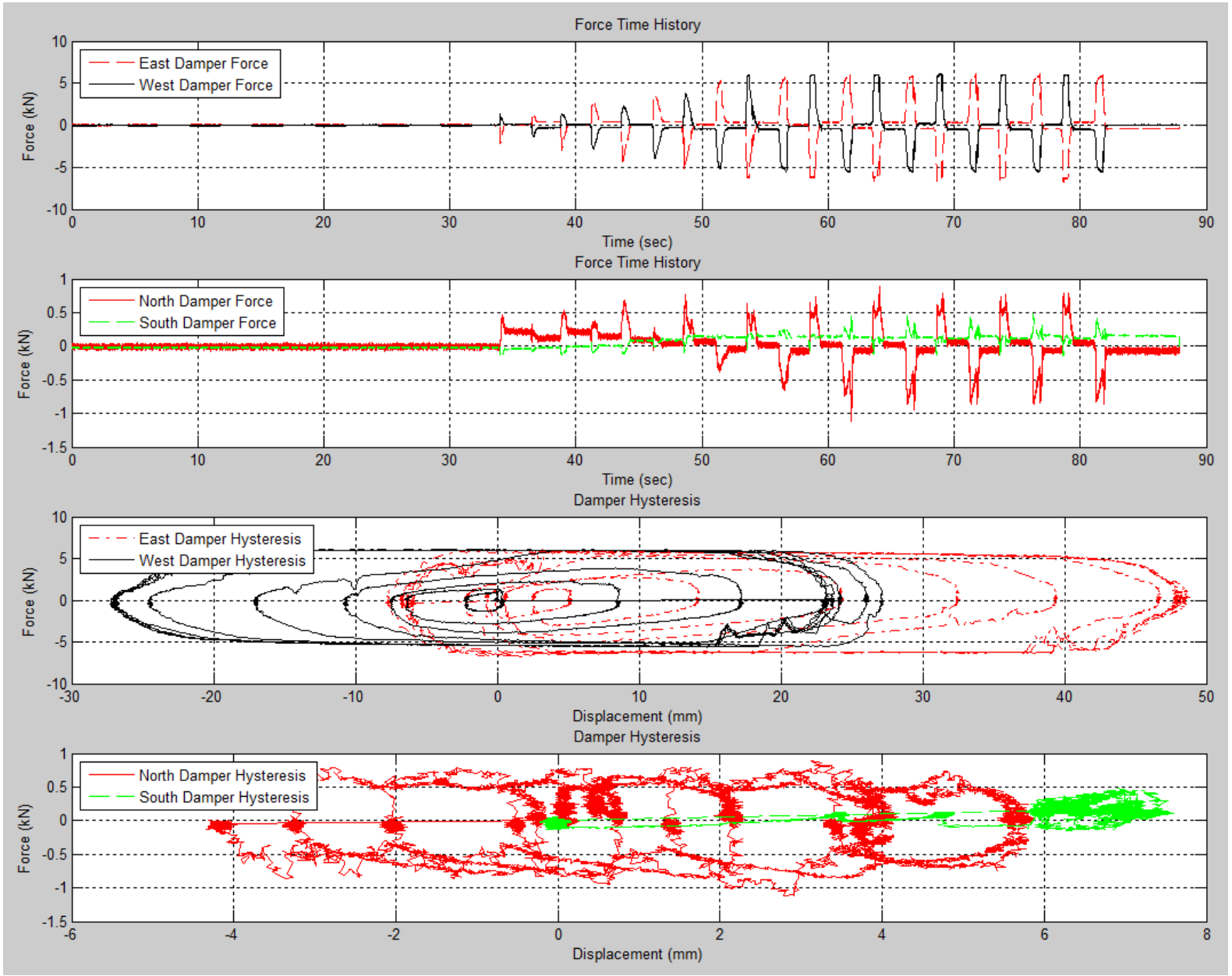
Force Time History
East Damper Force
West Damper Force
Force (kN)
Time (sec)
Force Time History
North Damper Force
South Damper Force
Force (kN)
Time (sec)
Damper Hysteresis
East Damper Hysteresis
West Damper Hysteresis
Force (kN)
Displacement (mm)
Damper Hysteresis
North Damper Hysteresis
South Damper Hysteresis
Force (kN)
Displacement (mm)

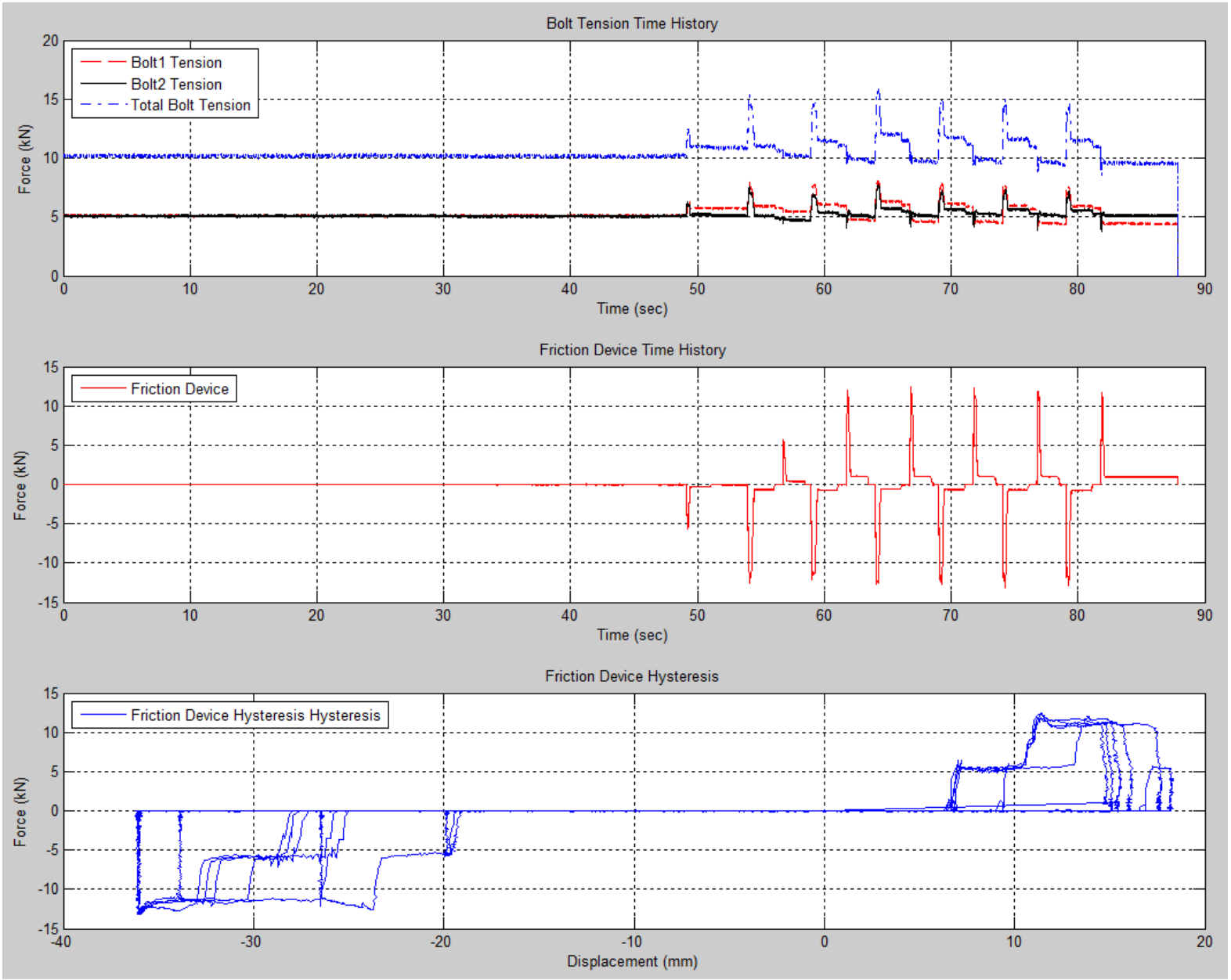
Bolt Tension Time History
Bolt1 Tension
Bolt2 Tension
Total Bolt Tension
Force (kN)
Time (sec)
Friction Device Time History
Friction Device
Force (kN)
Time (sec)
Friction Device Hysteresis
Friction Device Hysteresis Hysteresis
Force (kN)
Displacement (mm)